UNIVERSITY OF
Cincinnati

Reconstructing high-frequency Holocene glacial chronostratigraphies in the Himalayan-Tibetan orogen

Sourav Saha
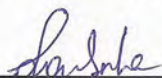
University of Cincinnati

Date: 11/2/2018

I, Sourav Saha, hereby submit this original work as part of the requirements for the degree of Doctor of Philosophy in Geology.
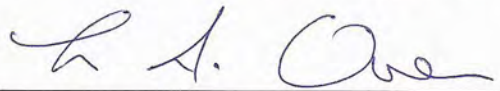
It is entitled:

Reconstructing high-frequency Holocene glacial chronostratigraphies in the Himalayan-Tibetan orogen
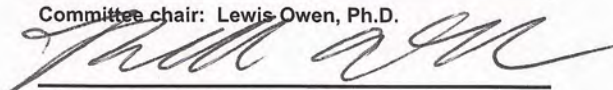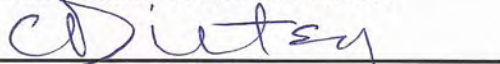
Student's signature: _____

This work and its defense approved by:
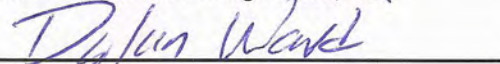
Committee chair: Lewis Owen, Ph.D.

Committee member: Richard Beck, Ph.D.

Committee member: Craig Dietsch, Ph.D.

Committee member: Dylan Ward, Ph.D.

UNIVERSITY OF Cincinnati

31702

Reconstructing high-frequency Holocene glacial chronostratigraphies in the Himalayan-Tibetan orogen

A dissertation submitted to the

Graduate School

of the University of Cincinnati

in partial fulfillment of the

requirements for the degree of

DOCTOR OF PHILOSOPHY

in the Department of Geology

of the McMicken College of Arts and Science

November 2nd, 2018
by

Sourav Saha

M.Phil., Jawaharlal Nehru University, New Delhi, 2013

M.A., Jawaharlal Nehru University, New Delhi, 2011

B.A., University of North Bengal, Raja Rammohanpur, 2009

Committee Chair: Lewis A. Owen, Ph.D.

Reconstructing high-frequency Holocene glacial chronostratigraphies in the Himalayan-Tibetan orogen

Academic dissertation for the Degree of Doctor of Philosophy in Geology at the University of Cincinnati to be publicly defended on Friday 2nd November 2018 at 1:00 PM in Geology-Physics Building, Cincinnati, Ohio 45221.

Abstract

The timing and extents of high-frequency Holocene glacier advances are reconstructed in the seven glaciated valleys of the NW and Central Himalaya using detailed geomorphic mapping, sedimentological analysis, ^{10}Be dating, equilibrium-line altitudes (ELAs), statistical analyses, and numerical modeling. Following the north-south (low to high) precipitation gradient the study areas include: Stok, Lato, Karzok, and Parkachik valleys in the Zanskar range; Hamtah and Kulti valleys in the Lahul Himalaya; and Bhagirathi valley in the Garhwal Himalaya. Eighty new ^{10}Be ages indicate that locally glaciers advanced extensively (ΔELA: ~260±100 m) during the late glacial in the Kulti valley (tentatively at ~14.7±2.1 ka) and the Early Holocene (ΔELA: ~180±60 m) in the Kulti (~13.0–10.9 ka) and Hamtah (~10.4±0.4 ka) valleys. Local glacier advances became progressively more restricted overtime during the Mid-Holocene (ΔELA: ~160±80 m) in the Karzok valley (~6.1–3.3 ka) and during the Late Holocene (ΔELA: ~4–140 m) in the Stok (~2.1–0.9 ka), Lato (~0.7–0.4, ~0.3±0.1 ka), Karzok (~2.6–0.5, ~1.0±0.1, ~0.7±0.1 ka), Hamtah (~0.2±0.1 ka), Kulti (~0.6–0.4 ka), Parkachik (~0.2–0.1 ka), and Bhagirathi (~2.4–1.9, ~1.7–0.5, ~0.5–0.1 ka) valleys. Furthermore, four hundred and sixty published ^{10}Be ages are compiled to reconstruct regional stages in the 73 glaciated valleys across the whole orogen to evaluate these new local glacial stages and to help understand the pattern of Holocene glaciation over the Himalayan-Tibetan orogen. The regional stages, stated here as the Himalayan-Tibetan Holocene stages (*HTHs*), indicate at least one late glacial (~15.3–11.8 ka) and five Holocene (~11.5–9.5, ~8.8–7.7, ~7.0–3.2, ~2.3–1.0, and <1 ka) glacier advances. Additional two Mid-Holocene substages or Himalayan Holocene stages (*HHs:* ~6.9–4.3 and ~4.5–2.8 ka) are defined for the NW Himalaya where ~40% of the total 80 valleys are studied for detailed glacial chronostratigraphies. Paleoglacier maps are also developed for these previously studied valleys for regional ELA reconstructions. Past temperature (*T*) profiles are modeled based on glacier geometry and using an

inverse glacier flow model in 66 of the total 80 valleys. Inter-regional comparisons of the timing and extents of these glacier advances are performed using a climate zonation map; developed using Cluster Analysis and Principal Component Analysis. These inter-regional comparisons support that the Early Holocene *HTHs* were likely driven by enhanced precipitation; the ~8.8–7.7 ka *HTHs* by regional cooling; the early Mid-Holocene *HTHs* by declining precipitation and low temperature; and the Late Holocene *HTHs* by overall regional cooling. Issues of high-degree of ^{10}Be age scattering due to prior exposure (i.e., inheritance) are also addressed by targeting two historically dated moraines in the upper Bhagirathi valley. Low concentrations of inherited ^{10}Be (age equivalent of ~0.05–0.13 ka) are measured in the independently dated moraines in the temperate Bhagirathi valley. In conjunction with the local glacial chronostratigraphies developed in the new study areas, it is evident that the melt-dominated highly active temperate and polythermal valley glaciers are relatively better candidates for reconstructing high-resolution Holocene glacial chronologies than the cold-based less erosive semiarid and arid valley glaciers.

Department of Geology

University of Cincinnati, OH 45221

UNIVERSITY OF
Cincinnati

Acknowledgments

seasons. I am fortunate to be part of this international family and will always be a proud alum.

SS also thanks to the Doctoral committee members that include Craig Dietsch, Dylan Ward, and Richard Beck and other past and present faculties of the Department including Tom Lowell, Dan Sturmer, Joshua Miller, and Eva Enkelmann for all the support and encouragement throughout the last four years. Time and again they have helped me to improve professionally and become a better scientist. Finally, none of my research works would have been possible without the support from my advisor, LAO. He is like a fatherly figure to me who have always understood me, given me plenty of freedom to undertake my independent research, and always cared for me, my future, and my family. You are a role model to me and always will be.

Portions of this dissertation were critically reviewed by Marc W. Caffee (Purdue University) and three anonymous reviewers. The committee members are also thanked for their improvements to earlier drafts of this work.

This work is dedicated to the following:

My family: my mom, my belated father, Mimi (my sister), and Abby (my girlfriend)—thank you for your infinite love and support.

Professor Amitabh Kundu who is currently a Distinguished Fellow at the Research and Information System for Developing Countries, New Delhi—I would not be able to come to the USA and complete my dream without your support during the most critical moment of my life. I dedicate this thesis as a small gift to your generosity.

Table of contents

Thesis content

This doctoral dissertation consists of a summary section and the three manuscripts listed below.

Paper I.

Saha, S., Owen, L.A., Orr, E.N., and Caffee, M.W., 2018. Timing and nature of Holocene glacier advances at the northwestern end of the Himalayan-Tibetan orogen: Quaternary Science Reviews, v. 187, p. 177–202.

Paper II.

Saha, S., Owen, L.A., Orr, E.N., and Caffee, M.W., *in prep*. High-frequency Holocene glacier fluctuations in the Himalaya and Tibet: Quaternary Science Reviews.

Paper III.

Saha, S., Owen, L.A., Orr, E.N., and Caffee, M.W., *in preparation*. Systematically inherited cosmogenic ^{10}Be in Late Holocene moraine boulders in the Bhagirathi catchment of the Garhwal Himalaya, northern India: *intend to submit in* Earth Surface Processes and Landforms.

Author contributions

The contributions from listed authors are divided as follows for each article.

I.   *My contribution*: I led the project, compiled the data, did the quantitative analyses, constructed all the tables, drew figures, and wrote the main body of the paper. My contribution also involved the field investigation including field mapping and sampling for cosmogenic ^{10}Be dating. I also prepared cosmogenic ^{10}Be samples in the Quaternary Geochronology Laboratories of the University of Cincinnati.

Other contributions: LAO initiated the project. LAO and ENO contributed to field mapping, sampling, and involved in the constructive discussion in the field. MWC AMS measured the ^{10}Be samples at the PRIME laboratory of Purdue University and additionally, provided constructed comments. All authors contributed to commenting on the paper, analyses, and discussion.

II.   *My contribution*: I initiated and led the project, compiled the data, did the quantitative analyses, constructed all the tables, drew figures, and wrote the main body of the paper. My contribution also involved the field investigation including field mapping and sampling for cosmogenic ^{10}Be dating. I also prepared cosmogenic ^{10}Be samples in the Quaternary Geochronology Laboratories of the University of Cincinnati and performed the inverse flow model.

Other contributions: LAO conducted an initial field investigation in the Kulti valley study area and obtained moraine boulders samples for ^{10}Be dating. LAO and MWC also provided constructed comments for the project. ENO contributed to field mapping, sampling, and involved in the constructive discussion in the field. MWC AMS

measured the ^{10}Be samples at the PRIME laboratory of Purdue University. All authors contributed to commenting on the paper, analyses, and discussion.

III.   *My contribution*: I led the project, compiled the data, did the quantitative analyses, constructed all the tables, drew figures, and wrote the main body of the paper. My contribution also involved the field investigation including field mapping and sampling for cosmogenic ^{10}Be dating. I also prepared cosmogenic ^{10}Be samples in the Quaternary Geochronology Laboratories of the University of Cincinnati.

Other contributions: LAO initiated the project. LAO and ENO contributed to field mapping, sampling, and involved in the constructive discussion in the field. MWC AMS measured the ^{10}Be samples at the PRIME laboratory of Purdue University and additionally, provided constructed comments. All authors contributed to commenting on the paper, analyses, and discussion.

1   Introduction

Over the past decade, compilations of young glacial chronologies have been used to help reconstruct and understand the nature of Holocene glaciation on a global scale (Grove, 2008; Davis et al., 2009; Solomina et al., 2015, 2016). Most of these studies conclude that long-term glacier advances during the Holocene in extratropical regions are broadly the consequence of climatic change driven by orbital forcing (Solomina et al., 2015). Changes in oceanic-atmospheric circulations in the North Atlantic (Denton and Broecker, 2008; Chiang and Friedman, 2012; Chiang et al., 2014; Wanner et al., 2015) represent another possible amplification mechanism. By way of contrast, long-term forcing behind Holocene glacier variability in the Himalaya has been attributed to distinct regional teleconnections, and do not correlate directly with orbital forcing (Solomina et al., 2015, 2016). Despite the impressive preservation of glacial landform assemblages throughout the Himalaya, this view has not been adequately tested due to the lack of well-defined Holocene glacial chronostratigraphies. We intend to resolve this issue in this thesis by contributing new glacial chronologies and improving the existing ones across the Himalayan-Tibetan orogen (Paper I).

In addition, studies that focused on 20th and 21st Century glacier fluctuations throughout the Himalayan-Tibetan orogen, indicate non-uniform retreat, and in some cases advance, of mountain glaciers due to warming and associated atmospheric changes (Bhambri et al., 2011, 2017; Bahuguna et al., 2014; Brun et al., 2017). Variable temporal and spatial responses of tropical-subtropical high-altitude valley glaciers to climate change present significant challenges for model predictions and environmental risk assessment (Barker, 2007; Cogley et al., 2010; IPCC, 2014). Defining past spatial fluctuations of high-altitude mountain glaciers across a variety of climatic and orographic settings in the orogen on millennial and sub-millennial timescales highlights issues relevant to the nature of future environmental change in Central Asia (Bolch et al., 2012; Vaux Jr. et al., 2012). We aim to address this issue by exploring further ways in which we can interpret ^{10}Be dated glacial chronostratigraphies locally and offer a robust inter-regional comparison of Holocene glaciations in the orogen (Paper II).

High-resolution glacial chronologies from valley glaciers in the Himalayan-Tibetan orogen can be used to test the hypothesis that the long-term pattern of Himalayan glacier advances is either in phase or out of phase with glacier advances throughout the Northern Hemisphere, and elsewhere. Detailed glacial chronologies may further provide critical insights into the relative controls of climatic factors, which include: insolation driven movement of Earth's thermal equator; maritime influences; upper atmospheric circulation change and ocean heat transfer (Solomina et al., 2015, 2016); and non-climatic factors specific to each locality such as microclimate variability, topography, debris cover of glaciers, and glacier type (Barr and Lovell, 2014; Anderson et al., 2014). Previous studies (e.g., Dortch et al., 2013; Murari et al., 2014; Owen and Dortch, 2014; Solomina et al., 2015, 2016) have compared Quaternary (mainly Pleistocene) glacial history across the Himalayan-Tibetan orogen, but a clear delineation of the inter-regional variability in glacier responses to identical climatic perturbation, especially during the Holocene, is lacking. In paper II we have tried to resolve this issue.

In this study, we, therefore, specifically targeted young moraines in seven glaciated valleys of the NW and central Himalaya and Transhimalaya following the orographically controlled precipitation gradient and glacial dynamics (Fig. 1; Bookhagen et al., 2005; Bookhagen and Burbank, 2006). From north to south (semiarid to humid) the study areas include: Stok, Lato, Karzok, and Parkachik valleys in the Zanskar range (paper I, II); Hamtah and Kulti valleys in the Lahul Himalaya (paper I, II); and Bhagirathi valley in the Garhwal Himalaya (paper III).

Due to the lack of preserved organic materials required for radiocarbon dating and limited radiocarbon (cf. Röthlisberger and Geyh, 1985a, b; Yi et al., 2008) and optically stimulated luminescence (OSL; cf. Bisht et al., 2017; Deswal et al., 2017) chronologies across the Himalaya and Tibet, orogen-wide comparisons of Holocene glaciation using these dating techniques are substantially challenging. However, since quartz-rich boulders on moraines are abundant in these settings, terrestrial cosmogenic nuclide (TCN) dating of multiple boulders are often preferred to determine the apparent age of individual landforms. Despite great promises, a considerable research gap exists in our understanding of the geological uncertainties of the TCN dating method. For instance, moraine boulders are assumed to have zero

concentration of TCNs before incorporating into the glacial system (cf. Gosse and Phillips, 2001; Gosse, 2005; Ivy-Ochs et al., 2007; Putkonen et al., 2008). However, if the boulders have previous inventory (i.e., concentration) of TCNs (e.g., ^{10}Be) due to prior exposures, known as inheritance, during part of the bedrock slopes and/or glacial transportation, they will systematically yield older apparent ages (Applegate et al., 2010, 2012; Heyman et al., 2011). Similarly, if post-depositional shielding or exhumation took place, incomplete exposures are expected, giving younger than true ages (ibid). Studies that investigated Late Quaternary glacial deposits argued that incomplete exposures are more important than prior exposures/inheritance (Applegate et al., 2012; Heyman et al., 2011). However, recent studies on young Holocene moraine boulders (Li et al., 2016) and from glacially modified landscapes (cf. Balco et al., 2002; Owen et al., 2009; Rinterknecht et al., 2006) and/or from areas dominated by non-erosive ice (cf. Fabel et al., 2002; Briner et al., 2006; Placzek et al., 2014; Orr et al., 2017, 2018), show that inheritance from prior exposures contribute to the high degree of scattering in exposure ages. Despite this recognition, the role of complex geological history (including the links between erosion, climate, topography, tectonics, and glacial dynamics) on prior exposures has not been adequately addressed (Scherler et al., 2011a, b, 2014; Bookhagen et al., 2005; Bookhagen and Burbank, 2006; Gruber and Haeberli, 2007; Dortch et al., 2011; Roe, 2011; Barr and Lovell, 2014). In this thesis, we also aim to address this issue by directly measuring inherited ^{10}Be concentrations in the two independently dated moraines (ten ^{10}Be dates) in the Bhagirathi valley.

Using a combination geomorphic mapping, sedimentological analysis, equilibrium-line altitudes (ELA) and ELA depressions (ΔELAs), and 80 new ^{10}Be ages, we aim to constrain new Holocene glacial chronostratigraphies in our seven study areas of the NW and central Himalaya and Transhimalaya. Additionally, we have also compiled and compared Holocene glacial chronostratigraphies in 73 previously studied glaciated valleys across the whole orogen (in 36 locations in Fig. 1) for which ^{10}Be ages (n=460) are available. We only compared ^{10}Be boulder ages sampled from ice-marginal laterofrontal, terminal/recessional, and lateral moraines in this thesis.

2 Study areas

Our study areas encompass several tectonic-lithologic domains (Honegger et al., 1982; Brookfield and Andrews-Speed,1984; Searle et al., 1987; Searle et al., 1997, 1999; Steck et al., 1998; Schlup et al., 2003) and are bounded by four major structures. From north to south these structures are: i) Indus-Tsangpo Suture Zone (ITSZ), ii) South Tibetan Detachment (STD), iii) Main Central Thrust (MCT), and iv) Main Boundary Thrust (MBT; Fig. 2; Epard and Steck, 2008). Continued crustal shortening, the result of the collision and partial subduction of the Indian and Eurasian continental lithospheric plates since the early Miocene, initiated the development of these foreland propagating thrust systems and uplifted mountain ranges (~400 to >7000 m above sea level) in the Himalaya (Searle et al., 1997; Fielding et al., 1994; Duncan et al., 2003). Lithotectonically the ITSZ defines the northernmost limit of the Tethyan Sedimentary Series (TSS), STD defines the northern limit of the High Himalayan Crystalline Series (HHCS), MCT the northern limit of the Lesser Himalayan Series (LHS), and MBT the northern limit of the Sub-Himalayan Series (SHS; Fig. 2; Searle et al., 1997, 1999; Steck et al., 1998; Epard and Steck, 2008).

Stok, Lato, and Karzok valleys (paper I) are located in the far NE and east of the semiarid Zanskar Range of the NW Himalaya and Transhimalaya, bounded by the Ladakh Batholith in the north and HHCS in the south (Kirstein, 2011). Regional tectonic collisions resulted in the folding and thrusting of Zanskar metasedimentary rocks and formed the Zanskar Suture Zone (ZSZ) and ITSZ (Searle, 1986; Steck et al., 1998; Schlup et al., 2003; Orr et al., 2017). The Stok study area consists of thick-bedded conglomerates with alternating coarse and fine-grained sandstone, siltstone, and shale known as the Stok Kangri (Kangri = glacier) molasse (Brookfield and Andrews-Speed, 1984; Fig. 2). The Karzok and Lato study areas, north of ZSZ, are composed of coarse-grained granite of the North Himalayan nappe system (Stutz and Thöni, 1987; Fuchs and Linner, 1996; Steck et al., 1998; Epard and Steck, 2008). Two glaciers in the Karzok valley (e.g., Mentok and Gomuche Kangri) and each in Lato (e.g., Amda kangri) and Stok (e.g., Stok Kangri) valleys are studied here (Fig. 1). These study areas presently receive annual precipitation ranging from 40 to 100 mm (Fig. 1; Bookhagen and Burbank, 2006). Most of these glaciers are predominantly cold-based

sub-polar types, they are smaller (0.6–2.5 km^2), mostly debris free, and are more precipitation-sensitive and sublimation dominated (Benn and Owen, 2002). Regional ELAs vary between ~5480 and 5900 m asl (Table 1).

In contrast to smaller sub-polar type glaciers elsewhere in Zanskar (Orr et al., 2017, 2018; Saha et al., 2018), the Nun Kun massif (paper II), in the far west of the Zanskar Range, has a few large glaciers, including the ~12-km-long Parkachik glacier (~48 km^2; Fig. 1). The major lithologies of the massif include intruded leucogranite and gneiss, and quartzite metamorphosed from the TSS sequence (Fig. 2; Fuchs, 1997; Vance and Harris, 1999). Parkachik glacier is located on north-facing flanks of the Nun Kun massif, polythermal in nature, and mantled by a thin layer of debris (Lee et al., 2014). Topography strongly influence the precipitation gradient in the valley, with present-day precipitation varying between ~150 and 700 mm a^{-1} from the valley floor to the higher reaches (Bookhagen and Burbank, 2006). Snow is delivered to the glaciers by avalanching and direct snowfall (Osmaston, 1994). Regional ELAs vary between ~5000 and 5600 m asl (Table 1). Presently glaciers in the NW Himalaya and Transhimalaya are fed by the winter mid-latitude westerlies system-driven snowfall and directly respond to changes in the strength of westerly-winds (Mölg et al., 2014). However, the Indian summer monsoon (ISM) also plays a significant role in modulating past and present glacier dynamics in the region (Finkel et al., 2003; Bookhagen et al., 2005; Owen, 2009).

The Hamtah and Kulti study areas (paper I, II) are located on the NW trending northern and southwestern slopes of the Greater Himalaya in Lahul, respectively (Fig. 1). Major lithologies of the Hamtah crystalline axis consists mostly of migmatites, and the Rohtang gneiss and granite (Fig. 2; Kumar et al., 1987). The Kulti valley, however, has neo-terminal Proterozoic black slate, phyllite, and fine-grained biotite-schist of the Batal Formation (Kumar et al., 1987; Rawat and Purohit, 1988; Bhargava, 2008), with Neoproterozoic to Permian granite (Steck, 2003). These study areas in Lahul, located in the rain shadow of the Pir Panjal Range, has an annual precipitation of ~200–900 mm from the valley floor to the higher reaches (Fig. 1; Bookhagen and Burbank, 2006; Azam et al., 2014), producing a wet and cool transitional climate, conducive for the growth of large (~4–18 km^2), melt-dominated, high-activity, debris-mantled

polythermal-to-temperate glaciers (Fig. 2; Owen et al., 1996, 1997; Benn and Owen, 2002). Hamtah glacier in the Hamtah valley and Sonapani glacier in the Kulti valley are studied here (Fig. 1). Contemporary steady-state ELAs vary between ~4500 and 4800 m asl in the region (Table 1), and glaciers are highly sensitive to changes in the ambient temperature (Su and Shi, 2002; Bisht et al., 2017).

The Bhagirathi valley (paper III) is also located on the NW trending northwestern slopes of the Greater Himalaya in Garhwal (Fig. 1). The valley is bounded by STD to the north and Vaikrita thrust (VT) to the south (Fig. 2; Searle et al., 1997, 1999) and carved mostly within the Shivling-Bhagirathi leucogranite-granodiorite body, and gneiss, and metasedimentary rocks in the upper reaches (>4000 m asl; Fig. 2; Agarwal & Kumar, 1973; Sharma, 1983; Chaujar et al., 1993; Bhambri et al., 2011). Presently the valley receives plenty of moisture, with contribution from ISM is ~1000–2500 mm a^{-1} (IMD, 1989; Burbank et al., 2003; Scherler et al., 2010; Thayyen and Gergan, 2010; Wulf et al., 2010) and mid-latitude westerlies is ~546 mm a^{-1} (Bhambri et al., 2011). Snow is supplied mostly indirectly in the form of avalanches from cornices on the steep bedrock slopes (Sharma and Owen, 1996; Tangri, 2004; Dhobal et al., 2008; Singh et al., 2008; Raina et al., 2015; Bhattacharya et al., 2016). Two glaciers, Gangotri (trunk) and Meru (tributary), in the Bhagirathi valley, are selected for this study. Gangotri glacier is the largest glacier in the Central Himalaya, covering an area of ~144 km^2, and largely a high-activity type, thick debris-mantled, temperate glacier (Srivastava, 2012; Raina et al., 2015). This glacier is highly sensitive to changes in the ambient temperature. The contemporary ELA of the glacier lies between ~4510 and 5160 m asl (Table 1; Owen and Sharma, 1998; Naithani et al., 2001; Ahmad and Hasnain, 2004, Burbank et al., 2003; Srivastava, 2012; Singh et al., 2017).

3   Methodologies

3.1.   Mapping and morphostratigraphy

We prepared detailed field geomorphic and surficial geologic maps using digital mapping techniques and handheld GPS with ±3 m spatial uncertainties at the scale of 1:20,000 (Paper I–III). We

employed the geomorphic and sedimentological techniques described in Benn and Owen (2002) and Benn and Evans (2010) to identify and differentiate landforms and sediments of different origins (Paper I–III). Multiple fieldworks are conducted in the summers of 2014–2016 (Fig. 3) including solo and group field trips.

We also defined morphostratigraphy and glacial stages based on position, morphology, cross-cutting relationship, vegetation, and relative weathering characteristics of individual moraines and associated landforms (Paper I–III; Owen et al., 1997). Using the scheme outlined in Owen and Derbyshire (1989), Owen et al. (1997), Hughes et al. (2005), and Hughes (2010), we used the letters 'M' (or 'm') to denote moraines and 'b' for glacially eroded bedrock. Subscript letters were used to indicate the study area, e.g., 'K' for the Kulti valley, 'H' for the Hamtah valley. Individual moraines and bedrock surfaces were also numbered using the subscript '1' for the morphostratigraphically youngest of all preserved sets of moraines, and the subscript letter 'a' for the youngest ridge of a moraine set. We assigned each glacier advance or still-stand position to a local glacial stage (Paper I–III).

3.2. GIS and remote sensing analysis

GIS and remote sensing techniques using ESRI ArcGIS 10.3 were extensively employed to refine the field maps (Paper I–III). We used Google Earth imagery, Advanced Spaceborne Thermal Emission and Reflection Radiometer (ASTER) global digital elevation models (GDEMs), and Landsat Enhanced Thematic Mapper Plus (ETM+) imagery to aid the field maps further. Glaciers were manually delineated and further assisted with a combination of terrain attributes derived from ASTER (30 m) DEM, ETM+ multispectral optical and/or thermal satellite remote sensing, and high-resolution images from Google Earth to detect ice-debris interface (Paper I–III; Bishop et al., 2001; Bolch et al., 2008; Kargel et al., 2005; Paul et al., 2004; Shukla et al., 2010). We also used satellite remote sensing and published geomorphic maps to develop contemporary and past glacier maps of all previously investigated (dated using [10]Be) glaciated valleys. Additionally, essential data for ELA measurements are generated using *3D Analyst* and *Conversion Tools* in ArcGIS, including glaciated area or polygons, elevations, triangular irregular networks (TINs), and

ASCII files (Benn et al., 2005; Osmaston, 2005). Basic terrain (e.g., relief, slope, aspect, length, cross profiles, hypsometry, contours, and hillshade) and hydrological data were also generated. We also used GIS to extract and interpolate climatic data. For example, ~42,511 glacier polygons (samples), derived from the Randolph Glacier Inventory (RGI 6.0), were converted into points and, subsequently, utilized to extract climate data from the gridded CRU CL 2.0 (10' latitude/longitude) reanalysis temperature (in °C) and the Tropical Rainfall Measuring Mission (TRMM) derived precipitation (in mm) datasets (4-km-horizontal x 250-m-vertical; Appendix A3).

3.3. Geochronology

3.3.1. Field sampling

Multiple moraine boulders (n = 2–9) from each moraine were sampled using a chisel and hammer after carefully considering the morphostratigraphy, physical setting, e.g., stability, degradation, hillslope contamination, and surficial characteristics (Paper I–III; cf. Gosse and Phillips, 2001). Well-inset stable boulders with no evidence of post-depositional surface deflections, detrital cover, surface spallation, pitting, fracturing, and/or extensive weathering were preferentially sampled. We also preferred to choose boulders with well-developed lichen cover and/or rock varnish, because they provide a measure of confidence that boulders had not been recently exhumed and/or toppled (Owen et al., 2006). Due to high wind speed (5–15 km h^{-1}; Singh et al., 2007; Ramanathan, 2011) in this high elevation settings, we argue that our sampled boulders with heights ranging from 0.5 to 3.5 m, likely had little snow cover that would have shielded them from cosmic rays (Balco et al., 2008; Heyman et al., 2016). Approximately 500 g of rock to a depth of ≤3 cm from the top of each boulder was collected. Topographic shielding from the boulder surface to the horizon was measured using a compass and an inclinometer at 10° interval (Gosse and Phillips, 2001; Balco et al., 2008).

3.3.2. Cosmogenic surface exposure dating

We used [10]Be terrestrial cosmogenic nuclides (TCNs) to estimate apparent moraine ages and

establish temporal constraints on the high-frequency Holocene glacial advances in the Himalayan-Tibetan orogen (Paper I–III). At Earth's surface, TCNs form in target minerals, in this study: quartz (SiO_2), because of its interaction with high energy cosmic rays (Gosse and Phillips, 2001). The production rate of TCNs in a target mineral depends on variety of factors including its latitude, atmospheric pressure, depth from the surface, density of the material, temporal changes in the geomagnetic strength and solar modulation, surface erosion rate, and shielding (Lal, 1991; Uppala et al., 2005; Lifton et al., 2005, 2008; Balco et al., 2008; Martin et al., 2016; Marrero et al., 2016; Lifton, 2016). Since (spallogenic) production rate of TCNs decreases with depth, the removal of prior TCNs on a boulder by glacier erosion results in resetting of the cosmogenic clock. These boulders are often deposited on the surfaces of ice-marginal moraines which are geomorphological markers in the terrain and signify ice margin geometries. Measuring the concentrations of TCNs in these moraine boulders provide a measure of the length of time the boulders were exposed to cosmic rays. In other words, the time (or year) may be defined as the minimum age of glacier advance (Gosse, 2005; Ivy-Ochs et al., 2007; Putkonen et al., 2008) and/or beginning of glacier retreat from the ice-marginal moraine (Applegate and Alley, 2011; O'Hara et al., 2017). Similarly, for bedrock surfaces, the TCN concentrations may represent the time that a glacier withdrew from a specific location during the retreat (cf. Ward et al., 2009, 2015). Solving for t (time) in the exposure age equation allows us to derive exposure time as (Gosse and Phillips, 2001),

$$N_{10} = \frac{P_{10}}{\lambda_{10}}\left[1 - exp^{-\lambda_{10}t}\right]$$

where N_{10} is a ^{10}Be concentration contains in SiO_2 sample (atoms g^{-1}), P_{10} is the site-specific production rate (atoms g^{-1} a^{-1}), and λ_{10} is the ^{10}Be decay constant (4.99 x 10^{-7}).

We crushed and sieved the boulder samples to attain the 250–500 μm fraction. Quartz extraction, dissolution, chromatography, isolation of Be and the preparation of BeO were executed at the Quaternary Geochronology Laboratories of the University of Cincinnati following the methods outlined in Kohl and Nishiizumi (1992) and Nishiizumi et al. (1994). We performed the AMS measurements at the Purdue Rare Isotope Measurement (PRIME) Laboratory at Purdue University (Sharma et al., 2000).

We calculated 80 new and recalculated 460 published moraine boulder and three bedrock ^{10}Be ages (Paper I–III; Appendices A1, A5, A6) using the community standard Cosmic Ray Exposure program (CREp) of Martin et al. (2016) and CRONUS-Earth V3 of Balco et al. (2008). The global sea-level high-latitude (SLHL) spallogenic ^{10}Be production rate of 4.08±0.23 atoms g^{-1} a^{-1} was used (Borchers et al., 2016; Martin et al., 2016; http://calibration.ice-d.org/). We calculated the apparent exposure ages using the scaling schemes of Lifton-Sato-Dunai (*LSD*; Lifton et al., 2014), time-dependent Lal and Stone (*Lm*; Balco et al., 2008), and time-independent Lal and Stone (*St*; Lal, 1991; Stone, 2000), but we only reported the CREp *LSD* ages (Appendices A2). We assumed zero-erosion rates and reported all the ages in thousands of years (ka) before AD 2016. However, to understand how erosion might affect our Holocene ages, we experimented with several different erosion rates. Our results suggest that even with a high steady-state erosion rate for arid and semi-arid environments, like our study areas, of 10 m Ma^{-1} (see Seong et al., 2007; Dietsch et al., 2015), the difference from zero erosion is <10% over the Holocene.

We followed the formal Holocene stratigraphic subdivision approved by The International Commission on Stratigraphy (ICS; Walker et al., 2012) to evaluate our regional stages. According to ICS, the Early Holocene span from 11.7–8.3 ka, the Mid-Holocene from 8.3–4.2 ka, and the Late Holocene from 4.2 ka to present.

3.4. Statistical analyses

We used arithmetic and weighted means, median, and mode as measures of central tendencies to calculate the apparent mean moraine ages with ±1σ uncertainties (Chapters/Papers I–III). Probability density distribution peaks are also reported as an additional measure of central age (Chapters/Papers I–III).

We used reduced chi-squared (χ^2) statistics (Paper I–III) to assess the distribution of age population following the methods/recommendation of Applegate et al. (2010, 2012), Kaplan et al. (2013), and Putnam et al. (2013b). Whenever a χ^2 value is >1 and falls outside 95% confidence interval, we treated the age population for outlier detection using community standard methods (e.g., Applegate et al., 2010, 2012; Putnam et al., 2013b). We used >2σ from the mean of the distribution (Putnam et al., 2013a) and

Chauvenet's criterion (Taylor, 1997; Dunai, 2010; Putnam et al., 2013b) to detect outliers. Outliers are only removed under following circumstances: i) independent age for the moraine strongly suggests age overestimation; ii) field evidence suggests possible post-depositional toppling, or exhumation, or slope (mass movement) contamination; and iii) ages do not follow morphostratigraphic and reconstructed chronologic order.

To detect distinct regional glacial stages (Paper I–III; Appendices A1, A5), we used a combination of radial plot analysis (using radial plotter of Galbraith, 1990, 2010; Galbraith and Roberts, 2012; Vermeesch, 2009), probability density function (using kernel density or *'ksdensity'* fit in MATLAB R2017a), and Student's t-test (cf. Dortch et al., 2013; Murari et al., 2014). For Student's t-test, a two-tailed p-value of <0.01 (at ≥99% confidence level) was used.

A primary climatic zone map was reconstructed by grouping glaciers (samples) with identical climate parameters (Paper II; Appendix A3; cf. Sagredo and Lowell, 2012). We used Cluster Analysis (CA; Zuming and Maohuan, 1989) and Principal Component Analysis (PCA; Seaby and Henderson, 2014) in the R statistical package (The R Core Team, 2018) to group glaciers. Using the Euclidean distance and the unweighted pair-group method with arithmetic averaging (UPGMA; Romesburg, 2004), we produced a cluster dendrogram (Paper II). We calculated the cophenetic distance between two samples (glaciers) in the cluster dendrogram and performed a Pearson's product-moment correlation between the sample Euclidean and cophenetic distances to test the significance of our clusters/groups (Seaby and Henderson, 2014). Also, we performed an analysis of similarities (ANOSIM; ibid) to test whether the samples (glaciers) within groups are more similar than would be expected by random chance.

3.5.   Equilibrium-line altitudes

Former ELAs are reported assuming a simplistic steady-state scenario (Sugden and John, 1976) and using area-altitude (AA), area accumulation ratio (AAR), and toe-headwall accumulation ratio (THAR) methods for each glacier advance (Paper I–III; Benn et al., 2005; Osmaston, 2005). The modern maximum elevations of lateral moraines (MELM; Nesje and Dahl, 1992) are reported to calculate present ELAs. We

obtained the AARs and THARs from the published literature for diverse climatic regions (Paper I–III). Herein we report the (arithmetic) mean ELA and ELA depression (ΔELA) with ± 1σ uncertainty, obtained from multiple indices and ratios (Paper I–III; Appendices A1, A5).

3.6. Inverse flow model

A linear inverse glacier flow model was used following the methods of Klok and Oerlemans (2003) and Oerlemans (2001, 2005) to estimate the inter-regional change of net temperature (ΔT) during Holocene glacial advances in the orogen (Paper II). This flow model is based on the first-order glacier dynamics (Oerlemans, 2001, 2005). Unlike more explicit numerical glacier/ice sheet models, that require many complex geologic, climatic, and energy balance variables (cf. Azam et al., 2014; Roe and Baker, 2014; Rounce et al., 2015) and are often catchment specific (cf. Carr et al., 2010; Eaves et al., 2016; Pellitero et al., 2016; Putnam et al., 2013b), the current model requires a limited number of variables and hence, is easy to reconstruct for a wide range of Himalayan glaciers and widely different climatic regions throughout the orogen. The linear flow model can be stated as,

$$T(t) = -\frac{1}{c}\left[L(t) + \tau \frac{dL(t)}{dt}\right]$$

where T is a temperature perturbation, t is time, L is the medial glacier length with respect to present snout position, dL is the linear interpolation per decade (dt), c and τ are climate sensitivity and response time, respectively (Paper II; see Appendix A4). Despite limitations, the model is applied to reconstruct the Holocene temperature changes (in K) for 66 glaciated valleys.

4   Summary of papers

4.1. Paper I

Saha, S., Owen, L.A., Orr, E.N., and Caffee, M.W., 2018, Timing and nature of Holocene glacier advances at the northwestern end of the Himalayan-Tibetan orogen: Quaternary Science Reviews, v. 187, p. 177–202.

In this study, we offer new Holocene glacial chronostratigraphies in the three semiarid glaciated valleys (Stok, Lato, and Karzok) and one transitional between humid to the semiarid glaciated valley (Hamtah) of the NW Himalaya. These valleys are chosen based on the orographically-controlled prevailing precipitation gradient which is decreasing northward and, in turn, influence the glacier dynamics. For example, Hamtah glacier, located in the transitional Greater Himalaya, are polythermal-to-temperate in nature. Whereas Stok, Lato, and Karzok valleys in the semiarid Zanskar region have smaller (<2.5 km^2) cirque glaciers that are more sublimation-dominated cold-based types. A succession of young moraines is preserved in these valleys. Since the moraine boulders are believed to derive directly from cirque walls, except Hamtah, we believed that the boulders would likely have low prior exposures or inheritance. This hypothesis led to examining the nature of Holocene glaciations and possible forcing factors behind glacier advances in the NW Himalaya. Using detailed geomorphic mapping and 49 TCN ^{10}Be dating, two Holocene local glacial stages are proposed in the Hamtah (~10.4±0.4, and ~0.2±0.1 ka), four in the Karzok (~6.1–3.3, ~2.1±0.4 [tentative], ~1.0±0.1, and ~0.7±0.1 ka), two in the Lato (~0.5±0.2 [tentative], and ~0.3±0.1 ka), one in the Stok valley (~2.1–0.9 ka). High-amplitude glacier advances are recorded during the Early Holocene (ΔELA ~182 m) and progressively restricted advances in the Mid- and Late Holocene (ΔELA ~4–65 m). We also compared these new ^{10}Be local glacial stages with the existing ones (187 published ages) in the adjacent NW part of the Himalayan-Tibetan orogen. Seven Himalayan Holocene regional stages (*HHs*) are defined; ~10.9–9.3, ~8.2–7.4, ~6.9–4.3, ~4.5–2.8, ~2.7–1.8, ~1.8–0.9, and <1 ka. Similar to local glacial stages, *HHs* also indicate regionally extensive Early Holocene glacier advances (ΔELA ~425±229 m) and progressively limited advances in the Mid-Holocene (ΔELA ~141±106 m) and Late Holocene (ΔELA ~124±121 m). Long-term orbital forcing amplified by large-scale migration of Earth's thermal equator and the associated hemispheric oceanic-atmospheric systems are proposed for such glacier behavior in the region. Additionally, a large scatter in ^{10}Be ages are evident for the majority of moraines in the cold-based semiarid glaciated valleys due to inheritance, indicating the inefficiency of these systems to erode and/or transport boulders from bedrock slopes to the moraine.

4.2. Paper II

Saha, S., Owen, L.A., Orr, E.N., and Caffee, M.W., *to be submitted*. High-frequency Holocene glacier fluctuations in the Himalaya and Tibet: Quaternary Science Reviews.

This study builds on the mapping, and chronological effort presented in Saha et al. (2018; Paper I) and provided a detailed reconstruction of high-frequency Holocene glacial chronostratigraphies throughout the Himalayan-Tibetan orogen. In contrast to Saha et al. (2018; Paper I), larger polythermal-to-temperate glaciers in the two new study areas of the NW Himalaya, the Kulti valley in the Lahul and Parkachik valley in the Nun Kun massif, are selected. To test the hypothesis as to whether moraine boulders in larger polythermal-to-temperate glaciers have less age scatter because of limited inherited TCNs and are, therefore, suitable for reconstructing high-frequency Holocene glacial advances, [10]Be dated 16 new moraine boulders are examined in the study areas. Additionally, to compare the Holocene regional glacial chronologies developed for the NW Himalaya (Paper I) with rest of the orogen, 503 published [10]Be ages from 77 valleys were compiled and recalculated; a primary climate zonation map was developed to objectively identify identical climatic regions; and changes in ΔELAs during past glacier advances were estimated. Finally, the net temperature change (*ΔT*) was modelled using a linear inverse flow model between periods of regional glacier advances to decipher inter-regional variations of climate. The study indicates tightly clustered three local glacier advances in the Kulti valley at ~14.7, ~12.2, and ~0.5 ka, and one in the Parkachik valley at ~0.2 ka. This support the hypothesis that larger polythermal-to-temperate glaciers with likely more erosive capacity are a better candidate to reconstruct Holocene apparent mean moraine ages relative to semiarid glaciers. The regional compilation and inter-regional comparisons also suggest at least one synchronous late glacial (~15.3–11.8 ka) and five Holocene glacial advances throughout the orogen at ~11.5–9.5, ~8.8–7.7, ~7.0–3.2, ~2.3–1.0, and <1 ka. Both reconstructed local and regional Early Holocene glacier stages indicate high-amplitude glaciations in the Early Holocene and progressively more restricted advances over time. The inter-regional ΔELA and *ΔT* comparisons also indicate the likely influence of enhanced monsoonal humidity in the Early Holocene glaciations, followed by relative cooling

and aridity in the Mid- and Late Holocene and overall restricted glaciations. This study also showed that cold-based glaciers in the north and NW are more affected during this transition than the temperate glaciers to the south of the orogen.

4.3. Paper III

Saha, S., Owen, L.A., Orr, E.N., and Caffee, M.W., *to be submitted*. Systematically inherited cosmogenic ^{10}Be in Late Holocene moraine boulders in the Bhagirathi catchment of the Garhwal Himalaya, northern India: Earth Surface Processes and Landforms.

This study presents the role of geomorphic processes in determining the systematic inheritance of TCNs in moraine boulders. This study updates two existing and proposed two new Late Holocene glacial chronologies in the Bhagirathi valley of the Garhwal (central) Himalaya. Saha et al. (2018; Paper I) showed that moraine boulders delivered by sublimation-dominated cold-based small glaciers have large scatter in young Holocene ages, largely due to prior exposures or inheritance. In contrast, Saha et al. (*in prep*; Paper II) targets only large polythermal-to-temperate glacier settings and successfully ^{10}Be dated Holocene moraine boulders with limited to no age scatter. In this study, moraines formed by the largest glacier system in the central Himalaya, Gangotri glacier system, which is highly active, erosive, and temperate are ^{10}Be dated. The moraine boulders in the valley are expected to have limited systematic inheritance. To estimate inheritance, ^{10}Be concentrations were measured in ten boulders sampled from the two young ice-marginal moraines that have been independently dated to AD 1780 and 1935 using historical descriptions and measurements, lichenometry, plane-table map, and photographs. If the obvious outlier of ~4.5 ka (i.e., ~14.9 x 10^4 at g^{-1}) is removed, the data suggest inherited ^{10}Be concentrations of only ~0.09–0.60 x10^4 at g^{-1} SiO$_2$ (equivalent age of ~0.05-0.13 ka) in the majority of moraine boulders. Such a low inheritance is, in fact, within the ±2σ uncertainties of the TCN ages of the respective moraines and supports the hypothesis that temperate high-erosive glacier settings are probably the best candidates to reconstruct high-resolution Holocene glacial chronostratigraphies. When compared with the previous studies (Paper I, II), this study also suggests that the TCN dating resolution in a valley glacier system may be less affected by the location

of the boulder supply (i.e., cirque wall vs. valley wall), but more by the erosion rate, existing geomorphic landforms, and boulder transport pathways in the active glacier. Additionally, the study reinforces the concept that moraine formation in debris mantled valley glaciers may occur on a decadal timescale in response to a combination of climate change and stochastic, interannual variability in mass balances. In addition, [10]Be dated nine new and recalculated six published moraine boulders from the trunk Gangotri and the tributary Meru glaciers are used to temporally constrain the Gangotri, Bhujbasa, and Meru local glacial stages to ~2.4–1.9, ~1.7–0.5, ~0.5–0.1 ka, respectively. The majority of these glacier advances are restricted (ΔELAs 16–28 m), similar to our findings in Saha et al. (2018, *in prep*; Paper I and II) for other regions of the orogen.

5   Discussion

This thesis concerns the high-frequency Holocene glaciations in the Himalayan-Tibetan orogen. Key issues addressed by previous researchers include the overall pattern of Late Quaternary glaciations across the orogen (Dortch et al., 2013, Murari et al., 2014, Owen and Dortch, 2014), extent of glaciations in some notable valleys (Seong et al., 2009; Lee et al., 2014), and proposal for regionally unique forcing over long-term orbital forcing in driving glaciation in the orogen (Solomina et al., 2015, 2016). Building on these early works, this study offers: i) a detailed reconstruction of Holocene glaciations in seven new glaciated valleys across melt-dominated to sublimation-types of glaciers; ii) a robust inter-regional comparison of timing and extent of Holocene glaciations in the whole orogen; iii) reinforces the long-term role of orbital forcing as a major driver behind these glaciations; and also iv) addresses key issues related to geological uncertainties in TCN dating including inheritance. I will discuss the key contributions presented in this thesis, the challenges, and outline potential future directions for paleoglacial research in the Himalaya and Tibet.

5.1. Dating uncertainties

This thesis addresses the issue of high-degree of age scattering due to prior exposures (i.e., inheritance) by targeting well-developed moraines from three different types of glaciers in the NW and central Himalaya and Transhimalaya, i.e., sublimation-dominated cold-based types, the polythermal-to-temperate types or intermediate, and melt-dominated temperate types. Most TCN moraine boulders ages in the sublimation-dominated cold-based, less erosive glacier settings (75% local glacial stages), that include Stok, Lato and Karzok valleys of the NW Himalaya and Transhimalaya (Paper I), indicate large dispersions (χ^2 >100), rendering them difficult for reconstructing high-resolution Holocene glacial chronologies and regional correlations. Majority of these TCN data (Paper I) display positive skewness, convex upward cumulative probability distribution, and older age tails, indicating the predominance of inherited [10]Be (cf. Applegate et al., 2012). Polythermal-to-temperate small Hamtah glacier in Lahul also indicate a large apparent age dispersion (χ^2 124) for its youngest moraine. However, the larger polythermal-to-temperate glaciers of Lahul and Nun Kun, that include Sonapnai and Parkachik glaciers, and the temperate glaciers of the Garhwal (i.e., Gangotri and Meru) have low to minimum scatter (χ^2 with 95% confidence interval) in their apparent moraine ages. In addition, inherited [10]Be measurements from the two historically dated moraines in the Bhagirathi valley show insignificant contribution (0.05–0.13 ka) from prior exposures. This tentatively suggests that melt-dominated highly active temperate and polythermal valley glaciers are relatively better candidates to reconstruct high-resolution Holocene glacial chronostratigraphies than the cold-based less erosive semiarid and arid valley glaciers.

A combination of boulder/block rotation during supraglacial transportation and/or deposition, high bedrock slope and boulder erosion, high-frequency rockfall events, and/or subglacial origin, may result in a low concentration of inherited [10]Be on moraines boulders in more temperate settings. However, this relation is not straightforward. When [10]Be ages are compiled and compared across the orogen, nearly 51% of the data display excess contribution from prior exposures. Inherited ages as high as 0.7–6.3 ka may be possible depending on the catchment microclimate, tectonic and geomorphic regimes, and glacier dynamics (cf. Heimsath and McGlynn, 2008). Additional complexity may be imposed by reworking of older glacial deposits and/or rock glacier deposits (cf. Shroder et al., 2000; Çiner et al., 2017). Supraglacial exposure

alone may systematically overestimate boulder ages by as much as ~0.1–0.3 ka in cold-based glaciers in the NW Himalaya and Transhimalaya and ~0.05–0.9 ka in the temperate glaciers elsewhere in the central and eastern Himalaya (Heimsath and McGlynn, 2008; Murari et al., 2014). Unlike LGM or older moraine boulders, this undetectable perturbation on the ^{10}Be inventory is potentially substantial for young Holocene boulders, which systematically contributes to the high degree of scattering. Any Holocene ^{10}Be chronological comparisons, therefore, should be made with extreme caution.

5.2. An interpretative framework

Before this project was initiated much of the research in the orogen was focused on reconstructing the Late Quaternary glaciations mainly using ^{10}Be TCN dating and interpreting the past glaciations in terms of either large regions, i.e., semiarid and monsoonal (Owen et al., 2012; Dortch et al., 2013, Murari et al., 2014, Owen and Dortch, 2014 and references therein) or at the catchment level (Abramowski et al., 2006; Gayer et al., 2006; Jiao and Shen, 2006; Seong et al., 2007, 2009; Meyer et al., 2009; Chevalier et al., 2011). Very few studies in the orogen were specifically focused on the detailed reconstruction of Holocene glaciations (Seong et al., 2007, 2009; Pratt-Sitaula et al., 2011), leaving huge research gap in the Holocene glacial chronostratigraphies in many regions of the orogen including the NW and central Himalaya (Owen and Dortch, 2014). With these challenges in mind, this thesis attempted to explore further ways in which we can interpret ^{10}Be dated glacial chronostratigraphies locally and offer a robust inter-regional comparison.

According to the analysis (see section 3) presented in this thesis (Paper I, II, III), local Holocene glacial stages based on ≥3 (outlier free) apparent ages are considered robust, whereas <3 (outlier free) moraine boulder ages are considered less reliable (tentative; Figs. 3, 4). While both sets of data (i.e., robust and tentative) are presented, most of the Holocene regional glacial stages are based on multiple local glacial stages across the orogen. Multiple statistical techniques (see section 3) also proved useful in separating distinct age population (Paper I, II). For inter-regional comparison, climatic regions (zones) are defined using CA and further refined by PCA. Five climatic subgroups are proposed as a framework for such a comparison. These regions are,

- *Group 1*: Arid and semiarid colder climatic zone—(a) Transhimalaya, NW Tibet, Pamir, and Tian Shan, and (b) southern and northeastern Tibet,

- *Group 2*: Transitional climatic zone—(a) western Himalaya, (b) central and eastern Himalaya, and

- *Group 3*: Wet and warm (temperate) climatic zone—central and eastern Himalaya.

This interpretation also assumes that the moisture sensitive arid and semiarid glaciers would have had high-amplitude response during stronger ISM which penetrates over the whole orogen (Rupper et al., 2009). Similarly, temperature sensitive temperate glaciers would have responded strongly during regional cooling, likely teleconnected via the mid-latitudinal westerlies (Mölg et al., 2014).

An extensive late glacial local glacier advance is evident in the Kulti valley (tentatively at ~14.7±2.1 ka). Coeval late glacial advances are also reconstructed in the arid and semiarid Transhimalaya, NW Tibet, Pamir, and Tian Shan (~13.5–12.9 ka), in the transitional western Himalaya (~15.3–11.8 ka), and tentatively in other regions where they often overlap with the Early Holocene advances (Fig. 4). High-amplitude glaciations are evident in the arid and semiarid regions (ΔELAs 400–1000 m) relative to their temperate counterpart (ΔELAs 100–300 m), suggesting a possible increase in moisture supply and corresponding diffusion reflection (albedo) cooling for this advance.

Extensive local glacier advances are also evident during the Younger Dryas (YD)–Early Holocene transition and Early Holocene in the Kulti (~13.0–10.9 ka) and Hamtah valleys (~10.4±0.4 ka) of Lahul. Coeval regional glaciations are also recorded in the transitional western (~11.1–10.3 ka) and central and eastern Himalaya (~11.5–10.1 ka), warm and wet central and eastern Himalaya (~13.0–10.9 ka), and tentatively in other regions (Fig. 5). Identical to late glacial, high-amplitude glacier advances are experienced in more arid and semiarid regions (ΔELAs 200–440 m) than in the temperate regions (ΔELAs 29–128 m). Stronger ISM is proposed as major forcing behind these advances.

The ~8 ka abrupt climate cooling in the North Atlantic is well documented in glaciated regions worldwide (Matero et al., 2017). Prominent regional glacier advances during this Early to Mid-Holocene transition are also identified in three regions (8.0–7.7, 8.8–8.3, and 9.5–8.7 ka) and tentatively in one region of the orogen (~8.0 ka; Fig. 5). In the transitional western Himalaya, the much restricted ΔELAs (~172±186

m) compared to the more temperate central Himalaya (~331±182 m), may be a result of regional cooling.

A Mid-Holocene local glacier advance at ~6.1–3.3 ka is reconstructed in the Karzok valley (Fig. 5). Regionally, the glacial records in the orogen show high-amplitude glacial activity in the wet and warm central and eastern Himalaya (ΔELA: ~515±269 m), followed by the arid and semiarid NW Tibet (ΔELA: ~273±141 m), transitional western (ΔELAs ~193±86 m) and central and eastern Himalaya (ΔELAs ~144±177 m), and the arid and semiarid NE Tibet (ΔELA of ~81±71 m). Based on the inter-regional pattern of ΔELA at ~7.0–3.2 ka, intensive glacial activity in the temperature sensitive wet and warm central and eastern Himalaya was likely at this time and may be linked to more cooling (Azharuddin et al., 2017; Srivastava et al., 2017). Furthermore, intensive glacier retreat since ~8 ka in the NW Himalaya and Tibet (or muted response in the NE Tibet) is likely associated with extreme aridity (Wünnemann et al., 2010; Berkelhammer et al., 2012; Shi et al., 2017).

Multiple submillennial-scale (restricted) Late Holocene local glacier advances are reconstructed in the study areas; Stok (~2.1–0.9 ka), Lato (~0.7–0.4, ~0.3±0.1 ka), Karzok (~2.6–0.5, ~1.0±0.1, ~0.7±0.1 ka), Hamtah (~0.2±0.1 ka), Kulti (~0.6–0.4 ka), Parkachik (~0.2–0.1 ka), and Bhagirathi valleys (~2.4–1.9, ~1.7–0.5, ~0.5–0.1 ka; Fig. 4) and elsewhere in the orogen (Fig. 5). Most of these advances are significantly restricted with ΔELAs ranging from only ~4–200 m (Fig. 5) and likely driven by North Atlantic cooling (Somolina et al., 2015, 2016). Due to high apparent age dispersions (18–79%) and systematic inheritance (Paper III), inter-regional correlations for the last 2 ka are arguably highly speculative and cautiously interpreted in this study.

5.3. Paleoclimate implications

The regional glacial chronostratigraphical reconstruction indicates one late glacial, and at least five Himalayan-Tibetan Holocene stages (*HTHs*). Additional substages may also be possible for some regions where [10]Be glacial chronologies are sufficient and widespread. For example, in Saha et al. (2018; Paper I), seven Himalayan Holocene stages (*HHs*) are proposed in the northwestern Himalaya and Tibet instead of five HTS. Therefore, to extract a robust Holocene paleoclimatic information across the orogen, many more

20

detailed glacial chronologies are required, in addition to continuous climate proxy records.

However, ΔELA reconstructions in this thesis (Paper I, II, III) suggest overall high glacial amplitude in the late glacial and Early Holocene, which coincide with the northerly shifted Earth's thermal equator (ITCZ) and increased ISM precipitation (Dykoski et al., 2005; Jennerjahn et al., 2004; Lea et al., 2003; Severinghaus et al., 2009; Wang et al., 2001, 2004), as well as abrupt North Atlantic cooling during Younger Dryas and ~8 ka (Denton and Broecker, 2008 ; Matero et al., 2017). Corresponding Early Holocene (~11.5–9.5 and ~8.8–7.7 ka) extensive glacier advances are also identified in glacial records in European Alps (Moran et al., 2016, 2015, Schimmelpfennig et al., 2014, 2012; Schindelwig et al., 2012), Greenland (O'Hara et al., 2017), Arctic Canada (Young et al., 2012), Svalbard (van der Bilt et al., 2015), tropical Andes, Africa, and Southern Hemispheric extratropical regions (Solomin, et al., 2015, 2016 and references therein).

Progressively restricted glacier advances over time are recorded during subsequent glacier advances in the orogen (Fig. 5). A considerable increase in $\varDelta T$ in the arid and semiarid regions also supports a major shift towards extreme aridity in the Mid-Holocene in the orogen (Paper II). Subsequent Late Holocene advances were accordingly restricted. These changes are attributed to reduced northern hemisphere insolation and corresponding north Atlantic cooling (Chiang et al., 2014; Denton and Broecker, 2008; Lund et al., 2006). The enhanced mid-latitude westerly winds likely teleconnected the Late Holocene cooling events in the Himalayan-Tibetan orogen (Mölg et al., 2014; Srivastava et al., 2017; Yancheva et al., 2007).

Overall, the study reinforces the concept that the orbital forcing primarily modulates the long-term pattern of Holocene glaciations in the Himalayan-Tibetan orogen. The relative strength/weakness of both ISM and mid-latitude westerlies, on the other hand, determine the amplitude of short-term Holocene glacier advances in different regions of the orogen.

5.4. Future outlook

This study provides a framework for future reconstruction of Holocene glaciations in the

Himalayan-Tibetan orogen. Despite the attempts to develop new glacial chronologies in the Zanskar, Lahul, and Garhwal Himalaya, and compilation of existing chronologies throughout the orogen, many questions are still unresolved. Even though the study has started to unravel the spatial pattern of timing and extent of glaciations, our knowledge is still incomplete regarding the complex interaction between erosion rates, depositional regime, terrain, climate, glacial dynamics, and scatter in TCN ages. Ambiguities, thus, remains in interpreting local glacial stages and their regional significance. Ambiguities also exist in the understanding of sensitivities of different types of glaciers including cold-based, polythermal, and temperate, and understanding the drivers and controls behind short-term glacial advances. Finally, cross-disciplinary efforts are needed to resolve these issues. Future studies, therefore, should consider the following areas of research.

First, a continued effort to evaluate Holocene geochronological constraints is required, especially in the arid and semiarid NE and central Tibet and temperate and transitional central and eastern Himalaya. The temporal constraints of past glaciations are poorly resolved for these regions. Additionally, a sincere effort will be dedicated to continuously update the recently developed web-based informal cosmogenic-nuclide exposure-age database (e.g., http://alpine.ice-d.org/, http://antarctica.ice-d.org/) for a wide-ranging audience. These databases are also equipped with continuous improvements and updates of the TCN dating technique.

Second, immediate attention is required to develop geomorphic process-driven models for inheritance (cf. Applegate et al., 2010, 2012; Heyman et al., 2011), especially to account for large age scatter in young geological materials/landforms. Future research must focus on quantifying the frequency of random rockfall events, fracture pattern in steep bedrock slopes, ^{10}Be concentrations in valley sidewalls and supraglacial debris across different grain sizes, and the erosion rate of supraglacial boulders during glacial transportation at the catchment-scale. The existing geomorphic process-driven inheritance model of Applegate et al. (2012), therefore, is a significant contribution but requires further improvement by incorporating additional geomorphic processes.

Third, a significant amount of paleoglacial data in this thesis has been generated including the

timing (e.g., TCN dates) and amplitude (lengths, ELAs and ΔELAs) of Holocene glacier advances across the Himalayan-Tibetan orogen. A simple linear glacier flow model (after Klok and Oerlemans, 2003; Oerlemans, 2001, 2005) is also used (Paper II) to estimate the regional net change in temperature between periods of glaciations. Despite limitations, the model offers some key points that need further investigation, including a major shift towards extreme aridity in the Mid-Holocene in the orogen (Paper II). This study also argues that enough well-constrained paleoglacier targets are now available as key boundary conditions in more sophisticated paleoclimatic models (cf. Rupper and Roe, 2008; Rupper et al., 2009). Future research, therefore, should use more advanced and complex climate models (e.g., 2-D coupled energy balance–ice flow model) at the orogen-scale and target specific time slices (e.g., late glacial, Early Holocene, or Mid-Holocene) to evaluate global and/or regional climate controls on Central Asian glacier fluctuations and sensitivity. These models may also offer insight into the future climate change and the fate of these mountain glaciers (Bolch et al., 2012).

6   Conclusions

The main conclusions of this thesis are:

- *[10]Be chronologies from the NW and central Himalaya and Transhimalaya show that understanding site-specific characteristics are important for defining the timing of Holocene local glacial stages.* The local glacial chronologies developed in the semiarid glaciers of the NW Himalaya and Transhimalaya that include Stok (~2.1–0.9 ka), Lato (~0.7–0.4, ~0.3±0.1 ka), and Karzok (~6.1–3.3, ~2.6–0.5, ~1.0±0.1, ~0.7±0.1 ka) valleys show a large age dispersion, mostly due to inheritance and a few due to boulder displacement or recent slope deposits. The age scatters in larger polythermal-to-temperate glaciers, for example, Kulti (~0.6–0.4 ka), Parlachik (~0.2–0.1 ka), and Bhagirathi (~2.4–1.9, ~1.7–0.5, ~0.5–0.1 ka) valleys, however, are very limited and hence, arguably suitable for developing Holocene glacial chronostratigraphies.

- *An evaluation of the robustness of the [10]Be Himalayan-Tibetan Holocene stages (HTHs)*

shows that at least five synchronous regional glacier advances (~11.5–9.5, ~8.8–7.7, ~7.0–3.2, ~2.3–1.0, and <1 ka) can be defined. Additional substages may be possible for regions with an improved number of well-defined local glacial stages. For instance, seven regional Himalayan Holocene stages (*HHs*) are defined for the NW Himalaya and Tibet (~10.9–9.3, ~8.2–7.4, ~6.9–4.3, ~4.5–2.8, ~2.7–1.8, ~1.8–0.9, and <1 ka), largely because ~42% of the total 77 valleys studied are located in this region, including a contribution from this study. Despite these cautions, ~51 and 28% the data (new + published) display significant scattering in moraine apparent (^{10}Be) ages due to inheritance and incomplete exposures, respectively. A further improvement, therefore, deemed necessary to understand the role of geomorphic process uncertainties in TCN geochronological research and refine the regional framework (*HTHs*) developed in this thesis.

- *Erosive temperate glaciers are a better candidate to reconstruct high-resolution Holocene glacial stages*. The inheritance measurements on ten boulders from the two independently dated moraines in the Bhagirathi valley shows inherited ages of only ~0.05–0.13 ka which is within the ±2σ uncertainties of the ^{10}Be ages of the respective moraines. Gangotri which is the largest (~30 km) and highly erosive (~2–5 mm a^{-1}) glacier in the central Himalaya, shows that inheritance is less of a problem in more dynamic temperate glacier settings than in the arid and semiarid less erosive (<0.01 mm a^{-1}) settings.

- *Regional climatic gradient and topography play a crucial role in the response and extent of past Holocene glacier advances.* The climate sensitivity and PCA vector analysis confirmed that most of the glaciers in the Himalaya and Tibet are regionally highly susceptible to precipitation and changes in this variable would likely result in highly variable responses of glaciers in respective climatic zones. The inter-regional variability in reconstructed past ELAs and ΔELAs, however, are attributed to variable glacier hypsometries and corresponding (altitudinal) temperature gradient. The pronounced north-south and east-west climatic transacts, mainly for precipitation, therefore, are argued to control the large-scale variability of Holocene glacial amplitudes across the orogen, whereas at the catchment-scale glacial hypsometries likely play the crucial role. This observation must be reconciled with future glacier-climate models to quantify variable glacier responses to identical climatic perturbation.

- *Reconstruction of spatiotemporal extents (ELAs and ΔELAs) of HTHs shows that the maximum extent of glacier advances took place during the late glacial and Early Holocene across all regions in the orogen.* Progressively restricted glacier advances over time are recorded in the Mid- and Late Holocene. However, in the arid and semiarid regions, glaciers retreated extensively in the Mid-Holocene from their last Early Holocene positions. Our modeled *ΔT* measurements and proxy climate records suggest a major shift towards aridity during the Mid-Holocene as the likely reason for such restricted glaciations.

- *Our study reinforces the concept that the orbital forcing primarily modulates the long-term pattern of Holocene glaciations in the Himalayan-Tibetan orogen*. The relative strength/weakness of both ISM and mid-latitude westerlies, on the other hand, determine the amplitude of short-term Holocene glacier advances in different regions of the orogen.
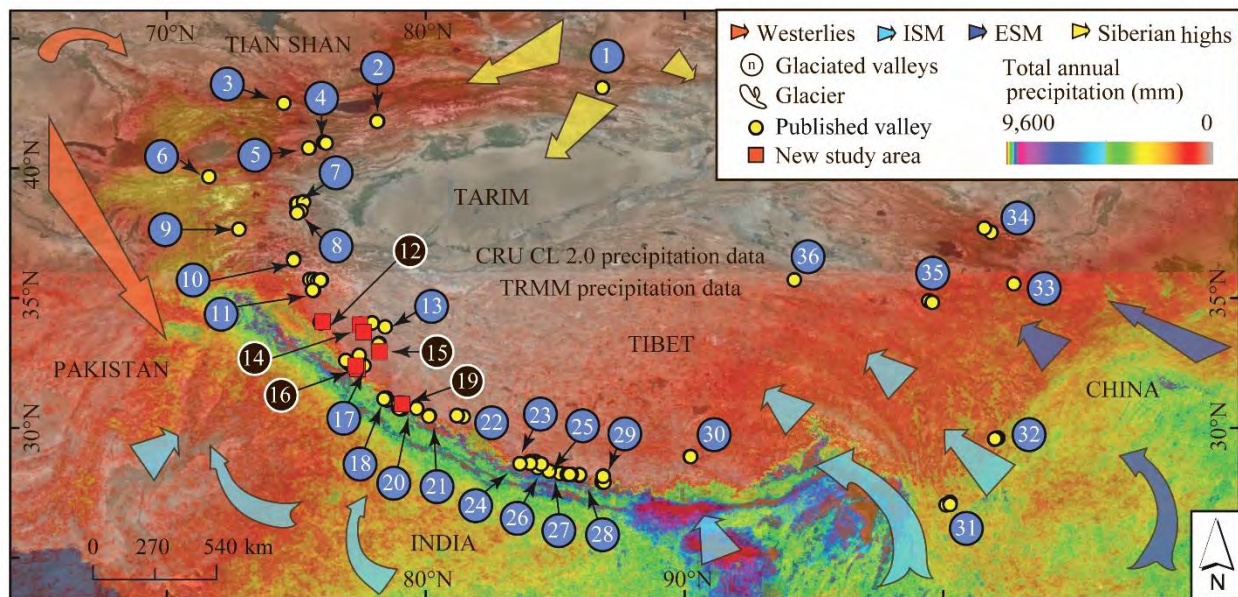
Fig. 1. Physical settings of the study areas. (A) TRMM and CRU CL 2.0 precipitation map, superimposed on hillshade map, showing the location of [10]Be dated (with ages <15 ka only) glaciated valleys across the Himalaya, the Tibet, the Pamir, and the Tian Shan. Seven new (in black circles—this study) and 73 published (in blue circles) valleys are presented in 36 locations. Arrows indicate the propagating directions of the prevailing climate systems (ISM – Indian Summer Monsoon; ESM – East Asia Summer Monsoon).

Valley locations are: (1) Daxi, Tian Shan; (2) Bordoo, Tian Shan; (3) Ala Archa, Tian Shan; (4) Aksai, Tian Shan; (5) Kitschi-Kurumdu, Tian Shan; (6) Koksu, Pamir; (7) Kongur Shan, Pamir; (8) Muztag Ata, Pamir; (9) Great Bogchigir, Karakoram; (10) Hunza valley, Karakoram; (11) Central Karakoram; (12) Parkachik, Sentic, Rantac, & Tarangoz, Nun Kun massif; (13) Chang & Pang, Ladakh; (14) Stok & Lato, Zanskar; (15) Puga & Karzok, Zanskar; (16) Kulti, Hamtah, & adjacent valleys, Lahul; (17) Yunam, Great Himalaya; (18) Tons, Garhwal; (19) Bhagirathi, Garhwal; (20) Bhillanganga & Dudhanga, Garhwal; (21) Nanda Devi, Garhwal; (22) Muguru, Gurla Mandhata; (23) Lete, Milarepa, Syaktan, Yak, Lyapche, Danfe & Dudh Khola, Annapurna; (24) Macha Khola, Gorkha Himal; (25) Mailun Khola, Ganesh Himal; (26) Langtang, Nepal; (27) Nyalam County, Southern Xixabangma; (28) Khumbu Himal, Nepal; (29) Rongbuk, N Mt. Everest; (30) Karola Pass, Mt. Kaluxung; (31) Renhe, Baishui, & Ganheba, Yulong and Ganheba mountains; (32) Hailuogou, Gonga Shan; (33) Dalijia Shan, NE Tibet; (34) Xiying He, Qilian Shan; (35) Anyemaqen mountains; (36) Kunlun Shan.

Table 1. A summary of glaciers in the study areas.

Glacier	Valley	Mountain Range	Climate	Length (km)	Glacier area (km²)	slope (°)	Aspect	Toe to cirque head (m asl)	Contemporary ELAs (m asl)	Annual precipitation (mm)
Stok Kangri	Stok valley	E Zanskar	Semiarid	~1.8	0.6	36	NE	5290–5720	5481±27	~40–100
Amda Kangri	Lato valley	E Zanskar	Semiarid	~2.9	1.1	22	ENE	5310–5740	5504±24	~40–100
Mentok Kangri	Karzok valley	E Zanskar	Semiarid	~1.5	2.5	33	NE	5480–6000	5709±31	~40–100
Gomuche Kangri	Karzok valley	E Zanskar W	Semiarid	~1.3	1.5	42	N	5380–6080	5773±117	~40–100
Parkachik	Parkachik	Zanskar	Transitional	~12.0	48.0	19	N	3600–7020	5361±202	~150–700
Hamtah	Hamtah valley	Greater Himalaya	Transitional	~5.7	4.0	27	NW	4056–5010	4456±70	~400–800
Sonapani	Kulti valley	Greater Himalaya	Transitional	~10.0	18.0	17	W	3900–5465	4749±127	~200–900
Gangotri	Bhagirathi	Greater Himalaya	Humid	~30.2	102.2	14	NW	4020–7000	5049±143	~1000–3000
Meru	Bhagirathi	Himalaya	Humid	~6.0	4.7	20	NE	4460–5940	5023±138	~1000–3000
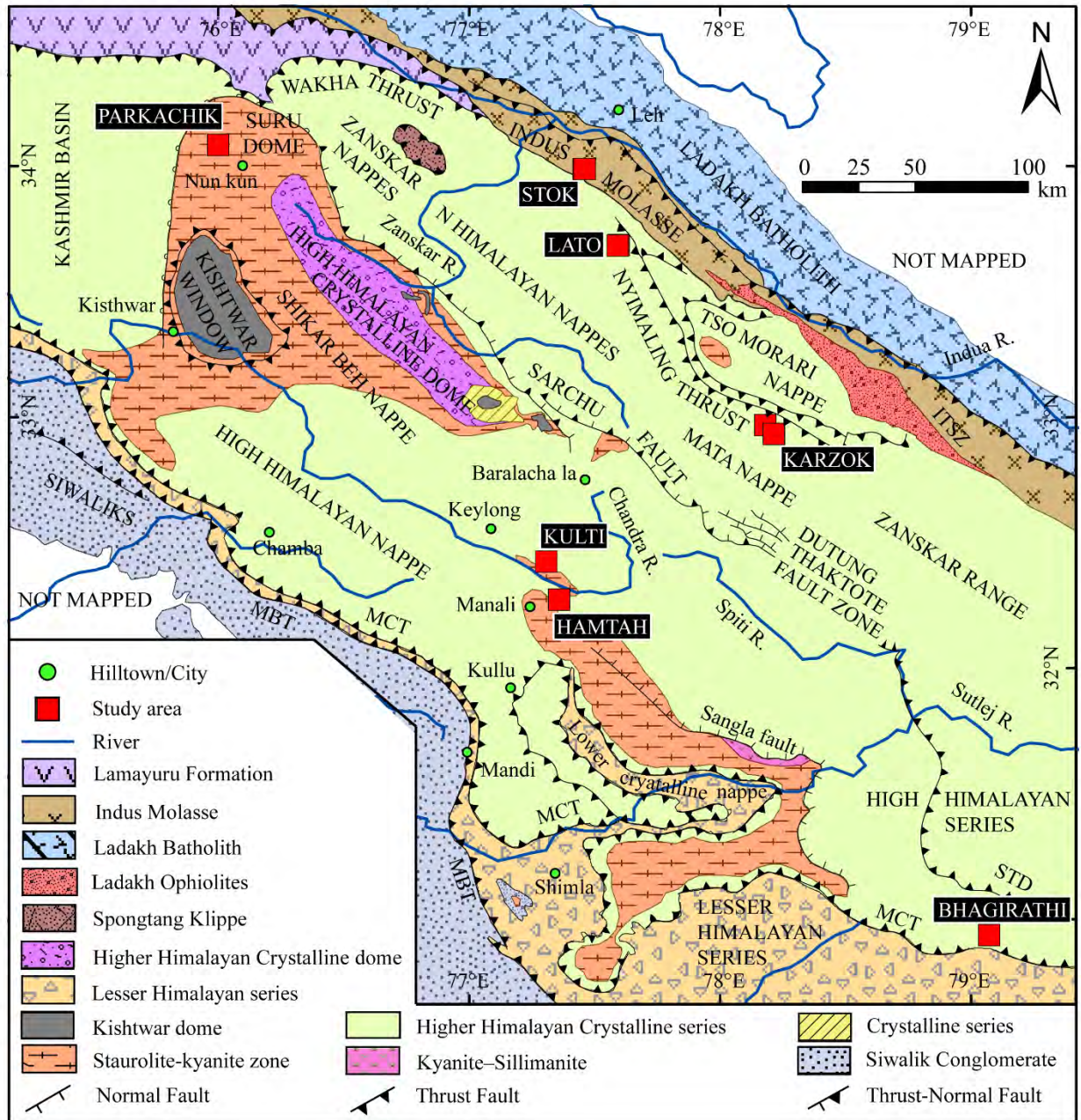
Fig. 2. Simplified geology map of the NW Himalaya and Transhimalaya showing Stok, Lato, Karzok, Parkachik, Kullu, and Hamtah study areas and the central Himalaya displaying the Bhagirathi study area; modified after Epard and Steck, 2008.

Fig. 3. Field camps in the summers of 2014–2016 in the NW Himalaya. A & B) Lato field camp with LAO & ENO (photo courtesy: LAO). C) Solang upper basecamp, south of Hamtah valley with LAO, ENO, and Madhav Murari (photo courtesy: LAO). D) Parkachik solo field camp with a tarp and erratic as a kitchen and a tent. E) Karzok field camp with ENO. F) Gangotri Tapovan basecamp with LAO, ENO, and Jim

Benton (photo courtesy: LAO).
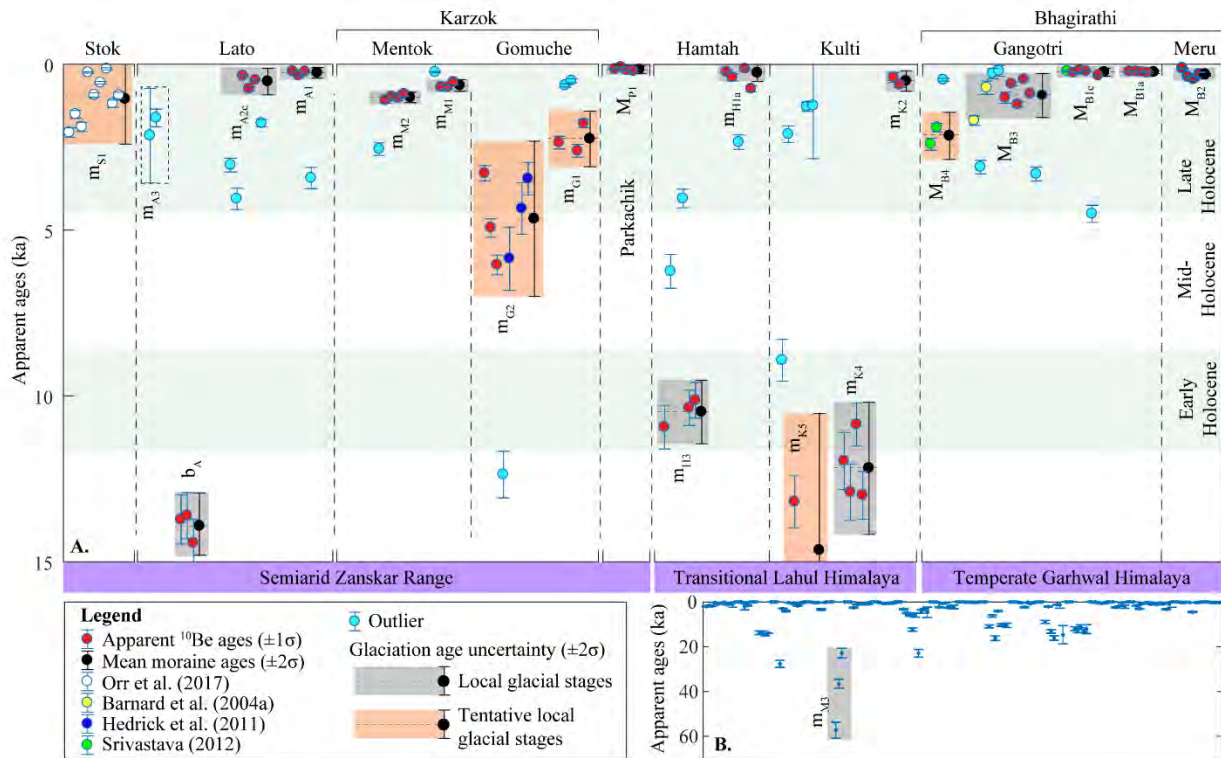
Fig. 4. The new Holocene ^{10}Be glacial chronologies showing all age clusters associated with ice-marginal moraines in the Himalaya. A. Local glacial stages in seven study areas are shown. Age clusters are organized morphostratigraphically from older to young in each valley. Samples are organized from north to south following the prevailing precipitation gradient. Outliers are highlighted along with prominent and tentative local glacial stages. B. The oldest (this study) ^{10}Be chronology of the m$_{M3}$ moraine from Mentok kangri is shown along with the older age outliers.
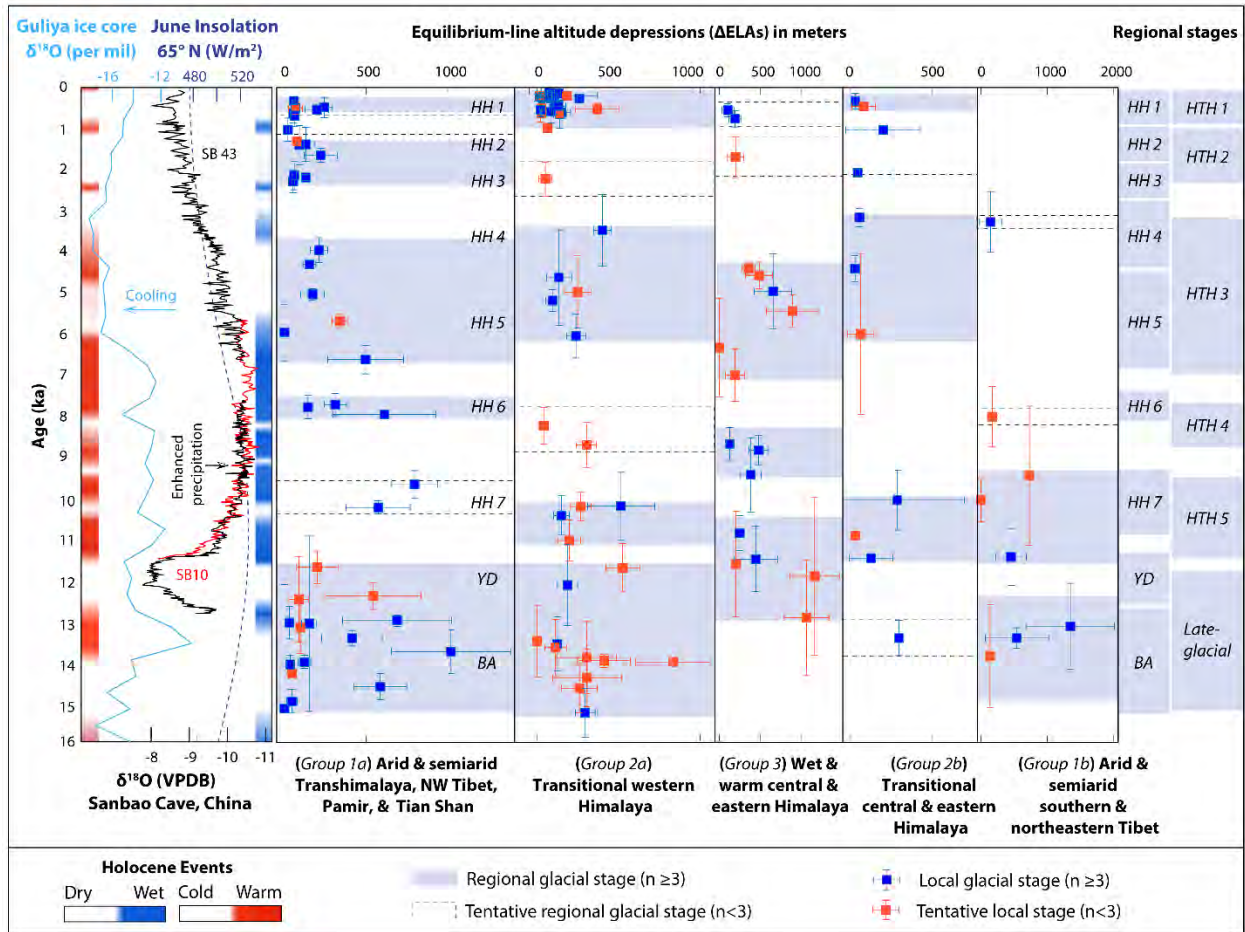
Fig. 5. Timing and amplitude of late glacial and Holocene regional glacier advances across the Himalayan-Tibetan orogen compared with continuous proxy records. Five climatic regions are used for inter-regional comparisons. Local glacial stages (mean [10]Be ages in x-axis) for each region are combined (S3) and compared against the corresponding ΔELA (in y-axis). Uncertainty bars are ±1σ. Regional Himalayan-Tibetan Holocene stages (*HTHs*) for the whole orogen (this study) are compared against Himalayan Holocene stages (*HHs*) reconstructed for the NW Himalaya and Tibet in Saha et al. (2018). A simplified summary of major late glacial-Holocene climatic events is shown by shaded blue and red bars, representing significant dry-wet and cold-warm periods, respectively. They are reconstructed after Demske et al. (2009), Wünnemann et al. (2010), Berkelhammer et al. (2012), Rawat et al. (2015a, 2015b), Srivastava et al. (2017). The color

scheme only represents the time range and not the magnitude. Reconstructed orbital trend at 65°N latitude (after Berger, 1978), oxygen isotopes from speleothems (Sanbao cave, China after Dong et al., 2010), and from Guliya ice cores (Guliya ice core, Tibet after Thompson et al., 1997) are shown at the bottom for climatic interpretation.

7   References

Abramowski, U., Bergau, Seebach, D., Zech, R., Glaser, B., Sosin, P., Kubik, P.W., Zech, W., 2006. Pleistocene glaciations of Central Asia: results from 10Be surface exposure ages of erratic boulders from the Pamir (Tajikistan), and the Alay–Turkestan range (Kyrgyzstan). Quat. Sci. Rev. 25, 1080–1096.

Agarwal, N.C., Kumar, G., 1973. Geology of the upper Bhagirathi and Yamuna valleys, Uttarkashi District, Kumaun Himalaya. Himalayan Geology 3, 1–23.

Ahmad, S. and Hasnain, S.I., 2004. Analysis of satellite imageries for characterization of glacio-morphological features of the Gangotri Glacier, Ganga headwater, Garhwal Himalayas. In Srivastava, D., Gupta. K.R. and Mukerji. S. (Editors), Geological Survey of India, Spl. Pub. No. 80, 61–67.

Anderson, L.S., Roe, G.H., Anderson, R.S., 2014. The effects of interannual climate variability on the moraine record. Geology 42, 55–58.

Applegate, P.J., Alley, R.B., 2011. Challenges in the Use of Cosmogenic Exposure Dating of Moraine Boulders to Trace the Geographic Extents of Abrupt Climate Changes: The Younger Dryas Example 111–122.

Applegate, P.J., Urban, N.M., Keller, K., Lowell, T. V., Laabs, B.J.C., Kelly, M. a., Alley, R.B., 2012. Improved moraine age interpretations through explicit matching of geomorphic process models to cosmogenic nuclide measurements from single landforms. Quat. Res. 77, 293–304.

Applegate, P.J., Urban, N.M., Laabs, B.J.C., Keller, K., Alley, R.B., 2010. Modeling the statistical distributions of cosmogenic exposure dates from moraines. Geosci. Model Dev. 3, 293–307.

Azam, M.F., Wagnon, P., Vincent, C., Ramanathan, A., Favier, V., Mandal, Pottakkal, J.G., 2014. Processes governing the mass balance of Chhota Shigri Glacier (western Himalaya, India) assessed by point-scale surface energy balance measurements. Cryosph. 8, 2195–2217.

Azharuddin, S., Govil, P., Singh, A.D., Mishra, R., Agrawal, S., Tiwari, A.K., Kumar, K., 2017. Monsoon-influenced variations in productivity and lithogenic flux along offshore Saurashtra, NE Arabian Sea during the Holocene and Younger Dryas: A multi-proxy approach. Palaeogeogr. Palaeoclimatol. Palaeoecol. 483, 136–146.

Bahuguna, I.M., Rathore, B.P., Brahmbhatt, R., Sharma, M., Dhar, S., Randhawa, S.S., Kumar, K., Romshoo, S., Shah, R.D., Ganjoo, R.K., Ajai, 2014. Are the Himalayan glaciers retreating? Curr. Sci. 106, 1008–1013.

Balco, G., Stone, J.O., Lifton, N. a., Dunai, T.J., 2008. A complete and easily accessible means of calculating surface exposure ages or erosion rates from 10Be and 26Al measurements. Quat. Geochronol. 3, 174–195.

Balco, G., Stone, J.O.H., Porter, S.C., Caffee, M.W., 2002. Cosmogenic-nuclide ages for New England coastal moraines, Martha's Vineyard and Cape Cod, Massachusetts, USA. Quat. Sci. Rev. 21, 2127–2135.

Barker, T., 2007. Climate Change 2007. An Assessment of the Intergovernmental Panel on Climate Change. Change, Synthesis Report 446, 12–17.

Barr, I.D., Lovell, H., 2014. A review of topographic controls on moraine distribution. Geomorphology.

Benn, D., Evans, D.J., 2010, Glaciers and glaciation, 2 eds. Routledge. P. 817.

Benn, D.I., Owen, L.A., 2002. Himalayan glacial sedimentary environments: a framework for reconstructing and dating the former extent of glaciers in high mountains 98, 3–25.

Benn, D.I., Owen, L.A., Osmaston, H.A., Seltzer, G.O., Porter, S.C., Mark, B., 2005. Reconstruction of equilibrium-line altitudes for tropical and sub-tropical glaciers 139, 8–21.

Berger, A.L., 1978. Long-Term Variations of Caloric Insolation from the Earth' s Orbital Elements'. Quat. Res. 9, 139–167.

Berkelhammer, M., Sinha, A., Stott, L., Cheng, H., Pausata, F.S.R., Yoshimura, K., 2012. An abrupt shift in the Indian Monsoon 4,000 years ago An Abrupt Shift in the Indian Monsoon 4000 Years Ago.

Bhambri, R., Bolch, T., Chaujar, R.K., Kulshreshtha, S.C., 2011. Glacier changes in the Garhwal Himalaya, India, from 1968 to 2006 based on remote sensing. J. Glaciol. 57, 543–556.

Bhambri, R., Hewitt, K., Kawishwar, P., Pratap, B., 2017. Surge-type and surge-modified glaciers in the Karakoram. Sci. Rep. 7, 1–14.

Bhargava, O.N., 2008. An updated introduction to the Spiti geology. J. Palaeontol. Soc. India 53, 113–129.

Bhattacharya, A., Bolch, T., Mukherjee, K., Pieczonka, T., Kropáček, J., Buchroithner, M.F., 2016. Overall recession and mass budget of Gangotri Glacier, Garhwal Himalayas, from 1965 to 2015 using remote sensing data. J. Glaciol. 62, 1115–1133.

Bishop, M.P., Bonk, R., Kamp, U., Shroder, J.F., 2001. Terrain analysis and data modeling for alpine glacier mapping. Polar Geogr. 25, 182–201.

Bisht, P., Nawaz Ali, S., Rana, N., Singh, S., Poonam, Sundriyal, Y.P., Bagri, D.S., Juyal, N., 2017. Pattern of Holocene glaciation in the monsoon-dominated Kosa Valley, central Himalaya, Uttarakhand, India. Geomorphology 284, 130–141.

Bolch, T., Buchroithner, M., Pieczonka, T., Kunert, A., 2008. Planimetric and volumetric glacier changes in the Khumbu Himal, Nepal, since 1962 using Corona, Landsat TM and ASTER data. J. Glaciol. 54, 592–600.

Bolch, T., Kulkarni, A., Kaab, A., Huggel, C., Paul, F., Cogley, J.G., Frey, H., Kargel, J.S., Fujita, K., Scheel, M., Bajracharya, S., Stoffel, M., 2012. The State and Fate of Himalayan Glaciers. Science (80). 336, 310–314.

Bookhagen, B., Burbank, D.W., 2006. Topography, relief, and TRMM-derived rainfall variations along the Himalaya. Geophys. Res. Lett. 33, L08405.

Bookhagen, B., Thiede, R.C., Strecker, M.R., 2005. Abnormal monsoon years and their control on erosion and sediment f lux in the high, arid northwest Himalaya 231, 131–146.

Borchers, B., Marrero, S., Balco, G., Caffee, M., Goehring, B., Lifton, N., Nishiizumi, K., Phillips, F., Schaefer, J., Stone, J., 2016. Geological calibration of spallation production rates in the CRONUS-Earth project. Quat. Geochronol. 31, 188–198.

Brookfield, M.E., Andrews-Speed, C.P., 1984. Sedimentology, petrography and tectonic significance of the shelf, flysch and molasse clastic deposits across the Indus Suture Zone, Ladakh, NW India. Sediment. Geol. 40, 249–286.

Brun, F., Berthier, E., Wagnon, P., Kääb, A., Treichler, D., 2017. A spatially resolved estimate of High Mountain Asia glacier mass balances from 2000 to 2016. Nat. Geosci. 10, 668–673.

Burbank, D.W., Blythe, A. E., Putkonen, J., Pratt-Sitaula, B., Gabet, E., Oskin, M., Barros, A., Ojha, T.P., 2003. Decoupling of erosion and precipitation in the Himalayas. Nature 426, 652–655.

Carr, S.J., Lukas, S., Mills, S.C., 2010. Glacier reconstruction and mass-balance modelling as a geomorphic and palaeoclimatic tool. Earth Surf. Process. Landforms 35, 1103–1115.

Chaujar, R.K., Mazari, R.K., and Gergan, J.T., 1993, Glacial geomorphology of the Gaumukh – the source of Ganga, with reference to its present state of environment, in Proceedings of Seminar on Ganga in the Service of the Nation, 12–13: Rorkee, University of Rorkee, p. 1–14.

Chevalier, M.-L., Hilley, G., Tapponnier, P., Van Der Woerd, J., Liu-Zeng, J., Finkel, R.C., Ryerson, F.J.,

Li, H., Liu, X., 2011. Constraints on the late Quaternary glaciations in Tibet from cosmogenic exposure ages of moraine surfaces. Quat. Sci. Rev. 30, 528–554.

Chiang, J.C.H., Friedman, A.R., 2012. Extratropical Cooling, Interhemispheric Thermal Gradients, and Tropical Climate Change. Annu. Rev. Earth Planet. Sci. 40, 383–412.

Chiang, J.C.H., Lee, S.Y., Putnam, A.E., Wang, X., 2014. South Pacific Split Jet, ITCZ shifts, and atmospheric North-South linkages during abrupt climate changes of the last glacial period. Earth Planet. Sci. Lett. 406, 233–246.

Çiner, A., Sarıkaya, M.A., Yıldırım, C., 2017. Misleading old age on a young landform? The dilemma of cosmogenic inheritance in surface exposure dating: Moraines vs. rock glaciers. Quat. Geochronol. 42, 76–88.

Cogley, J.G., Kargel, J.S., Kaser, G., van der Veen, C.J., 2010. Tracking the source of glacier misinformation. Science 327, 522.

Cronauer, S.L., Briner, J.P., Kelley, S.E., Zimmerman, S.R.H., Morlighem, M., 2016. 10Be dating reveals early-middle Holocene age of the Drygalski Moraines in central West Greenland. Quat. Sci. Rev. 147, 59–68.

Davis, P.T., Menounos, B., Osborn, G., 2009. Holocene and latest Pleistocene alpine glacier fluctuations: a global perspective. Quat. Sci. Rev. 28, 2021–2033.

Demske, D., Tarasov, P.E., Wünnemann, B., Riedel, F., 2009. Late glacial and Holocene vegetation, Indian monsoon and westerly circulation in the Trans-Himalaya recorded in the lacustrine pollen sequence from Tso Kar. Palaeogeogr. Palaeoclimatol. Palaeoecol. 279, 172–185.

Denton, G.H., Broecker, W.S., 2008. Wobbly ocean conveyor circulation during the Holocene? Quat. Sci. Rev. 27, 1939–1950.

Deswal, S., Sharma, M., Saini, R., Chand, P., Juyal, N., Singh, I., Srivastava, P., Ajai, Bahuguna, I.M., 2017. Late Holocene Glacier Dynamics in the Miyar Basin, Lahaul Himalaya, India. Geosciences 7, 64.

Dietsch, C., Dortch, J.M., Reynhout, S. a., Owen, L. a., Caffee, M.W., 2014. Very slow erosion rates and landscape preservation across the southwestern slope of the Ladakh Range, India. Earth Surf. Process. Landforms, 389–402.

Dobhal, D.P., Gergan, J.T., Thayyen, R.J., 2008. Mass balance studies of the Dokriani Glacier from 1992 to 2000, Garhwal Himalaya, India. Bull. Gaciological Res. 25, 9–17.

Dong, J., Wang, Y., Cheng, H., Hardt, B., Edwards, R.L., Kong, X., Wu, J., Chen, S., Liu, D., Jiang, X., Zhao, K., 2010. A high-resolution stalagmite record of the Holocene East Asian monsoon from Mt Shennongjia, central China. Holocene 20, 257–264.

Dortch, J.M., Owen, L. a., Caffee, M.W., 2013. Timing and climatic drivers for glaciation across semi-arid western Himalayan–Tibetan orogen. Quat. Sci. Rev. 78, 188–208.

Dortch, J.M., Owen, L. a., Schoenbohm, L.M., Caffee, M.W., 2011. Asymmetrical erosion and morphological development of the central Ladakh Range, northern India. Geomorphology 135, 167–180.

Dunai, T.J., 2010. Cosmogenic Nuclides: Principles, Concepts and Applications in the Earth Surface Sciences. Cambridge Univ. Press. Cambridge.

Duncan, C., Masek, J., Fielding, E., 2003. How steep are the Himalaya? Characteristics and implications of along-strike topographic variations. Geology 31, 75–78.

Dykoski, C.A., Edwards, R.L., Cheng, H., Yuan, D., Cai, Y., Zhang, M., Lin, Y., Qing, J., An, Z., Revenaugh, J., 2005. A high-resolution, absolute-dated Holocene and deglacial Asian monsoon record from Dongge Cave, China. Earth Planet. Sci. Lett. 233, 71–86.

Eaves, S.R., Mackintosh, A.N., Anderson, B.M., Doughty, A.M., Townsend, D.B., Conway, C.E., Winckler, G., Schaefer, J.M., Leonard, G.S., Calvert, A.T., 2016. The Last Glacial Maximum in the central North Island, New Zealand: Palaeoclimate inferences from glacier modelling. Clim. Past 12, 943–960.

Epard, J., Steck, A., 2008. Structural development of the Tso Morari ultra-high pressure nappe of the Ladakh Himalaya 451, 242–264.

Fabel, D., Stroeven, A.P., Harbor, J., Kleman, J., Elmore, D., Fink, D., 2002. Landscape preservation under fennoscandian ice sheets determined from in situ produced10Be and26Al. Earth Planet. Sci. Lett. 201, 397–406.

Fielding, E., Isacks, B., Barazangi, M., Duncan, C., 1994. How flat is Tibet? Geology 22, 163–167.

Finkel, R.C., Owen, L. a., Barnard, P.L., Caffee, M.W., 2003. Beryllium-10 dating of Mount Everest moraines indicates a strong monsoon influence and glacial synchroneity throughout the Himalaya. Geology 31, 561–564.

Fuchs, G., 1977. Traverse of Zanskar from the Indus to the Valley of Kashmir–a preliminary note. Jahrb. der Geol. Bundesanstalt 120, 219–229.

Fuchs, G., Linner, M., 1996. On the geology of the suture zone and Tso Morari Dome in Eastern Ladakh (Himalaya). Jahrb. der Geol. Bundesanstalt 139, 191–207.

Galbraith, R., 2010. On plotting OSL equivalent doses. Anc. TL 28, 1–10.

Galbraith, R.F., 1990. The radial plot: Graphical assessment of spread in ages. Int. J. Radiat. Appl. Instrumentation. Part 17, 207–214.

Galbraith, R.F., Roberts, R.G., 2012. Statistical aspects of equivalent dose and error calculation and display in OSL dating: An overview and some recommendations. Quat. Geochronol. 11, 1–27.

Gayer, E., Lavé, J., Pik, R., France-Lanord, C., 2006. Monsoonal forcing of Holocene glacier fluctuations in Ganesh Himal (Central Nepal) constrained by cosmogenic 3He exposure ages of garnets. Earth Planet. Sci. Lett. 252, 275–288.

Gosse, J.C., 2005. The contributions of cosmogenic nuclides to unraveling alpine paleo-glacier histories. In: Huber, U.M., Bugmann, H.K.M., Reasoner, M.A. (Eds.), Global Change and Mountain Regions. An Overview of Current Knowledge. Advances in Global Change Research, vol. 23. Springer, Dordrecht, pp. 39–50.

Gosse, J.C., Phillips, F.M., 2001. Terrestrial in situ cosmogenic nuclides: theory and application. Quat. Sci. Rev. 20, 1475–1560.

Grove, A. T., 2008. A brief consideration of climate forcing factors in view of the Holocene glacier record. Glob. Planet. Change 60, 141–147.

Gruber, S., Haeberli, W., 2007. Permafrost in steep bedrock slopes and its temperatures-related destabilization following climate change. J. Geophys. Res. Earth Surf. 112, 1–10.

Hedrick, K. a., Seong, Y.B., Owen, L. a., Caffee, M.W., Dietsch, C., 2011. Towards defining the transition in style and timing of Quaternary glaciation between the monsoon-influenced Greater Himalaya and the semi-arid Transhimalaya of Northern India. Quat. Int. 236, 21–33.

Heimsath, A.M., McGlynn, R., 2008. Quantifying periglacial erosion in the Nepal high Himalaya. Geomorphology 97, 5–23.

Heyman, J., Applegate, P.J., Blomdin, R., Gribenski, N., Harbor, J.M., Stroeven, A.P., 2016. Boulder height - exposure age relationships from a global glacial 10Be compilation. Quat. Geochronol. 34, 1–11.

Heyman, J., Stroeven, A.P., Caffee, M.W., Hättestrand, C., Harbor, J.M., Li, Y., Alexanderson, H., Zhou, L., Hubbard, A., 2011. Palaeoglaciology of Bayan Har Shan, NE Tibetan Plateau: exposure ages reveal a missing LGM expansion. Quat. Sci. Rev. 30, 1988–2001.

Honegger, K., Dietrich, V., Frank, W., Gansser, A., Thrni, M., Trommsdorff, V., 1982. Magmatism and metamorphism in the Ladakh Himalayas (the Indus-Tsangpo suture zone). Earth Planet. Sci. Lett. 60, 253–292.

Hughes, P.D., 2010. Geomorphology and Quaternary stratigraphy: The roles of morpho-, litho-, and allostratigraphy. Geomorphology 123, 189–199.

Hughes, P.D., Gibbard, P.L., Woodward, J., 2005. Quaternary glacial records in mountain regions: A formal stratigraphical approach Quaternary glacial records in mountain regions: A formal stratigraphical approach.

IMD (Indian Meteorological Department), 1989, Climate of Uttar Pradesh: Government of India Publication, p. 372–375.

IPCC, 2014. Climate Change 2013, the Fifth Assessment Report.

Ivy-Ochs, S., Kerschner, H., Schlüchter, C., 2007. Cosmogenic nuclides and the dating of Lateglacial and

Early Holocene glacier variations: The Alpine perspective. Quat. Int. 164–165, 53–63.

Jennerjahn, T.C., Ittekkot, V., Arz, H.W., Behling, H., Pätzold, J., Wefer, G., 2004. Asynchronous Terrestrial and Marine Signals of Climate Change During Heinrich Events Asynchronous Terrestrial and Marine Signals of Climate Change During Heinrich Events. Science (80). 306.

Jiao, K.Q., Shen, Y.P., 2006. Quaternary glaciations in Tanggulha Mountains. In: Shi, Y.F., Su, Z., Cui, Z.J. (Eds.), The Quaternary Glaciations and Environmental Variations in China. Science and Technology Press of Hebei Province, Shijiazhuang, pp. 326–356

Kaplan, M.R., Schaefer, J.M., Denton, G.H., Doughty, A.M., Barrell, D.J.A., Chinn, T.J.H., Putnam, A.E., Andersen, B.G., Mackintosh, A., Finkel, R.C., Schwartz, R., Anderson, B., 2013. The anatomy of long-term warming since 15 ka in New Zealand based on net glacier snowline rise. Geology 41, 887–890.

Kargel, J.S., Abrams, M.J., Bishop, M.P., Bush, A., Hamilton, G., Jiskoot, H., Kääb, A., Kieffer, H.H., Lee, E.M., Paul, F., Rau, F., Raup, B., Shroder, J.F., Soltesz, D., Stainforth, D., Stearns, L., Wessels, R., 2005. Multispectral imaging contributions to global land ice measurements from space. Remote Sens. Environ. 99, 187–219.

Kirstein, L. a., 2011. Thermal evolution and exhumation of the Ladakh Batholith, northwest Himalaya, India. Tectonophysics 503, 222–233.

Klok, E.J., Oerlemans, J., 2003. Deriving historical equilibrium-line altitudes from a glacier length record by linear inverse modelling. Holocene 13, 343–351.

Kohl, C.P., Nishiizumi, K., 1992. Chemical isolation of quartz for measurement of in-situ-produced cosmogenic nuclides. Geochim. Cosmochim. Acta 56, 3583–3587.

Kumar, G., Joshi, A., Mathur, V.K., 1987. Redlichid trilobites from the tal formation. Lesser Himalaya. India. Curr. Sci. 56, 659–663.

Lal, D., 1991. Cosmic ray labeling of erosion surfaces: in situ nuclide production rates and erosion models. Earth Planet. Sci. Lett. 104, 424–439.

Lea, D.W., Pak, D.K., Peterson, L.C., Hughen, K.A., 2003. Synchroneity of Tropical and High-Latitude Atlantic Temperatures over the Last Glacial Termination. Science (80). 301, 1361–1364.

Lee, S.Y., Seong, Y.B., Owen, L.A., Murari, M.K., Lim, H.S., Yoon, H. Il, Yoo, K.C., 2014. Late Quaternary glaciation in the Nun-Kun massif, northwestern India. Boreas 43, 67–89.

Li, Y., Li, Y., Harbor, J., Liu, G., Yi, C., Caffee, M.W., 2016. Cosmogenic 10Be constraints on Little Ice Age glacial advances in the eastern Tian Shan, China. Quat. Sci. Rev. 138, 105–118.

Lifton, N. a., Bieber, J.W., Clem, J.M., Duldig, M.L., Evenson, P., Humble, J.E., Pyle, R., 2005. Addressing solar modulation and long-term uncertainties in scaling secondary cosmic rays for in situ cosmogenic nuclide applications. Earth Planet. Sci. Lett. 239, 140–161.

Lifton, N., 2016. Implications of two Holocene time-dependent geomagnetic models for cosmogenic nuclide production rate scaling. Earth Planet. Sci. Lett. 433, 257–268.

Lifton, N., Sato, T., Dunai, T.J., 2014. Scaling in situ cosmogenic nuclide production rates using analytical approximations to atmospheric cosmic-ray fluxes. Earth Planet. Sci. Lett. 386, 149–160.

Lifton, N.A., Smart, D.F., Shea, M.A., 2008. Scaling time-integrated in situ cosmogenic nuclide production rates using a continuous geomagnetic model. Earth Planet. Sci. Lett. 268, 190–201.

Lund, D.C., Lynch-stieglitz, J., Curry, W.B., 2006. Gulf Stream density structure and transport during the past millennium 444, 601–604.

Marrero, S.M., Phillips, F.M., Borchers, B., Lifton, N., Aumer, R., Balco, G., 2016. Cosmogenic nuclide systematics and the CRONUScalc program. Quat. Geochronol. 31, 160–187.

Martin, L.C.P., Blard, P.H., Balco, G., Lavé, J., Delunel, R., Lifton, N., Laurent, V., 2017. The CREp program and the ICE-D production rate calibration database: A fully parameterizable and updated online tool to compute cosmic-ray exposure ages. Quat. Geochronol. 38, 25–49.

Matero, I.S.O., Gregoire, L.J., Ivanovic, R.F., Tindall, J.C., Haywood, A.M., 2017. The 8.2 ka cooling event caused by Laurentide ice saddle collapse. Earth Planet. Sci. Lett. 473, 205–214.

Mayewski, P.A., Rohling, E.E., Stager, J.C., Karl??n, W., Maasch, K.A., Meeker, L.D., Meyerson, E.A., Gasse, F., van Kreveld, S., Holmgren, K., Lee-Thorp, J., Rosqvist, G., Rack, F., Staubwasser, M.,

Schneider, R.R., Steig, E.J., 2004. Holocene climate variability. Quat. Res. 62, 243–255.

Meyer, M.C., Hofmann, C. C., Gemmell, A. M.D., Haslinger, E., Häusler, H., Wangda, D., 2009. Holocene glacier fluctuations and migration of Neolithic yak pastoralists into the high valleys of northwest Bhutan. Quat. Sci. Rev. 28, 1217–1237.

Mölg, T., Maussion, F., Scherer, D., 2014. Mid-latitude westerlies as a driver of glacier variability in monsoonal High Asia. Nat. Clim. Chang. 4, 68–73.

Moran, A.P., Ivy-Ochs, S., Schuh, M., Christl, M., Kerschner, H., 2016. Evidence of central Alpine glacier advances during the Younger Dryas–early Holocene transition period. Boreas 45, 398–410.

Moran, A.P., Kerschner, H., Ochs, S.I., 2015. Redating the moraines in the Kromer Valley (Silvretta Mountains) – New evidence for an early Holocene glacier advance. Holocene 26, 655–664.

Murari, M.K., Owen, L.A., Dortch, J.M., Caffee, M.W., Dietsch, C., Fuchs, M., Haneberg, W.C., Sharma, M.C., Townsend-Small, A., 2014. Timing and climatic drivers for glaciation across monsoon-influenced regions of the Himalayan–Tibetan orogen. Quat. Sci. Rev. 88, 159–182.

Naithani, A.K., Nainwal, H.C., Sati, K.K., Prasad, C., 2001. Geomorphological evidences of retreat of the Gangotri glacier and its characteristics. Curr. Sci. 80, 87–94.

Nesje, A., Dahl, S.O., 1992. Equilibrium-line altitude depressions of reconstructed Younger Dyras and Holocene glaciers in Fosdalen, inner Nordfjord, western Norway. Nor. Geol. Tidsskr. 72, 209–216.

Nishiizumi, K., Finkel, R.C., Caffee, M.W., Southon, J.R., Kohl, C.P., Arnold, J.R., Olinger, C.T., Poths, J., Klein, J., 1994. Cosmogenic Production of 10Be and 26Al on the Surface of the Earth and Underground. In: Eighth International Conference on Geochronology, Cosmochronology and Isotope Geochemistry. U.S. Geol. Surv. Circular 1107, Berkeley, California, p. 234.

O'Hara, S.L., Briner, J.P., Kelley, S.E., 2017. A10Be chronology of early Holocene local glacier moraines in central West Greenland. Boreas 46, 655–666.

Oerlemans, J., 2001, Glaciers and climate change: Lisse, Netherlands, Swets and Zeitlinger, 160 p.

Oerlemans, J., 2005. Extracting a climate signal from 169 glacier records. Science 308, 675–7.

Orr, E.N., Owen, L.A., Murari, M.K., Saha, S., Caffee, M.W., 2017. The timing and extent of Quaternary glaciation of Stok, northern Zanskar Range, Transhimalaya, of northern India. Geomorphology 284.

Orr, E.N., Owen, L.A., Saha, S., Caffee, M.W., Murari, M.K., 2018. Quaternary glaciation of the Lato Massif, Zanskar Range of the NW Himalaya. Quat. Sci. Rev. 183.

Osmaston, H., 1994. The geology, geomorphology and Quaternary history of Zangskar. In: Crook, J., Osmaston, H. (Eds.), Himalayan Buddhist Villages. University of Bristol Press, UK, pp. 1–36.

Osmaston, H., 2005. Estimates of glacier equilibrium line altitudes by the Area ?? Altitude, the Area ?? Altitude Balance Ratio and the Area ?? Altitude Balance Index methods and their validation. Quat. Int. 138–139, 22–31.

Owen, L. A. & Derbyshire, E. 1989: The Karakoram glacial depositional system. Zeitschrift f€ur Geomorphologie N.F., Supplement76, 33–73.

Owen, L. a., Caffee, M.W., Bovard, K.R., Finkel, R.C., Sharma, M.C., 2006. Terrestrial cosmogenic nuclide surface exposure dating of the oldest glacial successions in the Himalayan orogen: Ladakh Range, northern India. Bull. Geol. Soc. Am. 118, 383–392.

Owen, L. a., Chen, J., Hedrick, K. a., Caffee, M.W., Robinson, A.C., Schoenbohm, L.M., Yuan, Z., Li, W., Imrecke, D.B., Liu, J., 2012. Quaternary glaciation of the Tashkurgan Valley, Southeast Pamir. Quat. Sci. Rev. 47, 56–72.

Owen, L. a., Dortch, J.M., 2014. Nature and timing of Quaternary glaciation in the Himalayan–Tibetan orogen. Quat. Sci. Rev. 88, 14–54.

Owen, L. a., Thackray, G., Anderson, R.S., Briner, J., Kaufman, D., Roe, G., Pfeffer, W., Yi, C., 2009. Integrated research on mountain glaciers: Current status, priorities and future prospects. Geomorphology 103, 158–171.

Owen, L.A., Bailey, R.M., Rhodes, E.J., Holloway, R., 1997. Style and timing of glaciation in the Lahul Himalaya, northern India: a framework for reconstructing late Quaternary palaeoclimatic change in the western Himalayas 12, 83–109.

Owen, L.A., Derbyshire, E., Richardson, S., Benn, D.I., Evans, D.J.A., Mitchell, W.A., 1996. The quaternary glacial history of the Lahul Himalaya, northern India. J. Quat. Sci. 11, 25–42.

Owen, L.A., Sharma, M.C., 1998. Rates and magnitudes of paraglacial fan formation in the Garhwal Himalaya: Implications for landscape evolution. Geomorphology 26, 171–184.

Pellitero, R., Rea, B.R., Spagnolo, M., Bakke, J., Ivy-Ochs, S., Frew, C.R., Hughes, P., Ribolini, A., Lukas, S., Renssen, H., 2016. GlaRe, a GIS tool to reconstruct the 3D surface of palaeoglaciers. Comput. Geosci. 94, 77–85.

Placzek, C., Granger, D.E., Matmon, A., Quade, J., Ryb, U., 2014. Geomorphic process rates in the central atacama desert, Chile: Insights from cosmogenic nuclides and implications for the onset of hyperaridity. Am. J. Sci. 314, 1462–1512.

Pratt-Sitaula, B., Burbank, D.W., Heimsath, A.M., Humphrey, N.F., Oskin, M., Putkonen, J., 2011. Topographic control of asynchronous glacial advances: A case study from Annapurna, Nepal. Geophys. Res. Lett. 38, 1–6.

Putkonen, J., Connolly, J., Orloff, T., 2008. Landscape evolution degrades the geologic signature of past glaciations. Geomorphology 97, 208–217.

Putnam, A.E., Schaefer, J.M., Denton, G.H., Barrell, D.J.A., Andersen, B.G., Koffman, T.N.B., Rowan, A. V., Finkel, R.C., Rood, D.H., Schwartz, R., Vandergoes, M.J., Plummer, M.A., Brocklehurst, S.H., Kelley, S.E., Ladig, K.L., 2013. Warming and glacier recession in the Rakaia valley, Southern Alps of New Zealand, during Heinrich Stadial 1. Earth Planet. Sci. Lett. 382, 98–110.

Putnam, A.E., Schaefer, J.M., Denton, G.H., Barrell, D.J.A., Birkel, S.D., Andersen, B.G., Kaplan, M.R., Finkel, R.C., Schwartz, R., Doughty, A.M., 2013. The Last Glacial Maximum at 44??S documented by a 10Be moraine chronology at Lake Ohau, Southern Alps of New Zealand. Quat. Sci. Rev. 62, 114–141.

Raina, V.K., Shehmani, and Sangewar, C.V., 2015, Glacier snout monitoring in the Himalayas: Geological Society of India, Bengaluru, p. 227–251.

Ramanathan, A.L., 2011. Status Report on Chhota Shigri Glacier (Himachal Pradesh) Status Report on Chhota Shigri Glacier (Himachal Pradesh). Sci. Eng. Res. Counc. Dep. Sci. Technol. Gov. India 1–89.

Rawat, B.S. and Purohit, K.K., 1988. Geology of the area around Chhota Shigri glacier, Lahul and spiti district, (H.P.). Technical report on Multi-Disciplinary glacier expedition to Chhoat Shigri, Department of Science and Technology, 2: 152–157.

Rawat, S., Gupta, A.K., Sangode, S.J., Srivastava, P., Nainwal, H.C., 2015a. Late Pleistocene-Holocene vegetation and Indian summer monsoon record from the Lahaul, Northwest Himalaya, India. Quat. Sci. Rev. 114, 167–181.

Rawat, S., Gupta, A.K., Srivastava, P., Sangode, S.J., Nainwal, H.C., 2015b. A 13,000 year record of environmental magnetic variations in the lake and peat deposits from the Chandra valley, Lahaul: Implications to Holocene monsoonal variability in the NW Himalaya. Palaeogeogr. Palaeoclimatol. Palaeoecol. 440, 116–127.

RGI Consortium, 2017. Randolph Glacier Inventory (RGI) – A Dataset of Global Glacier Outlines: Version 6.0. Tech. Report, Glob. L. Ice Meas. from Space, Boulder, Color. USA.

Rinterknecht, V.R., Clark, P.U., Raisbeck, G.M., Yiou, F., Bitinas, A., Brook, E.J., Marks, L., Zelcs, V., Lunkka, J.P., Pavlovskaya, I.E., Piotrowski, J.A., Raukas, A., 2006. The Last Deglaciation of the Southeastern Sector of the Scandinavian Ice Sheet. Science (80). 331, 1449–1452.

Roe, G.H., 2011. What do glaciers tell us about climate variability and climate change? J. Glaciol. 57, 567–578.

Roe, G.H., Baker, M.B., 2014. Glacier response to climate perturbations: an accurate linear geometric model. J. Glaciol. 60, 670–684.

Romesburg, C., 2004. Cluster Analysis for Researchers. North Carolina, p. 330.

Röthlisberger, F., Geyh, M., 1985b. Glacier variations in Himalayas and Karakoram. Z. Gletsch. Glazialgeol. 21, 237–249.

Röthlisberger, F., Geyh, M.A., 1985a. Gletscherschwankungen der letzten 10.000 Jahre e Ein Verleich

zwischen Nordund Südhemisphare (Alpen, Himalaya, Alaska, Südamerika, Neuseeland). Verlag Sauerländer, Aarau.

Rounce, D.R., Quincey, D.J., McKinney, D.C., 2015. Debris-covered energy balance model for Imja-Lhotse Shar Glacier in the Everest region of Nepal. Cryosph. Discuss. 9, 3503–3540.

Rupper, S., Roe, G., 2008. Glacier Changes and Regional Climate: A Mass and Energy Balance Approach. J. Clim. 21, 5384–5401.

Rupper, S., Roe, G., Gillespie, A., 2009. Spatial patterns of Holocene glacier advance and retreat in Central Asia. Quat. Res. 72, 337–346.

Sagredo, E. a., Lowell, T.V., 2012. Climatology of Andean glaciers: A framework to understand glacier response to climate change. Glob. Planet. Change 86–87, 101–109.

Saha, S., Owen, L.A., Orr, E.N., and Caffee, M.W., 2018. Timing and nature of Holocene glacier advances at the northwestern end of the Himalayan-Tibetan orogen: Quaternary Science Reviews, v. 187, p. 177–202.

Saha, S., Owen, L.A., Orr, E.N., and Caffee, M.W., *in preparation*. Systematically inherited cosmogenic [10]Be in Late Holocene moraine boulders in the Bhagirathi catchment of the Garhwal Himalaya, northern India: *intend to submit in* Earth Surface Processes and Landforms.

Saha, S., Owen, L.A., Orr, E.N., and Caffee, M.W., *in prep*. High-frequency Holocene glacier fluctuations in the Himalaya and Tibet: Quaternary Science Reviews.

Scherler, D., Bookhagen, B., Strecker, M.R., 2011a. Hillslope-glacier coupling: The interplay of topography and glacial dynamics in High Asia. J. Geophys. Res. Earth Surf. 116, 1–21.

Scherler, D., Bookhagen, B., Strecker, M.R., 2011b. Spatially variable response of Himalayan glaciers to climate change affected by debris cover. Nat. Geosci. 4, 156–159.

Scherler, D., Bookhagen, B., Strecker, M.R., von Blanckenburg, F., Rood, D., 2010. Timing and extent of late Quaternary glaciation in the western Himalaya constrained by 10Be moraine dating in Garhwal, India. Quat. Sci. Rev. 29, 815–831.

Scherler, D., Munack, H., Mey, J., Eugster, P., Wittmann, H., Codilean, A.T., Kubik, P., Strecker, M.R., 2014. Ice dams, outburst floods, and glacial incision at the western margin of the Tibetan Plateau: A >100 k.y. chronology from the Shyok Valley, Karakoram. Geol. Soc. Am. Bull. 126, 738–758.

Schimmelpfennig, I., Schaefer, J.M., Akçar, N., Ivy-Ochs, S., Finkel, R.C., Schlüchter, C., 2012. Holocene glacier culminations in the Western Alps and their hemispheric relevance. Geology 40, 891–894.

Schimmelpfennig, I., Schaefer, J.M., Akçar, N., Koffman, T., Ivy-Ochs, S., Schwartz, R., Finkel, R.C., Zimmerman, S., Schlüchter, C., 2014. A chronology of Holocene and Little Ice Age glacier culminations of the Steingletscher, Central Alps, Switzerland, based on high-sensitivity beryllium-10 moraine dating. Earth Planet. Sci. Lett. 393, 220–230.

Schindelwig, I., Akçar, N., Kubik, P.W., Schlüchter, C., 2012. Lateglacial and early Holocene dynamics of adjacent valley glaciers in the Western Swiss Alps. J. Quat. Sci. 27, 114–124.

Schlup, M., Carter, A., Cosca, M., Steck, A., 2003. Exhumation history of eastern Ladakh revealed by Ar-40/Ar-39 and fission-track ages: the Indus River-Tso Morari transect, NW Himalaya. Jgsl 160,

Seaby, R., Henderson, P., 2014. Community Analysis Package 5.0: Searching for structure in community data. PISCES Conserv. Ltd., Engl.

Searle, A.M.P., Parrish, R.R., Hodges, K. V, Hurford, A., Ayres, M.W., Searle, M.P., Parrish, R.R., Hodges, K. V, Hurford, A., Ayres, M.W., Whitehouse, M.J., 1997. Shisha Pangma Leucogranite, South Tibetan Himalaya: Field Relations, Geochemistry, Age, Origin, and Emplacement. J. Geol. 105, 295–318.

Searle, M.P., Noble, S.R., Hurford, A.J., Rex, D.C., 1999. Age of crustal melting, emplacement and exhumation history of the Shivling leucogranite, Garhwal Himalaya. Geol. Mag. 136, 513–525.

Searle, M.P., Windley, B.F., Coward, M.P., Cooper, D.J.W., Rex, A. J., Rex, D., Tingdong, L., Xuchang, X., Jan, M.Q., Thakur, V.C., Kumar, S., 1987. The closing of Tethys and the tectonics of the Himalaya. Geol. Soc. Am. Bull. 98, 678–701.

Seong, Y.B., Owen, L. a., Bishop, M.P., Bush, A., Clendon, P., Copland, L., Finkel, R., Kamp, U., Shroder, J.F., 2007. Quaternary glacial history of the Central Karakoram. Quat. Sci. Rev. 26, 3384–3405.

Seong, Y.B., Owen, L.A., Yi, C., Finkel, R.C., 2009. Quaternary glaciation of Muztag Ata and Kongur Shan: Evidence for glacier response to rapid climate changes throughout the late glacial and holocene in westernmost Tibet. Bull. Geol. Soc. Am. 121, 348–365.

Severinghaus, J.P., Beaudette, R., Headly, M. a, Taylor, K., Brook, E.J., 2009. the Terrestrial Biosphere 1431–1434.

Sharma, K.K. (1983) Granitoid belts of the Himalaya, Karakoram, and Hindukush, Punjab University, Lahore. 11–37.

Sharma, M.C., Owen, L.A., 1996. Quaternary glacial history of NW Garhwal, Central Himalayas. Quat. Sci. Rev. 15, 335–365.

Sharma, P., Bourgeois, M., Elmore, D., Granger, D., Lipschutz, M.E., Ma, X., Miller, T., Mueller, K., Rickey, F., Simms, P., Vogt, S., 2000. PRIME lab AMS performance, upgrades and research applications. Nucl. Instruments Methods Phys. Res. Sect. B-Beam Interact. with Mater. Atoms 172, 112–123.

Shi, X., Kirby, E., Furlong, K.P., Meng, K., Robinson, R., Lu, H., Wang, E., 2017. Rapid and punctuated Late Holocene recession of Siling Co, central Tibet. Quat. Sci. Rev. 172, 15–31.

Shroder, J.F., Bishop, M.P., Copland, L., Sloan, V.F., 2000. Debris-covered glaciers and rock glaciers in the Nanga Parbat Himalaya, Pakistan. Geogr. Ann. Ser. A Phys. Geogr. 82, 17–31.

Shukla, A., Arora, M.K., Gupta, R.P., 2010. Synergistic approach for mapping debris-covered glaciers using optical-thermal remote sensing data with inputs from geomorphometric parameters. Remote Sens. Environ. 114, 1378–1387.

Singh, D. Sen, Tangri, A.K., Kumar, D., Dubey, C.A., Bali, R., 2017. Pattern of retreat and related morphological zones of Gangotri Glacier, Garhwal Himalaya, India. Quat. Int. 444, 172–181.

Singh, P., Haritashya, U.K., Kumar, N., 2007. Meteorological study for Gangotri Glacier and its comparison with other high altitude meteorological stations in central Himalayan region. Nord. Hydrol. 38, 59.

Singh, P., Haritashya, U.K., Kumar, N., 2008. Modelling and estimation of different components of streamflow for Gangotri Glacier basin, Himalayas. Hydrol. Sci. J. 53, 309–322.

Solomina, O.N., Bradley, R.S., Hodgson, D. a., Ivy-Ochs, S., Jomelli, V., Mackintosh, A.N., Nesje, A., Owen, L. a., Wanner, H., Wiles, G.C., Young, N.E., 2015. Holocene glacier fluctuations. Quat. Sci. Rev. 111, 9–34.

Solomina, O.N., Bradley, R.S., Jomelli, V., Geirsdottir, A., Kaufman, D.S., Koch, J., McKay, N.P., Masiokas, M., Miller, G., Nesje, A., Nicolussi, K., Owen, L.A., Putnam, A.E., Wanner, H., Wiles, G., Yang, B., 2016. Glacier fluctuations during the past 2000 years. Quat. Sci. Rev. 149, 61–90.

Srivastava, P., Kumar, A., Chaudhary, S., Meena, N., Sundriyal, Y.P., Rawat, S., Rana, N., Perumal, R.J., Bisht, P., Sharma, D., Agnihotri, R., Bagri, D.S., Juyal, N., Wasson, R.J., Ziegler, A.D., 2017. Paleofloods records in Himalaya. Geomorphology 284, 17–30.

Steck, A., 2003. Geology of the NW Indian Himalaya. Eclogae Geol. Helv. 96, 147-U13.

Steck, A., Epard, J.-L., Vannay, J.-C., Hunziker, J., Girard, M., Morard, A. and Robyr, M. 1998. Geological transect across the Tso Morari and Spiti areas—the nappe structures of the Tethys Himalaya. Eclogae Geologicae Helvetiae, 91, 103–121.

Stone, J.O., 2000. Air pressure and cosmogenic isotope production. 105, 23,753–759.

Stutz, E., Thöni, L.M., 1987. The lower Paleozoic Nyimaling x granite in the Indian Himalaya (Ladakh): new Rb/Sr data versus zircon typology. Geol. Rundschau 76, 307–315.

Su, Z., Shi, Y., 2002. Response of monsoonal temperate glaciers to global warming since the Little Ice Age. Quat. Int. 97–98, 123–131.

Sugden, D. E. and John, B. S. 1976. Glaciers and Landscape. A Geomorphological Approach. Edward Arnold, London.

Tangri, A.K., Chandra, R., Yadav, S.K.S., 2004. Temporal monitoring of the snout, Equilibrium line and Ablation zone of Gangotri Glacier through remote sensing and GIS techniques- an attempt at deciphering the climatic variability. Geological Survey of India (Special Publication) 80, 145–153

Taylor, J.R., 1997, An Introduction to Error Analysis: Second Edition, University Science Books, Sausalito, Calif.

Thayyen, R.J., Gergan, J.T., 2010. Role of glaciers in watershed hydrology: A preliminary study of a "himalayan catchment." Cryosphere 4, 115–128.

The R Core Team, 2018. R: A Language and Environment for Statistical Computing. Vienna, Austria. ISBN 3-900051-07-0.

Thompson, L.G., Tao, T., Davis, M.E., Henderson, A., Mosley-Thompson, E., Lin, P.N., Beer, J., Synal, H.A., Cole-Dai, J., Bolzan, J.F., 1997. Tropical Climate Instability: The Last Glacial Cycle from a Qinghai-Tibetan Ice Core. Science (80). 276, 1821–1825.

Uppala, S.M., KÅllberg, P.W., Simmons, A.J., Andrae, U., Bechtold, V.D.C., Fiorino, M., Gibson, J.K., Haseler, J., Hernandez, A., Kelly, G.A., Li, X., Onogi, K., Saarinen, S., Sokka, N., Allan, R.P., Andersson, E., Arpe, K., Balmaseda, M.A., Beljaars, A.C.M., Berg, L. Van De, Bidlot, J., Bormann, N., Caires, S., Chevallier, F., Dethof, A., Dragosavac, M., Fisher, M., Fuentes, M., Hagemann, S., Hólm, E., Hoskins, B.J., Isaksen, L., Janssen, P.A.E.M., Jenne, R., Mcnally, A.P., Mahfouf, J.-F., Morcrette, J.-J., Rayner, N.A., Saunders, R.W., Simon, P., Sterl, A., Trenberth, K.E., Untch, A., Vasiljevic, D., Viterbo, P., Woollen, J., 2005. The ERA-40 re-analysis. Q. J. R. Meteorol. Soc. 131, 2961–3012.

van der Bilt, W.G.M., Bakke, J., Vasskog, K., D'Andrea, W.J., Bradley, R.S., Ólafsdóttir, S., 2015. Reconstruction of glacier variability from lake sediments reveals dynamic Holocene climate in Svalbard. Quat. Sci. Rev. 126, 201–218.

Vance, D., Harris, N., 1999. Timing of prograde metamorphism in the Zanskar Himalaya. Geology 27, 395.

Vaux, Jr., H.J., Balk, D., Cook, E.R., Gleick, P., Lau, W.K.-M., Levy, M., Malone, E.L., Mcdonald, R., Shindell, D., Thompson, L.G., Wescoat, J.L., Williams, M.W., 2012. Himalayan Glaciers Climate Change, Water Resources, and Water Security. National Academy of Sciences, Washington, DC.

Vermeesch, P., 2009. RadialPlotter: A Java application for fission track, luminescence and other radial plots. Radiat. Meas. 44, 409–410.

Walker, M.J.C., Berkelhammer, M., Björck, S., Cwynar, L.C., Fisher, D.A., Long, A.J., Lowe, J.J., Newnham, R.M., Rasmussen, S.O., Weiss, H., 2012. Formal subdivision of the Holocene Series/Epoch: A Discussion Paper by a Working Group of INTIMATE (Integration of ice-core, marine and terrestrial records) and the Subcommission on Quaternary Stratigraphy (International Commission on Stratigraphy). J. Quat. Sci. 27, 649–659.

Wang, B., Wu, R., Lau, K.-M., 2001. Interannual Variability of the Asian Summer Monsoon: Contrasts between the Indian and the Western North Pacific – East Asian Monsoons *. J. Clim. 14, 4073–4090.

Wang, X., Auler, A.S., Edwards, R.L., Cheng, H., Cristalli, P.S., Smart, P.L., Richards, D.A., Shen, C.-C., 2004. Wet periods in northeastern Brazil over the past 210 kyr linked to distant climate anomalies. Nature 432, 740–743.

Wanner, H., Mercolli, L., Grosjean, M., Ritz, S.P., 2015. Holocene climate variability and change; a data-based review.

Ward, D.J., Anderson, R.S., Guido, Z.S., Briner, J.P., 2009. Numerical modeling of cosmogenic d??glaciation records, Front Range and San Juan mountains, Colorado. J. Geophys. Res. Earth Surf. 114.

Ward, D.J., Cesta, J.M., Galewsky, J., Sagredo, E., 2015. Late pleistocene glaciations of the arid subtropical Andes and new results from the Chajnantor Plateau, northern Chile. Quat. Sci. Rev. 128, 98–116.

Wulf, H., Bookhagen, B., Scherler, D., 2010. Seasonal precipitation gradients and their impact on fluvial sediment flux in the Northwest Himalaya. Geomorphology 118, 13–21.

Wünnemann, B., Demske, D., Tarasov, P., Kotlia, B.S., Reinhardt, C., Bloemendal, J., Diekmann, B., Hartmann, K., Krois, J., Riedel, F., Arya, N., 2010. Hydrological evolution during the last 15 kyr in the Tso Kar lake basin (Ladakh, India), derived from geomorphological, sedimentological and palynological records. Quat. Sci. Rev. 29, 1138–1155.

Yancheva, G., Nowaczyk, N.R., Mingram, J., Dulski, P., Schettler, G., Liu, J., Sigman, D.M., Peterson, L.C., Haug, G.H., 2007. Influence of the intertropical convergence zone on the East Asian monsoon 445, 3–6.

Yi, C., Chen, H., Yang, J., Liu, B., Fu, P., Liu, K., Li, S., 2008. Review of Holocene glacial chronologies based on radiocarbon dating in Tibet and its surrounding mountains. J. Quat. Sci. 23, 533–543.

Young, N.E., Briner, J.P., Rood, D.H., Finkel, R.C., 2012. Glacier extent during the Younger Dryas and 8.2-ka event on Baffin Island, Arctic Canada. Science (80). 337, 1330–1333.

Zuming, L.A.I., Maohuan, H., 1989. A numerical classification of glaciers in china by means of glaciological indices at the equilibrium line. Snow Cover Glacier Var. (Proceedings Balt. Symp. Maryland).

Paper I

Lahul, India

Timing and nature of Holocene glacier advances at the northwestern end of the Himalayan-Tibetan orogen

Sourav Saha [a] [1*]**, Lewis A. Owen** [a]**, Elizabeth N. Orr** [a]**, Marc W. Caffee** [b]

[a] *Department of Geology, University of Cincinnati, Cincinnati, OH 45221, USA*
[b] *Department of Physics, Department of Earth, Atmospheric and Planetary Sciences, Purdue University, West Lafayette, IN 47907, USA*

Abstract

Holocene glacial chronostratigraphies are developed for four glaciated valleys at the northwestern end of the Himalayan-Tibetan orogen using geomorphic mapping and cosmogenic [10]Be surface exposure dating. The study areas include the Hamtah valley in the Lahul Himalaya, and the Karzok, Lato and upper Stok valleys in Zanskar. Five local glacial stages are dated to ~10.4, ~6.1–3.3, ~2.1–0.9, ~0.7–0.4, and ~0.3–0.2 ka based on 49 new moraine boulder ages. Large age dispersions are evident for each of the local glacial stages. This is especially the case for ~6.1–3.3 and ~2.1–0.9 ka, which is likely a result of prior and/or incomplete exposures in very young moraine boulders. An additional compilation of 187 published [10]Be moraine boulder ages helps define seven Himalayan Holocene regional glacial stages (HHs) for the northwestern end of the Himalayan-Tibetan orogen. These HHs date to ~10.9–9.3, ~8.2–7.4, ~6.9–4.3, ~4.5–2.8, ~2.7–1.8, ~1.8–0.9, and <1 ka. Early Holocene glacier advances were generally more extensive and had larger equilibrium-line altitude depressions (ΔELA= ~425±229 m) than glacier advances during the mid-Holocene (ΔELA= ~141±106) and late Holocene (ΔELA= ~124±121 m). The early Holocene glacier advances likely to correspond to the orbitally-forced northerly migration of the Intertropical Convergence Zone and enhanced summer monsoon. The timing of the majority of HHs during mid- and late Holocene corresponds well with the North Atlantic cooling that is likely teleconnected via mid-latitude westerlies, particularly during ~8 ka and after ~5 ka. These chronostratigraphies suggest that Holocene

glaciation in the northwestern part of the Himalayan-Tibetan orogen is largely influenced by long-term orbital forcing amplified by large-scale migration of the Earth's thermal equator and the associated hemispheric oceanic-atmospheric systems.

1. Introduction

Over the past decade, several compilations of young glacial chronologies have been used to help reconstruct and understand the nature of Holocene glaciation on a global scale (Grove, 2008; Davis et al., 2009; Solomina et al., 2015, 2016). Most of these studies conclude that glacier advances during the Holocene in extratropical regions are broadly the consequence of climatic change driven by long-term orbital forcing, with occasional forcing by explosive volcanic eruptions and El Ninõ-Southern Oscillations (Solomina et al., 2015). Changes in oceanic-atmospheric circulations in the North Atlantic (Denton and Broecker, 2008; Chiang and Friedman, 2012, 2014; Wanner et al., 2015) represent another possible amplification mechanism. By way of contrast, long-term forcing behind Holocene glacier variability in the Himalaya has been attributed to distinct regional teleconnections, and do not correlate directly with orbital forcing (Solomina et al., 2015, 2016). Despite the impressive preservation of glacial landform assemblages throughout the Himalaya, this view has not been adequately tested due to the lack of well-defined Holocene glacial chronostratigraphies (Fig. 1A).

To examine the nature of Holocene glaciations and possible forcing factors behind glacier advances in the Himalaya, we developed Holocene glacial chronostratigraphies for four glaciated valleys at the northwestern end of the Himalayan-Tibetan orogen using remote sensing and field mapping, geomorphic techniques, and cosmic-ray-produced (cosmogenic) [10]Be surface exposure age dating. We also compare these new studies with existing glacial chronostratigraphies developed using [10]Be dating in adjacent regions of the Himalayan-Tibetan orogen (Fig. 1B). These include: the Chandra valley in Lahul, (Owen et al.,

2001); the Yunam (Saha et al., 2016), Puga (Hedrick et al., 2011) and Stock valleys (Orr et al., 2017) and Nun Kun massif (Lee et al., 2014) in Zanskar; the northern slopes of the Ladakh range (Dortch et al., 2013); several valleys in the eastern and central Karakoram (Owen et al., 2002; Seong et al., 2007); Muztag Ata (Seong et al., 2009) and the Great Bogchigir valley in the Pamir (Röhringer et al., 2012); and the Koksu valley in Alay Range (Abramowski et al., 2006) (Fig. 1B). These study areas are within the contemporary transition between the Indian summer monsoon and mid-latitudinal westerly climate systems. Together these represent a key natural laboratory for investigating the relative influence of these climate systems in the region (Fig. 1B).

Previous studies of Quaternary glaciation, utilizing optically stimulated luminescence (OSL) and cosmogenic [10]Be surface exposure ages, have shown that glacier advances at the northwestern end of the Himalayan-Tibetan orogen are likely influenced by both oscillations in the Indian summer monsoon and mid-latitude westerlies (Taylor and Mitchell, 2000; Owen et al., 2001; Hedrick et al., 2011; Dortch et al., 2013; Lee et al., 2014; Saha et al., 2016; Eugster et al., 2016; Sharma et al., 2016; Orr et al., 2017, 2018). Dortch et al. (2013) and Owen and Dortch (2014 and references therein) using [10]Be dating have summarized the regional Quaternary glacier advances in the northwestern end of Himalaya and Tibet. Their semi-arid western Himalayan-Tibetan stages (SWHTS) date to 311±32 (SWHTS 9), ~234±44 (SWHTS 7), 146±18 (SWHTS 6), 121±11 (SWHTS 5E), 80±5 (SWHTS 5A), 72±8 (SWHTS 5A), 61±5 (SWHTS 4), 46±4 (SWHTS 3), 30±3 (SWHTS 2F), 20±2 (SWHTS 2E), 16.9±0.7 (SWHTS 2D), 14.9±0.8 (SWHTS 2C), 13.9±0.5 (SWHTS 2B), 12.2±0.8 (SWHTS 2A), ~8.8±0.3 (SWHTS 1E), ~6.9±0.2 (SWHTS 1D), 3.8±0.6 (SWHTS 1C), 1.7±0.2 (SWHTS 1B), and 0.4±0.1 ka (SWHTS 1A). Recently, new moraine chronologies using [10]Be (Saha et al., 2016, Eugster et al., 2016; Orr et al., 2017, 2018) and OSL (Sharma et al., 2016) are also added to improve further and corroborate the existing regional stages of Quaternary glacier advances. While detailed Pleistocene chronologies are reconstructed in several valleys in the northwestern Himalaya, only a few attempts have been made to reconstruct Holocene glacial chronostratigraphies in the Lahul and Zanskar regions (see Owen and Dortch, 2014). These studies have delineated how small temperate to sub-polar glaciers in these regions oscillated throughout the Holocene.

We, therefore, selected areas across the northwestern end of the Himalayan-Tibetan orogen which have a strong precipitation gradient, ranging from ~800 to ~40 mm a^{-1}, to help examine Holocene glacier oscillations. From wettest to driest, our study areas include the Hamtah valley in the Lahul Himalaya, and the Karzok, Lato, and upper Stok valleys in Zanskar (Fig. 1). We use ^{10}Be dating because this method has been applied extensively due to the scarcity of suitable organic materials necessary for radiocarbon dating and/or the lack of well-bleached non-glacial sediments suitable for OSL dating (Owen and Dortch, 2014). The primary goals of our study are to refine previously proposed regional glacial stages (Dortch et al., 2013; Owen and Dortch, 2014; Solomina et al., 2015) and to assess whether Holocene glacier advances at the northwestern end of the Himalayan-Tibetan orogen were driven by regionally unique forcing factors that are not directly be influenced by long-term orbital trends, and/ or global changes in the oceanic-atmospheric circulation system.

2.   Regional setting

Our study areas encompass several tectonic-lithologic domains (Honegger et al., 1982; Brookfield and Andrews-Speed, 1984; Searle et al., 1987; Steck et al., 1998; Schlup et al., 2003) and are defined by three major structures. From south to north these structures are: i) the Main Central Thrust (MCT); ii) the Zanskar Shear Zone (ZSZ) and the Sarchu fault; and iii) Indus-Tsangpo Suture Zone (ITSZ) (Fig. 1C; Epard and Steck, 2008). North of the MCT, the Hamtah crystalline axis consists mostly of migmatites, and the Rohtang gneiss and granite (Kumar et al., 1987). The Karzok and Lato study areas, located north of ZSZ in the Zanskar range, are composed of coarse-grained granite of the North Himalayan nappe system (Stutz and Thöni, 1987; Fuchs and Linner, 1996; Steck et al., 1998; Epard and Steck, 2008). The upper reaches of the Stok study area that is located in the northwestern part of this nappe system and consists of thick-bedded conglomerates with alternating coarse and fine-grained sandstone, siltstone, and shale known as the Stok Kangri (Kangri glacier) molasse (Brookfield and Andrews-Speed, 1984).

The Himalayan-Tibetan orogen imposes a formidable physical barrier to the Indian summer monsoon, the East Asian monsoon, and the northern mid-latitude westerlies (Fig. 1B). The present-day total

annual precipitation derived from Tropical Rainfall Measurement Mission (TRMM) data for 1998 to 2005 shows a northward decline from 1500 to 3000 mm in the high mountain ranges of the Himalaya, to slightly >100 mm over much of the interior of the Tibetan Plateau (Fig. 1B; Bookhagen and Burbank, 2006). These prevailing climate systems and precipitation gradient are responsible for tropical climates in the forelands of the eastern Himalaya to sub-tropical arid climate into the interior of the Tibetan Plateau (Spicer, 2017). According to Rupper and Roe (2008) and Rupper et al. (2009), stronger monsoons are often associated with abundant moisture supply from the Indian Ocean and South China Sea (Owen and Benn, 2005) and enhanced cloud albedo. Orographically modulated increased cloud albedo often favors a decrease in incoming shortwave radiation (dynamic response) and in association with evaporative/sublimation cooling foster positive mass balance. This dynamic energy balance response to increased cloud cover and latent heat transfer are one of the most crucial physical mechanisms that have been argued for significantly effecting the amplitude and timing of contemporary and past Himalayan glacier oscillations (Rupper and Roe, 2008; Rupper et al., 2009). The northern mid-latitude westerlies, in contrast, teleconnect cooling events in the North Atlantic and Mediterranean regions to the Himalayan-Tibetan orogen helping regulate the supply of winter snow and fostering colder temperature (Srivastava et al., 2017). Mölg et al. (2014) have even argued that large-scale mid-latitude westerly waves play a crucial role in modulating present-day May-June precipitation and summer air temperature over monsoonal High Asia.

A strong latitudinal-temperature gradient also exists along the south-north transect, coupled with local altitudinal changes in temperature within each mountain range (CRU CL 2.0 reanalysis surface climate data derived from New et al., 2002). The contemporary regional equilibrium-line altitudes (ELAs) broadly follow the climatic gradient, rising from ~3000 m asl in the Lesser Himalaya to ~6000 m asl to the interior of Tibetan Plateau, and declining again to <4800 m asl in the northeastern part of Tibet (Benn and Owen, 1998; Zhou et al., 2011).

Most of the present-day precipitation in the study areas occurs during the summer monsoon (60–80% of annual precipitation), but both the Indian summer monsoon and the mid-latitude westerlies influence the glacier mass balance and the types of glaciers in all the study areas (Azam et al., 2014; Mölg et al.,

2014). The Hamtah study area in Lahul, located in the rain shadow of the Pir Panjal range, has an annual

precipitation of ~400–800 mm (Fig. 1B). The Karzok, Lato, and Stok study areas, to the north of the

Transhimalaya, have annual precipitation ranging from 40 to 100 mm (Fig. 1B and C). Temperate glaciers

in the Greater Himalaya, to the south, including Lahul, are larger, more erosive, melt-dominated, and

support a thick debris-mantle in the ablation zone (Benn and Owen, 2002). These glaciers presently receive

abundant snowfall during the summer monsoon and are more susceptible to changes in temperature (see Su

and Shi, 2002). In contrast, glaciers in the northern and northwestern parts of the study areas, that include

the northern Zanskar and Ladakh ranges, Central Karakoram, the Pamir, and Alay Ranges (Fig. 1B) are

predominantly of cold-based sub-polar types, they are smaller, mostly debris free, and are more

precipitation-sensitive and sublimation dominated (Benn and Owen, 2002). Presently most of these glaciers

are fed by the snowfall associated with the winter mid-latitude westerlies system (Fig. 1B), and directly

respond to changes in the strength of westerly-winds.

3. Methods

3.1. Geomorphic mapping

Former glacier extents in each of the study areas were reconstructed by mapping glacial and

associated landforms in the field using a handheld GPS at the scale of 1:20,000 (uncertainty ±3 m; Fig. 2).

High-resolution Google Earth imagery, Advanced Spaceborne Thermal Emission and Reflection

Radiometer (ASTER) global digital elevation models (V002, resolution of 30 m), and Landsat Enhanced

Thematic Mapper Plus (ETM) imagery (resolution 30 m) were used to aid in reconnaissance and final field

mapping (http://glovis.usgs.gov/next/). Contemporary and past glacier maps of all previously investigated

(dated using [10]Be) glaciated valleys (Fig. 1B; Supplementary material S1) were also prepared using the

satellite imagery and published geomorphic maps.

3.2. Morphostratigraphy

Moraines and associated landforms in the four study areas were assigned to glacial stages based on morphostratigraphy using the scheme proposed by Hughes et al. (2005) and Hughes (2010). We used the letters *m* to denote moraines and *b* for glacially eroded bedrock. Subscript letters are used to indicate the study area, e.g., *H* for Hamtah study area (Fig. 2A). Individual moraines and bedrock surfaces were also numbered using a subscript (*1, 2 ... n*) from youngest to oldest. Furthermore, individually mapped moraine ridges (ice-contact ridges) within a moraine set of a particular glacial stage were assigned a subscript letter *a, b ... n* (with increasing age). For instance, the m_{H1a} is a moraine (*m*) in the Hamtah study area (subscript *H*), it is the youngest moraine (subscript *1*) and the youngest ridge (subscript *a*), whereas the m_{H3a} is a moraine with a single ridge (subscript *a*) and is the oldest of a set of three moraines (subscript *3*).

3.3. Sampling for cosmogenic ^{10}Be

Moraine boulders and glacially sculpted bedrock surfaces were sampled based on the morphostratigraphic considerations; only sharp-crested, relatively well-preserved moraines with little evidence of erosion and/or degradation were sampled (Table 1; Fig. 3; Supplementary material S2). Multiple (9–3) boulder samples were obtained from individual moraines. We only sampled quartz-rich large boulders (>50 cm high) that were inset into the crest of moraines and showed no evidence of post-depositional toppling and little, if any, weathering (Table 2; Fig. 3). We generally avoided sampling boulders close to hillslopes, on moraine slopes, or within depressions that might be affected by post-depositional toppling, exhumation, and shielding. Intensely jointed, fractured, pitted, and/or sediment covered boulders were avoided to reduce the possibility that the boulders might have had complex exposure histories. Boulders with well-developed rock varnish and/or lichen cover were preferentially sampled; these features provide a measure of confidence that the boulders had not recently toppled and/or have been recently exhumed.

Approximately 500 g of rock from the top (to a depth of ≤3) of each boulder/bedrock surface were collected using a hammer and chisel (Table 2). Topographic shielding was recorded using a clinometer and compass, measuring the skyline angles above the horizontal to the skyline at azimuth intervals of 10° (Gosse

and Phillips, 2001; Balco et al., 2008). Boulders were photographed from several perspectives, and their locations were recorded using a handheld GPS (Fig. 3; Supplementary material S2). The width, length, and height of each boulder were documented using a tape measure (Table 2).

3.4. [10]Be extraction and AMS measurements

Quartz extraction and [10]Be sample preparation were performed in the Geochronology Laboratories at the University of Cincinnati using the community standard methods of Nishiizumi et al. (1994) and Kohl and Nishiizumi (1992). All AMS measurements were performed at the Purdue Rare Isotope Measurement (PRIME) Laboratory at Purdue University (Sharma et al., 2000). Be isotopic measurements were normalized using the 07KNSTD standard (Nishiizumi et al., 2007). We used the appropriate standard correction factors available at http://hess.ess.washington.edu/ for recalculating published ages. Residual boron contamination was considered negligible, and no correction for boron was made in the age calculation (cf. Putnam et al., 2013b; Corbett et al., 2016). Blank corrections ranged from 0.1 to 23.1% (averaging 3%) for a [10]Be concentration of >20,000 atoms g^{-1} SiO_2 and from 15.7 to 32.4% for a [10]Be concentration of <20,000 atoms g^{-1} SiO_2. Analytical uncertainties were generally 5.8±5.1% (±1σ), but larger than 10% for five very young samples (<0.6 ka; Table 2).

3.5. Exposure age calculations

Exposure ages were determined using the CRONUScale (Marrero et al., 2016), Cosmic Ray Exposure program (CREp; Martin et al., 2016) and CRONUS-Earth V3 (http://hess.ess.washington. edu/math/v3/v3_age_in.html) online calculators (Supplementary material S3). There are several notable differences among these recent age calculators, most prominent being the sea-level high- latitude (SLHL) spallogenic production rates. In the absence of a locally calibrated in situ [10]Be production rate (Heyman, 2014), we used the global SLHL production rates of ~3.92±0.17 atoms g^{-1} a^{-1} in the CRONUScale (Borchers et al., 2016; Marrero et al., 2016) and 4.08±0.23 atoms g^{-1} a^{-1} in the CREp and CRONUS-Earth V3 calculators that are linked to the online ICE-D database (Martin et al., 2016). All available scaling models,

i.e., Lifton-Sato-Dunai (LSD; Lifton et al., 2014 [SA and SF in Marrero et al., 2016]), Lal and Stone time-dependent (Lm; Balco et al., 2008), Lal and Stone time-independent (St; Lal, 1991; Stone, 2000), Desilets (De; Desilets et al., 2006), Dunai (Du; Dunai, 2001), Lifton (Li; Lifton et al., 2005, 2008) were used to calculate [10]Be ages (Supplementary material S3). Holocene [10]Be age differences among different scaling frameworks computed using different age calculators were <10% (Supplementary material S4). For our study, we used the CREp LSD model when discussing the ages because the model does not have systematic neutron monitor-based biases and incorporates both time-varying dipolar and non-dipolar geomagnetic components (cf., Lifton et al., 2008) and solar modulation framework (cf., Lifton et al., 2005, 2008). The CREp (LSD and Lm) ages were calculated using the ERA40 atmospheric model (Uppala et al., 2005) and Lifton-VDM2016 geomagnetic database (Lifton, 2016). All the ages are reported in thousands of years (ka) before 2016 CE (the year that the new samples were processed and measured).

We assume a zero-erosion rate when calculating the ages because most of the sampled boulders exhibited little, if any, signs of weathering (e=0 in Table 2). However, to understand how erosion might affect our Holocene ages, we experimented with several different erosion rates (Supplementary material S5). Our results suggest that even with a high steady-state erosion rate for arid and semi-arid environments, similar to our study areas, of 10 m Ma[-1] (see Seong et al., 2007; Dietsch et al., 2015), the difference from zero erosion is <10% over the Holocene (see Supplementary material S5). No correction was made for snow cover. We argue that this is valid because most of the sampled boulders have prominent relief (rising >50 cm above the moraine surface) and likely remained snow free due to windswept conditions throughout the winter (Fig. 3). We also recalculated, using the same methods as for all new ages, the previously published [10]Be ages for Holocene moraines at the northwestern end of the Himalayan-Tibetan orogen (Fig. 1B; Supplementary material S6).

3.6. Moraine/bedrock ages

Geologic uncertainties including differential erosion, prior-exposure, reworking, and/or incomplete exposure histories due to the exhumation of moraine boulders, that influence exposure ages often outweigh

analytical and production rate uncertainties (Putkonen and Swanson, 2003; Applegate et al., 2010, 2012). These geologic uncertainties affect a mean ^{10}Be exposure age of a single landform based on multiple (9–3) samples (Table 2). Reduced chi-squared (χ^2) statistics were used to assess the distribution of ages (Applegate et al., 2010, 2012; Kaplan et al., 2013; Putnam et al., 2013b). The χ^2 values if >1, indicates high dispersion of ages and geologic factors other than analytical uncertainties are likely accounted for. Moraine ages with χ^2>1 are then further treated to identify outliers. Outliers were initially identified if an individual boulder age uncertainty was >2σ from the arithmetic mean age of the distribution (Putnam et al., 2013a). We further verified any outliers using Chauvenet's criterion as advocated in Taylor (1997), Dunai (2010), and Putnam et al. (2013b). Any outliers identified by these methods were additionally verified using our field records and applied only when compelling field evidence supported our statistical outliers. We were not able to apply the field verification methods for published data and hence, relied entirely on our statistical interpretation and description in the respective literature (Supplementary material S3). Chosen outliers (66 out of a total of 236 ^{10}Be ages) were discarded from further statistical treatment. Finally, we report the weighted mean and 1σ uncertainties to define the true age of the moraine (Barrows, 2007). The weighted mean is usually applied in scenarios where samples are dispersed, and arithmetic mean age is likely influenced by longer tail skewed distribution (cf. Applegate et al., 2012). We have used the word 'tentative' throughout our paper as a cautionary note given possible large uncertainty associated with some of the age interpretations, especially when defining a mean based on <3 samples and/or ages for largely dispersed data.

We assume that the mean moraine ^{10}Be age is a minimum age of a local glacial stage/glacier advance as it represents the last time that boulders were deposited on the moraine before the glacier began to thin and/or retreat (cf. Gosse, 2005; Ivy-Ochs et al., 2007; Putkonen et al., 2008). We interpret bedrock ages to represent the time that a glacier withdrew from a specific location during the retreat (cf. Ward et al., 2009, 2015). Moraine preservation is poor in high- energy glaciated environments such as the Himalaya due to post-depositional denudation and/or obliteration of older landscape features by advancing younger glaciers (Kirkbride and Winkler, 2012). Likewise, local microclimate, topography, hypsometry, and aspect

make glaciers in some valleys more likely to respond to climate change and/or have a better-preserved record of glaciation (Roe, 2011; Barr and Lovell, 2014). Probabilistic models applied in several studies (e.g., Gibbons et al., 1984; Kirkbride and Brazier, 1998; Kirkbride and Winkler, 2012) also suggest that it is unlikely to preserve more than three sets of moraines in a single/local glaciated valley (~30% probability). We used the term local glacial stage to define a morphostratigraphically distinct glacier advance within any one of our four study areas. Several local glacial chronologies with similar climatic and glacial landform characteristics constitute a regional glacial stage in our study. We argue that regional glacial stages are helpful to reconstruct a complete glacial history in a region and furthermore to examine whether moraine formation has taken place due to widespread changes in climate or is due to intrinsic climate variability in individual valleys (see Roe, 2011).

3.7. Regional glacial stages

We employed radial plots (Galbraith, 1990, 2010; Galbraith and Roberts, 2012; Vermeesch, 2009) to identify different populations (local glacial stages) in preference to probability density functions (Supplementary material S3). A combination of radial plot analysis and statistical tests (Student's t-test) were used to test whether hypothesized age distributions were distinct from each other. A threshold two-tailed p-value of <0.01 (at ≥99% confidence level) was used to define distinct regional glacial stages/chronozones. We used both the upper and lower tail distributions of the lumped age population, i.e., local glacial stages, including their uncertainties to define the chronozone of each regional glacial stage. Most regional glacial stages are based on ≥3 local glacial stages.

3.8. Equilibrium-line altitudes

We calculated former ELAs and ELA depressions (ΔELAs) for each of our study areas using detail reconstruction of former glaciers derived from our geomorphic maps, as well as all ELAs of previously [10]Be dated glaciated valleys using glacial maps for the northwestern end of the Himalayan-Tibetan orogen (Supplementary material S1). Assuming a simplistic steady-state scenario (Sugden and John, 1976; Putnam

et al., 2013b), former ELAs were calculated using area-altitude (AA), area accumulation ratio (AAR), and toe-headwall accumulation ratios (THAR) methods for each glacier advance, as recommended by Benn et al. (2005) and Osmaston (2005; Table 3). We also used the modern maximum elevation of lateral moraines (MELM; cf. Dahl and Nesje, 1992) of studied valleys to further reconstruct modern ELAs. Calculating past ELAs based on MELM is more uncertain due to poor preservation and/or post-depositional burial of lateral moraines. Therefore, this method was not used for past glacier advances. Many of the glaciers within our study areas have widely different geometries, micro-climates, glacier hypsometries, debris mantles, and slopes, so to help address this variability we use several ELA methods. Application of multiple ELA methods also helped us to evaluate and eliminate some of the uncertainties associated with each method.

The AAR and THAR ratios used in our study were obtained from the published literature for consistency and comparisons (Table 3). A selected summary of recommended AAR and THAR values are provided in Table 3. AARs vary between 0.5 and 0.7 with THARs between 0.3 and 0.5 for the majority of glacier types. When the modern AAR and THAR values (ratios) were calibrated with respect to modern MELM, the AAR and THAR had mean and 1σ values of 0.66 ± 0.13 and 0.31 ± 0.18, respectively. We calculated our ELAs based on three commonly recommended AAR (0.5, 0.6, 0.7) and THAR (0.3, 0.4, 0.5) values (Supplementary material S7). Mean ELAs and ΔELAs were calculated based on all these methods and ratio values.

4. Geomorphology of the study areas

4.1. Hamtah study area

The Hamtah study area is a north-trending ~13-km-long glaciated valley that rises from 3700 m asl to the peak of Indrasan at 6223 m asl and covers an area of ~36 km^2 (Fig. 2A). The major stream, Hamtah Nala, drains from Hamtah glacier at 4070 m asl and flows into the Chandra river. The 5.7-km-long, debris-mantled Hamtah glacier and two small glaciers occupy the valley and have contemporary ELAs of

~4456±70 m asl. While smaller hanging glaciers are located well above the present ELA and have very limited to no discernible ablation zone, the ablation zone of Hamtah glacier is large and covers ~70% (MELM derived; Shukla et al., 2015) of the total glaciated area.

Four sets of moraines are preserved in the Hamtah valley: m_{H1a}, m_{H1b}, m_{H2}, and m_{H3} (Table 1; Fig. 2A). $m_{H1}a$ is the innermost latero-frontal moraine that has a sharp crest and extends along the valley between 3960 and 4575 m asl (Figs. 2A and 4A). The frontal section of the moraine is located at ~1 km downstream from Hamtah glacier. The western lateral moraine is discontinuous over a length of 6.3 km and covered by talus in many places (Fig. 2A). The eastern lateral moraine is a ~6-km-long, a well-preserved ridge that rises ~26 m from the present valley floor. The eastern lateral moraine also preserves a distinct ablation valley parallel to its length, which helps prevent the burial of the moraine by hillslope deposits. Five large boulders were sampled along this ridge (Table 1; Fig. 3A).

The outermost lateral moraine, m_{H3}, is situated ~2.4 km down the valley of the m_{H1a} extending between ~3730 and 3880 m asl (Table 1; Figs. 2A and 4B). The western lateral ridge of the moraine is discontinuous over a length of ~500 m and buried by debris flows from the hillslopes. An ablation valley separates the western lateral moraine from the steep hillslope deposits in its lower reaches. Four samples were collected from this section of the moraine (Figs. 2A and 4B). The eastern lateral ridge is 660 m long with a mean height of ~10 m. While this moraine is better preserved, it is partially buried under thick rockfall deposits upstream at an altitude of >3880 m asl and downstream below <3805 m asl, where the valley narrows from ~3 to 0.4 km in width (Figs. 2A and 4B). Two large stable boulders (>1 m height) were sampled from this moraine ridge away from the hillslopes (Table 1; Fig. 3B).

4.2. Karzok study area

The Karzok study area is a broad bowl-shaped valley (~80 km^2) except for a narrow eastern outlet to Tso (Lake) Moriri (Fig. 2B). The valley is ~15-km-long and ranges between ~3 and 10 km wide. Eight small debris-free cirque glaciers are present in the valley (Fig. 2B). The youngest moraines, which are ice-

contact, help form small lakes along most of these small glaciers. Moraines along Mentok Kangri to the south and Gomuche Kangri to the west of the valley were examined in this study (Figs. 2B and 4C, D).

Mentok Kangri is the largest glacier (~1.5 km in length) in this study area, and it extends to 5487 m asl with an ELA of ~5710±30 m asl (Fig. 2B). Three sets of latero-frontal moraines are present: m_{M1}, m_{M2}, and m_{M3} (Table 1; Fig. 2B). m_{M1} is a 2.5-km-long well-preserved, steep, sharp-crested latero-frontal moraine with four recessional ice-contact ridges. The frontal section of the moraine is ~300 m downstream from Mentok Kangri and rises ~50 m above the present valley floor. Four boulders were sampled over its four ridges of the moraine (Table 1; Fig. 3C). Another well preserved but relatively subdued (~17-m-high) moraine, m_{M2}, is present ~380 m downstream of m_{M1} at 5350 m asl (Table 1; Fig. 4C). This latero-frontal moraine is discontinuous and consists of four ice-contact ridges over a length of 7 km. Five boulders were sampled on this moraine (Fig. 2B). Three additional boulders were also sampled from m_{M3} latero-frontal moraine, ~500 m downstream of m_{M2} at 5220 m asl (Fig. 2B). This 2.4-km-long moraine consists of a single ridge with a rounded crest (Table 1).

Gomuche Kangri is the second largest glacier (~1.3-km-long) in the valley with an ELA of ~5770±120 m asl that is ~270 m above the elevation of its snout (Fig. 2B). We mapped two sets of moraines, $m_{G1,}$ and m_{G2} (Table 1; Fig. 2B). m_{G1} is a 2.2-km-long latero-frontal moraine, located 220 m downstream from its snout at 5350 m asl (Fig. 4D). Three ice-contact (recessional) ridges with a mean height of 23 m are present above the valley floor on this moraine (Fig. 2B). Five samples were collected from the three ridges (Fig. 3D). m_{G2} consists of multiple recessional and hummocky ridges that are tens of meters long (Fig. 4E). This moraine ridge complex, extending between 5200 and 5380 m asl, is discontinuous and highly degraded and associated with a dead-ice zone (Table 1). We sampled four boulders and additionally recalculated four published [10]Be ages of Hedrick et al. (2011) from the most stable three farthest recessional ridge crests (~0.3 km downstream from m_{G1}; Figs. 2B and 3E; Table 1). The ridges in the moraine complex are not well defined, and the degree of weathering is not significant enough to allow us to differentiate them into different substages.

4.3. Lato study area

The Lato study area is a ~13-km-long, and ~3 km-wide valley extending between 4200 and 6200 m asl and has small debris-free glaciers in its upper reaches (Fig. 2C). The 2.9-km-long Amda Kangri and three small glaciers contribute water to the ephemeral Amda Chu that drains the valley. Amda Kangri has an ELA of ~5500±20 m asl and extends to 5340 m asl. Six sets of moraines including a set of round-crested hummocky moraines are present in the valley, of which three sets of sharp-crested young moraines, m_{A1}, m_{A2} (m_{A2a}, m_{A2b}, m_{A2c}), and m_{A3} were examined in detail (Table 1; Fig. 2C). Orr et al. (2018) assign these moraines to the Kyambu glacial stage.

m_{A1}, adjacent to the snout of Amda Kangri at 5326 m asl, is a 154-m-long and 20-m-high end moraine that trends northeast and exhibits little, if any, signs of erosion/degradation (Fig. 4F). The five granitic boulders that were sampled on the moraine were relatively stable and freshly fractured (Table 1; Fig. 3F). Two subdued recessional moraines, m_{A2a} and m_{A2b} are present at an elevation of 5299 and 5298 m asl, respectively. These two moraines are inset into a 2.2- km-long north trending lateral moraine of Amda Kangri (Figs. 2C and 4F). This lateral moraine grades into a relatively well-preserved 346-m-long and 10-m-high end moraine, m_{A2c}, at 5285 m asl (Figs. 3G and 4F). We sampled six boulder samples from this ridge.

Three bedrock samples were collected from glacially sculpted striated bedrock (b_A) ~1.4 km downstream from the m_{A2c} at an elevation of 5180 m asl (Figs. 2C and 4H). A 10-m-high end moraine (m_{A3}) was also mapped and sampled some 1.6 km down the valley from glacially sculpted bedrock at 5113 m asl (Fig. 2C). This end moraine has a rounded crest with steep slopes and stretches perpendicular to the valley for a length of ~130 m (Fig. 4G). The northern part of the moraine is subdued and has subangular/sub-rounded denuded boulders that have undergone slight granular weathering. Many lodged striated boulders are also present on the surface of the moraine. We sampled two boulders from the southern section of the crest that consist of relatively less denuded boulders (Table 1). The northern face of the moraine is arcuate and most likely has shaped by the post-depositional river incision and/or the formation of a debris fan. A

57

broad braided channel is developed right behind the end moraine with largely dispersed young boulders (Fig. 2C).

4.4. Stok study area

Stok Kangri and four debris-free cirque glaciers are present in the upper reach of the Stok valley (Fig. 2D). This sub-polar type glacier is ~1.8 km long with an ELA of ~5480±30 m asl. Building on the work of Orr et al. (2017), we recognize four sets of moraines in the upper Stok valley: m_{S1}, m_{S2}, m_{S3}, m_{S4}, and m_{S5} (Table 1; Fig. 2D). For our study, we have only targeted the m_{S1} moraine complex for dating (Fig. 2D). Orr et al. (2017) discuss the discrepancies between the exposure ages of the moraine complex and their morphostratigraphic contexts. The southern latero-frontal ridges (their M_{S2}) are interpreted as older than northern latero-frontal ridges (their M_{S1}) of m_{S1} moraine complex. Our new study updates the field map and morphostratigraphic interpretation presented in Orr et al. (2017).

The m_{S1} moraine complex is at ~5230–5450 m asl (Fig. 2D) and is composed of diamicton containing highly fractured boulders and cobbles supported by a coarse gravel-sandy matrix (Table 1). The southern latero-frontal moraine of m_{S1} has a length of ~1.5 km and consists of >4 recessional ridges, whereas the northern latero-frontal moraine is ~1.3-km-long and consist of ~3 inner recessional ridges (Fig. 2D). The mean relief of these ridges is similar (~30 m high) (Fig. 2D). Four boulder samples (STOK-1401 to 1404) were collected by Orr et al. (2017) from the distant ridge of the north latero-frontal moraine (Fig. 4I), and five samples including a new one (STOK-1405 to 1408 and 1516) were collected from the inner ridges of the south latero-frontal moraine (Fig. 2D). The distant ridge of north latero-frontal moraine also consists of more weathered boulders (Table 1). Based on its morphostratigraphic position and relative weathering, we reinterpreted the distant northern ridge (M_{S1} of Orr et al., 2017) of the moraine complex to be older than inner southern ridges (M_{S2} of Orr et al., 2017). A summary of characteristics of all moraines, bedrock, and sampled boulders in our study areas are provided in Table 1.

5. Dating results

5.1. Hamtah study area

m_{H3} is correlated with Kulti glacial stage moraines of Owen et al. (1996, 1997, 2001) in Lahul. Ages for m_{H3} range from ~16.2 to 4.0 ka (χ^2 value of 98.3; Fig. 5A; Table 2). Three outliers (Hamtah 1402, 1403, and 1404) were identified and discarded from the final analysis (Table 2; Fig. 5A). The remaining three samples have a weighted mean age of 10.4±0.4 ka (Table 4; Fig. 6A). This early Holocene glacier advance overlaps (at ±2σ) with the previously reported Kulti glacial stage of Owen et al. (2001) at 11.6±0.6 ka in the Chandra valley, Lahul (n=2; recalculated here in Supplementary material S3). However, using different in situ ^{10}Be production rates Eugster et al. (2016) assigned the Kulti glacial stage to 13.7±1.3 ka.

Ages for m_{H1a} range from ~2.4 to 0.14 ka (Fig. 5B; Table 2) with a high degree of dispersion (i.e., χ^2 is 124.9; Fig. 6B). Since most of the samples were collected away from slope deposits and they show no sign of post-depositional modification, one possibility is that the age range is due to varying prior-exposure histories. The skewed distribution toward the younger ages (skewed 2.13) further suggests that the older ages are due to inherited ^{10}Be (Ivy-Ochs et al., 2007). Although we have assumed no production of ^{10}Be during glacial transport, a horizontal surface flow velocity of ~20–14 m yr^{-1} (Shukla et al., 2015) could account for the inheritance of as much as ~0.3–0.1 ka. Two outliers (Hamtah 1408 and 1502 in Table 2) were identified and removed, leaving an age range of ~0.4 to 0.1 ka. The tentative weighted mean moraine age based on three boulders is ~0.2±0.1 ka (Table 4; Fig. 6B).

5.2. Karzok study area

The ages for m_{M3} range from ~57.2 to 22.9 ka with a χ^2 value of 124.0 (Fig. 5C; Table 2). Since, most of the granitic boulders on this moraine exhibit spheroidal weathering, the ages may be affected by post-depositional modification of the boulders (Supplementary material S2). We tentatively associate the moraine age with oldest boulder age (57.2±3.5 ka).

m_{M2} has five ages that are similar except for one outlier, KO-1 (Fig. 5C, Table 2). The outlier-free distribution yields a weighted mean age of 1.0±0.1 ka (Table 4; Fig. 6C). These ages are similar across all the four ice-contact ridges of the m_{M2} moraine, which suggests that all the moraine ridges may have all formed within several decades.

Four ages for m_{M1} are tightly clustered, except for one outlier, KO-7 at ~0.2 ka (Fig. 5C; Table 2). After eliminating the outlier, the moraine has a weighted mean age of 0.7±0.1 ka (Table 4; Fig. 6D). The four ages for m_{G2}, when combined with four additional ages from Hedrick et al. (2011), range from ~23 to 3.3 ka (χ^2=111.3; Fig. 5D; Table 2). Two outliers are evident (KO 1502: 12.4±0.7 ka and TM-C: 22.9±1.7 ka). After omitting the outliers, the remaining six ages have an overlapping multimodal normal kernel density distribution (Fig. 6E). m_{G2} appeared to be a detached dead-ice section of the main glacier which was likely unstable during the past (Fig. 4E). Some of the young ages are possibly the result of the post-depositional toppling of moraine boulders. It is not possible to assign a mean age to this moraine with confidence, but we suggest that this moraine likely formed between ~6.1 and 3.3 ka (Table 4; Fig. 6E).

The five ages for m_{G1} range from ~2.6 to 0.5 ka with a χ^2 value of 181.7 (Fig. 5D; Table 2). Two young outliers (KO 15 at ~0.6 ka and KO16 at ~0.5 ka), which are morphostratigraphically inconsistent (Fig. 5D), were omitted (Fig. 6F, Table 2). Field observations of the sampled boulders (Supplementary material S2) indicate that they are inset a little off-the-crest of the moraine. It is highly possible that this moraine is the unstable and post-depositional toppling of some boulders may have occurred. Due to the smaller length of the glacier (~1.3 km), inherited [10]Be production during transport is probably less (>0.2 ka; assuming horizontal surface flow velocity of the glacier is 7–4m yr^{-1} after Scherler et al., 2011) than the uncertainty of moraine formation. We tentatively assign a weighted mean age of 2.1±0.4 ka to this moraine (n=3; Table 4; Fig. 6F).

5.3. Lato study area

The older moraine, m_{A3}, has young exposure ages (2.1±1.4 and 1.6±0.3 ka). These ages are also reported in Orr et al. (2018), and they have assigned these moraine ages to their Kyambu glacial stage.

However, these ages are morphostratigraphically inconsistent and have very high uncertainties (>66%). The moraine should be much older than the bedrock ages (b_A: ~14 ka) sampled further upstream from this moraine (Fig. 5E; Table 2). Since we preferentially sampled larger fresh boulders from the southern face of the moraine, that appears overridden by recent hillslope deposits, one possibility is that we may have sampled boulders deposited much later than the stabilization of the moraine and hence may represent hillslope activity than the absolute age of the moraine. We are unable to assign a numerical age to this moraine.

The three bedrock ages for b_A are consistent (Fig. 5E; Table 2) and have a weighted mean age of 13.9±0.4 ka (Fig. 6G).

The ages for m_{A2c} range from ~27.6 to 0.4 ka (Fig. 5F; Table 2). Even after three outliers (Lato 1409, 1410, and 1411) were omitted from the age distribution, the dispersion is still high with a χ^2 value of 24.3 (Fig. 6H). There was no sign of differential surface erosion and/or post-depositional modification of these boulders, and the surface of the moraine ridge is stable with a rounded crest. While it is possible that two older age outliers (~4 and ~3 ka) from m_{A2c} may have undergone different prior-exposure histories in this low erosion rate setting, the possibility of boulder toppling is very unlikely (Supplementary material S2). We, therefore, discarded the two outliers (Table 2), and the outlier free population ranges between ~0.7 and ~0.4 ka with a tentative weighted mean moraine age of 0.5±0.2 ka (Table 4; Fig. 6H).

Five ages for m_{A1} range from ~3.4 to 0.2 ka (Fig. 5F; Table 2). After omitting two older outliers (Lato 1415 at ~1.8 and LATO 1419 at ~3.4 ka), we assign a weighted mean age of 0.3±0.1 ka to this moraine (Table 4; Fig. 6I).

5.4. Stok study area

Four ages for the distant northern ridge of m_{S1} that were determined by Orr et al. (2017) range from ~2.1 to 0.3 ka, whereas five ages for the southern moraine, that include one new and four previously published ages in Orr et al. (2017), range between ~0.9 and ~0.1 ka (Fig. 5G; Table 2). A young outlier (Stok 1404 with an age of ~0.3 ka) from the northern latero-frontal moraine and two young outliers (Stok

1406 and 1407 at ~0.6 and ~0.1 ka, respectively) from the southern latero-frontal moraine are evident and excluded from the subsequent analysis (Table 2). Field evidence (see Supplementary material S2) suggests possible toppling and displacement (i.e., incomplete exposures) of these young outlier samples. The recessional moraine ridges of m_{S1} also appeared unstable at several places. Although we avoided sampling unstable locations, the stability of the moraine complex in the recent past is not entirely clear. In contrast to boulder toppling, an inherited [10]Be concentration during supraglacial transport may result in age overestimation by ~0.3–0.1 ka (assuming the same glacier surface velocity as Gomuche Kangri). Similarly, since some of the older age boulders at the northern ridge are close to cirque walls (Fig. 4I), they are likely to be affected by reworking and hillslope deposits and therefore, may be biased by inheritance. The outlier free distribution shows overlapping multimodal relative probabilities (Table 4; Fig. 6J). Thus we refrain from assigning any mean age to this moraine complex; its age is likely bracketed between ~2.1 and ~0.9 ka (Table 4; Fig. 6J).

6. Equilibrium-line altitudes

The reconstructed steady-state ELAs for our study areas, in general, reflect gradual altitudinal rise of ~180–4 m since the early Holocene in the Lahul and the Zanskar study areas. Hamtah glacier in Lahul was the most extensive (~10.7-km-long) during the early Holocene at ~10.4 ka with ΔELA of ~182±57 m (Table 5). The next dated glacier advance, at ~0.2 ka, had a ΔELA of ~57±28 m (Table 5).

In the Karzok valley, Gomuche Kangri experienced relatively larger (extending ~0.8 km) Neoglacial glacier advances during ~6.1–3.3 ka, with a ΔELA of ~159±77 m. The ΔELA was ~64±50 m during a later restricted advance (extending ~0.2 km) at ~2.1 ka (Table 5). The adjacent Mentok Kangri, however, only extended ~0.5 and 0.3 km during the late Holocene, at ~1.0 and ~0.7 ka, with ΔELAs of ~63±6 and 21±3 m, respectively (Table 5).

In the Lato valley, Amda Kangri advanced at ~0.5 and ~0.3 ka and was restricted to ~0.4 km (ΔELAs of ~21±7 m) and ~0.04 km (ΔELAs of ~4±4 m) from its contemporary glacier terminus, respectively (Table 5).

The late Holocene moraine complex (m_{s1} at ~2.1–0.9 ka) of the Stok Kangri represents a glacier advance of ~0.3 km from its contemporary terminus, with a ΔELAs of ~65±11 m (Table 5).

7. Discussion

7.1. Local glacial stages in study areas

The young moraines in our study exhibit scattering in [10]Be ages (16 outliers out of 49; Fig. 7A; Table 2). These scattering manifests themselves in χ^2 of >1, positive skewness, and convex upward cumulative probability density distributions (cf. Applegate et al., 2012). Our interpretation of the cosmogenic [10]Be measurements is that for especially young features, inherited [10]Be could represent a substantial fraction of the cosmogenic [10]Be inventory. Likewise, the instability of many of the sample surfaces increases the possibility that some samples have not been exposed to cosmic rays continuously since the deposition time of the surface. Since, most of the glaciers in our study are cold-based sub-polar types that are not substantially erosive in nature (except Hamtah glacier), the limited erosion of bedrock cliffs (>0.6 m of bedrock erosion is required to obtain rock with no [10]Be) that overhang these glaciers, and/or reworking of older glacial deposits, could help explain the presence of inheritance (cf. Applegate et al., 2012). An additional complication is the possibility of [10]Be production in boulders *en transit* to deposition. Supraglacial exposure might lead to an overestimate of moraine ages by as much as ~0.3–0.1 ka as well as adding scatter. Recent studies which date supraglacial boulders on glacier surfaces (cf. Ward and Anderson, 2011), suggest age inheritance ranging between ~0.9 and ~0.05 ka for more humid glaciers in the Central and Eastern Himalaya (Heimsath and McGlynn, 2008; Murari et al., 2014). Post-depositional boulder toppling could also contribute to scattering by exposing fresh surfaces after deposition of the moraine. These processes are likely present in all glacial settings, but for LGM or older features the production of [10]Be in supraglacial boulders or the toppling of a boulder in the first ~1 ka of a moraine represents an undetectable perturbation on the [10]Be inventory. For Holocene glaciation, the impact of these processes is potentially substantial and may be a major contributor to scatter in our results (Supplementary materials S3). The m_{S1} complex in Stok Kangri supports the view that instability and possible post-

depositional boulder toppling (incomplete-exposures) may contribute to the spread of [10]Be ages on moraines. Post-depositional hillslope contamination, e.g., the supply of rock fall debris to moraines, however, is a possibility for age scatter for the m_{H3} in Hamtah and m_{A3} in Lato (Supplementary materials S8).

Despite the scatter introduced by these geologic factors, we identify five Holocene local glacial stages using the 49 new and 12 published (Hedrick et al., 2011; Orr et al., 2017) [10]Be ages. These date to ~10.4, ~6.1–3.3, ~2.1–0.9, ~0.7–0.4, and ~0.3–0.2 ka, with three synchronous advances at ~2.1–0.9, ~0.7–0.4, and ~0.3–0.2 ka (Table 4; Fig. 7A).

A large glacier advance occurred in the early Holocene in the Hamtah study area, which is the wettest (~800–400 mm) of our study areas. Hamtah glacier extended >10 km in Lahul at ~10.4 ka (Fig. 7A, Bi) with a ΔELA of ~182±57 m (Tables 4 and 5). Similar extensive early Holocene local glacial stages are evident in the semi-arid Muztag Ata-Kong Shan region of the northwestern Tibet (Seong et al., 2009), but with larger ΔELAs of between ~797±129 and 574±181 m (Supplementary materials S7, S9).

Neoglacial glacier advances at ~6.1–3.3 and ~2.1–0.9 ka in our semi-arid study areas of the Zanskar Range were restricted in extent (<1.0 km; Fig. 7A, Biii; Table 4). Gomuche Kangri in the Karzok valley advanced ~0.8 km (~159±77 m) at ~6.1–3.3 ka; we cannot assign a precise age to this glacier advance. Coeval local glacial advances also occurred in other areas of Zanskar, e.g., in the Puga valley (Hedrick et al., 2011), in the mid-latitude westerlies dominated Central Karakoram (Seong et al., 2007), and in semi-arid Muztag Ata (Seong et al., 2009), with ΔELAs ranging from ~650 to 150 m (Supplementary materials S7, S9).

Restricted (~0.3 km) local glacier advances at ~2.1 ka occurred in the Karzok valley (Fig. 7A, Biii), Ladakh (Dortch et al., 2013) and Muztag Ata (Seong et al., 2009), with a ΔELAs ranging between ~130 and 56 m (Supplementary materials S3, S7). An equally restricted glacier advance (~0.3 km) occurred at ~2.1 to 0.9 ka in the Stok valley (Fig. 7A, Bv). We are unable to assign a precise age to this local glacier advance. Another restricted (~0.5 km) local glacier advance at ~1.0 ka occurred in the Mentok Kangri valley, with a ΔELA of ~63±6m (Fig. 7A, Bii). Corresponding glacier advances are also proposed for the

Central Karakoram and northwestern Tibet at between ~1.7 and 1.1 and ~1.0–0.9 ka, respectively (Supplementary material S3 and references therein).

Two local glacial stages with limited extent (<0.4 km) occurred during the late Holocene, at ~0.7–0.4 ka in the Karzok and Lato study areas (Fig. 7A, Bii, Biv) and at ~0.3–0.2 ka in the Hamtah and Lato study areas (Fig. 7A, Bi, Biv). These local glacial stages probably represent Little Ice Age (LIA) glacier advances with ΔELAs ranging between ~57 and ~4 m (Supplementary materials S7, S9). Coeval LIA stages are also recognized in the other valleys in Zanskar (Hedrick et al., 2011; Dortch et al., 2013; Saha et al., 2016), Ladakh (Lee et al., 2014), and in Mustag Ata (Seong et al., 2007, 2009; Supplementary material S3).

7.2. Himalayan Holocene regional glacial stages (HH)

We propose seven Himalayan Holocene regional glacial stages (HHs) using our 49 new and 187 published [10]Be ages from a total 32 glaciated valleys across the northwestern end of the Himalaya and Tibet (Figs. 8 and 9; Table 4; Supplementary material S3). The modern distribution of moraine successions is being utilized as proxy for paleoclimate (e.g., Benn and Ballantyne, 2005; Ballantyne et al., 2007; Owen and Dortch, 2014), but this approach has been questioned because several additional non-climatic factors are also believed to influence moraine formation (Warren and Hulton, 1990; Kaplan et al., 2009; Roe and O'Neal, 2009; Roe, 2011; Anderson et al., 2012; Barr and Clark, 2012; Barr and Lovell, 2014) and their preservation (Putkonen and O'Neal, 2006; Kirkbride and Winkler, 2012). These factors include: moraines formed by valley glaciers that are significantly impacted by topography (Barr and Lovell, 2014); micro-climate (Oerlemans, 2010); glacier response time (Oerlemans, 2005); erosional censoring (Kirkbride and Winkler, 2012); altered glacier flow by the presence of pre-existing landforms/deposits (Owen et al., 2001); and intrinsic climate variability (Roe and O'Neal, 2009; Roe, 2011).

While these non-climatic geologic factors undoubtedly impact glacial activity, they may have only a limited effect on Holocene timescales. For instance, erosion censoring (or eradication) of geomorphic records and self-defeating feedback mechanisms (see Macgregor et al., 2000; Kaplan et al., 2009) are unlikely since we use mostly small cirque and valley glaciers in relatively semi-arid/arid climate (except

transitional climate in Hamtah valley) in our study. The progressively decreasing extent of glacier advances over the Holocene are least likely to be modified by erosional feedback mechanisms (see Barr and Lovell, 2014). Limited range-scale uplift (<20 m in 10 ka after Lavé and Avouac, 2001) during the Holocene makes it unlikely that any significant topographic/tectonic controls have occurred (see Barr and Lovell, 2014). However, a complex combination of other stochastic factors specific to each locality, including climatic and microclimatic regimes, climate variability, pre-existing topography, debris cover, glacial history, and geologic setting, could influence the timing and extent of Holocene glaciation and the preservation of glacial evidence in our study areas (Hobley et al., 2010; Dortch et al., 2011; Dietsch et al., 2015).

Despite these limitations, glacial chronologies represent a significant archive of climate and considerable effort continues to be made to link timing and extent of past glacier advances (Gillespie et al., 2003; Grove, 2008; Davis et al., 2009; Dortch et al., 2013) to climate change (Dyke and Savelle, 2000; Putnam et al., 2013b), including ELA reconstructions (Benn and Lehmkuhl, 2000; Kaplan et al., 2013). Reconstructing regional glacial stages based on multiple local stages, thus provide an opportunity to address these issues and the large-scale assessment of glaciation, which may differ locally. In our study, a regional assessment helps us to compare changes in ELAs between more monsoonal glaciers to the south and more arid sub-polar type glaciers to the north (Supplementary material S9). The glaciers in the south are more sensitive to changes in temperature and therefore, likely more extensive during colder events. The opposite is true for the more cold-based glaciers in the northern regions, which are more sensitive to changes in moisture supply (Benn and Owen, 2002).

Each HH is discussed below, and broad-scale possible forcing factors for glaciation are considered (Fig. 8). However, correlating discrete glacial records with continuous climate proxy records is challenging and should be interpreted cautiously (see Roe, 2011). Here, we speculate on possible climate forcing by considering the high-resolution proxy records as a guide to assess climatic integrity, spatial coherence, and chronological robustness of our HHs, as generally proposed by Kirkbride and Winkler (2012).

7.2.1.   Regional glacial stages for the late glacial

Two late glacial regional glacial stages, i.e., ~15.4–12.7 and ~12.6–11.4 ka, are evident in our analysis (Figs. 8A and 9; Supplementary material S3). These late glacial advances often extend into the Holocene and are also crucial to understand the long-term possible forcing factors. The weighted means of these glacier advances are at 13.9±0.7 and 11.9±0.5 ka.

Our limited analysis of ΔELAs in thirteen glaciated valleys broadly indicates extensive glacier advances during ~15.4–12.7 ka in the Central Karakoram (except in the Hunza valley) and Muztag Ata (~1105–491 m). In comparison, temperate glaciers in Lahul to the south are relatively restricted (ΔELA ~490–340 m), possibly indicating enhanced moisture supply further north. Moisture supply may be orographically restricted (ΔELA ~122–97 m) in the Pamir and Alay Ranges during these glacier advances, which is in the extreme northwest of our study areas (see Supplementary materials S9). We speculate that these glacial advances may be coeval with the enhanced monsoon in the orogen during Bølling-Allerød Interstadial (~14.7–12.7 ka; Fig. 9).

Glacier advances are also dated during ~12.6–11.4 ka in Lahul, Central Karakoram, and Muztag Ata. Relatively larger ΔELAs are evident for Lahul and Central Karakoram (~580–667 m) compared to those in the Muztag Ata-Kong Shan region (~201±117 m) (see Supplementary materials S9). However, our data is too limited to confirm any climatic influence during this stage. We speculate that the timing of this glacier advance might be coincident with the Younger Dryas (YD) Stadial (12.9–11.7 ka) and North Atlantic cooling (Denton and Broecker, 2008; Chiang et al., 2014).

These glacier advances closely match with the proposed semi-arid western Himalayan-Tibetan stages (SWHTS) 2B (13.9±0.5 ka) and 2A (12.2±0.8 ka) of Dortch et al. (2013) and the monsoonal Himalayan-Tibetan stages (MOHITS) 2A (12.9±0.9 ka) and 1K (11.4±0.7 ka) of Murari et al. (2014 and references therein).

7.2.2.   HH 7 (~10.9–9.3 ka)

A short-term but relatively extensive early Holocene glacier advance is recognized from three local glacial stages with ages ranging from ~10.9 to 9.3 ka and a weighted mean of 10.1±0.4 ka, which we call

HH 7 (Figs. 8A and 9; Table 4). This regional glacial chronostratigraphy matches closely with the MOHITS 1J at 10.1±0.5 ka of Murari et al. (2014 and references therein) for the monsoonal eastern and central Himalaya. Larger changes in ELAs (~797–574 m) are evident in northern sub-polar glaciers in Muztag Ata (Seong et al., 2009) than in southern temperate/monsoonal glaciers in Lahul (~182±57 m; see Supplementary materials S9). We speculate, given dataset size, that this is largely because of relatively enhanced moisture supply and associated cloud albedo and radiative cooling in the cold-based northwestern Tibetan glaciers (cf., Rupper et al., 2009). The onset and rapid increase in monsoonal precipitation following a northerly shift of the Intertropical Convergence Zone (ITCZ) is also widely suggested during this time on the basis of speleothem (Fleitmann et al., 2003, 2007; Dykoski et al., 2005; Wang et al., 2005; Hu et al., 2008), and glacial and pluvial lake records (Ji et al., 2005a, 2005b; Yu et al., 2006; Herzschuh, 2006; Zhu et al., 2009; Mischke and Zhang, 2010; Leipe et al., 2014) in Oman, China and India (Fig. 9). We tentatively associate this possible climatic linkage recorded widely in multiple proxy records with glacial advances in the northwestern Himalaya and Tibet.

7.2.3. *HH 6 (~8.2–7.4 ka)*

HH 6 has a weighted mean age of 7.8±0.2 ka with local glacial stages ranging from ~8.2 to 7.4 ka (Figs. 8B and 9; Table 4). This stage is recorded in three valleys in Muztag Ata with ΔELAs ranging between ~612 and 144 m (see Supplementary materials S9). Coeval glacier advances were also recorded in the semi-arid Zanskar (Sharma et al., 2016), the monsoonal southeastern and central Himalaya (Bisht et al., 2015), and arid northern Tibet (MOHITS 1H at 8.1±0.8 ka and MOHITS 1G at 7.7±0.6 ka of Murari et al., 2014 and references therein), but the ΔELAs have not be determined for these regions. Abrupt temperature lowering with aridity during this time is also recorded extensively in several lake records from Tibet and has been linked to abrupt North Atlantic cooling between 8.5 and 8.2 ka (Ji et al., 2005a, 2005b; Kramer et al., 2010; Mischke and Zhang, 2010).

7.2.4. *HH 5 (~6.9–4.3 ka)*

HH 5 has a weighted mean of 5.1±1.1 ka and is evident in four glaciated valleys (Figs. 8B and 9; Table 4). The ΔELAs in Lahul and Muztag Ata are comparable (~172–160 m), but relatively larger in the Central Karakoram (~622±250 m; see Supplementary materials S9). Equivalent glacier advances are also reported in the more monsoonal central Himalaya and southeastern Tibet (MOHITS 1F at 5.4±0.6 ka of Murari et al., 2014 and references therein). However, our local glacial stages are limited and highly scattered (19% dispersion) to decipher the role of climate during this regional stage. Recently, Srivastava et al. (2017) suggested a cold-dry period in the Himalaya at ~5.4–3.8 ka with the high-frequency oscillation of short-term wet-warm periods. Catchment specific variable climatic responses are also reported in several lakes in Tibet during this time (see the review of Herzschuh, 2006; and Zhang and Mischke, 2009; Mischke et al., 2010). Whether this stage is associated with stronger Indian Summer monsoon (moisture) in the early phase (~6 ka in Fig. 9) or later with North Atlantic cooling (temperature) that is teleconnected via mid-latitude westerlies cannot be determined.

7.2.5. *HH 4 (~4.5–2.8 ka)*

HH 4 has a weighted mean age of 3.9±0.6 ka; its local glacial stages range from ~4.5 to 2.8 ka (Figs. 8C and 9; Table 4). Dortch et al. (2013) also identified a glacial stage at 3.8±0.6 ka (SWHTS 1C). A larger ΔELA is reconstructed in the Puga valley of Zanskar (~426±58 m) in the south relative to Muztag Ata (~212–153 m; see Supplementary materials S9). The onset of a cold reversal during this time, associated with North Atlantic cooling (Mayewski et al., 2004; Solomina et al., 2015), is also recorded in glacial records in the central Himalaya (MOHITS 1E at 3.5±0.4 ka in Murari et al., 2014 and references therein), peat records in the Garhwal Himalaya (Phadtare, 2000; Srivastava et al., 2017), the marine record in the Arabian Sea (von Rad et al., 1999), and several lake records in eastern (Mischke et al., 2010; Kramer et al., 2010; Mischke and Zhang, 2010), central (Herzschuh et al., 2006), and southwest Tibet (Gasse et al., 1996; Yanhong et al., 2006).

7.2.6. *HH 3 (~2.7–1.8 ka)*

HH 3 has a weighted mean age of 2.2±0.2 ka with local glacial stages ranging from ~2.7 to 1.8 ka (Figs. 8C and 9; Table 4). The ΔELAs are generally very small, but larger in Muztag Ata (~131±24 m) than in Ladakh and Zanskar (~64–56 m; see Supplementary materials S9). Coeval glacier advances are also reported from the monsoonal central Himalaya (MOHITS 1D at 2.3±0.1 ka of Murari et al., 2014 and references therein), although overall cold and dry conditions have been proposed during ~3.0–1.4 ka in the Garhwal Himalaya (Srivastava et al., 2017; Fig. 9). Due to a small number of local glacial stages (n=3), we cannot resolve the potential climate forcing for these glacier advances.

7.2.7.   *HH 2 (~1.8–0.9 ka)*

With local glacial stages ranging from ~1.8 to 0.9 ka and a weighted mean of 1.2±0.4 ka, HH 2 was restricted in extent and is recorded in six glaciated valleys (Figs. 8D and 9; Table 4). The age dispersion for this HH is large (25%) indicating greater age scatter. ΔELAs are relatively large in Muztag Ata (~222–130 m) compared to the central Karakoram and Zanskar (~65–24 m; see Supplementary materials S9). The relative ΔELA differences between different types of glaciers in the north and south support the view that moisture supply increased in the northwestern Tibet occurred during this time. This stage correlates with MOHITS 1C at 1.5±0.2 ka of Murari et al. (2014) in the humid eastern Himalaya. Whether stage 2 is associated with two cold events at ~1.7 and ~1.3 ka (Liu and Thompson, 1998; Mischke and Zhang, 2010; Yu et al., 2006) and/or intensified summer monsoon in the beginning of the Medieval Warm Period (Gupta et al., 2003; Dixit and Tandon, 2016; Srivastava et al., 2017) is impossible to resolve presently.

7.2.8.   *HH 1 (<1.0 ka)*

Restricted local glacier advances are reconstructed during the last 1 ka in ten glaciated valleys, with HH stage 1 having a mean age of 0.4±0.2 ka (Figs. 8D and 9; Table 4). Due to large age dispersion (43%) and overlapping ages, smaller sub-stages (e.g., MOHITS 1B at 0.7±0.1 and MOHITS 1A at 0.4±0.1 ka of Murari et al., 2014 in the monsoonal central Himalaya and southeastern Tibet) are speculative in our study areas. We suggest that this HH might correspond to LIA cooling episodes associated with North Atlantic

sea ice expansion and weakening of AMOC (Bond et al., 2001; Grove, 2004, 2008; Denton and Broecker, 2008) and is likely teleconnected by mid-latitude westerlies (Rowan, 2016). However, ΔELA were quite variable during this stage in our study areas. From south to north, ΔELAs range from ~167 to 57 m in Lahul, ~400–4 m in Zanskar, ~230 m in Ladakh, to ~68–63 m in Muztag Ata-Kongur Shan region (see Supplementary materials S9). Large-scale regional variations in ΔELAs also suggest catchment specific climate response during this time and corroborate with the view that LIA was both cold and dry and cold and wet depending upon the catchment in the western Himalaya (Demske et al., 2009; Wünnemann et al., 2010; Rawat et al., 2015a, 2015b; Liang et al., 2015; Srivastava et al., 2017).

7.3. Holocene glacier advances and hemispheric climate linkages

We compare our Himalayan regional glacial chronostratigraphies to global glaciation datasets (see Mayewski et al., 2004; Grove, 2008; Davis et al., 2009; Luetscher et al., 2011; Schindelwig et al., 2012; Schimmelpfennig et al., 2012; Schimmelpfennig et al., 2014; Solomina et al., 2015, 2016 and references therein; Le Roy et al., 2015, 2017; Moran et al., 2015, 2016, 2017) and climate proxies derived from ice cores, lakes, and speleothems to help decipher the long-term climate forcing behind HHs (Fig. 9). These correlations are based on timing/chronozones, so they are accordingly speculative. We identify two regional late glacial and seven HHs (Fig. 9). The extent of glaciation varies significantly between each HH (see Supplementary material S9). Detailed studies of ΔELAs suggest relatively restricted glacial advances over time in each valley from Lateglacial/early Holocene through to the LIA (Fig. 10; see Supplementary material S1).

During the early Holocene (~10.9–9.3 ka) extensive glacial advances (ΔELA of ~425±229 m), relative to their LIA advance, are recorded in the northwestern Himalaya and Tibet. Similar early Holocene extensive glacier advances (~11.0–9.6 ka), larger than LIA maximum, are also recorded in European Alps (Schindelwig et al., 2012; Schimmelpfennig et al., 2012; Schimmelpfennig et al., 2014; Moran et al., 2015, 2016), Greenland (O'Hara et al., 2017), Arctic Canada (Young et al., 2012), Svalbard (van der Bilt et al., 2015), tropical Andes, Africa, and Southern Hemispheric extra-tropical regions (Fig. 10; Solomina et

al., 2015, 2016 and references therein). Most of these early Holocene glacier advances in the high-latitudes of northern hemisphere are being attributed to cooling associated with the YD and short-term Preboreal Oscillation (PBO) in the Nordic Seas (Schindelwig et al., 2012; Moran et al., 2015, 2016), or regional freshwater input to North Atlantic subpolar gyre (O'Hara et al., 2017). In contrast, early Holocene glacier advances in our study areas are most likely modulated by tropical/subtropical hydro-climatic changes and increased moisture supply and radiative cooling (see Rupper et al., 2009) corresponding to a northerly shifted Earth's thermal equator (ITCZ) and stronger monsoon (Wang et al., 2001, 2004; Lea et al., 2003; Jennerjahn et al., 2004; Dykoski et al., 2005; Severinghaus et al., 2009). Northward migration of large-scale atmospheric circulation systems associated with long-term orbital forcing likely favored high amplitude glacier advances in the northern hemisphere sub-tropics (e.g., our study area) and low-latitude tropical Andean and African glacier-systems (Levermann et al., 2009; Frierson and Hwang, 2011; Ceppi et al., 2013).

The subsequent early Holocene glacier advances, at ~8.2–7.4 ka, are also extensive in the northwestern Tibet compared to their LIA advance. Similar widespread high-amplitude glacial advances are also dated in the northern hemisphere extratropical glaciers (Solomina et al., 2015, 2016 and references therein; Cronauer et al., 2016) and attributed to changes in the North Atlantic Ocean condition (Alley et al., 1997; Davis et al., 2009; Eynaud et al., 2009). Possible teleconnection via mid-latitude westerlies is proposed for cooling during this time on the Tibetan Plateau (Thompson et al., 1997, 2003; Seong et al., 2009; Dortch et al., 2013).

Five HHs are recognized between the mid-Holocene and LIA (~6.9–0.2 ka; Figs. 9 and 10). These glacier advances are comparatively more restricted in extent than early Holocene ones (ΔELA of ~141±106 and ~124±121 m in mid- and late-Holocene, respectively). Many extensive glacier advances, as large as the LIA maximum or larger (Luetscher et al., 2011; Moran et al., 2017; Le Roy et al., 2015, 2017), are also evident since at least ~4.3 ka in the northern hemisphere extratropical regions (Fig. 10). These glacier advances are attributed to reduced northern hemisphere insolation (Fig. 9) and corresponding north Atlantic sea-ice expansion, weakening of the Atlantic Meridional Overturning Circulation (Lund et al., 2006;

Denton and Broecker, 2008; Chiang et al., 2014), and southerly shifted ITCZ and westerly wind belts (Haug et al., 2001; Sachs et al., 2009). The enhanced mid-latitude westerly winds likely teleconnected the cooling events in our study areas, but at subdued amplitude (Yancheva et al., 2007; Mölg et al., 2014; Srivastava et al., 2017). Our study, therefore, reinforces the concept of long-term orbitally influenced Holocene glaciation in the northwestern part of the Himalayan-Tibetan orogen and the possible amplification by large-scale migration of Earth's thermal equator and the associated hemispheric oceanic-atmospheric systems.

8. Conclusions

We define the long-term pattern of Holocene glacier advances at the northwestern end of the Himalayan-Tibetan orogen using 49 new and 187 recalculated published [10]Be moraine boulder ages from 32 glaciated valleys. Despite the large dispersion of individual [10]Be boulder ages on young moraines, our results suggest that in our four study areas, five Holocene glacial stages are locally recorded, including three synchronous advances. These date to ~10.4, ~6.1–3.3, ~2.1–0.9, ~0.7–0.4, and ~0.3–0.2 ka.

An extensive (>10 km) glacier advance and larger ΔELA (~182±57 m) occurred in the early Holocene at ~10.4 ka in the more humid Hamtah study area in the Lahul Himalaya. Relative to early Holocene, middle and late Holocene glacier advances in our study areas were progressively restricted with ΔELAs ranging from ~160 to ~4 m. Glaciers advanced at ~0.2 ka in the Hamtah valley, at ~6.1–3.3 and ~2.1 ka in the Gomuche Kangri and at ~1.0 and ~0.7 ka in the Mentok Kangri valleys of Karzok, at ~0.5 and ~0.3 ka in the Lato study area and at ~2.1–0.9 ka in the Stok valley during the Holocene.

Seven HHs were determined by compiling 32 local glacial chronologies (new and published ages) for the northwestern end of the Himalayan-Tibetan orogen. These date to ~10.9–9.3, ~8.2–7.4, ~6.9–4.3, ~4.5–2.8, ~2.7–1.8, ~1.8–0.9, and <1 ka. These regional glacier advances are highly variable in each valley during different stages, but in general are relatively extensive for the early Holocene with mean ΔELAs of ~425±229 m, compared to middle Holocene (mean ΔELA of ~141±106 m), and late Holocene (mean ΔELA of ~124±121 m). The spatial distribution of ΔELAs during different HHs indicate a complex interplay of topography, hypsometry, and moisture and temperature associated with the prevailing summer monsoon

and mid-latitude winter westerlies. Based on the amplitude of Holocene glacier advances in the northwestern Himalaya and Tibet, we argue that they are analogous to glacier advances in the low latitudinal Andes, Africa, Peruvian Andes, and some extratropical regions in the Northern Hemisphere, i.e., progressively restricted from early to late Holocene. Nevertheless, the timing of majority of HHs during mid- and late Holocene indicates close correspondence with the North Atlantic cooling that is likely teleconnected via mid-latitude westerlies, especially during ~8 ka and after ~5 ka. In contrast, early Holocene glacier advances are driven by a northerly shifted ITCZ and enhanced monsoon activities in the region. We interpret this long-term pattern of Holocene glacier advances to be likely influenced by orbital forcing and amplified by large-scale migration of Earth's thermal equator and the associated hemispheric oceanic-atmospheric systems. Future studies should verify these findings with high-frequency Holocene glacier advances across the entire orogen.

Appendix A1. Supplementary data

Supplementary data related to this article can also be found at https://doi.org/10.1016/j.quascirev.2018.03.009.
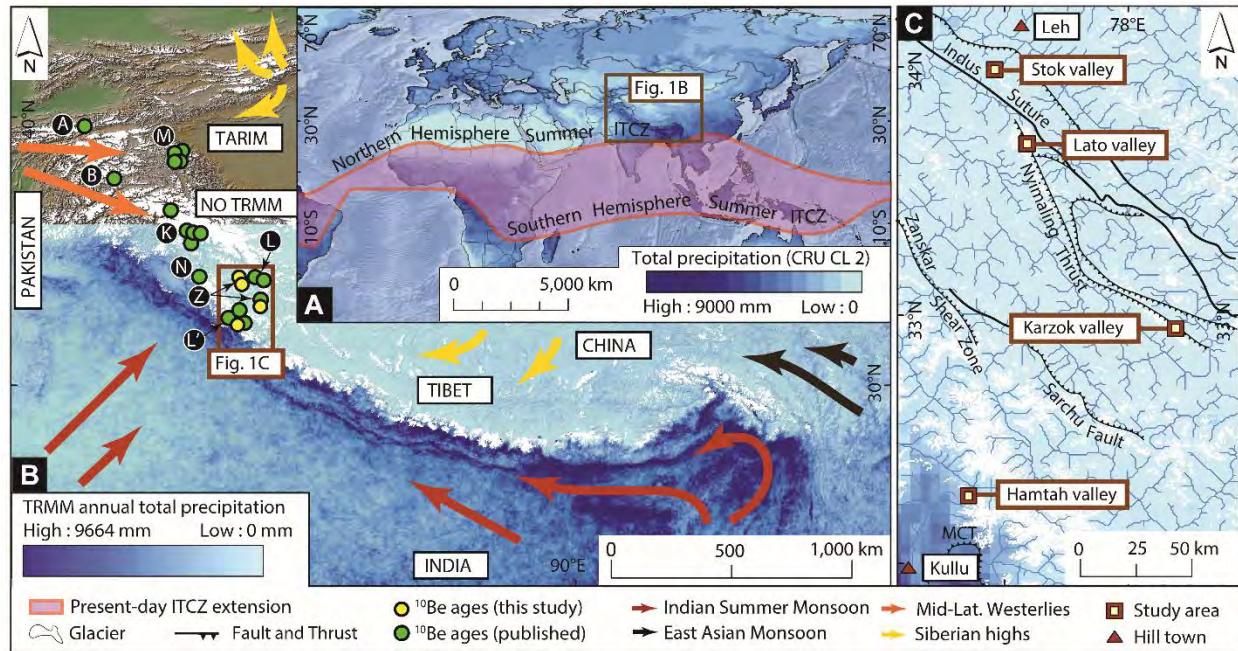
Fig. 1. Regional context and location of the study areas. (A) Present-day seasonal distribution of the Intertropical Convergence Zone (ITCZ) with respect to the Himalayan-Tibetan orogen (in brown rectangle). (B) Tropical Rainfall Measuring Mission (TRMM) precipitation imagery (averaged from 1998 to 2005) superimposed on a hillshade map, showing the study area (brown rectangle) and locations of new (yellow circles) and published (green circles) ^{10}Be ages. New and published study areas are highlighted in black circles as A=Alay Range (Koksu), B=Great Bogchigir, M=Muztag Ata, K=Karakoram, L=Ladakh (Chang, Pang), N=Nun Kun, Z=Zanskar (Stok, Lato, Karzok), L'= Lahul Himal. The region is dominated by four major climate systems: the Indian summer and East Asian monsoons (during the summer), the northern mid-latitude westerlies, and the Siberian high-pressure system (during winter). (C) Locations of the new study areas showing TRMM derived strong annual total precipitation regimes from south to north. See the text for regional geology.
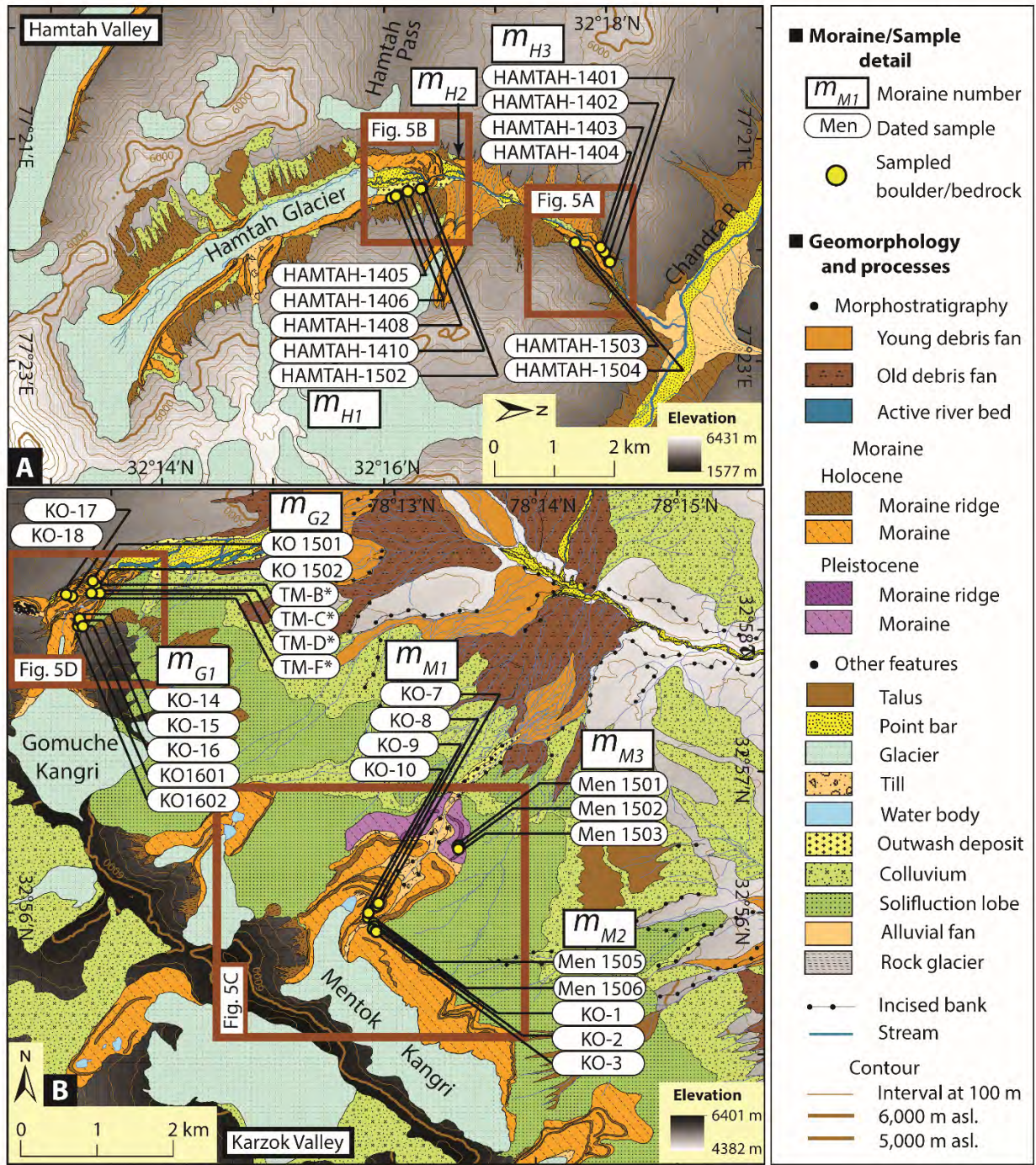
Fig. 2. (continued).
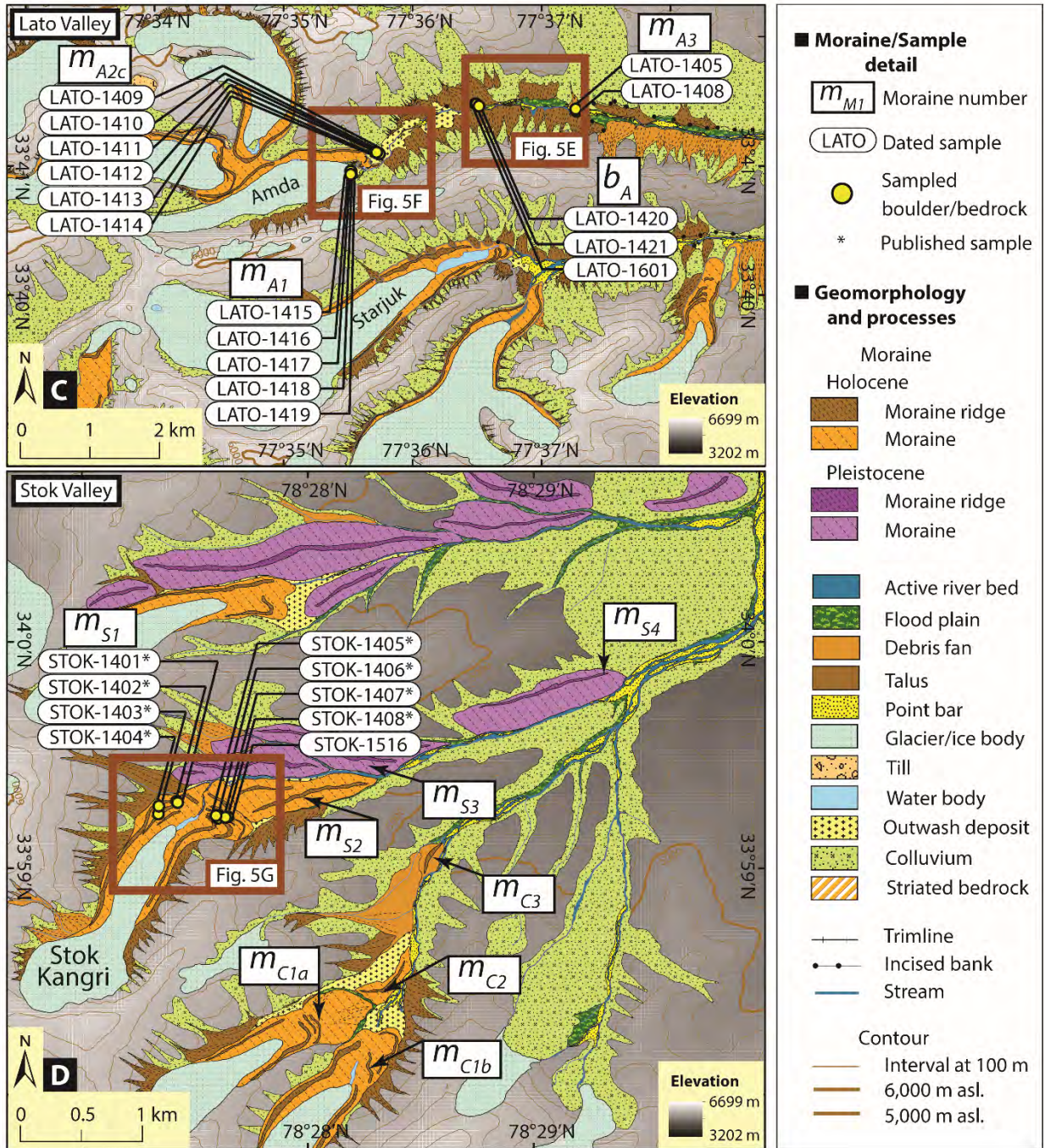
Fig. 2. Geomorphology of the study areas. (A) Hamtah valley showing locations of moraine boulders. (B) Karzok valley highlighting the sample locations. Four published samples (*) on older m_{G2} moraine are adapted from Hedrick et al. (2011). (C) Landforms and locations of sampled moraine boulders in the Lato valley. (D) Stok valley showing sampling locations for m_{S1} moraine complex. Published samples (*) for m_{S1}

are adapted from Orr et al. (2017). Note: the map is based on UTM projection (Zone 43N) and WGS 1984 datum.
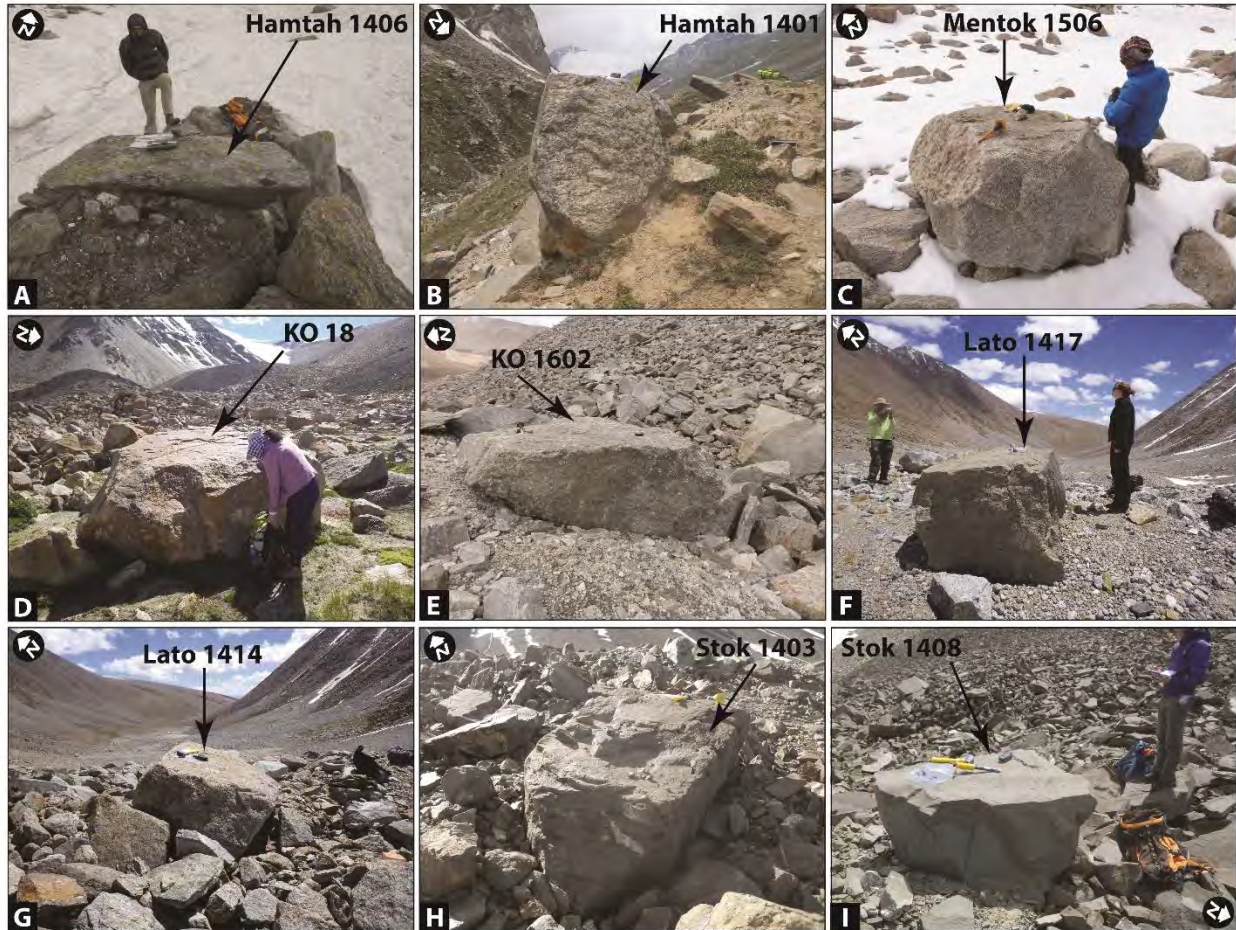
Fig. 3. Examples of sampled boulders for ^{10}Be exposure dating. Boulders inset into m_{H1a} latero-frontal (A) and m_{H3} lateral (B) moraines of the Hamtah study area. (C) A large tabular boulder resting on m_{M1} latero-frontal moraine of Mentok Kangri. (D) A boulder resting on the innermost m_{G1} latero-frontal moraine of Gomuche Kangri. (E and F) Boulders standing upright at the crest of m_{A1} and m_{A2c} end moraines in Lato study area, respectively. (G and H) Views of boulders embedded into the crest of young m_{S1} moraine complex of Stok study area.
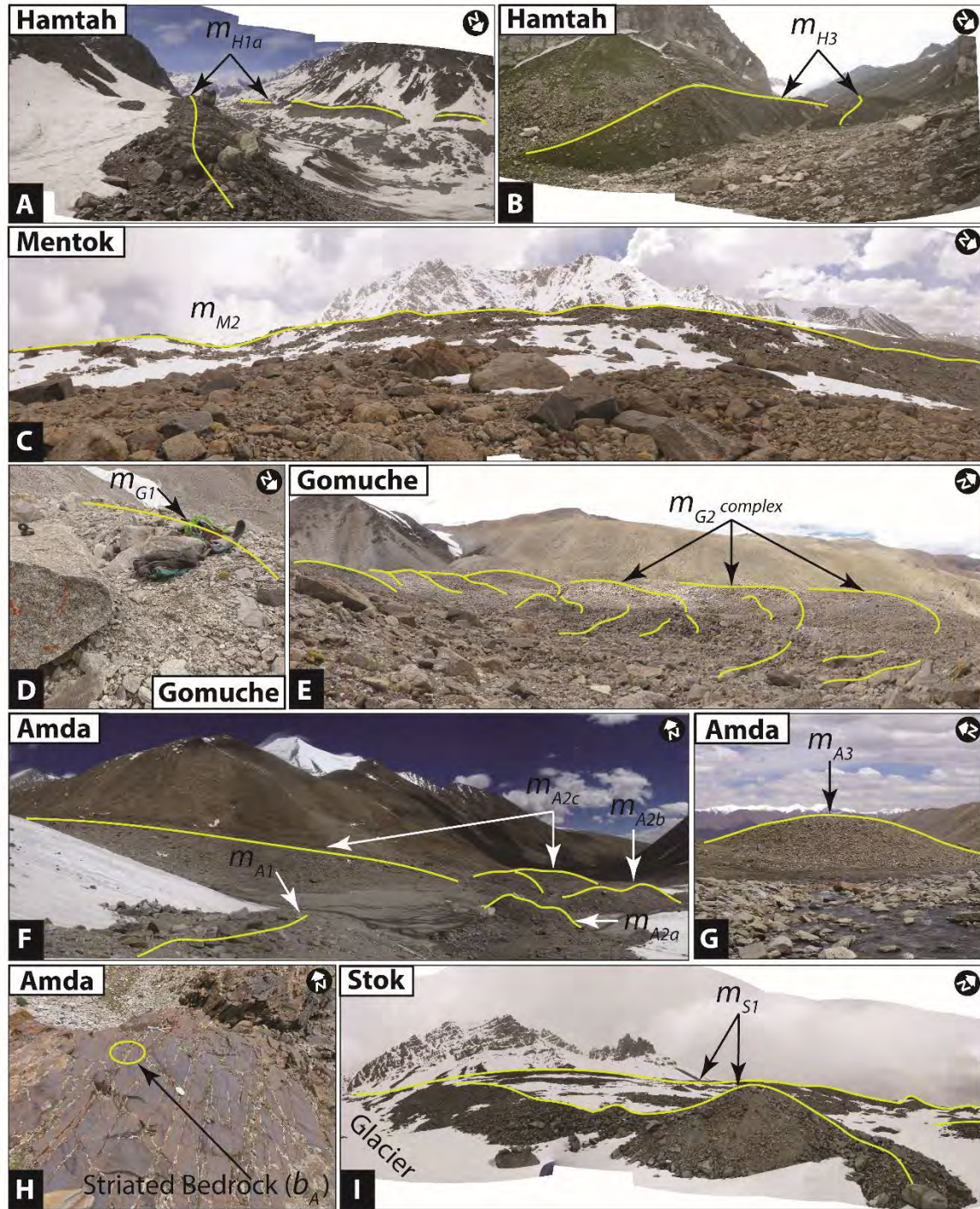
Fig. 4. Characteristics of the moraines. (A) Youngest latero-frontal moraine, m_{H1a} and (B) oldest m_{H3} lateral moraines in Hamtah valley. (C) Older Holocene m_{M2} latero-frontal moraine of Mentok Kangri in the Karzok study area. (D) Youngest m_{G1} latero-frontal moraine and (E) older m_{G2} recessional moraine complex of Gomuche Kangri in the Karzok study area. (F) Youngest moraine complex (m_{A1}, m_{A2a}, m_{A2b}, m_{A2c}) and (G) older m_{A3} end moraine of Amda Kangri in the Lato study area. (H) Striated and polished bedrock in the

Lato study area. (I) Youngest m_{S1} latero-frontal moraine complex of Stok Kangri in the Stok study area. Distant and inner ridges are highlighted.
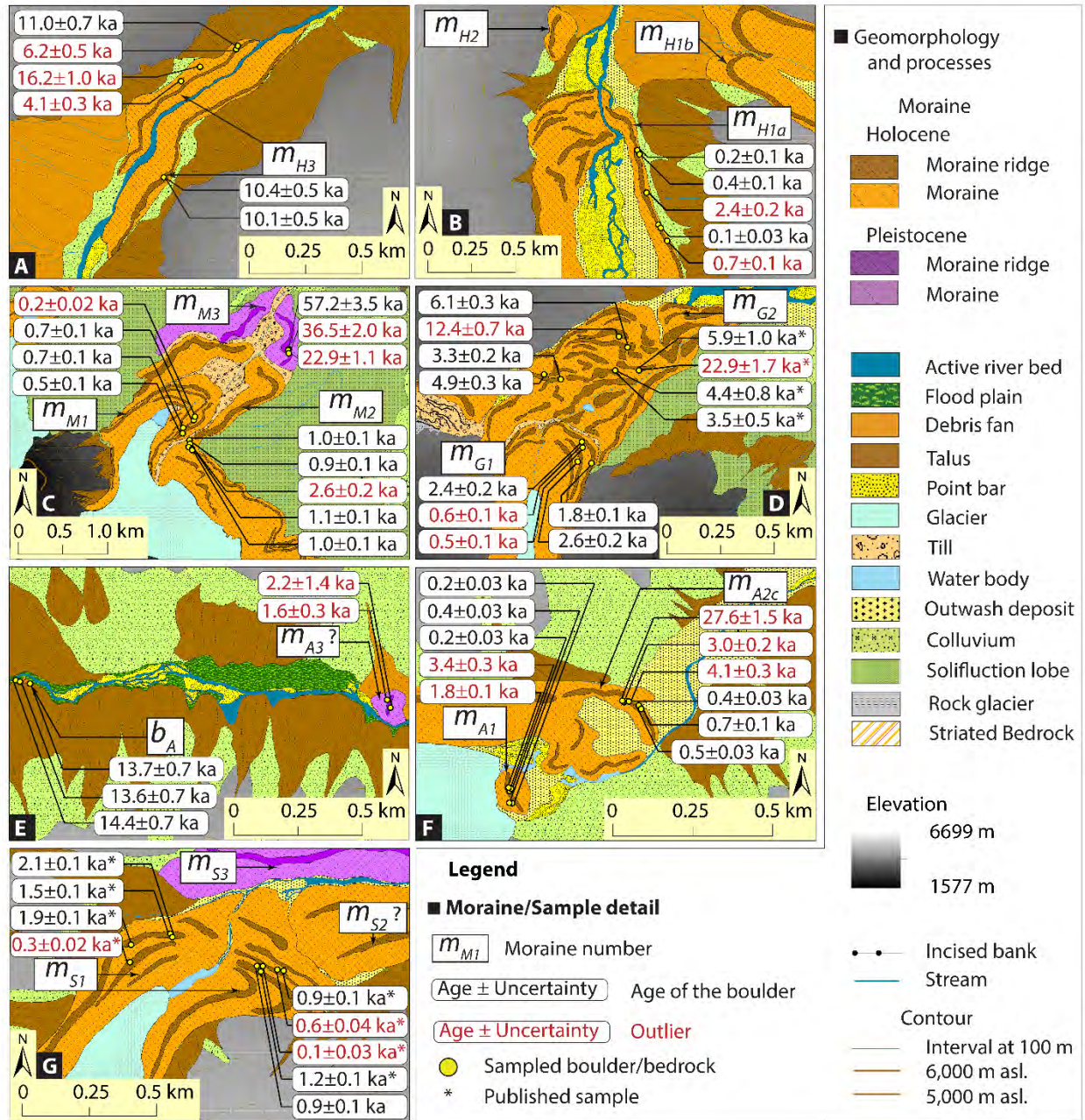
Fig. 5. Geomorphology of the study areas with cosmogenic [10]Be surface exposure ages. (A) Enlarged Hamtah valley showing the [10]Be ages on the oldest (m_{H3}) and (B) youngest (m_{H1a}) moraines. (C) Mentok Kangri with [10]Be ages. (D) Gomuche Kangri with new and published [10]Be ages (*). (E) Enlarged section of the Amda Kangri showing oldest moraine, m_{A3}, and bedrock samples with [10]Be ages shown in boxes and

(F) youngest moraine (m_{A1}) showing [10]Be ages. (G) Stok moraine complex ($m_{S1)}$ with [10]Be ages. Note that the map is based on UTM projection (Zone 43N) and WGS 1984 datum.
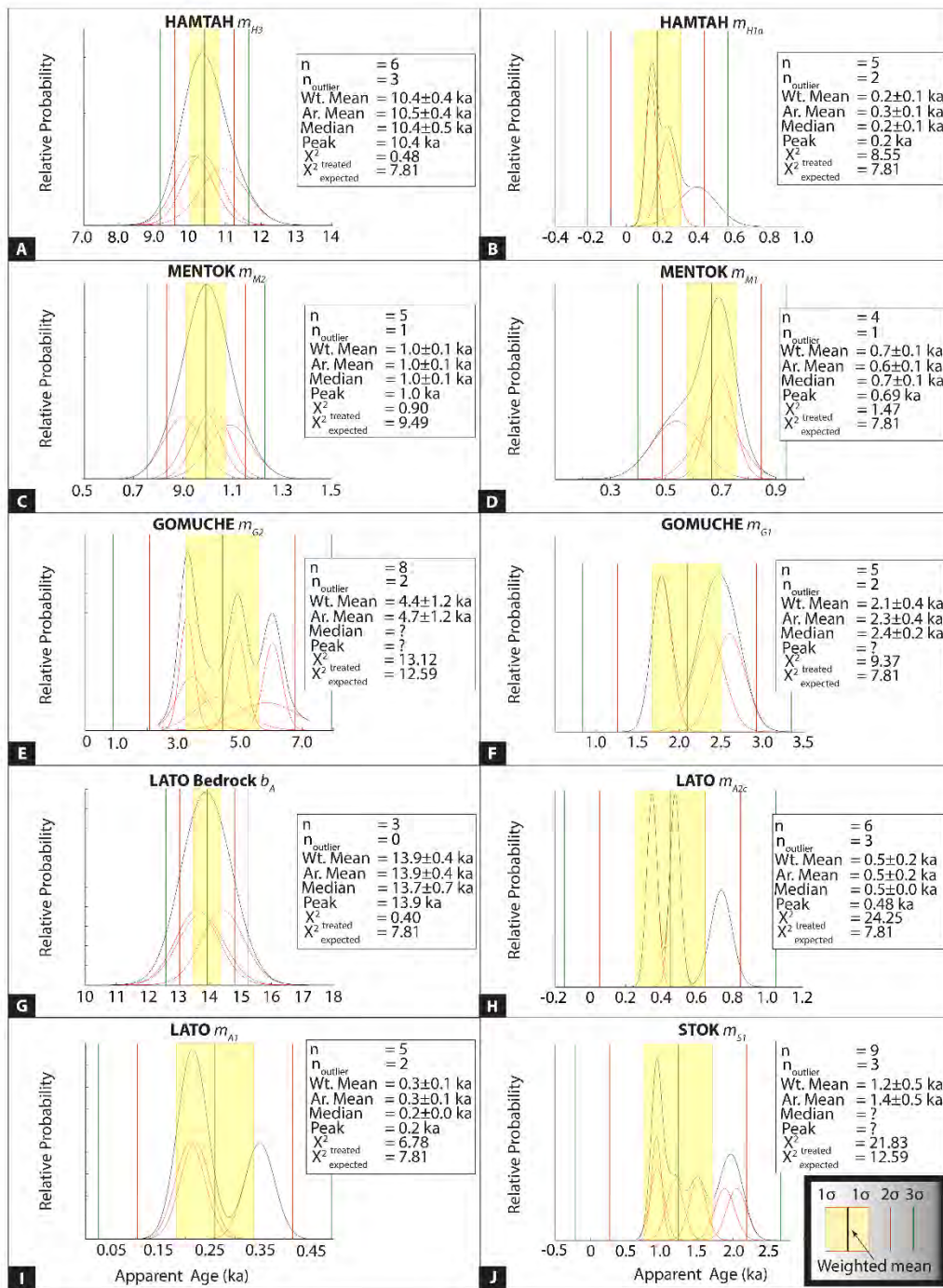
Fig. 6. Probability density plots showing outlier-free age distributions for each dated moraine in the study areas. Relevant age statistics are enclosed in boxes of each members. Age uncertainties (1σ, 2σ, and 3σ)

81

are represented by vertical lines. This statistical treatment proved robust for moraines with χ^2 of outlier-free population (called here as $\chi^2_{treated}$) within expected 95% confidence interval of a normal kernel density functions (which we called $\chi^2_{expected}$). The moraines with $\chi^2_{treated} > \chi^2_{expected}$ are interpreted as tentative (lower confidence) in this study.
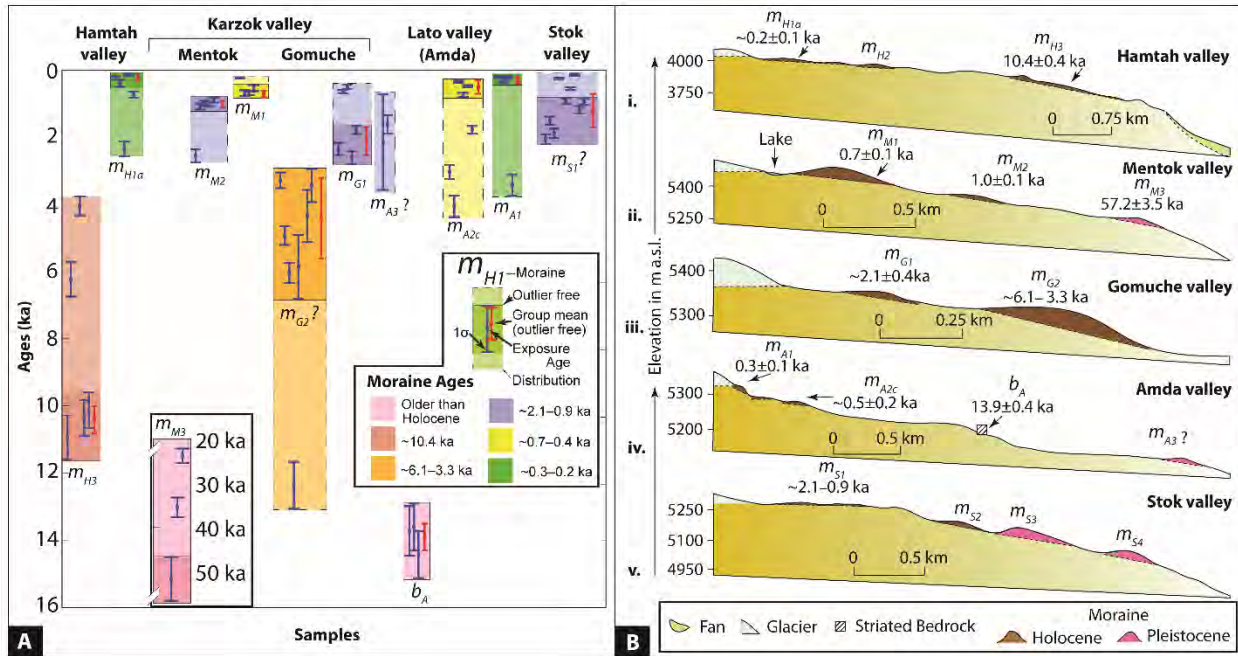
Fig. 7. [10]Be ages for new study areas. (A) Scatter plot with error bars showing local glacial stages from four study areas. Moraine boulder ages are arranged by morphostratigraphy from oldest to youngest for each valley. (B) Schematic longitudinal topographical profiles of each of the studied glaciated valley with their (weighted) mean±1σ moraine exposure ages.
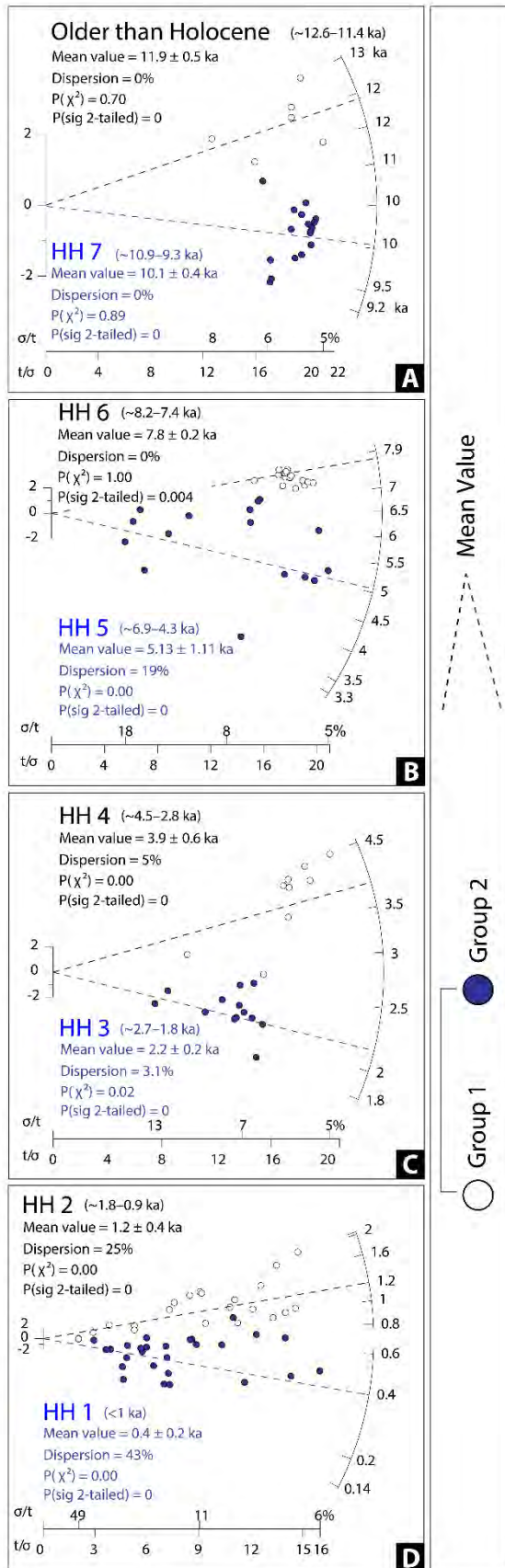
Fig. 8. Radial plots for outlier-free individual boulder ages comparing statistically significant two nearest age clusters, reported here as regional glacial stages, per selected timescale. We separately plotted two adjacent groups in each plot to demonstrate the statistical differences including their mean ages. Note: open and closed-blue circles represent two nearest but different age population in each plot. Regional glacial stages are arranged in descending chronological order from A through D. These results also show insignificant $P_{(sig\ 2\text{-tailed})}$ distributions. Dashed lines represent the weighted mean of each population. Note that 1σ uncertainties for regional glacial stages are reported.

83
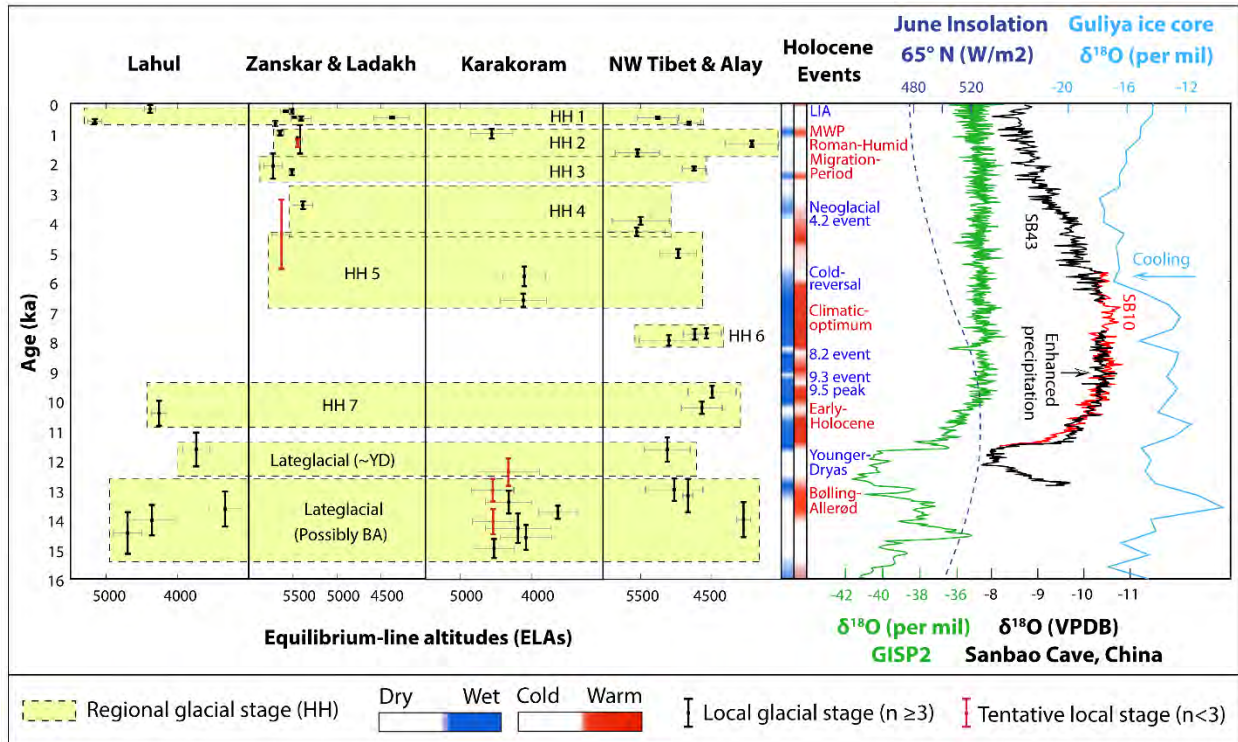
Fig. 9. Chronostratigraphies for Holocene regional glacial stages (HHs) in the northwestern end of the Himalaya and Tibet and coeval short-term climatic changes recorded in proxy records. HHs are arranged based on ELAs (x-axis) and organized according to (four) regions. A simplified summary of major Holocene climatic events is shown in the central part of the diagram and is reconstructed after Demske et al. (2009), Wünneman et al. (2010), Berkelhammer et al. (2012), Rawat et al. (2015a, 2015b), and Srivastava et al. (2017). Note that the color scheme doesn't correspond to magnitude of the change, but only the time range. Reconstructed orbital trend at 65ºN lat. (after Berger, 1978), oxygen isotopes from Greenland ice cores—a proxy for temperature (Grootes and Stuiver, 1997.), from speleothems –a proxy for regional precipitation (Sanbao cave, China after Dong et al., 2010), and form Guliya ice cores—a proxy for regional temperature (Guliya ice core, Tibet after Thompson et al., 1997) are shown in the right for climatic interpretation.
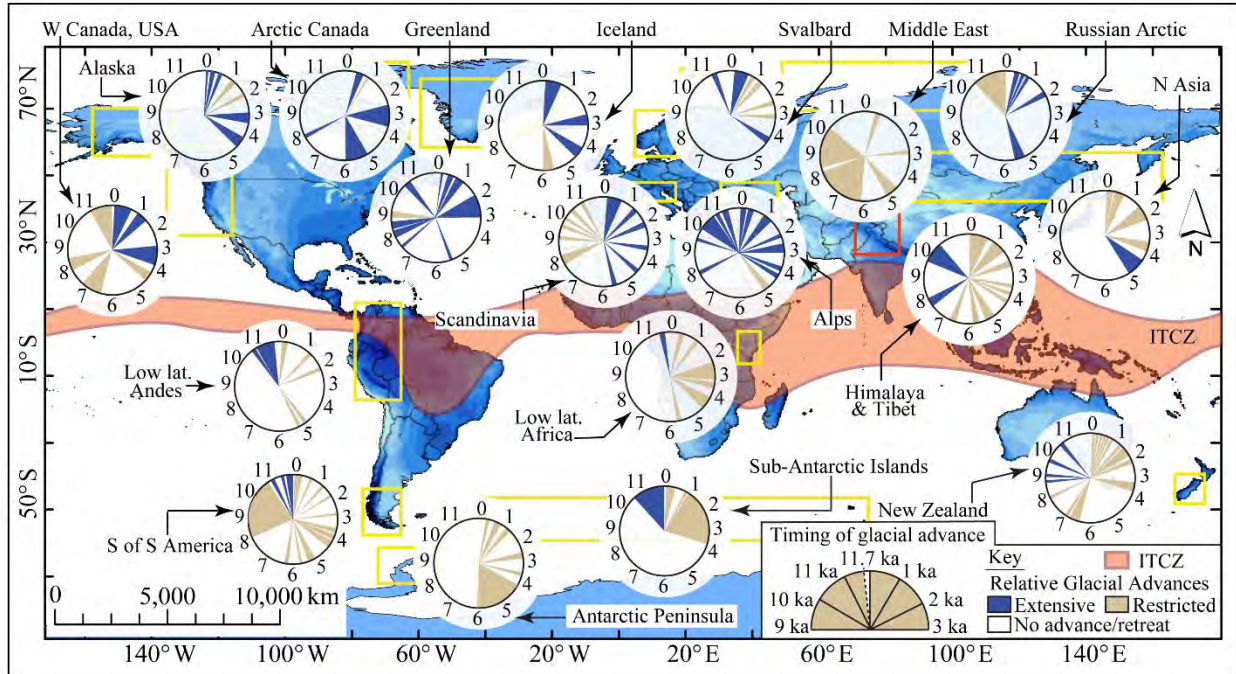
Fig. 10. Global seasonal distribution of ITCZ (see also Fig 1A) and Holocene glacial chronostratigraphies compiled after Mayewski et al. (2004), Grove (2008), Davis et al. (2009), Luetscher et al. (2011), Schindelwig et al. (2012), Schimmelpfennig et al. (2012), Schimmelpfennig et al. (2014), Solomina et al., (2015, 2016 and references therein), Le Roy et al. (2015, 2017), and Moran et al. (2015, 2016, 2017). Clock diagrams showing the timing of glacier advances (in ka) with qualitative comparison of glacier extents during each chronozone. Here blue indicates *extensive advances* and pale brown *restricted glacier advances* relative to their LIA maximum. Our results for the northwestern Himalaya and Tibet are solely based on [10]Be dates with likely denote minimum age of glacial advance, whereas glacial records for other regions are based on variety of proxy climatic and glacial records, and hence partial obliteration of glacial records during subsequent extensive advances is likely minimum. To be consistent in our interpretation, only records of glacial advances (and not retreats) are shown here. Note also that here we present only Holocene glacial records (i.e., 11,700 years) and hence YD records are not shown for focused discussion.

85

Table 1. Descriptions of morphostratigraphically defined glacial landforms in our study areas.

Glacial Stage	Moraine/bedrock characteristics	Boulder characteristics
Hamtah valley, Lahul		
m_{H1a}	– Innermost latero-frontal moraine with sharp crest; pebbly/boulder diamicton with sandy-gravel matrix; prominent ablation valley separates the morainic boulder from the debris fans/talus; several hummocky ridges are present in the frontal section of the moraine; grasses are present.	— Angular to subangular large boulders along the crests of the moraine; tabular and moderately to well inset; slightly dip down the ablation valley supporting its glacial origin; no sign of slope deposition; very coarse grained leucogranite; several lichen-covered large boulders are present.
m_{H1b}	– ~2-km-long sharp-crested latero-frontal moraine; ~20 m relief from the valley floor; next to one of the hanging glaciers to the east; situated ~200 m above the present main valley floor at an altitude of 4,150–4,540 m asl.	— Not dated; mostly angular to subangular boulders.
m_{H2}	– A lateral moraine remnant ~ 200 m down valley from $mH1a$ and is at an altitude of 3,980–3,990 m asl. The western lateral moraine is mostly buried under debris flow fans and scree, although there is a <100-m-long stretch that is only partially buried.	— Not dated; no suitable boulders are available.
m_{H3}	– ~2.4-km-long outermost lateral moraine; presently the frontal section of the moraine is being eroded/incised; extensively covered by grasses and soil development; pebbly diamicton with sandy-gravel matrix; prominent ablation valley is present to the west.	— Subangular/subrounded leucogranite boulders distributed along the crests of the two moraine ridges; mostly stable, tabular and well inset; largely covered by lichens.
Mentok Kangri, Karzok		
m_{M1}	– ~2.5-km-long, well-preserved, steep, sharp-crested latero-frontal moraine with four recessional ice-contact ridges; samples are collected from all four ridges; pebbly diamicton with sandy-gravel matrix.	— Angular to subangular fresh, large, tabular granitic and metagranitic boulders; little to no weathering and/or toppling; inset on the crest of the moraine, especially well interlocked with other boulders.
m_{M2}	– ~7-km-long discontinuous latero-frontal moraine; consists of four ice-contact ridges; pebbly till deposit with sandy-gravel matrix; a few very small localized patches of xerophytic shrubs and grasses.	— Little to slightly weathered and fresh granitic and metagranitic rocks; large tabular boulders on the crest of the moraine; stable fresh fracture faces (angular/subangular) and distinct from older fracture faces; mostly well interlocked with other boulders.
m_{M3}	– Single lateral ridge with a rounded crest; rock varnish present in most boulders; patches of xerophytic shrubs, grasses, mosses and lichens are present; sandy-gravelly matrix.	— Well inset large granitic boulders into the moraine crest; moderate to high granular weathering with rounded top; the protruding top portion were sampled; hard to sample.
Gomuche Kangri, Karzok		
Contemporary (unstable)	– Very unstable micro-ridge close to present glacier snout; buried ice is exposed at many places; probably-boulder surface till is constantly degrading, likely turn into ground till in future; sandy matrix is present in exposed sections; geometry of the moraine ridges and presence of boulder tables indicate that this section was once part of the main glacier body.	— Not dated; boulders are not stable and suitable for exposure dating.
m_{G1}	– ~2.2-km-long latero-frontal moraine; pebbly till deposit with sandy-gravelly matrix; three prominent ridges were mapped; average height of the ridges is 23 m above the valley floor; mosses and lichens are present in patches but less.	— Fresh angular and subangular metagranitic boulders mostly well interlocked with other boulders and stable at the crest; little to not weathered.
m_{G2} (or KM-4)	– The moraine ridge complex is discontinuous and highly degraded with multiple tens of meters long recessional and hummocky ridges; likely part of a dead-ice zone; samples collected on the farthest downstream recessional ridges; fresh boulder surface with pebbly diamicton and supported by sand-gravelly matrix.	— large (~2-m-tall), tabular, and well-inset porphyritic granitic boulders from the most stable ridge crests; subangular/angular large blocks; patches of mosses and lichens are present but not extensive; some to no weathering was identified; hard to sample.
Amda valley, Lato		
m_{A1}	– ~154-m-long and 20-m-high end moraine; exhibits little, if any, signs of erosion/degradation; diamicton of boulders and cobbles present with clasts supported by coarse gravel-sandy matrix; stable ridge.	— Freshly fractured and tabular granitic boulders; no sign of weathering; very limited to no detrital materials on the boulders surface; lodged on the crest of the end moraine.
m_{A2a}	– A ~120-m-long subdued (~8 m relief) recessional moraine, located ~75 m downstream of $mA1$; slightly unstable and presently is being incised by anastomosing outwash streams.	— Not dated; lack of suitable boulders.
m_{A2b}	– ~110-m-long and ~6-m-high subdued dissected ridge; slightly unstable.	— Not dated; lack of suitable boulders.
m_{A2c}	– ~346-m-long and 10-m-high end moraine; diamicton of boulders and cobbles present with clasts supported by coarse gravel-sandy matrix; stable ridge with rounded surface; some very small patches of some xerophytic shrubs and grasses are present.	— Fresh angular and subangular porphyritic granite boulders; boulder inset on the crests away from the depression; boulders are mostly well interlocked with other boulders.
b_a	– Glacially sculpted striated bedrock; highly polished and striated flat surface; striations are parallel to ice flow.	— Samples were collected from smooth polished surfaces at different elevations; extensive lichen cover and rock varnish present.
m_{A3}	– 10-m-high end moraine; northern part of the moraine is subdued; striated boulders are lodged on the surface with diamicton of boulders and cobbles; south facing slope likely covered by post-depositional slope deposits; some xerophytic shrubs and grasses present.	— Larger tabular granitic boulders; subangular/subrounded; some boulders are slightly lichen covered; some boulders are slightly denuded.
Stok valley, Zanskar		
m_{S1}	– ~30-m-high and 2.8-km-long latero-frontal moraine complex; consisting of >4 ice-contact inner recessional ridges; outer ridge is narrow, steep and more prominent; inner frontal ridges are subdued; diamicton of highly fractured boulders and cobbles with coarse gravel-sandy matrix; slight lichen cover.	— Angular to subangular boulders; large vein-quartz dominated conglomerate boulders; fresh fractures and sharp edges indicate slightly to moderately denudated; partially inset but appeared stable; boulder fracturing due to thermal shock and post-depositional block displacement is evident.
m_{S2}	– Consisting of two rounded/denudated ice-contact ridges and is located ~400 m downstream of m_{S1}; coarse gravel-sandy matrix supported.	— Not dated; highly denudated rounded boulders; mostly large and stable but highly pitted and fractured granites; rock varnish and extensive lichen cover exists.
Stok companion glacier, Zanskar		
m_{C1a}	– Slightly unstable; freshly exposed laterofrontal moraine ridge; pebbly-boulder diamicton with sandy-gravel matrix.	— Not dated; angular to subangular fresh tabular boulders; well inset on the crest; highly fractured due to its lithology.
m_{C1b}	– Slightly unstable young laterofrontal moraine ridge; pebbly-boulder diamicton with sandy-gravel matrix.	— Not dated; angular to subangular fresh tabular boulders; highly fractured due to its lithology.
m_{C2}	– Stable lateral moraine ridge; pebbly-boulder diamicton with sandy-gravel matrix.	— Not dated; angular to subangular fresh tabular boulders.
m_{C3}	– Round crested lateral moraine remnant; well stable, but denudated surface; some xerophytic shrubs and grasses present.	— Not dated; highly denudated conglomerate boulders; mostly large and stable but highly pitted and fractured granites; rock varnish and extensive lichen cover exists.

Table 2. Holocene moraine/bedrock surface-exposure sample details and [10]Be ages (in thousands of years before AD2016, labeled 'ka'±1σ) for the four study areas of the northwestern Himalaya.

Area	Moraine morpho-stratigraphy	Sample ID	Latitude (DD N)	Longitude (DD E)	Elevation (m a.s.l.)	Boulder size (LxWxH) (cm)	Sample thickness (cm)	Shielding correction	Quartz weight (g)	Carrier added (g)	[10]Be/[9]Be ± 1σ (10^{-14})[g]	[[10]Be] ± 1σ (10^4 atoms g^{-1})[h]	LSD Age ± 1σ (ka)[i]	Lm Age ± 1σ (ka)[j]
Hamtah valley	m_{H1a}	HAMTAH-1405	32.2725	77.3574	4,014	410 x 390 x 120	2.0	0.943	28.9662	0.3515[d]	10.74±2.32	0.89±0.19	0.23±0.05	0.21±0.05
	m_{H1a}	HAMTAH-1406	32.2722	77.3575	4,023	190 x 80 x 60	1.0	0.944	29.5368	0.3510[d]	19.17±5.08	1.56±0.41	0.40±0.11	0.37±0.10
	m_{H1a}	HAMTAH-1408[a]	32.2686	77.3585	4,111	160 x 100 x 60	2.5	0.954	25.6686	0.3515[e]	96.62±5.90	9.06±0.55	2.35±0.22	2.21±0.18
	m_{H1a}	HAMTAH-1410	32.2678	77.3589	4,125	130 x 80 x 70	2.5	0.948	25.3997	0.3503[d]	6.30±1.08	0.60±0.10	0.14±0.03	0.13±0.03
	m_{H1a}	HAMTAH-1502[a]	32.2703	77.3579	3,861	300 x 210 x 200	2.0	0.923	22.1344	0.3518[f]	24.13±2.31	2.57±0.25	0.74±0.09	0.70±0.07
	m_{H3}	HAMTAH-1401	32.3005	77.3684	3,783	110 x 100 x 110	1.5	0.897	25.6264	0.3501[d]	398.76±20.43	37.33±1.91	10.94±0.66	10.48±0.62
	m_{H3}	HAMTAH-1402[a]	32.3006	77.3685	3,769	160 x 120 x 60	2.0	0.887	26.2449	0.3503[d]	217.14±18.51	19.86±1.69	6.24±0.51	5.93±0.48
	m_{H3}	HAMTAH-1403[a]	32.2998	77.3670	3,808	250 x 150 x 80	1.0	0.879	27.8189	0.3513[d]	670.80±27.12	58.05±2.35	16.18±1.03	15.67±0.87
	m_{H3}	HAMTAH-1404[a]	32.2992	77.3662	3,808	360 x 270 x 100	2.0	0.879	25.2556	0.3523[e]	128.03±6.02	12.21±0.57	4.05±0.28	3.79±0.23
	m_{H3}	HAMTAH-1503	32.2942	77.3647	4,112	270 x 180 x 100	3.0	0.898	7.7449	0.3506[e]	131.06±2.72	41.47±0.86	10.36±0.53	10.02±0.47
	m_{H3}	HAMTAH-1504	32.2954	77.3655	4,083	570 x 270 x 220	3.0	0.879	23.2097	0.3497[f]	384.84±7.21	38.89±0.73	10.13±0.54	9.77±0.47
Lato valley	m_{A1}	LATO-1415[a]	33.6822	77.5920	5,366	200 x 130 x 90	3.0	0.95	22.2096	0.3518[f]	125.27±2.91	13.31±0.31	1.78±0.11	1.72±0.11
	m_{A1}	LATO-1416	33.6822	77.5921	5,358	590 x 290 x 110	4.0	0.95	25.2732	0.3498[d]	17.46±1.86	1.66±0.18	0.21±0.03	0.20±0.03
	m_{A1}	LATO-1417	33.6826	77.5920	5,348	185 x 140 x 100	2.0	0.951	28.3242	0.3506[d]	32.31±1.17	2.74±0.10	0.35±0.03	0.34±0.03
	m_{A1}	LATO-1418	33.6826	77.5921	5,351	70 x 40 x 70	3.0	0.946	24.7312	0.3505[d]	18.41±1.47	1.79±0.14	0.22±0.03	0.22±0.03
	m_{A1}	LATO-1419[a]	33.6827	77.5920	5,339	110 x 80 x 40	3.0	0.952	23.038	0.3523[f]	240.38±18.05	24.66±1.85	3.43±0.32	3.31±0.32
	m_{A2c}	LATO-1409[a]	33.6851	77.5953	5,314	180 x 150 x 60	3.0	0.959	11.5494	0.3505[e]	1274.75±27.10	265.10±5.64	27.56±1.52	29.25±1.52
	m_{A2c}	LATO-1410[a]	33.6851	77.5953	5,321	180 x 110 x 50	2.5	0.959	28.05	0.3511[d]	254.86±10.13	21.86±0.87	3.04±0.21	2.93±0.21
	m_{A2c}	LATO-1411[a]	33.6851	77.5952	5,315	250 x 160 x 90	2.0	0.959	27.7016	0.3512[d]	341.11±20.48	29.63±1.78	4.06±0.32	3.92±0.32
	m_{A2c}	LATO-1412	33.6850	77.5957	5,315	210 x 80 x 70	1.0	0.958	24.1378	0.3514[e]	27.71±1.47	2.76±0.15	0.35±0.03	0.34±0.03
	m_{A2c}	LATO-1413	33.6849	77.5957	5,317	170 x 80 x 60	2.0	0.959	23.0324	0.3501[f]	56.57±2.00	5.77±0.20	0.74±0.06	0.73±0.06
	m_{A2c}	LATO-1414	33.6851	77.5954	5,314	200 x 130 x 100	2.0	0.96	27.964	0.3509[d]	43.71±2.12	3.76±0.18	0.48±0.03	0.46±0.03
	b_A	LATO1420[b]	33.6914	77.6081	5,191	Bedrock	2.5	0.951	11.888	0.3516[e]	544.04±14.91	110.02±3.02	13.73±0.74	13.9±0.74
	b_A	LATO1421[b]	33.6913	77.6083	5,180	Bedrock	3.0	0.951	17.4754	0.3489[e]	790.62±16.30	107.92±2.22	13.61±0.7	13.77±0.7
	b_A	LATO1601[b]	33.6911	77.6086	5,171	Bedrock	2.0	0.942	12.0054	0.3521[e]	560.06±8.24	114.80±1.69	14.43±0.7	14.65±0.7
	m_{A3}	LATO1405[a]	33.6905	77.6211	5,134	150 x 130 x 50	2.0	0.968	27.9485	0.3502[e]	172.80±114.18	14.80±9.78	2.15±1.42	2.08±1.42
	m_{A3}	LATO1408[a]	33.6907	77.6211	5,136	120 x 90 x 50	1.0	0.971	28.7324	0.3502[e]	137.57±20.37	11.46±1.70	1.62±0.27	1.57±0.27
Stok valley	m_{S1}	STOK-1405[c]	33.9872	77.4601	5,370	140 x 70 x 70	2.0	0.98	25.0795	0.3522[e]	79.59±3.26	7.64±0.31	0.93±0.07	0.92±0.07
	m_{S1}	STOK-1406[a c]	33.9870	77.4600	5,314	160 x 80 x 100	2.5	0.98	25.6799	0.3507[d]	48.48±2.35	4.54±0.22	0.56±0.04	0.55±0.04
	m_{S1}	STOK-1407[a c]	33.9871	77.4608	5,340	290 x 200 x 190	3.0	0.978	26.4547	0.3514[d]	13.71±2.35	1.25±0.21	0.14±0.03	0.14±0.03
	m_{S1}	STOK-1408[c]	33.9871	77.4606	5,308	190 x 130 x 100	3.0	0.978	10.6812	0.3483[d]	41.68±3.21	9.31±0.72	1.19±0.11	1.17±0.11
	m_{S1}	STOK-1516	33.9872	77.4599	5,303	160 x 120 x 70	3.0	0.977	22.944	0.3519[f]	71.67±6.36	7.37±0.65	0.94±0.1	0.92±0.1
	m_{S1}	STOK-1401[c]	33.9873	77.4557	5,329	120 x 90 x 100	3.0	0.964	25.5582	0.3505[e]	165.80±5.43	15.57±0.51	2.06±0.14	2.00±0.14
	m_{S1}	STOK-1402[c]	33.9879	77.4557	5,330	180 x 160 x 100	3.0	0.967	25.2641	0.3498[e]	123.78±6.10	11.72±0.58	1.51±0.12	1.48±0.12
	m_{S1}	STOK-1403[c]	33.9883	77.4570	5,323	140 x 70 x 70	1.0	0.969	26.8263	0.3503[e]	164.10±7.28	14.65±0.65	1.89±0.14	1.84±0.14
	m_{S1}	STOK-1404[a c]	33.9882	77.4571	5,328	280 x 130 x 80	2.0	0.969	25.2253	0.3509[d]	21.87±0.90	2.08±0.09	0.25±0.02	0.25±0.02
Karzok valley	m_{M1}	KO-7[a]	32.9328	78.2136	5,524	250 x 160 x 100	6.0	1.000	25.6596	0.3513[e]	21.74±1.45	2.04±0.14	0.24±0.02	0.23±0.02
	m_{M1}	KO-8	32.9333	78.2136	5,516	170 x 130 x 90	2.5	1.000	25.4739	0.3497[e]	63.04±5.85	5.92±0.55	0.69±0.08	0.68±0.08
	m_{M1}	KO-9	32.9341	78.2147	5,503	380 x 240 x 260	1.0	1.000	25.2789	0.3497[e]	63.36±2.49	6.00±0.24	0.70±0.05	0.68±0.05
	m_{M1}	KO10	32.9345	78.2148	5,503	160 x 130 x 90	1.0	1.000	22.2821	0.3489[e]	44.16±6.22	4.73±0.67	0.54±0.09	0.53±0.09

m_{M2}	KO1[a]	32.9321	78.2143	5,532	300 x 160 x 80	3.0	1.000	22.4344	0.3504[e]	191.11±6.14	20.44±0.66	2.56±0.19	2.46±0.19
m_{M2}	KO-2	32.9317	78.2143	5,541	400 x 325 x 140	6.0	1.000	21.9943	0.3507[d]	82.65±4.89	9.03±0.53	1.09±0.09	1.07±0.09
m_{M2}	KO-3	32.9314	78.2142	5,548	140 x 60 x 100	4.0	0.991	25.8534	0.3530[e]	87.60±4.20	8.18±0.39	0.98±0.07	0.95±0.07
m_{M2}	MENTOK-1505	32.9312	78.2145	5,569	190 x 130 x 90	2.0	0.991	22.3311	0.3503[f]	83.27±3.05	8.76±0.32	1.02±0.07	1.00±0.07
m_{M2}	MENTOK-1506	32.9311	78.2145	5,574	190 x 160 x 110	1.0	0.992	22.115	0.3517[f]	73.53±4.69	7.84±0.50	0.90±0.08	0.88±0.08
m_{M3}	MENTOK-1501	32.9413	78.2242	5,331	200 x 170 x 90	2.0	1.000	24.3921	0.3530[f]	5669.39±54.77	550.34±5.32	57.21±3.51	60.02±3.51
m_{M3}	MENTOK-1502[a]	32.9411	78.2242	5,335	340 x 170 x 100	2.0	1.000	24.2451	0.3519[f]	3694.63±69.15	359.70±6.73	36.49±1.99	38.32±1.99
m_{M3}	MENTOK-1503[a]	32.9408	78.2242	5,339	410 x 300 x 320	2.0	1.000	24.5983	0.3515[f]	2302.94±27.85	220.73±2.67	22.86±1.08	23.76±1.08
m_{G1}	KO-14	32.9672	78.1794	5,374	200 x 190 x 150	3.0	0.961	19.5522	0.3513[d]	138.87±5.85	17.10±0.72	2.36±0.19	2.27±0.19
m_{G1}	KO-15[a]	32.9678	78.1796	5,366	270 x 240 x 110	3.0	0.966	29.9259	0.3504[d]	61.45±3.22	4.93±0.26	0.64±0.05	0.62±0.05
m_{G1}	KO-16[a]	32.9678	78.1796	5,366	400 x 300 x 270	4.0	0.966	15.4506	0.3513[d]	24.82±2.04	3.87±0.32	0.5±0.06	0.48±0.06
m_{G1}	KO1601	32.9680	78.1796	5,374	270 x 210 x 100	2.0	0.966	25.5064	0.3503[e]	139.61±4.08	13.40±0.39	1.79±0.12	1.73±0.12
m_{G1}	KO1602	32.9671	78.1800	5,388	200 x 120 x 140	1.5	0.954	9.4984	0.3524[e]	73.03±2.75	18.94±0.71	2.61±0.19	2.51±0.19
m_{G2}	KO-17	32.9706	78.1787	5,331	307 x 109 x 190	3.0	0.984	16.6632	0.3505[d]	163.54±6.74	23.57±0.97	3.29±0.23	3.16±0.23
m_{G2}	KO-18	32.9708	78.1780	5,337	290 x 190 x 180	2.0	0.985	27.5274	0.3519[d]	419.49±13.55	36.75±1.19	4.93±0.28	4.74±0.28
m_{G2}	KO-1501	32.9720	78.1815	5,327	370 x 290 x 150	1.0	0.99	22.2012	0.3514[f]	451.84±11.51	47.97±1.22	6.05±0.3	5.92±0.3
m_{G2}	KO-1502[a]	32.9724	78.1812	5,334	300 x 260 x 220	2.0	0.99	24.2361	0.3510[f]	1090.46±13.90	105.93±1.35	12.37±0.7	12.42±0.7

[a] Outliers are identified and removed. Detail statistics are discussed in Table S1
[b] Bedrock samples
[c] Published [10]Be ages from Orr et al., 2017
[d] Carrier [9]Be concentration is 1,025.5 ppm
[e] Carrier [9]Be concentration is 1,023.2 ppm
[f] Carrier [9]Be concentration is 1,003.8 ppm
[g] Ratios are corrected from background [10]Be detected in procedural blanks
[h] Reported ([10]Be) values have been corrected from background [10]Be detected in procedural blanks
[i] Lifton-Sato-Dunai (LSD) scaling model using CREp online calculator
[j] Lal and Stone time-dependent (Lm) scaling model using CREp online calculator
Note: Density value of 2.7 g cm^{-3}, erosion rate of 0.00 cm a[-1], and AMS standard of 07KNSTD were used for all samples to calculate surface exposure ages.
       Lato [10]Be ages are also reported in Orr et al., 2018 which was submitted parallel with this manuscript.

Table 3. The common AAR and THAR ratios recommended in published literature.

Study	Region	AAR	THAR
Porter (1970)	Swat Himalaya	0.6±0.1	-
Andrew (1975)	Garhwal Himlaya	1.3	-
Kulkarni (1992)	Debris covered glaciers in the Western Himalaya	0.43–0.47	-
Sharma and Owen (1996)	Gangotri galcier in the Garhwal Himal	0.6 & 1.3	0.5
Burbank and Fort (1985)	Sub-polar glaciers in Ladakh region.	0.65	0.4
Fort (1995), Burbank and Cheng (1991)	Debris covered glaciers in the Nepal Himalaya	0.6–0.65	-
Tylor and Mitchel (2000)	Zanskar	-	0.4–0.5
Benn and Lehmkuhl (2000)	Debris covered glaciers in Karakoram to clean glaciers in Tibet	0.44–0.67	-
Kaser and Osmaston (2002)	Tropical debris-covered glaciers	0.65–0.70	-
Owen and Benn (2005)	Variety of glaciers in the Himalaya and Tibet	0.5–0.8	0.3–0.5
Scherler et al. (2011)	Western Himalaya	0.48±26	-
Orr et al. 2017, 2018	Zanskar	0.4, 0.5 & 0.6	0.4–0.5

Table 4. A summary of Holocene local and regional stages of glacial advances based on cosmogenic ^{10}Be surface exposure age data.

Regional glacial stage	Local glacial stage	Local stage age (ka)[a]	Regional stage age range (ka)	n (outlier free)	Chi-squared value[b]	Mean regional glacial stage age (ka)[c]	P (sig 2-tailed) between regional glacial stages
HH 7	m_{H3} (This study)	10.42±0.34	~10.9—9.3	3	0.48	10.06±0.42	0.000
	Olimde 3 stage (Seong et al., 2009)	10.25±0.15		6	0.10		
	Olimde 3 stage (Seong et al., 2009)	9.80±0.32		8	0.43		
HH 6	Olimde 4 Stage (Seong et al., 2009)	7.98±0.09	~8.2—7.4	6	0.06	7.83±0.23	0.004
	Olimde 4 Stage (Seong et al., 2009)	7.77±0.26		5	0.48		
	Olimde 4 Stage (Seong et al., 2009)	7.74±0.24		6	0.41		
HH 5	Mungo 2 stage (Seong et al., 2007)	6.63±0.30	~6.9—4.3	4	0.68	5.13±1.11	0.000
	Askole 2 stage (Seong et al., 2007)	5.83±0.60		4	0.92		
	Olimde 5 stage (Seong et al., 2009)	5.06±0.12		3	0.33		
	KM-4 stage/m_{G2} (Hedrick et al., 2011; This study)	4.94±0.28		6	13.12		
HH 4	Olimde 6 stage (Seong et al., 2009)	4.32±0.09	~4.5—2.8	3	0.19	3.87±0.58	0.000
	Olimde 6 stage (Seong et al., 2009)	3.95±0.25		3	2.17		
	PM-2 stage (Hedrick et al., 2011)	3.42±0.71		3	17.79		
HH 3	Ladakh Chang La cirque (Dortch et al., 2013)	2.31±0.24	~2.7—1.8	4	2.01	2.19±0.22	0.000
	Olimde 7 stage (Seong et al., 2009)	2.19±0.07		6	0.19		
	m_{G1} (This study)	2.10±0.34		3	9.37		
HH 2	m_{S1} (This study)	1.20±0.05	~1.8—0.9	6	21.83	1.15±0.39	0.000
	Olimde 7 stage (Seong et al., 2009)	1.66±0.14		3	0.75		
	Olimde 7 stage (Seong et al., 2009)	1.35±0.36		4	4.58		
	m_{G1} (Orr et al., 2017)	1.33±0.12		1	?		
	Askole 3 stage (Seong et al., 2007)	1.03±0.28		5	0.82		
	m_{M2} (This study)	0.99±0.07		4	0.90		
HH 1	m_{M1} (This study)	0.67±0.07	<1 ka	3	1.47	0.37±0.20	0.000
	Olimde 8 stage (Seong et al., 2009)	0.66±0.22		3	10.19		
	Upper Yunam (Saha et al., 2016)	0.59±0.11		3	2.13		
	Pangong high cirque (Dortch et al., 2013)	0.50±0.09		3	0.63		
	Olimde 8 stage (Seong et al., 2009)	0.48±0.13		4	4.19		
	Lonp stage (Lee et al., 2014)	0.47±0.10		2	12.53		
	m_{A2c} (This study)	0.45±0.16		3	24.25		
	m_{A1} (This study)	0.26±0.06		3	6.78		
	PM-3 stage (Hedrick et al., 2011)	0.26±0.04		3	2.22		
	m_{H1a} (This study)	0.18±0.11		3	8.55		

[a] All local stage age uncertainties are reported in 1σ.
[b] Corrected Chi-squared values are from outlier free distribution.
[c] All regional stage age uncertainties are reported in 1σ.

Table 5. A summary of ELAs and ΔELAs in our four study areas.

Glacial Stage	Mean moraine age (ka)	Glacier area (~km^2)	Mean slope (~°)	Mean Aspect	Head (m asl)	Toe (m asl)	MELM (m asl)	Area-Altitude AA (m asl)	Area-Accumulation ratio			Toe-Headwall altitude ratio			Mean ELA (m a.s.l.)	ΔELA (m)
									AAR (0.5)	AAR (0.6)	AAR (0.7)	THAR (0.3)	THAR (0.4)	THAR (0.5)		
Hamtah Valley, Lahul																
Present		4.0	27	NW	5,011	4,056	4,569	4,459	4,479	4,429	4,380	4,347	4,443	4,540	4,456±70	
m$_{H1a}$	0.18±0.13	5.6	29	NW	5,063	3,941	-	4,407	4,429	4,389	4,259	4,285	4,397	4,510	4,382±79	57±28
m$_{H3}$	10.42±0.42	6.6	30	NNW	5,063	3,688	-	4,332	4,389	4,240	4,119	4,103	4,241	4,380	4,258±108	182±57
Mentok Kangri, Karzok																
Present		2.5	33	NE	6,003	5,482	5,659	5,740	5,739	5,719	5,689	-	-	-	5,709±31	
m$_{M1}$	0.67±0.09	2.8	34	NE	6,003	5,447	-	5,714	5,720	5,699	5,669	-	-	-	5,701±20	21±3
m$_{M2}$	0.99±0.08	4.1	30	NE	6,003	5,378	-	5,685	5,679	5,650	5,620	5,568	5,631	5,695	5,647±41	63±6
Gomuche Kangri, Karzok																
Present		1.5	42	N	6,084	5,381	5,649	5,873	5,929	5,889	5,839	5,599	5,669	5,740	5,773±117	
m$_{G1}$	2.10±0.42	1.8	42	N	6,084	5,332	-	5,805	5,889	5,819	5,660	5,564	5,639	5,715	5,727±107	64±50
m$_{G2}$ (or KM-4)	4.40±1.17	2.1	39	NNE	6,084	5,206	-	5,732	5,829	5,649	5,530	5,473	5,561	5,650	5,632±113	159±77
Amda Kangri, Lato																
Present		1.1	22	ENE	5,743	5,312	5,489	5,538	5,529	5,509	5,469	-	-	-	5,504±24	
m$_{A1}$	0.26±0.08	1.4	25	ENE	5,764	5,298	-	5,533	5,529	5,499	5,469	-	-	-	5,511±27	4±4
m$_{A2c}$	0.45±0.02	1.6	25	ENE	5,764	5,264	-	5,511	5,519	5,479	5,439	-	-	-	5,487±31	21±7
Stok Kangri, Zanskar																
Present		0.6	36	NE	5721	5288	5459	5,507	5,509	5,489	5,439	-	-	-	5,481±27	
m$_{S1}$	1.20±0.48	0.9	34	NE	5748	5234	-	5,456	5,439	5,409	5,379	-	-	-	5,421±29	65±11

Note: The present here refers to year 2016 AD;
m asl is meter above sea level.
'-' indicates reconstructed ELAs are ambiguous/erroneous.

90

References

Abramowski, U., Bergau, A., Seebach, D., Zech, R., Glaser, B., Sosin, P., Kubik, P.W., Zech, W., 2006. Pleistocene glaciations of Central Asia: results from [10]Be surface exposure ages of erratic boulders from the Pamir (Tajikistan), and the Alay–Turkestan range (Kyrgyzstan). Quat. Sci. Rev. 25, 1080–1096.

Alley, R.B., Cuffey, K.M., Evenson, E.B., Strasser, J.C., Lawson, D.E., Larsonh, G.J., 1997. How glaciers entrain and transport basal sediment: Physical constraints. Quat. Sci. Rev. 16, 1017–1038.

Anderson, R.S., Dühnforth, M., Colgan, W., Anderson, L., 2012. Far-flung moraines: Exploring the feedback of glacial erosion on the evolution of glacier length. Geomorphology 179, 269–285.

Andrews. J. T., 1975: Glacial Systems. An Approach to G/aciers and Their Enrironments. 191 pp. Duxbury Press, North Scituate.

Applegate, P.J., Urban, N.M., Keller, K., Lowell, T. V., Laabs, B.J.C., Kelly, M. a., Alley, R.B., 2012. Improved moraine age interpretations through explicit matching of geomorphic process models to cosmogenic nuclide measurements from single landforms. Quat. Res. 77, 293–304.

Applegate, P.J., Urban, N.M., Laabs, B.J.C., Keller, K., Alley, R.B., 2010. Modeling the statistical distributions of cosmogenic exposure dates from moraines. Geosci. Model Dev. 3, 293–307.

Azam, M.F., Wagnon, P., Vincent, C., Ramanathan, A., Favier, V., Mandal, A., Pottakkal, J.G., 2014. Processes governing the mass balance of Chhota Shigri Glacier (western Himalaya, India) assessed by point-scale surface energy balance measurements. Cryosph. 8, 2195–2217.

Balco, G., Stone, J.O., Lifton, N. a., Dunai, T.J., 2008. A complete and easily accessible means of calculating surface exposure ages or erosion rates from [10]Be and [26]Al measurements. Quat. Geochronol. 3, 174–195.

Ballantyne, C.K., McCarroll, D., Stone, J.O., 2007. The Donegal ice dome, northwest Ireland: dimensions and chronology. J. Quat. Sci. 22, 773–783.

Barr, I.D., Clark, C.D., 2012. Late Quaternary glaciations in Far NE Russia; combining moraines, topography and chronology to assess regional and global glaciation synchrony. Quat. Sci. Rev. 53, 72–87.

Barr, I.D., Lovell, H., 2014. A review of topographic controls on moraine distribution. Geomorphology 226, 44–64.

Barrows, T.T., 2007. Absence of Cooling in New Zealand. Geology 86, 86–9.

Benn, D.I., Ballantyne, C.K., 2005. Palaeoclimatic reconstruction from Loch Lomond Readvance glaciers in the West Drumochter Hills, Scotland. J. Quat. Sci. 20, 577–592.

Benn, D.I., Lehmkuhl, F., 2000. Mass balance and equilibrium-line altitudes of glaciers in high-mountain environments. Quat. Int. 65–66, 15–29.

Benn, D.I., Owen, L. A., 1998. The role of the Indian summer monsoon and the mid-latitude westerlies in Himalayan glaciation: review and speculative discussion. J. Geol. Soc. London. 155, 353–363.

Benn, D.I., Owen, L.A., 2002. Himalayan glacial sedimentary environments: a framework for reconstructing and dating former glacial extents in high mountain regions. Quaternary International, 97-98, 3-26.

Benn, D.I., Owen, L.A., Osmaston, H.A., Seltzer, G.O., Porter, S.C., Mark, B., 2005. Reconstruction of equilibrium-line altitudes for tropical and sub-tropical glaciers 139, 8–21.

Berger, A., 1978. Long-term variations of caloric insolation resulting from the earth's orbital elements. Quat. Res. 9, 139–167.

Berkelhammer, M., Sinha, A., Stott, L., Cheng, H., Pausata, F.S.R., Yoshimura, K., 2012. An abrupt shift in the Indian Monsoon 4 , 000 years ago An Abrupt Shift in the Indian Monsoon 4000 Years Ago.

Bisht, P., Ali, S.N., Shukla, A.D., Negi, S., Sundriyal, Y.P., Yadava, M.G., Juyal, N., 2015. Chronology of late Quaternary glaciation and landform evolution in the upper Dhauliganga valley, (Trans Himalaya), Uttarakhand, India. Quat. Sci. Rev. 129, 147–162.

Bond, G., Kromer, B., Beer, J., Muscheler, R., Evans, M.N., Showers, W., Hoffmann, S., Lotti-Bond, R., Hajdas, I., Bonani, G., 2001. Persistent solar influence on North Atlantic climate during the Holocene. Science 294, 2130–2136.

Bookhagen, B., Burbank, D.W., 2006. Topography, relief, and TRMM-derived rainfall variations along the Himalaya. Geophys. Res. Lett. 33, L08405.

Borchers, B., Marrero, S., Balco, G., Caffee, M., Goehring, B., Lifton, N., Nishiizumi, K., Phillips, F., Schaefer, J., Stone, J., 2016. Geological calibration of spallation production rates in the CRONUS-Earth project. Quat. Geochronol. 31, 188–198.

Brookfield, M.E., Andrews-Speed, C.P., 1984. Sedimentology, petrography and tectonic significance of the shelf, flysch and molasse clastic deposits across the Indus Suture Zone, Ladakh, NW India. Sediment. Geol. 40, 249–286.

Burbank, D.W., Cheng, K.J., 1991. Relative dating of Quaternary moraines, Rongbuk valley, Mount Everest, Tibet: Implications for an ice sheet on the Tibetan Plateau. Quat. Res. 36, 1–18

Burbank, D.W., Fort, M.B., 1985. Bedrock control on glacial limits: examples from the ladakh and zanskar ranges, north-western Himalaya, India. J. Glaciol. 31, 143–149.

Ceppi, P., Hwang, Y.T., Liu, X., Frierson, D.M.W., Hartmann, D.L., 2013. The relationship between the ITCZ and the Southern Hemispheric eddy-driven jet. J. Geophys. Res. Atmos. 118, 5136–5146.

Chiang, J.C.H., Friedman, A.R., 2012. Extratropical Cooling, Interhemispheric Thermal Gradients, and Tropical Climate Change. Annu. Rev. Earth Planet. Sci. 40, 383–412.

Chiang, J.C.H., Lee, S.Y., Putnam, A.E., Wang, X., 2014. South Pacific Split Jet, ITCZ shifts, and atmospheric North-South linkages during abrupt climate changes of the last glacial period. Earth Planet. Sci. Lett. 406, 233–246.

Corbett, L.B., Bierman, P.R., Rood, D.H., 2016. An approach for optimizing in situ cosmogenic ^{10}Be sample preparation. Quat. Geochronol. 33, 24–34.

Cronauer, S.L., Briner, J.P., Kelley, S.E., Zimmerman, S.R.H., Morlighem, M., 2016. 10Be dating reveals early-middle Holocene age of the Drygalski Moraines in central West Greenland. Quat. Sci. Rev. 147, 59–68.

Dahl, S.O., Nesje, A., 1992. Paleoclimatic implications based on equilibrium-line altitude depressions of reconstructed Younger Dryas and Holocene cirque glaciers in inner Nordfjord, western Norway. Palaeogeogr. Palaeoclimatol. Palaeoecol. 94, 87–97.

Davis, P.T., Menounos, B., Osborn, G., 2009. Holocene and latest Pleistocene alpine glacier fluctuations: a global perspective. Quat. Sci. Rev. 28, 2021–2033.

Demske, D., Tarasov, P.E., Wünnemann, B., Riedel, F., 2009. Late glacial and Holocene vegetation , Indian monsoon and westerly circulation in the Trans-Himalaya recorded in the lacustrine pollen sequence from Tso Kar ,. Palaeogeogr. Palaeoclimatol. Palaeoecol. 279, 172–185.

Denton, G.H., Broecker, W.S., 2008. Wobbly ocean conveyor circulation during the Holocene? Quat. Sci. Rev. 27, 1939–1950.

Desilets, D., Zreda, M., Prabu, T., 2006. Extended scaling factors for in situ cosmogenic nuclides: New measurements at low latitude. Earth Planet. Sci. Lett. 246, 265–276.

Dietsch, C., Dortch, J., Reynhout, S., Owen, L., Caffee, M., 2015. Very slow erosion and topographic evolution of the Southern Ladakh Range, India. Earth Surface Processes and Landforms 40, 3, 389-402.

Dixit, Y., Tandon, S.K., 2016. Hydroclimatic variability on the Indian subcontinent in the past millennium: Review and assessment. Earth-Science Rev. 161, 1–15.

Dong, J., Wang, Y., Cheng, H., Hardt, B., Edwards, R.L., Kong, X., Wu, J., Chen, S., Liu, D., Jiang, X., Zhao, K., 2010. A high-resolution stalagmite record of the Holocene East Asian monsoon from Mt Shennongjia, central China. Holocene 20, 257–264.

Dortch, J., Owen, L., Schoenbohm, L., Caffee, M., 2011. Asymmetrical erosion and morphological development of the central Ladakh Range, northern India. Geomorphology 135, 167-180.

Dortch, J.M., Owen, L.A., Caffee, M.W., 2013. Timing and climatic drivers for glaciation across semi-arid western Himalayan–Tibetan orogen. Quat. Sci. Rev. 78, 188–208.

Dunai, T.J., 2001. Influence of secular variation of the geomagnetic field on production rates of in situ produced cosmogenic nuclides. Earth Planet. Sci. Lett.193, 197–212.

Dunai, T.J., 2010. Cosmogenic Nuclides: Principles, Concepts and Applications in the Earth Surface Sciences. Cambridge Univ. Press. Cambridge.

Dyke, A.S., Savelle, J.M., 2000. Major end moraines of Younger Dryas age on Wollaston Peninsula, Victoria Island, Canadian Arctic: implications for paleoclimate and for formation of hummocky moraine. Can. J. Earth Sci. 37, 601–619.

Dykoski, C.A., Edwards, R.L., Cheng, H., Yuan, D., Cai, Y., Zhang, M., Lin, Y., Qing, J., An, Z., Revenaugh, J., 2005. A high-resolution, absolute-dated Holocene and deglacial Asian monsoon record from Dongge Cave, China. Earth Planet. Sci. Lett. 233, 71–86.

Epard, J.L., Steck, A., 2008. Structural development of the Tso Morari ultra-high pressure nappe of the Ladakh Himalaya. Tectonophysics 451, 242–264.

Eugster, P., Scherler, D., Thiede, R.C., Codilean, A.T., Strecker, M.R., 2016. Rapid last glacial maximum deglaciation in the Indian Himalaya coeval with mid-latitude glaciers: New insights from [10]Be-dating of ice-polished bedrock surfaces in the Chandra Valley, NW Himalaya. Geophys. Res. Lett. n/a-n/a.

Eynaud, F., de Abreu, L., Voelker, A., Schönfeld, J., Salgueiro, E., Turon, J.L., Penaud, A., Toucanne, S., Naughton, F., Sánchez Goñi, M.F., Malaizé, B., Cacho, I., 2009. Position of the Polar Front along the western Iberian margin during key cold episodes of the last 45 ka. Geochem. Geophys. Geosyst. 10, Q07U05.

Eynaud, F., de Abreu, L., Voelker, A., Schönfeld, J., Salgueiro, E., Turon, J.-L., Penaud, A., Toucanne, S., Naughton, F., Sánchez Goñi, M.F., Malaizé, B., Cacho, I., 2009. Position of the Polar Front along the western Iberian margin during key cold episodes of the last 45 ka. Geochem. Geophys. Geosyst. 10, Q07U05.

Fleitmann, D., Burns, S.J., Mangini, A., Mudelsee, M., Kramers, J., Villa, I., Neff, U., Al-Subbary, A.A., Buettner, A., Hippler, D., Matter, A., 2007. Holocene ITCZ and Indian monsoon dynamics recorded in stalagmites from Oman and Yemen (Socotra). Quat. Sci. Rev. 26, 170–188.

Fleitmann, D., Burns, S.J., Mudelsee, M., Neff, U., Kramers, J., Mangini, A., Matter, A., 2003. Holocene Forcing of the Indian Monsoon Recorded in a Stalagmite from Southern Oman. Science (80). 300, 1737–1739.

Fort, M., 1995. The Himalayan glaciation: myth and reality. Journal of Nepal Geological Society Special Issue 11, 257–272.

Frierson, D.M.W., Hwang, Y.T., 2011. Extratropical Influence on ITCZ Shifts in Slab Ocean Simulations of Global Warming. J. Clim. 25, 720–733.

Fuchs, Gerhard., Linner, Manfred., 1996. On the Geology of the Suture Zone and Tso Morari Dome in Eastern Ladakh (Himalaya). Jb. Geol. Bundesanstalt, Wien 139. 191-207.

Galbraith, R. F., 1990. The radial plot: Graphical assessment of the spread in ages, Nucl. Tracks Radiat. Meas., 17, 207–214.

Galbraith, R. F., 2010. On plotting OSL equivalent doses. Anc. TL 28, 1–10.

Galbraith, R.F., Roberts, R.G., 2012. Statistical aspects of equivalent dose and error calculation and display in OSL dating: An overview and some recommendations. Quat. Geochronol. 11, 1–27.

Gasse, F., Fontes, J.C., Campo, E. Van, Wei, K., 1996. Holocene environmental changes in Bangong Co basin (Western Tibet). Part 4: Discussion and conclusions 120, 79–92.

Gibbons, A.B., Megeath, J.D., Pierce, K.L., 1984. Probability of moraine survival in a succession of glacial advances. Geology 12, 327–330.

Gillespie, A., Rupper, S., Roe, G., 2003. Climatic interpretation from mountain glaciations in Central Asia. XVI INQUA Congress Programs with Abstracts, DRI, Reno, Nv., p. 170.

Gosse, J.C., 2005. The contributions of cosmogenic nuclides to unraveling alpine paleo-glacier histories. In: Huber UM, Bugmann HKM, and Reasoner MA (eds.) Global Change and Mountain Regions. An Overview of Current Knowledge. Advances in Global Change Research, vol. 23, pp. 39–50. Dordrecht: Springer.

Gosse, J.C., Phillips, F.M., 2001. Terrestrial in situ cosmogenic nuclides: theory and application, Quat. Sci. Rev. 20, 1475–1560.

Grootes, P.M., Stuiver, M., 1997. Oxygen 18/16 variability in Greenland snow and ice with 10^{-3}- to 10^5-year time resolution. J. Geophys. Res. 102, 26455–26470.

Grove, A.T., 2008. A brief consideration of climate forcing factors in view of the Holocene glacier record. Glob. Planet. Change 60, 141–147.

Grove, J.M., 2004. Little Ice Ages Ancient and Modern, 2nd edition. Routledge, London. 2 vols.

Gupta, A.K., Anderson, D.M., Overpeck, J.T., 2003. Abrupt changes in the Asian southwest monsoon during the Holocene and their links to the North Atlantic Ocean. Nature 421, 354–357.

Haug, G.H., Hughen, K.A., Sigman, D.M., Peterson, L.C., Ro, U., 2001. Southward migration of the Intertropical Convergence Zone through the Holocene. Science 293, 1304–1308.

Hedrick, K. A., Seong, Y.B., Owen, L. A., Caffee, M.W., Dietsch, C., 2011. Towards defining the transition in style and timing of Quaternary glaciation between the monsoon-influenced Greater Himalaya and the semi-arid Transhimalaya of Northern India. Quat. Int. 236, 21–33.

Heimsath, A.M., McGlynn, R., 2008. Quantifying periglacial erosion in the Nepal high Himalaya. Geomorphology 97, 5–23.

Herzschuh, U., 2006. Palaeo-moisture evolution in monsoonal Central Asia during the last 50,000 years. Quat. Sci. Rev. 25, 163–178.

Herzschuh, U., Winter, K., Wünnemann, B., Li, S., 2006. A general cooling trend on the central Tibetan Plateau throughout the Holocene recorded by the Lake Zigetang pollen spectra. Quat. Int. 154–155, 113–121.

Heyman, J., 2014. Paleoglaciation of the tibetan plateau and surrounding mountains based on exposure ages and ELA depression estimates. Quat. Sci. Rev. 91, 30–41.

Hobley, D., Sinclair, H., Cowie, P., 2010. Processes, rates, and timescales of fluvial response in an ancient postglacial landscape of the northwest Indian Himalaya. Geological Society of America Bulletin 122, 1569–1584.

Honegger, K., 1983. Struktur und Metamorphose im Zanskar Kristall9in. Ph.D. Thesis, ETH-Zürich.

Hu, C., Henderson, G.M., Huang, J., Xie, S., Sun, Y., Johnson, K.R., 2008. Quantification of Holocene Asian monsoon rainfall from spatially separated cave records. Earth and Planetary Science Letters 266, 221–232.

Hughes, P.D., 2010. Geomorphology and Quaternary stratigraphy: The roles of morpho-, litho-, and allostratigraphy. Geomorphology 123, 189–199.

Hughes, P.D., Gibbard, P.L., Woodward, J., 2005. Quaternary glacial records in mountain regions: A formal stratigraphical approach. Episodes, 28, 85-92.

Ivy-Ochs, S., Kerschner, H., Schlüchter, C., 2007. Cosmogenic nuclides and the dating of Lateglacial and Early Holocene glacier variations: The Alpine perspective. Quat. Int. 164–165, 53–63.

Jennerjahn, T.C., Ittekkot, V., Arz, H.W., Behling, H., Pätzold, J., Wefer, G., 2004. Asynchronous Terrestrial and Marine Signals of Climate Change During Heinrich Events Asynchronous Terrestrial and Marine Signals of Climate Change During Heinrich Events. Science (80). 306.

Ji, J., Shen, J., Balsam, W., Chen, J., Liu, L., Liu, X., 2005a. Asian monsoon oscillations in the northeastern Qinghai-Tibet Plateau since the late glacial as interpreted from visible reflectance of Qinghai Lake sediments. Earth Planet. Sci. Lett. 233, 61–70.

Ji, S., Xingqi, L., Sumin, W., Matsumoto, R., 2005b. Palaeoclimatic changes in the Qinghai Lake area during the last 18,000 years. Quat. Int. 136, 131–140.

Kaplan, M.R., Hein, A.S., Hubbard, A., Lax, S.M., 2009. Can glacial erosion limit the extent of glaciation? Geomorphology 103, 172–179.

Kaplan, M.R., Schaefer, J.M., Denton, G.H., Doughty, A.M., Barrell, D.J.A., Chinn, T.J.H., Putnam, A.E., Andersen, B.G., Mackintosh, A., Finkel, R.C., Schwartz, R., Anderson, B., 2013. The anatomy of long-term warming since 15 ka in New Zealand based on net glacier snowline rise. Geology 41, 887–890.

Kaser, G., Osmaston, H., 2002. Tropical Glaciers. Cambridge University Press, Cambridge, 207 pp.

Kirkbride, M.P., Brazier, V., 1998. A critical evaluation of the use of glacier chronologies in climate reconstruction, with reference to New Zealand. Quaternary Proceedings 6, 55-64.

Kirkbride, M.P., Winkler, S., 2012. Correlation of Late Quaternary moraines: Impact of climate variability, glacier response, and chronological resolution. Quat. Sci. Rev. 46, 1–29.

Kohl, C.P., Nishiizumi, K., 1992. Chemical isolation of quartz for measurement of in-situ produced cosmogenic nuclides. Geochim. Cosmochim. Acta 56, 3583–3587.

Kramer, A., Herzschuh, U., Mischke, S., Zhang, C., 2010. Holocene treeline shifts and monsoon variability in the Hengduan Mountains (southeastern Tibetan Plateau), implications from palynological investigations. Palaeogeogr. Palaeoclimatol. Palaeoecol. 286, 23–41.

Kulkarni, A. V, 1992. Mass balance of Hilnalayan glaciers using AAR and ELA Methods. J. Glaciol. 38, 101–104.

Kumar. G., Joshi. A., Mathur. V. K., 1987. Redlichid trilobites from the Tal Formation. Lesser Himalaya. India. Current Science 56, 659-663.

Lal, D., 1991. Cosmic ray labeling of erosion surfaces: in situ nuclide production rates and erosion models. Earth Planet. Sci. Lett. 104, 424–439.

Lavé, J., Avouac, J.P., 2001. Fluvial incision and tectonic uplift across the Himalayas of central Nepal. J. Geophys. Res. 106, 26561–26591.

Le Roy, M., Deline, P., Carcaillet, J., Schimmelpfennig, I., Ermini, M., ASTER Team, 2017. 10Be exposure dating of the timing of Neoglacial glacier advances in the Ecrins-Pelvoux massif, southern French Alps. Quat. Sci. Rev. 178, 118–138.

Le Roy, M., Nicolussi, K., Deline, P., Astrade, L., Edouard, J.L., Miramont, C., Arnaud, F., 2015. Calendar-dated glacier variations in the western European Alps during the Neoglacial: The Mer de Glace record, Mont Blanc massif. Quat. Sci. Rev. 108, 1–22.

Lea, D.W., Pak, D.K., Peterson, L.C., Hughen, K.A., 2003. Synchroneity of Tropical and High-Latitude Atlantic Temperatures over the Last Glacial Termination. Science, 301, 1361–1364.

Lee, S.Y., Seong, Y.B., Owen, L. a., Murari, M.K., Lim, H.S., Yoon, H. Il, Yoo, K.C., 2014. Late Quaternary glaciation in the Nun-Kun massif, northwestern India. Boreas 43, 67–89.

Leipe, C., Demske, D., Tarasov, P.E., 2014. A Holocene pollen record from the northwestern Himalayan lake Tso Moriri: Implications for palaeoclimatic and archaeological research. Quat. Int. 348, 93–112.

Levermann, A., Schewe, J., Petoukhov, V., Held, H., 2009. Basic mechanism for abrupt monsoon transitions. PNAS, 106. 20572–20577.

Liang, F., Brook, G.A., Kotlia, B.S., Railsback, L., B., Hardt, B., Cheng, H., Edwards, R.L., Kandasamy, S., 2015. Panigarh cave stalagmite evidence of climate change in the Indian Central Himalaya since AD 1256: Monsoon breaks and winter southern jet depressions. Quat. Sci. Rev. 124, 145–161.

Lifton, N., 2016. Implications of two Holocene time-dependent geomagnetic models for cosmogenic nuclide production rate scaling. Earth Planet. Sci. Lett. 433, 257–268.

Lifton, N., Sato, T., Dunai, T.J., 2014. Scaling in situ cosmogenic nuclide production rates using analytical approximations to atmospheric cosmic-ray fluxes. Earth Planet. Sci. Lett. 386, 149–160.

Lifton, N.A., Bieber, J.W., Clem, J.M., Duldig, M.L., Evenson, P., Humble, J.E., Pyle, R., 2005. Addressing solar modulation and long-term uncertainties in scaling secondary cosmic rays for in situ cosmogenic nuclide applications. Earth Planet. Sci. Lett. 239, 140–161.

Lifton, N.A., Smart, D.F., Shea, M.A., 2008. Scaling time-integrated in situ cosmogenic nuclide production rates using a continuous geomagnetic model. Earth Planet. Sci. Lett. 268, 190–201.

Liu, K., Thompson, L.G., 1998. A pollen record of Holocene climatic changes from the Dunde ice cap, Qinghai-Tibetan Plateau. Geology 1986, 135–138.

Luetscher, M., Hoffmann, D.L., Frisia, S., Spötl, C., 2011. Holocene glacier history from alpine speleothems, Milchbach cave, Switzerland. Earth Planet. Sci. Lett. 302, 95–106.

Lund, D.C., Lynch-stieglitz, J., Curry, W. B., 2006. Gulf Stream density structure and transport during the past millennium. Nature 444, 601–604.

Macgregor, K.R., Anderson, R.S., Program, E.D.W.G., 2000. Numerical simulations of glacial-valley longitudinal profile evolution. Geology, 28. 1031–1034.

Marrero, S., Phillips, F., Borchers, B., Lifton, N., 2016. Cosmogenic Nuclide Systematics and the CRONUScalc Program. Quat. Geochronol. 31, 1–72.

Martin, L.C.P., Blard, P.H., Balco, G., Lavé, J., Delunel, R., Lifton, N., Laurent, V., 2016. The CREp program and the ICE-D production rate calibration database: A fully parameterizable and updated online tool to compute cosmic-ray exposure ages. Quat. Geochronol. 38, 25–49.

Mayewski, P. a, Rohling, E., Curtstager, J., Karlén, W., Maasch, K., Davidmeeker, L., Meyerson, E., Gasse, F., Vankreveld, S., Holmgren, K., 2004. Holocene climate variability. Quat. Res. 62, 243–255.

Mischke, S., Zhang, C., 2010. Holocene cold events on the Tibetan Plateau. Glob. Planet. Change 72, 155–163.

Mischke, S., Zhang, C., Börner, A., Herzschuh, U., 2010. Lateglacial and Holocene variation in aeolian sediment flux over the northeastern Tibetan Plateau recorded by laminated sediments of a saline meromictic lake. J. Quat. Sci. 25, 162–177.

Mölg, T., Maussion, F., Scherer, D., 2014. Mid-latitude westerlies as a driver of glacier variability in monsoonal High Asia. Nat. Clim. Chang. 4, 68–73.

Moran, A.P., Ivy Ochs, S., Christl, M., Kerschner, H., 2017. Exposure dating of a pronounced glacier advance at the onset of the late-Holocene in the central Tyrolean Alps. Holocene 27, 1350–1358.

Moran, A.P., Ivy-Ochs, S., Schuh, M., Christl, M., Kerschner, H., 2016. Evidence of central Alpine glacier advances during the Younger Dryas–early Holocene transition period. Boreas 45, 398–410.

Moran, A.P., Kerschner, H., Ochs, S.I., 2015. Redating the moraines in the Kromer Valley (Silvretta Mountains) – New evidence for an early Holocene glacier advance. Holocene 26, 655–664.

Murari, M.K., Owen, L.A., Dortch, J.M., Caffee, M.W., Dietsch, C., Fuchs, M., Haneberg, W.C., Sharma, M.C., Townsend-Small, A., 2014. Timing and climatic drivers for glaciation across monsoon-influenced regions of the Himalayan–Tibetan orogen. Quat. Sci. Rev. 88, 159–182.

New, M., Lister, D., Hulme, M., Makin, I., 2002. A high-resolution data set of surface climate over global land areas. Clim. Res. 21, 1–25.

Nishiizumi, K., Finkel, R.C., Caffee, M.W., Southon, J.R., Kohl, C.P., Arnold, J.R., Olinger, C.T., Poths, J., Klein, J., 1994. Cosmogenic production of ^{10}Be and ^{26}Al on the surface of the earth and underground, Eighth International Conference on Geochronology, Cosmochronology and Isotope Geochemistry (U.S. Geol. Surv. Circular 1107), Berkeley, California, 234 pp.

Nishiizumi, K., Imamura, M., Caffee, M.W., Southon, J.R., Finkel, R.C., Mcaninch, J., 2007. Be AMS standards. Nuclear Instruments and Methods in Physics Research B, 258. 403–413.

O'Hara, S.L., Briner, J.P., Kelley, S.E., 2017. A10Be chronology of early Holocene local glacier moraines in central West Greenland. Boreas 46, 655–666.

Oerlemans, J., 2005. Extracting a Climate Signal from 169 Glacier Records. Science, 308, 675–677.

Oerlemans, J., 2010. The Microclimate of Valley Glaciers. Igitur, Utrecht Publishing & Archiving Services, Universiteitsbibliotheek Utrecht, The Netherlands. 138 pp.

Orr, E.N., Owen, L.A., Murari, M.K., Saha, S., Caffee, M.W., 2017. Geomorphology The timing and extent of Quaternary glaciation of Stok, northern Zanskar. Geomorphology 284, 142–155.

Orr, E.N., Owen, L.A., Saha, S., Caffee, M.W., Muraria, M.K., 2018. Quaternary glaciation of the Lato Massif, Zanskar Range of the NW Himalaya.

Osmaston, H., 2005. Estimates of glacier equilibrium line altitudes by the Area x Altitude, the Area x Altitude Balance Ratio and the Area x Altitude Balance Index methods and their validation. Quat. Int. 138–139, 22–31.

Owen, L.A, Finkel, R.C., Caffee, M.W., 2002. A note on the extent of glaciation throughout the Himalaya during the global Last Glacial Maximum. Quat. Sci. Rev. 21, 147–157.

Owen, L.A., Benn, D.I., 2005. Equilibrium-line altitudes of the Last Glacial Maximum for the Himalaya and Tibet: An assessment and evaluation of results. Quat. Int. 138–139, 55–78.

Owen, L.A., Derbyshire, E., Richardson, S., Benn, D.I., Evans, D.J.A., Mitchell, W.A., 1996. The Quaternary glacial history of the Lahul Himalaya, Northern India. Jour. Quat. Sci. 11, 25–42.

Owen, L.A., Dortch, J.M., 2014. Nature and timing of Quaternary glaciation in the Himalayan–Tibetan orogen. Quat. Sci. Rev. 88, 14–54.

Owen, L.A., Gualtieri, L., Finkel, R.C., Caffee, M.W., Benn, D.I., Sharma, M.C., 2001. Cosmogenic radionuclide dating of glacial landforms in the Lahul Himalaya, northern India: defining the timing of Late Quaternary glaciation. J. Quat. Sci. 16, 555–563.

Owen, L.A., Mitchell, W., Bailey, R.M., Coxon, P., Rhodes, E., 1997. Style and timing of Glaciation in the Lahul Himalaya, northern India: a framework for reconstructing late Quaternary palaeoclimatic change in the western Himalayas. Jour. Quat. Sci. 12, 83-109.

Phadtare, N.R., 2000. Sharp Decrease in Summer Monsoon Strength 4000–3500 cal yr B.P. in the Central Higher Himalaya of India Based on Pollen Evidence from Alpine Peat. Quaternary Research, 129, 122–129.

Porter, S.C., 1970. Quaternary Glacial Record in Swat Kohistan, West Pakistan. Geol. Soc. Am. Bull. 81, 1421–1446.

Putkonen, J., O'Neal, M., 2006. Degradation of unconsolidated Quaternary landforms in the western North America. Geomorphology, 75, 408–419.

Putkonen, J., Swanson, T., 2003. Accuracy of cosmogenic ages for moraines. Quat. Res. 59, 255–261.

Putkonen, J., Connolly, J., Orloff, T., 2008. Landscape evolution degrades the geologic signature of past glaciations. Geomorphology 97, 208–217.

Putnam, A.E., Schaefer, J.M., Denton, G.H., Barrell, D.J.A., Andersen, B.G., Koffman, T.N.B., Rowan, A. V., Finkel, R.C., Rood, D.H., Schwartz, R., Vandergoes, M.J., Plummer, M.A., Brocklehurst, S.H., Kelley, S.E., Ladig, K.L., 2013a. Warming and glacier recession in the Rakaia valley, Southern Alps of New Zealand, during Heinrich Stadial 1. Earth Planet. Sci. Lett. 382, 98–110.

Putnam, A.E., Schaefer, J.M., Denton, G.H., Barrell, D.J.A., Birkel, S.D., Andersen, B.G., Kaplan, M.R., Finkel, R.C., Schwartz, R., Doughty, A.M., 2013b. The Last Glacial Maximum at 44ºS documented by a [10]Be moraine chronology at Lake Ohau, Southern Alps of New Zealand. Quat. Sci. Rev. 62, 114–141.

Rawat, S., Gupta, A.K., Sangode, S.J., Srivastava, P., Nainwal, H.C., 2015a. Late Pleistocene-Holocene vegetation and Indian summer monsoon record from the Lahaul, Northwest Himalaya, India. Quat. Sci. Rev. 114, 167–181.

Rawat, S., Gupta, A.K., Srivastava, P., Sangode, S.J., Nainwal, H.C., 2015b. A 13,000 year record of environmental magnetic variations in the lake and peat deposits from the Chandra valley, Lahaul: Implications to Holocene monsoonal variability in the NW Himalaya. Palaeogeogr. Palaeoclimatol. Palaeoecol. 440, 116–127.

Roe, G.H., 2011. What do glaciers tell us about climate variability and climate change? J. Glaciol. 57, 567–578.

Roe, G.H., O'Neal, M.A., 2009. The response of glaciers to intrinsic climate variability: observations and models of late-Holocene variations in the Pacific Northwest. J. Glaciol. 55, 839-854.

Röhringer, I., Zech, R., Abramowski, U., Sosin, P., Aldahan, A., Kubik, P.W., Zöller, L., Zech, W., 2012. The late Pleistocene glaciation in the Bogchigir Valleys (Pamir, Tajikistan) based on [10]Be surface exposure dating. Quat. Res. 78, 590–597.

Rowan, A.V., 2016. The 'Little Ice Age in the Himalaya: A review of glacier advance driven by Northern Hemisphere temperature change. The Holocene, 1-17.

Rupper, S., Roe, G., 2008. Glacier Changes and Regional Climate: A Mass and Energy Balance Approach. J. Clim. 21, 5384–5401.

Rupper, S., Roe, G., Gillespie, A., 2009. Spatial patterns of Holocene glacier advance and retreat in Central Asia. Quat. Res. 72, 337–346.

Sachs, J.P., Sachse, D., Smittenberg, R.H., Zhang, Z., Battisti, D.S., Golubic, S., 2009. Southward movement of the Pacific intertropical convergence zone AD 1400–1850. Nat. Geosci. 2, 519–525.

Saha, S., Sharma, M.C., Murari, M.K., Owen, L.A., Caffee, M.W., 2016. Geomorphology, sedimentology and minimum exposure ages of streamlined subglacial landforms in the NW Himalaya, India 2016. Boreas, 45, 284–303.

Scherler, D., Bookhagen, B., Strecker, M.R., 2011. Hillslope-glacier coupling: The interplay of topography and glacial dynamics in High Asia. J. Geophys. Res. Earth Surf. 116, 1–21.

Schimmelpfennig, I., Schaefer, J.M., Akçar, N., Ivy-Ochs, S., Finkel, R.C., Schlüchter, C., 2012. Holocene glacier culminations in the Western Alps and their hemispheric relevance. Geology 40, 891–894.

Schimmelpfennig, I., Schaefer, J.M., Akçar, N., Koffman, T., Ivy-Ochs, S., Schwartz, R., Finkel, R.C., Zimmerman, S., Schlüchter, C., 2014. A chronology of Holocene and Little Ice Age glacier culminations of the Steingletscher, Central Alps, Switzerland, based on high-sensitivity beryllium-10 moraine dating. Earth Planet. Sci. Lett. 393, 220–230.

Schindelwig, I., Akçar, N., Kubik, P.W., Schlüchter, C., 2012. Lateglacial and early Holocene dynamics of adjacent valley glaciers in the Western Swiss Alps. J. Quat. Sci. 27, 114–124.

Schlup, M., Carter, A., Cosca, M., Steck, A., 2003. Exhumation history of eastern Ladakh revealed by Ar-40/Ar-39 and fission-track ages: the Indus River-Tso Morari transect, NW Himalaya. Jgsl 160, 385–399.

Searle, M.P., Windley, B.F., Coward, M.P., Cooper, D.J.W., Rex, A.J., Rex, D., Tingdong, L., Xuchang, X., Jan, M.Q., Thakur, V.C., Kumar, S., 1987. The closing of Tethys and the tectonics of the Himalaya. Geol. Soc. Am. Bull. 98, 678–701.

Seong, Y.B., Owen, L.A., Bishop, M.P., Bush, A., Clendon, P., Copland, L., Finkel, R., Kamp, U., Shroder, J.F., 2007. Quaternary glacial history of the Central Karakoram. Quat. Sci. Rev. 26, 3384–3405.

Seong, Y.B., Owen, L.A., Yi, C., Finkel, R.C., 2009. Quaternary glaciation of Muztag Ata and Kongur Shan: Evidence for glacier response to rapid climate changes throughout the Late Glacial and Holocene in westernmost Tibet. GSA Bulletin, 121, 348–365.

Severinghaus, J.P., Beaudette, R., Headly, M.A., Taylor, K., Brook, E.J., 2009. The Terrestrial Biosphere. Science, 324, 1431–1434.

Sharma, M.C., Owen, L.A., 1996. Quaternary glacial history of NW Garhwal, Central Himalayas. Quat. Sci. Rev. 15, 335–365.

Sharma, P., Bourgeois, M., Elmore, D., Granger, D., Lipschutz, M.E., Ma, X., Miller, T., Mueller, K., Rickey, F., Simms, P., Vogt, S., 2000. PRIME lab AMS performance, upgrades and research applications. Nucl. Instruments Methods Phys. Res. Sect. B-Beam Interact. with Mater. Atoms 172, 112–123.

Sharma, S., Chand, P., Bisht, P., Shukla, A.D., Bartarya, S.K., Sundriyal, Y.P., Juyal, N., 2016. Factors responsible for driving the glaciation in the Sarchu Plain, eastern Zanskar Himalaya, during the late Quaternary. J. Quat. Sci. 31, 495–511.

Shukla, S.P., Mishra, R., Chitranshi, A., 2015. Dynamics of Hamtah Glacier, Lahul & Spiti district, Himachal Pradesh. J. Ind. Geophys. Union. 19, 414–421.

Solomina, O.N., Bradley, R.S., Hodgson, D.A., Ivy-Ochs, S., Jomelli, V., Mackintosh, A.N., Nesje, A., Owen, L.A., Wanner, H., Wiles, G.C., Young, N.E., 2015. Holocene glacier fluctuations. Quat. Sci. Rev. 111, 9–34.

Solomina, O.N., Bradley, R.S., Jomelli, V., Geirsdottir, A., Kaufman, D.S., Koch, J., McKay, N.P., Masiokas, M., Miller, G., Nesje, A., Nicolussi, K., Owen, L.A., Putnam, A.E., Wanner, H., Wiles, G., Yang, B., 2016. Glacier fluctuations during the past 2000 years. Quat. Sci. Rev. 149, 61–90.

Spicer, Robert A., 2017. Tibet, the Himalaya, Asian monsoons and biodiversity – In what ways are they related? Plant Diversity. 39, 233–244.

Srivastava, P., Agnihotri, R., Sharma, D., Meena, N., Sundriyal, Y.P., Saxena, A., Bhushan, R., Sawlani, R., Banerji, U.S., Sharma, C., Bisht, P., Rana, N., Jayangondaperumal, R., 2017. 8000-year monsoonal record from Himalaya revealing reinforcement of tropical and global climate systems since mid-Holocene. Sci. Rep. 7, 1–10.

Steck, A., Epard, J.L., Vannay, J.C., Hunziker, J., Girard, M., Morard, A., Robyr, M., 1998. Geological transect across the Tso Morari and Spiti areas: the nappe structures of the Tethys Himalaya. Eclogae Geologicae Helveticae, 91, 103–121.

Stone, J.O., 2000. Air pressure and cosmogenic isotope production. Journal of Geophysical Research, 105, 23,753-23,759.

Stutz, E., Thöni, L.M., 1987. The lower Paleozoic Nyimaling x granite in the Indian Himalaya (Ladakh): new Rb/Sr data versus zircon typology. Geol. Rundschau 76, 307–315.

Su, Z., Shi, Y., 2002. Response of monsoonal temperate glaciers to global warming since the Little Ice Age. Quat. Int. 97–98, 123–131.

Sugden, D.E., John, B.S., 1976. Glaciers and Landscape. Edward Arnold: London.

Taylor, J.R., 1997. An Introduction to Error Analysis, 2nd edn. University Science Books, Sausalito, CA.

Taylor, P.J., Mitchell, W.A., 2000. The Quaternary glacial history of the Zanskar Range, north-west Indian Himalaya. Quaternary International, 65/66, 81-99.

Thompson, L.G., Mosley-thompson, E., Davis, M.E., Lin, P., Henderson, K., Mashiotta, T.A., 2003. Tropical glacier and ice core evidence of climate change on annual to millennial time scales. Climatic Change, 59, 137–155.

Thompson, L.G., Tao, T., Davis, M.E., Henderson, A., Mosley-Thompson, E., Lin, P.N., Beer, J., Synal, H. A., Cole-Dai, J., Bolzan, J. F., 1997. Tropical climate instability: the last glacial cycle from a Qinghai-Tibetan ice core. Science (80). 276, 1821–1825.

Uppala, S.M., Kållberg, P.W., Simmons, A.J., Andrae, U., Bechtold, V.D.C., Fiorino, M., Gibson, J.K., Haseler, J., Hernandez, A., Kelly, G.A., Li, X., Onogi, K., Saarinen, S., Sokka, N., Allan, R.P., Andersson, E., Arpe, K., Balmaseda, M.A., Beljaars, A.C.M., Berg, L. Van De, Bidlot, J., Bormann, N., Caires, S., Chevallier, F., Dethof, A., Dragosavac, M., Fisher, M., Fuentes, M., Hagemann, S., Hólm, E., Hoskins, B.J., Isaksen, L., Janssen, P.A.E.M., Jenne, R., Mcnally, A.P., Mahfouf, J.F., Morcrette, J.J., Rayner, N.A., Saunders, R.W., Simon, P., Sterl, A., Trenberth, K.E., Untch, A., Vasiljevic, D., Viterbo, P., Woollen, J., 2005. The ERA-40 re-analysis. Q. J. R. Meteorol. Soc. 131, 2961–3012.

van der Bilt, W.G.M., Bakke, J., Vasskog, K., D'Andrea, W.J., Bradley, R.S., Ólafsdóttir, S., 2015. Reconstruction of glacier variability from lake sediments reveals dynamic Holocene climate in Svalbard. Quat. Sci. Rev. 126, 201–218.

Vermeesch, P., 2009. RadialPlotter: A Java application for fission track, luminescence and other radial plots. Radiat. Meas. 44, 409–410.

von Rad, U., Schaaf, M., Michels, K.H., Schulz, H., Berger, W.H., Sirocko, F., 1999. A 5000-yr Record of Climate Change in Varved Sediments from the Oxygen Minimum Zone off Pakistan, Northeastern Arabian Sea. Quat. Res. 51, 39–53.

Wang, X., Auler, A.S., Edwards, R.L., Cheng, H., Cristalli, P.S., Smart, P.L., Richards, D.A., Shen, C.C., 2004. Wet periods in northeastern Brazil over the past 210 kyr linked to distant climate anomalies. Nature 432, 740–743.

Wang, Y., Cheng, H., Edwards, R.L., He, Y., Kong, X., An, Z., Wu, J., Kelly, M.J., Dykoski, C.A., Li, X., 2005. The Holocene Asian Monsoon: Links to Solar Changes and North Atlantic Climate. Science, 308, 854–858.

Wang, Y.J., Cheng, H., Edwards, R.L., An, Z.S., Wu, J.Y., Shen, C.C., Dorale, J.A., 2001. A high-resolution absolute-dated late Pleistocene Monsoon record from Hulu Cave, China. Science 294, 2345–2348.

Wanner, H., Mercolli, L., Grosjean, M., Ritz, S.P., 2015. Holocene climate variability and change: a data-based review. J. Geol. Soc. London. 172, 254–263.

Ward, D.J., Anderson, R.S., 2011. The use of ablation-dominated medial moraines as samplers for 10Be-derived erosion rates of glacier valley walls, Kichatna Mountains, AK. Earth Surf. Process. Landforms 36, 495–512.

Ward, D.J., Anderson, R.S., Guido, Z.S., Briner, J.P., 2009. Numerical modeling of cosmogenic deglaciation records, Front Range and San Juan mountains, Colorado. J. Geophys. Res. Earth Surf. 114.

Ward, D.J., Cesta, J.M., Galewsky, J., Sagredo, E., 2015. Late pleistocene glaciations of the arid subtropical Andes and new results from the Chajnantor Plateau, northern Chile. Quat. Sci. Rev. 128, 98–116.

Warren, C.R., Hulton, N.R.J., 1990. Topographic and glaciological controls on Holocene ice-sheet margin dynamics, central west Greenland. Ann. Glaciol. 14, 307–310.

Wünnemann, B., Demske, D., Tarasov, P., Kotlia, B.S., Reinhardt, C., Bloemendal, J., Diekmann, B., Hartmann, K., Krois, J., Riedel, F., 2010. Hydrological evolution during the last 15kyr in the Tso Kar

lake basin (Ladakh, India), derived from geomorphological, sedimentological and palynological records. Quat. Sci. Rev. 29, 1138–1155.

Yancheva, G., Nowaczyk, N.R., Mingram, J., Dulski, P., Schettler, G., Liu, J., Sigman, D.M., Peterson, L.C., Haug, G.H., 2007. Influence of the intertropical convergence zone on the East Asian monsoon. Nature 445, 3–6.

Yanhong, W., Lücke, A., Zhangdong, J., Sumin, W., Schleser, G.H., Battarbee, R.W., Weilan, X., 2006. Holocene climate development on the central Tibetan Plateau: A sedimentary record from Cuoe Lake. Palaeogeogr. Palaeoclimatol. Palaeoecol. 234, 328–340.

Young, N.E., Briner, J.P., Rood, D.H., Finkel, R.C., 2012. Glacier extent during the Younger Dryas and 8.2-ka event on Baffin Island, Arctic Canada. Science. 80, 337, 1330–1333.

Yu, Y., Yang, T., Li, J., Liu, J., An, C., Liu, X., Fan, Z., Lu, Z., Li, Y., Su, X., 2006. Millennial-scale Holocene climate variability in the NW China drylands and links to the tropical Pacific and the North Atlantic. Palaeogeogr. Palaeoclimatol. Palaeoecol. 233, 149–162.

Zhang, C., Mischke, S., 2009. A Lateglacial and Holocene lake record from the Nianbaoyeze Mountains and inferences of lake, glacier and climate evolution on the eastern Tibetan Plateau. Quat. Sci. Rev. 28, 1970–1983.

Zhou, S., Li, J., Zhao, J., Wang, J., Zheng, J., 2011. Quaternary Glaciations. Extent and Chronology in China. Dev. Quat. Sci. 15, 981–1002.

Zhu, L., Zhen, X., Wang, J., Lü, H., Xie, M., Kitagawa, H., Possnert, G., 2009. A ~30,000-year record of environmental changes inferred from Lake Chen Co, Southern Tibet. J. Paleolimnol. 42, 343–358.

Paper II

Solang, India

Photo credit: LAO

High-frequency Holocene glacier fluctuations in the Himalaya and Tibet

Sourav Saha [a] [1][*]**, Lewis A. Owen** [a]**, Elizabeth N. Orr** [a]**, Marc W. Caffee** [b]

[a] *Department of Geology, University of Cincinnati, Cincinnati, OH 45221, USA*
[b] *Department of Physics, Department of Earth, Atmospheric and Planetary Sciences, Purdue University, West Lafayette, IN 47907, USA*

ABSTRACT

Using a landsystems approach, sedimentology, detailed geomorphic mapping and 16 new and 503 published [10]Be surface exposure dating, we reconstruct Holocene glacial chronostratigraphies in 77 previously studied glaciated valleys spread across the Himalaya, Tibet, Pamir, and the Tian Shan. New studies in the Kulti valley of Lahul and Parkachik valley of the Nun Kun massif of the Himalaya of northern India indicate three advances at ~14.7, 12.2, 0.5 ka, in addition to one historically dated (late 19th Century) advance in the Kulti valley, and one Late Holocene advance at ~0.2 ka in the Parkachik valley. Our regional analyses suggest at least one late glacial (~15.3–11.8 ka) and five *Himalayan-Tibetan Holocene stages (HTHs)* at ~11.5–9.5, ~8.8–7.7, ~7.0–3.2, ~2.3–1.0, and <1 ka. The extent (amplitude) of glacier advances in 77 glaciated valleys has been reconstructed using equilibrium-line altitudes (ELAs). To objectively identify glaciated regions with comparable climatic characteristics and to evaluate the timing and extent of Holocene glacier advances across these regions, we also defined three major climatic groups (or five *climatic regions*) across the orogen using Cluster Analysis (CA) and Principal Component Analysis (PCA). Modern glacier hypsometries are also assessed to help explain the intra-regional variations in glacier amplitudes during each regional advance. Finally, a linear inverse glacier flow model was used to decipher the net changes in temperature (ΔT) between periods of reconstructed regional glacier advances in 66 glaciated valleys across different *climatic regions* of the orogen. The [10]Be, ELAs, and ΔT data suggest enhanced monsoonal humidity in the Early Holocene, followed by relative cooling and aridity in the Mid-

---

[1] * Corresponding author. 500, Geology-Physics, University of Cincinnati, Cincinnati, Oh 45221, USA.
E-mail address: sahasv@mail.uc.edu (S. Saha).

and Late Holocene. The sublimation-dominated cold-based glaciers in the north are more affected during this shift than the temperate glaciers in the south of the orogen.

1. Introduction

Studies of 20th and 21st Century glacier fluctuations throughout the Himalayan-Tibetan orogen indicate non-uniform retreat, and in some cases advance, of mountain glaciers due to warming and associated atmospheric changes (Bhambri et al., 2011; Bahuguna et al., 2014; Bhambri et al., 2017; Brun et al., 2017). Variable temporal and spatial responses of tropical-subtropical high-altitude glaciers to climate change present significant challenges for model predictions and environmental risk assessment (Barker, 2007; Cogley et al., 2010; IPCC, 2014). Defining past spatial fluctuations of high-altitude mountain glaciers across a variety of climatic and orographic settings in the orogen on millennial and sub-millennial timescales highlights issues relevant to the nature of future environmental change in Central Asia (Bolch et al., 2012; Vaux Jr. et al., 2012).

High-resolution glacial chronologies from glaciers in the Himalayan-Tibetan orogen can be used to test the hypothesis that the long-term pattern of Himalayan glacier advances is either in phase (or out) with glacier advances throughout the Northern Hemisphere, and elsewhere. Solomina et al. (2015, 2016) have proposed that the long-term pattern of Holocene glacier advances in the Himalayan-Tibetan orogen is not modulated by orbital forcing, but by regionally unique forcing factors. Recent studies by Saha et al. (2018), on the other hand, show that orbital forcing plays a significant role in driving Holocene glaciations in the northwestern part of the Himalayan-Tibetan orogen. Further research is required in other regions of the orogen to confirm these conflicting conclusions. Detailed glacial chronologies from other regions may further provide critical insights into the relative roles of climatic factors, which include: insolation driven movement of Earth's thermal equator; maritime influences; upper atmospheric circulation change and

ocean heat transfer (Solomina et al., 2015; Solomina et al., 2016; Saha et al., 2018); and non-climatic factors specific to each locality such as microclimate variability, topography, debris cover of glaciers, and glacier type (Barr and Lovell, 2014; Anderson et al., 2014). Previous studies (e.g., Dortch et al., 2013; Murari et al., 2014; Owen and Dortch, 2014; Solomina et al., 2015; Solomina et al., 2016) have compared Quaternary (mainly Pleistocene) glacial history across the Himalayan-Tibetan orogen, but a clear delineation of the inter-regional variability in glacier responses to identical climatic perturbation, especially during the Holocene, is lacking.

Holocene glacial records are generally better-preserved, can be dated to a higher precision than those for the Pleistocene, and may have a better potential for examining detailed glacier successions (Blomdin et al., 2016; Saha et al., 2018). Since we are specifically looking for variations in timing and amplitude of glacier fluctuations between glacial events, we treat every event individually and do not group events together, a technique employed for Pleistocene glaciation (cf. Zech et al., 2005; Schaefer et al., 2008). Given the lack of preserved organic materials required for radiocarbon dating, but the abundance of quartz-rich boulders on moraines, we use cosmic-ray-produced (cosmogenic) [10]Be surface exposure dating of multiple boulders to determine the age of individual landforms. Limited optically stimulated luminescence (OSL) studies also preclude us comparing glacial chronologies at the orogen-scale (cf. Bisht et al., 2017; Deswal et al., 2017). In this study, we have reconstructed Holocene glacial chronostratigraphies in two new study areas, as well as examining all previously published glaciated valleys throughout the orogen for which Holocene [10]Be ages are available (Fig. 1).

The two new study areas are located in the transitional northwestern Himalaya and include the Kulti valley in the Lahul Himalaya and the Parkachik valley in Nun Kun massif (Fig. 1A). These study areas preserve a series of young moraines and contain relatively large glaciers (>10-km-long). These glaciers are arguably more-erosive because they form broad U-shaped valleys, are melt-dominated, debris mantled, and located in a moderately wet micro-climatic zone with annual precipitation of ~200–900 mm/a (Bookhagen and Burbank, 2006; Azam et al., 2014). These study areas are well suited to test the hypothesis of Saha et al. (2018) that smaller cold-based sub-polar glaciers located in the semiarid climate setting of the

northwestern Himalaya tend to produce more scatter in the Holocene exposure ages. Additionally, glaciers in these two study areas are dominated by two prevailing climatic systems, the Indian summer monsoon (ISM) and the mid-latitude westerlies (Benn and Owen, 1998). The complex interplay of these systems influenced both the present and late Quaternary glacier advances/retreats in the adjacent valleys (Lee et al., 2014; Owen et al., 2001; L. A. Owen et al., 1997). These study areas may be key in evaluating the relative roles of the two dominant climate systems during Holocene glacial advances. Sediments and landforms of different origins are distinguished and mapped using a landsystems approach (Benn and Owen, 2002; Benn and Evans, 2010). Comprehensive Holocene glacial chronologies are developed in both the valleys using equilibrium-line altitudes (ELAs) and 16 [10]Be surface exposure dating.

We have also recalculated published [10]Be exposure ages from dated moraines in 77 valleys, shown in 36 locations of Figure 1, across the whole orogen. Using these published exposure ages (n=519) in conjunction with maps, equilibrium-line altitudes (ELAs), and ELA depressions (ΔELAs), we reconstruct the timing and amplitudes of Holocene glacial advances. We also measured present-day glacier hypsometries to explain variations in glacier amplitudes within a single climatic region. In conjunction with geomorphic maps, glacier geometry (Fig. 1B), [10]Be ages of moraines, and assuming that each moraine formation represents a steady-state scenario in 66 glaciated valleys, we also modeled the net change in past temperature in our study. We used a linear inverse glacier flow model of Klok and Oerlemans (2003) and Oerlemans (2001, 2005).

Our approach provides a comprehensive framework to i) examine the timing and spatial variability of Himalayan-Tibetan glacier fluctuations to Holocene climate change, ii) unravel the long-term and short-term forcings behind Holocene glacier fluctuations, iii) understand the climatic sensitivity of the high-altitude mountain glaciers in Central Asia, and perhaps; and iv) predict the response of these glaciers to future climate changes.

2. Physical Setting

Continued crustal shortening, the result of the collision and partial subduction of the Indian and Eurasian continental lithospheric plates since the early Miocene, initiated the development of a series of foreland propagating thrust systems and uplifted mountain ranges in the Himalaya (Searle et al., 1997). These mountain ranges throughout the Himalaya extend from ~400 to >7000 m above sea level (asl; Fielding et al., 1994; Duncan et al., 2003). The Greater Himalayan and Zanskar Ranges, bounded by the Main Central Thrust (MCT) to the south and the Indus-Tsangpo Suture Zone (ITSZ) to the north, constitute one of the highest mountain regions in the world (average >6000 m asl; Duncan et al., 2003). These mountains have had and continue to have a significant influence on past and present moisture supply; they are a barrier to incoming air masses (Owen et al., 1996; Burbank et al., 2012; Lee et al., 2014; Li et al., 2017).

Our two new study areas, the Kulti valley in Lahul and Parkachik valley in Nun Kun massif (Fig. 1A), are located in northern India on the NW trending southwestern slopes of the Greater Himalaya and northern flanks of the Zanskar Range, respectively. Kulti valley lies north of the Rohtang Pass (Fig 2A) and consists mostly of neo-terminal Proterozoic black slate, phyllite, and fine-grained biotite-schist of the Batal Formation (Kumar et al., 1987; Rawat and Purohit, 1988; Bhargava, 2008), with occasional Neoproterozoic to Permian granite (Steck, 2003). Leucogranite dated to 24–18 Ma and gneiss and quartzite metamorphosed from Paleo-Mesozoic Tethyan sedimentary rocks are present in the Nun Kun massif (Fuchs, 1997; Vance and Harris, 1999). Both study areas have abundant glacial and fluvial landforms, including U-shaped valley, moraines, debris and alluvial fans, talus slopes, glacially molded bedrock, river terraces, lacustrine and outwash plains, and glacial trimlines (Fig. 2).

The Kulti valley is in the rain shadow of the Pir Panjal Range. The valley presently receives most of its precipitation (>65%) from the ISM (Fig. 1A; Bookhagen and Burbank, 2006). Precipitation varies between ~200 and 900 mm/a from the valley floor to the higher reaches (Bookhagen and Burbank, 2006; Azam et al., 2014), producing a wet and cool transitional climate, conducive for the growth of steep, high-activity, debris-mantled glaciers (Fig. 2A; Owen et al., 1996, 1997). Contemporary steady-state ELAs vary

between ~4500 and 4800 m asl in the region (ibid; Chand et al., 2017) and glaciers are highly sensitive to changes in the ambient temperature (Bisht et al., 2017).

The Parkachik valley, a tributary of Suru valley, is located on north-facing slopes of the Nun Kun massif in the far west of the semiarid Zanskar Range (Fig. 1A, 2B). Topography strongly influence the precipitation gradient in the valley (Lee et al., 2014), with present-day precipitation varying between ~150 and 700 mm/a from the valley floor to the higher reaches (Bookhagen and Burbank, 2006). The massif has very steep slopes (>45°) rising to the high peaks of Nun at 7,135 and Kun at 7,077 m asl. Snow is delivered to the glaciers by avalanching and direct snowfall (Osmaston, 1994). In contrast to smaller sub-polar type glaciers elsewhere in Zanskar (Orr et al., 2017, 2018; Saha et al., 2018), the Nun Kun massif has a few large glaciers, including the ~12-km-long Parkachik glacier (Fig. 2A). Currently, the mid-latitudinal westerlies contribute ~55–58% of the total annual precipitation to the region (Fig. 1; Lee et al., 2014). Regional ELAs vary between ~5000 and 5600 m asl (Damm, 2006). A thin layer of debris mantles these glaciers.

Glacial chronostratigraphies for both study areas are poorly defined (Owen and Dortch, 2014). Previous studies have attempted to reconstruct glacial chronostratigraphies in the Chandra and adjacent valleys using cosmogenic (Owen et al., 2001; Eugster et al., 2016; Saha et al., 2018) and luminescence dating (Deswal et al., 2017; Saini et al., 2016). These studies show complex but extensive glaciation during ~20–17 ka (ca. global last glacial maximum [LGM] or ~chronozone 2 of Mix et al., 2001 or ~28–23 ka of Hughes and Gibbard, 2015), ~16–14 ka (ca. late glacial), and ~11.7–10 ka (ca. Early Holocene; supplementary material Fig. S1A). The oldest glacial stage in the Chandra valley, the Chandra glacial stage, as evidenced by ice-sculpted bedrock surfaces and bedrock benches at the altitude of 3150–4400 m asl, was not dated (Owen et al., 2001). Site-specific deglaciation, as recorded in polished bedrock and lodged boulders on drumlin surfaces, commenced between ~18 and 13 ka (Eugster et al., 2016; Saha et al., 2016). Our regional compilation, as shown in Figure S1A, also illustrates a sub-millennial-scale site-specific glacial response (advance/retreat) during ~18–13 ka. Besides, [10]Be dated glacier advances (recalculated in this study) at ~12.3±0.6 ka (the Kulti glacial stage of Owen et al., 2001), at ~10.1±0.4 ka (m_{H3} of Saha et al., 2018), at ~3.8±0.1 ka (Sonapani I stage of Owen et al., 2001) and <0.2 ka (m_{H1} of Saha et al., 2018),

are also proposed in the region. Historical photographs and trigonometrical maps of Geological Survey of India further indicate restricted glacier advances between 18th and 19th century (Walker and Pascoe, 1907; Owen et al., 1996, 1997, 2001; Harcourt et al., 2010; Raina et al., 2015; Saini et al., 2016).

In the Nun Kun massif, the ^{10}Be dated glacial history (recalculated in this study) indicates an extensive glacier advance which predates ~64.2–39.0 ka (Achambur glacial stage of Lee et al., 2014; Fig. S1B). Subsequent glacier advances are restricted and dated to ~21.2–17.0 (Tongul glacial stage), ~17.0– 15.0 and ~14.0–13.0 (Amantick glacial stage), and ~0.7–0.5 ka (Lomp glacial stage of Lee et al., 2014; Fig. S1B). The youngest set of lateral moraines which Lee et al. (2014) assigned to their Tanak glacial stage, were not dated in the massif. We have targeted these youngest set of moraines (M_{P1}) in this study.

Three biomes may be recognized within the study areas; sporadic coniferous trees (<3550 m asl); alpine meadow at the lower reaches (~3550–4850 m asl); and alpine tundra on the snow-free rock surfaces (>4850 m asl; Lee et al., 2014; Owen et al., 1996). Alpine meadows are dominated by grasses and shrubs, whereas lichens and mosses are the main alpine tundra vegetation.

3. Methods

3.1. Mapping and morphostratigraphy

Detailed geomorphic and surficial geologic maps were prepared using a GPS and digital mapping techniques in the field at the scale of 1:20,000 (±3m; Fig. 2). Google Earth imagery, Advanced Spaceborne Thermal Emission and Reflection Radiometer (ASTER) global digital elevation models (GDEMs), and Landsat Enhanced Thematic Mapper Plus (ETM+) imagery were used to refine these maps. We used the scheme proposed by Owen and Derbyshire (1989), Owen et al. (1997), Hughes et al. (2005), and Hughes (2010) to define our morphostratigraphy and its nomenclature. The letter 'M' refers to a moraine, with the subscript letter 'K' for Kulti and 'P' for Parkachik valleys, respectively. We used subscript '1' for the (morphostratigraphically) youngest of all preserved sets of moraines and the subscript letter 'a' for the

youngest ridge of a moraine set. A detailed account of these methods can be found in Orr et al. (2018) and Saha et al. (2018)

3.2. Geochronology

We carefully considered the morphostratigraphy, physical setting, e.g., stability, degradation, hillslope contamination, and surficial characteristics when choosing moraine boulders to sample. We avoided post-depositional surface deflection effects by choosing well-inset boulders on the crest of moraines (Fig. 3). The strong winds (5–15 km h^{-1}; Ramanathan, 2011) in this high-altitude environment likely preclude accumulation of snow and loess above boulders with heights of ~1 m or more (except for few samples; Table 1), minimizing the impact of shielding (<1%) on the cosmogenic nuclide inventory (Heyman et al., 2016). No sampled boulder showed any evidence of surface spallation, pitting, fracturing, and/or extensive weathering (see Fig. S2 for detailed characteristics). Approximately 500 g of rock to a depth of ≤5 cm from the top of each boulder was collected using a hammer and chisel (Table 1). We used compass and inclinometer to measure shielding from the boulder surface to the horizon at 10° interval. A detailed account of our field sampling procedure is provided in Orr et al. (2018) and Saha et al. (2018).

We performed quartz extraction and ^{10}Be sample preparation at the Quaternary Geochronology Laboratories of the University of Cincinnati following the methods outlined in Kohl and Nishiizumi (1992) and Nishiizumi et al. (1994). AMS measurements were performed at the Purdue Rare Isotope Measurement (PRIME) Laboratory at the Purdue University (Sharma et al., 2000). See supplementary material S3 and Saha et al. (2018) for more details.

Beryllium-10 exposure ages were calculated, and published ages were recalculated, using the community standard Cosmic Ray Exposure program (CREp) of Martin et al. (2017) and CRONUS-Earth V3 of Balco et al. (2008; Table S4). A global ^{10}Be production rate at sea level of 4.13±0.20 atoms/g SiO$_2$/a was used (Borchers et al., 2016; Martin et al., 2017). The relative differences among different age calculators are outlined in Saha et al. (2018). Exposure ages were calculated using the scaling schemes of Lifton-Sato-Dunai (*LSD*; Lifton et al., 2014), time-dependent Lal and Stone (*Lm*; Balco et al., 2008), and

time-independent Lal and Stone (*St*; Lal, 1991; Stone, 2000), but we only reported the CREp *LSD* ages in the text below. Saha et al. (2018) showed that the differences among different scaling schemes for Holocene [10]Be age are <10%. We assume zero-erosion rates and report all the ages in thousands of years (ka) before AD 2016 (Table 1; supplementary material S3, Table S4).

In our two new study areas, multiple boulders (2–6) were sampled from each moraine to constrain the exposure age of the moraine, and hence the minimum age of glacier advance (Gosse, 2005; Ivy-Ochs et al., 2007; Putkonen et al., 2008). For moraine ages from literature data we only used data if ≥2 concordant boulder ages were measured. We applied reduced chi-squared (χ^2) statistics to assess the distribution of ages (Applegate et al., 2010, 2012; Kaplan et al., 2013; Putnam et al., 2013b). Any age population with $\chi^2 > 1$ were believed to have outliers, and further statistical treatment was performed (cf. Saha et al., 2018). Chauvenet's criterion (Taylor, 1997; Dunai, 2010; Putnam et al., 2013b) was used to detect outliers. Outliers for our new study areas were only removed if convincing field evidence supports our statistical results, e.g., possible hillslope contamination, shallow burial, and/or toppling. We relied on statistical treatment and author's recommendations for published studies (see Table S4 for references) to detect and remove outliers. The simple arithmetic mean ± 1σ was used to define the mean moraine age and the age uncertainty.

Each morphostratigraphically distinct mean moraine age in a valley are reported here as *local glacial stages* (cf. Owen and Dortch, 2014; Saha et al., 2018). Probabilistic models suggest that each valley likely has ~30% probability (as recorded in moraines) to preserves its repeated advances from the same source (Gibbons et al., 1984; Kirkbride and Brazier, 1998; Kirkbride and Winkler, 2012). We, therefore, first defined climate regions (see section 'Climate Zonation'), i.e., regions with similar climatic characteristics and then compiled all *local glacial stage*s for each climatic region to reconstruct a complete regional glacial history. Using a combination of radial plotter and probability density function (kernel density or *'ksdensity'* fit in MATLAB), discrete population/Gaussians of local glacial stages are first identified. Student's t-test analysis is then applied to verify whether these selected population/Gaussians are statistically significant (≥95% confidence) and defined as *regional glacial stages* (cf. Dortch et al., 2013; Murari et al., 2014). We followed the formal Holocene stratigraphic subdivision approved by The

International Commission on Stratigraphy (ICS; Walker et al., 2012) to evaluate our *regional stages*. According to ICS, the Early Holocene span from 11.7–8.3 ka, the Mid-Holocene from 8.3–4.2 ka, and the Late Holocene from 4.2 ka to present. Additionally, we used the word *Himalayan-Tibetan Holocene stages or HTHs* to define our orogen-wide inter-regional glacial stages.

3.3. Equilibrium-line altitudes

Former ELAs are reported assuming a simplistic steady-state scenario (Sugden and John, 1976) and using area-altitude (AA), area accumulation ratio (AAR), and toe-headwall accumulation ratio (THAR) methods for each glacier advance (Table 2; Benn et al., 2005; Osmaston, 2005). The modern maximum elevations of lateral moraines (MELM; Nesje and Dahl, 1992) are reported to calculate present ELAs (Table 2). We obtained the AARs and THARs from the published literature for diverse *climatic regions* (see section 5.2.1 and Table S5). Different combinations of AARs (e.g., ranging from 0.45 to 0.80) and THARs (e.g., varies from 0.3 to 0.6) were used depending on the glacier setting, physical characteristics, and climate. See Table S6 for detailed ratios used for different *climatic regions* in this study. Herein we report the (arithmetic) mean ELA and ELA depression (ΔELA) with ± 1σ uncertainty, obtained from multiple indices and ratios (Table 2, S6).

We also evaluated the spatiotemporal distribution of ΔELAs across the orogen to get a clear insight into the relative strength of precipitation and temperature as a major forcing behind glacier oscillations (cf., Saha et al., 2018). We expect precipitation-sensitive cold-based sub-polar types of Himalayan-Tibetan glaciers (Fig. 4) to likely have significant ΔELAs during periods of increased precipitation and cloud albedo (diffusion radiation). Enhanced cloud albedo favors a decrease in incoming shortwave radiation and in conjunction with evaporative/sublimation cooling (latent heat transfer) foster negative energy balance, i.e., cooling by the dynamic response (Rupper and Roe, 2008; Rupper et al., 2009). Relative to cold-based glaciers, temperature-sensitive wet-warm temperate glaciers (Fig. 4) may likely respond with high ΔELAs during cold-dry climatic relapses (Bisht et al., 2017).

3.4. Glacier hypsometry

Modern glacier hypsometry was generated using ASTER GDEM (Fig. S7) for every 68 of the total 77 glaciated valleys for which present glacier ice and [10]Be ages are available. Herein they are designated as sampled glaciers and grouped (as in section 5.2.1). Since sizes of present glaciers vary widely across the orogen, glaciated areas were normalized using Z-Score (Mahmood, 2016) for comparison.

3.5. Climate zonation

To better compare the relative influence of prevailing climate systems on glaciers (Fig. 1) and inter-regional variances in the Himalayan-Tibetan orogen, a primary climatic zone map was reconstructed using >42500 mapped Central Asian glaciers, extracted from Randolph Glacier Inventory (RGI 6.0; RGI Consortium, 2017), and climate data (Fig. 4; New et al., 2002).

Monthly surface temperature maps were generated using the CRU CL 2.0 (10' latitude and longitude) reanalysis dataset for the period 1961–1990 (ibid). Due to poor resolution of the reanalysis data (ibid), we generated monthly precipitation maps from the Tropical Rainfall Measuring Mission (TRMM) data (4-km-horizontal x 250-m-vertical) for the period 1998–2009 (Bookhagen and Burbank, 2006). Nine climate parameters including annual mean temperature, annual temperature range, annual total precipitation, annual precipitation range, total summer monsoon precipitation, total winter precipitation, seasonality concentration index (SCI), dimensionless seasonality index (DSI), and relative entropy (RE), were derived from the monthly temperature and precipitation data (see supplementary material S8 for more details).

Sample glaciers used in our study extend from ~27° N to ~35° N and ~103°E to ~67 °E (Figs. 5A, S9)—the focus of our study. The climate data of the [10]Be dated sample glaciers that fall north of latitude ~35° N, i.e., valley locations 1–10 of Figure 1, are extracted separately from the CRU CL 2.0 dataset, largely because the gridded TRMM data is only generated up to 36° N (ibid). They are then included in the analysis.

Glaciers with identical climate were grouped using Cluster Analysis (CA; Zuming and Maohuan, 1989) and refined by Principal Component Analysis (PCA; Sagredo and Lowell, 2012; Seaby and Henderson, 2014) in the R statistical package (The R Core Team, 2018). Using the Euclidean distance and the unweighted pair-group method with arithmetic averaging (UPGMA; Romesburg, 2004), we produced a cluster dendrogram (supplementary material S8) by grouping the most analogous samples (glaciers). To test the significance of our clusters (groups), we calculated the cophenetic distance between two samples (glaciers) in the cluster dendrogram and performed a Pearson's product-moment correlation between the sample Euclidean and cophenetic distances (Seaby and Henderson, 2014; supplementary material S8). Also, we performed an analysis of similarities (ANOSIM; ibid) to test whether the samples (glaciers) within groups are more similar than would be expected by random chance (supplementary material S8).

3.6. Modeling past temperature

We reconstructed the Holocene temperature changes (T in K) for 66 of the total 77 high-altitude Himalayan-Tibetan glaciated valleys using the medial length, average slope, and annual total precipitation of the respective glacier. Past atmospheric temperatures (T) were not reconstructed for the remainder 11 study areas because essential parameters, e.g., existing glacier ice cover, well-defined laterofrontal and/or end moraines to reconstruct glacier geometry, moraine (^{10}Be) ages, and availability of reliable (contemporary) climate variables, were not met.

A linear inverse glacier flow model was used following the methods of Klok and Oerlemans (2003) and Oerlemans (2001, 2005). This flow model is based on the first-order glacier dynamics (Oerlemans, 2001, 2005); the constants are generated using data from 169 globally distributed glaciers since AD 1700 (ibid). The constants do not vary significantly across different glacier types and different regions (see ibid). We, therefore, use these constants for this study. Unlike more explicit numerical glacier/ice sheet models, that require many complex geologic, climatic, and energy balance variables (cf. Azam et al., 2014; Roe and Baker, 2014; Rounce et al., 2015) and are often catchment specific (cf. Carr et al., 2010; Eaves et al., 2016; Pellitero et al., 2016; Aaron E. Putnam et al., 2013), the current model requires a limited number of variables

113

and hence it is easy to reconstruct for a wide range of Himalayan glaciers and widely different *climatic regions* throughout the orogen. Although the model has its limitations for site-specific applications and should be used cautiously (Oerlemans, 2005), we argue that we are more interested in capturing the inter-regional pattern of net temperature (Δ*T*) change during Holocene glacier advances throughout the orogen and hence, is suitable for average broadscale spatiotemporal analysis.

Also, the linear flow model considers climate sensitivity (*c*) and response time (τ) of the glacier to estimate the lag time (see supplementary material S10 for more details about *c* and τ). If ambient temperature primarily drives glacier fluctuations on a continental scale, climate sensitivity (*c*), therefore, can be defined as the decrease in equilibrium glacier length per degree (Kelvin) increase in temperature (ibid). A simple linear response equation is, therefore, proposed (ibid):

$$\frac{dL(t)}{dt} = -\frac{1}{\tau}\left[cT(t) + L(t)\right] \qquad (1)$$

Here, *T* is a temperature perturbation (e.g., annual mean), *t* is time, *L* is the medial glacier length with respect to present snout position. Assuming a simple glacier advance scenario, we measured respective mean moraine age and distance from the snout to calculate *t* and *L*, respectively. *dL* is the linear interpolation over ten years (*dt*) interval. *c* and τ were determined from a first-order glacier dynamics theory (see supplementary material S10 for details) and explicitly explained in Schmeits and Oerlemans (1997), Oerlemans (1997, 2001), and Oerlemans et al., (1998). We individually calculated *c* and τ for each glacier, and hence, distinct for cold-based/polythermal/temperate glaciers.

The inverse model to solve for *T*, thus, can be stated as:

$$T(t) = -\frac{1}{c}\left[L(t) + \tau\frac{dL(t)}{dt}\right] \qquad (2)$$

This linear inverse glacier flow model uses present annual precipitation to estimate *c* and τ of the individual sample glacier; see supplementary material S10 to measure *c* and τ. Past change in annual

precipitation would, therefore, likely result in changes in c and τ. Proxy and model studies based on lake shorelines and $\delta^{18}O$ also showed that precipitation increase in the western and interior Tibet was ~55–200% higher than present during the Early Holocene (Huth et al., 2015; Li et al., 2017; Shi et al., 2017). Since it is challenging to quantify the spatiotemporal evolution of past precipitation, we added ±30% uncertainties to c and τ to account for this unknown error of the model. Additional limitations of the model are also presented in Oerlemans (2005). Further error estimate was made by combing T for sample glaciers in a climatic region and measuring a mean±1σ from the data (see supplementary material S10). Following the recommendation of Putnam et al. (2013), we only present net temperature (ΔT) change in the text.

4. Detailed study areas

4.1. Kulti valley

Kulti valley is flanked by <10-km-long Sonapani (Sona=Golden, Pani=Water) glacier in the upper reaches (>4000 m asl). This debris-mantled glacier, covering ~32.5 km^2, consists of five hanging glaciers that merge into a valley glacier that tapers into a narrow ice fall at ~3860 m asl and creates a V-shaped gorge above the icefall (Figs. 2A, 5A, S11A, B). Five sets of morphostratigraphically distinct moraines were identified and mapped in the valley (Figs. 2A, S2). These five sets of moraines (e.g., M_{K1}, M_{K2}, M_{K3}, M_{K4}, M_{K5}) in Kulti valley are traversed by a ~9-km-long meltwater stream, called Dugli Nala (Figs. 2A, S11C, D, I, J).

M_{K1}, located at ~3700–4000 m asl, is a ~1.8-km-long discontinuous SE trending laterofrontal moraine set (Fig. S11A). The furthest laterofrontal ridge of the moraine is ~2.9 km from the glacier snout (Fig 2A). Glacial trimlines are present in the opposite flank of the valley (Figs. 2A, S11A). Inset within the moraine is several <5-m-high NE-SW trending ~100-m-long hummocks (Fig. S11B). No stable, suitable boulders were found to sample for dating. Figure S2 presents detailed moraine and boulder characteristics.

Two subdued NE trending ~5-m-high and ~150-m-long rounded lateral moraine ridges are present ~0.9 km from M_{K1}, at altitudes of ~3669–3676 m asl. M_{K2} moraine ridges (M_{K2a}, M_{K2b}) are covered with grasses (Figs. S2, S11C, D). Two boulders were sampled from the M_{K2b} ridge (Figs. 2A, B; 3C, D).

An NW trending terminal moraine ridge, M_{K3}, is present ~2.14 km from M_{K2}, at an altitude of ~3638–3640 m asl (Figs. 2A, S11E). This ~30-m-high and ~450-m-long moraine ridge is referred to as Rataskal terminal moraine by Raina et al. (2015). No samples for dating were collected from M_{K3}, since post-depositional hillslope deposits may have superimposed the original terminal moraine (Figs. S2, S11E, F). A broad braided channel with lacustrine deposits is present upstream of M_{K3}, likely formed by damming of the moraine (Raina et al., 2015).

M_{K4} moraine set, ~0.9 km from M_{K3} at an altitude of ~3426–3500 m asl consists of three NE trending rounded lateral ridges (Fig. S11G, H). Four boulder samples were collected from M_{K4b} and M_{K4c} lateral ridges (Figs. 2A, C, 3A, B, S2). These ridges are ~20-m-high and ~500-m-long and mainly preserved in the NW of Dugli Nala. A subdued lateral moraine ridge to the SE is mostly buried under hillslope deposits (Fig. 2C).

A sharp-crested laterofrontal moraine set, M_{K5}, ~1.25 km from M_{K4}, is at an altitude of ~3164–3270 m asl. The moraine set trends NE with a sharp westward swing at the front (Fig. S11I). While the NW ridge is ~0.45-km-long and does not contain any large boulders, the SE ridge is ~1.1-km-long and contains several larger boulders (Figs. S2, S11J). We sampled six boulders from this grass-covered ridge (Fig 2A, C). Because of the narrow valley mouth, we expect hillslope contamination on the moraine surface (Fig. S11I). The moraine morphology and presence of lacustrine sediments capped with fluvial and debris flow sediments to the east of the moraine, likely indicate blocking of the main Chandra valley by the glacier (Owen et al., 1997).

4.2. Parkachik Valley

A large accumulation area (74%) and high steep peaks of Nun and Kun feed the ~12-km-long Parkachik glacier in the Parkachik Valley, the largest glacier in the massif (Figs. 2D, S11K). This glacier

is unique in the Zanskar Range due to its large size and extent (Lee et al., 2014). The glacier extends into four tributaries in the higher reaches (Fig. 2D). There are three other cirque glaciers on the northern flanks of the Nun Kun massif, from west to east these include Tarangoz, Rantac, and Sentick glaciers. The moraines of these glaciers were previously dated by Lee et al. (2014) using ^{10}Be. Two moraine sets of Parkachik glacier were mapped based on morphostratigraphy, M_{P1}, and M_{P2}.

M_{P1} is the youngest laterofrontal moraine set with two ice contact ridges at an elevation of ~3595–3730 m asl (Figs. 2D, E, S11K, L). M_{P1a} is closest to the glacier and presently unstable (Fig. S11L). The ~0.6-km-long sharp-crested west lateral ridge of M_{P1b} was sampled (Figs. 2D, E, 3E, F, S2). This moraine ridge is well preserved and stabilized by a bedrock ridge (Fig. S11K), away from hillslope deposits, and steep (20–42°) and ~70 m high. The moraine flank facing the glacier is currently undergoing base erosion by the meltwater stream (Fig. S11L). We sampled four stable tabular boulders from this ridge (Fig. 3E, F). The eastern lateral ridges are ~1.3 km long with no suitable boulders for sampling.

M_{P2} moraine set, located outside of M_{P1} to the east, consists of four grass-covered rounded ridges (Fig. S11K, M). These are steep, ~30-m-high, <0.35-km-long and discontinuous, and more of bedrock-cored ridges than moraines. One of the outer bedrock-cored ridges supports the west lateral ridge of M_{P1} moraine (Fig. S11K). The bedrock-cored ridges contain thin veneer of matrix-supported pebbly diamicton that overlay the polished and weathered bedrock surfaces. Due to the lack of suitable boulders for dating, we did not collect any samples from this moraine (Fig. S2).

5. Results

5.1. Local glacial analyses

5.1.1. Dating results: Kulti valley

The oldest M_{K5} laterofrontal moraine ridges were previously assigned to the Kulti glacial stage by Owen et al., (1996, 1997, 2001) based on their morphostratigraphic position and relative dating. Their Kulti

glacial stage was dated, using ^{10}Be (recalculated here), elsewhere in Lahul to ~12.3±0.6 ka (or 13.7±1.3 ka of Eugster et al., 2016). We have dated six boulders from the SE moraine ridge (Fig. 5A). Our ^{10}Be ages range from ~16.1–1.2 ka (Table 1, S4) showing large dispersion (χ^2=464) and possible (expected) hillslope contamination. We discarded four young ages (samples S19, S20, S23, and S24) from further analysis. Remaining ages offer a tentative (with only two ages) mean age of 14.7±2.1 ka.

Four sampled boulders on the M_{K4} moraine present an age clustering with a χ^2 of 2 (Table S4). Ages in the distant moraine ridges (M_{K4b} and M_{K4c}) spread between ~13.0 and 10.9 ka (Table 1), with a mean age of 12.2±1.0 ka (Fig. 5A).

No ages are available for our M_{K3} terminal moraine (Fig. 5A), which Owen et al. (1996, 1997, 2001) previously ascribed to the Sonapani I glacial stage based on relative dating.

Two boulders were dated on the young M_{K2} moraine. The ages range from ~0.6 to 0.4 ka (Table 1; S 4). We have ascribed a tentative (since only two boulders were dated) mean age of 0.5±0.2 ka to this moraine set (Fig. 5A).

The formation of the M_{K1} moraine complex predates AD 1906 (Fig. 4A) based on the photograph taken by Walker and Pascoe (1907 in Raina et al., 2015). According to their description, the glacier snout was at ~3711 m in AD 1906, only a few hundred meters up-valley from the lowest moraine ridges of M_{K1} moraine complex (see Fig. 15, page 38 of Owen et al., 1996). Owen et al. (1996, 1997, 2001) assigned this moraine to their Sonapani II glacial stage, a late 19th Century advance.

5.1.2.   Dating results: Parkachik valley

Ages for the ice-contact M_{P1} moraine form a tight cluster within the age range of ~0.2 to 0.1 ka (Table 1, S4) and a χ^2 value is 5.4 (acceptable at 95% confidence interval). We calculate a mean age of ~0.2±0.1 ka for this lateral moraine (Fig. 5B). Lee et al. (2014) could not date the youngest ice-contact moraine (TG4) in the Tarangoz valley in the Nun Kun massif, adjacent to Parkachik glacier (Fig. 2D). Their youngest dated moraine, TG3, is dated to ~0.6±0.1 ka (Table S4). We suggest that the M_{P1} moraine likely represents the youngest local glacial advance in the massif.

Röthlisberger and Geyh (1985a, b) used ^{14}C dating of humic acid to date the Parkachik moraine to 5055±381 cal yr BP (recalibrated using CALIB 7.1 of Stuiver et al. 2018). We were unable to find any organic materials in both M_{P1} and M_{P2} moraine sets to verify these ^{14}C ages.

5.1.3. Reconstructed ELAs and net temperature change

Sonapani glacier in the Kulti valley extended ~10 km from its present position (Fig. 1B) at ~14.7 ka with a ΔELA of 259±109 m (Table 2; Fig. 5A).

A subsequent ~7.6 km advance (Fig. 1B) at ~12.2 ka represents a ΔELA of 186±62 m (Table 2; Fig. 5A) in the valley and comparable to the Early Holocene glacier advance (ΔELA ~182 ± 57 m at ~10.5 ka) in the adjacent Hamtah valley (Saha et al., 2018). According to the inverse glacier flow model, between ~14.7 and ~12.2 ka a net temperature increase of 2.7±0.2 K is estimated (58.7% of the total increase).

Our undated Rataskal terminal moraine (M_{k3}), located ~6.5 km (Fig. 1B) from the present snout, had a ΔELA of 127±38 m.

Sonapani glacier also advanced ~4 and ~3 km (Fig. 1B) from the present snout during the Late Holocene at ~0.5 ka and late 19th Century, resulting in restricted ΔELAs of 106±30 and 92±31 m, respectively. We calculated a net ambient temperature increase of 0.9±0.2 (-7.3±0.4 to -6.4±0.2 K; 19.6%) and 1.0±0.2 K (-6.4±0.2 to -5.4±0.0 K; 21.7%) for ~12.2–0.5 ka and ~0.5–0.1 ka, respectively. Between ~0.1 ka advance and present, a net temperature increase of ~0.5 K.

The glacier only extended ~0.3 km (Fig. 1B) from its present snout at ~0.2 ka with a ΔELA of 20±9 m in the Parkachik valley (Table 2; Fig. 5B). We calculated a net temperature increase of 0.5±0.1 K since ~0.2 ka.

5.2. Regional analyses

5.2.1. Climatic groups and climatic regions

Previous studies have shown a latitudinal gradient of contemporary snowlines (Benn and Owen, 1998; Owen and Benn, 2005; Yao et al., 2012) and longitudinal and latitudinal variations of prevailing climatic systems (Vaux, Jr. et al., 2012) across the Himalaya and Tibet. While the winter mid-latitude westerlies significantly influence the western end of the Himalaya and Tibet (Mölg et al., 2014), the ISM and East Asian Summer Monsoon (ESM) largely dominate the southern and eastern (maritime) regions, and to a limited extent the interior (continental) portions of the orogen (Fig. 1A; Jin et al., 2014). Three broad types of glaciers have been proposed which include wet and warm temperate glaciers, sub-polar (cold) arid-semiarid glaciers, and polythermal transitional glaciers (Fig. 4; Derbyshire et al., 1991; Yang et al., 2009; Shangzhe et al., 2010; Yao et al., 2012; Zhu et al., 2013). The temperate glaciers are mostly melt-dominated, thick debris-mantled and have low-altitude snowlines (ibid). They are more susceptible to changes in temperature. The cold arid-semiarid glaciers, in contrast, are sublimation dominated, usually debris-free, and located at higher altitudes (ibid). These types of glaciers are more sensitive to changes in precipitation. Polythermal transitional glaciers are intermediate between cold and temperate glaciers.

While local altitude, relief, aspect, hypsometry, microclimate, pre-existing topography, debris cover, and slope deposits play a crucial role in determining individual glacier dynamics at the catchment-scale (Roe, 2011; Barr and Lovell, 2014), climate likely plays a first-order role in defining glacier characteristics at the scale of $>10^3$ km (cf. Sagredo and Lowell, 2012). We capture these glacier-types using a comprehensive climatic zone (group) map (Fig. 6).

Our CA dendrogram shows five major groups of glaciers (Fig 6A). These include:

- *Group 1* includes mostly sub-polar cold arid-semiarid glaciers, spreading across the NW Himalaya; the western and interior Tibet, and parts of Pamir and Tian Shan (Fig. 6B). Nearly 59.6% of sample glaciers fall in this group.

- *Group 2* encompasses 32.9% of the sample glaciers. These glaciers are transitional and distributed across the Karakoram, the Great Himalaya, and edges of the south, eastern and NE (maritime) Tibet (Fig. 6B).

- *Group 3* consists typically of warm-wet temperate glaciers, spreading across the southern edges of *Group 2*, i.e., along the Lesser Himalaya, SE Tibet, and in sporadic pockets of high precipitation. Approximately 3.4% of sample glaciers fall into this group (Fig. 6B).

- *Group 4* which consists of 3.5% of the sample glaciers, are mainly a humid transitional type and located in the further south and pockets of very high precipitation (Fig. 6B).

- *Group 5* is likely the most warm-wet type of glaciers (0.6%) and distinctly located along the southern Nepalese Himalaya and in some small locus of regionally high-peaks (Fig. 6B).

A strong positive correlation (0.69 at 95% confidence level) exists between Euclidian and cophenetic distances in the dendrogram, further supporting the CA clustering (Fig. 6A). An ANOSIM test also yielded a high R-value (0.73) at 99% confidence level which supports the hypothesis that the samples within groups are more similar than by random chance.

We have also refined our CA groups by running PCA (Table 3; Fig. 6C). Our first three principal components (PCs) explain ~88% of the total variance in the sample glaciers. We infer that PC1 (53% of the total variance) corresponds strongly and positively to annual total precipitation, annual precipitation range, and DSI (Fig. 6D, Table 3). The influence of temperature parameters is only partial and limited (Fig. 6D). Similarly, PC2 (26%) agrees more closely and negatively to summer monsoonal precipitation, RE, and SCI and positively to winter (westerlies) precipitation (Fig. 6D, Table 3). PC1 appears to track the climate at the glacier locations whereas PC2 reflects the seasonal variability. Based on the sensitivity analysis, the groups at the regional-scale are more susceptible to changes in precipitation parameters.

The PCA yielded similar results to the CA (see Fig. 6), suggesting robustness in the analysis. The first three principal components (Fig. 5C; Table 3) also suggest that the groups are distinct from each other except for *Group 4*. The *Group 4* (humid transitional climate) overlaps closely with *Group 2* (Fig. 6C). Similarly, *Group 5* only encloses a few (0.6%) warm-wet southern glacier, possibly representing end members. For the purpose of this study, we, therefore, ignore *Group 4* and *5* and focus on latitudinally distinct *Group 1–3* for the rest of the analysis.

Our statistical treatment does not capture the longitudinal climate zonation, i.e., maritime versus continental. The glaciers located in the NE and SE of the orogen are more sensitive to tropical maritime changes than the glaciers in the NW. Similarly, glaciers in the southern central part receive more moisture than glaciers in the NW part of the orogen. Sutlej river basin is considered the maximum extent of the mid-latitudinal westerlies (Vaux, Jr. et al., 2012). Since the longitudinal climatic gradient is crucial for our inter-regional analysis, additional climate variables, such as annual snowfall and $\delta^{18}O$ distribution, may be required to refine our initial climate groups.

Similarly, the published and new [10]Be dated moraines used in this study are limited (0.002% of the total 42511 glaciers) and disproportionately distributed with large longitudinal gaps (i.e., sample glaciers) across the orogen (Figs. 1A, 6B). For example, a large longitudinal hiatus exists between NW and western Himalayan sampled glaciers. The longitudinal gap is also prominent between western and central Himalayan glaciers. We, therefore, did not group, e.g., all the arid and semiarid glaciers of the NW and NE part of the orogen into a single category, but further subdivided the *Group 1–3* to accomplish the objective of the analysis, that is to compare Holocene glacier advances inter-regionally. Based on the availability of [10]Be dated moraines, following climatic subdivision, thus, is proposed and defined herein as *climatic regions*. This framework (five *climatic regions*) is used throughout the text.

- *Group 1*: Arid and semiarid colder climatic region—(a) Transhimalaya, NW Tibet, Pamir, and Tian Shan, and (b) southern and northeastern Tibet,

- *Group 2*: Transitional climatic region—(a) western Himalaya, (b) central and eastern Himalaya, and

- *Group 3*: Wet and warm climatic region—central and eastern Himalaya (since no moraines in the western Himalaya are [10]Be dated).

5.2.2. *Regional glacial stages, ELAs, and hypsometries*

Within a broad climatic region, variability in reconstructed past and contemporary ELAs at the catchment-scale may be attributed to variable glacier hypsometries and corresponding (altitudinal)

temperature gradient (Blomdin et al., 2016). Since glacier hypsometry is arguably influenced by a variety of factors including relief and terrain conditions, and microclimate, we further evaluated the intra-regional variability of glacier extents by assessing the average glacier hypsometries and ELAs (Table 4; Fig. S7).

Group 1(a): Arid and semiarid colder climatic region— *Transhimalaya, NW Tibet, Pamir, and Tian Shan*. Based on average hypsometry and contemporary ELA distributions of the sampled (^{10}Be dated) glaciers in the climatic region, we identified four distinct subgroups of glaciers (Table 4; Fig. S7). These include the Muztag Ata massif of the NW Tibet, the Pamir and the Tian Shan, the Karakoram, and the Ladakh and the Zanskar ranges; the major orographic barriers. A summary of ELAs and hypsometric distributions (toe to cirque head) of these glaciers is provided in Table 4 and Figure S7. These wide-ranging glacier hypsometries and ELAs likely play a crucial role in determining variable glacier responses and amplitudes to identical climatic perturbations.

Two tentative and five major stages of glacier advances are identified using 47 local glacial stages from 15.0 to 0.2 ka (Table 5; Fig. 7). A distinct (7.5% age dispersion) regional glacier advance occurred during the late glacial (15.2–11.7 ka; Figs. S12A, S13A); a tentative (n=2) one in the Early Holocene (10.3–9.7 ka with 0% age dispersion; Figs. S12A, S13B); a well clustered (0% age dispersion) one in the upper Mid-Holocene at 8.0–7.7 ka (Figs. S12B, S13C); in the latter part of the Mid-Holocene and Late Holocene at 6.6–3.5 ka (23% age dispersion; Fig. S12B); and three during the Late Holocene at 2.3–1.3, ~1 (tentative), and <1 ka (28–39% age dispersion; Figs. S12C, D, S13E). For the <1 ka regional advance, we argue that multiple overlapping local glacier advances at the century-timescale are probable (Fig. S12D). We are unable to distinguish further regional sub-stages for this period (Fig. 7). A summary of our glacial stage statistics including local mean moraine ages, regional stages, probability peaks, probability density fit using ksdensity function, and P $_{(sig2-tailed)}$ are provided in Table 5.

Extensive ΔELAs are recorded in the late glacial (~300±300 m) and Early Holocene (~670±160 m; Table S6, Fig. 7). Subsequent ΔELAs are progressively restricted over time (i.e., ~355±235, ~270±140, ~100±65, ~40±30, and ~100±95 m; Table S6, Fig. 7).

Group 1(b): Arid and semiarid colder climatic region—*southern and northeastern Tibet.* The sample glaciers in this region, from the toe-to-cirque head, have a hypsometric distribution between ~4500 and 6590 m asl (Fig. S7) and ELA distribution between ~4407 and 5259 m asl (Table S6).

Based on only eight local glacial stages, two prominent and two tentative regional stages are reconstructed (Fig. 7). Regional glacier advances are recorded during the late glacial (13.5–12.9 ka; Fig. S12K), Early Holocene (11.5–9.5 ka; Fig. S12K), Mid-Holocene (~8.0 ka; Fig. S12L), and Late Holocene (~3.3 ka; Fig. S12L). The ~8.0 and ~3.3 ka regional glacial stages are tentative (n=1; Table 5).

Extensive ΔELAs are recorded in the late glacial (~590±200 m), followed by progressively restricted glacier advances in the Holocene (ΔELAs: ~160±35, ~170±70, and ~80±70 m; Table S6, Fig. 7).

Group 2(a): Transitional climatic region—*western Himalaya.* We have identified two distinct hypsometric subgroups of glaciers in this region based on their average toe-to-cirque head distribution (Table 4; Fig. S7) and ELAs (Table S6). They are more monsoon-influenced glaciers in the Garhwal Himalaya and transitional glaciers in the Nun Kun, Lahul, and Gurla Mandhata (Table 4; Fig. S7).

Two tentative and four major stages of regional glacier advances are identified based on 37 local advances during the late glacial and Holocene (Fig. 7; Table 5). Glaciers advanced extensively between 15.3 and 11.8 ka (ΔELAs 335±215 m; Table S6, Figs. 7, S12E, S13H), progressively restricted during the Early Holocene at 11.1–10.3 (ΔELAs 285±165 m; Table S6, Figs. 7, S12E, S13I) and 8.8–8.3 ka (ΔELAs 170±185 m; Table S6, Figs. 7, S12F), the Mid-Holocene at 6.1–5.0 ka (9.3% age dispersion; ΔELAs 190±85 m; Table S6, Fig. 7), and the Late Holocene at ~2.2 and <1 ka in the region (ΔELAs 30±10 m; Table 5, S6, Figs. S8G).

The ~2.2 ka advance in highly tentative (n=1) and hence, are not considered here (Fig. 7). The 16 local glacier advances during <1 ka, however, are highly scattered (79% dispersion) and bimodal (Fig. S12G). We refrain from assigning any peak stage/sub-stage.

Group 2(b): Transitional climatic region—central and eastern Himalaya. Two subgroups of glaciers are demarcated based on their general hypsometries (Table 4; Fig. S7) and ELAs (Table S6). They are the Central Himalayan transitional glaciers (e.g., Nyalam, Khumbu, and Rongbuk) and the Eastern Himalayan transitional glaciers (e.g., Renhe, Baishui, Ganheba, and Hailuogou).

The number of reconstructed local glacial stages for this region is limited (n=11; Table 5). Based on the available ^{10}Be ages, three tentative (~13.5, ~2.1–1.0, and <1 ka) and two prominent (11.5–10.1 and 6.0–3.2 ka) regional glacial stages are recognized (Table 5; Figs. 7, S12J).

The estimated ΔELAs are ~145±180 m at 6.0–3.2 and only ~65±55 m during the last 1 ka (Fig. 7). The ΔELAs during rest of the regional stages are highly speculative and tentative (Table S6).

Group 3(a): Wet and warm climatic region—central and eastern Himalaya. All sample glaciers in the region have average hypsometric distribution from ~3930–6590 m asl (toe-to-cirque head) and ELA distribution (~4440–5584 m asl; Table S6), except few smaller cirque glaciers (Table 4).

Two tentative and three major regional stages of glacier advances are reconstructed between the late glacial and the Late Holocene using 18 local glacier stages (Table 5; Fig. 7). Extensive local glacier advances are reconstructed during the late glacial-Early Holocene transition at 13.0–10.9 ka (ΔELAs ~625±455 m; Table S6, Figs. 7, S12H), followed by restricted advances in the Early Holocene at 9.5–8.7 ka (age dispersion 6.3%; ΔELAs ~330±180 m; Table S6, Figs. 7, S12H, S13M). However, the Mid-Holocene glacier advances at 7.0–4.4 ka (dispersion 9.2%; Figs. S12I, S13N) are significantly more extensive (ΔELAs ~515±270 m; Table S6, Figs. 7,) than the two tentative Late Holocene advances at ~1.7 (n=1) and <1 (n=2) ka (ΔELAs ~150±65 m; Table 5, S6, Figs. 7, S12I) in the climatic region. An Early Holocene regional advance (~10 ka) might have occurred which is distinct from the late glacial (~12.5 ka) advance. Additional numerical ages are required to improve the chronostratigraphy further.

5.2.3. *Past Atmospheric Temperature Changes*

The modeled past temperature change based on glacier geometry is relatively better reconstructed for ages <9.5 ka for all *climatic regions* (Fig. 8). For ages >9.5 ka, the number of glaciers (n) used is very low (1–5), except in the Transitional (*Group 2*) and Humid (*Group 3*) *climatic regions* (Fig. 8), giving overall lower confidence in our model results for late glacial advances. Since enhanced precipitation, relative to the present, prevailed during the Early to Mid-Holocene (Fig. 7), we also argue that 30% positive precipitation increase scenario is likely a better representative for the modeled *T*.

Group 1(a): Arid and semiarid colder climatic region— Transhimalaya, NW Tibet, Pamir, and Tian Shan. The reconstructed regional atmospheric temperature (n=24) for this region indicates a net temperature (*ΔT*) change of -3.1±0.1, +1.7±0.2, -1.1±0.2, and -2.1±0.5 °C (note: for the ease of interpretation, *ΔT* K is expressed as *ΔT* °C) during 14.0 to 12.7, 12.7 to 11.7, 11.7 to 9.7, and 9.7 to 7.7 ka, respectively (Fig. 8). Because very few suitable older local glacial stages (n=2–4) are used to estimate regional *T* for these periods, our model results are tentative. We recommend further research to verify our initial model results.

We estimated a significant *ΔT* increase ranging from ~1.9 (±1.1) to 6.0 (±0.7) °C between the early Mid- (8.0–7.7 ka) and Mid- to early Late Holocene (6.6–3.5 ka) regional glacial advances (Fig. 8). During the subsequent Late Holocene regional glacial stages, i.e., ~3.5 to 2.3–1.3 ka and 2.3–1.3 to 1.0 ka, the *ΔT* increase is estimated to ~1.0±1.3 and ~0.5±0.3 °C, respectively (Fig. 8). During the latest 1.0 to 0.2 ka regional glacial advance, however, the *ΔT* rise is unprecedented in the climatic region (~1.4±0.9 °C; Fig. 8).

Group 1(b): Arid and semiarid colder climatic region—southern and northeastern Tibet. Only four suitable (glacier) geometric data were used to reconstruct regional past temperature change in the region (Fig. 8). A tentative (n=1) regional *ΔT* decrease of 0.9±0.1 °C is estimated during the Early and Mid-Holocene regional glacial advances, i.e., between 10.0–9.5 and ~8.0 ka, respectively (Fig. 8). However, a *ΔT* rise ranging from ~1.9 (±1.1) to 2.7 (±0.7) °C is reconstructed between the Mid- (~8.0 ka) and Late Holocene (~3.3 ka) regional glacial advances (Fig. 8).

Group 2(a): Transitional climatic region—western Himalaya. Based on 20 local glacial advances, we modeled the past temperature change in the region. The ΔT increase is estimated to ~0.7±2.9 °C between the Younger Dryas (12.7–11.8 ka) and Early Holocene (11.1–10.3 ka; Fig. 8). During the two Early Holocene advances (11.1–10.3 to 8.8–8.3 ka), the ΔT increase is estimated to ~1.6±0.0 °C (Fig. 8). The ΔT increase during the Early (8.8–8.3 ka) to Mid-Holocene (6.1–5.0 ka) glacier advances is measured to ~1.2±00 °C (Fig. 8). During the three Late Holocene advances in the region (i.e., 6.1–5.0 to ~2.2 ka, ~2.2 to ~1.0 ka, and ~1.0 to 0.13 ka), the ΔT rise is estimated to ~1.9±00, ~0.7±1.5, and ~0.8±0.4 °C, respectively (Fig. 8).

Group 2(b): Transitional climatic region—central and eastern Himalaya. We used seven local glacier advances to estimate the past temperature change in the region. During the late glacial (~13.0 ka) and Early Holocene (11.5–10.1 ka) regional glacier advances, a ΔT increase of ~2.9±2.2 °C is calculated, which is relatively higher than the ΔT increase in the Transitional western Himalaya (i.e., ~1.8±1.0 °C; Fig. 8). Since only 1–2 local glacial stages are used for ages >10.1 ka, the sharp fluctuation in temperature during 11.5–10.1 ka, is likely due to lack of available data (Fig. 8).

From Early (11.5–10.1 ka) to Mid-Holocene (6.0–3.2 ka), the ΔT increase range from ~1.3 (±1.3) to 2.5 (±1.9) °C in the region (Fig. 8). During the subsequent three Late Holocene advances, i.e., ~3 to ~2.1, ~2.1 to ~1, and ~1 to 0.14 ka, the ΔT increase is nearly analogous (~0.6±1.6, ~0.6±0.9, and ~0.7±00 °C, respectively; Fig. 8) in the region.

Group 3: Wet and warm climatic region—central and eastern Himalaya. The reconstructed temperature profile for the last 11.4 ka for this region is robust (n=11). A ΔT increase of ~1.6±0.0 °C is modeled between the two Early Holocene advances (11.4–10.9 and 9.5–8.7 ka) in the region (Fig. 8). A similar ΔT increase of ~1.5±0.2 °C is also estimated from the Early (9.5–8.7 ka) to Mid-Holocene (7.0–4.4 ka; Fig. 8). Between

Mid- (7.0–4.4 ka) and Late Holocene (~1.7 ka), the ΔT increase is estimated to ~1.5±0.1 °C (Fig. 8). During the last ~1.0 to 0.2 ka, ΔT increase is recorded to ~0.8±0.7 °C in the region (Fig. 8).

6. Discussion

6.1. Dating uncertainties

We have rejected 125 outliers [10]Be ages from a total age population of 519 in our study. A very high degree of scattering in our young ages (<15 ka) is evident from the high reduced chi-square (χ^2) values (Fig. 9A). Nearly 21% of our data have $\chi^2 \leq 1$, indicating that the scatter is largely a result of laboratory analytical uncertainties. The rest of the data, with $\chi^2 > 1$, shows a high-degree of age dispersion, and could be explained by geomorphic process-uncertainties (Applegate et al., 2012, 2010; Owen and Dortch, 2014). Nearly 51% of our data (Fig. 9A) display positive skewness, convex upward cumulative probability distribution, and older age tails that are likely influenced by inherited [10]Be (cf. Applegate et al., 2012). Recent studies on young Holocene moraine boulders in the NW Himalaya have also emphasized the problem of inherited [10]Be (cf. Saha et al., 2018). There are two possible ways prior exposures, known as inheritance, are possible, 1) as a part of the bedrock slope system before incorporation into the glacier system (Heimsath and McGlynn, 2008); and 2) the [10]Be production in boulders *en transit* to deposition in a supraglacial system (Shroder et al., 2000; Ward and Anderson, 2011; Lukas et al., 2012; Gibson et al., 2017; Scherler and Egholm, 2017). Bedrock inheritance depends on several factors including, but not limited to catchment erosion rates, the frequency of stochastic rockfalls and avalanche debris, and periglacial weathering rates (cf. Dühnforth et al., 2010; Ward and Anderson, 2011).

Inherited ages as high as 0.7–6.3 ka may be possible depending on the microclimate, tectonic and geomorphic regimes, and glacier dynamics (cf. Heimsath and McGlynn, 2008). Additional complexity may be imposed by reworking of older glacial deposits and/or rock glacier deposits especially in cold-based semiarid and arid glacier settings with low erosion rates (cf. Shroder et al., 2000; Çiner et al., 2017). Wherein supraglacial exposure may overestimate boulder ages by as much as ~0.3–0.1 ka in cold-based

glaciers in the NW Himalaya (ibid) to ~0.9–0.05 ka in the humid glaciers in the central and eastern Himalaya (Heimsath and McGlynn, 2008; Murari et al., 2014). Alternatively, instability in young moraines, including post-depositional boulder toppling, may be responsible for a deficit in ^{10}Be concentration, called incomplete exposures (28% of the total 121 moraines; Fig. 9A), yielding apparent ages younger than the true exposure age. Unlike LGM or older moraine boulders, this undetectable perturbation on the ^{10}Be inventory can be substantial for young Holocene boulders, which systematically contributes to the high degree of scattering (Fig. 9). Any Holocene ^{10}Be chronological comparisons, therefore, should be made with extreme caution.

Additionally, inter-regional comparisons of the χ^2-values also suggest that more erosive temperate glaciers in the humid and transitional central and eastern Himalaya have less scatter relative to less-erosive glaciers in the arid and semiarid interior and western Tibetan Plateau, Transhimalaya, and NW Himalaya (Fig. 9B). In contrast to our previous studies (e.g., Orr et al., 2017, 2018; Saha et al., 2018), we targeted larger polythermal-to-temperate broad valley glaciers in the NW Himalaya (Fig. 1A). Our ^{10}Be results largely indicate tight age clustering (except hillslope contamination on M_{K5}), and χ^2-values are within the 95% confidence interval (Table S4). We, thus, argue that high-resolution Holocene chronostratigraphies may be better reconstructed in more erosive glacier setting where geological uncertainties contributing towards inheritance are comparatively limited. Less-erosive and high-preservation glacier settings may be more suitable for reconstructing detailed Pleistocene glacial chronologies.

6.2. Local glacier advances

We obtained chronologies for three new ^{10}Be dated local glacier advances in the Kulti valley and one new local glacier advance in the Parkachik valley of the NW Himalaya (Fig. 5). The oldest local glacier advance in the Kulti valley is dated to ~14.7±2.1 ka in the late glacial (Fig. 5A) when the reconstructed glacier extent was the highest (ΔELA of 259±109 m). Coeval late glacial local glacier advances with similar amplitude (ΔELA of ~340±61 m) are also defined in the adjacent glaciated valleys of the upper Chandra (Fig. S1A; Owen et al., 2001; Eugster et al., 2016) and the upper Yunam catchments (Saha et al., 2015),

indicating catchment-wide glaciation during this period. Additionally, a few overlapping (^{10}Be) drumlin and polished bedrock ages also suggest site-specific glacier retreat during this time in the upper Chandra catchment (Fig. S1A). The late glacier advances are also remarkably widespread throughout the Himalayan-Tibetan orogen, and stronger summer monsoons are recorded in several proxy records (Figs. 7, 10; Owen et al., 2001, 2002; Lasserre, 2002; Barnard et al., 2004a; Abramowski et al., 2006; Seong et al., 2007, 2009; Schaefer et al., 2008; Röhringer et al., 2012; Wang et al., 2013; Murari et al., 2014).

Subsequently, during the Early Holocene (~12.2±1.0 ka), the reconstructed glacier amplitude was slightly restricted (ΔELA of ~186±62 m) in the Kulti valley compared to their late glacial advance (Fig 5A). Equivalent ΔELAs (~180 m) are also recorded during ~12.3–10.4 ka in two other valleys of the upper Chandra catchment (Figs. 7, 10; Owen et al., 2001; Saha et al., 2018). These local glacial stages in the basin overlap at ±2σ and are likely coeval (Fig. S1A). Recent OSL dated lacustrine samples, inset within the moraines in the Miyar Valley, ~100 km downstream of the Kulti valley, indicate a glacier advance predating ~10–8 ka (Deswal et al., 2017). In the adjacent Yunam catchment, an OSL dated (~9 ka) outwash terrace also indicate an Early Holocene glacier advance (Sharma et al., 2016). Early Holocene local glacier advances are, therefore, regionally widespread and similar in amplitudes in the Lahul region. Between the late glacial and Early Holocene, the $\mathit{\Delta T}$ increase in the Kulti valley is highest (58% of the total increase) than subsequent local glacier advances. This warming may be linked to the initiation of peat accumulation near the adjacent Chandra Tal (Lake) at ~12.9±0.2 ka (Owen et al., 1997; Rawat et al., 2015a, 2015b) and also suggest wetter condition. Sharma et al. (2016) proposed stronger Early Holocene monsoons as the major driving force for these widespread glacial advances of equal amplitudes in the region (Sharma et al., 2016).

We could not date the Rataskal terminal moraine (~6.5 km from the snout) of the Kulti valley but based on the ages of other moraines, we speculate that it may have formed during the Early to Mid-Holocene.

Like several restricted local glacier advances at ~0.5±0.2 ka in the Lahul (ΔELAs: ~57–167 m) and elsewhere in the Himalayan-Tibetan orogen (ΔELAs: ~1–370 m; Figs. 7, 10; Saha et al., 2018 and

references therein), the late Holocene advance in the Kulti valley was also limited in extent (ΔELA: ~106±30 m; Fig. 5A), suggesting a drastic change in the forcing factors from Early to Late Holocene (ibid). Historical data from the Geological Survey of India (Walker and Pascoe, 1907; Owen et al., 1996, 1997, 2001; Raina et al., 2015) further indicates a glacier still-stand and formation of subdued hummocky moraine complex (M_{K1}) in the Kulti valley during the late 19th Century, ~3 km from the snout of Sonapani glacier (Fig. 5A). Our dated ice-contact moraine (M_{P1}) in the Parkachik valley of the Nun Kun massif also has a mean moraine age of ~0.2±0.1 ka (Fig. 5B). This late Holocene glacier advance in the Parkachik valley, however, is relatively more restricted (ΔELA: ~20 m) than the Kulti valley (~95 m), suggesting a further decline in the strength of the forcing factors northwestward. Equivalent Late Holocene glacier advances/still-stands are also historically (maps) recorded in the Miyar valley (Harcourt et al., 2010; Saini et al., 2016), the upper Bhagirathi valley (Raina et al, 2015 and references therein), and dated in the adjacent Hamtah valley (Saha et al., 2018; Fig. S1). There is additional research based on ice cores, tree rings, lake sediments, and historical documents elsewhere in the orogen which further supports glacier advances during the ~18th–19th centuries (Yang et al., 2009a, 2009b; Xu and Yi, 2014; Liang et al., 2015). We argue that the late 19th Century advance/still-stand in the region is widespread and may be distinct from the ~0.5 ka advances.

6.3. Regional glacier advances

An extensive list of limitations and merits of Holocene glacial chronological reconstructions is outlined in Saha et al. (2018). With those challenges in mind, we have expanded our chronological and ELA reconstructions in this study and also added a climatic framework for inter-regional comparisons and modeled the past temperature changes across the whole Himalaya and Tibet.

We have developed an objective criterion to group glaciers with similar climatic characteristics and provided a robust climate zonation map for the orogen (Figs. 6, S9; New et al., 2002; Bookhagen and Burbank, 2006). Three major groups of glaciers (*Group 1–3*) are identified and grouped using CA and PCA (Fig. 6), which remarkably capture the orographically influenced latitudinal climatic gradient (cf. Li et al.,

2017). Pearson's correlation and ANOSIM tests further confirm that the sample grouping is not by random chance. Since we only used temperature and precipitation that are largely affected by the latitudinal distribution of topography (Fig. 4), we are unable to capture the longitudinal climatic gradient (maritime vs. continental). This suggests that additional work is required to improve our initial climatic groups. For the purpose of this study and based on our limited [10]Be dated local glacial stages, we further subdivided our three climatic groups and defined five *climatic regions* as a framework for analysis. They include, *Group 1a* (Transhimalaya, NW Tibet, Pamir, and Tian Shan), *Group 1b* (Arid and semiarid southern and NE Tibet), *Group 2a* (Transitional western Himalaya), *Group 2b* (Transitional central and eastern Himalaya), and *Group 3* (Wet and warm central and eastern Himalaya; Fig. 7). Both our PCA vector results (Fig. 6D; Table 3) and sensitivity analysis confirmed that most of the glaciers in the Himalaya and Tibet are highly susceptible to precipitation/moisture at the regional-scale and changes in this variable would likely results in highly variable responses of glaciers in respective *climatic regions* (cf. Bookhagen and Burbank, 2010).

Our modeled *T* profiles are reconstructed for a wide variety of glaciers across the entire orogen and regionally averaged to account for the limitations associated with the individual catchments (cf. Pratt-Sitaula, et al., 2011). However, the model is probably not so well constrained for the past mass-balance effect (*c* and *τ*) of individual glacier, because *P* increase in some areas of the western and interior Tibet was much higher (~55–200%) than present during the Early Holocene (Huth et al., 2015; Li et al., 2017; Shi et al., 2017). The actual *P* increase, therefore, may exceed our assumed ±30% change in *P* in the semi-arid and arid regions and probably suggest that the actual *T* increase was much less than our modeled *T* from the Early to Mid-Holocene (Fig. 8). We also assumed a simplistic glacier advance scenario (cf. Putnam et al., 2013b) where glaciers are progressively more restricted over time, or in other words, continuous rise in *T*. The detailed geologic records of glacier fluctuations (advance and retreat) are not available for this study and hence, relative warming and cooling is not captured by the model. Additional limitations of the model include: 1) simplified energy and mass-balance relationship, 2) the influence of meteorological variables other than *T* and *P* are not considered, 3) the number of glacier length records and degree of spatiotemporal

coverage varies across all the *climatic regions*, 4) our assumption is violated for the Mid-Holocene when *P* decrease in the semi-arid regions was substantial than *T*.

The model *T*, therefore, may not accurately capture the exact perturbation in ambient temperature, but the sense of change (*ΔT*) is significant, especially when compared inter-regionally. We, thus, interpret the results from glacial chronologies, ΔELAs, and model *T* results to show that the long-term changes in glacier geometries have taken place differently across discrete *climatic regions* of the orogen and likely modulated by changes in *P* in the Early to Mid-Holocene and changes in *T* from Mid- to Late Holocene. Whereas at the catchment-scale, individual glacier hypsometries may determine the relative change in their glacier geometries during the Holocene (cf. Pratt-Sitaula et al., 2011).

Based on 121 local glacial stages, we have reconstructed one late glacial and five inter-regional *Himalayan-Tibetan Holocene stages (HTHs)* across the orogen during the to Late Holocene. These include:

Late glacial advance (~15.3–11.8 ka)

Extensive regional glacier advances are recorded during this time throughout the Himalayan-Tibetan orogen (Figs. 7, 10) with regional mean ΔELAs ranging from 270–600 m (Figs. 7, 10). Due to widely variable glacier hypsometries and corresponding temperature gradient in the Transhimalaya, NW Tibet, Pamir, and Tian Shan (*Group 1a*; Fig. S7), ΔELA uncertainties are also very high at the catchment-scale in these areas (ΔELAs 30–1020 m). However, in general, regional glacier advances are more extensive (ΔELAs are ~100–400 m lower) in the colder arid and semiarid regions (*Group 1*) during this stage relative to the transitional *climatic regions* (*Group 2*; Fig. 10). We suggest locally variable but relatively enhanced moisture supply and corresponding radiative cooling likely favored extensive late glacial glaciations among the arid and semiarid glaciers relative to the southerly transitional temperate glaciers. While Saha et al. (2018) identified two discrete glacial advances at this time in the NW Himalaya and Tibet, e.g., ~15.4–12.7 and ~12.6–11.4 ka, such distinction is not clear in the arid and semiarid NE Tibet (*Group 1b*), transitional

(*Group 2b*) and wet-warm (*Group 3*) central and eastern Himalaya due to limited robust local glacial stages (Fig. 10). Additional chronological works, thus, are paramount to refine this stage.

The regional glacier advances at this stage also coincide with the climatic relapses associated with warm-wet Bølling-Allerød Interstadial and cold-dry Younger Dryas Stadial (Chiang et al., 2014; Denton and Broecker, 2008) in the orogen. Evidence of glaciations are widely detected in lake records in Lahul (Rawat et al., 2015a, 2015b), Zanskar (Demske et al., 2009), the NE Tibet (J. Ji et al., 2005; Thomas et al., 2016), and the SE Tibet (Kramer et al., 2010a) and further corroborate our results.

HTHs 5 (~11.5–9.5 ka)

Extensive Early Holocene *HTHs* are identified in all *climatic regions* (Fig. 7). We estimated the highest glacier extent among the moisture-sensitive glaciers of the arid and semiarid Transhimalaya, NW Tibet, Pamir, and Tian Shan (*Group 1a;* Fig. 7) with the average ΔELA ~300–400 m lower than the transitional western Himalaya (*Group 2a*) and the wet and warm central and eastern Himalaya (*Group 3*). The average ΔELA is estimated to ~400–600 m lower in the arid and semiarid Transhimalaya, NW Tibet, Pamir, and Tian Shan (*Group 1a*) compared to the transitional central Himalaya (*Group 2b*), and the arid and semiarid NE Tibet (*Group 1b*; Fig. 10). Enhanced moisture supply to the NW of the orogen and corresponding radiative cooling are suggested to explain such spatial pattern of glaciation and ΔELAs (Rupper and Roe, 2008; Rupper et al., 2009). However, *HTHs 5* (equivalent to *HH 7* in Saha et al., 2018) consist of several tentative local glacial stages in *Group 1a, 1b, 2b,* and *3 climatic regions* (Fig. 7) and require significant future improvement with additional chronologies.

Early Holocene wetter-warmer climate associated with strong summer monsoon is widely evident in several continuous proxy records in the orogen (Dong et al., 2010b; Dykoski et al., 2005; Fleitmann et al., 2007, 2003; Gasse et al., 1996; Herzschuh et al., 2006; Hu et al., 2008; Hudson et al., 2016; Thompson et al., 1997; Wang et al., 2005). Sediment core records from the Arabian Sea also support wetter-colder phase during this time (Rawat et al., 2015a, 2015b; Azharuddin et al., 2017).

134

Our model results also indicate that the net temperature increase between the late glacial and *HTHs 5* in the transitional central and eastern Himalaya (*Group 2b*) is ~1.8±1.0 °C higher than that of transitional western Himalaya (*Group 2a*; Fig. 8). Comparatively greater Early Holocene warming in *Group 2b climatic region*, therefore, is likely responsible for this restricted glaciation.

Colder but drier Early Holocene climate is detected in several lake records of the central (J. Ji et al., 2005; Yanhong et al., 2006; Yu et al., 2006), eastern (Mischke and Zhang, 2010), and NE Tibet (J. Ji et al., 2005). This relative dryness may be responsible for the subdued Early Holocene glacial advances in the arid and semiarid NE Tibet (*Group 1a*; Figs. 7, 10).

HTHs 4 (~8.8–7.7 ka)

Prominent regional glacier advances during this Early to Mid-Holocene transition are evident in two (*Group 1a and 3*) and tentatively in two (*Group 1b and 2a*) *climatic regions* of the orogen (Table 5; Fig. 7). This stage coincides with the ~8 ka abrupt climate cooling in the North Atlantic (Matero et al., 2017). Glaciers in the more westerlies-dominated arid and semiarid NW Tibet (*Group 1a*) advanced extensively during this time leading to mean ΔELA ~50–400 m lower than the glaciers in the distant arid and semiarid NE Tibet (*Group 1b*; Figs. 7, 10). More moisture and colder climate teleconnected via the mid-latitudinal westerlies possibly favored high glacier activity in *Group 1a*. Whereas, aridity in the east may be responsible for the muted glacier response in *Group 1b*. Although our model results indicate net temperature decrease (e.g., ~2.1±0.5 and ~0.9±0.1 °C, respectively) in both the arid and semiarid regions between *HTHs 5* and *4*, given the limited data set, we are unable to confirm this cooling in the Early Holocene.

Similarly, in the more temperature-sensitive wet and warm central Himalaya (*Group 3*), extensive regional glaciation is recorded with average ΔELA ~90–200 m lower than the transitional western Himalaya (*Group 2a*; Fig. 10), a pattern anticipated during large-scale ambient cooling. However, since our *HTHs 4* is tentative to absent in most of the *climatic regions*, additional chronologies are needed to evaluate our results.

However, lacustrine and pollen (proxy) records indicate a widespread cold-wet spell during this phase in the NW (Wünnemann et al., 2010b) and western Himalaya (Phadtare, 2000), and in the southern Tibet (Hudson et al., 2016). Similarly, a cold-dry (aridity) spell prevailed in the central (Dong et al., 2010b), NE (Ji, et al., 2005a, 2005b; Mischke and Zhang, 2010), and SE Tibet (Kramer et al., 2010a) during this stage, which further supports our initial inferences.

HTHs 3 (~7.0–3.2 ka)

The glacial records in the orogen show extensive glacial activities during this stage in the more temperature- sensitive wet and warm central and eastern Himalayan glaciers (*Group 3*; Fig. 10). In *Group 3*, the mean ΔELA is 60–400 m lower than the arid and semiarid NW Tibet (*Group 1a*) and 100–400 m lower than the transitional western (*Group 2a*) and central and eastern Himalaya (*Group 2b*; Fig. 7). The least glacier activities are recorded tentatively in the arid and semiarid NE Tibet with ΔELA of only ~81±71 m (*Group 1b*; Fig. 10). Enhanced cooling, as also recorded in other proxy records (Bisht et al., 2017; Azharuddin et al., 2017; Srivastava et al., 2017), is suggested to explain such spatial pattern of glaciation across all *climatic regions*. However, *HTHs 3*, in general, shows high age dispersions (9–23%) with poor chronologies for *Group 2b* and *3*.

The majority of the proxy records in the orogen indicate intensified warming and stronger monsoon at the at ~7.0–6.0 ka, followed by a decline in monsoonal strength (Phadtare, 2000; Ji et al., 2005a, 2015b; Wünnemann et al., 2010; Srivastava et al., 2017). An abrupt shift is detected during ~5.5–4.8 ka towards colder and drier climate over the orogen (ibid). A decline in monsoon intensity and strengthening of mid-latitudinal westerlies associated with North Atlantic cooling are proposed for this shift (Clift et al., 2012; Leipe et al., 2014). This regional glacial stage, which encompasses both *HH 5* and *4* stages of Saha et al. (2012) for the NW Himalaya (Table 5, Fig. 7), therefore, coincides with the strengthening of monsoon (associated albedo and dynamic cooling of Rupper et al., 2009) and subsequently westerlies (cooling of Mölg et al., 2013).

From Early to Mid-Holocene, our model results indicate a significant ΔT increase of ~1.9–6.0 °C in *Group 1a* (Fig. 8), whereas the ΔT rise in other regions are comparable (e.g., *Group 1b*: ~1.9–2.7 °C, *Group 2b*: ~1.3–2.5 °C, and *Group 2a*: ~1.2–1.5 K; Fig. 8). This unprecedented temperature increase modeled after glacier length in *Group 1a* is not supported by proxy data. We rather speculate that part of the intensive glacier retreat since ~8 ka in *Group 1a* (or muted response in *Group 1b*) is associated with extreme aridity (Ji et al., 2005a, 2005b; Herzschuh et al., 2006; Zhu et al., 2009; Kramer et al., 2010; Mischke and Zhang, 2010; Wünnemann et al., 2010; Berkelhammer et al., 2012; Huang et al., 2016; Shi et al., 2017). This also suggests that our model assumption that ambient temperature primarily drives glacier fluctuations on a continental scale is not always true.

HTHs 2 (~2.3–1.0 ka)

Mostly tentative and restricted glacial advances (ΔELAs of 21–222 m) are recorded during this time in the orogen. Saha et al. (2018) recently proposed two stages (their *HH 3* and *2*) in the NW Himalaya, which encompass *HTHs 2*. We speculate that two substages (~2.3–1.7 and ~1 ka) are possible, but given the systematic inheritance for ages <2 ka, we cannot verify these individual substages. They may also represent geologic noise (e.g., older deposits) in the data. For instance, neither lake proxy records (cf. Huang et al., 2016) nor any glacier records are detected during *HTHs 2* in the arid and semiarid NE Tibet (*Group 1b*). Detailed Late Holocene chronological reconstructions are required to evaluate *HTHs 2* and assess any climate forcing (J. Ji et al., 2005; S. Ji et al., 2005; Phadtare, 2000; Srivastava et al., 2017; Wünnemann et al., 2010a).

HTHs 1 (<1 ka)

Approximately 30 local glacier stages (25%) have exposure ages <1.0 ka. Due to high age dispersions (18–79%) and systematic inheritance, we are unable to define any substages for this period. Individual advances including Little Ice Age (LIA) can be reconstructed at the catchment-scale (see section *6.2*), but at the regional-scale large uncertainties preclude us from further analysis.

The extent of glaciation for *HTHs 1* is generally very restricted across all *climatic regions* (average ΔELA ~100–150 m; Fig. 10). High-glacier amplitudes are evident in the wet and warm central Himalaya (*Group 3*) with mean ΔELA ~40–100, ~50–100, and ~90–150 m lower than the transitional western Himalaya (*Group 2a*), the arid and semiarid Transhimalaya, NW Tibet, Pamir, and Tian Shan (*Group 1a*), and the transitional central and eastern Himalaya, respectively (*Group 2b*; Fig. 10).

ΔT increase is approximately identical (~0.8 °C) in all regions of the orogen (Fig. 8) from ~1.0 to 0.2 ka, except in *Group 1a* where the *ΔT* rise is ~1.4±0.9 °C (Fig. 8).

Based on the spatial distribution of ΔELAs and net temperature change for this period, we suggest possible cold-dry climate in the arid and semiarid NW Tibet, and cold-wet climate in the Transhimalaya and transitional western Himalaya. Proxy records also corroborate this general pattern (Liu and Thompson, 1998; Netajirao R. Phadtare, 2000; Srivastava et al., 2017; Thompson et al., 1997; Wünnemann et al., 2010a).

7. Global Holocene glacial signal?

Our regional glacial chronostratigraphical reconstruction indicates one late glacial, and at least five synchronous *HTHs*. Additional substages may also be possible for some regions where [10]Be glacial chronologies are sufficient and widespread. For example, Saha et al. (2018) proposed seven Himalayan Holocene stages (*HHs*) in the northwestern Himalaya and Tibet. We herein complemented this previous study and provided a detailed orogen-wide Holocene glacial chronostratigraphical reconstruction. Detailed studies of ΔELA suggest overall high glacial amplitude in the late glacial and Early Holocene, which coincide with the northerly shifted Earth's thermal equator (ITCZ) and increased monsoonal precipitation (Dykoski et al., 2005; Jennerjahn et al., 2004; Lea et al., 2003; Severinghaus et al., 2009; Wang et al., 2001, 2004), as well as abrupt North Atlantic cooling during Younger Dryas and ~8 ka (Denton and Broecker, 2008 ; Matero et al., 2017). Corresponding Early Holocene (~11.5–9.5 and ~8.8–7.7 ka) extensive glacier advances are also identified in glacial records in European Alps (Moran et al., 2016, 2015, Schimmelpfennig et al., 2014, 2012; Schindelwig et al., 2012), Greenland (O'Hara et al., 2017), Arctic

Canada (Young et al., 2012), Svalbard (van der Bilt et al., 2015), tropical Andes, Africa, and Southern Hemispheric extratropical regions (Solomin, et al., 2015, 2016 and references therein).

Progressively restricted glacier advances over time are recorded during subsequent glacier advances in the orogen (Figs. 7, 8, 9). A considerable Mid-Holocene regional glacier retreat is evident in the arid and semiarid regions and supports a major shift towards extreme aridity in the orogen (Fig. 8). Subsequent Late Holocene advances, including LIA, were accordingly restricted (Fig. 9). These changes are attributed to reduced northern hemisphere insolation and corresponding north Atlantic cooling (Chiang et al., 2014; Denton and Broecker, 2008; Lund et al., 2006). The enhanced mid-latitude westerly winds likely teleconnected the Late Holocene cooling events in the Himalayan-Tibetan orogen (Mölg et al., 2014; Srivastava et al., 2017; Yancheva et al., 2007).

Overall, our study reinforces the inferences made in Saha et al. (2018) that the orbital forcing primarily modulates the long-term pattern of Holocene glaciation in the Himalayan-Tibetan orogen. The relative strength/weakness of both summer monsoon and mid-latitude westerlies, on the other hand, determine the amplitude of short-term Holocene glacier advances in different regions of the orogen.

8. Conclusions

Our geomorphic mapping, cosmogenic ^{10}Be surface exposure dating, ELAs, glacial hypsometry, and inverse linear flow model approach yielded the following conclusions.

i.   The Kulti valley in the Lahul Himalaya and the Parkachik valley in Nun Kun massif, located in the transitional northwestern Himalaya, had relatively large (>10-km-long) and broad U-shaped polythermal-to-temperate valley glaciers that produced a series of young moraines. Three sets of morphostratigraphically distinct moraines in the Kulti valley are dated to ~14.7 (M_{K5}), ~12.2 (M_{K4}), and ~0.5 ka (M_{K2}), whereas the youngest moraine complex (M_{K1}) is historically dated to the late 19th century. The ΔELA was 259±109 m during the late glacial in the valley. The glacier cover became

progressive less throughout the Holocene. The modeled $\mathit{\Delta T}$ increase in the valley is maximum (58% of the total increase) between the late glacial and Early Holocene.

ii.   A new LIA local glacial advance (M_{P1}: ~0.2 ka) with ΔELA of ~92±31 m is also reconstructed using cosmogenic [10]Be dating in the Parkachik valley of the Nun Kun massif. Based on our analysis and dating results, we accept the hypothesis that high-resolution Holocene chronostratigraphies may be better reconstructed in more erosive glacier settings where geological uncertainties are comparatively limited.

iii.   Three major *climatic regions* (*Group 1–3*) are defined and used for inter-regional comparisons based on mountain glaciers with contrasting temperature and precipitation regime across the orogen. These *climatic regions* include, (*1a*) arid and semiarid Transhimalaya, NW Tibet, Pamir, and Tian Shan; (*1b*) arid and semiarid southern and NE Tibet; (*2a*) transitional western Himalaya; and (*2b*) transitional central and eastern Himalaya, and (*3*) Wet and warm central and eastern Himalaya.

Initially, five groups of glaciers with comparable climatic characteristics are identified in our study using CA and further refined by PCA. These groups are statistically robust at the 95% confidence level. Additionally, ANOSIM analysis indicates similarities within groups are not a result of random chance. Our PCA vectors and sensitivity analysis also confirm that most of Himalayan-Tibetan glaciers are highly susceptible to changes in precipitation at the regional scale. The pronounced north-south and east-west climatic transacts, mainly for precipitation, therefore, are argued to control the large-scale variability of contemporary and Holocene glacial extents across the orogen. In contrast, at the catchment-scale glacial hypsometries likely play the crucial role. This observation must be reconciled with future glacier-climate models to quantify variable glacier responses to identical climatic perturbation.

iv. Building on Saha et al. (2018) and using 121 *local glacial stages*, we reconstructed *regional glacial stages* from the late glacial to Late Holocene in five discrete *climatic regions* across the orogen. These are assigned to: 15.2–11.7, 10.3–9.7, 8.0–7.7, 6.6–3.5, 2.3–1.3, ~1, and <1 ka in the arid and semiarid Transhimalaya, NW Tibet, Pamir, and Tian Shan (n=47); 13.5–12.9, 11.5–9.5, ~8.0 and ~3.3 ka in arid and semiarid southern and NE Tibet (n=8); 15.3–11.8, 11.1–10.3, 8.8–8.3, 6.1–5.0, ~2.2 and <1 ka in the transitional western Himalaya (n=37); ~13.5, 11.5–10.1, 6.0–3.2, ~2.1–1.0, and <1 ka in the transitional central and eastern Himalaya (n=11); and ~13.0–10.9, 9.5–8.7, 7.0–4.4, ~1.7, and <1 ka in the wet and warm central and eastern Himalaya (n=18).

v. The spatial distribution of ΔELAs in the orogen during ~15.3–11.8 ka (ca. late glacial) shows locally variable but relatively enhanced monsoonal moisture supply and amplified cooling in the arid and semiarid regions.

The enhanced monsoon during ~11.5–9.5 ka (ca. Early Holocene) may also result in relatively extensive glacier advances in the moisture sensitive arid and semiarid Transhimalaya, NW Tibet, Pamir, and Tian Shan. Whereas higher net temperature increase between the late glacial and Early Holocene advances in the transitional central and eastern Himalaya may be responsible for its comparatively subdued response during the Early Holocene than the transitional western Himalaya; the *ΔT* difference is ~1.8±1.0 K.

The subsequent glacier advances during ~8.8–7.7 ka (ca. Early to Mid-Holocene transition) suggest wet-cold climate in the arid and semiarid NW Tibet, enhanced cooling in the wet-warm central Himalaya, and extreme aridity in the arid and semiarid NE Tibet.

During ~7.0–3.2 ka (ca. Mid-Holocene) regional glacier advances, we propose intensified cooling in the wet and warm central and eastern Himalaya, based on ΔELAs. The unprecedented modeled net temperature increase (~1.9–6.0 K) in the arid and semiarid regions, from Early to Mid-Holocene, however, suggests extreme aridity in these regions.

The overall cold-dry climate is detected in ΔELAs and modeled temperature in the (tentative) Late Holocene regional glacier advances in the orogen during ~2.3–1.0 ka.

Between the last 1.0 and 0.2 ka, we suggest possible cold-dry climate in the arid and semiarid NW Tibet, and cold-wet climate in the Transhimalaya and transitional western Himalaya. The net temperature increase in the last 1 ka is remarkably identical (~0.8 K) in all the *climatic regions* of the orogen.

vi. Overall, [10]Be, ΔELAs and *ΔT* show a major regional shift in the relative strength of the prevailing climate systems in the orogen during the Mid- and Late Holocene transition. Generally, enhanced monsoonal humidity is likely replaced by relative cooling and aridity driven by North Atlantic changes and teleconnected by mid-latitude westerlies. Northerly sub-polar glaciers are more affected during this latter part of Mid- and the early part of the Late Holocene than the southerly temperate glaciers in the orogen. We, therefore, further reinforces the concept of long-term orbitally influenced Holocene glaciation in the Himalayan-Tibetan orogen.

ACKNOWLEDGMENTS

Fig. 1. Physical settings of the study areas. (A) TRMM and CRU CL 2.0 precipitation map, superimposed on hillshade map, showing the location of [10]Be dated (with ages <15 ka only) glaciated valleys across the Himalaya, the Tibet, the Pamir, and the Tian Shan. Two new (in black circles—this study) and 77 published (in blue circles) valleys are presented. Arrows indicate the propagating directions of the prevailing climate systems (ISM – Indian Summer Monsoon; ESM – East Asia Summer Monsoon). Valley locations are: (1) Daxi, Tian Shan, (2) Bordoo, Tian Shan, (3) Ala Archa, Tian Shan, (4) Aksai, Tian Shan, (5) Kitschi-Kurumdu, Tian Shan, (6) Koksu, Pamir, (7) Kongur Shan, Pamir, (8) Muztag Ata, Pamir, (9) Great Bogchigir, Karakoram, (10) Hunza valley, Karakoram, (11) Central Karakoram, (12) Parkachik, Sentic, Rantac, & Tarangoz, Nun Kun massif, (13) Chang & Pang, Ladakh, (14) Stok & Lato, Zanskar, (15) Puga & Karzok, Zanskar, (16) Kulti, Hamtah, & adjacent valleys, Lahul, (17) Yunam, Great Himalaya, (18) Tons, Garhwal, (19) Bhagirathi, Garhwal, (20) Bhillanganga & Dudhanga, Garhwal, (21) Nanda Devi,

Garhwal, (22) Muguru, Gurla Mandhata, (23) Lete, Milarepa, Syaktan, Yak, Lyapche, Danfe & Dudh Khola, Annapurna, (24) Macha Khola, Gorkha Himal, (25) Mailun Khola, Ganesh Himal, (26) Langtang, Nepal, (27) Nyalam County, Southern Xixabangma, (28) Khumbu Himal, Nepal, (29) Rongbuk, N Mt. Everest, (30) Karola Pass, Mt. Kaluxung, (31) Renhe, Baishui, & Ganheba, Yulong and Ganheba mountains, (32) Hailuogou, Gonga Shan, (33) Dalijia Shan, NE Tibet, (34) Xiying He, Qilian Shan, (35) Anyemaqen mountains, (36) Kunlun Shan. (B) Diagram showing present (blue circle) and past (diamonds) lengths of glaciers from their respective headwall in each location. Each location often contains >1 valley and are represented near to their location number, e.g., adjacent valleys at location 7 are shown in between 7 and <8.
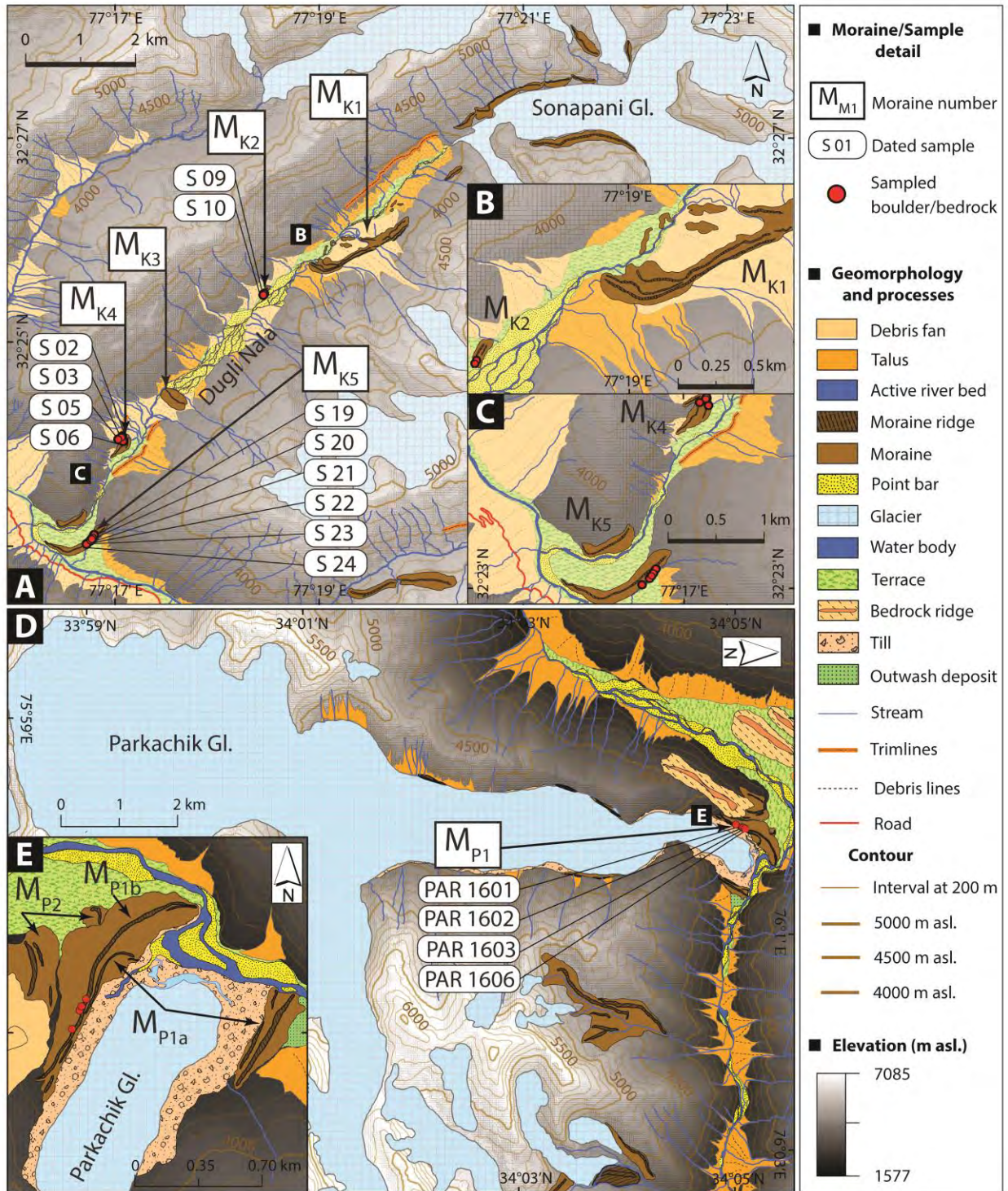
Fig. 2. Geomorphology of the study areas. (A) Kulti valley showing landforms and locations of moraine boulders. (B) Highlighted M_{K1} and M_{K2} moraine ridges. (C) Zoomed in view of M_{K4} and M_{K5} moraines. (D) Sampling locations of M_{P1b} moraine and associated landforms in the Parkachik valley. (E) Highlighted M_{P1} moraine ridges.

145
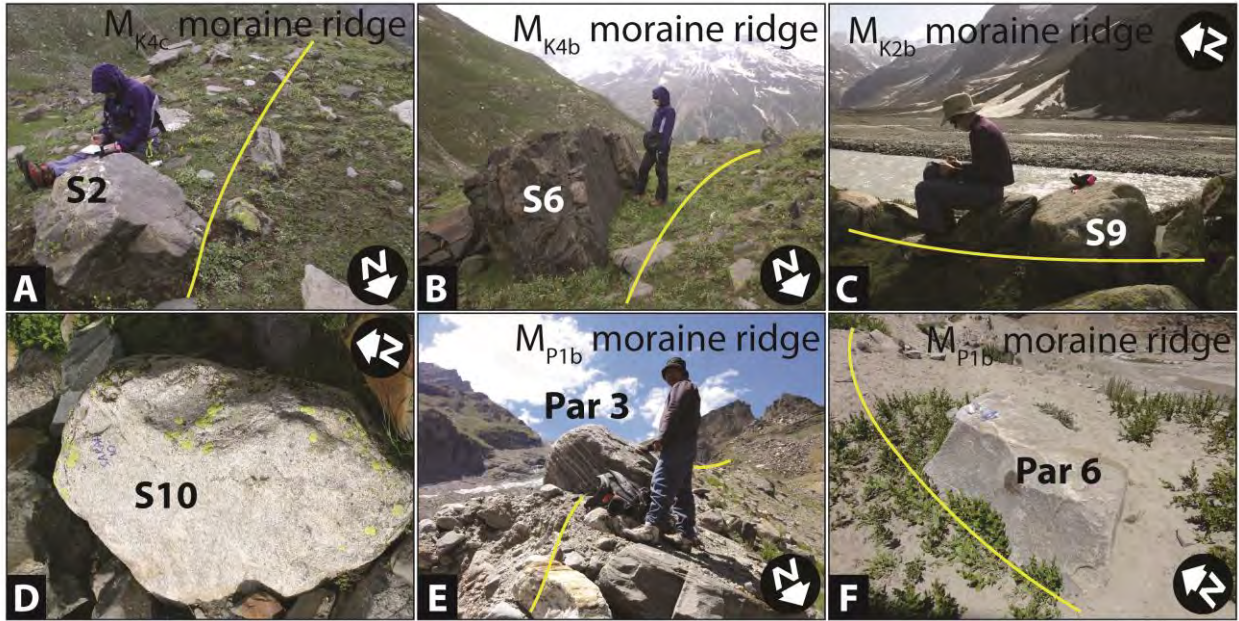
Fig. 3. Examples of sampled boulders for ^{10}Be exposure dating. Boulders inset into M_{K4C} (A) and M_{K4b} (B) lateral rides in the Kulti valley. (C and D) Relative to M_{K4} moraine, subdued boulders are present on the young M_{K2b} lateral ridge in the valley. (E and F) Boulders are large, fresh, and well inset into the crest of the M_{P1b} lateral ridge in the Parkachik valley.
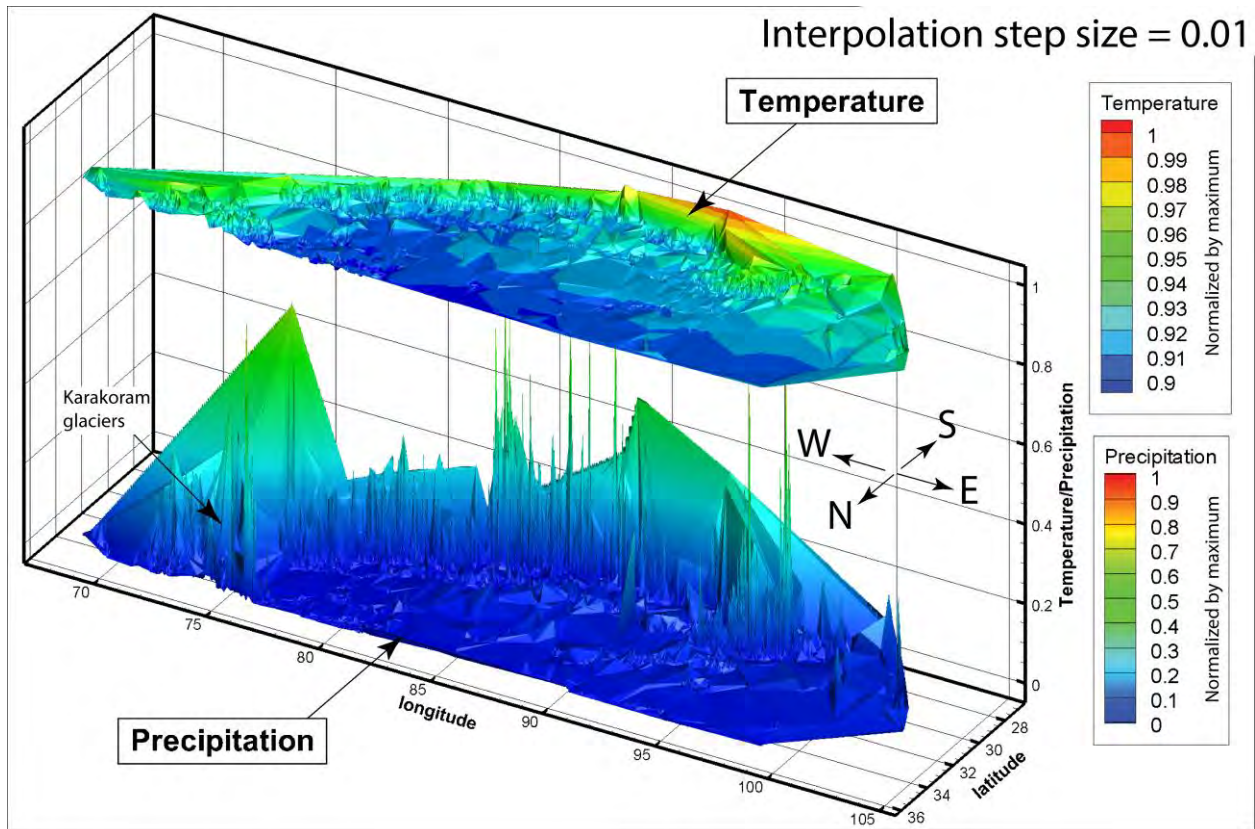
Fig. 4. Distribution of temperature (source: CRU CL. 2.0) and precipitation (source: TRMM) variables across the Himalayan-Tibetan orogen. Climate variables are extracted using glaciers as points (see supplementary material S8). The southern Himalayan glaciers, in general, are wet-warm temperate types, whereas the glaciers further north in the Transhimalaya and Tibetan Plateau are broadly cold-dry sub-polar types.
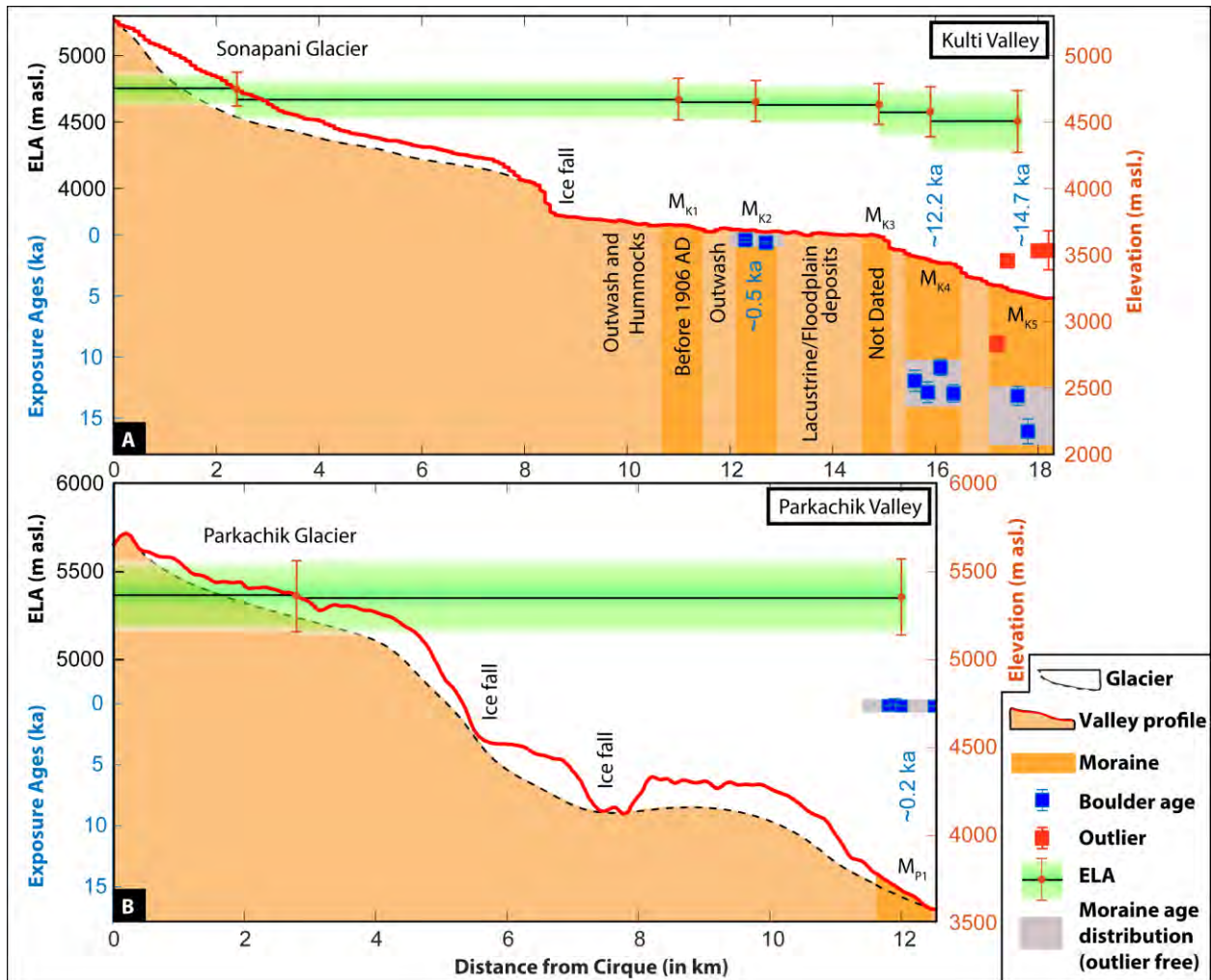
Fig. 5. Cross-valley profiles showing topography, major landforms, reconstructed ELAs, and [10]Be moraine chronologies for the Kulti (A) and the Parkachik (B) valleys in the NW Himalaya of northern India. The mean moraine ages with 1σ uncertainties that are morphostratigraphically distinct represent the local glacial stages in respective valleys. Both valleys show typical stair-case topography with steep ice falls.
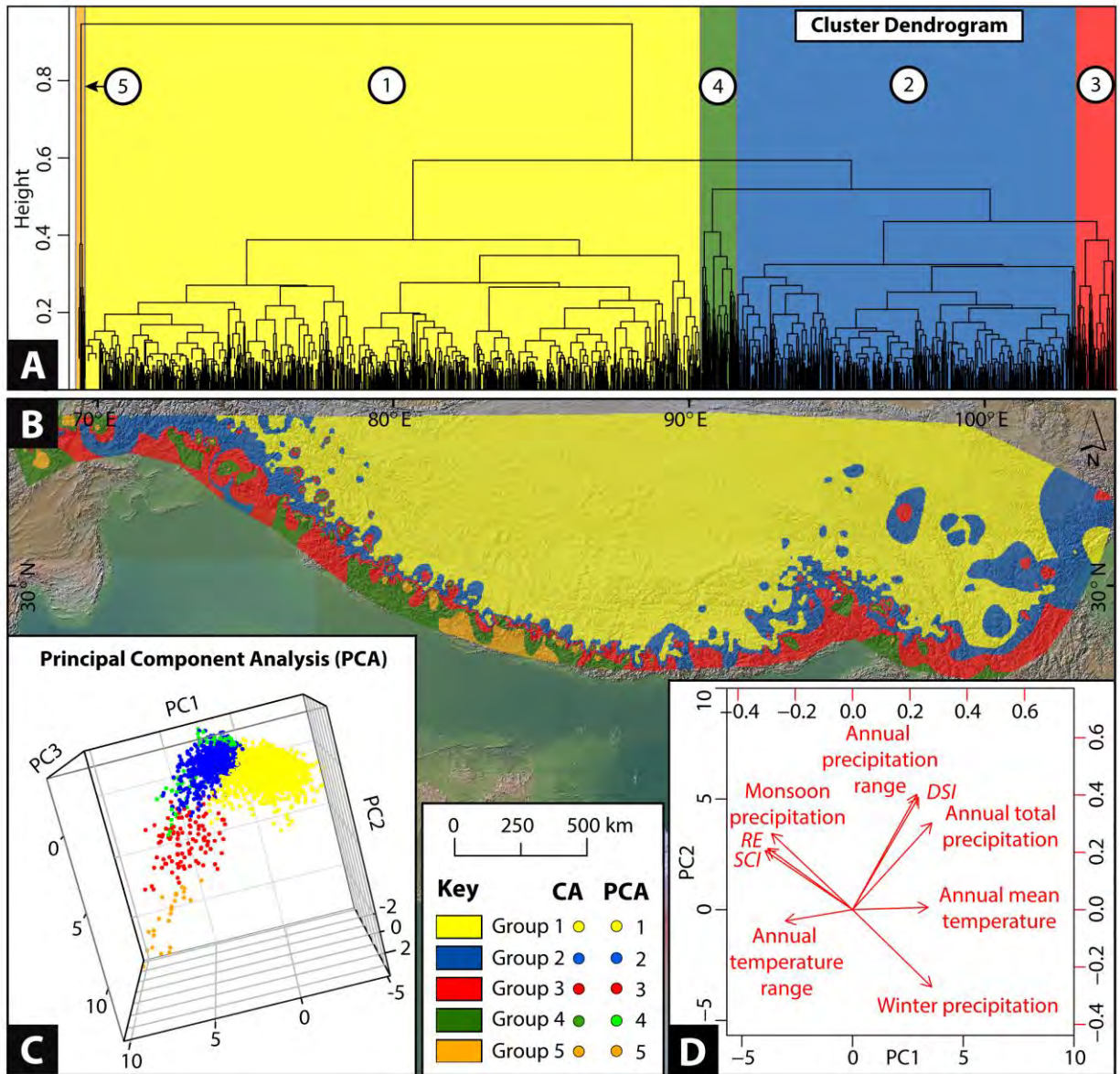
Fig. 6. Cluster and Principal Component Analyses of Himalayan-Tibetan glaciers to identify identical climate zones. (A) The dendrogram (hierarchical tree) representing groups of most similar glaciers based on the climate parameters. Each terminal of the hierarchical tree represents a single glacier (n = 42,511). Each vertical line joins the groups at the certain level of similarity. Five major climate groups are identified. (B) Each glacier point, based on its cluster, is interpolated over the region to generate a climate zone map and superimposed over a hillshade map. (C) PCA results are shown in three dimensions (PC1, PC2, PC3). These three axes explain 88% of the total variance (PC1 53%, PC2 26% and PC3 9%). The groups derived

149

in CA and PCA methods are identical (see the key). (D) Biplot is showing the magnitude and sign of each parameter's contribution to the PC1 and PC2 (Table 3).
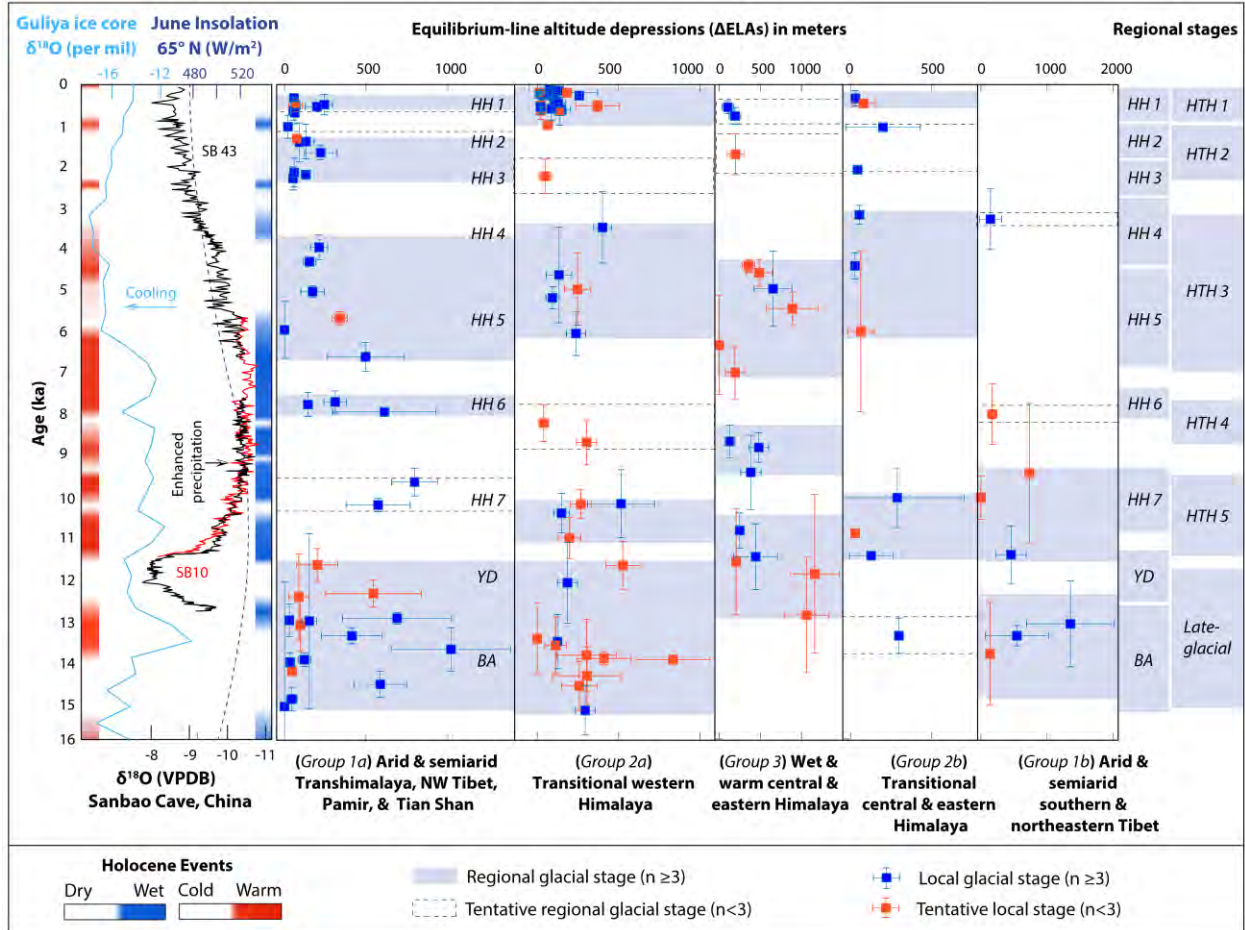
Fig. 7. Timing and amplitude of late glacial and Holocene regional glacier advances across the Himalayan-Tibetan orogen compared with continuous proxy records. Five regions are used (see section *5.2.1*) for inter-regional comparisons. Local glacial stages (mean [10]Be ages in x-axis) for each region are combined (Table S4) and compared against the corresponding ΔELA (in y-axis; Table S6). Uncertainty bars are ±1σ. Regional Himalayan-Tibetan Holocene stages (*HTHs*) for the whole orogen (this study) are compared against Himalayan Holocene stages (*HHs*) reconstructed for the NW Himalaya and Tibet in Saha et al. (2018). A simplified summary of major late glacial-Holocene climatic events is shown by shaded blue and red bars, representing significant dry-wet and cold-warm periods, respectively. They are reconstructed after Demske et al. (2009), Wünnemann et al. (2010), Berkelhammer et al. (2012), Rawat et al. (2015a, 2015b),

150

Srivastava et al. (2017). *T*he color scheme only represents the time range and not the magnitude. Reconstructed orbital trend at 65°N latitude (after Berger, 1978), oxygen isotopes from speleothems (Sanbao cave, China after Dong et al., 2010), and from Guliya ice cores (Guliya ice core, Tibet after Thompson et al., 1997) are shown at the bottom for climatic interpretation.

Fig. 8. Reconstructed past temperatures in different *climatic regions* using the inverse linear flow model (after Oerlemans, 2001, 2005). Sixty-six local glacier geometries are used. Ages >9.5 ka have overall lower confidence due to a limited number of glaciers used. We added ±30% precipitation uncertainties to account

for the errors associated with c and τ. Since this is a linear model, the sharp jumps are associated with the number of data available. Regional net temperatures (ΔT) are estimated after theses modeled temperature graphs.
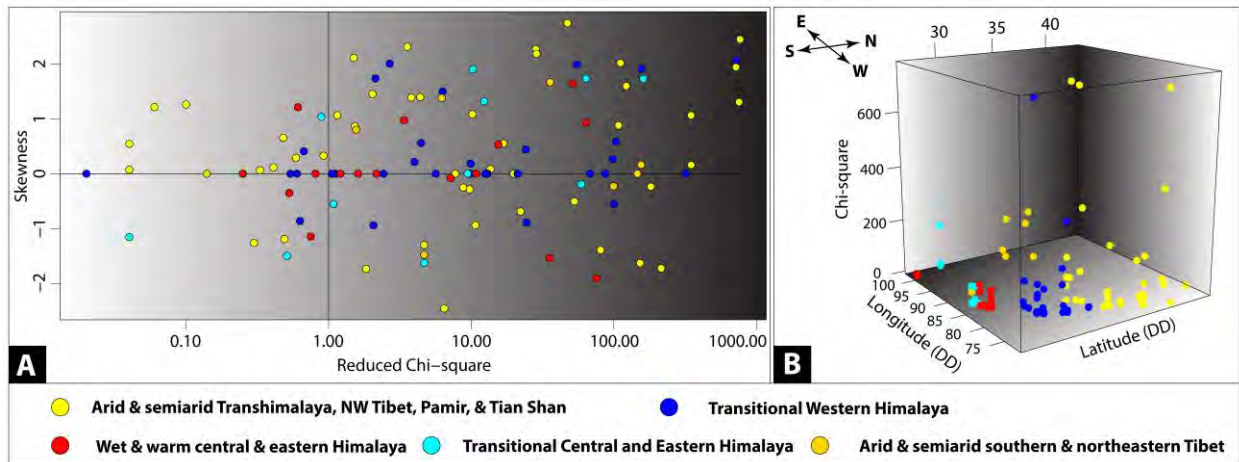
Fig. 9. Scatter diagrams showing reduced χ^2 values. A. Scatter diagram showing χ^2 and skewness distribution. Positive skewness with $\chi^2 > 1$ indicates older tail distribution (e.g., likely inheritance) and vice-versa. B. Latitudinal and longitudinal distribution of χ^2 values of 121 local glacial stages in the Himalayan-Tibetan orogen from late glacial to Late Holocene. More erosive temperate glaciers in the wet-warm and transitional central and eastern Himalaya show overall low χ^2 values compared to less erosive glaciers in the arid and semiarid regions.
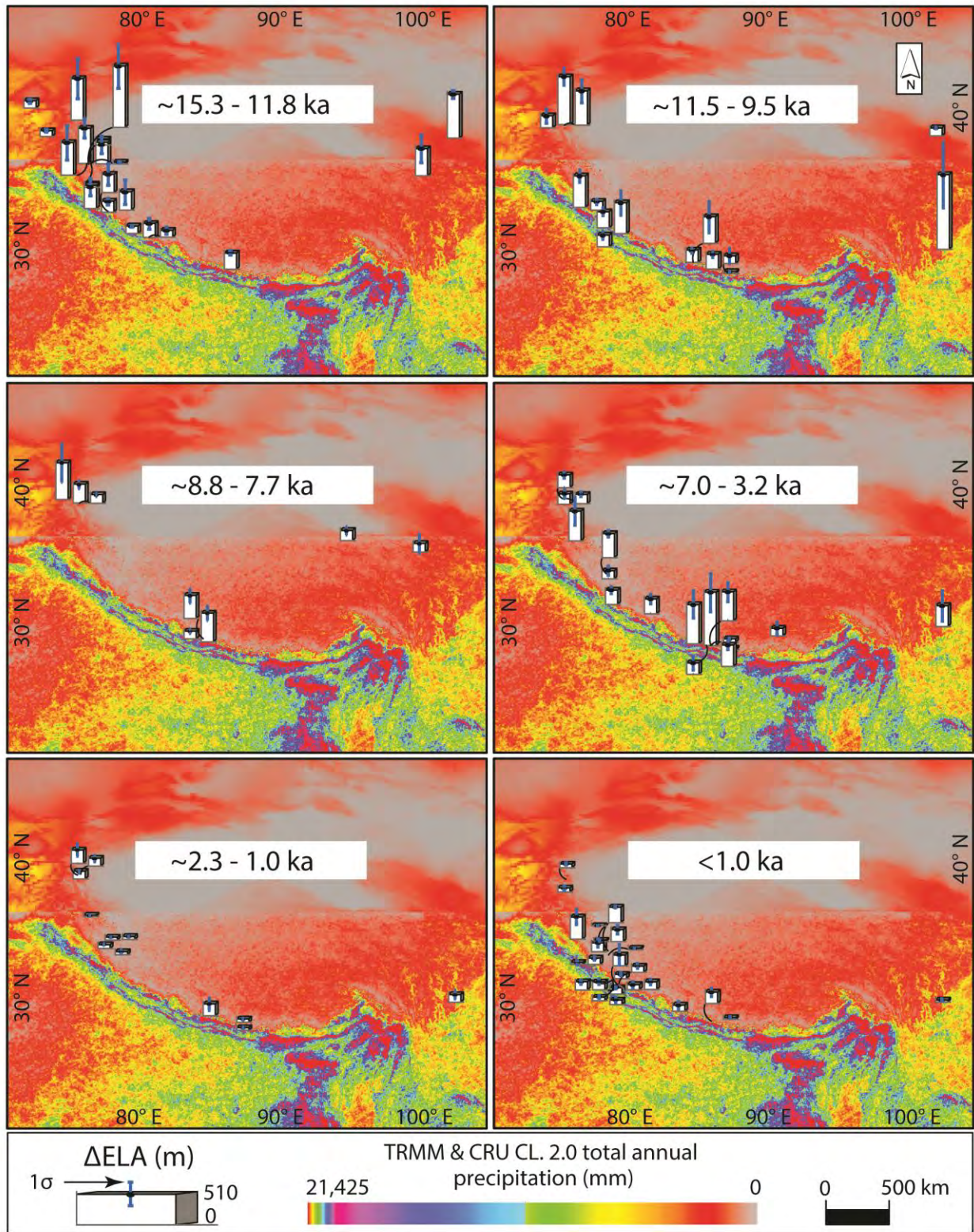
Fig. 10. Spatial distribution of ΔELAs in the Himalayan-Tibetan orogen during coeval regional glacier advances from late glacial to Late Holocene.

Table 1. Holocene moraine surface-exposure sample details and [10]Be ages (in thousands of years before AD 2016, labeled 'ka'±1σ) for the Kulti valley of the Lahul Himalaya.

Moraine morpho-stratigraphy	Sample ID	Latitude (DD N)	Longitude (DD E)	Elevation (m asl)	Boulder size (L x W x H) (cm)	Sample thickness (cm)	Shielding correction	Quartz weight (g)	[9]Be Carrier added (g)	[10]Be/[9]Be ± 1σ (10^{-14})	[[10]Be] ± 1σ (10^4 atoms g^{-1})	LSD Age ± 1σ (ka)[h]	Lm Age ± 1σ (ka)[i]
Kulti valley, Lahul													
M_{K5}	S19[a]	32.3833	77.2783	3255	300 x 290 x 90	2.0	1.000	31.090	1.0107[b]	21.20±0.64[d]	22.80±0.69	8.92±0.63	8.33±0.46
M_{K5}	S20[a]	32.3833	77.2783	3258	240 x 190 x 50	2.0	1.000	27.090	0.9400[b]	4.12±0.39[d]	4.73±0.45	2.11±0.25	1.95±0.22
M_{K5}	S21	32.3833	77.2783	3256	330 x 290 x 130	2.0	1.000	10.521	0.4221[b]	9.48±0.34[e]	32.03±1.14	13.19±0.78	12.54±0.72
M_{K5}	S22	32.3833	77.2783	3268	140 x 60 x 90	2.0	1.000	24.678	0.9505[b]	35.20±1.40[e]	44.85±1.78	16.11±1.01	15.33±0.86
M_{K5}	S23[a]	32.3833	77.2783	3272	160 x 80 x 30	2.0	1.000	30.900	0.9912[b]	2.98±0.28[d]	3.16±0.30	1.28±0.14	1.20±0.13
M_{K5}	S24[a]	32.3833	77.2783	3274	150 x 130 x 40	3.0	1.000	29.690	0.9855[b]	2.79±3.58[d]	3.06±3.93	1.25±1.6	1.16±1.49
M_{K4}	S2	32.4000	77.2850	3522	130 x 80 x 60	2.0	0.913	29.717	0.9440[b]	34.87±1.83[e]	36.64±1.92	11.96±0.86	11.42±0.71
M_{K4}	S3	32.4000	77.2850	3527	135 x 120 x 160	2.0	0.915	29.220	0.9990[b]	35.05±1.49[d]	39.64±1.69	12.90±0.85	12.29±0.76
M_{K4}	S5	32.4000	77.2850	3526	260 x 160 x 120	2.0	0.915	29.240	0.9820[b]	29.39±1.49[d]	32.65±1.65	10.86±0.65	10.33±0.63
M_{K4}	S6	32.4000	77.2850	3528	140 x 130 x 70	2.0	0.915	26.440	1.0140[b]	31.53±0.67[d]	39.99±0.85	12.99±0.72	12.40±0.63
M_{K2}	S9	32.4233	77.3067	3676	60 x 30 x 35	2.0	0.917	28.900	0.9635[b]	1.15±0.42[d]	1.27±0.46	0.40±0.15	0.37±0.14
M_{K2}	S10	32.4233	77.3067	3678	75 x 35x 30	2.0	0.913	32.592	0.9560[b]	2.01±0.20[e]	1.95±0.19	0.62±0.08	0.59±0.07
Parkachik valley, Nun Kun													
M_{P1}	PAR 1601	34.0835	75.9998	3700	500x400x150	2.0	0.968	21.065	0.3548[c]	0.48±0.05[f]	0.56±0.06	0.15±0.02	0.14±0.02
M_{P1}	PAR 1602	34.0844	76.0001	3687	100x60x100	3.0	0.973	13.654	0.3502[c]	0.18±0.04[f]	0.33±0.08	0.09±0.02	0.08±0.02
M_{P1}	PAR 1603	34.0846	76.0002	3678	180x50x80	3.5	0.974	9.665	0.3536[c]	0.28±0.02[g]	0.71±0.05	0.19±0.02	0.19±0.02
M_{P1}	PAR 1606	34.0850	76.0004	3667	210x115x70	2.0	0.969	7.905	0.3531[c]	0.24±0.04[g]	0.74±0.12	0.21±0.04	0.19±0.04

Note: Density value of 2.7 g cm^{-3}, the erosion rate of 0.00 cm a^{-1}, and AMS standard of 07KNSTD were used for all samples to calculate surface exposure ages; weathering is limited to none

[a] Outliers are identified and removed
[b] Carrier [9]Be concentration is 495 ppm
[c] Carrier [9]Be concentration is 1045.9 ppm
[d] Ratios are corrected from background [10]Be: 5.72±0.48 ([10]Be/[9]Be ± 1σ (10^{-14}))
[e] Ratios are corrected from background [10]Be: 3.13±0.21 ([10]Be/[9]Be ± 1σ (10^{-14}))
[f] Ratios are corrected from background [10]Be: 0.12±0.05 ([10]Be/[9]Be ± 1σ (10^{-14}))
[g] Ratios are corrected from background [10]Be: 0.08±0.03 ([10]Be/[9]Be ± 1σ (10^{-14}))
[h] Lifton-Sato-Dunai (LSD) scaling model using CREp online calculator
[i] Lal and Stone time-dependent (Lm) scaling model using CREp online calculator

Table 2. A summary of ELAs and ΔELAs in our study areas

Glacial Stage	Mean moraine age (ka)	Glacier area (~km²)	Mean slope (~°)	Mean aspect	Head (m asl)	Toe (m asl)	MELM (m asl)	Area-Altitude (m asl)	Area-Accumulation ratio AAR (0.45)	AAR (0.55)	AAR (0.65)	Toe-Headwall altitude ratio THAR (0.40)	THAR (0.50)	THAR (0.60)	Mean ELA (m asl)	ΔELA (m)
Kulti valley, Lahul																
Present	-	17.7	17	W	5465	3901	4640	4815	4929	4819	4719	4533	4690	4846	4749±127	-
M_{K1}	~0.12±0.01 (Historical)	22.9	18	W, SW	5478	3601	-	4727	4879	4759	4590	4403	4585	4766	4673±157	92±31
M_{K2}	0.51±0.16	23.4	18	W, SW	5478	3662	-	4704	4859	4739	4569	4397	4580	4762	4659±154	106±30
M_{K3}	N/A?	24.4	17	W, SW	5498	3631	-	4662	4839	4709	4529	4387	4575	4762	4638±153	127±38
M_{K4}	12.18±0.99	24.9	17	W, SW	5498	3432	-	4641	4829	4699	4500	4255	4460	4664	4578±188	186±62
M_{K5}	15.30±0.60	25.7	17	W, SW	5498	3151	-	4598	4809	4659	4469	4099	4335	4570	4506±232	259±109
Parkachik valley, Nun Kun																
Present	-	47.5	19	N	7014	3592	5251	5437	5510	5419	5339	4967	5310	5652	5361±202	
M_{P1}	0.16±0.05	48.6	19	N	7014	3556	-	5401	5499	5409	5319	4943	5290	5636	5357±216	20±9
M_{P2}	N/A?	-	-	-	-	-	-	-	-	-	-	-	-	-	-	-

Note: The present here refers to the year 2016 AD

m asl is a meter above sea level

N/A? indicates numerical dates are not available

Table 3. Principal component (PC) loading for all the variables used in this study.

Variables	PC1	PC2	PC3	PC4	PC5	PC6	PC7	PC8	PC9
Annual mean temperature	0.33	0.01	0.52	-0.26	-0.74	-0.03	0.01	0.00	-0.02
Annual temperature range	-0.29	-0.05	-0.73	-0.13	-0.60	0.06	0.02	0.01	-0.01
Annual total precipitation	0.35	0.38	-0.24	0.06	-0.01	-0.77	-0.23	-0.16	0.03
Annual precipitation range	0.29	0.49	-0.14	-0.08	0.03	0.50	0.02	-0.43	0.46
Total summer monsoon precipitation	-0.35	0.33	0.18	0.43	-0.18	0.02	-0.38	0.45	0.42
Total winter precipitation	0.35	-0.34	-0.18	-0.47	0.17	0.05	-0.40	0.44	0.36
SCI	-0.38	0.26	0.14	-0.47	0.09	0.09	-0.59	-0.23	-0.36
RE	-0.37	0.27	0.12	-0.53	0.11	-0.29	0.52	0.17	0.33
DSI	0.28	0.50	-0.14	-0.05	0.05	0.23	0.17	0.57	-0.49

Table 4. Average hypsometric and contemporary ELAs across five *climatic regions*.

Glacier subgroups	Toe (m asl)	Cirque head (m asl)	Present ELAs (m asl)
Group 1(a): Arid and semiarid colder climatic region— Transhimalaya, NW Tibet, Pamir, and Tian Shan.			
Muztag Ata, NW Tibet	~4500	~7000	~4017–5749
Pamir & the Tian Shan	~3550	~4500	~3963–4144
Karakoram[a]	~3930	~6000	~4713–5057
Ladakh & Zanskar	~5450	~6210	~5489–5870
Group 1(b): Arid and semiarid colder climatic region—southern and northeastern Tibet			
Southern & northeastern Tibet	~4500	~6590	~4407–5259
Group 2(a): Transitional climatic region—western Himalaya			
Garhwal Himalaya	~3740	~6020	~4611–5062
Nun Kun, Lahul, & Gurla Mandhata	~4000	~6780	~4500–6152
Group 2(b): Transitional climatic region—central and eastern Himalaya			
Central Himalaya	~4880	~6780	~5390–5809
Eastern Himalaya	~2980	~7000	-
Group 3(a): Wet and warm climatic region—central and eastern Himalaya			
Central & Eastern Himalaya[b]	~3930	~6590	~4440–5584

[a] Batura & Hunza glaciers are the largest (~57 km-long) and extending from ~2600–7540 m asl.
[b] Some smaller cirque glaciers (e.g., Syaktan, Yak Upper, Danfe, Macha Khola, and Mailun Khola) have an altitudinal range from snout-to-cirque between ~4690 and 5450 m asl.

Table 5. A summary of late glacial and Holocene local and regional stages of glacial advances based on recalculated cosmogenic [10]Be surface exposure age data.

Location number shown in Figure 1	Local glacial stage	Local stage age (ka)[a]	Regional stage age range (ka)	n (outlier free)	χ^2 value[b]	Peak of the stage (ka)[c]	Kernel Density fit (ka)[d]	P (sig2-tailed) between stages
Group 1(a). Arid and semiarid Transhimalaya, NW Tibet, Pamir, and Tian Shan								
5	Kitschi-Kurumdu-M2 (Zech, 2012)	15.16±3.03	15.2–11.7	4	17.74	13.9±0.1	14.0±0.9	0.0
11	Mungo 2 stage-m_{1I} (Seong et al., 2007)	14.98±0.29		5	0.17			
11	Mungo 2 stage-m_{1D} (Seong et al., 2007)	14.62±0.32		3	0.19			
10	Batura stage-t6 (Owen et al., 2002)	14.30±0.01		2				
11	Mungo 2 stage-m_{1I} (Seong et al., 2007)	14.08±0.23		3	0.11			
6	AV (Abramowski et al., 2006)	14.02±0.16		3	0.04			
11	Mungo 2 stage-m_{1G} (Seong et al., 2007)	13.77±0.53		10	0.56			
11	Mungo 2 stage-m_{1F} (Seong et al., 2007)	13.44±0.19		3	0.08			
9	BO8 stage (Röhringer et al., 2012)	13.18±0.64		2	0.65			
2	BOR 2 stage (Blomdin et al. (2016)	13.08±2.13		3	10.59			
11	Mungo 2 stage-m_{3I} (Seong et al., 2007)	13.06±0.40		3	0.33			
7	Olimde 2 stage-m_{3H} (Seong et al., 2009)	13.01±0.14		3	0.04			
10	Batura stage-t6 (Owen et al., 2002)	12.49±1.05		2				
11	Mungo 2 stage-m_{1E} (Seong et al., 2007)	12.41±0.33		2	0.25			
8	Olimde 2 stage-m_{5C} (Seong et al., 2009)	11.71±0.40		2	0.46			
8	Olimde 3 stage-m_{3F} (Seong et al., 2009)	10.25±0.16	10.3–9.7	6	0.10	10.3±0.1	10.2±0.3	0.0
8	Olimde 3 stage-$m_{3F'}$ (Seong et al., 2009)	9.69±0.34	(tentative)	8	0.43			
7	Olimde 4 Stage-m_{4H} (Seong et al., 2009)	7.98±0.10	8.0–7.7	6	0.06	7.4±0.1	8.0±0.2	0.0
8	Olimde 4 Stage-m_{6A} (Seong et al., 2009)	7.80±0.29		5	0.48			
8	Olimde 4 Stage-m_{5A} (Seong et al., 2009)	7.74±0.27		6	0.41			
11	Mungo 2 stage-m_{2G} (Seong et al., 2007)	6.64±0.35	6.6–3.5	4	0.68	4.4±0.1	5.7±0.8	0.0
11	Askole 2 stage-m_{2b} (Seong et al., 2007)	5.98±0.69		4	0.92			
3	Aksai (Koppes et al., 2008)	5.70±0.16		2				
8	Olimde 5 stage-$m_{6C'}$ (Seong et al., 2009)	5.05±0.14		3	0.33			
15	KM-4 stage/mG2 (Hedrick et al., 2011)	4.66±1.17		6	13.12			
7	Olimde 6 stage-m_{5H} (Seong et al., 2009)	4.32±0.11		3	0.19			
7	Olimde 6 stage-m_{6H} (Seong et al., 2009)	3.97±0.30		3	2.17			
15	PM-2 stage (Hedrick et al., 2011; Saha et al., 2018)	3.50±0.87		3	17.79			
13	Ladakh Chang La cirque (Dortch et al., 2013)	2.29±0.28	2.3–1.3	4	2.02	2.1±0.0	2.2±0.4	0.0
15	m_{G1} (Saha et al., 2018)	2.25±0.42		3	9.37			
8	Olimde 7 stage-m7A (Seong et al., 2009)	2.20±0.07		6	0.19			
7	Olimde 7 stage-m7H (Seong et al., 2009)	1.66±0.17		3	0.75			
14	m_{S2} (Orr et al., 2017; Saha et al., 2018)	1.42±0.48		6	21.83			
7	Olimde 7 stage-m_{3I} (Seong et al., 2009)	1.39±0.42		4	4.58			
15	m_{G1} (Orr et al., 2017)	1.33±0.12		1	-			
11	Askole 3 stage-m_{1H} (Seong et al., 2007)	1.03±0.28	~1.0 (tentative)	5	0.82	1.0±0.0	1.0±0.1	0.0
15	m_{M2} (Saha et al., 2018)	1.00±0.08		4	0.9			
8	Olimde 8 stage-m_{8A} (Seong et al., 2009)	0.69±0.27	<1.0	3	10.19	?	0.6±0.1	0.0
15	m_{M1} (Saha et al., 2018)	0.64±0.09		3	1.47			
2	BOR 1 (Blomdin et al., 2016)	0.64±0.23		3	10.96			
13	Pangong high cirque (Dortch et al., 2013)	0.54±0.11		3	0.63			
14	m_{A2c} (Saha et al., 2018)	0.52±0.20		3	24.25			
8	Olimde 8 stage-m_{6C} (Seong et al., 2009)	0.51±0.15		4	4.19			

3	Ala Archa (Koppes et al., 2008)	0.49±0.25		2				
1	Daxi (Li et al., 2014)	0.33±0.02		4	0.49			
15	PM-3 stage (Hedrick et al., 2011)	0.28±0.05		3	2.22			
14	m_{A1} (Saha et al., 2018)	0.26±0.08		3	6.78			

Group 2(a). Transitional western Himalaya

22	M5 (Owen et al., 2010)	15.30±0.60	15.3–11.8	3	0.54	14.0±0.2	13.7±1.2	0.0
16	M_{k5} (This study)	14.65±2.06		2				
16	Kulti glacial stage (Owen et al., 2001)	14.45±0.70		1	-			
18	Tons Valley-location C (Scherler et al., 2010)	14.06±0.10		2				
16	Kulti glacial stage (Owen et al., 2001)	14.03±0.16		2	0.05			
16	Kulti glacial stage (Owen et al., 2001)	13.95±0.88		2	1.11			
21	Moraine m2 (Barnard et al., 2004b)	13.71±0.69		1	-			
20	mm1 (Murari et al., 2014)	13.62±0.66		4	0.67			
12	Anantick stage-ST-3 (Lee et al., 2014)	13.55±0.88		2				
16	M_{k4} (This study)	12.18±0.99		4	2.06			
16	Kulti glacial stage (Owen et al., 2001)	11.76±0.59		2	0.54			
18	Tons Valley-location D (Scherler et al., 2010)	11.09±0.50	11.1–10.3	1	-	10.6±0.2	10.8±0.5	0.0
16	m_{H3} (Saha et al., 2018)	10.48±0.48		3	0.48			
18	Tons Valley-location F' (Scherler et al., 2010)	10.26±0.35		2				
20	mk1 (Murari et al., 2014)	10.25±0.83		5	0.64			
22	M7 (Owen et al., 2010)	8.75±0.55	8.8–8.3	2		7.8±0.2	8.4±0.5	0.0
19	Kedar glacial stage (Barnard et al., 2004a)	8.28±0.45	(tentative)	2				
18	Tons Valley-Location F (Scherler et al., 2010)	6.09±0.54	6.1–5.0	4	4	5.5±0.1	5.5±0.2	0.0
19	Shivling glacial stage (Srivastava, 2012; Sci. report)	5.22±0.27		7	0.63			
22	M8 (Owen et al., 2010)	5.01±0.88		2				
19	Gangotri glacial stage (Srivastava, 2012; Sci. report)	2.16±0.35	~2.2 (tentative)	2		2.2±0.4	?	
18	Tons Valley-Location G (Scherler et al., 2010)	0.66±0.34	<1	2		?	0.3±0.1	0.0
17	Yn (Saha et al., 2016)	0.62±0.15		2	2.13			
21	Moraine m4 (Barnard et al., 2004b)	0.60±0.28		2				
19	Gangotri stage (Barnard et al., 2004a; Srivastava, 2012)	0.56±0.30		5	4.45			
12	Lonp stage-TG-3 (Lee et al., 2014)	0.53±0.13		2	12.53			
16	M_{k2} (This study)	0.51±0.16		2				
22	M9 (Owen et al., 2010)	0.46±0.10		4	2.57			
20	mk2 (Murari et al. (2014)	0.31±0.17		3	19.33			
16	m_{H1a} (Saha et al., 2018)	0.26±0.13		3	8.55			
18	Tons Valley-Location E (Scherler et al., 2010)	0.26±0.08		2				
22	M10 (Owen et al., 2010)	0.24±0.15		3	10.04			
19	Bhujbas glacial stage (Srivastava, 2012; Sci. report)	0.21±0.02		1	-			
20	mbd1 (Murari et al., 2014)	0.21±0.02		3	0.61			
20	mbd2 (Murari et al., 2014)	0.16±0.15		5	103.54			
20	mbd3 (Murari et al., 2014)	0.15±0.10		3	71.63			
20	mbd4 (Murari et al., 2014)	0.13±0.11		2				

Group 3(a). Wet and warm central and eastern Himalaya

31	Ganhaizi (Kong et al., 2009)	12.97±1.41	13.0–10.9	2			12.0±1.0	0.0
31	Ganheba (Kong et al., 2009)	11.96±1.94		2				
31	Yulong (Kong et al., 2009)	?		0				
23	Yak Glacier lower (Pratt-Sitaula, 2005)	11.66±1.29		2				

23	Lyapche Glacier (Pratt-Sitaula, 2005)	11.54±0.80		3	2.02			
24	LT3: Langtang Stage (Abramowski, 2004)	10.90±0.43		3	0.55			
23	Syaktan Glacier (Pratt-Sitaula, et al., 2011)	9.48±0.91	9.5–8.7	4	3.38		8.9±0.5	0.0
23	Danfe Glacier (Pratt-Sitaula, et al., 2011)	8.87±0.36		7	0.53			
23	Yak upper (Pratt-Sitaula, 2005)	8.72±0.40		5	0.75			
25	M3 (Gayer et al., 2006)	7.04±0.64	7.0–4.4	2			4.6±0.6 and	
23	Lete (Zech et al., 2009)	6.36±1.21		1			6.2±0.5	
26	Langtang glacial stage (Barnard et al., 2006)	5.47±0.40		2				0.0
26	MK4: LIA (Abramowski, 2004)	4.99±0.92		4	2.83			
26	Langtang glacial stage (Barnard et al., 2006)	4.60±0.33		1				
26	LT6 (Abramowski, 2004)	4.42±0.15		2				
23	Neoglacial (Zech et al., 2009)	1.70±0.50	~1.7 (tentative)	2		1.7±0.5	?	
26	Yala I glacial stage (Barnard et al., 2006)	0.76±0.20	<1 (tentative)	6	0.61	?	0.7±0.1	
23	E moraine crest (Heimsath and McGlynn, 2008)	0.55±0.16		5	5.54			0.0

Group 2(b). Transitional central and eastern Himalaya

27	Puluo 2 moraine (Schaefer et al., 2008)	13.47±0.58	~13.5 (tentative)	4	0.41		?	
28	Chhukung glacial stage (Finkel et al., 2003)	11.52±0.11	11.5–10.1	3	0.04		9.8±0.7 and	0.0
28	Chhukung glacial stage (Finkel et al., 2003)	10.97±0.03		2			11.3±0.7	
30	Local LGM moraines (Owen et al., 2005)	10.10±0.73		5	0.89			
30	Recessional moraine (Owen et al., 2005)	6.03±1.97	6.0–3.2	2			4.6±0.7	0.0
28	Thuklha glacial stage (Finkel et al., 2003)	4.43±0.32		3	1.08			
29	T5c (Owen et al., 2009)	3.18±0.23		5	1.18			
29	T6 (Owen et al., 2009)	2.08±0.09	~2.1–1.0	3	0.51	2.1±0.1	1.0±0.2 and	0.0
30	Neoglacial moraines (Owen et al., 2005)	1.04±0.10	(tentative)	4	0.31		2.1±0.2	
30	Little Ice Age moraines (Owen et al., 2005)	0.46±0.06	<1	2			0.5±0.2	0.0
29	T7 (Owen et al., 2009)	0.33±0.19		3	12.31			

Group 1(b). Arid and semiarid southern and northeastern Tibet

33	Group D moraines (Wang et al., 2013)	13.45±0.25	13.5–12.9	2			13.2±0.7	0.0
34	LLL (Lasserre et al., 2002)	13.16±1.05		6	1.66			
35	Halong glacial stage (Owen et al., 2003a)	12.89±1.26		6	4.68			
32	PR (Owen et al., 2005)	11.47±0.70	11.5–9.5	4	1.56		10.8±1.0	0.0
35	Holocene moraine (Owen et al., 2003b)	10.08±0.53		1	-			
35	Halong glacial stage (Owen et al., 2003a)	9.48±1.70		2				
36	M2 moraines (Owen et al., 2006)	8.04±0.74	~8.0 (tentative)	2		8.0±0.7	?	
32	Youngest (Owen et al., 2005)	3.28±0.74	~3.3 (tentative)	3	6.20	3.3±0.7	?	

[a] All local stage age uncertainties are reported in 1σ.
[b] Corrected Chi-squared values are from outlier free distribution.
[c] All regional stage age uncertainties are reported in 1σ.
[d] Kernel Density fit is performed using ksdensity function in MATLAB and using the PDF model after Dortch et al. (2013) and Murari et al. (2014)

Appendix A2. Supplementary data

REFERENCE CITED

Abramowski, D., 2004. exposure dating of erratic boulders in the reconstruction of the late Pleistocene glaciation history of mountainous regions, with examples from Nepal and Central Asia. Deposit.Ddb.De.

Abramowski, U., Bergau, A., Seebach, D., Zech, R., Glaser, B., Sosin, P., Kubik, P. W., Zech, W., 2006. Pleistocene glaciations of Central Asia: results from [10]Be surface exposure ages of erratic boulders from the Pamir (Tajikistan), and the Alay–Turkestan range (Kyrgyzstan). Quat. Sci. Rev. 25, 1080–1096.

Anderson, L. S., Roe, G. H., Anderson, R. S., 2014. The effects of interannual climate variability on the moraine record. Geology 42, 55–58.

Applegate, P. J., Urban, N. M., Keller, K., Lowell, T. V., Laabs, B. J. C., Kelly, M. A., Alley, R. B., 2012. Improved moraine age interpretations through explicit matching of geomorphic process models to cosmogenic nuclide measurements from single landforms. Quat. Res. 77, 293–304.

Applegate, P. J., Urban, N. M., Laabs, B. J. C., Keller, K., Alley, R. B., 2010. Modeling the statistical distributions of cosmogenic exposure dates from moraines. Geosci. Model Dev. 3, 293–307.

Azam, M. F., Wagnon, P., Vincent, C., Ramanathan, A., Favier, V., Mandal, A., Pottakkal, J. G., 2014. Processes governing the mass balance of Chhota Shigri Glacier (western Himalaya, India) assessed by point-scale surface energy balance measurements. Cryosph. 8, 2195–2217.

Azharuddin, S., Govil, P., Singh, A. D., Mishra, R., Agrawal, S., Tiwari, A. K., Kumar, K., 2017. Monsoon-influenced variations in productivity and lithogenic flux along offshore Saurashtra, NE Arabian Sea during the Holocene and Younger Dryas: A multi-proxy approach. Palaeogeogr. Palaeoclimatol. Palaeoecol. 483, 136–146.

Bahuguna, I. M., Rathore, B. P., Brahmbhatt, R., Sharma, M., Dhar, S., Randhawa, S. S., Kumar, K., Romshoo, S., Shah, R. D., Ganjoo, R. K., Ajai, 2014. Are the Himalayan glaciers retreating? Curr. Sci. 106, 1008–1013.

Balco, G., Stone, J. O., Lifton, N. A., Dunai, T. J., 2008. A complete and easily accessible means of calculating surface exposure ages or erosion rates from [10]Be and [26]Al measurements. Quat. Geochronol. 3, 174–195.

Barker, T., 2007. Climate Change 2007 : An Assessment of the Intergovernmental Panel on Climate Change. Change, Synthesis Report 446, 12–17.

Barnard, P. L., Owen, L. A, Sharma, M. C., Finkel, R. C., 2004b. Late Quaternary (Holocene) landscape evolution of a monsoon-influenced high Himalayan valley, Gori Ganga, Nanda Devi, NE Garhwal. Geomorphology 61, 91–110.

Barnard, P.L., Owen, L. A., Finkel, R.C., 2006. Quaternary fans and terraces in the Khumbu Himal south of Mount Everest: their characteristics, age and formation. J. Geol. Soc. London. 163, 383–399.

Barnard, P.L., Owen, L.A., Finkel, R.C., 2004. Style and timing of glacial and paraglacial sedimentation in a monsoon-influenced high Himalayan environment , the upper Bhagirathi Valley , Garhwal Himalaya. Sediment. Geol. 165, 199–221.

Barr, I. D., Lovell, H., 2014. A review of topographic controls on moraine distribution. Geomorphology.

Benn, D. I., Owen, L. A., 1998. The role of the Indian summer monsoon and the mid-latitude westerlies in Himalayan glaciation: review and speculative discussion. J. Geol. Soc. London. 155, 353–363.

Benn, D. I., Owen, L. A., 2002. Himalayan glacial sedimentary environments : a framework for reconstructing and dating the former extent of glaciers in high mountains 98, 3–25.

Benn, D. I., Owen, L. A., Osmaston, H. A., Seltzer, G. O., Porter, S. C., Mark, B., 2005. Reconstruction of equilibrium-line altitudes for tropical and sub-tropical glaciers. Quat. Int. 138–139, 8–21.

Benn, D., Evans, D. J, 2010. Glaciers and glaciation, 2 eds. Routledge, p. 817.

Berger, A. L., 1978. Long-Term Variations of Caloric Insolation from the Earth's Orbital Elements'. Quat. Res. 9, 139–167.

Berkelhammer, M., Sinha, A., Stott, L., Cheng, H., Pausata, F. S. R., Yoshimura, K., 2012a. An abrupt shift in the Indian Monsoon 4 , 000 years ago An Abrupt Shift in the Indian Monsoon 4000 Years Ago.

Berkelhammer, M., Sinha, A., Stott, L., Cheng, H., Pausata, F. S. R., Yoshimura, K., 2012b. An Abrupt Shift in the Indian Monsoon 4000 Years Ago.

Bhambri, R., Bolch, T., Chaujar, R. K., Kulshreshtha, S. C., 2011. Glacier changes in the Garhwal Himalaya, India, from 1968 to 2006 based on remote sensing. J. Glaciol. 57, 543–556.

Bhambri, R., Hewitt, K., Kawishwar, P., Pratap, B., 2017. Surge-type and surge-modified glaciers in the Karakoram. Sci. Rep. 7, 1–14.

Bhargava, O. N., 2008. An updated introduction to the Spiti geology. J. Palaeontol. Soc. India 53, 113–129.

Bisht, P., Nawaz Ali, S., Rana, N., Singh, S., Poonam, Sundriyal, Y. P., Bagri, D. S., Juyal, N., 2017. Pattern of Holocene glaciation in the monsoon-dominated Kosa Valley, central Himalaya, Uttarakhand, India. Geomorphology 284, 130–141.

Blomdin, R., Stroeven, A. P., Harbor, J. M., Lifton, N. A., Heyman, J., Gribenski, N., Petrakov, D. A., Caffee, M. W., Ivanov, M. N., Hättestrand, C., Rogozhina, I., Usubaliev, R., 2016. Evaluating the timing of former glacier expansions in the Tian Shan: A key step towards robust spatial correlations. Quat. Sci. Rev. 153, 78–96.

Bolch, T., Kulkarni, A., Kaab, A., Huggel, C., Paul, F., Cogley, J. G., Frey, H., Kargel, J. S., Fujita, K., Scheel, M., Bajracharya, S., Stoffel, M., 2012. The State and Fate of Himalayan Glaciers. Science (80). 336, 310–314.

Bookhagen, B., Burbank, D. W., 2006. Topography, relief, and TRMM-derived rainfall variations along the Himalaya. Geophys. Res. Lett. 33, L08405.

Bookhagen, B., Burbank, D. W., 2010. Toward a complete Himalayan hydrological budget: Spatiotemporal distribution of snowmelt and rainfall and their impact on river discharge. J. Geophys. Res. 115, F03019.

Borchers, B., Marrero, S., Balco, G., Caffee, M., Goehring, B., Lifton, N., Nishiizumi, K., Phillips, F., Schaefer, J., Stone, J., 2016. Geological calibration of spallation production rates in the CRONUS-Earth project. Quat. Geochronol. 31, 188–198.

Brun, F., Berthier, E., Wagnon, P., Kääb, A., Treichler, D., 2017. A spatially resolved estimate of High Mountain Asia glacier mass balances from 2000 to 2016. Nat. Geosci. 10, 668–673.

Burbank, D. W., Bookhagen, B., Gabet, E. J., Putkonen, J., 2012. Modern climate and erosion in the Himalaya. Comptes Rendus-Geosci. 344, 610–626.

Carr, S. J., Lukas, S., Mills, S. C., 2010. Glacier reconstruction and mass-balance modelling as a geomorphic and palaeoclimatic tool 1115, 1103–1115.

Chand, P., Sharma, M. C., Bhambri, R., Sangewar, C. V., Juyal, N., 2017. Reconstructing the pattern of the Bara Shigri Glacier fluctuation since the end of the Little Ice Age, Chandra valley, north-western Himalaya. Prog. Phys. Geogr. 41, 643–675.

Chiang, J. C. H., Lee, S. Y., Putnam, A. E., Wang, X., 2014. South Pacific Split Jet, ITCZ shifts, and atmospheric North-South linkages during abrupt climate changes of the last glacial period. Earth Planet. Sci. Lett. 406, 233–246.

Çiner, A., Sarıkaya, M. A., Yıldırım, C., 2017. Misleading old age on a young landform? The dilemma of cosmogenic inheritance in surface exposure dating: Moraines vs. rock glaciers. Quat. Geochronol. 42, 76–88.

Clift, P. D., Carter, A., Giosan, L., Durcan, J., Duller, G. A. T., Macklin, M. G., Alizai, A., Tabrez, A. R., Danish, M., VanLaningham, S., Fuller, D. Q., 2012. U-Pb zircon dating evidence for a Pleistocene Sarasvati River and capture of the Yamuna River. Geology 40, 211–214.

Cogley, J. G., Kargel, J. S., Kaser, G., van der Veen, C. J., 2010. Tracking the source of glacier misinformation. Science 327, 522.

Damm, B., 2006. Late Quaternary glacier advances in the upper catchment area of the Indus River (Ladakh and Western Tibet). Quat. Int. 154–155, 87–99.

Demske, D., Tarasov, P. E., Wünnemann, B., Riedel, F., 2009. Late glacial and Holocene vegetation , Indian monsoon and westerly circulation in the Trans-Himalaya recorded in the lacustrine pollen sequence from Tso Kar. Palaeogeogr. Palaeoclimatol. Palaeoecol. 279, 172–185.

Denton, G. H., Broecker, W. S., 2008. Wobbly ocean conveyor circulation during the Holocene? Quat. Sci. Rev. 27, 1939–1950.

Derbyshire, E., Shi, Y., Li, J., Zheng, B., Li, S., Wang, J., 1991. Quaternary glaciation of tibet: The geological evidence. Quat. Sci. Rev. 10, 485–510.

Deswal, S., Sharma, M., Saini, R., Chand, P., Juyal, N., Singh, I., Srivastava, P., Ajai, Bahuguna, I. M., 2017. Late Holocene Glacier Dynamics in the Miyar Basin, Lahaul Himalaya, India. Geosciences 7, 64.

Dong, J., Wang, Y., Cheng, H., Hardt, B., Edwards, R. L., Kong, X., Wu, J., Chen, S., Liu, D., Jiang, X., Zhao, K., 2010a. A high-resolution stalagmite record of the Holocene East Asian monsoon from Mt Shennongjia, central China. Holocene 20, 257–264.

Dong, J., Wang, Y., Cheng, H., Hardt, B., Edwards, R. L., Kong, X., Wu, J., Chen, S., Liu, D., Jiang, X., Zhao, K., 2010b. A high-resolution stalagmite record of the Holocene East Asian monsoon from Mt Shennongjia , central China 2, 257–264.

Dortch, J. M., Owen, L. A., Caffee, M. W., 2013. Timing and climatic drivers for glaciation across semi-arid western Himalayan–Tibetan orogen. Quat. Sci. Rev. 78, 188–208.

Dühnforth, M., Anderson, R. S., Ward, D., Stock, G. M., 2010. Bedrock fracture control of glacial erosion processes and rates. Geology 38, 423–426.

Dunai, T. J., 2010. Cosmogenic Nuclides: Principles, Concepts and Applications in the Earth Surface Sciences. Cambridge Univ. Press. Cambridge.

Duncan, C., Masek, J., Fielding, E., 2003. How steep are the Himalaya? Characteristics and implications of along-strike topographic variations. Geology 31, 75–78.

Dykoski, C. A., Edwards, R. L., Cheng, H., Yuan, D., Cai, Y., Zhang, M., Lin, Y., Qing, J., An, Z., Revenaugh, J., 2005. A high-resolution, absolute-dated Holocene and deglacial Asian monsoon record from Dongge Cave, China. Earth Planet. Sci. Lett. 233, 71–86.

Eaves, S. R., Mackintosh, A. N., Anderson, B. M., Doughty, A. M., Townsend, D. B., Conway, C. E., Winckler, G., Schaefer, J. M., Leonard, G. S., Calvert, A. T., 2016. The Last Glacial Maximum in the central North Island, New Zealand: Palaeoclimate inferences from glacier modelling. Clim. Past 12, 943–960.

Eugster, P., Scherler, D., Thiede, R. C., Codilean, A. T., Strecker, M. R., 2016. Rapid last glacial maximum deglaciation in the Indian Himalaya coeval with mid-latitude glaciers: New insights from [10]Be-dating of ice-polished bedrock surfaces in the Chandra Valley, NW Himalaya. Geophys. Res. Lett. 43, 1589–1597

Fielding, E., Isacks, B., Barazangi, M., Duncan, C., 1994. How flat is Tibet? Geology 22, 163–167.

Finkel, R.C., Owen, L. A., Barnard, P.L., Caffee, M.W., 2003. Beryllium-10 dating of Mount Everest moraines indicates a strong monsoon influence and glacial synchroneity throughout the Himalaya. Geology 31, 561–564.

Fleitmann, D., Burns, S. J., Mangini, A., Mudelsee, M., Kramers, J., Villa, I., Neff, U., Al-Subbary, A. A., Buettner, A., Hippler, D., Matter, A., 2007. Holocene ITCZ and Indian monsoon dynamics recorded in stalagmites from Oman and Yemen (Socotra). Quat. Sci. Rev. 26, 170–188.

Fleitmann, D., Burns, S. J., Mudelsee, M., Neff, U., Kramers, J., Mangini, A., Matter, A., 2003. Holocene Forcing of the Indian Monsoon Recorded in a Stalagmite from Southern Oman. Science (80). 300, 1737–1739.

Fujita, K., 2008. Effect of precipitation seasonality on climatic sensitivity of glacier mass balance. Earth Planet. Sci. Lett. 276, 14–19.

Gasse, F., Fontes, J. C., Campo, E. Van, Wei, K., 1996. Holocene environmental changes in Bangong Co basin (Western Tibet). Part 4 : Discussion and conclusions 120, 79–92.

Gayer, E., Lavé, J., Pik, R., France-Lanord, C., 2006. Monsoonal forcing of Holocene glacier fluctuations in Ganesh Himal (Central Nepal) constrained by cosmogenic [3]He exposure ages of garnets. Earth Planet. Sci. Lett. 252, 275–288.

Gibbons, A. B., Megeath, J. D., Pierce, K. L., 1984. Probability of moraine survival in a succession of glacial advances. Geology 12, 327–330.

Gibson, M. J., Glasser, N. F., Quincey, D. J., Mayer, C., Rowan, A. V., Irvine-Fynn, T. D. L., 2017. Temporal variations in supraglacial debris distribution on Baltoro Glacier, Karakoram between 2001 and 2012. Geomorphology 295, 572–585.

Gosse, J. C., 2005. The contributions of cosmogenic nuclides to unraveling alpine paleo-glacier histories, in Huber, U. M., et al., eds., Global Change and Mountain Regions. An Overview of Current Knowledge: Advances in Global Change Research, vol. 23. Springer, Dordrecht, 39–50.

Harcourt, A. F. P. T. R., 2010. Geographical Society, B. B. and Publishing: On the Himalayan Valleys: Kooloo, Lahoul, and Spiti, Journal of the Royal Geographical Society, 41(1871), 245–257.

Hedrick, K. a., Seong, Y.B., Owen, L. A., Caffee, M. W., Dietsch, C., 2011. Towards defining the transition in style and timing of Quaternary glaciation between the monsoon-influenced Greater Himalaya and the semi-arid Transhimalaya of Northern India. Quat. Int. 236, 21–33.

Heimsath, A. M., McGlynn, R., 2008. Quantifying periglacial erosion in the Nepal high Himalaya. Geomorphology 97, 5–23.

Herzschuh, U., Winter, K., Wünnemann, B., Li, S., 2006. A general cooling trend on the central Tibetan Plateau throughout the Holocene recorded by the Lake Zigetang pollen spectra. Quat. Int. 154–155, 113–121.

Heyman, J., Applegate, P. J., Blomdin, R., Gribenski, N., Harbor, J. M., Stroeven, A. P., 2016. Boulder height - exposure age relationships from a global glacial ^{10}Be compilation. Quat. Geochronol. 34, 1–11.

Hu, C., Henderson, G. M., Huang, J., Xie, S., Sun, Y., Johnson, K. R., 2008. Quantification of Holocene Asian monsoon rainfall from spatially separated cave records. Earth Planet. Sci. Lett. 266, 221–232.

Huang, L., Zhu, L., Wang, J., Ju, J., Wang, Y., Zhang, J., Yang, R., 2016. Glacial activity reflected in a continuous lacustrine record since the early Holocene from the proglacial Laigu Lake on the southeastern Tibetan Plateau. Palaeogeogr. Palaeoclimatol. Palaeoecol. 456, 37–45.

Hudson, A. M., Olsen, J. W., Quade, J., Lei, G., Huth, T. E., Zhang, H., 2016. A regional record of expanded Holocene wetlands and prehistoric human occupation from paleowetland deposits of the western Yarlung Tsangpo valley, southern Tibetan Plateau. Quat. Res. (United States) 86, 13–33.

Hughes, P. D., 2010. Geomorphology and Quaternary stratigraphy: The roles of morpho-, litho-, and allostratigraphy. Geomorphology 123, 189–199.

Hughes, P. D., Gibbard, P. L., 2015. A stratigraphical basis for the Last Glacial Maximum (LGM). Quat. Int. 383, 174–185.

Hughes, P. D., Gibbard, P. L., Woodward, J., 2005. Quaternary glacial records in mountain regions : A formal stratigraphical approach Quaternary glacial records in mountain regions : A formal stratigraphical approach.

Huth, T., Hudson, A. M., Quade, J., Guoliang, L., Hucai, Z., 2015. Constraints on paleoclimate from 11.5 to 5.0 ka from shoreline dating and hydrologic budget modeling of Baqan Tso, southwestern Tibetan Plateau. Quat. Res. (United States) 83, 80–93.

IPCC, 2014. Climate Change 2013, the Fifth Assessment Report.

Ivy-Ochs, S., Kerschner, H., Schlüchter, C., 2007. Cosmogenic nuclides and the dating of Lateglacial and Early Holocene glacier variations: The Alpine perspective. Quat. Int. 164–165, 53–63.

Jennerjahn, T. C., Ittekkot, V., Arz, H. W., Behling, H., Pätzold, J., Wefer, G., 2004. Asynchronous Terrestrial and Marine Signals of Climate Change During Heinrich Events Asynchronous Terrestrial and Marine Signals of Climate Change During Heinrich Events. Science (80). 306.

Ji, J., Shen, J., Balsam, W., Chen, J., Liu, L., Liu, X., 2005. Asian monsoon oscillations in the northeastern Qinghai-Tibet Plateau since the late glacial as interpreted from visible reflectance of Qinghai Lake sediments. Earth Planet. Sci. Lett. 233, 61–70.

Ji, S., Xingqi, L., Sumin, W., Matsumoto, R., 2005. Palaeoclimatic changes in the Qinghai Lake area during the last 18,000 years. Quat. Int. 136, 131–140.

Jin, L., Schneider, B., Park, W., Latif, M., Khon, V., Zhang, X., 2014. The spatial–temporal patterns of Asian summer monsoon precipitation in response to Holocene insolation change: a model-data synthesis. Quat. Sci. Rev. 85, 47–62.

Kaplan, M. R., Schaefer, J. M., Denton, G. H., Doughty, A. M., Barrell, D. J. A., Chinn, T. J. H., Putnam, A. E., Andersen, B. G., Mackintosh, A., Finkel, R. C., Schwartz, R., Anderson, B., 2013. The anatomy of long-term warming since 15 ka in New Zealand based on net glacier snowline rise. Geology 41, 887–890.

Kirkbride, M. P., Brazier, V., 1998. A critical evaluation of the use of glacier chronologies in climatic reconstruction, with reference to New Zealand. In Owen, I.A. (Ed.), Mountain glaciations, Quaternary Proceedings, 6. Wiley, Chichester, U.K., 55–64.

Kirkbride, M. P., Winkler, S., 2012. Correlation of Late Quaternary moraines: Impact of climate variability, glacier response, and chronological resolution. Quat. Sci. Rev. 46, 1–29.

Klok, E. J., Oerlemans, J., 2003. Deriving historical equilibrium-line altitudes from a glacier length record by linear inverse modelling. Holocene 13, 343–351.

Kohl C. P., Nishiizumi K., 1992. Chemical isolation of quartz for measurement of in-situ-produced cosmogenic nuclides. Geochimica et Cosmochimica Acta 56, 3583–3587.

Kohl, C. P., Nishiizumi, K., 1992. Chemical isolation of quartz for measurement of in-situ-produced cosmogenic nuclides. Geochim. Cosmochim. Acta 56, 3583–3587.

Kong, P., Na, C., Fink, D., Zhao, X., Xiao, W., 2009. Moraine dam related to late Quaternary glaciation in the Yulong Mountains, southwest China, and impacts on the Jinsha River. Quat. Sci. Rev. 28, 3224–3235.

Koppes, M., Gillespie, A. R., Burke, R. M., Thompson, S. C., Stone, J., 2008. Late Quaternary glaciation in the Kyrgyz Tien Shan. Quat. Sci. Rev. 27, 846–866.

Kramer, A., Herzschuh, U., Mischke, S., Zhang, C., 2010a. Holocene treeline shifts and monsoon variability in the Hengduan Mountains (southeastern Tibetan Plateau), implications from palynological investigations. Palaeogeogr. Palaeoclimatol. Palaeoecol. 286, 23–41.

Kramer, A., Herzschuh, U., Mischke, S., Zhang, C., 2010b. Late glacial vegetation and climate oscillations on the southeastern Tibetan Plateau inferred from the Lake Naleng pollen profile. Quat. Res. 73, 324–335.

Kumar, G., Joshi, A., Mathur, V. K., 1987. Redlichid trilobites from the Tal formation. Lesser Himalaya. India. Curr. Sci. 56, 659–663.

Lal, D., 1991. Cosmic ray labeling of erosion surfaces: in situ nuclide production rates and erosion models. Earth Planet. Sci. Lett. 104, 424–439.

Lasserre, C., 2002. Fast late Pleistocene slip rate on the Leng Long Ling segment of the Haiyuan fault, Qinghai, China. J. Geophys. Res. 107, 2276.

Lea, D. W., Pak, D. K., Peterson, L. C., Hughen, K. A., 2003. Synchroneity of Tropical and High-Latitude Atlantic Temperatures over the Last Glacial Termination. Science (80). 301, 1361–1364.

Lee, S. Y., Seong, Y. B., Owen, L. A., Murari, M. K., Lim, H. S., Yoon, H. Il, Yoo, K.-C., 2014. Late Quaternary glaciation in the Nun-Kun massif, northwestern India. Boreas 43, 67–89.

Leipe, C., Demske, D., Tarasov, P. E., 2014. A Holocene pollen record from the northwestern Himalayan lake Tso Moriri: Implications for palaeoclimatic and archaeological research. Quat. Int. 348, 93–112.

Li, J., Ehlers, T. A., Werner, M., Mutz, S. G., Steger, C., Paeth, H., 2017. Late quaternary climate, precipitation δ18O, and Indian monsoon variations over the Tibetan Plateau. Earth Planet. Sci. Lett. 457, 412–422.

Li, Y., Wang, N., Zhou, X., Zhang, C., Wang, Y., 2014. Synchronous or asynchronous Holocene Indian and East Asian summer monsoon evolution: A synthesis on Holocene Asian summer monsoon simulations, records and modern monsoon indices. Glob. Planet. Change 116, 30–40.

Liang, F., Brook, G. A., Kotlia, B. S., Railsback, L., B., Hardt, B., Cheng, H., Edwards, R. L., Kandasamy, S., 2015. Panigarh cave stalagmite evidence of climate change in the Indian Central Himalaya since AD 1256: Monsoon breaks and winter southern jet depressions. Quat. Sci. Rev. 124, 145–161.

Lifton, N., 2016. Implications of two Holocene time-dependent geomagnetic models for cosmogenic nuclide production rate scaling. Earth Planet. Sci. Lett. 433, 257–268.

Lifton, N., Sato, T., Dunai, T. J., 2014. Scaling in situ cosmogenic nuclide production rates using analytical approximations to atmospheric cosmic-ray fluxes. Earth Planet. Sci. Lett. 386, 149–160.

Liu, K., Thompson, L. G., 1998. A pollen record of Holocene climatic changes from the Dunde ice cap , Qinghai-Tibetan Plateau. Geology 1986, 135–138.

Lukas, S., Graf, A., Coray, S., Schlüchter, C., 2012. Genesis, stability and preservation potential of large lateral moraines of Alpine valley glaciers - towards a unifying theory based on Findelengletscher, Switzerland. Quat. Sci. Rev. 38, 27–48.

Lund, D. C., Lynch-stieglitz, J., Curry, W. B., 2006. Gulf Stream density structure and transport during the past millennium 444, 601–604.

Mahmood, A., 2016. Statistical methods in geographical studies. Rajesh Publications, New Delhi, p. 88

Martin, L. C. P., Blard, P. H., Balco, G., Lavé, J., Delunel, R., Lifton, N., Laurent, V., 2017a. The CREp program and the ICE-D production rate calibration database: A fully parameterizable and updated online tool to compute cosmic-ray exposure ages. Quat. Geochronol. 38, 25–49.

Matero, I. S. O., Gregoire, L. J., Ivanovic, R. F., Tindall, J. C., Haywood, A. M., 2017. The 8.2 ka cooling event caused by Laurentide ice saddle collapse. Earth Planet. Sci. Lett. 473, 205–214.

Mischke, S., Zhang, C., 2010. Holocene cold events on the Tibetan Plateau. Glob. Planet. Change 72, 155–163.

Mix, A. C., Bard, E., Schneider, R., 2001. Environmental processes of the ice age: Land, oceans, glaciers (EPILOG). Quat. Sci. Rev. 20, 627–657.

Mölg, T., Maussion, F., Scherer, D., 2013. Mid-latitude westerlies as a driver of glacier variability in monsoonal High Asia. Nat. Clim. Chang. 4, 68–73.

Mölg, T., Maussion, F., Scherer, D., 2014. Mid-latitude westerlies as a driver of glacier variability in monsoonal High Asia. Nat. Clim. Chang. 4, 68–73.

Moran, A. P., Ivy-Ochs, S., Schuh, M., Christl, M., Kerschner, H., 2016. Evidence of central Alpine glacier advances during the Younger Dryas–early Holocene transition period. Boreas 45, 398–410.

Moran, A. P., Kerschner, H., Ochs, S. I., 2015. Redating the moraines in the Kromer Valley (Silvretta Mountains) – New evidence for an early Holocene glacier advance. Holocene 26, 655–664.

Murari, M. K., Owen, L. A., Dortch, J. M., Caffee, M. W., Dietsch, C., Fuchs, M., Haneberg, W. C., Sharma, M. C., Townsend-Small, A., 2014. Timing and climatic drivers for glaciation across monsoon-influenced regions of the Himalayan–Tibetan orogen. Quat. Sci. Rev. 88, 159–182.

Nesje, A., Dahl, S. O., 1992. Equilibrium-line altitude depressions of reconstructed Younger Dyras and Holocene glaciers in Fosdalen, inner Nordfjord, western Norway. Nor. Geol. Tidsskr. 72, 209–216.

New, M., Lister, D., Hulme, M., Makin, I., 2002. A high-resolution data set of surface climate over global land areas. Clim. Res. 21, 1–25.

Nishiizumi, K, Finkel, R. C, Caffee, M. W, Southon, J. R, Kohl, C. P, Arnold, J. R, Olinger, C. T, Poths, J, Klein, J. 1994. Cosmogenic Production of [10]Be and [26]Al on the Surface of the Earth and Underground, in Eighth International Conference on Geochronology, Cosmochronology and Isotope Geochemistry. U.S. Geol. Surv. Circular 1107, Berkeley, California, p. 234.

Nishiizumi, K., Imamura, M., Caffee, M. W., Southon, J. R., Finkel, R. C., Mcaninch, J., 2007. Be AMS standards 258, 403–413.

O'Hara, S. L., Briner, J. P., Kelley, S. E., 2017. A [10]Be chronology of early Holocene local glacier moraines in central West Greenland. Boreas 46, 655–666.

Oerlemans, J., 1997. Climate Sensitivity of Franz Josef Glacier, New Zealand, as Revealed by Numerical Modeling. Arct. Alp. Res. 29, 233–239.

Oerlemans, J., 2001, Glaciers and climate change. Lisse, Netherlands, Swets and Zeitlinger, p. 160.

Oerlemans, J., 2005a. Extracting a climate signal from 169 glacier records. Science 308, 675–7.

Oerlemans, J., 2005b. Extracting a Climate Signal from 169 Glacier Records 308, 675–677.

Oerlemans, J., Anderson, B., Hubbard, A., Huybrechts, P., Jóhannesson, T., Knap, W. H., Schmeits, M., Stroeven, A. P., van de Wal, R. S. W., Wallinga, J., Zuo, Z., 1998. Modelling the response of glaciers to climate warming. Clim. Dyn. 14, 267–274.

Ohio Supercomputer Center. 1987. Ohio Supercomputer Center. Columbus OH: Ohio Supercomputer Center. http://osc.edu/ark:/19495/f5s1ph73.

Orr, E. N., Owen, L. A., Murari, M. K., Saha, S., Caffee, M. W., 2017. The timing and extent of Quaternary glaciation of Stok, northern Zanskar Range, Transhimalaya, of northern India. Geomorphology 284.

Orr, E. N., Owen, L. A., Murari, M. K., Saha, S., Caffee, M. W., 2017. Geomorphology The timing and extent of Quaternary glaciation of Stok , northern Zanskar. Geomorphology 284, 142–155.

Orr, E. N., Owen, L. A., Saha, S., Caffee, M. W., Murari, M. K., 2018. Quaternary glaciation of the Lato Massif, Zanskar Range of the NW Himalaya. Quat. Sci. Rev. 183, 140–156.

Orr, E., Owen, L. A., Saha, S., 2017. Determining the rates and drivers of headwall erosion within glaciated catchments in the NW Himalaya, EP33F. Presented at 2017 Fall Meeting, AGU, New Orleans, LA.

Osmaston, H., 1994. The geology, geomorphology and Quaternary history of Zangskar. In Crook, J., Osmaston, H. (Eds.), Himalayan Buddhist Villages. University of Bristol Press, UK, 1–36.

Osmaston, H., 2005. Estimates of glacier equilibrium line altitudes by the Area ?? Altitude, the Area ?? Altitude Balance Ratio and the Area ?? Altitude Balance Index methods and their validation. Quat. Int. 138–139, 22–31.

Owen, L. A, Derbyshire, E., 1989. The Karakoram glacial depositional system. Zeitschrift f€ur Geomorphologie N.F., Supplement 76, 33–73.

Owen, L. A., Bailey, R. M., Rhodes, E. J., Holloway, R., 1997. Style and timing of glaciation in the Lahul Himalaya , northern India : a framework for reconstructing late Quaternary palaeoclimatic change in the western Himalayas 12, 83–109.

Owen, L. A., Bailey, R. M., Rhodes, E. J., Mitchell, W. A., Coxon, P., 1997. Style and timing of glaciation in the Lahul Himalaya, northern India: a framework for reconstructing late Quaternary palaeoclimatic change in the western Himalayas. J. Quat. Sci. 12, 83–109.

Owen, L. A., Benn, D. I., 2005. Equilibrium-line altitudes of the Last Glacial Maximum for the Himalaya and Tibet : an assessment and evaluation of results 139, 55–78.

Owen, L. A., Derbyshire, E., Richardson, S., Benn, D., Evans, D. I., Mitchell, W. A., 1996. The Quaternary glacial history of the Lahul Himalaya , northern India 11, 25–42.

Owen, L. A., Dortch, J. M., 2014. Nature and timing of Quaternary glaciation in the Himalayan–Tibetan orogen. Quat. Sci. Rev. 88, 14–54.

Owen, L. A., Finkel, R. C., Barnard, P. L., Haizhou, M., Asahi, K., Caffee, M. W., Derbyshire, E., 2005. Climatic and topographic controls on the style and timing of Late Quaternary glaciation throughout Tibet and the Himalaya defined by ^{10}Be cosmogenic radionuclide surface exposure dating. Quat. Sci. Rev. 24, 1391–1411.

Owen, L. A., Finkel, R. C., Caffee, M. W., Gualtieri, L., 2002. Timing of multiple late Quaternary glaciations in the Hunza Valley, Karakoram Mountains, northern Pakistan: Defined by cosmogenic radionuclide dating of moraines. Bull. Geol. Soc. Am. 114, 593–604.

Owen, L. A., Finkel, R. C., Haizhou, M., Barnard, P. L., 2006. Late Quaternary landscape evolution in the Kunlun Mountains and Qaidam Basin, Northern Tibet: A framework for examining the links between glaciation, lake level changes and alluvial fan formation. Quat. Int. 154–155, 73–86.

Owen, L. A., Finkel, R. C., Haizhou, M., Spencer, J. Q., Derbyshire, E., Barnard, P. L., Caffee, M. W., 2003. Timing and style of Late Quaternary glaciation in northeastern Tibet. Bull. Geol. Soc. Am. 115, 1356–1364.

Owen, L. A., Finkel, R. C., Minnich, R. A., Perez, A. E., 2003. Extreme southwestern margin of late Quaternary glaciation in North America: Timing and controls. Geology 31, 729–732.

Owen, L. A., Gualtieri, L., Finkel, R. C., Caffee, M. W., Benn, D. I., Sharma, M. C., 2001. Cosmogenic radionuclide dating of glacial landforms in the Lahul Himalaya, northern India: defining the timing of Late Quaternary glaciation. J. Quat. Sci. 16, 555–563.

Owen, L. A., Robinson, R., Benn, D. I., Finkel, R. C., Davis, N. K., Yi, C., Putkonen, J., Li, D., Murray, A.S., 2009. Quaternary glaciation of Mount Everest. Quat. Sci. Rev. 28, 1412–1433.

Owen, L. A., Yi, C., Finkel, R. C., Davis, N. K., 2010. Quaternary glaciation of Gurla Mandhata (Naimon'anyi). Quat. Sci. Rev. 29, 1817–1830.

Pascale, S., Lucarini, V., Feng, X., Porporato, A., Hasson, S. ul, 2014. Analysis of rainfall seasonality from observations and climate models. Clim. Dyn. 3281–3301.

Pellitero, R., Rea, B. R., Spagnolo, M., Bakke, J., Ivy-Ochs, S., Frew, C. R., Hughes, P., Ribolini, A., Lukas, S., Renssen, H., 2016. GlaRe, a GIS tool to reconstruct the 3D surface of palaeoglaciers. Comput. Geosci. 94, 77–85.

Phadtare, N. R., 2000. Sharp Decrease in Summer Monsoon Strength 4000–3500 cal yr B . P . in the Central Higher Himalaya of India Based on Pollen Evidence from Alpine Peat 129, 122–129.

Phadtare, N. R., 2000. Sharp decrease in summer monsoon strength 4000-3500 cal yr B.P. in the central Higher Himalaya of India based on pollen evidence from alpine peat. Quat. Res. 53, 122–129.

Pratt-Sitaula, B., 2005. Glaciers, Climate, and Topography in the Nepalese Himalaya (PhD thesis). University of California, Santa Barbara.

Pratt-Sitaula, B., Burbank, D. W., Heimsath, A. M., Humphrey, N. F., Oskin, M., Putkonen, J., 2011. Topographic control of asynchronous glacial advances: A case study from Annapurna, Nepal. Geophys. Res. Lett. 38, 1–6.

Putkonen, J., Connolly, J., Orloff, T., 2008. Landscape evolution degrades the geologic signature of past glaciations. Geomorphology 97, 208–217.

Putnam, A. E., Schaefer, J. M., Denton, G. H., Barrell, D. J. A., Andersen, B. G., Koffman, T. N. B., Rowan, A. V., Finkel, R. C., Rood, D. H., Schwartz, R., Vandergoes, M. J., Plummer, M. A., Brocklehurst, S. H., Kelley, S. E., Ladig, K. L., 2013. Warming and glacier recession in the Rakaia valley , Southern Alps of New Zealand , during Heinrich Stadial 1. Earth Planet. Sci. Lett. 382, 98–110.

Putnam, A. E., Schaefer, J. M., Denton, G. H., Barrell, D. J. A., Birkel, S. D., Andersen, B. G., Kaplan, M. R., Finkel, R. C., Schwartz, R., Doughty, A. M., 2013. The Last Glacial Maximum at 44??S documented by a [10]Be moraine chronology at Lake Ohau, Southern Alps of New Zealand. Quat. Sci. Rev. 62, 114–141.

Raina, V. K, Shehmani, Sangewar, C. V., 2015. Glacier snout monitoring in the Himalayas. Geological Society of India, Bengaluru, 227–251.

Ramanathan, A. L., 2011. Status Report on Chhota Shigri Glacier (Himachal Pradesh) Status Report on Chhota Shigri Glacier (Himachal Pradesh). Sci. Eng. Res. Counc. Dep. Sci. Technol. Gov. India 1–89.

Rawat, B. S. Purohit, K. K., 1988. Geology of the area around Chhota Shigri glacier, Lahul and spiti district, (H.P.). Technical report on Multi-Disciplinary glacier expedition to Chhoat Shigri, Department of Science and Technology, 2, 152–157.

Rawat, S., Gupta, A. K., Sangode, S. J., Srivastava, P., Nainwal, H. C., 2015a. Late Pleistocene-Holocene vegetation and Indian summer monsoon record from the Lahaul, Northwest Himalaya, India. Quat. Sci. Rev. 114, 167–181.

Rawat, S., Gupta, A. K., Srivastava, P., Sangode, S. J., Nainwal, H. C., 2015b. A 13,000 year record of environmental magnetic variations in the lake and peat deposits from the Chandra valley, Lahaul: Implications to Holocene monsoonal variability in the NW Himalaya. Palaeogeogr. Palaeoclimatol. Palaeoecol. 440, 116–127.

Rawat, S., Gupta, A. K., Srivastava, P., Sangode, S. J., Nainwal, H. C., 2015c. A 13,000 year record of environmental magnetic variations in the lake and peat deposits from the Chandra valley, Lahaul: Implications to Holocene monsoonal variability in the NW Himalaya. Palaeogeogr. Palaeoclimatol. Palaeoecol. 440, 116–127.

RGI Consortium, 2017. Randolph Glacier Inventory (RGI) – A Dataset of Global Glacier Outlines: Version 6.0. Tech. Report, Glob. L. Ice Meas. from Space, Boulder, Color. USA.

Roe, G. H., 2011. What do glaciers tell us about climate variability and climate change? J. Glaciol. 57, 567–578.

Roe, G. H., Baker, M. B., 2014. Glacier response to climate perturbations : an accurate linear geometric model. J. Glaciol. 60, 670–684.

Röhringer, I., Zech, R., Abramowski, U., Sosin, P., Aldahan, A., Kubik, P. W., Zöller, L., Zech, W., 2012. The late Pleistocene glaciation in the Bogchigir Valleys (Pamir, Tajikistan) based on [10]Be surface exposure dating. Quat. Res. 78, 590–597.

Romesburg, C., 2004. Cluster Analysis for Researchers. North Carolina, p. 330.

Röthlisberger, F., Geyh, M. A., 1985a. Gletscherschwankungen der letzten 10.000 Jahre e Ein Verleich zwischen Nordund Südhemisphare (Alpen, Himalaya, Alaska, Südamerika, Neuseeland). Verlag Sauerländer, Aarau.

Röthlisberger, F., Geyh, M., 1985b. Glacier variations in Himalayas and Karakoram. Z. Gletsch. Glazialgeol. 21, 237–249.

Rounce, D. R., Quincey, D. J., McKinney, D. C., 2015. Debris-covered energy balance model for Imja-Lhotse Shar Glacier in the Everest region of Nepal. Cryosph. Discuss. 9, 3503–3540.

Rupper, S., Roe, G., 2008. Glacier Changes and Regional Climate: A Mass and Energy Balance Approach. J. Clim. 21, 5384–5401.

Rupper, S., Roe, G., Gillespie, A., 2009a. Spatial patterns of Holocene glacier advance and retreat in Central Asia. Quat. Res. 72, 337–346.

Rupper, S., Roe, G., Gillespie, A., 2009b. Spatial patterns of Holocene glacier advance and retreat in Central Asia. Quat. Res. 72, 337–346.

Sagredo, E. A., Lowell, T. V., 2012. Climatology of Andean glaciers: A framework to understand glacier response to climate change. Glob. Planet. Change 86–87, 101–109.

Saha, S., Owen, L. A., Orr, E. N., Caffee, M. W., 2018. Timing and nature of Holocene glacier advances at the northwestern end of the Himalayan-Tibetan orogen. Quat. Sci. Rev. 187, 177–202.

Saha, S., Owen, L. A., Orr, E. N., Caffee, M. W., 2018. Timing and nature of Holocene glacier advances at the northwestern end of the Himalayan-Tibetan orogen. Quat. Sci. Rev. 187, 177–202.

Saha, S., Owen, L. A., Orr, E. N., Caffee, M. W., *in preparation*. Systematically inherited cosmogenic [10]Be in Late Holocene moraine boulders in the Bhagirathi catchment of the Garhwal Himalaya, northern India: *intend to submit in* Earth Surface Processes and Landforms.

Saha, S., Sharma, M. C., Murari, M. K., Owen, L. A., Caffee, M. W., 2016. Geomorphology, sedimentology and minimum exposure ages of streamlined subglacial landforms in the NW Himalaya, India. Boreas 45.

Saha, S., Sharma, M. C., Murari, M. K., Owen, L. A., Caffee, M. W., 2015. Geomorphology, sedimentology and minimum exposure ages of streamlined subglacial landforms in the NW Himalaya, India. Boreas 2016.

Saini, R., Sharma, M. C., Deswal, S., Barr, I. D., Kumar, P., 2016. Glacio-archaeological evidence of warmer climate during the Little Ice Age in the Miyar basin, Lahul Himalaya, India. Clim. Past Discuss. 1–24.

Schaefer, J. M., Oberholzer, P., Zhao, Z., Ivy-Ochs, S., Wieler, R., Baur, H., Kubik, P. W., Schlüchter, C., 2008. Cosmogenic beryllium-10 and neon-21 dating of late Pleistocene glaciations in Nyalam, monsoonal Himalayas. Quat. Sci. Rev. 27, 295–311.

Scherler, D, Egholm, 2017. Debris supply to mountain glaciers and how it effects their sensitivity to climate change–A case study from the Chhota Shigri Glacier, India, 206444. Presented at 2017 Fall Meeting, AGU, New Orleans, LA.

Scherler, D., Bookhagen, B., Strecker, M. R., von Blanckenburg, F., Rood, D., 2010. Timing and extent of late Quaternary glaciation in the western Himalaya constrained by [10]Be moraine dating in Garhwal, India. Quat. Sci. Rev. 29, 815–831.

Schimmelpfennig, I., Schaefer, J. M., Akçar, N., Ivy-Ochs, S., Finkel, R. C., Schlüchter, C., 2012. Holocene glacier culminations in the Western Alps and their hemispheric relevance. Geology 40, 891–894.

Schimmelpfennig, I., Schaefer, J. M., Akçar, N., Koffman, T., Ivy-Ochs, S., Schwartz, R., Finkel, R. C., Zimmerman, S., Schlüchter, C., 2014. A chronology of Holocene and Little Ice Age glacier

culminations of the Steingletscher, Central Alps, Switzerland, based on high-sensitivity beryllium-10 moraine dating. Earth Planet. Sci. Lett. 393, 220–230.

Schindelwig, I., Akçar, N., Kubik, P. W., Schlüchter, C., 2012. Lateglacial and early Holocene dynamics of adjacent valley glaciers in the Western Swiss Alps. J. Quat. Sci. 27, 114–124.

Schmeits, M. J., Oerlemans, J., 1997. Simulation of the historical variations in length of Unterer Grindelwaldgletscher, Switzerland. J. Glaciol. 43, 152–164.

Seaby, R., Henderson, P., 2014. Community Analysis Package 5.0: Searching for structure in community data. PISCES Conserv. Ltd., Engl.

Searle, A. M. P., Parrish, R. R., Hodges, K. V, Hurford, A., Ayres, M. W., Searle, M. P., Parrish, R. R., Hodges, K. V, Hurford, A., Ayres, M. W., Whitehouse, M. J., 1997. Shisha Pangma Leucogranite, South Tibetan Himalaya: Field Relations, Geochemistry, Age, Origin, and Emplacement. J. Geol. 105, 295–318.

Seong, Y. B., Owen, L. A., Bishop, M. P., Bush, A., Clendon, P., Copland, L., Finkel, R., Kamp, U., Shroder, J. F., 2007. Quaternary glacial history of the Central Karakoram. Quat. Sci. Rev. 26, 3384–3405.

Seong, Y. B., Owen, L. A., Yi, C., Finkel, R. C., 2009. Quaternary glaciation of Muztag Ata and Kongur Shan: Evidence for glacier response to rapid climate changes throughout the Late Glacial and Holocene in westernmost Tibet. Geol. Soc. Am. Bull. 121, 348–365.

Severinghaus, J. P., Beaudette, R., Headly, M. A., Taylor, K., Brook, E. J., 2009. the Terrestrial Biosphere 1431–1434.

Shangzhe, Z., Jie, W., Liubing, X., Xiaoli, W., Colgan, P. M., Mickelson, D. M., 2010. Glacial advances in southeastern Tibet during late Quaternary and their implications for climatic changes. Quat. Int. 218, 58–66.

Sharma, P., Bourgeois, M., Elmore, D., Granger, D., Lipschutz, M. E., Ma, X., Miller, T., Mueller, K., Rickey, F., Simms, P., Vogt, S., 2000. PRIME lab AMS performance, upgrades and research applications. Nucl. Instruments Methods Phys. Res. Sect. B-Beam Interact. with Mater. Atoms 172, 112–123.

Sharma, S., Chand, P., Bisht, P., Shukla, A. D., Bartarya, S. K., Sundriyal, Y. P., Juyal, N., 2016. Factors responsible for driving the glaciation in the Sarchu Plain, eastern Zanskar Himalaya, during the late Quaternary. J. Quat. Sci. 31, 495–511.

Shi, X., Kirby, E., Furlong, K. P., Meng, K., Robinson, R., Lu, H., Wang, E., 2017. Rapid and punctuated Late Holocene recession of Siling Co, central Tibet. Quat. Sci. Rev. 172, 15–31.

Shroder, J. F., Bishop, M. P., Copland, L., Sloan, V. F., 2000. Debris-covered glaciers and rock glaciers in the Nanga Parbat Himalaya, Pakistan. Geogr. Ann. Ser. A Phys. Geogr. 82, 17–31.

Solomina, O. N., Bradley, R. S., Hodgson, D. A., Ivy-Ochs, S., Jomelli, V., Mackintosh, A. N., Nesje, A., Owen, L. A., Wanner, H., Wiles, G. C., Young, N. E., 2015a. Holocene glacier fluctuations. Quat. Sci. Rev. 111, 9–34.

Solomina, O. N., Bradley, R. S., Hodgson, D. A., Ivy-ochs, S., Jomelli, V., Mackintosh, A. N., Nesje, A., Owen, L. A., Wanner, H., Wiles, G. C., Young, N. E., 2015. Holocene glacier fl uctuations. Quat. Sci. Rev. 111, 9–34.

Solomina, O. N., Bradley, R. S., Hodgson, D. A., Ivy-Ochs, S., Jomelli, V., Mackintosh, A. N., Nesje, A., Owen, L. A., Wanner, H., Wiles, G. C., Young, N. E., 2015b. Holocene glacier fluctuations. Quat. Sci. Rev. 111, 9–34.

Solomina, O. N., Bradley, R. S., Jomelli, V., Geirsdottir, A., Kaufman, D. S., Koch, J., McKay, N. P., Masiokas, M., Miller, G., Nesje, A., Nicolussi, K., Owen, L. A., Putnam, A. E., Wanner, H., Wiles, G., Yang, B., 2016. Glacier fluctuations during the past 2000 years. Quat. Sci. Rev. 149, 61–90.

Srivastava, D., 2012. Status Report on Gangotri Glacier, Science and Engineering Research Board, Department of Science and Technology, New Delhi. Himal. Glaciol. Tech. Rep. 1–102.

Srivastava, P., Agnihotri, R., Sharma, D., Meena, N., Sundriyal, Y. P., Saxena, A., Bhushan, R., Sawlani, R., Banerji, U. S., Sharma, C., Bisht, P., Rana, N., Jayangondaperumal, R., 2017. 8000-year

monsoonal record from Himalaya revealing reinforcement of tropical and global climate systems since mid-Holocene. Sci. Rep. 7, 1–10.

Steck, A., 2003. Geology of the NW Indian Himalaya. Eclogae Geol. Helv. 96, 147-U13.

Stone, J. O., 2000. Air pressure and cosmogenic isotope production. 105, 23,753-23,759.

Stuiver, M., Reimer, P. J., Reimer, R. W., 2018. CALIB 7.1 [WWW program] at http://calib.org, accessed 2018-10-20.

Sugden, D. E., John, B. S., 1976. Glaciers and Landscape. A Geomorphological Approach. Edward Arnold, London.

Taylor, J. R., 1997. An Introduction to Error Analysis. Second Edition, University Science Books, Sausalito, Calif.

The R Core Team, 2018. R : A Language and Environment for Statistical Computing. Vienna, Austria. ISBN 3-900051-07-0,.

Thomas, E. K., Huang, Y., Clemens, S. C., Colman, S. M., Morrill, C., Wegener, P., Zhao, J., 2016. Changes in dominant moisture sources and the consequences for hydroclimate on the northeastern Tibetan Plateau during the past 32 kyr. Quat. Sci. Rev. 131, 157–167.

Thompson, L. G., Tao, T., Davis, M. E., Henderson, A., Mosley-Thompson, E., Lin, P. N., Beer, J., Synal, H. A., Cole-Dai, J., Bolzan, J. F., 1997. Tropical Climate Instability: The Last Glacial Cycle from a Qinghai-Tibetan Ice Core. Science (80). 276, 1821–1825.

Uppala, S. M., KÅllberg, P. W., Simmons, A. J., Andrae, U., Bechtold, V. D. C., Fiorino, M., Gibson, J. K., Haseler, J., Hernandez, A., Kelly, G. A., Li, X., Onogi, K., Saarinen, S., Sokka, N., Allan, R. P., Andersson, E., Arpe, K., Balmaseda, M. A., Beljaars, A. C. M., Berg, L. Van De, Bidlot, J., Bormann, N., Caires, S., Chevallier, F., Dethof, A., Dragosavac, M., Fisher, M., Fuentes, M., Hagemann, S., Hólm, E., Hoskins, B. J., Isaksen, L., Janssen, P. A. E. M., Jenne, R., Mcnally, A. P., Mahfouf, J. -F., Morcrette, J. -J., Rayner, N. A., Saunders, R. W., Simon, P., Sterl, A., Trenberth, K. E., Untch, A., Vasiljevic, D., Viterbo, P., Woollen, J., 2005. The ERA-40 re-analysis. Q. J. R. Meteorol. Soc. 131, 2961–3012.

van der Bilt, W. G. M., Bakke, J., Vasskog, K., D'Andrea, W. J., Bradley, R. S., Ólafsdóttir, S., 2015. Reconstruction of glacier variability from lake sediments reveals dynamic Holocene climate in Svalbard. Quat. Sci. Rev. 126, 201–218.

Vance, D., Harris, N., 1999. Timing of prograde metamorphism in the Zanskar Himalaya. Geology 27, 395.

Vaux, Jr., H. J., Balk, D., Cook, E. R., Gleick, P., Lau, W. K. -M., Levy, M., Malone, E. L., Mcdonald, R., Shindell, D., Thompson, L. G., Wescoat, J. L., Williams, M. W., 2012. Himalayan Glaciers Climate Change , Water Resources , and Water Security. National Academy of Sciences, Washington, DC.

Walker, H., Pascoe, E. N., 1907. Notes on certain glaciers in Lahaul. Rec. Geol. Surv. India 35, 139–147.

Walker, M. J. C., Berkelhammer, M., Björck, S., Cwynar, L. C., Fisher, D. A., Long, A. J., Lowe, J. J., Newnham, R. M., Rasmussen, S. O., Weiss, H., 2012. Formal subdivision of the Holocene Series/Epoch: A Discussion Paper by a Working Group of INTIMATE (Integration of ice-core, marine and terrestrial records) and the Subcommission on Quaternary Stratigraphy (International Commission on Stratigraphy). J. Quat. Sci. 27, 649–659.

Wang, B., Wu, R., Lau, K. -M., 2001. Interannual Variability of the Asian Summer Monsoon : Contrasts between the Indian and the Western North Pacific–East Asian Monsoons*. J. Clim. 14, 4073–4090.

Wang, J., Kassab, C., Harbor, J. M., Caffee, M. W., Cui, H., Zhang, G., 2013. Cosmogenic nuclide constraints on late Quaternary glacial chronology on the Dalijia Shan, northeastern Tibetan Plateau. Quat. Res. 79, 439–451.

Wang, X., Auler, A. S., Edwards, R. L., Cheng, H., Cristalli, P. S., Smart, P. L., Richards, D. A., Shen, C.-C., 2004. Wet periods in northeastern Brazil over the past 210 kyr linked to distant climate anomalies. Nature 432, 740–743.

Wang, Y., Cheng, H., Edwards, R. L., He, Y., Kong, X., An, Z., Wu, J., Kelly, M. J., Dykoski, C. A., Li, X., 2005. The Holocene Asian Monsoon : Links to Solar Changes and North Atlantic Climate 854–858.

Ward, D. J., Anderson, R. S., 2011. The use of ablation-dominated medial moraines as samplers for [10]Be-derived erosion rates of glacier valley walls, Kichatna Mountains, AK. Earth Surf. Process. Landforms 36, 495–512.

Wünnemann, B., Demske, D., Tarasov, P., Kotlia, B. S., Reinhardt, C., Bloemendal, J., Diekmann, B., Hartmann, K., Krois, J., Riedel, F., 2010a. Hydrological evolution during the last 15kyr in the Tso Kar lake basin (Ladakh, India), derived from geomorphological, sedimentological and palynological records. Quat. Sci. Rev. 29, 1138–1155.

Wünnemann, B., Demske, D., Tarasov, P., Kotlia, B. S., Reinhardt, C., Bloemendal, J., Diekmann, B., Hartmann, K., Krois, J., Riedel, F., Arya, N., 2010b. Hydrological evolution during the last 15 kyr in the Tso Kar lake basin (Ladakh, India), derived from geomorphological, sedimentological and palynological records. Quat. Sci. Rev. 29, 1138–1155.

Xu, X., Yi, C., 2014. Little Ice Age on the Tibetan Plateau and its bordering mountains: Evidence from moraine chronologies. Glob. Planet. Change 116, 41–53.

Yancheva, G., Nowaczyk, N. R., Mingram, J., Dulski, P., Schettler, G., Liu, J., Sigman, D. M., Peterson, L. C., Haug, G. H., 2007. Influence of the intertropical convergence zone on the East Asian monsoon 445, 3–6.

Yang, B., Bräuning, A., Liu, J., Davis, M. E., Yajun, S., 2009a. Temperature changes on the Tibetan Plateau during the past 600 years inferred from ice cores and tree rings. Glob. Planet. Change 69, 71–78.

Yang, B., Kang, X., Liu, J., Bräuning, A., Qin, C., 2009b. Annual temperature history in southwest Tibet during the last 400 years recorded by tree rings. Int. J. Climatol. 971, 962–971.

Yanhong, W., Lücke, A., Zhangdong, J., Sumin, W., Schleser, G. H., Battarbee, R. W., Weilan, X., 2006. Holocene climate development on the central Tibetan Plateau: A sedimentary record from Cuoe Lake. Palaeogeogr. Palaeoclimatol. Palaeoecol. 234, 328–340.

Yao, T., Thompson, L., Yang, W., Yu, W., Gao, Y., Guo, X., Yang, X., Duan, K., Zhao, H., Xu, B., Pu, J., Lu, A., Xiang, Y., Kattel, D. B., Joswiak, D., 2012. Different glacier status with atmospheric circulations in Tibetan Plateau and surroundings. Nat. Clim. Chang. 2, 663–667.

Young, N. E., Briner, J. P., Rood, D. H., Finkel, R. C., 2012. Glacier extent during the Younger Dryas and 8.2-ka event on Baffin Island, Arctic Canada. Science (80). 337, 1330–1333.

Yu, Y., Yang, T., Li, J., Liu, J., An, C., Liu, X., Fan, Z., Lu, Z., Li, Y., Su, X., 2006. Millennial-scale Holocene climate variability in the NW China drylands and links to the tropical Pacific and the North Atlantic. Palaeogeogr. Palaeoclimatol. Palaeoecol. 233, 149–162.

Zech, R., 2012. A late Pleistocene glacial chronology from the Kitschi-Kurumdu Valley, Tien Shan (Kyrgyzstan), based on [10]Be surface exposure dating. Quat. Res. 77, 281–288.

Zech, R., Abramowski, U., Glaser, B., Sosin, P., Kubik, P. W., Zech, W., 2005. Late Quaternary glacial and climate history of the Pamir Mountains derived from cosmogenic [10]Be exposure ages. Quat. Res. 64, 212–220.

Zech, R., Zech, M., Kubik, P. W., Kharki, K., Zech, W., 2009. Deglaciation and landscape history around Annapurna, Nepal, based on [10]Be surface exposure dating. Quat. Sci. Rev. 28, 1106–1118.

Zhu, H., Xu, P., Shao, X., Luo, H., 2013. Little Ice Age glacier fluctuations reconstructed for the southeastern Tibetan Plateau using tree rings. Quat. Int. 283, 134–138.

Zhu, L., Zhen, X., Wang, J., Lü, H., Xie, M., Kitagawa, H., Possnert, G., 2009. A ~30,000-year record of environmental changes inferred from Lake Chen Co, Southern Tibet. J. Paleolimnol. 42, 343–358.

Zuming, L. A. I., Maohuan, H., 1989. A numerical classification of glaciers in china by means of glaciological indices at the equilibrium line. Snow Cover Glacier Var. (Proceedings Balt. Symp. Maryland).

Gangotri, India

Paper III

Photo credit: LAO

171

Systematically inherited cosmogenic ^{10}Be in Late Holocene moraine boulders in the Bhagirathi catchment of the Garhwal Himalaya, northern India

Sourav Saha[†][1]**, Lewis A. Owen** [a]**, Elizabeth N. Orr** [a]**, Marc W. Caffee** [b]

[a] *Department of Geology, University of Cincinnati, Cincinnati, OH 45221, USA*
[b] *Department of Physics, Department of Earth, Atmospheric and Planetary Sciences, Purdue University, West Lafayette, IN 47907, USA*

ABSTRACT

Excess inventories of (^{10}Be) terrestrial cosmogenic nuclides due to prior exposure often precludes accurate exposure dating of recent geological materials, especially for materials/landforms that are < 2 ka. Here, we directly measure the inherited ^{10}Be concentrations in ten boulders from two moraines, which have been independently historically dated, in one of the largest and erosive glaciers of the Garhwal Himalaya, northern India. We choose the ~30-km-long Gangotri glacier in the Bhagirathi catchment to investigate systematically inherited ^{10}Be concentrations during glacier transportation and inclusion by random rockfall events from the valley walls. In conjunction with detailed geomorphic mapping and ^{10}Be dating, we show that even for an erosive (2–5 mm a^{-1}) high-velocity glacier (48±5 m a^{-1}) with a large ablation area (93 km^2 or 64% of total glacier area), a minimum of 0.09–0.60 x10^4 ^{10}Be atoms/g SiO$_2$ (equivalent age of 0.05–0.13 ka) of systematic excess in ^{10}Be concentration is expected, with an obvious outlier that could be as old as ~4.5 ka (equivalent ^{10}Be concentration of ~14.9 x 10^4 atoms/g SiO$_2$). Several key geomorphic process uncertainties are proposed. In addition, we also dated (using ^{10}Be) nine new and recalculated six published moraine boulders from the trunk Gangotri and the tributary Meru glaciers to help improve the Late Holocene local glacial chronostratigraphies in the catchment and to help understand the role of inheritance during past glaciations. Morphostratigraphically, from oldest to youngest, the Late Holocene moraines are dated to ~2.4–1.9, ~1.7–0.5, ~0.5–0.1 ka.

[†]* Corresponding author. 500, Geology-Physics, University of Cincinnati, Cincinnati, Oh 45221, USA.
E-mail address: sahasv@mail.uc.edu (S. Saha).

1. Introduction

The precession and accuracy of terrestrial cosmogenic nuclide (TCN) exposure dating are primarily governed by the physical principles of the method (Fabel and Harbor, 1999; Gosse and Phillips, 2001; Lal, 1991; Nishiizumi et al., 2007) and geological uncertainties (Briner et al., 2005; Hallet and Putkonen, 1994; Putkonen and Swanson, 2003; Zech et al., 2005b; Heyman et al., 2011, 2016). While significant advances have been made in recent years to reduce systematic analytical uncertainties (Nishiizumi et al., 2007; Corbett et al., 2016), model the physical processes (Lifton et al., 2005, 2008; Uppala et al., 2005; Lifton, 2016), improving the regional production rates (Heyman, 2014; Martin et al., 2017), and scaling schemes (Balco et al., 2008; Lifton et al., 2014; Martin et al., 2017; Borchers et al., 2016; Marrero et al., 2016), very few studies in exposure dating have tried to address the uncertainties associated with geomorphic processes, especially in glaciated settings (Applegate et al., 2010, 2012; Heyman et al., 2011; Valletta et al., 2017). An enormous amount of TCN exposure age data on glacial deposits worldwide are available, including for the high-altitude glaciers of the Himalayan-Tibetan orogen (http://alpine.ice-d.org/; Balco, 2011). To apply these TCN data at their fullest potential to help reconstruct paleoclimatic and to understand glacial dynamics, an adequate understanding of geological scatter is paramount (Applegate et al., 2010, 2012; Heyman et al., 2011; Balco, 2011).

Key assumptions on the geological history of the samples that have been dated using TCN methods have has rarely been tested (Çiner et al. 2017). For instance, moraine boulders are assumed to have no TCNs before incorporating into the glacial system (cf. Gosse and Phillips, 2001; Gosse, 2005; Ivy-Ochs et al., 2007; Putkonen et al., 2008). However, if the boulders have previous inventory, i.e., TCN concentration due to prior exposures, known as inheritance, during glaciation and/or glacial transportation, they will systematically yield older apparent ages (Applegate et al., 2010, 2012; Heyman et al., 2011). Similarly, if post-depositional shielding or exhumation takes place, incomplete exposures are expected, giving younger

173

than true ages (ibid). Studies that investigated Late Quaternary glacial deposits argued that incomplete exposure is a more significant problem than prior exposures/inheritance (Applegate et al., 2012; Heyman et al., 2011). However, recent studies on young Holocene (<2 ka) moraine boulders (Li et al., 2016; Saha et al., 2018, submitted) and from glacially modified landscapes (cf. Balco et al., 2002; Owen et al., 2009; Rinterknecht et al., 2006) and/or from areas dominated by non-erosive ice (cf. Fabel et al., 2002; Briner et al., 2006; Placzek et al., 2014; Orr et al., 2017, 2018), show that inheritance from prior exposures contribute to a high degree of scattering in exposure ages. Despite this recognition, the role of complex geological history including the links between erosion, climate, topography, tectonics, and glacial dynamics on prior exposures has not been adequately addressed (Scherler et al., 2011a, b, 2014; Bookhagen et al., 2005; Bookhagen and Burbank, 2006; Gruber and Haeberli, 2007; Dortch et al., 2011; Roe, 2011; Barr and Lovell, 2014). In this study, we aim to address this issue by directly measuring inherited ^{10}Be concentrations in moraine boulders. We also use new and published ^{10}Be ages to refine the Late Holocene glacial chronostratigraphy for an important area of the Himalaya, in the upper Bhagirathi valley of Garhwal in the Central Himalaya, northern India.

To test the assumption of zero inheritance of TCNs in boulders before deposition into a moraine system, we selected two recessional moraines in front of Gangotri glacier in Garhwal (Fig. 1). These moraines were independently dated by lichenometry, historical descriptions and plane table mapping, sketches, and photographs (Hodgson, 1822; Auden, 1937; Sharma and Owen, 1996; Srivastava et al., 2004a, b; Srivastava, 2012; Bhambri et al., 2012; Raina et al., 2015). Gangotri glacier is a ~30.2-km-long erosive temperate glacier (erosion rates of 2–5 mm a^{-1}; Orr et al., in prep.) with high mean velocity (~48±4.8 m a^{-1}; Bhattacharya et al., 2016). Nine new boulders were sampled from the two historical moraines, dated to AD 1780 and 1935, to measure the ^{10}Be concentrations. In addition, one previously published ^{10}Be age on one of the moraines was examined. Any excess ^{10}Be concentration beyond that expected from its historic age would be considered to have been inherited before deposition. We expect a minimum systematic inheritance of ^{10}Be in these extremely young moraine boulders given the very high erosion and abundant supraglacial activity (Raina et al., 2015). We also compared the relative ^{10}Be concentrations in moraine

boulders with supra- and proglacial sediments from Gangotri glacier from Orr et al. (in prep.) and Barnard et al. (2004a), respectively, and medial moraine debris samples from the nearby central and western Himalayan glaciated catchments (Heimsath and McGlynn, 2008; Seong et al., 2009a; Ward and Anderson, 2011; Murari et al., 2014).

Additionally, to test whether systematic inheritance remained minimum during past glacier advances (cooling), which may result in changes in glacial dynamics and mass balances, periglacial processes, mass movements, and catchment sediment flux, and thickness of debris mantle (Church and Slaymaker, 1989; Watanabe et al., 1998; Ballantyne, 2002a, b; Thiede et al., 2005; Moore et al., 2009; Montgomery, 2002; Sanders et al., 2012; Gibson et al., 2017; Scherler and Egholm, 2017), we also dated nine boulders using ^{10}Be and recalculated six published boulders ^{10}Be ages from the three Late Holocene laterofrontal moraines (Barnard et al., 2004a; Srivastava, 2012). A high-resolution geomorphic and surface unit map is developed, and the extent of glacier advances are reconstructed using ELAs and ΔELAs to help understand the paleoglacial history in the catchment.

2. Study area

2.1. Regional Settings

The NW trending Bhagirathi catchment is located in the north of Uttarkashi district of Uttarakhand, in Garhwal (Fig. 1). Geologically the Garhwal Himalaya comprises three main lithotectonic units: i) the Tethyan sedimentary sequence to the NE; ii) central High Himalayan series; and iii) the Lesser Himalayan sequence to the SW (Searle et al., 1997, 1999; Bassi 2004; Vannay et al., 2004). The upper Bhagirathi catchment, however, is bounded by NW trending South Tibetan Detachment (STD) to the north and Vaikrita thrust (VT) to the south (Searle et al., 1997, 1999). Despite the absence of a clear-cut single shear zone, Searle et al. (1997, 1999) argued that STD normal fault(s) divides the sillimanite grade gneiss of the crystalline series below from the Tethyan sedimentary sequence above (Fig. 2; Agarwal and Kumar 1973; Metcalfe, 1993; Owen et al., 1995, 1996; Searle et al., 1997, 1999). The Jhala normal fault, a late brittle

structure, further separates the quartzo-feldspathic gneiss below from the Harshil metasedimentary rock above (Fig. 2; ibid). The Harshil Series is overlain by the unmetamorphosed Tethyan sedimentary rock of the Martoli Group (Fig. 2; ibid).

The Bhagirathi catchment is carved mostly within the Shivling-Bhagirathi leucogranite-granodiorite body in its upper reaches (>4000 m asl; Fig. 2; Agarwal & Kumar, 1973; Sharma, 1983) which likely intruded along the STD (Searle et al., 1999). The deep glacial erosion (~2–5 mm a^{-1} in Awasti et al., 2004; Haritashy et al., 2006; Orr et al. in prep.) and denudation of bedrock slopes (Gabet et al., 2004; Anders and Roe, 2006), and high regional uplift (~4–5.7 mm a^{-1} in Barnard et al., 2004a; Scherler et al., 2014) are proposed for impressive vertical exposures in excess of 2–3 km, and the high mountain peaks (>6500 m asl; Figs. 1, 2; Searle et al., 1999) in the upper reaches of the catchment. The supraglacial debris that predominantly covers the ablation zones of these glaciers are, therefore, mostly composed of leucogranite, granitic gneiss, and metasedimentary rock (Bhambri et al., 2011; Chaujar et al., 1993).

Numerous topographic and geomorphic features including high relative relief (~1.0–3.0 km), steep (>45°) asymmetrical bedrock slopes (Fig. 2), large alluvium/debris fans, and steep box-shaped gorges (~20–30 m deep) are preserved in the catchment, indicating its influence in the recent topographic rejuvenation (Vohra, 1971; Searle et al., 1987; Validya, 1991; Rajendra et al., 2000; Barnard et al., 2001; Bali et al., 2004; Srivastava, 2012; Singh et al., 2017). Other prominent landforms include small rock glaciers, hanging valleys, strath terraces, river and paraglacial fan terraces, outwash and glaciofluvial terraces and planes, moraines, talus, point bars, and braided stream beds along the catchment floors (Fig. 3). Mass movements are particularly prevalent throughout the study area because of the steep topography, glacial and fluvial erosion, heavy monsoon rains and storms, and earthquakes (Owen et al., 1995; 1996; Barnard et al., 2001, 2004a).

The Indian summer monsoon (ISM) and the northern mid-latitude westerlies are the two major climatic systems that currently dominate the Bhagirathi catchment (Finkel et al., 2003; Bookhagen et al., 2005; Owen, 2009). The ISM provides most of the annual precipitation (1000–2500 mm a^{-1}) between July and September with significant annual variability (IMD, 1989; Burbank et al., 2003; Scherler et al., 2010;

Thayyen and Gergan, 2010; Wulf et al., 2010). Despite that, the glaciers in the catchment are predominantly fed by westerly-dominated winter snow from December to March (~546 mm a^{-1}), mostly indirectly in the form of avalanches from cornices on the steep bedrock slopes (Sharma and Owen, 1996; Tangri, 2004; Dhobal et al., 2008; Singh et al., 2008; Bhambri et al., 2011; Raina et al., 2015; Bhattacharya et al., 2016). Significant micro-climatic variations, mainly precipitation, exists within the catchment, controlled by elevation, aspects, terrain, geomorphic regimes, and proximity to glaciers (Sharma and Owen, 1996; Barnard et al., 2004a; Barros et al., 2006; Singh et al., 2007; Srivastava, 2012). Recently, installed manned (from AD 1999) and automatic (from AD 2000) meteorological stations at Bhujbasa (~3780 m asl), ~4 km from the snout of Gangotri glacier, provides a more detailed records of monthly precipitation and temperature at the site (Bhambri et al., 2011; Srivastava, 2012; Singh et al., 2017). Annual mean monthly temperature ranges between -2.3° and 11°C (ibid).

The Bhagirathi catchment favors the growth of dense coniferous trees, e.g., cedar and pine, up to ~3000 m asl. The coniferous forest is more open between ~3000 and 3700 m asl and is replaced by alpine tundra vegetation, e.g., alpine shrubs, grasses, lichens, and mosses, above 3700 m asl (Schweinfurth 1968; Sharma and Owen, 1996).

The upper reaches of the Bhagirathi catchment have several major glaciers (Raina and Srivastava, 2008), extending from ~1400 to 7200 m asl. Gangotri glacier is the largest glacier in the Central Himalaya, covering an area of ~144 km^2 (Srivastava, 2012; Raina et al., 2015). Since this high-activity type temperate glacier is fed by a series of large tributary glaciers including Raktavarn, Chaturangi, Swachhand, Ghonohim and Kirti glaciers; often the term glacier system is used to define Gangotri glacier (Fig. 1; ibid). The cirques of Gangotri glacier are at the northern flanks of the Chaukhamba group of peaks at ~5600 m asl (Figs. 1, 2; Srivastava, 2012). The contemporary equilibrium-line altitude (ELA) of Gangotri glacier lies between 4510 and 5160 m asl (Owen and Sharma, 1998; Naithani et al., 2001; Ahmad and Hasnain, 2004, Burbank et al., 2003; Srivastava, 2012; Singh et al., 2017). The accumulation zone is steep (~20–25°) with an average ice thickness of >300 m (Srivastava, 2012; Gantayat et al., 2014; Singh et al., 2017). The ablation zone is 26 km long covering 64% of the total glaciated area (Tangri et al., 2004; Singh et al., 2017). The average slope

of the ablation zone is ~5° and has numerous longitudinal and transverse or curved crevasses (Tewari, 1972), sharp serac faces (Raina et al., 2015), thick but variable debris mantle, six distinct medial moraines, meltwater channels, ponds, and ice collapse features (Haritashya et al., 2010; Scherler et al., 2011a; Satyabala, 2012; Orr et al., in prep.), indicating the predominance of supraglacial transport pathways (Sharma and Owen, 1996). Gangotri glacier presently (AD 2017) terminate at ~4070 m asl; the snout is called Gaumukh (Tangri et al., 2004; Srivastava, 2012; Raina et al., 2015). The velocity of Gangotri glacier for the period AD 1993–2014 varies between 50 and 70 m a^{-1} in the accumulation zone to <40 m a^{-1} near snout yielding an average velocity of ~48±5–50±7 m a^{-1} (Bhattacharya et al., 2016).

The NE trending Meru glacier (also referred to as Meru bamak) is a tributary glacier and is located west of Gangotri glacier some 300 m higher than the snout of the main Gangotri trunk glacier (4370–5564 m asl) (Fig. 3; Shankar and Srivastava, 2001). Meru glacier is 6 km long and 0.5 km wide, covering an area of ~17 km^2, and is enclosed by laterofrontal moraine ridges that partially overrides the laterofrontal moraines of the main Gangotri glacier near Gaumukh (~4200 m asl; Figs. 3, 4C). Meru glacier also has a thick but variable mantle of supraglacial debris in its ablation zone (Fig. S1C, D, E). The meltwater stream from Meru glacier is incising both the moraine ridges and has created a large funnel-like depression at the mouth of the tributary valley (Fig. 3). Several hummocks that are also undergoing erosion by the meltwater stream formed in front of the snout indicate the continuous down wasting of the glacier (Fig. S1D). An old dried glacial lake, known as Tapovan, formed where the laterofrontal moraines of Meru glacier override moraines of Gangotri glacier (~4300 m asl; Figs. 3, 4C; Ranhotra and Bhattacharya, 2004).

Chorabari and a companion glacier (30.75°N, 79.06°E) in the Mandakini catchment are located south of the Bhagirathi catchment (Singh, 2014). Each of these glaciers is ~7 km long and have cirques in the south-facing flanks of the Kedarnath peak (Fig. 1). These glaciers are also high activity-type with the comparable microclimatic regime (ibid).

2.2. Past Glaciations

Based on several preserved glacial landforms including ice-sculpted granitic bedrock slopes, moraines, erratics, and extent of U-shaved valley, six stages of glacial advances are proposed in the main Bhagirathi and Kedar hanging valleys (Sharma and Owen, 1996; Dutta et al., 2004; Puri et al., 2004; Singh, 2004; Srivastava, 2004; Barnard et al., 2004a; Srivastava, 2012; Raina et al., 2015). From oldest to youngest, these glacial stages include the: i) Bhagirathi (OSL dated to ~63.0 ka); ii) Sudarshan (OSL and [10]Be dated to ~20.8–15.8 ka); iii) Kedar ([10]Be dated to ~8.3 ka); iv) Shivling (OSL and [10]Be dated to ~5.2 ka), v) Gangotri stage (tentatively [10]Be dated to ~2.4–1.9 ka); and vi) Bhujbasa (tentatively [10]Be dated to ~0.4–2.0 ka; Fig. 1; ibid). Note all the [10]Be ages have been recalculated from the original publications using the schemes described below.

Glaciers extended to Jhala (~2465 m asl) some 43 km from the present glacier positions during the Bhagirathi glacial stage (Fig. 1). Evidences of this local glacial stage include a sharp-ridge end moraine and transition from U- to V-shaped valley near Jhala, and high elevation (>4100 m asl) ice-sculpted surfaces on the south facing bedrock flanks (MI01 in Figs. 1, 4A; Sharma and Owen, 1996; Barnard et al., 2004a; Srivastava, 2012; Raina et al., 2015). In addition, Sharma and Owen (1996) OSL dated an older deformed glaciofluvial deposit to ~85 ka (MI04 in Fig. 1), which is believed to be a section of valley fill before the glacial advance. This evidence supports an extensive local glacial maximum at ~63 ka in the catchment.

Discontinuous lateral moraines from west of Gangotri town some 24 km from Gangotri glacier to Bhaironghati (~2790 m asl) indicate a subsequent glacier advance at ~20.8–15.8 ka, called the Sudarshan glacial stage (Fig. 1; Barnard et al., 2004a; Srivastava, 2012). Sharma and Owen (1996) OSL dated the moraine to ~17.0 ka (MI05 in Fig. 1). Subsequently, Barnard et al. (2004a) also [10]Be dated (recalculated here) a degraded lateral moraine to ~20.8 and 15.8 ka (BH35B and 36 in Fig. 1), close to south facing bedrock slopes at ~4100 m asl and ~2.5 km from the snout of Gangotri glacier. This moraine is morphostratigraphically correlated with Sudarshan glacial stage (Figs. 3, S1A).

A well-defined laterofrontal moraine that can be traced from the cirque of the Kedar glacier up to ~2.4 km down the valley from the snout was [10]Be dated (recalculated here) to ~8.3 ka in the hanging Kedar

valley (BH19 and 20 in Fig. 1; Barnard et al., 2004). This moraine represents an early Mid-Holocene glacier advance and is assigned to Kedar glacial stage.

Seven erratic boulders (Milap 4–13 in Fig. 3) were ^{10}Be dated (recalculated here) to ~5.2 ka from an ice-polished bedrock pavement some 18 km down valley from Gangotri glacier and ~1.5 km west of Gangotri town at ~3010 m asl, (Srivastava, 2012; Saha et al., submitted). The pavement which is in 20–30 m above present river level, is covered by dense cedar and pine forests and can be traced for ~0.8 km (Sharma and Owen, 1996). The glacier advance that produced these landforms is assigned to the Shivling glacial stage and is also OSL dated to ~5.1 ka using the aeolian silt that caps a remnant lateral moraine near Bhujbasa (MI03 in Fig. 1; ibid).

Two prominent sets of lateral moraines, at ~3 and ~2 km from Gangotri glacier are assigned to the Gangotri and Bhujbasa glacial stages, respectively (Barnard et al., 2004a; Srivastava, 2012). These are tentatively ^{10}Be dated to ~2.4–1.9 and ~0.4–0.2 ka, respectively (ibid). The Late Holocene glacial chronostratigraphies are poorly defined in the Bhagirathi catchment (ibid) because only a few boulders (1–2) with scattered ^{10}Be ages ($\chi^2 > 52$) are dated from different ridge surfaces and from locations where contamination by slope deposits are prominent. We, therefore, targeted these young moraines to refine and provide new glacial chronostratigraphies.

2.3. Validating the Historical Moraine Ages

Captain J.A. Hodgson and Lieutenant Herbert of the British Army surveyed the Bhagirathi catchment in AD 1817 and documented a detail description of the glacier snout (Gaumukh), its distance from the town of Gangotri (~17 km) and altitude (~3913 m asl; Hodgson, 1822). Based on their description of the snout's position and moraine ridges of the trunk glacier (Hodgson, 1822) and later validation using lichenometric dating by the Geological Survey of India (GSI; Srivastava et al., 2004a, b), an age of AD 1780 was proposed for the distant recessional ridge, inset within the Bhujbasa stage moraines (Figs. 3, 4; Raina et al., 2015). Subsequent sketches and photographs that were taken by artists and GSI geologists

(Raina et al., 2015 and references therein) further validate the pre AD 1817 formation of the distant recessional moraine.

The AD 1935 moraine was validated using the plane-table survey map at the scale of 1:4800 by Auden (1937) of the GSI in October 1935 (see Fig. 3). He also provided photographs of the snout position (shown in Raina et al., 2015, pp. 235–240). This historical evidence strongly supports the independent age of AD 1935 for the recessional moraine (Fig. 4; Bhambri et al., 2012).

3. Methods

3.1. Mapping and Sedimentology

We prepared detailed geomorphic and surficial geologic maps using a handheld GPS with ±3 m spatial uncertainties and digital mapping techniques at the scale of 1:20,000 (Fig. 3). Field maps are further refined using Google Earth imagery, Advanced Spaceborne Thermal Emission and Reflection Radiometer (ASTER) global digital elevation models (GDEMs), and Landsat Enhanced Thematic Mapper Plus (ETM+) imagery in ArcGIS 10.3.

3.2. Morphostratigraphy and Assigning Local Glacial Stages

We defined morphostratigraphy and glacial stages based on position, morphology, cross-cutting relationship, and relative weathering characteristics of individual moraines and associated landforms (Owen et al., 1997). We were also able to verify the ages of some of the young moraines in the field based on lichenometry, historical descriptions and measurements, plane table map, sketches, and photographs (Hodgson, 1822; Auden, 1937; Sharma and Owen, 1996; Srivastava et al., 2004a, b; Srivastava, 2012; Bhambri et al., 2012; Raina et al., 2015), which further strengthen our morphostratigraphic reconstructions. Using the scheme outlined in Owen and Derbyshire (1989), Owen et al. (1997), Hughes et al. (2005), and Hughes (2010), we used the letters 'M' to denote moraines, the subscript letter 'B' for the Bhagirathi catchment, the subscript '1' for the morphostratigraphically youngest of all preserved sets of moraines, and

the subscript letter 'a' for the youngest ridge of a moraine set. We assigned each glacier advance or still-stand position to a local glacial stage (Sharma and Owen, 1996; Dutta et al., 2004; Puri et al., 2004; Singh, 2004; Srivastava, 2004a; Barnard et al., 2004a; Srivastava, 2012; Raina et al., 2015).

3.3. Geochronology

Multiple (4–5) boulders from each moraine were sampled (Figs. 5; S2) using a chisel and hammer after carefully considering the morphostratigraphy, physical setting, e.g., stability, degradation, hillslope contamination, and surficial characteristics (cf. Gosse and Phillips, 2001). Well-inset stable boulders with no evidence of post-depositional surface deflections, detrital cover, surface spallation, pitting, fracturing, and/or extensive weathering were preferentially sampled. We also preferred to choose boulders with well-developed lichen cover, because lichens like rock varnish also provide a measure of confidence that boulders had not been recently exhumed and/or toppled (Owen et al., 2006). Due to high wind speed (>10 km hr^{-1}; Singh et al., 2007) in this high elevation settings, we argue that our sampled boulders with heights ranging from 0.7 to 3.5 m (Figs. 5; S2), likely had little snow cover that would have shielded them from cosmic rays (Balco et al., 2008; Heyman et al., 2016). Approximately 500 g of rock to a depth of ≤3 cm from the top of each boulder was collected (Table S3). Topographic shielding from the boulder surface to the horizon was measured using a compass and an inclinometer at 10° interval (Gosse and Phillips, 2001; Balco et al., 2008).

Quartz extraction and ^{10}Be sample preparation were executed at the Quaternary Geochronology Laboratories of the University of Cincinnati following the methods outlined in Kohl and Nishiizumi (1992) and Nishiizumi et al. (1994). A detailed account of the laboratory procedure can be found in Dortch et al. (2009, 2013) and Saha et al., (2015). We performed the AMS measurements at the Purdue Rare Isotope Measurement (PRIME) Laboratory at Purdue University. The average blank (^{10}Be/^{9}Be ratio) correction was 18±17%, and analytical uncertainty was 8±8% in these extremely young samples. No correction for residual boron (Corbett et al., 2016), radioactive decay, and muongenic production (Brown et al., 1995; Braucher et al., 2003) were made as they are deemed negligible for the timescale of this study. The native ^{9}Be (cf.

Portenga et al., 2015), as measured in ~5 g fractions of clean quartz form boulders and sediments, were insignificant (1.5±1.1 x 10^{-4} to 1.9±1.6 x 10^{-4} ppm; this study and Orr et al. in prep.) and hence, no adjustment to the $^{10}Be/^9Be$ ratios were made.

We calculated new 18 new and recalculated 22 published ^{10}Be ages using the community standard Cosmic Ray Exposure program (CREp) of Martin et al. (2017) and CRONUS-Earth V3 of Balco et al. (2008). The global sea-level high- latitude (SLHL) spallogenic ^{10}Be production rate of 4.08±0.23 atoms g^{-1} a^{-1} was used (Borchers et al., 2016; Martin et al., 2017; http://calibration.ice-d.org/). We calculated the apparent exposure ages using the scaling schemes of Lifton-Sato-Dunai (*LSD*; Lifton et al., 2014), time-dependent Lal and Stone (*Lm*; Balco et al., 2008), and time-independent Lal and Stone (*St*; Lal, 1991; Stone, 2000), but we only reported the CREp *LSD* ages in the text below. We assumed zero-erosion rates and reported all the ages in thousands of years (ka) before AD 2017.

Moraine exposure ages are often defined as the minimum age of glacier advance (Gosse, 2005; Ivy-Ochs et al., 2007; Putkonen et al., 2008) and/or beginning of glacier retreat (Applegate and Alley, 2011; O'Hara et al., 2017). We applied this definition throughout our paper. The inherited ^{10}Be ages for moraine boulders are estimated by subtracting from the independent age and inherited concentrations are recalculated using the *LSD* scale. To assess the distribution of age population, we used reduced chi-squared (χ^2) statistics (Applegate et al., 2010, 2012; Kaplan et al., 2013; Putnam et al., 2013b). Whenever a χ^2 value is >1 and falls outside 95% confidence interval, we treated the age population for outlier detection using community stand methods (Applegate et al., 2010, 2012; Putnam et al., 2013b). For example, we used >2σ from the arithmetic mean of the distribution (Putnam et al., 2013a) and Chauvenet's criterion (Taylor, 1997; Dunai, 2010; Putnam et al., 2013b) to detect outliers. Outliers are only removed under following circumstances: i) independent age for the moraine strongly suggests age overestimation; ii) field evidence, mainly for published samples, suggests possible post-depositional toppling, or exhumation, or slope (mass movement) contamination; and iii) ages do not follow morphostratigraphic and reconstructed chronologic order. Finally, arithmetic mean ± 1σ was calculated to define the apparent moraine age and the age

uncertainty after discarding the outlier. We also reported weighted mean $\pm 1\sigma$ (Applegate et al., 2010, 2012) and probability density peaks (Dortch et al., 2013) as additional measures of central tendency.

3.4. Equilibrium-Line Altitudes (ELAs)

Assuming a simplistic steady-state scenario (Sugden and John, 1976; Putnam et al., 2013b), we estimated former ELAs and ELA depressions (ΔELAs) in the Bhagirathi and Kedar valleys. We used area-altitude (AA), area accumulation ratio (AAR), and toe-headwall accumulation ratios (THAR) methods for each glacier advance, as recommended by Benn et al. (2005) and Osmaston (2005) and calculated the mean ELAs with $\pm 1\sigma$. We also applied the modern maximum elevation of lateral moraines (MELM; Dahl and Nesje, 1992) to estimate the present ELAs of the glaciers. Multiple ELA indices are used to help us evaluate and eliminate uncertainties associated with each method.

We obtained the AAR and THAR ratios from published literature in the Garhwal region (Table 1; Andrew, 1975; Sharma and Owen, 1996; Barnard et al., 2004a; Nainwal et al., 2006; Schaefer et al., 2008; Dhobal et al., 2008; Scherler et al., 2010; Mehta et al., 2012; Srivastava, 2012). Based on these recommendations, the AARs of 0.45, 0.55, and 0.65 and the THAR of 0.4 are used in our study. We individually estimated former ELAs for each glacier following the recommendation of Sharma and Owen (1996).

4. Description of landforms

We have mainly focused on the geomorphology and sedimentology of landforms within ~4 km from Gaumukh down to Bhujbasa (Figs. 3, 4). We choose this area because: i) a succession of young moraine sets are best preserved along this stretch; ii) the exposure age chronologies are poorly reconstructed, because either a single boulder is dated (n=1), or dated boulders are collected from ridges mostly influenced by post-depositional mass movement processes (e.g., Barnard et al. 2004a; Srivastava, 2012); iii) previous attempts were unsuccessful to understand the systematically inherited cosmogenic nuclide (e.g., [10]Be) inventory in these young (<2 ka) moraine boulders (e.g., Barnard et al. 2004a); iv) this part of the Bhagirathi catchment has a wealth of historical maps, field sketches, and photographs for >200

years (Sharma and Owen, 1996; Srivastava, 2012; Raina et al., 2015). This location provides an excellent opportunity to independently date moraines and evaluate the concentration of inherited TCNs.

Four sets of moraines are identified along this ~4 km forefield from the snout of Gangotri glacier. From (morphostratigraphically) oldest to youngest they include: M_{B4}, M_{B3}, M_{B2}, and M_{B1}, of which moraine M_{B2} is part of Meru glacier (Table 2; Figs. 3, 4).

The NW trending M_{B4} laterofrontal moraine set is better preserved at ~600 m upstream from Bhujbasa (~4150–3810 m asl) and consists of two prominent moraine ridges (M_{B4a} and M_{B4b}), each ~2.7 km long (Figs. 3, 4A). The moraine front (~4000–3810 m asl) is mostly buried and dissected by the debris flow fans and the streams traversing the debris flow fans, respectively. The Bhagirathi river also dissects the moraine front at ~3810 m asl (Fig. 3, 4A). The M_{B4} is ~120–180 m above the glacier forefield, close to the bedrocks slopes, and, therefore, extensively influenced by post-depositional slope contamination (Fig. S1A, B). No new samples were collected from this moraine. Small talus cones formed at the base of the moraine, indicating the ongoing paraglacial transition of the catchment (Fig. S1A). Based on morphostratigraphy, a continuation of the M_{B4} is evident up-valley near Tapovan (~4310–4500 m asl), where the lateral moraine set is ~4 km long (Figs. 3, 4B,C). Two or more (discontinuous) moraine ridges of the M_{B4}, proximal to the north facing slopes of the catchment near Tapovan, have a ridge height of ~20 m higher than the M_{B3} and is separated by an ~30-m-wide distinct ablation valley (Fig. 4C). Srivastava (2012) provided three ^{10}Be ages (Milap2, 3, and 7) for the M_{B4} moraine (Fig. 3).

The M_{B3} laterofrontal moraine set ends ~1.3 km up-valley from Bhujbasa (Figs. 3, 4A). This NW trending moraine, stretching between ~3856 and 4420 m asl, is inset within M_{B4}. Two prominent ridges are evident (M_{B3a} and M_{B3b}) all along the moraine (Fig. 4B, C). The western lateral section of the M_{B3} continues all along Gangotri glacier and its tributaries, but the eastern lateral section is fragmented, because of the sharp NW bend of the trunk glacier at ~4400 m asl (Fig. 3). Like M_{B4}, the frontal section (3856–4000 m asl) of M_{B3} is also intensely dissected by debris/alluvium fans and meltwater streams (Figs. 3, 4A), and developed a chain of talus cones at the base (Fig. S1A). While Barnarad et al. (2004) sampled six boulders from the ~1.7-km-long frontal section (~3900 m asl) of the northern ridge (M_{B3a}) of the moraine, our field

observation indicates extensive recent debris and rockfall deposits all along the section (Figs. 3; S1A). We did not sample the frontal section of the moraine because we could not differentiate the moraine boulders from the boulders deposited by mass movements. However, five ^{10}Be samples were collected from the western lateral ridge of the moraine near Tapovan (~4200–4440 m asl) where it is best preserved and away from any slope deposits (Table 3; Figs. 3, 5A, B).

M_{B2} is an NE trending, >4-km-long laterofrontal moraine set which runs on both sides of Meru glacier. M_{B2} overrides the M_{B3} and M_{B4} stage moraines of Gangotri glacier at the front (~4200 m asl; Figs. 3, 4C), and hence, morphostratigraphically younger. In addition to the main ridge (M_{B2b}), a subdued ice contact ridge also formed between the snout (4466 m asl) and the front (4244 m asl) of the moraine (Fig. S1D). This ridge (M_{B2a}) likely formed as a result of continuous downwasting of Meru glacier. Several small (~10^1 m) hummocky ridges also formed in between the snout and the front, further supporting recent retreat and/or downwasting of the glacier (Fig. S1D). Four samples were collected from the east moraine ridge of M_{B2b} (Table 3; Figs. 3, 5C, D). Distinct ablation valleys prevent slope contamination from nearby talus deposits (Fig. S1C; Ranhotra and Bhattacharya, 2004; Haritashya et al., 2010).

The M_{B1} recessional/hummocky moraine complex is inset into M_{B3} (~3920–3875 m asl; Table 2; Figs. 3, 4D, E). M_{B1} ridges are small (10–40 m long) and subdued in size (<10 m high), indicating a rapid retreat of Gangotri glacier after the M_{B3} advance/still-stand. The distant moraine ridges of M_{B1c}, located ~2.4 km down the valley from the snout, are assigned a historical age of AD 1780 (i.e., 0.24 ka; Hodgson, 1822; Sharma and Owen, 1996; Srivastava et al., 2004a, 2004b; Raina et al., 2015; Figs. 3, 4D). Srivastava (2012) previously proposed an apparent exposure age for M_{B1c} based on a single ^{10}Be age (Milap 1 in Fig. 3). Since this moraine has an independent historical age, we collected five boulder samples from M_{B1c} to estimate the systematic inheritance of ^{10}Be (Table 3; Figs. 3. 5E, F). We also collected four additional boulders from another sharp crested terminal moraine ridge (M_{B1a}) to assess inheritance (Table 3; Figs. 3, 5G, H, I). The M_{B1a} is located ~1.7 km down-valley from the snout (Figs. 3, 4E). A historical age of AD 1935 (i.e., 0.08 ka) is assigned to this moraine (Auden, 1937; Sharma and Owen, 1996; Srivastava et al., 2004a, b; Srivastava, 2012; Bhambri et al., 2012; Raina et al., 2015; Figs. 3, 4E). The recessional moraines

that are older than AD 1971 have prominent ridges, strong clast fabrics, and suitable for TCN dating (Sharma and Owen, 1996; Fig. 4D, E). Table 2 provides additional moraine morphological, sedimentary, and boulder characteristics.

5. Results

5.1. Inherited ^{10}Be

We estimated the inherited ^{10}Be in the M_{B1c} and M_{B1a} recessional moraines (Hodgson, 1822; Auden, 1937; Sharma and Owen, 1996; Srivastava et al., 2004a, b; Srivastava, 2012; Bhambri et al., 2012; Raina et al., 2015). ^{10}Be concentrations of five new (Table 3; Fig. 6A) and a published boulder(s) (Srivastava, 2012) for the M_{B1c} range between ~0.7 and 14.9 x 10^4 atoms/g SiO_2 (equivalent exposure ages of ~0.2–4.5 ka; Fig. 6A). If we remove the ~4.5 ka outlier (Gang18), the remaining samples provide inherited ^{10}Be concentrations ranging from ~0 to 0.4 x 10^4 atoms/g SiO_2 (equivalent ages of 0–0.13 ka; Table 5; Fig. 6A).

Four new boulder samples from the M_{B1c} give consistent ^{10}Be concentrations ranging from ~0.8–0.9 x10^4 atoms/g SiO_2 (equivalent exposure ages of ~0.2 ka; Table 3; Figs. 3, 6A). The estimated inherited ^{10}Be range between ~0.4 and 0.6 x10^4 atoms/g SiO_2 (equivalent age overestimation of ~0–0.05 ka; Table 5). The ^{10}Be ages for these moraines, therefore, indicate age overestimation by as low as 0.05–0.13 ka, i.e., within the uncertainty range (±2σ) of the TCN dating, to as high as ~4.5 ka if the obvious outlier is considered (Table 5).

However, the ^{10}Be concentrations in the supraglacial (i.e., active ice) and proglacial sediments from Gangotri glacier (Figs. 2, 6A; Barnard et al., 2004a; Orr et al., in prep.) are reported to be higher and measured to ~1.1–2.7 x 10^4 and ~3.9 x 10^4 atoms/g SiO_2, respectively (equivalent ages of ~0.2–0.6 ka and ~1.1 ka, respectively; Table 5; Fig. 6B). Additionally, we also inferred the maximum ^{10}Be concentrations in those supraglacial (Orr et al., in prep.) and proglacial sediment(s) (Table 5; Barnard et al., 2004a). Maximum concentration is expected if a sample is exposed to cosmic rays steadily since its emplacement on the glacier surface and traveled in the ablation zone to its respective medial moraine or proglacial

position. Our results indicate ^{10}Be concentrations ranging between ~1.8 and 2.9 x 10^4 atoms/g SiO_2 for supraglacial sediments and ~4 and 7 x 10^4 atoms/g SiO_2 (i.e., ~0.5–0.7 ka) for proglacial sediments. These estimated maximum ^{10}Be concentrations are, therefore, comparable ($\pm 2\sigma$) with the actual measured ^{10}Be concentration.

Previous studies in the Himalayan high-mountain settings (Barnard et al., 2004a; Heimsath and McGlynn, 2008; Seong et al., 2009a; Orr et al., in prep.) and in Alaska (Ward and Anderson, 2011), that targeted medial moraine supraglacial debris, specifically to measure erosion rates using ^{10}Be (Fig. 6B), also indicate that moraine boulder samples for Gangotri glacier are usually much younger (0.2–0.3 ka) than the active ice supraglacial debris (0.1–2.6 ka ;Fig. 6B). The ages of these supraglacial debris are calculated assuming respective average catchment-wide ^{10}Be production rate.

Three supraglacial boulders (active ice) are also ^{10}Be dated from Chorabari glacier, Kedarnath (Fig. 6B; Murari et al., 2014) with inherited ages (recalculated here) of only ~0.06, ~0.22 and ~0.62 ka (Fig. 6B).

5.2. Dating Results and Local Glacial Stages

Three published boulder samples from M_{B4} (Gangotri stage) have ^{10}Be ages ranging from ~2.4 to 0.5 ka (recalculated in Table 3; Srivastava, 2012). Among these, sample Milap7 (~0.5 ka; ibid) was collected from the frontal section of the moraine which is heavily covered by fresh slope deposits and dissected by seasonal streams. We identify the sample as an outlier (Fig. 7A). The remaining two samples (Table 3) that were collected from the distant western lateral moraines near Tapovan (Fig. 7B) gives a tentative (because n=2) mean age of ~2.2±0.4 ka (χ^2 of 5.6; Table 6). We, therefore, reassigned the Gangotri glacier stage to ~2.4–1.9 ka (Fig. 8).

Five new boulder samples from the M_{B3} (Bhujbasa glacial stage) yielded ages ranging from ~3.3 to 0.5 ka (χ^2 of 30.6 and age dispersion 64%; Fig. 7B). Statistically and given the age range of M_{B4}, the ~3.3 ka sample (Gang5) is identified as an outlier (Fig. 7B). The remaining ages range from ~1.2–0.5 ka with a mean age of ~0.8±0.3 ka (Fig 7B). Barnard et al. (2004a) also ^{10}Be dated six samples from the frontal section of M_{B3} with ages of ~3.1–0.3 ka (recalculated here; Fig. 7A). The younger ages (~0.26 and ~0.34

ka) are likely outliers because recent slope deposits cover the frontal section of M_{B3}. Similarly, the ~3.1 ka age may also be an outlier based on M_{B4} ages (Fig. 7A). We, therefore, reassign the Bhujbasa glacial stage to ~1.7–0.5 ka (n=8; Fig. 8).

The apparent exposure ages (n=4) for M_{B2} of Meru glacier range between ~0.5 and 0.1 ka, with a mean age of ~0.3±0.1 ka (Fig. 7B). Even though χ^2 is as high as 36.5 and age dispersion is 49%, none of the sampled boulders show any signs of toppling or exhumation (Fig. 5C, D). We, therefore, assign M_{B2} to ~0.5–0.1 ka (Fig. 8). Since M_{B2} is on top of M_{B3}, i.e., it is younger, our morphostratigraphy is supported by chronostratigraphical reconstructions and further support the removals of young outliers for M_{B3} (Fig. 7B). We propose this as a new stage and name it the Meru glacial stage.

Several recessional M_{B1} moraines are inset into M_{B3} and are independently dated by lichenometry, historical descriptions and measurements, plane table map, sketches, and photographs (Hodgson, 1822; Auden, 1937; Sharma and Owen, 1996; Srivastava et al., 2004a, b; Srivastava, 2012; Bhambri et al., 2012; Raina et al., 2015) to the last two centuries (Figs. 7, 8). We assign these moraines to the Gaumukh glacial stage.

5.3. ELA Reconstructions

Meru glacier extended ~1.3 km during ~0.5–0.1 ka (Meru glacial stage) resulting in ΔELA of ~138±57 m (Fig. 8; Table 4). Gangotri glacier advanced ~2 km from the snout during the Bhujbasa glacial stage at ~1.7–0.5 ka resulting in a ΔELA of ~16±4 m (Fig. 8). The ΔELA is estimated to only ~28±20 m during the Gangotri glacial stage at ~2.4–1.9 ka when the trunk glacier extended ~3 km (Fig. 8).

Among older glacial stages, the Shivling glacial stage at ~5 ka had a ΔELAs of ~185±207 m, the Sudarshan glacial stage at ~20.1–15.9 ka had a ΔELAs of ~298±221 m, and the Bhagirathi glacial stage at ~63 ka had a ΔELAs of ~508±252 m (Table 4; Fig. 8). The hanging Kedar glacier during the Kedar glacial stage at ~8.6–8.0 ka advanced <3 km, having a ΔELA of 126±60 (Table 4).

6. Discussion

6.1. The Role of Inheritance in the Bhagirathi catchment

Boulders often with prior exposures are deposited at moraines, yielding apparent ages that are too old (Applegate et al., 2010, 2012). For the two youngest recessional moraine ridges (AD 1780 and 1935) in our study, we found negligible systematic inventory of inherited ^{10}Be (~0.4–0.6 x10^4 atoms/g SiO$_2$; Table 5), yielding excess apparent ages of only ~0.05–0.13 ka, which is approximately within the analytical uncertainties of ^{10}Be dating (±2σ). While large boulders (0.7–3.5 m), which are ^{10}Be dated in this study, are mostly delivered by random rockfall and avalanche events (Heimsath and McGlynn, 2008; Seong et al., 2009a), and periglacial processes (Shroder et al., 2000; Matsuoka, 2001; Owen et al., 2003; Hales and Roering, 2005; Sanders et al., 2012; Gibson et al., 2017), supraglacial and proglacial sediments (grain size <64 mm) may experience more complex geological history over 10^{1-2} year timescales, including, if not limited to, reworking from previous moraines (cf. Carson and Kirkby, 1972; Ballantyne, 2002a, b). While we are cautious to derive conclusions from two different grain sizes, our comparisons between moraine boulders (this study) and supraglacial (Orr et al., in prep.) and proglacial sediments (Barnard et al., 2004) from the same glacier indicate that systematic ^{10}Be concentrations during glacial transportation (i.e., *en route*) are always higher in the sediments than in moraine boulders in a very erosive glacial setting (~2.1–5.3 mm/a; Fig. 6A). This contrasts with semiarid to hyperarid settings that have low erosion rates (<0.01 mm/a), where boulders generally have an excessive prior inventory of ^{10}Be than sediments (Fabel et al., 2002; Briner et al., 2006; Placzek et al., 2014).

We also estimated the maximum ^{10}Be concentration in the supraglacial samples assuming a constant ^{10}Be production rate, glacial velocity, and distance along medial moraines (see Fig. 6A). The estimated ^{10}Be concentrations are comparable with the measured concentration. This may indicate a steady exposure of supraglacial sediments during glacial transportation relative to boulders. Further, comparison with other ^{10}Be dated supraglacial boulders (Murari et al., 2014) and erosion rate studies that specifically targeted supraglacial debris along medial moraines (Barnard et al., 2004a; Heimsath and McGlynn, 2008; Seong et al., 2009a; Ward and Anderson, 2011; Orr et al., in prep.), also concurs with our above inference.

While the measured ^{10}Be concentrations and apparent ages in different catchments are largely influenced by latitude, altitude, glacier length and velocity, and most profoundly erosion rates (e.g., erosion rates for Gangotri = 2.1–5.3 mm/a, Annapurna = 0.20±0.05 mm/a, Baltoro = 0.7–2.5 mm/a, and Alaska =0.5–1.33 mm/a; ibid), our comparisons only tentatively corroborate the idea that moraine boulders in more erosive settings (≥2 mm/a) may have minimum ^{10}Be inventory than active ice supraglacial sediments and debris (Fig. 6).

The prior accumulation of ^{10}Be in moraine boulders may depend on several geologic factors which may be broadly categorized into i) inheritance during the non-glacier system; and ii) inheritance during the glacier system. In the non-glacier system, excess prior inventory may occur in boulders when part of a bedrock flanks before detachment and as a sediment storage, e.g., slope deposits, rock glaciers, before reworked into the glacier system (Table 6; Shroder et al., 2000; Heimsath and McGlynn, 2008; Seong et al., 2009a; Applegate et al., 2010, 2012; Heyman et al., 2011; Çiner et al., 2017). In the glacier system, supraglacial transportation of debris likely results in excess ^{10}Be inventory (Table 6; Heyman et al., 2011).

A brief discussion on several geomorphic processes during each system are elaborated in Table 6, along with the estimated maximum ^{10}Be inheritance during each subsystem. If the moraine boulders used in this study had steady-exposures during both the systems, much higher inherited ^{10}Be would be expected (Table 6). Several geomorphic processes, however, may explain why our sampled boulders have lower concentrations of inherited ^{10}Be. These include:

1) Constant boulder/block rotation and toppling during supraglacial transportation preclude steady-exposures and hence, low systematically inherited ^{10}Be (Fig. 9). The dynamic and high-activity type supraglacial environment of Gangotri glacier system consisting of rugged surface, variable but thick blanket of debris mantle, large crevasses and ice collapse structures, supports high-instability of supraglacial boulder on the glacier surface (Fig. 9; Tewari, 1972; Haritashya et al., 2010; Scherler et al., 2011a; Satyabala, 2012; Raina et al., 2015).

2) Higher-frequency stochastic rockfall events from bedrock flanks with homogeneous ^{10}Be production than that inferred through ^{10}Be erosion rates (~2.1–5.3 mm/a; Orr et al., in prep.), may

systematically contribute to low inherited [10]Be in moraine boulders. However, no such studies to our knowledge exist for the upper Bhagirathi catchment (cf. Bali et al., 2003; Scherler et al., 2014) to corroborate this hypothesis.

3) Majority of the moraine boulders are derived from steep sidewalls than from ridges. Studies showed that erosion at ridge crests is much slower than on the sidewalls (cf. Heimsath and McGlynn, 2008; Placzek et al., 2014), contributing to systematically lower inherited [10]Be. Since greater slope angles and steep relief promote a larger debris flux (Finlayson et al., 2002; Burbank et al., 2003; Ouimet et al., 2009; Scherler et al., 2011b, 2014) by facilitating high-frequency rockfalls and avalanches (Luckman, 1977; Anderson, 2005; Gruber and Haerberli, 2007; Matsuoka and Murton, 2008; Foster et al., 2010; Bernhardt and Schulz, 2010; Nagai et al., 2013), and since the south facing slopes of the upper Bhagirathi catchment is incredibly steep and ~2–3 km tall (Fig. 2), it may be possible that our sampled moraine boulders are predominantly derived from the south-facing slopes.

4) High erosion rates of boulders during supraglacial transportation may also reduce the surface accumulation of spallogenic [10]Be (Gosse and Phillips, 2001). If we assume a [10]Be production rate of ~95.4 atoms/g SiO_2/a, density of 2.7 g cm^{-3}, decay constant of 4.99 x 10^{-7}, erosion rate of 0.2–0.5 mm a^{-1}, and spent ~0.5 ka on the supraglacial zone, a maximum spallogenic [10]Be concentration at the surface of a boulder would still range between ~1.2 x 10^4–3.1 x 10^4 atoms/g SiO_2 (i.e., ~0.1–0.3 ka; Fig. S4). We argue that while high supraglacial boulder erosion by interclast abrasion and attrition are very likely (Fig. 9; Owen et al., 2003; Benn and Evans, 2010; Benn et al., 2012), this may be one of the facilitating factors, if not primary, for the low [10]Be concentrations on our sampled boulders.

5) The majority of boulders if transported sub- and/or englacially and later transported to the surface of the glacier, may have zero to limited inherited [10]Be (Table 6). We argue that while it may be possible for some boulders given the high activity of Gangotri glacier (Sharma and Owen, 1996), it is unreasonable to assume for all the large sampled boulders (Table 3).

6) Sampled boulders might have derived from nearby slopes during glacial to paraglacial transition and transported at a much faster speed during the recession in the last 0.2 ka. While we cannot verify if this

is the case, no major geomorphic evidence or topographic scars, e.g., rock avalanches, were observed upglacier in the catchment that suggests extensive localized sediment evacuation in the recent past (cf. Shugar and Clague, 2011; Reznichenko et al., 2011; Shugar et al., 2018).

7) Boulders originating from locations with heterogeneous production rates (Scherler and Egholm, 2017) and/or low production rates due to high shielding (Zweck et al., 2013) may also contribute to low inherited ^{10}Be in moraine boulders systematically. We argue that this could be a key factor, but not a primary one.

Additional factors may also add geological complexity to the process. For example, assessing the relative roles of fracture patterns, jointing (Hallet et al., 1999; Murton et al., 2006; Hales and Roering, 2007), and local fault systems (Validya, 1991; Sorkhabi et al., 1996; Bali et al., 2003) on the susceptibility of the rock to failure are beyond the scope of this paper, but have profound impact in determining inherited ^{10}Be in moraine boulders. Although we have argued that moraine boulders in more monsoon dominated erosive settings likely have minimum inherited ^{10}Be, caution should be drawn when applying such conclusions over the catchment-scale because this relation may vary with lithology, structural architecture, microclimate, slope, aspects, terrain geometry, and the geomorphic history (Sharma and Owen, 1996; Barros et al., 2006; Singh et al., 2007; Srivastava, 2012). Similarly, the frequency and depth of wet-dry episodes, seasonal and diurnal temperature fluctuations, and periglacial processes (Hales and Roering, 2007; Humphreys and Wilkinson, 2007; Moores et al., 2008; Dühnforth et al., 2010; Fischer et al., 2010, 2012; West et al., 2014; Eppes and Keanini, 2017), also influence the strength of bedrock (Murton et al., 2006; Eppes and McFadden, 2008), and in turn moderate hillslope debris flux. These factors, although, crucial, are not quantified in this study. Scherler and Egholm (2017) also proposed the significance of dynamic evolution of debris mantle with changing climate, and topography in determining ^{10}Be concentration on medial moraine debris. We argue that these changes even at 10^{1-2} year timescale are critical in controlling systematically inherited ^{10}Be in boulders. Equally significant roles on systematic inheritance are played by changing glacier mass balance regime, velocity, hydrology, and subglacial stick-slip processes (Benn and Evans, 2010; Evans et al., 2006) during glacial and paraglacial transitions (Ballantyne

and Benn, 1994; Owen and Sharma, 1998; Ballantyne, 2002a, b; Barnard et al., 2004a). Chemical weathering of moraine boulders, however, are insignificant to consider in this context (Tripathy and Singh, 2010). Further research on the frequency of random rockfall events, fracture patterns in steep bedrock slopes, [10]Be concentrations in valley sidewalls and supraglacial debris across different grain sizes and the erosion rate of supraglacial boulders *en route* are required to decipher the role of geomorphic process uncertainties on prior exposures.

Although discrete geomorphic processes may result in extremely low inheritance in boulders, we propose that a combination of complex geomorphic processes are the more plausible cause. This study further supports that more erosive temperate glaciers likely are better candidates to reconstruct high-resolution terrestrial Late Holocene glacial chronostratigraphies than semiarid and arid glaciers (Saha et al., 2018, submitted). Insignificant inherited [10]Be in our study also reinforces the concept that moraine formation in debris mantled valley glaciers may occur on a decadal timescale in response to a combination of climate change and stochastic, interannual variability in mass balances (cf. Roe, 2011; Anderson et al., 2014).

6.2. Implications for Late Holocene Chronologies

We improve the previously proposed two Late Holocene local glacial stages, i.e., Gangotri and Bhujbasa glacial stages (Figs. 7, 8; Sharma and Owen, 1996; Barnard et al., 2004a; Srivastava, 2012) and proposed two new local glacial stages (Meru and Gaumukh glacial stages) for the Bhagirathi catchment. Gangotri glacier stage is tentatively assigned to ~2.4–1.9 ka and Bhujbasa glacial stage to ~1.7–0.5 ka. ΔELAs for these local stages were small (~16–28 m; Table 4; Fig. 8). Coeval to Gangotri glacial stage are restricted glacier advances in the semiarid and arid regions of the NW Himalaya and Tibet (Seong et al., 2009b; Dortch et al., 2013; Orr et al., 2018; Saha et al., 2018) and in the monsoon-dominated central Himalaya (Owen et al., 2009; Zech et al., 2009). Similarly, contemporaneous to Bhujbasa glacial stage, restricted glacier advances are evident in the semiarid NE Himalaya (Seong et al., 2009b; Orr et al., 2017; 2018; Saha et al., 2018), the temperate western (Scherler et al., 2010; Saha et al., 2015) and central

Himalaya (Owen et al., 2005; Barnard et al., 2006; Zech et al., 2009; Heimsath and McGlynn, 2008). We assigned the Meru local glacial stage to ~0.5–0.1 ka, which has a ΔELA of ~140 m in the tributary valley (Table 4; Fig. 8), suggesting an accelerated recession of the tributary glacier since the last advance (Fig. 7). Our field investigation further corroborates the recent rapid downwasting of Meru glacier (Fig, S1C, D).

However, most notable in our reconstructed local glacial stages is the age dispersion (64%; χ^2 ~31) of the Bhujbasa glacial stage; excluding published ages of Barnard et al. (2004a; Table 3). While AD 1780 and 1935 recessional moraines (M_{B1}) and Meru stage moraines (M_{B2}) have consistent apparent [10]Be ages and lower inheritance, systematic inheritance is likely high for the Bhujbasa stage (M_{B3}) moraine at the 10^{2-3}-year timescale (Fig. 7). We argue that this may likely be associated with selective sediment evacuation from older gentler slopes and moraine deposits, and/or rock glaciers, i.e., sediment storage (cf. Carson and Kirkby, 1972; Ballantyne, 2000a, b) during periods of glacier advances. For examples, several protalus and morainic rock glaciers (cf. Owen and England, 1998) are observed on the gentler north-facing slopes of the trunk valley and west facing slopes for the tributary valleys of the upper Bhagirathi catchment (Fig. 2). Rock glaciers are inefficient agents of sediment transfer (Shroder et al., 2000) and therefore, often yield seemingly maximum ages associated with inheritance (cf. Çiner et al., 2017). While these inherited ages are not a significant statistical issue for the Mid-Holocene moraine boulders of M_{B5} (~5.2 ka, 0% dispersion) in the catchment, they represent quite a big spread in apparent ages for moraines < 2 ka. The distinct ~4.5 ka outlier of AD 1780 (M_{Bc1}) moraine may also be explained using this argument.

6.3. Implications for Dating Young Moraines

We further compare the apparent [10]Be ages of youngest set of moraines from several semiarid glaciers of the northwestern Himalaya (Dortch et al., 2013; Hedrick et al., 2011; Orr et al., 2018; Saha et al., 2018) with our study area and adjacent temperate glaciers of the central Himalaya (Fig. 10; Barnard et al., 2004a; Owen et al., 2010; Murari et al., 2014). The cumulative probability density distributions (CDFs; Applegate et al., 2012) of youngest moraine ages in the cold-based semiarid glaciers systemically show very high spread (range: >1 ka) in the apparent [10]Be ages, making it impossible to identify outliers (Fig.

10A). In contrast, [10]Be ages for temperate glaciers, including this study, show a narrow age distribution (range:<1 ka) for most boulders and outliers are distinct from rest of the age distribution. Continuing from our ongoing discussion, we, therefore, propose that studies which solely use single TCN (e.g., [10]Be) ages to define youngest glacial chronologies, such as Little Ice Age (LIA), especially in the semiarid and arid settings (cf. Yang et al., 2008; Li et al., 2016; Rowan, 2016; Saha et al., 2018), should carefully consider the geomorphic process uncertainties and implications of age spread due to systematic inheritance. Undoubtedly the precession of apparent TCN exposure ages is increasing because of ongoing improvements in analytical, production rate, and scaling scheme uncertainties (Nishiizumi et al., 2007; Balco et al., 2008; Lifton et al., 2014; Martin et al., 2017; Borchers et al., 2016; Marrero et al., 2016), but geological uncertainties are rarely addressed (Heyman et al., 2011).

7. Conclusions

The inherited [10]Be concentrations for AD 1780 moraine range between ~0 and 0.4×10^4 atoms/g SiO_2 (equivalent to an age of ~0 and 0.13 ka) and AD 1935 moraine between ~0.8 and 0.9×10^4 atoms/g SiO_2 (equivalent to an age of ~0 and 0.05 ka). The significantly low systematic inheritance in our moraine boulders may be because of a combination of complex geomorphic processes. This includes boulder/block rotation during supraglacial transportation and/or deposition, high bedrock slope and boulder erosion, high-frequency rockfall events, and/or subglacial origin, which likely offset some of the excess inventory of [10]Be on the sampled surface. When compared with supraglacial and proglacial sediments, overall low [10]Be concentrations were measured in moraine boulders, further suggesting that moraine boulders may likely have low inheritance than sediments in the more erosive, high-activity temperate glacier settings. We, therefore, argued that these glaciers including Gangotri likely are better candidates for reconstructing high-resolution terrestrial Late Holocene glacial chronostratigraphies than semiarid and arid glaciers. Additionally, this study stresses that a careful consideration of the geomorphic process uncertainties and systematic inheritance are crucial when estimating high-resolution apparent exposure ages using a single TCN.

Using nine new and six published [10]Be ages, we further improved the timing of the Late Holocene Gangotri and Bhujbasa local glacial stages and proposed two new local stage, the Meru and Gaumukh glacial stages, in the catchment. The Gangotri, Bhujbasa, Meru, and Gaumukh glacial stages are assigned to ~2.4–1.9, ~1.7–0.5, ~0.5–0.1, and ~0.2 ka, respectively. The estimated ΔELAs of the Late Holocene glacial stages in the trunk (~16–28 m) and the tributary Meru valley (ΔELA: ~140 m) are significantly restricted. This study, thus, further support muted Late Holocene glacier advances in the Himalaya relative to glacier advances elsewhere in the extratropics of the northern hemisphere (Solomina et al., 2015, 2016 and references therein).

In future, we intend to measure the [10]Be concentrations in rockfall debris to quantify rockfall frequency and cliff retreat rates in the catchment. We will also quantify the [10]Be concentrations in supraglacial debris across different grain sizes with the aim of developing an improved geomorphic process model for inheritance.
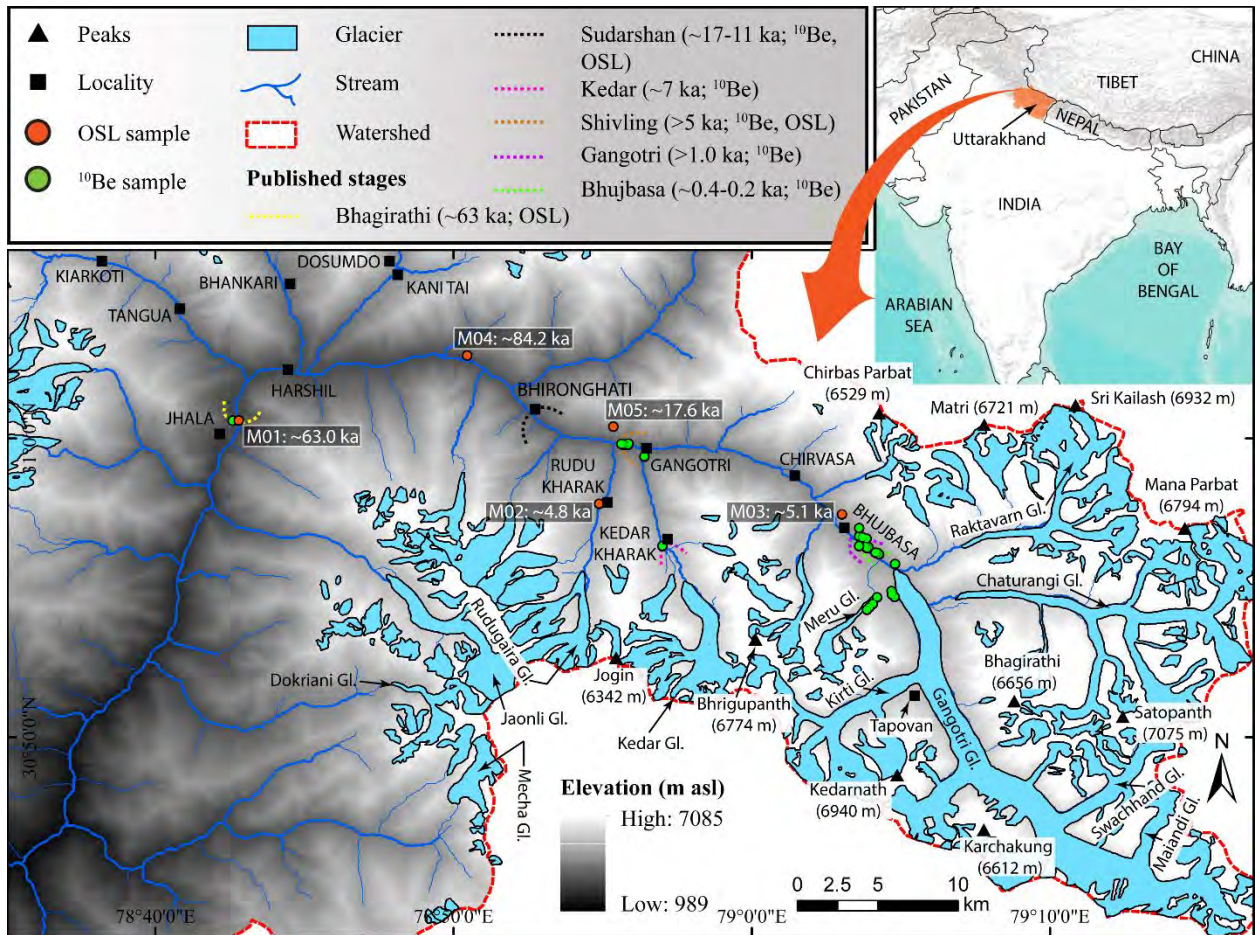
Fig. 1. Study area map is showing upper reaches of the Bhagirathi catchment and major glaciers. Inset map showing the location of the Bhagirathi catchment. Published glacial stages and available optically stimulated luminescence (OSL) ages (after Sharma and Owen, 1996) are also shown.
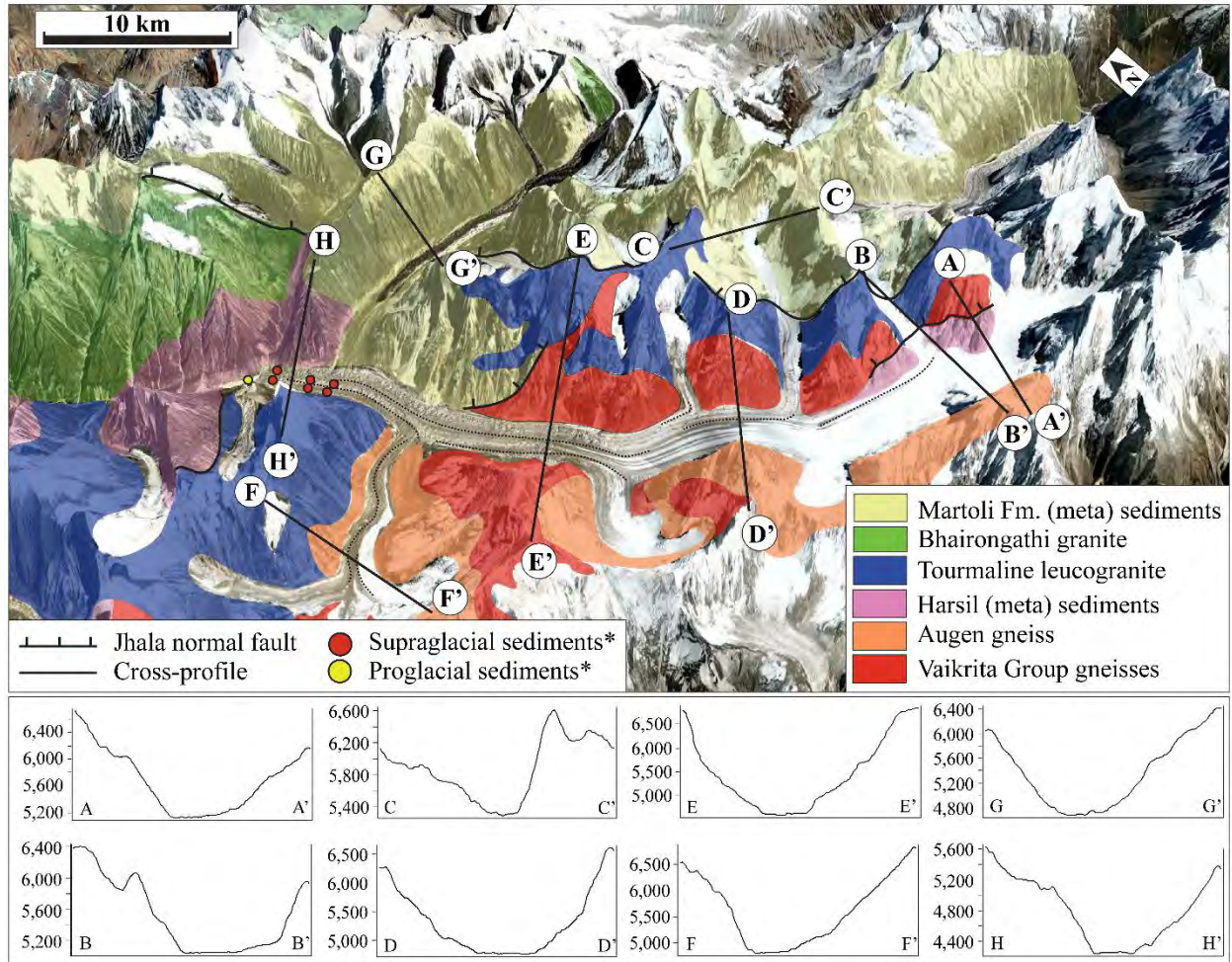
Fig. 2. Geology map that is superimposed on Google Earth terrain map, showing the steep (>45°) bedrock reliefs and asymmetrical valley cross-profiles. Periglacial processes and denudation along these steep bedrock slopes contribute to thick debris mantle on Gangotri glacier. Medial moraines are highlighted (dotted lines) and supraglacial (Orr et al., in prep.) and proglacial (Barnard et al., 2004a) sediment samples are shown.
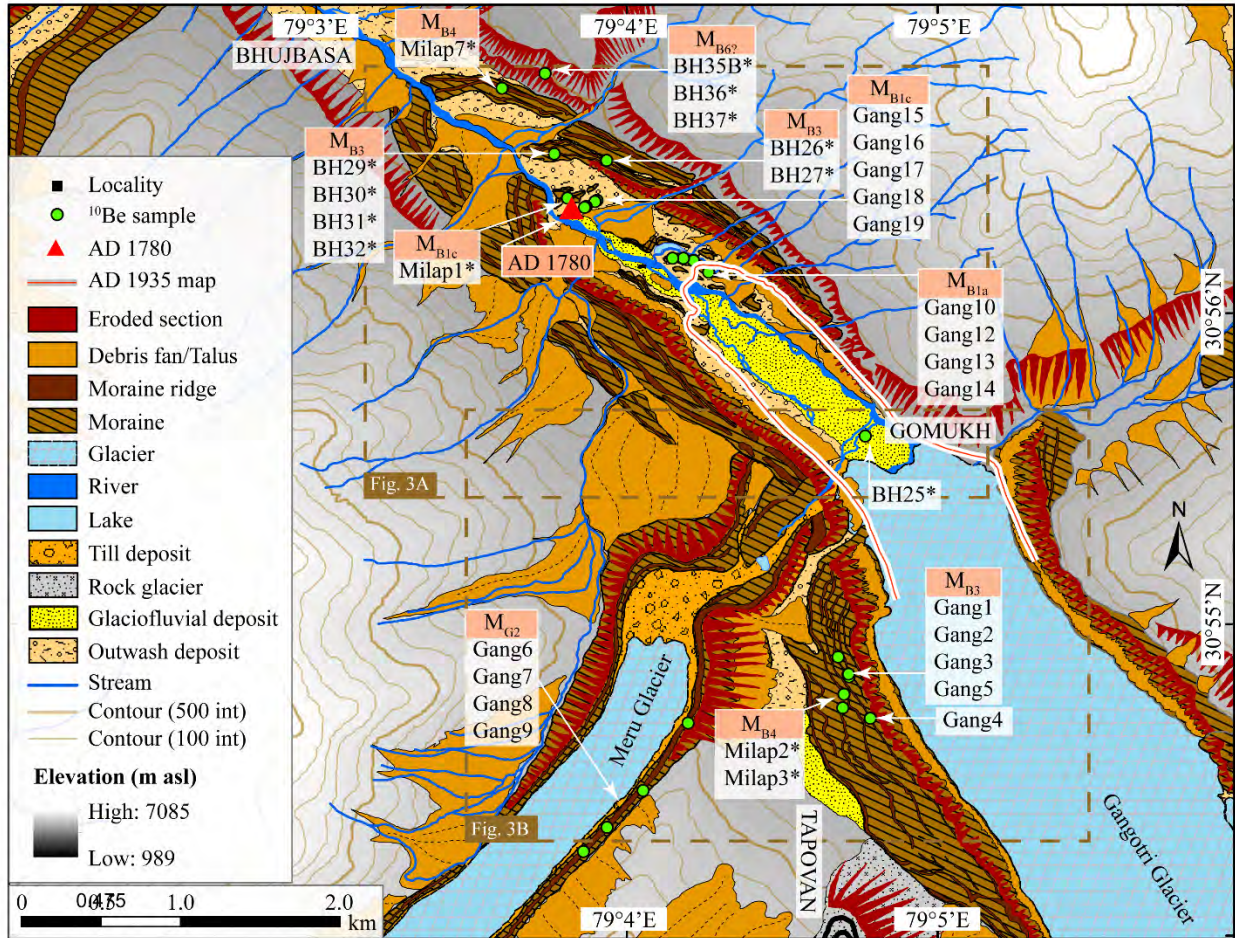
Fig. 3. Study area geomorphology and a surficial unit map showing the location of new and published [10]Be samples. Each moraine/moraine set is morphostratigraphically defined. AD 1780 and 1935 positions are obtained from Raina et al. (2015) and Bhambri et al. (2011), respectively.
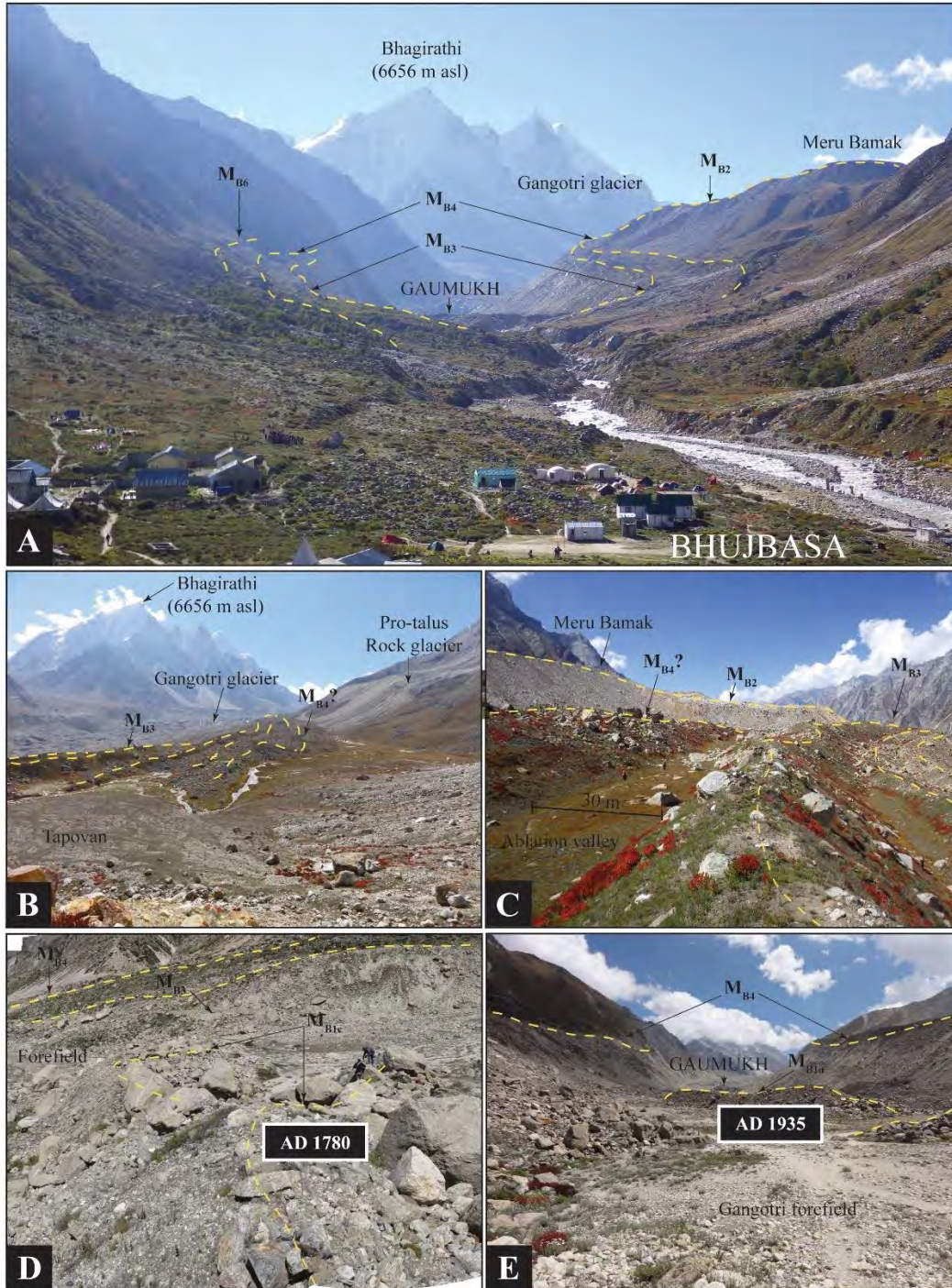
Fig. 4. Views of the moraines sampled for ^{10}Be. A) Forefield of Gangotri glacier with M_{B6} (Sudarshan stage), M_{B4} (Gangotri stage), M_{B3} (Bhujbasa stage), and M_{B2} (Meru stage) moraines. B) Western lateral part of the M_{B4} and M_{B3} near Tapovan. C) Prominent ablation valleys separate high relief M_{B4} and subdued M_{B3} moraines. M_{B2} moraine near Tapovan is also highlighted. AD 1780 (D) and AD 1935 (E) end moraines of the M_{B1} recessional stage are also shown.

201

Fig. 5. Selected examples of moraine boulders sampled for [10]Be measurements. Sampled boulders A–D are used for [10]Be chronology, whereas E–I are measured for inherited [10]Be concentration.
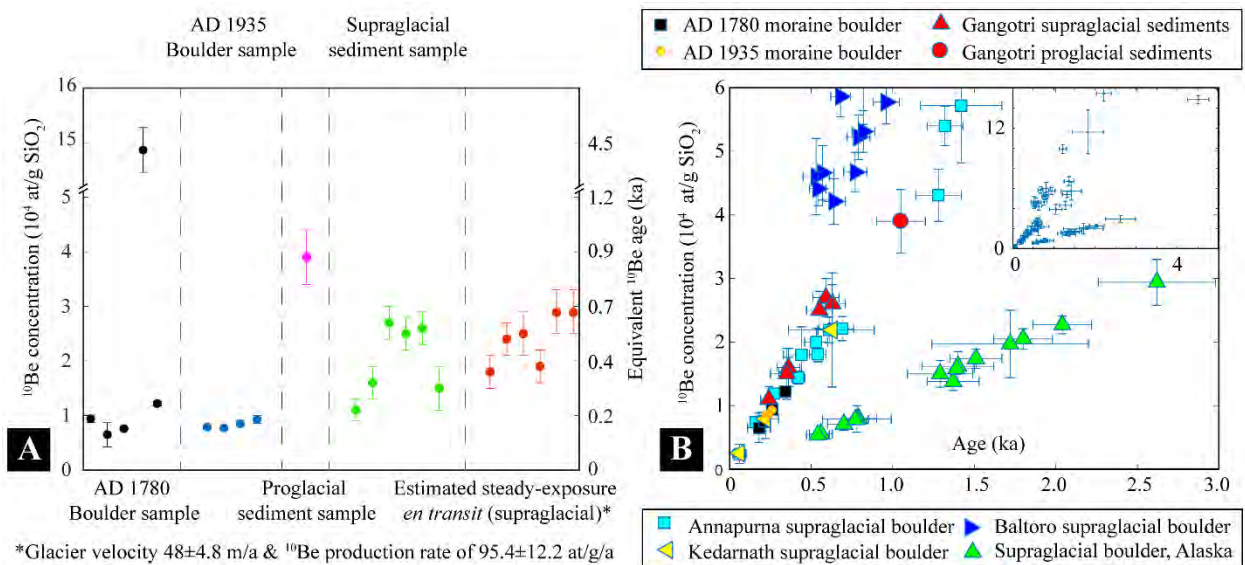
Fig. 6. Prior inventory of [10]Be in moraine boulders and sediments. A) The inherited [10]Be concentration for boulders measured in this study from historical Gangotri moraines (Fig. 3) and compared with supraglacial (along medial moraine; after Orr et al., in prep.) and proglacial (after Barnard et al., 2004; Fig. 2) sediments from Gangotri glacier. The samples are within ~325±90 m altitudinal range from each other. Assuming a steady-state, we also modeled inherited [10]Be in the supraglacial sediments (red) using a glacier velocity of ~48±5 m/a (Bhattacharya et al., 2016), [10]Be production rate of ~95.4±12.2 atoms/g SiO_2/a (Orr et al., in prep.), and measuring the distance along the respective medial moraines (Fig. 2). B) Comparing inherited [10]Be ages from moraine deposits across different glacial systems and different glaciers in the Himalaya (Barnard et al., 2004a; Heimsath and McGlynn, 2008; Seong et al., 2009a; Murari et al., 2014; Orr et al., in prep.) and Alaska (Ward and Anderson, 2011) with different bedrock slope erosion rates. See the text for details. Note: [10]Be concentrations are not normalized and cannot be directly compared, but ages are estimated by respective catchment production rates, and hence are compared.
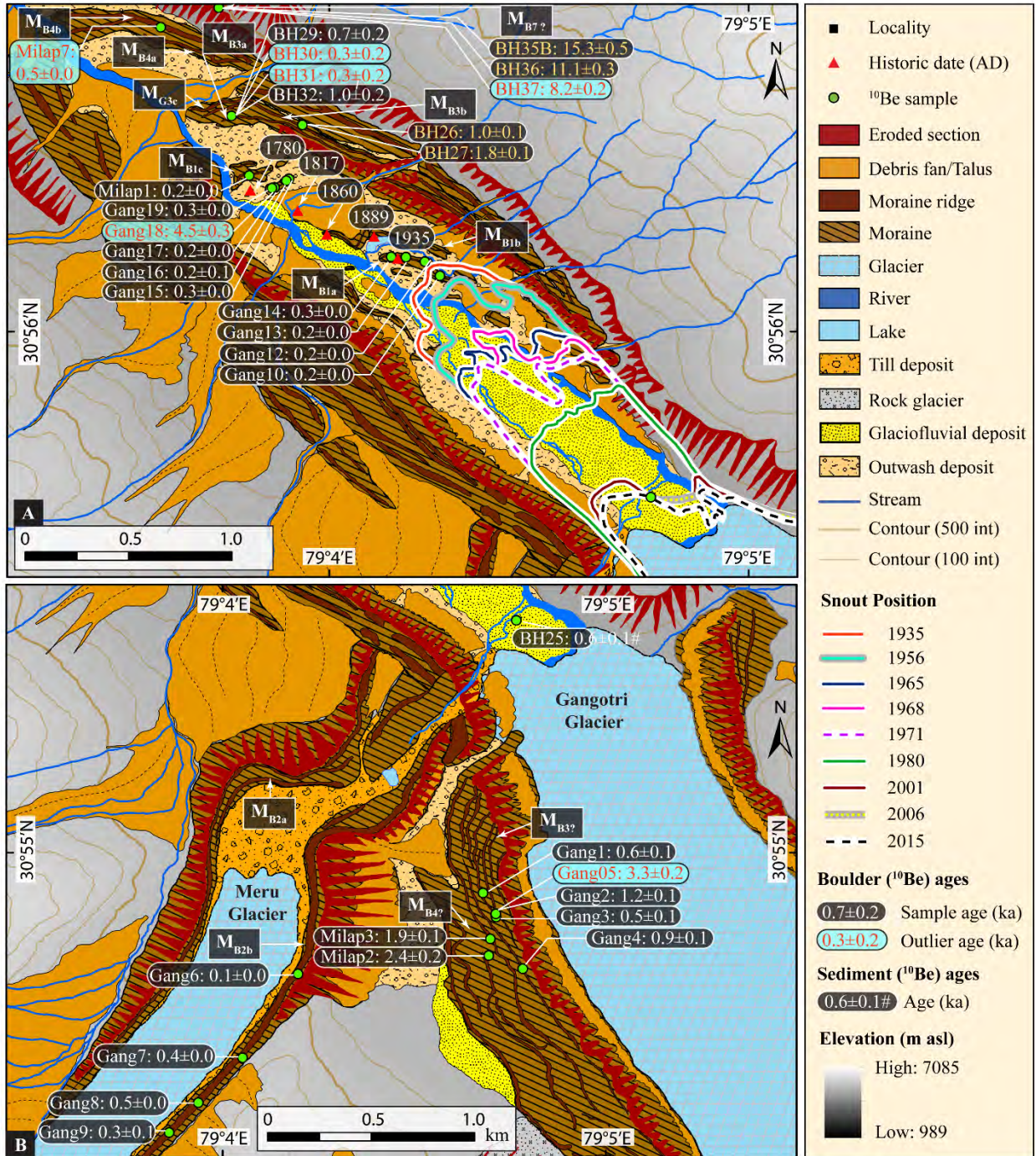
Fig. 7. Study area geomorphology and a surficial unit map showing the location of new and published [10]Be samples and their apparent exposure ages. A) Historical dates and maps of glacier snouts are shown along with [10]Be ages near Gaumukh. Historical dates and maps are modified after Raina et al. (2015) and Bhambri et al. (2012), respectively. B) [10]Be ages are shown for Meru Bamak and M_{B3} and M_{B4} moraines.

204
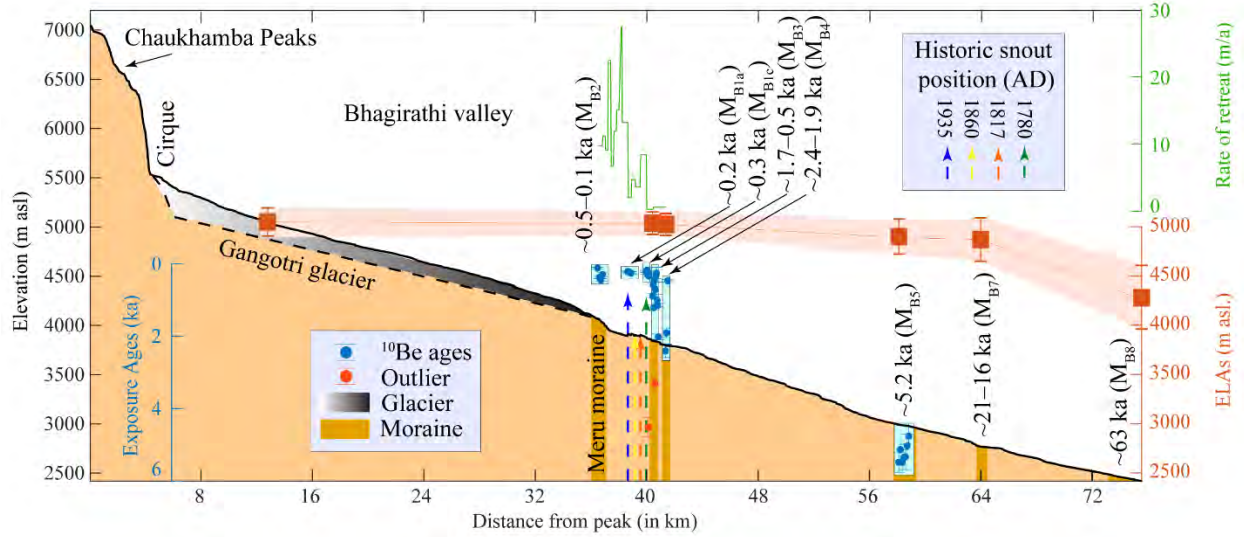
Fig. 8. Longitudinal profile down the Bhagirathi catchment from the valley head to Jhala. Moraine locations and chronologies are shown, coupled with ELAs and recent rate of retreat of Gangotri glacier. Historic snout positions are derived from Raina et al. (2015).

Fig. 9. Photographs showing supraglacial boulder instabilities on the Gangotri glacier. Humans for scale. Photographs are taken ~1–4 km upglacier from the snout.
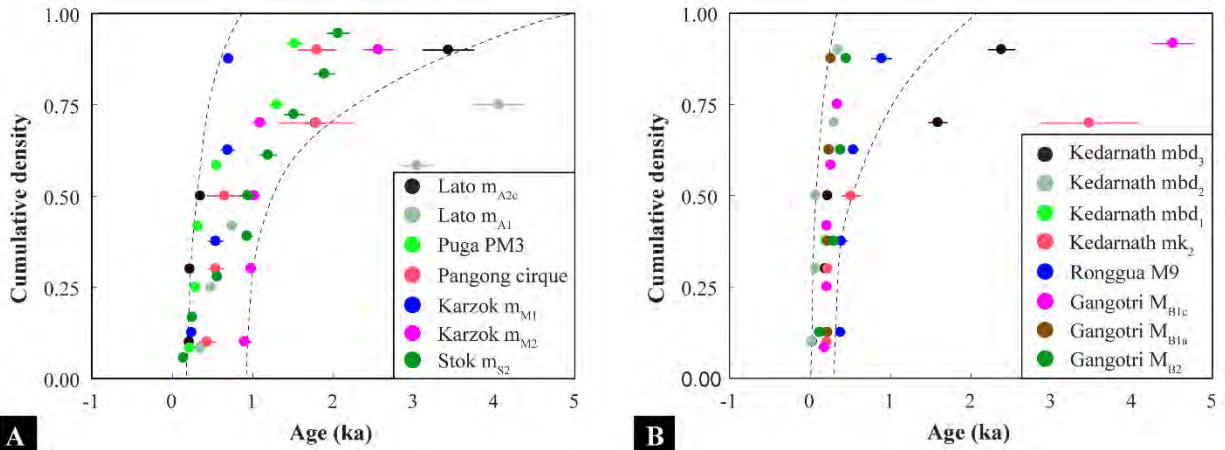
Fig. 10. Cumulative density distribution of sorted (ascending order) apparent [10]Be ages with ±1σ uncertainties of youngest moraines. Ages are shown for (A) cold-based semi-arid cirque glaciers and (B) monsoon-dominated temperate glaciers. Note that moraine ages with no age scatter would have cumulative density increase (y-axis) along a straight line (x-axis). In other words, the samples ages would have incremental vertical progression with no convex upward (for inheritance) or downward (for incomplete exposures) distribution (cf. Applegate et al., 2012). Samples with high age scatter due to inheritance would show smooth convex upward distribution because of systematically older ages. In contrast, samples with minimum inheritance would have a slight convex upward distribution with occasional discrete older (tail end) ages. Here ages are recalculated for Lato, Karzok, Stok (Orr et al., 2018; Saha et al., 2018), Puga (Hedrick et al., 2011), Pangong (Dortch et al., 2013), Kedarnath (Murari et al., 2014), Ronggua (Owen et al., 2010), and Bhagirathi (Barnard et al., 2004a) valleys.

Table 1: Published AAR and THAR ratios used in this study for the Garhwal region.

Study	Region	AAR	THAR
Schaefer et al. (2008)	Garhwal Himalaya	-	0.40–0.50
Andrew (1975), Sharma and Owen (1996), Barnard et al. (2004a)	Garhwal Himalaya	0.60, 1.3	0.5
Dhobal et al. (2008)	Garhwal Himalaya (debris-covered)	~0.61–0.70	0.50–0.60
Nainwal et al. (2008)	Garhwal Himalaya	0.60±0.05	-
Mehta et al. (2012)	Garhwal Himalaya	~0.45	-
Scherler et al. (2010)	Garhwal Himalaya	0.45, 0.55, 0.65	0.50–0.60
Srivastava (2012)	Garhwal Himalaya	0.36	-

Table 2: Moraine and boulder characteristics in the study area.

Morpho stat.	Moraine characteristics	Moraine boulder characteristics
Gangotri moraines		
M_{B4}	NW trending laterofrontal moraine set; consists of two prominent moraine ridges (M_{B4a} and M_{B4b}); mostly buried and dissected by the debris fans and the streams traversing the fans, respectively; extensively influenced by post-depositional slope contamination; mostly covered by grasses and shrubs and relatively thick grasses near the south facing slopes of the catchment; composed of matrix-supported pebbly diamicton.	Angular to subangular boulders are predominant, but subrounded boulders are present near debris fans and dissecting streams; limited rock varnish and moderate lichen cover; fan geomorphic processes likely supply fresh boulders; Lithology: gneisses and granites.
M_{B3}	NW trending laterofrontal moraine set; two prominent ridges are distinguished (M_{B3a} and M_{B3b}); presently located ~100 m above the glacier bed; only shrubs, lichens, mosses are found along the moraine set; composed of massive matrix supported pebbly/boulder diamicton.	Lithology: gneisses; moderate to well inset on the create and little off the crest, but no sign of toppling; poorly-developed to no varnish; thick lichen cover is present; little to not weathered; sub-angular freshly fractured large boulders (1–3 m-high).
$\underline{M_{B1}}$	Small (10–40 m long and <10 m high); sharp-crested recessional/hummocky moraine complex; these moraines are devoid of any vegetation and composed of matrix-supported pebbly diamicton.	Lithology: gneisses; cubic to oblate shaped; mostly angular to subangular; massive (0.6–3.5 m-high) tabular boulders with sharp fracture faces; little to no weathering; some have slight brown stain; mostly on the crest of the moraine and wedged between other boulders; no slope contamination.
Meru moraines		
M_{B2}	NE trending; >4 km-long laterofrontal moraine; the main moraine ridge (M_{B2b}) is >15 m thick above the glacier bed, >150 m thick above Tapovan, and >200 m thick above the M_{B3} and M_{B4} moraines; has steep slopes (>30°) and sharp ridges; no vegetation, except sporadic distribution of grasses and shrubs; massive sandy matrix supported by pebbly/boulder diamicton.	Lithology: Tourmaline granite; angular to subangular freshly fractured boulders; limited rock varnish and moderate lichen cover; large (~1–6 m high), flat-topped, cubic-shaped boulders were sampled from the moraine crest; little to no sign of weathering; moderate to well inset to well balanced.

Table 3. Holocene moraine [10]Be sample details, concentrations and apparent ages (in ka before AD 2017, ±1σ) for the Bhagirathi catchment in the Garhwal Himalaya.

Moraine morpho-stratigraphy	Sample ID	Latitude (DD N)	Longitude (DD E)	Elevation (m a.s.l.)	Boulder size (L x W x H) (cm)	Sample thickness (cm)	Shielding correction	[10]Be/[9]Be ± 1σ (10^{-15})	[[10]Be] ± 1σ (10[4] atoms g[-1])	LSD Age ± 1σ (ka)[i]	Lm Age ± 1σ (ka)[j]
Sudarshan stage											
M_{B7}	BH35B[a]	30.9500	79.0600	4093	-	5.0	0.970	-	94.00±2.80	20.82±1.01	20.34±0.96
M_{B7}	BH36[a]	30.9500	79.0600	4112	-	5.0	0.970	-	69.50±1.90	15.83±0.88	15.30±0.74
M_{B7}	BH37[ac]	30.9500	79.0600	4098	-	5.0	0.970	-	51.30±1.50	12.15±0.76	11.63±0.58
Kedar stage											

207

Group	Sample	Lat	Long	Elev	Dimensions						
M_{B6}	BH19[a]	30.9400	78.9500	4323	-	5.0	0.970	-	49.30±1.20	8.59±0.48	9.06±0.63
M_{B6}	BH20[a]	30.9400	78.9500	4242	-	5.0	0.970	-	43.80±1.00	7.96±0.4	8.31±0.52

Shivling stage

Group	Sample	Lat	Long	Elev	Dimensions						
M_{B5}	Milap4[b]	30.9964	78.9308	3029	-	5.0	0.918	62.24±3.51	10.70±0.38[g]	5.48±0.28	5.04±0.28
M_{B5}	Milap5[b]	30.9971	78.9274	3012	-	5.0	0.907	37.91±2.53	9.66±0.31[g]	5.13±0.29	4.68±0.29
M_{B5}	Milap8[b]	30.9971	78.9311	3021	-	2.0	0.899	103.83±7.19	10.68±0.61[g]	5.48±0.35	5.04±0.35
M_{B5}	Milap10[b]	30.9968	78.9289	3017	-	2.0	0.911	59.44±4.71	10.50±0.62[g]	5.35±0.35	4.89±0.35
M_{B5}	Milap11[b]	30.9967	78.9284	3022	-	2.0	0.907	91.46±6.33	10.44±0.58[g]	5.33±0.35	4.89±0.35
M_{B5}	Milap12[b]	30.9968	78.9277	3017	-	2.0	0.905	98.63±5.62	9.68±0.43[h]	5.02±0.32	4.57±0.32
M_{B5}	Milap13[b]	30.9969	78.9272	3039	-	2.0	0.907	52.36±4.42	9.25±0.57[g]	4.76±0.36	4.33±0.36

Gangotri stage

Group	Sample	Lat	Long	Elev	Dimensions						
M_{B4}	Milap2[b]	30.7633	79.0775	4343	-	5.0	0.980	93.27±4.09	9.83±0.29[h]	2.41±0.18	2.22±0.14
M_{B4}	Milap3[b]	30.9129	79.0783	4335	-	5.0	0.980	84.55±4.04	7.98±0.26[h]	1.91±0.13	1.80±0.11
M_{B4}	Milap7[b]	30.9454	79.0600	3935	-	2.0	0.949	13.45±1.80	1.69±0.07[g]	0.47±0.04	0.44±0.03

Bhujbasa stage

Group	Sample	Lat	Long	Elev	Dimensions						
M_{B3}	BH26[a]	30.9400	79.0600	3917	-	5.0	0.97	-	5.80±0.30	1.70±0.14	1.58±0.11
M_{B3}	BH27[a]	30.9400	79.0600	3918	-	5.0	0.97	-	10.20±0.40	3.10±0.21	2.86±0.18
M_{B3}	BH29[a]	30.9400	79.0600	3973	-	5.0	0.97	-	3.30±0.90	0.71±0.20	0.75±0.21
M_{B3}	BH30[ae]	30.9400	79.0600	3956	-	5.0	0.97	-	1.60±0.70	0.34±0.16	0.37±0.16
M_{B3}	BH31[ae]	30.9400	79.0600	3973	-	5.0	0.97	-	1.20±0.70	0.26±0.16	0.24±0.15
M_{B3}	BH32[a]	30.9400	79.0600	3956	-	5.0	0.97	-	4.60±0.70	1.01±0.17	1.07±0.19
M_{B3}	Gang1	30.9149	79.0780	4294	400x260x260	1.5	0.963	13.05±1.05	2.57±0.15[d]	0.59±0.05	0.56±0.05
M_{B3}	Gang2	30.9140	79.0785	4328	240x160x95	3.0	0.960	39.62±1.64	5.17±0.17[d]	1.21±0.08	1.14±0.08
M_{B3}	Gang3	30.9139	79.0786	4327	300x270x140	2.5	0.960	13.59±1.52	2.05±0.16[e]	0.46±0.05	0.43±0.05
M_{B3}	Gang4	30.9116	79.0797	4337	500x300x300	1.0	0.964	26.95±1.43	3.90±0.13[e]	0.89±0.06	0.83±0.06
M_{B3}	Gang5[c]	30.9140	79.0785	4329	135x120x100	3.0	0.960	41.53±1.57	13.29±0.43[f]	3.31±0.21	3.09±0.21

Meru stage

Group	Sample	Lat	Long	Elev	Dimensions						
M_{B2}	Gang6	30.9114	79.0699	4519	350x295x170	3.0	0.958	2.32±0.47	0.63±0.08[f]	0.12±0.02	0.11±0.02
M_{B2}	Gang7	30.9078	79.0675	4569	200x160x220	3.0	0.916	14.29±1.24	1.79±0.10[e]	0.38±0.03	0.35±0.03
M_{B2}	Gang8	30.9058	79.0656	4598	500x500x600	2.5	0.910	18.16±1.37	2.21±0.11[e]	0.45±0.04	0.43±0.04
M_{B2}	Gang9	30.9045	79.0643	4614	300x100x110	2	0.909	6.12±1.23	1.49±0.30[d]	0.30±0.06	0.29±0.06

Gaumukh resessional stage

Group	Sample	Lat	Long	Elev	Dimensions						
M_{B1c}	Milap1[b]	30.9395	79.0635	3908	-	5	0.947	10.59±1.98	0.71±0.05[h]	0.21±0.02	0.19±0.02
M_{B1c}	Gang15	30.9394	79.0651	3914	470x370x260	2.0	0.936	5.92±0.70	0.94±0.07[d]	0.26±0.03	0.24±0.03
M_{B1c}	Gang16	30.9393	79.0650	3915	250x170x170	2.0	0.936	2.87±0.71	0.65±0.23[d]	0.18±0.07	0.17±0.07
M_{B1c}	Gang17	30.9391	79.0645	3912	240x200x120	2.0	0.952	7.30±0.72	0.76±0.02[e]	0.21±0.02	0.20±0.02
M_{B1c}	Gang18[c]	30.9390	79.0644	3911	230x170x85	2.0	0.948	67.91±2.10	14.86±0.41[f]	4.51±0.26	4.18±0.26
M_{B1c}	Gang19	30.9390	79.0644	3911	240x190x65	2.5	0.952	11.56±0.91	1.22±0.04[e]	0.34±0.03	0.32±0.03
M_{B1a}	Gang10	30.9355	79.0711	3932	210x140x90	1.0	0.918	7.90±0.87	0.79±0.04[e]	0.22±0.02	0.21±0.02

M_{B1a}	Gang12	30.9362	79.0702	3932	180x100x125	1.0	0.919	5.57±0.59	0.77±0.01[e]	0.22±0.01	0.20±0.01
M_{B1a}	Gang13	30.9363	79.0697	3924	390x260x190	2.0	0.935	5.27±0.55	0.85±0.05[f]	0.24±0.02	0.22±0.02
M_{B1a}	Gang14	30.9363	79.0691	3927	580x550x350	3.0	0.937	3.22±0.44	0.93±0.07[f]	0.26±0.03	0.24±0.03

Note: Density value of 2.7 g cm^{-3}, erosion rate of 0.00 cm a-1, and AMS standard of 07KNSTD were used for all samples, except BH samples (LLNL3000), to calculate apparent surface exposure ages

[a] Data from Barnard et al. (2004a)

[b] Data from Srivastava (2012)

[c] Outliers removed

[d] Ratios are corrected from background ^{10}Be: 1.51±0.41 and 2.49±0.39 (^{10}Be/^{9}Be ± 1σ (10^{-15}))

[e] Ratios are corrected from background ^{10}Be: 1.37±0.68 and 1.04±0.39 (^{10}Be/^{9}Be ± 1σ (10^{-15}))

[f] Ratios are corrected from background ^{10}Be: 0.87±0.29 and 0.64±0.24 (^{10}Be/^{9}Be ± 1σ (10^{-15}))

[g] Ratios are corrected from background ^{10}Be: 2.39±1.01 (^{10}Be/^{9}Be ± 1σ (10^{-15}))

[h] Ratios are corrected from background ^{10}Be: 4.33±2.18 and 3.10±1.03 (^{10}Be/^{9}Be ± 1σ (10^{-15}))

[i] Lifton-Sato-Dunai (LSD) scaling model using CREp online calculator

[j] Lal and Stone time-dependent (Lm) scaling model using CREp online calculator

[-] No data available

Table 4. A summary of ELAs and ΔELAs in the Garhwal Himalaya.

Glacial Stage	Mean moraine age (ka)	Glacier area (~km²)	Mean slope (~°)	Mean Aspect	Head (m asl)	Toe (m asl)	MELM (m asl)	Area-Altitude AA (m asl)	Area-Accumulation ratio AAR 0.45	AAR 0.55	AAR 0.65	Toe-Headwall altitude ratio THAR 0.40	Mean ELA (m asl)	ΔELA (m)
Gangotri glacier														
Present	-	102.2	14	NW	7003	4017	4900	5151	5149	5000	4879	5145	5049±143	-
M_{B3}	~1.7–0.5	115.1	15	NW	7004	3874	-	5132	5130	4990	4859	5131	5050±124	16±4
M_{B4}	~2.4–1.9	116.1	15	NW	7004	3792	-	5122	5129	4989	4859	5083	5036±114	28±20
M_{B5}	5.22±0.27	125.8	16	NW, WNW	7010	2980	-	4998	5079	4939	4789	4596	4880±191	185±207
M_{B6}	~20.1–15.9	141.3	18	NW, WNW	7010	2766	-	4840	4989	4839	4699	4469	4767±196	298±221
M_{B7}	~63.0	165.0	20	NW, WNW, SW	7010	2416	-	4538	4869	4709	4409	4259	4557±240	508±252
Meru Bamak														
Present	-	4.7	20	NE	5940	4462	4772	5107	5169	5049	4979	5061	5023±138	-
M_{B2}	~0.5–0.1	5.6	20	NE	5940	4137	-	5007	5059	4969	4779	4862	4935±113	138±57
Kedar Bamak														
Present	-	18.5	20	ENE	6429	4581	4920	5234	5260	5089	4979	5329	5135±165	-
Kedar glacial stage	~8.6–8.0	22.0	19	ENE, NE	6429	4218	-	5139	5119	4989	4909	5107	5053±99	126±60

Note: The present here refers to year AD 2017
m asl is a meter above sea level

Table 5. A summary of ^{10}Be concentrations, inherited ^{10}Be concentrations, and equivalent ages.

Sample	Independent age (ka)[a]	Measured concentration±1σ (10⁴ at/g/SiO₂)	Inherited concentration±1σ (10⁴ at/g/SiO₂)	Equivalent age (ka)
Moraine M$_{B1c}$[†]	0.24	~0.7–14.9 (or ~0.7–1.2)[b]	0–14.2 (or 0–0.13)[b]	~0-4.5 (or ~0–0.13)[b]
Moraine M$_{B1a}$[†]	0.08	~0.8–0.9	~0.4–0.6	~0–0.05
Supraglacial sediments[§]	-	~1.1–2.7	-	~0.2–0.6
Supraglacial sediments[#] (max exposure)	-	~1.8–2.9	-	~0.4–0.7
Proglacial sediments[*]		~3.9	-	~1.1
Proglacial sediments[#] (max exposure)	-	~4–7	-	~0.5–0.7

[†] ^{10}Be measured (this study)

[§] ^{10}Be recalculated from Orr et al. in prep.

[#] ^{10}Be estimated assuming ^{10}Be production rate of ~95.4±12.2 at/g/a/ (Orr et al., in prep.) and average glacier velocity of ~48±4.8 m/a (Bhattacharya et al., 2016)

[*] ^{10}Be recalculated from Barnard et al., 2004a

[a] Historical age

[b] Sample outlier Gang18 removed

Table 6 Geomorphic process uncertainties in glacial settings yielding too-old (inherited) ^{10}Be concentrations.

Geomorphic systems	Geomorphic processes	Max inherited concentration (10⁴ at/g)[ab]	Max inherited age (ka)[ab]
Inheritance during the non-glacier system			
Bedrock slopes (before detachment)	Periglacial weathering processes (e.g., frost cracking, freeze-thaw, & ice wedging) supply large volumes of rockfall & avalanche debris, sediments	~0.9–4.0	0.1—0.5
Sediment storage (e.g., debris and talus fans separated by ablation valleys, rock glaciers); erosion & reworking of older moraines/deposits	Sediment storage & remobilization is largely affected when sediments, clasts, & boulders are stored in the system for a longer duration before incorporating into the (latest) glacier system	>4.0 (even >15 is possible)	>0.5
Inheritance during the glacier system			
Supraglacial transportation in the ablation zone	Transport the rockfall & avalanche debris & sediments supraglacial along the medial moraines; inheritance *en route*	~1.8–7.0	~0.2—0.7
Incorporation into the englacial & subglacial system after detached from bedrock	Rockfall & avalanche debris & sediments are delivered to en- & subglacial zones via crevasses, moulins, meltwater channels, & collapsed ponds	~0.9–4.0	0.1—0.5
Basal erosion (e.g., abrasion, quarrying) & transported through the supraglacial zone (*en route*)	Subglacial erosion by abrasion, quarrying, & attrition generate sediments and boulders; transport them to supraglacial zone; ultimately deliver them via supraglacial processes; inheritance *en route*	~1.8–7.0	~0.2—0.7
Basal erosion & transported through en- & subglacial zones	Subglacial erosion by abrasion, quarrying, & attrition generate sediments & boulders; deliver them via subglacial channel conduits &/or by basal stick-slip motion, or englacially; not exposed to cosmic rays	~0	~0

[a] Estimated using erosion rates (e=) of 2—5 mm/a (calculated for 1 m thick boulder) & ^{10}Be production rate of ~95.4±12.2 at/g/a (Orr et al. in prep.); Glacier flow velocity ~48±4.8 m/a (Bhattacharya et al., 2011).

[b] Length of the ablation zone is ~26 km; slope 45°—60°; strike 30°—300°; shielding factor 0.6—0.8.

Note: No adjustments were made to changes in climate and glacier dynamics while calculating inherited concentrations.

Appendix A3. Supplementary data

REFERENCE CITED

Aggarwal, NC, Kumar, G. 1973. Geology of the upper Bhagirathi and Yamuna Valleys, Uttarkashi District, Kumaun Himalaya. Himalayan Geology 3: 1–23.

Ahmad, S. Hasnain, SI. 2004. Analysis of satellite imageries for characterization of glacio-morphological features of the Gangotri Glacier, Ganga headwater, Garhwal Himalayas. In Srivastava, D., et al., eds., Geological Survey of India, Spl. Pub. No. 80: 61–67.

Anders A, Roe G. 2006. Spatial patterns of precipitation and topography in the Himalaya. Special Papers-2398: 39–53.

Anderson LS, Roe GH, Anderson RS. 2014. The effects of interannual climate variability on the moraine record. Geology 42: 55–58.

Anderson SP. 2005. Glaciers show direct linkage between erosion rate and chemical weathering fluxes. Geomorphology 67: 147–157.

Andrews, JT. 1975. Glacial Systems. Duxbury, North Scituate, Massachusetts: p. 191.

Applegate PJ, Alley RB. 2011. Challenges in the Use of Cosmogenic Exposure Dating of Moraine Boulders to Trace the Geographic Extents of Abrupt Climate Changes: The Younger Dryas Example: 111–122.

Applegate PJ, Urban NM, Keller K, Lowell T V., Laabs BJC, Kelly M a., Alley RB. 2012. Improved moraine age interpretations through explicit matching of geomorphic process models to cosmogenic nuclide measurements from single landforms. Quaternary Research 77: 293–304.

Applegate PJ, Urban NM, Laabs BJC, Keller K, Alley RB. 2010. Modeling the statistical distributions of cosmogenic exposure dates from moraines. Geoscientific Model Development 3: 293–307.

Auden, JB. 1937. The snout of the Gangotri glacier, Tehri Garhwal. Records of the Geological Survey of India, 72 (II): p. 135–140.

Awasthi, DD, Bali, R, Tewari, NK. 2004. Growth rate of lichen Dimelaena oreina in the Gangotri glacier valley, Uttarkashi District, Uttaranchal: Some significant observations. In Srivastava, D., et al., eds., Geological Survey of India, Spl. Pub. No. 80: 161–165.

Balco G, Stone JO, Lifton N a., Dunai TJ. 2008. A complete and easily accessible means of calculating surface exposure ages or erosion rates from ^{10}Be and ^{26}Al measurements. Quaternary Geochronology 3: 174–195.

Balco G, Stone JOH, Porter SC, Caffee MW. 2002. Cosmogenic-nuclide ages for New England coastal moraines, Martha's Vineyard and Cape Cod, Massachusetts, USA. Quaternary Science Reviews 21: 2127–2135.

Balco G. 2011. Contributions and unrealized potential contributions of cosmogenic-nuclide exposure dating to glacier chronology, 1990–2010. Quaternary Science Reviews 30: 3–27.

Bali R, Awasthi DD, Tiwari NK. 2003. Neotectonic control on the geomorphic evolution of the Gangotri Glacier Valley, Garhwal Himalaya. Gondwana Research 6: 829–838.

Ballantyne CK. 2002a. Paraglacial geomorphology. Quaternary Science Reviews 21: 1935–2017.

Ballantyne CK. 2002b. The Loch Lomond Readvance on the Isle of Mull, Scotland: glacier reconstruction and palaeoclimatic implications. 17: 759–771.

Barnard PL, Owen L a., Finkel RC, Asahi K. 2006. Landscape response to deglaciation in a high relief, monsoon-influenced alpine environment, Langtang Himal, Nepal. Quaternary Science Reviews 25: 2162–2176.

Barnard PL, Owen LA, Finkel RC. 2004a. Style and timing of glacial and paraglacial sedimentation in a monsoon-influenced high Himalayan environment, the upper Bhagirathi Valley, Garhwal Himalaya. Sedimentary Geology 165: 199–221.

Barnard PL, Owen LA, Sharma MC, Finkela RC. 2001. Natural and human-induced landsliding in the Garhwal Himalaya of Northern India. Geomorphology 40: 21–35.

Barr ID, Lovell H. 2014. A review of topographic controls on moraine distribution. Geomorphology 226: 44–64.

Barros, AP, Chiao, S, Lang, TJ, Burbank, D, Putkonen, J. 2006. From weather to climate-seasonal and interannual variability of storms and implications for erosion processes in the Himalaya: Special Papers-Geological Society of America, 398: p. 17.

Bassi, UK, 2004. Geology of the Gangotri-Gaumukh area, Uttarkashi District, Uttaranchal. In Srivastava, D., et al., eds. Geological Survey of India, Spl. Pub. No. 80: 235–239.

Benn DI, Bolch T, Hands K, Gulley J, Luckman A, Nicholson LI, Quincey D, Thompson S, Toumi R, Wiseman S. 2012. Response of debris-covered glaciers in the Mount Everest region to recent warming, and implications for outburst flood hazards. Earth-Science Reviews 114: 156–174.

Benn DI, Owen LA, Osmaston HA, Seltzer GO, Porter SC, Mark B. 2005. Reconstruction of equilibrium-line altitudes for tropical and sub-tropical glaciers. Quaternary International 138–139: 8–21.

Benn, D, Evans, DJ, 2010. Glaciers and glaciation, 2 eds. Routledge. p. 817.

Bernhardt M, Schulz K. 2010. SnowSlide: A simple routine for calculating gravitational snow transport. Geophysical Research Letters 37: 1–6.

Bhambri R, Bolch T, Chaujar RK, Kulshreshtha SC. 2011. Glacier changes in the Garhwal Himalaya, India, from 1968 to 2006 based on remote sensing. Journal of Glaciology 57: 543–556.

Bhambri R, Bolch T, Chaujar RK. 2012. Frontal recession of Gangotri Glacier, Garhwal Himalayas, from 1965–2006, measured through high resolution remote sensing data. Current Science 102: 489–494.

Bhattacharya A, Bolch T, Mukherjee K, Pieczonka T, Kropáček J, Buchroithner MF. 2016. Overall recession and mass budget of Gangotri Glacier, Garhwal Himalayas, from 1965 to 2015 using remote sensing data. Journal of Glaciology 62: 1115–1133.

Bjornson J, Lauriol B. 2001. Microgelivation versus macrogelivation: Towards bridging the gap between laboratory and field frost weathering. Permafrost and Periglacial Processes 12: 299–313.

Bookhagen B, Burbank DW. 2006. Topography, relief, and TRMM-derived rainfall variations along the Himalaya. Geophysical Research Letters 33: L08405.

Bookhagen B, Thiede RC, Strecker MR. 2005. Late Quaternary intensified monsoon phases control landscape evolution in the northwest Himalaya. Geology 33: 149.

Borchers B, Marrero S, Balco G, Caffee M, Goehring B, Lifton N, Nishiizumi K, Phillips F, Schaefer J, Stone J. 2016. Geological calibration of spallation production rates in the CRONUS-Earth project. Quaternary Geochronology 31: 188–198.

Braucher R, Brown ET, Bourlès DL, Colin F. 2003. In situ produced ^{10}Be measurements at great depths: Implications for production rates by fast muons. Earth and Planetary Science Letters 211: 251–258.

Briner J, Gosse J, Bierman P. 2006. Applications of cosmogenic nuclides to Laurentide Ice Sheet history and dynamics. Geological Society of America 2415: 29–41.

Briner JP, Kaufman DS, Manley WF, Finkel RC, Caffee MW. 2005. Cosmogenic exposure dating of late Pleistocene moraine stabilization in Cosmogenic exposure dating of late Pleistocene moraine stabilization in Alaska: 1108–1120.

Brown ET, Stallard RF, Larsen MC, Raisbeck GM, Yiou F. 1995. Denudation rates determined from the accumulation of in situ-produced ^{10}Be in the luquillo experimental forest, Puerto Rico. Earth and Planetary Science Letters 129: 193–202.

Burbank DW, Blythe A E, Putkonen J, Pratt-Sitaula B, Gabet E, Oskin M, Barros A, Ojha TP. 2003. Decoupling of erosion and precipitation in the Himalayas. Nature 426: 652–655.

Carson, MA. Kirkby, MJ. 1972. Hillslope form and process.

Chaujar, RK, Mazari, RK, Gergan, JT. 1993. Glacial geomorphology of the Gaumukh–the source of Ganga, with reference to its present state of environment. In Proceedings of Seminar on Ganga in the Service of the Nation, 12–13. Rorkee, University of Rorkee: 1–14.

Church M, Slaymaker O. 1989. Disequilibrium of Holocene sediment yield in glaciated British Columbia. Nature: 452–454.

Çiner A, Sarıkaya MA, Yıldırım C. 2017. Misleading old age on a young landform? The dilemma of cosmogenic inheritance in surface exposure dating: Moraines vs. rock glaciers. Quaternary Geochronology 42: 76–88.

Corbett LB, Bierman PR, Rood DH. 2016. An approach for optimizing in situ cosmogenic [10]Be sample preparation. Quaternary Geochronology 33: 24–34.

Dahl SO, Nesje A. 1992. Paleoclimatic implications based on equilibrium-line altitude depressions of reconstructed Younger Dryas and Holocene cirque glaciers in inner Nordfjord, western Norway. Palaeogeography, Palaeoclimatology, Palaeoecology 94: 87–97.

Dortch JM, Dietsch C, Owen LA, Caffee MW, Ruppert K. 2011. Episodic fluvial incision of rivers and rock uplift in the Himalaya and Transhimalaya. Journal of the Geological Society 168: 783–804.

Dortch JM, Owen LA, Caffee MW. 2013. Timing and climatic drivers for glaciation across semi-arid western Himalayan–Tibetan orogen. Quaternary Science Reviews 78: 188–208.

Dortch JM, Owen LA, Haneberg WC, Caffee MW, Dietsch C, Kamp U. 2009. Nature and timing of large landslides in the Himalaya and Transhimalaya of northern India. 28: 1037–1054.

Dühnforth M, Anderson RS, Ward D, Stock GM. 2010. Bedrock fracture control of glacial erosion processes and rates. Geology 38: 423–426.

Dunai TJ. 2010. Cosmogenic Nuclides: Principles, Concepts and Applications in the Earth Surface Sciences. Cambridge University Press, Cambridge.

Dutta, SS, Sangewar, CV, Shukla, SP, Chitranshi, A, Puri, VMK, Hampaiah, P. 2004. Some observation on physiography and geomorphology of Gangotri glacier area, Bhagirathi basin, Uttaranchal. Geological Survey of India Special Publication, 80: 69–78.

Eppes MC, Keanini R. 2017. Mechanical weathering and rock erosion by climate-dependent subcritical cracking. Reviews of Geophysics 55: 470–508.

Eppes MC, McFadden L. 2008. The influence of bedrock weathering on the response of drainage basins and associated alluvial fans to Holocene climates, San Bernardino Mountains, California, USA. Holocene 18: 895–905.

Evans DJA, Phillips ER, Hiemstra JF, Auton CA. 2006. Subglacial till: Formation, sedimentary characteristics and classification. Earth-Science Reviews 78: 115–176.

Fabel D, Harbor J. 1999. The use of in-situ produced cosmogenic radionuclides in glaciology and glacial geomorphology. Annals of Glaciology 28: 103–110.

Fabel D, Stroeven AP, Harbor J, Kleman J, Elmore D, Fink D. 2002. Landscape preservation under fennoscandian ice sheets determined from in situ produced [10]Be and [26]Al. Earth and Planetary Science Letters 201: 397–406.

Finkel RC, Owen L a., Barnard PL, Caffee MW. 2003. Beryllium-10 dating of Mount Everest moraines indicates a strong monsoon influence and glacial synchroneity throughout the Himalaya. Geology 31: 561–564.

Finlayson DP, Montgomery DR, Hallet B. 2002. Spatial coincidence of rapid inferred erosion with young metamorphic massifs in the Himalayas. Geology 30: 219–222.

Fischer L, Amann F, Moore JR, Huggel C. 2010. Assessment of periglacial slope stability for the 1988 Tschierva rock avalanche (Piz Morteratsch, Switzerland). Engineering Geology 116: 32–43.

Fischer L, Purves RS, Huggel C, Noetzli J, Haeberli W. 2012. On the influence of topographic, geological and cryospheric factors on rock avalanches and rockfalls in high-mountain areas. Natural Hazards and Earth System Science 12: 241–254.

Foster D, Brocklehurst SH, Gawthorpe RL. 2010. Glacial-topographic interactions in the Teton Range, Wyoming. Journal of Geophysical Research 115: F01007.

Gabet EJ, Burbank DW, Putkonen JK, Pratt-Sitaula BA, Ojha T. 2004. Rainfall thresholds for landsliding in the Himalayas of Nepal. Geomorphology 63: 131–143.

Gantayat P, Kulkarni A V., Srinivasan J. 2014. Estimation of ice thickness using surface velocities and slope: Case study at Gangotri Glacier, India. Journal of Glaciology 60: 277–282.

Gibson MJ, Glasser NF, Quincey DJ, Mayer C, Rowan A V., Irvine-Fynn TDL. 2017. Temporal variations in supraglacial debris distribution on Baltoro Glacier, Karakoram between 2001 and 2012. Geomorphology 295: 572–585.

Gosse JC, Phillips FM. 2001. Terrestrial in situ cosmogenic nuclides:theory and application. Quaternary Science Reviews 20: 1475–1560.

Gosse, JC. 2005. The contributions of cosmogenic nuclides to unraveling alpine paleo-glacier histories, in Huber, U.M.., et al., eds., Global Change and Mountain Regions. An Overview of Current Knowledge: Advances in Global Change Research, vol. 23. Springer, Dordrecht: 39–50.

Gruber S, Haeberli W. 2007. Permafrost in steep bedrock slopes and its temperatures-related destabilization following climate change. Journal of Geophysical Research: Earth Surface 112: 1–10.

Hales TC, Roering JJ. 2005. Climate-controlled variations in scree production, Southern Alps, New Zealand. Geology 33: 701–704.

Hales TC, Roering JJ. 2007. Climatic controls on frost cracking and implications for the evolution of bedrock landscapes. Journal of Geophysical Research: Earth Surface 112: 1–14.

Hallet B, Putkonen J. 1994. Surface dating of dynamic landforms: Young boulders on aging moraines. Science (New York, N.Y.) 265: 937–940.

Haritashya UK, Kumar A, Singh P. 2010. Geomorphology Particle size characteristics of suspended sediment transported in meltwater from the Gangotri Glacier, central Himalaya — An indicator of subglacial sediment evacuation. Geomorphology 122: 140–152.

Haritashya UK, Singh P, Kumar N, Gupta RP. 2006. Suspended sediment from the Gangotri Glacier: Quantification, variability and associations with discharge and air temperature. Journal of Hydrology 321: 116–130.

Hedrick KA, Seong YB, Owen LA, Caffee MW, Dietsch C. 2011. Towards defining the transition in style and timing of Quaternary glaciation between the monsoon-influenced Greater Himalaya and the semi-arid Transhimalaya of Northern India. Quaternary International 236: 21–33.

Heimsath AM, McGlynn R. 2008. Quantifying periglacial erosion in the Nepal high Himalaya. Geomorphology 97: 5–23.

Heyman J, Applegate PJ, Blomdin R, Gribenski N, Harbor JM, Stroeven AP. 2016. Boulder height - exposure age relationships from a global glacial [10]Be compilation. Quaternary Geochronology 34: 1–11.

Heyman J, Stroeven AP, Harbor JM, Caffee MW. 2011. Too young or too old: Evaluating cosmogenic exposure dating based on an analysis of compiled boulder exposure ages. Earth and Planetary Science Letters 302: 71–80.

Heyman J. 2014. Paleoglaciation of the Tibetan plateau and surrounding mountains based on exposure ages and ELA depression estimates. Quaternary Science Reviews 91: 30–41.

Hodgson. 1822. Journey of a survey to the heads of the rivers, Ganges and Jamna in the year 1817. Asiatic Research, 14: 60–152.

Hughes PD, Gibbard PL, Woodward J. 2005. Quaternary glacial records in mountain regions: A formal stratigraphical approach Quaternary glacial records in mountain regions: A formal stratigraphical approach. Episodes 28: 85–92.

Hughes PD. 2010. Geomorphology and Quaternary stratigraphy: The roles of morpho-, litho-, and allostratigraphy. Geomorphology 123: 189–199.

Humphreys GS, Wilkinson MT. 2007. The soil production function: A brief history and its rediscovery. Geoderma 139: 73–78.

IMD (Indian Meteorological Department). 1989. Climate of Uttar Pradesh. Government of India Publication: 372–375.

Ivy-Ochs S, Kerschner H, Schlüchter C. 2007. Cosmogenic nuclides and the dating of Lateglacial and Early Holocene glacier variations: The Alpine perspective. Quaternary International 164–165: 53–63.

Ivy-Ochs S, Kerschner H, Schlüchter C. 2007. Cosmogenic nuclides and the dating of Lateglacial and Early Holocene glacier variations: The Alpine perspective. Quaternary International 164–165: 53–63.

Kaplan, MR, Schaefer, JM, Denton, GH, Doughty, AM, Barrell, DJA, Chinn, TJH, Putnam, AE, Andersen, BG, Mackintosh, A, Finkel, RC, Schwartz, R, Anderson, B. 2013. The anatomy of long-term warming since 15 ka in New Zealand based on net glacier snowline rise. Geology 41: 887–890.

Kohl CP, Nishiizumi K. 1992. Chemical isolation of quartz for measurement of in-situ-produced cosmogenic nuclides. Geochimica et Cosmochimica Acta 56: 3583–3587.

Lal D. 1991. Cosmic ray labeling of erosion surfaces: in situ nuclide production rates and erosion models. Earth and Planetary Science Letters 104: 424–439.

Li Y, Li Y, Harbor J, Liu G, Yi C, Caffee MW. 2016. Cosmogenic [10]Be constraints on Little Ice Age glacial advances in the eastern Tian Shan, China. Quaternary Science Reviews 138: 105–118.

Lifton N a., Bieber JW, Clem JM, Duldig ML, Evenson P, Humble JE, Pyle R. 2005. Addressing solar modulation and long-term uncertainties in scaling secondary cosmic rays for in situ cosmogenic nuclide applications. Earth and Planetary Science Letters 239: 140–161.

Lifton N. 2016. Implications of two Holocene time-dependent geomagnetic models for cosmogenic nuclide production rate scaling. Earth and Planetary Science Letters 433: 257–268.

Lifton NA, Smart DF, Shea MA. 2008. Scaling time-integrated in situ cosmogenic nuclide production rates using a continuous geomagnetic model. Earth and Planetary Science Letters 268: 190–201.

Lifton, N., Beel, C., Hättestrand, C., Kassab, C., Rogozhina, I., Heermance, R., Oskin, M., Burbank, D., Blomdin, R., Gribenski, N., Caffee, M., Goehring, B.M., Heyman, J., Ivanov, M. 2014. Constraints on the late Quaternary glacial history of the Inylchek and Sary-Dzaz valleys from in situ cosmogenic [10]Be and [26]Al, eastern Kyrgyz Tian Shan. Quaternary Science Reviews 101: 77–90.

Luckman, BH. 1977. The geomorphic activity of snow avalanches. Geografiska Annaler. Series A, Physical Geography, 59(1-2): 31–48.

Marrero SM, Phillips FM, Borchers B, Lifton N, Aumer R, Balco G. 2016. Cosmogenic nuclide systematics and the CRONUScalc program. Quaternary Geochronology 31: 160–187.

Martin LCP, Blard PH, Balco G, Lavé J, Delunel R, Lifton N, Laurent V. 2017. The CREp program and the ICE-D production rate calibration database: A fully parameterizable and updated online tool to compute cosmic-ray exposure ages. Quaternary Geochronology 38: 25–49.

Matsuoka, N, Murton, J. 2008. Frost weathering: recent advances and future directions. Permafrost and Periglacial Processes, 19(2): 195–210.

Mehta M, Majeed Z, Dobhal DP, Srivastava P. 2012. Geomorphological evidences of post LGM glacial advancements in the Himalaya: study from Chorabari Glacier, Garhwal Himalaya, India: 149–163.

Metcalfe, RP. 1993. Pressure, temperature and time constraints on metamorphism across the Main Central Thrust zone and High Himalayan slab in the Garhwal Himalaya, in Himalayan Tectonics, edited by Treloar, P.J., and, Searle, MP. Geol. Soc. Spec. Publ., 74: 485–509.

Montgomery DR. 2002. Valley formation by fluvial and glacial erosion. Geology 30: 1047–1050.

Moore RD, Fleming SW, Menounos B, Wheate R, Fountain A, Stahl K, Holm K, Jakob M. 2009. Glacier change in western North America: influences on hydrology, geomorphic hazards and water quality. HYDROLOGICAL PROCESSES 23: 42–61.

Moores JE, Pelletier JD, Smith PH. 2008. Crack propagation by differential insolation on desert surface clasts. Geomorphology 102: 472–481.

Murari MK, Owen LA, Dortch JM, Caffee MW, Dietsch C, Fuchs M, Haneberg WC, Sharma MC, Townsend-Small A. 2014. Timing and climatic drivers for glaciation across monsoon-influenced regions of the Himalayan–Tibetan orogen. Quaternary Science Reviews 88: 159–182.

Murton, JB, Peterson, R, Ozouf, JC. 2006. Bedrock fracture by ice segregation in cold regions. Science, 314 (5802): 1127–1129.

Nagai H, Fujita K, Nuimura T, Sakai A. 2013. Southwest-facing slopes control the formation of debris-covered glaciers in the Bhutan Himalaya. Cryosphere 7: 1303–1314.

Nainwal HC, Negi BDS, Chaudhary M. 2008. Temporal changes in rate of recession: Evidences from Satopanth and Bhagirath Kharak glaciers, Uttarakhand, using Total Station Survey. Research Communications 94: 653–660.

Naithani AK, Nainwal HC, Sati KK, Prasad C. 2001. Geomorphological evidences of retreat of the Gangotri glacier and its characteristics. Current Science 80: 87–94.

Nishiizumi K, Imamura M, Caffee MW, Southon JR, Finkel RC, Mcaninch J. 2007. Be AMS standards. 258: 403–413.

Nishiizumi, K, Finkel, RC, Caffee, MW, Southon, JR, Kohl, CP, Arnold, JR, Olinger, CT, Poths, J, Klein, J. 1994. Cosmogenic Production of [10]Be and [26]Al on the Surface of the Earth and Underground, in Eighth International Conference on Geochronology, Cosmochronology and Isotope Geochemistry. U.S. Geol. Surv. Circular 1107, Berkeley, California: p. 234.

O'Hara SL, Briner JP, Kelley SE. 2017. A [10]Be chronology of early Holocene local glacier moraines in central West Greenland. Boreas 46: 655–666.

Orr EN, Owen LA, Murari MK, Saha S, Caffee MW. 2017. Geomorphology The timing and extent of Quaternary glaciation of Stok, northern Zanskar. Geomorphology 284: 142–155.

Orr EN, Owen LA, Saha S, Caffee MW, Murari MK. 2018. Quaternary glaciation of the Lato Massif, Zanskar Range of the NW Himalaya. Quaternary Science Reviews 183: 140–156.

Orr, EN, Owen, LA, Saha S, Caffee, MW. *in prep*. Rates of bedrock slope erosion of the upper Bhagirathi catchment, Garhwal, northern India. Earth and Planetary Sciences.

Osmaston H. 2005. Estimates of glacier equilibrium line altitudes by the Area ?? Altitude, the Area ?? Altitude Balance Ratio and the Area ?? Altitude Balance Index methods and their validation. Quaternary International 138–139: 22–31.

Ouimet WB, Whipple KX, Granger DE. 2009. Beyond threshold hillslopes: Channel adjustment to base-level fall in tectonically active mountain ranges. Geology 37: 579–582.

Owen LA, Bailey RM, Rhodes EJ, Holloway R. 1997. Style and timing of glaciation in the Lahul Himalaya, northern India: a framework for reconstructing late Quaternary palaeoclimatic change in the western Himalayas. 12: 83–109.

Owen LA, Derbyshire E, Scott CH. 2003. Contemporary sediment production and transfer in high-altitude glaciers. 155: 13–36.

Owen LA, England J. 1998. Observations on rock glaciers in the Himalayas and Karakoram Mountains of northern Pakistan and India. Geomorphology 26: 199–213.

Owen LA, Finkel RC, Barnard PL, Haizhou M, Asahi K, Caffee MW, Derbyshire E. 2005. Climatic and topographic controls on the style and timing of Late Quaternary glaciation throughout Tibet and the Himalaya defined by [10]Be cosmogenic radionuclide surface exposure dating. Quaternary Science Reviews 24: 1391–1411.

Owen LA, Robinson R, Benn DI, Finkel RC, Davis NK, Yi C, Putkonen J, Li D, Murray AS. 2009. Quaternary glaciation of Mount Everest. Quaternary Science Reviews 28: 1412–1433.

Owen LA, Sharma MC. 1998. Rates and magnitudes of paraglacial fan formation in the Garhwal Himalaya: implications for landscape evolution. Geomorphology 26: 171–184.

Owen LA, Yi C, Finkel RC, Davis NK. 2010. Quaternary glaciation of Gurla Mandhata (Naimon'anyi). Quaternary Science Reviews 29: 1817–1830.

Owen LA. 2009. Latest Pleistocene and Holocene glacier fluctuations in the Himalaya and Tibet. Quaternary Science Reviews 28: 2150–2164.

Owen, L, Benn, D, Derbyshire, E, Evans, D, Mitchell, W, Thompson, D, Richardson, S, Lloyd, M, Holden, C. 1995. The geomorphology and landscape evolution of the Lahul Himalaya, Northern India. Zeitschrift für Geomorphologie 39: 145– 174.

Owen, LA, Caffee, MW, Bovard, KR, Finkel, RC, Sharma, MC. 2006. Terrestrial cosmogenic nuclide surface exposure dating of the oldest glacial successions in the Himalayan orogen: Ladakh Range, northern India. GSA Bulletin 118: 383–392.

Owen, LA, Derbyshire, E. 1989. The Karakoram glacial depositional system. Zeitschrift f€ur Geomorphologie N.F., Supplement 76: 33–73.

Owen, LA, Sharma, MC, Bigwood, R. 1996. Mass movement hazard in the Garhwal Himalaya: the effects of the 20 October 1991 Garhwal earthquake and the July–August 1992 monsoon season. Geomorphology and Land Management in a Changing Environment. Wiley, Chichester, UK: 69–88.

Placzek C, Granger DE, Matmon A, Quade J, Ryb U. 2014. Geomorphic process rates in the central Atacama Desert, Chile: Insights from cosmogenic nuclides and implications for the onset of hyperaridity. American Journal of Science 314: 1462–1512.

Portenga EW, Bierman PR, Duncan C, Corbett LB, Kehrwald NM, Rood DH. 2015. Erosion rates of the Bhutanese Himalaya determined using in situ-produced [10]Be. Geomorphology 233: 112–126.

Puri, VMK, Srivastava, D, Sangewar, CV, Mukerjee, BP, Swaroop, S. 2004. Palaeo-glaciation and glacier recession during quaternary period in Himalaya with special reference to Bhagirathi basin, Ganga catchment. In Srivastava, D., et al., eds., Geological Survey of India, Spl. Pub. No. 80: 167–177.

Putkonen J, Connolly J, Orloff T. 2008. Landscape evolution degrades the geologic signature of past glaciations. Geomorphology 97: 208–217.

Putkonen J, Swanson T. 2003. Accuracy of cosmogenic ages for moraines. Quaternary Research 59: 255–261.

Putnam AE et al. 2013a. Warming and glacier recession in the Rakaia valley, Southern Alps of New Zealand, during Heinrich Stadial 1. Earth and Planetary Science Letters 382: 98–110.

Putnam AE, Schaefer JM, Denton GH, Barrell DJA, Birkel SD, Andersen BG, Kaplan MR, Finkel RC, Schwartz R, Doughty AM. 2013b. The Last Glacial Maximum at 44??S documented by a [10]Be moraine chronology at Lake Ohau, Southern Alps of New Zealand. Quaternary Science Reviews 62: 114–141.

Raina, VK, Shehmani, Sangewar, CV. 2015. Glacier snout monitoring in the Himalayas. Geological Society of India, Bengaluru: 227–251.

Raina, VK, Srivastava, D. 2008. Glacier atlas of India. Bangalore, Geological Society of India.

Rajendran K, Rajendran CP, Jain SK, Murty CVR, Arlekar JN. 2000. The Chamoli earthquake, Garhwal Himalaya: Field observations and implications for seismic hazard. Current Science 78: 45–51.

Ranhotra, PS, Bhattacharyya, A. 2013. Modern vegetational distribution and pollen dispersal study within Gangotri glacier valley, Garhwal Himalaya. Journal of the Geological Society of India, 82(2): 133–142.

Reznichenko N V., Davies TRH, Alexander DJ. 2011. Effects of rock avalanches on glacier behaviour and moraine formation. Geomorphology 132: 327–338.

Rinterknecht VR et al. 2006. The Last Deglaciation of the Southeastern Sector of the Scandinavian Ice Sheet. Science 331: 1449–1452.

Roe GH. 2011. What do glaciers tell us about climate variability and climate change? Journal of Glaciology 57: 567–578.

Rowan A V. 2016. The 'Little Ice Age in the Himalaya: A review of glacier advance driven by Northern Hemisphere temperature change. The Holocene: 1–17.

Saha S, Owen LA, Orr EN, Caffee MW. 2018. Timing and nature of Holocene glacier advances at the northwestern end of the Himalayan-Tibetan orogen. Quaternary Science Reviews 187: 177–202.

Saha S, Owen, LA, Orr, EN, Caffee, MW. submitted., High-frequency Holocene glacier fluctuations in the Himalaya and Tibet. Quaternary Science Reviews.

Saha S, Sharma MC, Murari MK, Owen LA, Caffee MW. 2015. Geomorphology, sedimentology and minimum exposure ages of streamlined subglacial landforms in the NW Himalaya, India. Boreas 45: 284–303.

Sanders JW, Cuffey KM, Moore JR, MacGregor KR, Kavanaugh JL. 2012. Periglacial weathering and headwall erosion in cirque glacier bergschrunds. Geology 40: 779–782.

Satyabala, SP. 2016. Spatiotemporal variations in surface velocity of the Gangotri glacier, Garhwal Himalaya, India. Study using synthetic aperture radar data: Remote sensing of environment, 181: 151–161.

Schaefer JM, Oberholzer P, Zhao Z, Ivy-Ochs S, Wieler R, Baur H, Kubik PW, Schlüchter C. 2008. Cosmogenic beryllium-10 and neon-21 dating of late Pleistocene glaciations in Nyalam, monsoonal Himalayas. Quaternary Science Reviews 27: 295–311.

Scherler D, Bookhagen B, Strecker MR, von Blanckenburg F, Rood D. 2010. Timing and extent of late Quaternary glaciation in the western Himalaya constrained by ^{10}Be moraine dating in Garhwal, India. Quaternary Science Reviews 29: 815–831.

Scherler D, Bookhagen B, Strecker MR. 2011a. Hillslope-glacier coupling: The interplay of topography and glacial dynamics in High Asia. Journal of Geophysical Research: Earth Surface 116: 1–21.

Scherler D, Bookhagen B, Strecker MR. 2011b. Spatially variable response of Himalayan glaciers to climate change affected by debris cover. Nature Geoscience 4: 156–159.

Scherler D, Bookhagen B, Strecker MR. 2014. Tectonic control on 10 Be-derived erosion rates in the Garhwal Himalaya, India. Journal of Geophysical Research: Earth Surface 119: 83–105.

Scherler, D, Egholm. 2017. Debris supply to mountain glaciers and how it effects their sensitivity to climate change–A case study from the Chhota Shigri Glacier, India, 206444. Presented at 2017 Fall Meeting, AGU, New Orleans, LA.

Schweinfurth, U. 1968. Vegetation of the Himalaya. V: Mountains and Rivers of India, in 21st International Geographical Congress, India. Calcutta, National Committee for Geography: 110–136.

Searle MP, Noble SR, Hurford AJ, Rex DC. 1999. Age of crustal melting, emplacement and exhumation history of the Shivling leucogranite, Garhwal Himalaya. Geological Magazine 136: 513–525.

Searle, AMP, Parrish, RR, Hodges, KV, Hurford, A, Ayres, MW., Searle, MP, Parrish, RR, Hodges, KV, Hurford, A, Ayres, MW, Whitehouse, MJ. 1997. Shisha Pangma Leucogranite, South Tibetan Himalaya: Field Relations, Geochemistry, Age, Origin, and Emplacement. The Journal of Geology 105: 295–318.

Searle, MP, Windley, BF, Coward, MP, Cooper, DJW, Rex, AJ, Rex, D, Tingdong, L, Xuchang, X, Jan, MQ, Thakur, VC, Kumar, S. 1987. The closing of Tethys and the tectonics of the Himalaya. Geological Society of America Bulletin 98: 678–701.

Sen Singh, D. 2014. Surface processes during flash floods in the glaciated terrain of Kedarnath, Garhwal Himalaya and their role in the modification of landforms. Current Science 106: 594–597.

Seong YB, Owen LA, Caffee MW, Kamp U, Bishop MP, Bush A, Copland L, Shroder JF. 2009a. Rates of basin-wide rockwall retreat in the K2 region of the Central Karakoram defined by terrestrial cosmogenic nuclide [10]Be. Geomorphology 107: 254–262.

Seong YB, Owen LA, Yi C, Finkel RC. 2009b. Quaternary glaciation of Muztag Ata and Kongur Shan: Evidence for glacier response to rapid climate changes throughout the late glacial and holocene in westernmost Tibet. Bulletin of the Geological Society of America 121: 348–365.

Shankar, R, Srivastava, D. 2001. Glaciated regime and environmental interaction and Himalayan ecosystem. Geological Survey of India, Spl. Pub. 53: 17–21.

Sharma MC, Owen LA. 1996. Quaternary glacial history of NW Garhwal, Central Himalayas. Quaternary Science Reviews 15: 335–365.

Shroder JF, Bishop MP, Copland L, Sloan VF. 2000. Debris-covered glaciers and rock glaciers in the Nanga Parbat Himalaya, Pakistan. Geografiska Annaler, Series A: Physical Geography 82: 17–31.

Shugar DH, Clague JJ, McSaveney MJ. 2018. Late Holocene activity of Sherman and Sheridan glaciers, Prince William Sound, Alaska. Quaternary Science Reviews 194: 116–127.

Shugar DH, Clague JJ. 2011. The sedimentology and geomorphology of rock avalanche deposits on glaciers. Sedimentology 58: 1762–1783.

Singh D Sen, Tangri AK, Kumar D, Dubey CA, Bali R. 2017. Pattern of retreat and related morphological zones of Gangotri Glacier, Garhwal Himalaya, India. Quaternary International 444: 172–181.

Singh P, Haritashya UK, Kumar N. 2007. Meteorological study for Gangotri Glacier and its comparison with other high altitude meteorological stations in central Himalayan region. Nordic Hydrology 38: 59.

Singh P, Haritashya UK, Kumar N. 2008. Modelling and estimation of different components of streamflow for Gangotri Glacier basin, Himalayas. Hydrological Sciences Journal 53: 309–322.

Singh, SD. 2004. Late quaternary morpho-sedimentary processes in the Gangotri glacier area, Garhwal Himalayas, India. In Srivastava, D., et al., eds., Geological Survey of India, Spl. Pub. No. 80: 97–103.

Soekhabi RB, Stump E, Foland KA, Jain AK. 1996. Fission-track and 4°Ar/39Ar evidence for episodic denudation of the Gangotri granites in the Garhwal Higher Himalaya, India. Tectonophysics 260: 187–199.

Srivastava D. 2012. Status Report on Gangotri Glacier, Science and Engineering Research Board, Department of Science and Technology, New Delhi. Himalayan Glaciology Technical Report: 1–102.

Srivastava, D, Shukla, SP, Bhattacharya, DN. 2004b. Lichens: a tool for dating the moraines of Gangotri glacier area. In Srivastava, D., Gupta, K.R. and Mukerji, S., (Editors), Geological Survey of India, Spl. Pub. 80: 155–160.

Srivastava, D. 2004a. Recession of Gangotri glacier. In Srivastava, D., Gupta, K.R. and Mukerji, S., (Editors), Geological Survey of India, Spl. Pub. 80: 21–31.

Stone JO. 2000. Air pressure and cosmogenic isotope production. 105: 23,753-23,759.

Sugden, DE, John, BS. 1976. Glaciers and Landscape. A Geomorphological Approach. Edward Arnold, London.

Tangri, AK, Chandra, R, Yadav, SKS. 2004. Temporal monitoring of the snout, Equilibrium line and Ablation zone of Gangotri Glacier through remote sensing and GIS techniques- an attempt at deciphering the climatic variability. Geological Survey of India (Special Publication) 80: 145–153.

Taylor, JR. 1997. An Introduction to Error Analysis. Second Edition, University Science Books, Sausalito, Calif.

Tewari, AP. 1972. Study of the Gangotri glacier, Uttarkashi district, (Central Himalaya), Uttar Pradesh. Misc. Pub. of Geological Survey of India, 15: 69–74.

Thayyen, RJ, Gergan, JT. 2010. Role of glaciers in watershed hydrology: A preliminary study of a "himalayan catchment." Cryosphere 4: 115–128.Stone, J.O., 2000, Air pressure and cosmogenic isotope production.: v. 105, p. 23,753-23,759.

Thiede RC, Arrowsmith JR, Bookhagen B, McWilliams MO, Sobel ER, Strecker MR. 2005. From tectonically to erosionally controlled development of the Himalayan orogen. Geology 33: 689.

Tripathy GR, Singh SK. 2010. Chemical erosion rates of river basins of the Ganga system in the Himalaya: Reanalysis based on inversion of dissolved major ions, Sr, and 87Sr/86Sr. Geochemistry, Geophysics, Geosystems 11: 1–20.

Uppala, S.M., KÅllberg, P.W., Simmons, A.J., Andrae, U., Bechtold, V.D.C., Fiorino, M., Gibson, J.K., Haseler, J., Hernandez, A., Kelly, G.A., Li, X., Onogi, K., Saarinen, S., Sokka, N. 2005. The ERA-40 re-analysis. Quarterly Journal of the Royal Meteorological Society 131: 2961–3012.

Valdiya, KS. 1991. The Uttarkashi earthquake of 20 October: implications and lessons. Curr. Sci. 61: 801–803.

Valletta RD, Willenbring JK, Lewis AR. 2017. "Difference Dating": A novel approach towards dating alpine glacial moraines. Quaternary Geochronology 41: 1–10.

Vannay JC, Grasemann B, Rahn M, Frank W, Carter A, Baudraz V, Cosca M. 2004. Miocene to Holocene exhumation of metamorphic crustal wedges in the NW Himalaya: Evidence for tectonic extrusion coupled to fluvial erosion. Tectonics 23: 1–24.

Vohra, CP. 1971. Report of the Training-Cum-Study Expedition to the Gangotri glacier. INCH, CSIR, New Delhi.

Vohra, CP. 1988. Gangotri glacier. Indian Mountaineer, Indian Mountaineering Foundation: 1–8.

Ward DJ, Anderson RS. 2011. The use of ablation-dominated medial moraines as samplers for [10]Be-derived erosion rates of glacier valley walls, Kichatna Mountains, AK. Earth Surface Processes and Landforms 36: 495–512.

Watanabe T, Dali L, Shiraiwa T. 1998. Slope denudation and the supply of debris to cones in Langtang Himal, Central Nepal Himalaya. Geomorphology 26: 185–197.

West N, Kirby E, Bierman P, Clarke BA. 2014. Aspect-dependent variations in regolith creep revealed by meteoric [10]Be. Geology 42: 507–510.

Wulf H, Bookhagen B, Scherler D. 2010. Seasonal precipitation gradients and their impact on fluvial sediment flux in the Northwest Himalaya. Geomorphology 118: 13–21.

Yang B, Bräuning A, Dong Z, Zhang Z, Keqing J. 2008. Late Holocene monsoonal temperate glacier fluctuations on the Tibetan Plateau. Global and Planetary Change 60: 126–140.

Zech R, Glaser B, Sosin P, Kubik PW, Zech W. 2005. Evidence for long-lasting landform surface instability on hummocky moraines in the Pamir Mountains (Tajikistan) from [10]Be surface exposure dating. Earth and Planetary Science Letters 237: 453–461.

Zech R, Zech M, Kubik PW, Kharki K, Zech W. 2009. Deglaciation and landscape history around Annapurna, Nepal, based on [10]Be surface exposure dating. Quaternary Science Reviews 28: 1106–1118.

Zweck C, Zreda M, Desilets D. 2013. Snow shielding factors for cosmogenic nuclide dating inferred from Monte Carlo neutron transport simulations. Earth and Planetary Science Letters 379: 64–71.

Appendices

Solang, India

Photo credit: LAO

11.1 Appendix A1 (Supplementary materials for Paper I)

List of supplementary materials

S1: Present and former extents of glaciers for steady-state ELA reconstruction (Kmz format – not included here).

S2: Holocene glacial chronostratigraphies were reconstructed using ^{10}Be surface dating of moraine boulders in the NW Himalaya.

S3: ^{10}Be surface-exposure ages (in thousands of years before AD2016, labeled 'ka'±1σ) form 32 glaciated valleys at the NW end of the Himalaya and Tibet.

S4: Holocene boulder ages (published and new) are compared using different online age calculators and scaling schemes with reference to the LSD (Lifton-Sato-Dunai) scheme using the CREp calculator (used in this study).

S5: Comparison of the influence of different erosion rates using the 57 Holocene ^{10}Be surface exposure ages in our study.

S6: Location of ^{10}Be samples used in this study (Kmz format – not included here).

S7: Reconstructed steady-state ELAs and ΔELAs in the numerically dated (^{10}Be) glaciated valleys at the NW end of the Himalaya and Tibet.

S8: Evidence showing post depositional hillslope contamination in the Hamtah m_{H3} and Lato m_{A3} moraines.

S9: Maps showing equilibrium line altitude depressions (ΔELAs) in the NW Himalaya and Tibet during different regional stages of glacier advances.

S2: Holocene glacial chronostratigraphies were reconstructed using ^{10}Be surface dating of moraine boulders in the NW Himalaya. Whenever possible large boulders from moraine crests were chosen for sampling. Arrows indicate the sample location on the boulder surface. Details are provided in Table S1.

46 — Lato 1420

47 — Lato 1421

48 — Lato 1601

49 — Stok 1401

50 — Stok 1402

51 — Stok 1403

52 — Stok 1404

53 — Stok 1405

54 — Stok 1406

55 — Stok 1407

56 — Stok 1408

57 — Stok 1516

Table S3 Be-10 surface-exposure ages (in thousands of years before AD2016, labeled 'ka'±1σ) from 32 glacited valleys at the NW end of the Himalaya and Tibet. Sample data, regional and local glacial stages, and associated age statistics are highlighted.

Reference	Local Glacial Stage	Glacial stage or moraine name	Sample ID	Latitude (DD)	Longitude (DD)	Elevation (m a.s.l.)	Sample thickness (cm)	Density (g cm-3)	Erosion (cm a-1)	Shielding correction	[10Be] ± 1σ (104 atoms g-1)a	AMS std	Regional glacial stage	Local glacial stage (based on LSD ages in ka)	LSD Age ± 1σ (ka) [CREp]	Basic Statistics	Lm Age ± 1σ (ka)	SA Age ± 1σ (ka)	SF Age ± 1σ (ka)	Lm Age ± 1σ (ka)	St Age ± 1σ (ka)	De Age ± 1σ (ka)	Du Age ± 1σ (ka)	Li Age ± 1σ (ka)	LSD Age ± 1σ (ka) [CRONUS EARTH 3.0]	Lm Age ± 1σ (ka)	St Age ± 1σ (ka)
Seong et al., 2007	Mungo 2 stage	m1I	K2-72	35.703	75.953	4209	2.0	2.70	0.0	1.000	82.28±1.81	KNSTD			14.65±0.68	Chi-squared: 0.17	14.4±0.74	15.30±1.10	15.50±1.20	14.60±1.10	14.50±1.20	15.00±2.00	15.00±2.00	14.80±1.80	13.86±0.31	14.23±0.31	14.23±0.3
Seong et al., 2007	Mungo 2 stage	m1I	K2-73	35.704	75.952	4213	2.0	2.70	0.0	1.000	84.09±1.81	KNSTD			14.91±0.69		14.66±0.75	15.50±1.10	15.80±1.20	14.80±1.10	14.80±1.30	15.30±2.10	15.60±2.10	15.10±1.80	14.06±0.30	14.50±0.31	14.52±0.3
Seong et al., 2007	Mungo 2 stage	m1I	K2-74	35.703	75.952	4212	2.0	2.70	0.0	1.000	84.99±1.81	KNSTD			15.04±0.7	Skewness: +0.97	14.81±0.76	15.70±1.10	16.00±1.30	15.00±1.10	14.90±1.30	15.50±2.10	15.80±2.10	15.20±1.80	14.21±0.30	14.66±0.31	14.66±0.3
Seong et al., 2007	Mungo 2 stage	m1I	K2-75	35.703	75.948	4215	3.0	2.70	0.0	1.000	83.19±2.71	KNSTD		14.98±0.26	14.87±0.76	Outlier: 1	14.62±0.81	15.50±1.10	15.70±1.30	14.80±1.20	14.70±1.30	15.30±2.10	15.60±2.10	15.00±1.90	14.01±0.46	14.45±0.47	14.47±0.4
Seong et al., 2007	Mungo 2 stage	m1I	K2-76	35.703	75.947	4211	3.0	2.70	0.0	1.000	107.60±2.71	KNSTD			18.89±0.91	Wt. mean: 14.98±0.26 ka	18.4±1	19.30±1.20	19.60±1.30	18.90±1.40	19.10±1.60	19.20±2.30	19.40±2.30	18.90±2.20	17.70±0.45	18.36±0.47	18.77±0.4
Seong et al., 2007	Mungo 2 stage	m1I	K2-77	35.703	75.943	4211	3.0	2.70	0.0	1.000	86.80±1.81	KNSTD			15.44±0.72	Ar. mean: 14.98±0.26 ka / Peak: 14.95 ka	15.15±0.79	16.10±1.20	16.40±1.30	15.40±1.20	15.40±1.30	15.90±2.20	16.20±2.20	16.00±2.00	14.62±0.31	15.04±0.31	15.13±0.3
Seong et al., 2007	Mungo 2 stage	m1D (bedrock)	K2-23	35.718	75.520	2646	3.0	2.70	0.0	0.960	33.46±0.90	KNSTD			14.96±0.74	Chi-squared: 0.19	15.51±0.85	16.50±1.20	16.50±1.30	14.90±1.20	14.80±1.30	16.80±2.30	17.00±2.30	16.00±2.20	14.96±0.41	14.52±0.39	14.55±0.40
Seong et al., 2007	Mungo 2 stage	m1D (bedrock)	K2-24	35.718	75.520	2631	3.0	2.70	0.0	0.960	31.65±0.90	KNSTD			14.33±0.71	Skewness: +0.70	14.92±0.83	15.80±1.10	15.90±1.30	14.30±1.10	14.20±1.20	16.10±2.30	16.30±2.30	16.00±2.00	14.37±0.41	13.91±0.40	13.89±0.40
Seong et al., 2007	Mungo 2 stage	m1D (bedrock)	K2-25	35.718	75.520	2631	3.0	2.70	0.0	0.960	30.74±0.90	KNSTD		14.61±0.26	13.96±0.72	Outlier: 1	14.55±0.8	15.40±1.10	15.50±1.20	13.90±1.10	13.80±1.20	15.70±2.20	15.90±2.20	16.00±2.00	13.98±0.41	13.60±0.40	13.49±0.40
Seong et al., 2007	Mungo 2 stage	m1D (bedrock)	K2-26	35.719	75.520	2650	3.0	2.70	0.0	0.960	32.55±0.90	KNSTD			14.57±0.71	Wt. mean: 14.61±0.26 ka / Ar. mean: 14.62±0.26 ka / Peak: 14.62 ka	15.09±0.84	16.00±1.20	16.10±1.30	14.50±1.20	14.40±1.30	16.40±2.30	16.60±2.30	16.20±2.10	14.58±0.41	14.11±0.39	14.12±0.3
Owen et al. (2001)	Kulti glacial stage	N/A	L44	32.400	77.600	4070	5.0	2.70	0.0	0.990	66.21±1.90	LLNL3000		14.45±0.70	14.45±0.7	!	14.83±0.8	15.60±1.20	15.80±1.30	14.40±1.10	14.30±1.30	15.10±2.10	15.60±2.10	15.00±1.80	14.08±0.41	14.07±0.41	14.02±0.4
Owen et al., 2002	Batura stage	t6	KK98-34a	36.510	74.890	2600	5.0	2.70	0.0	0.990	28.00±0.86	LLNL3000			12.69±0.68	Chi-squared: 0.00	13.14±0.76	14.00±1.10	14.10±1.20	12.50±1.10	12.40±1.10	14.30±2.00	15.00±2.00	14.10±1.80	12.88±0.40	12.49±0.38	12.16±0.3
Owen et al., 2002	Batura stage	t6	KK98-34b	36.510	74.890	2610	5.0	2.70	0.0	0.990	32.24±0.86	LLNL3000		14.30±0.01	14.31±0.7	Skewness: !	14.81±0.81	15.60±1.20	15.70±1.30	14.30±1.10	14.20±1.20	16.10±2.30	16.30±2.30	15.90±2.10	14.28±0.38	13.90±0.37	13.88±0.3
Owen et al., 2002	Batura stage	t6	KK98-35	36.510	74.890	2595	5.0	2.70	0.0	0.990	31.90±0.86	LLNL3000			14.29±0.71	Peak: 14.30 ka	14.8±0.81	15.60±1.20	15.70±1.20	14.20±1.10	14.10±1.20	16.10±2.30	16.30±2.30	15.90±2.10	14.28±0.39	13.88±0.38	13.86±0.3
Seong et al., 2007	Mungo 2 stage	m1I	K2-78	35.695	75.957	4225	2.0	2.70	0.0	1.000	84.99±1.81	KNSTD			14.96±0.69	Chi-squared: 0.11	14.73±0.76	15.00±1.10	15.90±1.20	14.90±1.10	14.80±1.30	15.40±2.10	15.70±1.80	15.10±1.80	14.12±0.30	14.57±0.31	14.59±0.3
Seong et al., 2007	Mungo 2 stage	m1I	K2-79	35.694	75.958	4221	3.0	2.70	0.0	1.000	80.47±1.81	KNSTD			14.26±0.67	Skewness: -1.29	14.02±0.76	15.00±1.00	15.20±1.10	14.20±1.00	14.10±1.20	15.00±1.90	15.00±1.90	14.50±1.80	13.59±0.31	13.89±0.31	13.84±0.3
Seong et al., 2007	Mungo 2 stage	m2I	K2-80	35.694	75.958	3823	3.0	2.70	0.0	0.810	64.20±1.81	KNSTD			17.14±0.87	Outlier: 5	16.99±0.96	18.00±1.30	18.20±1.40	17.10±1.40	17.20±1.50	18.00±2.40	18.30±2.40	17.70±2.20	16.31±0.46	16.61±0.47	16.86±0.4
Seong et al., 2007	Mungo 2 stage	m2I	K2-81	35.693	75.960	3821	3.0	2.70	0.0	0.810	66.01±1.81	KNSTD		14.08±0.19	17.43±0.98		17.43±0.98	18.40±1.30	18.70±1.40	17.60±1.40	17.70±1.50	18.40±2.40	18.60±2.40	18.10±2.30	16.75±0.46	17.07±0.47	17.35±0.4
Seong et al., 2007	Mungo 2 stage	m2I	K2-82	35.692	75.960	3818	2.0	2.70	0.0	0.810	63.29±1.81	KNSTD			16.83±0.86	Wt. mean: 14.08±0.19 ka	16.66±0.96	17.70±1.30	17.90±1.40	16.80±1.40	16.80±1.50	17.70±2.40	17.90±2.40	17.40±2.20	16.02±0.46	16.33±0.47	16.53±0.4
Seong et al., 2007	Mungo 2 stage	m2I	K2-83	35.692	75.961	3779	3.0	2.70	0.0	1.000	231.48±5.43	KNSTD			48.51±3.17	Ar. mean: 14.08±0.19 ka	48.8±3.44	44.50±3.30	45.30±3.70	46.00±3.90	51.80±4.50	46.90±6.80	45.60±6.80	45.50±6.20	44.03±1.04	46.56±1.10	50.89±1.2
Seong et al., 2007	Mungo 2 stage	m2I	K2-84	35.689	75.941	3768	2.0	2.70	0.0	1.000	61.49±1.81	KNSTD			13.82±0.71	Peak: 14.09 ka	13.82±0.78	14.70±1.10	14.90±1.10	13.70±1.10	13.60±1.20	15.00±1.90	15.00±1.90	14.50±1.80	13.40±0.40	13.50±0.40	13.36±0.3
Seong et al., 2007	Mungo 2 stage	m2I	K2-85	35.689	75.941	3766	2.0	2.70	0.0	1.000	62.39±2.71	KNSTD			14.15±0.82		14.13±0.88	15.00±1.20	15.20±1.20	14.10±1.20	14.00±1.30	14.90±2.20	15.00±2.00	14.70±1.80	13.68±0.60	13.79±0.60	13.73±0.6
Abramowski et al., 2006	N/A	AV	AV1	39.680	71.620	3440	4.0	2.70	0.0	1.000	56.57±3.65	S555	Regional glacial stage: ~15.4–12.7 ka; Weighted mean: 13.88±0.68 ka; n: 44; Dispersion: 0 %; P(sig 2-tailed): 0.00		13.82±1.02	Chi-squared: 0.04	13.24±1.05	14.10±1.30	14.30±1.40	13.80±1.40	13.70±1.50	14.60±2.10	14.80±2.10	14.00±2.00	13.17±0.85	13.53±0.88	13.48±0.8
Abramowski et al., 2006	N/A	AV	AV2	39.680	71.620	3440	4.0	2.70	0.0	1.000	57.48±3.65	S555		14.02±0.17	14.02±1.01	Skewness: +0.07 / Outlier: 0 / Wt. mean: 14.02±0.17 ka / Ar. Mean: 14.02±0.17 ka	13.45±1.04	14.30±1.30	14.50±1.40	14.10±1.40	13.90±1.50	14.90±2.20	15.00±2.20	15.00±2.00	13.35±0.85	13.71±0.87	13.69±0.8
Abramowski et al., 2006	N/A	AV	AV3	39.680	71.620	3440	4.0	2.70	0.0	1.000	58.39±3.65	S555			14.23±1.02	Peak: 14.02 ka	13.65±1.03	14.50±1.30	14.70±1.40	14.30±1.40	14.20±1.50	15.10±2.20	15.20±2.20	15.00±2.00	13.53±0.85	13.89±0.87	13.91±0.8
Owen et al. (2001)	Kulti glacial stage	N/A	L24	32.500	77.000	2985	5.0	2.70	0.0	0.860	7.09±0.35	LLNL3000			3.6±0.23	Chi-squared: 0.05	3.93±0.28	3.76±0.39	3.79±0.42	3.40±0.30	3.16±0.31	3.72±0.74	4.06±0.74	3.71±0.56	3.74±0.18	3.47±0.17	3.10±0.1
Owen et al. (2001)	Kulti glacial stage	N/A	L25	32.500	77.000	2985	5.0	2.70	0.0	0.930	8.04±0.52	LLNL3000			3.77±0.28	Skewness: !	4.11±0.34	3.96±0.47	4.00±0.50	3.57±0.35	3.31±0.36	3.90±0.79	4.28±0.79	3.90±0.64	3.92±0.25	3.66±0.24	3.25±0.2
Owen et al. (2001)	Kulti glacial stage	N/A	L28	32.500	77.000	3000	5.0	2.70	0.0	0.970	33.02±1.04	LLNL3000		14.02±0.12	14.14±0.73	Outlier: 2 / Wt. mean: 14.02±0.12 ka / Ar. Mean: 14.03±0.12 ka	14.95±0.84	15.80±1.20	15.90±1.30	14.10±1.20	14.00±1.20	15.70±2.30	16.00±2.30	16.00±2.00	14.24±0.45	13.58±0.37	13.47±0.3
Owen et al. (2001)	Kulti glacial stage	N/A	L29	32.500	77.000	2985	5.0	2.70	0.0	0.970	34.66±0.95	LLNL3000			13.91±0.7	Peak: 14.03 ka	14.76±0.8	15.50±1.20	15.60±1.20	13.80±1.10	13.70±1.20	15.40±2.20	15.80±2.20	15.30±1.90	14.02±0.39		
Seong et al., 2007	Mungo 2 stage	m1G	K2-48	35.671	75.799	3633	2.0	2.70	0.0	1.000	54.25±1.81	KNSTD			13.26±0.77	Chi-squared: 0.56	13.26±0.77	14.40±1.10	14.50±1.10	13.10±1.10	12.90±1.20	14.00±1.90	14.40±1.90	14.10±1.80	12.94±0.43	12.68±0.4	
Seong et al., 2007	Mungo 2 stage	m1G	K2-49	35.671	75.799	3631	2.0	2.70	0.0	1.000	55.16±1.81	KNSTD			13.39±0.69	Skewness: -0.20	13.48±0.76	14.30±1.10	14.50±1.10	13.30±1.10	13.10±1.20	14.00±1.90	14.60±1.90	14.10±1.80	13.09±0.43	13.10±0.4	
Seong et al., 2007	Mungo 2 stage	m1G	K2-50	35.671	75.799	3640	2.0	2.70	0.0	1.000	58.77±1.81	KNSTD			14.12±0.73	Outlier: 1	14.17±0.8	15.10±1.10	15.20±1.10	14.10±1.10	13.90±1.20	15.00±2.00	15.00±2.00	14.60±1.90	13.71±0.42	13.69±0.4	
Seong et al., 2007	Mungo 2 stage	m1G	K2-51	35.671	75.799	3644	2.0	2.70	0.0	1.000	54.25±1.81	KNSTD			13.1±0.7		13.18±0.77	14.00±1.10	14.20±1.10	13.00±1.10	12.80±1.10	14.00±1.90	14.40±1.90	14.10±1.80	12.88±0.43	12.60±0.4	
Seong et al., 2007	Mungo 2 stage	m1G	K2-52	35.667	75.798	3636	2.0	2.70	0.0	1.000	54.25±1.81	KNSTD		13.76±0.50	13.24±0.77		13.24±0.77	14.10±1.10	14.30±1.20	13.00±1.10	12.90±1.20	14.00±1.90	14.40±1.90	14.10±1.80	12.93±0.43	12.66±0.4	
Seong et al., 2007	Mungo 2 stage	m1G	K2-53	35.667	75.797	3643	4.0	2.70	0.0	1.000	58.77±1.81	KNSTD			14.33±0.72		14.38±0.79	15.20±1.10	15.40±1.20	14.30±1.20	14.10±1.20	15.00±2.00	15.20±2.10	15.00±1.90	13.92±0.43	13.90±0.4	
Seong et al., 2007	Mungo 2 stage	m1G	K2-54	35.666	75.797	3824	3.0	2.70	0.0	1.000	43.40±0.90	KNSTD			9.86±0.47	Wt. mean: 13.76±0.50 ka	9.96±0.54	10.40±0.86	10.56±0.93	9.47±0.84	9.39±0.79	10.30±1.60	10.80±1.60	10.10±1.40	10.16±0.21	10.02±0.21	9.23±0.1
Seong et al., 2007	Mungo 2 stage	m1G	K2-55	35.666	75.796	3825	3.0	2.70	0.0	1.000	64.20±1.81	KNSTD			14.32±0.7	Ar. mean: 13.77±0.50 ka	15.10±1.10	15.00±1.10	13.90±1.10	13.80±1.20	15.00±2.00	15.00±2.00	14.90±1.80	13.78±0.39	13.89±0.3	
Seong et al., 2007	Mungo 2 stage	m1G	K2-56	35.668	75.797	3881	2.0	2.70	0.0	1.000	66.01±1.81	KNSTD			13.96±0.7	Peak: 13.80 ka	13.9±0.78	15.00±1.00	15.00±1.00	13.90±1.10	13.80±1.10	15.00±2.00	14.50±1.80	13.48±0.37	13.52±0.3		
Seong et al., 2007	Mungo 2 stage	m1G	K2-58	35.694	75.719	3879	2.0	2.70	0.0	1.000	65.10±2.71	KNSTD			13.8±0.79		13.75±0.84	15.00±1.10	14.80±1.20	13.70±1.20	13.60±1.30	14.50±2.20	15.00±2.00	14.80±1.90	13.33±0.56	13.48±0.5	
Seong et al., 2007	Mungo 2 stage	m1G	K2-59	35.694	75.719	3811	2.0	2.70	0.0	1.000	65.10±1.81	KNSTD			14.38±0.7		14.32±0.77	15.20±1.10	15.40±1.10	14.30±1.10	14.20±1.20	15.10±2.00	15.00±1.90	13.82±0.39	13.96±0.3		
Owen et al. (2001)	Kulti glacial stage	N/A	L10	32.300	77.200	2390	5.0	2.70	0.0	0.990	25.76±1.99	LLNL3000		13.64±0.62	14.57±1.18	Chi-squared: 1.11 / Skewness: ! / Outlier: 0 / Wt. mean: 13.64±0.62 ka / Ar. Mean: 13.95±0.62 ka	15.67±1.35	16.60±1.80	16.60±1.90	14.50±1.60	14.40±1.70	16.70±2.60	16.90±2.60	16.60±2.50	14.98±1.16	14.11±1.09	14.15±1.10
Owen et al. (2001)	Kulti glacial stage	N/A	L12	32.300	77.200	2415	5.0	2.70	0.0	0.990	23.77±0.78	LLNL3000			13.33±0.68	Peak: 13.47 ka	14.41±0.8	15.20±1.10	15.20±1.20	13.20±1.10	13.10±1.10	15.20±2.10	15.50±2.10	15.10±1.90	13.79±0.45	13.05±0.43	12.85±0.4
Seong et al., 2007	Mungo 2 stage	m1F (bedrock)	K2-60	35.694	75.719	3031	2.0	2.70	0.0	0.940	37.07±0.90	KNSTD			13.43±0.64	Chi-squared: 0.08	13.81±0.75	15.00±1.00	14.80±1.10	13.30±1.10	13.20±1.10	14.30±2.00	15.00±2.00	14.60±1.80	13.38±0.33	13.12±0.32	12.94±0.3
Seong et al., 2007	Mungo 2 stage	m1F (bedrock)	K2-61	35.694	75.718	3032	2.0	2.70	0.0	0.930	36.17±0.90	KNSTD			13.25±0.64	Skewness: +0.16	13.63±0.74	14.00±1.00	14.60±1.10	13.10±1.10	13.00±1.10	15.00±1.90	14.90±1.90	14.50±1.80	13.21±0.33	12.98±0.32	12.75±0.3
Seong et al., 2007	Mungo 2 stage	m1F (bedrock)	K2-62	35.672	75.814	3017	2.0	2.70	0.0	0.940	34.36±1.81	KNSTD		13.42±0.16	12.63±0.86	Outlier: 1	13.02±0.93	13.80±1.20	13.90±1.30	12.50±1.20	12.30±1.20	14.00±2.00	14.00±2.00	13.80±1.90	12.75±0.67	12.46±0.66	12.10±0.6
Seong et al., 2007	Mungo 2 stage	m1F (bedrock)	K2-63	35.672	75.814	2944	2.0	2.70	0.0	0.690	26.22±0.90	KNSTD			13.63±0.72	Wt. mean: 13.42±0.16 ka / Ar. mean: 13.44±0.16 ka / Peak: 13.43 ka	14.03±0.83	14.90±1.10	15.00±1.00	13.50±1.20	13.40±1.20	15.10±2.10	15.40±2.10	14.90±1.90	13.57±0.47	13.26±0.46	13.10±0.4
Röhringer et al., 2012	BO8 stage	N/A	BH12	37.649	72.780	4451	3.0	2.70	0.0	0.960	108.28±7.07	S555			16.81±1.26	Chi-squared: 0.65	15.79±1.21	16.80±1.60	17.10±1.60	16.80±1.70	16.90±1.80	16.80±2.50	17.00±2.50	16.40±2.30	15.30±1.00	16.32±1.07	16.58±1.0
Röhringer et al., 2012	BO8 stage	N/A	BH13	37.649	72.780	4451	2.0	2.70	0.0	0.960	87.05±3.45	S555		13.21±0.45	13.63±0.76	Skewness: !	12.96±0.83	13.80±1.10	14.10±1.20	13.60±1.20	13.40±1.20	14.00±1.90	14.00±1.90	13.40±1.80	12.79±0.51	13.31±0.53	13.21±0.5
Röhringer et al., 2012	BO8 stage	N/A	BH14	37.649	72.780	4449	4.0	2.70	0.0	0.960	79.38±3.73	S555			12.73±0.82	Outlier: 1 / Wt. mean: 13.21±0.45 ka / Ar. mean: 13.18±0.45 ka / Peak: 13.20 ka	12.02±0.84	12.90±1.10	13.10±1.20	12.60±1.20	12.50±1.20	13.00±1.90	13.10±1.90	12.50±1.70	12.11±0.57	12.56±0.59	12.25±0.5
Seong et al., 2007	Mungo 2 stage	m3I	K2-86	35.689	75.941	3445	3.0	2.70	0.0	0.980	46.11±0.90	KNSTD			13.0±0.72	Chi-squared: 0.33	12.82±0.62	13.81±0.99	14.20±1.10	13.00±1.00	12.90±1.00	13.00±1.90	14.20±1.90	13.70±1.80	12.74±0.25	12.63±0.25	12.29±0.2
Seong et al., 2007	Mungo 2 stage	m3I	K2-87	35.689	75.941	3442	3.0	2.70	0.0	0.980	48.83±1.81	KNSTD			13.52±0.73	Skewness: +1.72	13.69±0.8	14.50±1.10	14.70±1.20	13.40±1.20	13.30±1.20	14.60±2.00	15.00±2.00	14.40±1.80	13.27±0.49	13.21±0.49	13.04±0.4
Seong et al., 2007	Mungo 2 stage	m3I	K2-88	35.688	75.927	3447	3.0	2.70	0.0	0.980	52.44±1.81	KNSTD		13.02±0.32	14.4±0.75	Outlier: 1	14.56±0.82	15.40±1.10	15.60±1.30	14.30±1.20	14.20±1.30	15.50±2.20	15.80±2.20	15.30±1.90	13.98±0.48	13.98±0.48	13.97±0.4
Seong et al., 2007	Mungo 2 stage	m3I	K2-89	35.688	75.927	3441	3.0	2.70	0.0	0.980	46.11±0.90	KNSTD			12.85±0.62	Wt. mean: 13.02±0.32 ka / Ar. mean: 13.06±0.32 ka / Peak: 12.98 ka	13.02±0.71	14.00±1.00	14.00±1.10	13.00±1.00	12.50±1.10	14.00±1.90	14.20±1.90	13.70±1.80	12.76±0.25	12.65±0.25	12.32±0.2
Seong et al., 2009	Olimde 2 stage	m3H	KONG_5	38.642	74.995	3539	3.0	2.70	0.0	1.000	53.17±1.45	KNSTD			12.88±0.67	Chi-squared: 0.04	12.48±0.75	13.00±1.00	13.50±1.10	12.80±1.10	12.70±1.10	14.00±1.90	13.90±1.90	13.50±1.80	12.68±0.35	12.43±0.35	
Seong et al., 2009	Olimde 2 stage	m3H	KONG_6	38.642	74.995	3539	5.0	2.70	0.0	1.000	53.71±1.45	KNSTD		13.01±0.11	12.99±0.66	Skewness: +0.54 / Outlier: 0 / Wt. mean: 13.01±0.11 ka / Ar. mean: 13.01±0.11 ka	12.6±0.76	13.00±1.00	13.60±1.10	12.90±1.10	12.80±1.10	14.00±1.90	14.00±1.90	13.60±1.80	12.60±0.34	12.78±0.35	12.55±0.3
Seong et al., 2009	Olimde 2 stage	m3H	KONG_7	38.642	74.995	3542	5.0	2.70	0.0	1.000	54.61±1.45	KNSTD			13.15±0.66	Peak: 13.01 ka	12.8±0.76	14.00±1.00	13.80±1.10	13.10±1.10	13.00±1.10	14.00±1.90	14.20±1.80	13.70±1.80	12.74±0.34	12.93±0.34	12.74±0.3
Seong et al., 2007	Mungo 2 stage	m1E	K2-31	35.721	75.676	3164	2.0	2.70	0.0	0.940	36.17±0.90	KNSTD			12.18±0.65	Chi-squared: 0.25	12.52±0.74	13.00±1.00	13.40±1.10	12.05±0.97	12.00±1.00	13.00±1.90	13.80±1.90	13.20±1.80	12.36±0.31	12.09±0.30	11.67±0.2
Seong et al., 2007	Mungo 2 stage	m1E	K2-32	35.722	75.674	3166	3.0	2.70	0.0	0.940	5.43±0.90	KNSTD		12.41±0.23	1.99±0.36	Skewness: ! / Outlier: 1 / Wt. mean: 12.41±0.23 ka / Ar. mean: 12.41±0.23 ka / Peak: 12.41 ka	2.11±0.4	2.23±0.47	2.24±0.48	1.96±0.41	1.79±0.36	2.23±0.53	2.50±0.53	2.22±0.53	1.93±0.32	1.86±0.31	1.76±0.2
Seong et al., 2007	Mungo 2 stage	m1E (bedrock)	K2-33	35.724	75.672	3052	4.0	2.70	0.0	0.960	35.26±0.90	KNSTD			12.64±0.65		12.99±0.75	14.00±1.00	13.90±1.10	12.00±1.00	12.30±1.10	14.00±1.90	14.30±1.90	13.80±1.80	12.73±0.33	12.46±0.32	12.10±0.3
Seong et al., 2009	Olimde 2 stage	m5C	MUST-72	38.287	75.011	4295	5.0	2.70	0.0	1.000	80.65±1.99	KNSTD	Regional glacial stage: ~12.6–11.4 ka; Weighted mean: 11.92±0.45 ka; n: 7; Dispersion: 0 %; P(sig 2-tailed): 0.00		12.32±0.64	Chi-squared: 0.64	12.49±0.74	13.00±1.00	13.00±1.10	12.40±1.00	12.30±1.10	13.00±1.90	13.70±1.90	13.00±1.90	12.50±0.31	12.97±0.32	12.79±0.3
Seong et al., 2009	Olimde 2 stage	m5C	MUST-73	38.286	75.011	4298	5.0	2.70	0.0	1.000	69.62±1.72	KNSTD			11.43±0.54	Skewness: !	10.92±0.56	11.60±0.89	12.27±0.91	11.37±0.95	11.24±0.94	11.60±1.60	12.00±1.60	11.40±1.50	11.22±0.28	11.50±0.28	11.02±0.2
Seong et al., 2009	Olimde 2 stage	m5C	MUST-74	38.286	75.011	4292	2.0	2.70	0.0	1.000	72.97±1.81	KNSTD		11.66±0.28	11.99±0.64	Outlier: 2 / Wt. mean: 11.66±0.28 ka / Ar. mean: 11.71±0.28 ka / Peak: 11.62 ka	11.34±0.59	12.13±0.88	12.85±0.99	11.94±0.97	11.81±0.99	12.10±1.70	12.50±1.70	11.90±1.50	11.61±0.29	11.97±0.30	11.59±0.2
Seong et al., 2009	Olimde 2 stage	m5C	MUST-75	38.286	75.011	4293	5.0	2.70	0.0	1.000	74.14±2.89	KNSTD			12.19±0.73		11.48±0.69	12.30±0.98	13.00±1.10	12.00±1.00	12.00±1.10	12.30±1.80	12.70±1.80	12.10±1.60	11.73±0.46	12.13±0.48	11.77±0.4

Study	Stage	Code	Sample	Lat	Long	Elev (m)	Thick	Dens	—	Shield	Age (ka)	Std	Group mean	Age1	Stats / Regional	A1	A2	A3	A4	A5	A6	A7	A8	A9	A10	A11
Owen et al. (2001)	Kulti glacial stage	N/A	L20	32.600	76.900	2865	5.0	2.70	0.0	0.900	24.20±1.30	LLNL3000	11.64±0.42	11.34±0.71	Chi-squared: 0.54 Skewness: ! Outlier: 0 Wt. mean: 11.64±0.42 ka Ar. mean: 11.76±0.42 ka Peak: 11.54 ka	12.1±0.89	12.80±1.20	12.90±1.30	11.20±1.10	11.00±1.10	13.00±2.00	13.00±2.00	12.70±1.80	11.93±0.64	11.40±0.61	10.83±0.58
		N/A																							12.11±0.84	11.69±0.81
Owen et al. (2001)	Kulti glacial stage		L21	32.600	76.900	2700	5.0	2.70	0.0	1.000	26.28±1.82	LLNL3000		12.18±0.96		13.08±1.08	13.80±1.40	13.90±1.50	12.10±1.30	11.90±1.40	13.80±2.10	14.20±2.10	14.00±2.00	12.74±0.88		
This study	Early Holocene	mH3	HAMTAH-1401	32.300	77.368	3783	1.5	2.7	0.0	0.897	37.33±1.91	07KNSTD	10.42±0.34	10.94±0.66	Chi-squared: 0.48 Skewness: +1.16 Outlier: 3 Wt. mean: 10.42±0.34 ka Ar. mean: 10.48±0.34 ka Peak: 10.37 ka	10.48±0.62	11.40±1.10	11.60±1.10	10.00±1.00	10.02±0.96	11.10±1.70	11.00±1.60		9.83±0.51	10.69±0.55	11.03±0.5
This study	Early Holocene	mH3	HAMTAH-1402	32.301	77.368	3769	2.0	2.7	0.0	0.887	19.86±1.69	07KNSTD		6.24±0.51		5.93±0.48	6.18±0.75	6.26±0.77	5.61±0.57	5.45±0.64	6.00±1.30	6.50±1.30	5.95±0.94	5.35±0.46	6.00±0.51	6.33±0.5
This study	Early Holocene	mH3	HAMTAH-1403	32.300	77.367	3808	1.0	2.7	0.0	0.879	58.05±2.35	07KNSTD		16.1±1.03		15.67±0.87	17.10±1.30	17.30±1.40	15.60±1.30	15.70±1.40	16.70±2.30	17.10±2.30	16.50±2.20	15.36±0.62	15.24±0.62	15.36±0.6
This study	Early Holocene	mH3	HAMTAH-1404	32.299	77.366	3808	2.0	2.7	0.0	0.879	12.21±0.57	07KNSTD		4.05±0.28		3.79±0.23	3.87±0.38	3.90±0.40	3.60±0.30	3.31±0.31	3.70±0.73	4.12±0.73	3.72±0.54	3.25±0.15	3.71±0.18	3.87±0.1
This study	Early Holocene	mH3	HAMTAH-1503	32.294	77.365	4112	3.0	2.7	0.0	0.898	41.47±0.86	07KNSTD		10.36±0.53		10.02±0.47	10.76±0.89	10.91±0.97	9.57±0.86	9.50±0.80	10.30±1.60	10.90±1.60	10.20±1.50	9.33±0.19	10.21±0.21	10.48±0.2
This study	Early Holocene	mH3	HAMTAH-1504	32.295	77.366	4083	3.0	2.7	0.0	0.879	38.89±0.73	07KNSTD		10.13±0.54		9.77±0.47	10.46±0.86	10.61±0.94	9.28±0.82	9.23±0.77	10.00±1.60	10.60±1.60	9.90±1.40	9.07±0.17	10.01±0.19	10.23±0.1
Seong et al., 2009	Olimde 3 stage	m3F	MUST-1	38.467	75.061	3689	5.0	2.70	0.0	1.000	45.30±1.18	KNSTD	10.25±0.15	10.31±0.5	Chi-squared: 0.10 Skewness: +1.26 Outlier: 0 Wt. mean: 10.25±0.15 ka Ar. mean: 10.25±0.15 ka Peak: 10.24 ka	10.04±0.57	10.56±0.87	10.68±0.95	10.02±0.87	9.91±0.86	10.80±1.60	11.10±1.60	10.50±1.50	10.34±0.27	10.40±0.27	9.79±0.2
Seong et al., 2009	Olimde 3 stage	m3F	MUST-2	38.467	75.062	3681	5.0	2.70	0.0	1.000	44.85±1.18	KNSTD		10.26±0.5	Regional glacial stage: ~10.9–9.3 ka, Weighted mean: 10.06±0.42 ka, n: 17, Dispersion: 0 %, P(sig 2-tailed): 0.00	10±0.57	10.50±0.86	10.68±0.95	10.02±0.87	9.91±0.86	10.70±1.60	11.10±1.60	10.50±1.50	10.30±0.27	10.34±0.27	9.73±0.2
Seong et al., 2009	Olimde 3 stage	m3F	MUST-3	38.465	75.065	3700	5.0	2.70	0.0	1.000	46.66±1.45	KNSTD		10.54±0.53		10.22±0.59	10.81±0.91	11.00±1.00	10.33±0.92	10.20±0.90	11.00±1.60	11.40±1.60	10.60±1.50	10.66±0.33	10.02±0.3	
Seong et al., 2009	Olimde 3 stage	m3F	MUST-4	38.464	75.065	3709	5.0	2.70	0.0	1.000	45.12±1.18	KNSTD		10.18±0.5		9.91±0.57	10.40±0.87	10.58±0.94	9.93±0.87	9.82±0.85	10.60±1.60	11.00±1.60	10.40±1.40	10.22±0.27	10.27±0.27	9.65±0.2
Seong et al., 2009	Olimde 3 stage	m3F	MUST-5	38.466	75.062	3688	5.0	2.70	0.0	1.000	44.31±1.18	KNSTD		10.12±0.5		9.85±0.58	10.33±0.86	10.51±0.93	9.86±0.87	9.75±0.84	10.50±1.60	11.00±1.60	10.40±1.40	10.17±0.27	10.21±0.27	9.58±0.2
Seong et al., 2009	Olimde 3 stage	m3F	MUST-6	38.467	75.061	3685	5.0	2.70	0.0	1.000	44.12±1.09	KNSTD		10.1±0.5		9.83±0.58	10.31±0.85	10.49±0.93	9.83±0.86	9.73±0.83	10.50±1.60	10.90±1.60	10.30±1.40	10.16±0.25	10.19±0.25	9.56±0.2
Seong et al., 2009	Olimde 3 stage	m3F'	MUST-7	38.511	75.034	3535	5.0	2.70	0.0	1.000	42.23±1.54	KNSTD	9.80±0.32	10.43±0.55	Chi-squared: 0.43 Skewness: +0.21 Outlier: 1 Wt. mean: 9.71±0.32 ka Ar. mean: 9.69±0.32 ka Peak: 9.70 ka	10.2±0.62	10.76±0.95	10.91±1.00	10.22±0.93	10.10±0.92	11.00±1.60	11.40±1.60	10.60±1.50	10.55±0.39	10.54±0.39	9.92±0.3
Seong et al., 2009	Olimde 3 stage	m3F'	MUST-8	38.516	75.032	3534	5.0	2.70	0.0	1.000	41.32±1.09	KNSTD		10.23±0.51		10.02±0.58	10.54±0.87	10.71±0.94	10.00±0.87	9.89±0.85	10.80±1.60	11.20±1.60	10.60±1.50	10.32±0.27	10.32±0.27	9.71±0.2
Seong et al., 2009	Olimde 3 stage	m3F'	MUST-9	38.520	75.031	3521	5.0	2.70	0.0	1.000	39.69±0.99	KNSTD		9.94±0.49		9.73±0.58	10.20±0.82	10.36±0.92	9.66±0.86	9.56±0.82	10.50±1.60	11.00±1.40	10.08±0.25	10.06±0.25	9.39±0.2	
Seong et al., 2009	Olimde 3 stage	m3F'	MUST-10	38.521	75.032	3517	5.0	2.70	0.0	1.000	36.89±0.99	KNSTD		9.25±0.54		8.99±0.63	9.49±0.79	9.60±0.90	8.96±0.79	8.91±0.77	9.70±1.50	10.20±1.50	9.60±1.40	9.44±0.26	9.52±0.26	8.75±0.2
Seong et al., 2009	Olimde 3 stage	m3F'	MUST-11	38.520	75.034	3494	5.0	2.70	0.0	1.000	36.62±0.99	KNSTD		9.31±0.54		9.55±0.81	9.71±0.91	9.00±0.80	8.96±0.78	9.80±1.50	10.20±1.50	9.60±1.40	9.58±0.26	9.49±0.26	8.79±0.2	
Seong et al., 2009	Olimde 3 stage	m3F'	MUST-12	38.521	75.034	3490	5.0	2.70	0.0	1.000	38.34±0.99	KNSTD		9.78±0.5		9.56±0.61	10.04±0.81	10.20±0.87	9.48±0.84	9.40±0.81	10.30±1.60	10.70±1.60	10.10±1.40	9.98±0.26	9.92±0.26	9.23±0.2
Seong et al., 2009	Olimde 3 stage	m3F'	MUST-13	38.514	75.035	3511	5.0	2.70	0.0	1.000	38.07±1.27	KNSTD		9.6±0.56		9.37±0.66	9.84±0.88	10.00±0.94	9.30±0.85	9.22±0.82	10.10±1.60	10.50±1.60	9.90±1.40	9.83±0.33	9.77±0.33	9.06±0.30
Seong et al., 2009	Olimde 3 stage	m3F'	MUST-14	38.513	75.035	3521	5.0	2.70	0.0	1.000	38.70±0.99	KNSTD		9.71±0.51		9.48±0.62	9.95±0.85	10.10±0.90	9.40±0.83	9.30±0.80	10.20±1.60	10.60±1.60	10.00±1.40	9.92±0.26	9.86±0.25	9.16±0.24
Seong et al., 2009	Olimde 4 Stage	m4H	KONG_8	38.640	75.003	3639	5.0	2.70	0.0	0.980	33.55±0.99	KNSTD	7.98±0.09	7.95±0.44	Chi-squared: 0.06 Skewness: +1.21 Outlier: 0 Wt. mean: 7.98±0.09 ka Ar. mean: 7.98±0.09 ka Peak: 7.99 ka	7.68±0.44	8.14±0.64	8.30±0.70	7.72±0.65	7.65±0.67	8.30±1.30	8.70±1.30	8.10±1.10	8.03±0.24	8.08±0.24	7.56±0.2
Seong et al., 2009	Olimde 4 Stage	m4H	KONG_9	38.640	75.004	3637	5.0	2.70	0.0	0.980	33.09±0.99	KNSTD		7.86±0.42	Regional glacial stage: ~8.2–7.4 ka, Weighted mean: 7.83±0.23 ka, n: 17, Dispersion: 0 %, P(sig 2-tailed): 0.004	7.59±0.43	8.05±0.62	8.17±0.67	7.63±0.64	7.60±0.67	8.20±1.30	8.70±1.30	8.10±1.10	7.92±0.24	7.98±0.24	7.47±0.2
Seong et al., 2009	Olimde 4 Stage	m4H	KONG_10	38.640	75.004	3638	5.0	2.70	0.0	0.980	33.82±0.99	KNSTD		8.01±0.44		7.63±0.44	8.21±0.65	8.34±0.73	7.79±0.66	7.73±0.68	8.40±1.30	8.90±1.30	8.20±1.10	8.15±0.24	8.15±0.24	7.58±0.2
Seong et al., 2009	Olimde 4 Stage	m4H	KONG_11	38.641	75.005	3639	5.0	2.70	0.0	0.980	33.64±1.09	KNSTD		7.97±0.44		7.71±0.45	8.16±0.63	8.29±0.75	7.74±0.66	7.72±0.68	8.40±1.30	8.80±1.30	8.20±1.10	8.05±0.24	8.10±0.24	7.58±0.2
Seong et al., 2009	Olimde 4 Stage	m4H	KONG_12	38.641	75.005	3641	5.0	2.70	0.0	0.980	34.54±0.99	KNSTD		8.17±0.44		7.90±0.46	8.36±0.66	8.50±0.79	7.94±0.67	7.92±0.69	8.60±1.30	9.00±1.30	8.40±1.30	8.30±0.24	8.30±0.24	7.78±0.2
Seong et al., 2009	Olimde 4 Stage	m4H	KONG_13	38.641	75.006	3652	5.0	2.70	0.0	0.980	33.73±1.63	KNSTD		7.94±0.51		7.66±0.5	8.12±0.72	8.25±0.78	7.71±0.73	7.69±0.75	8.30±1.30	8.70±1.30	8.10±1.10	8.01±0.39	8.07±0.39	7.55±0.3
Seong et al., 2009	Olimde 4 Stage	m6A	MUST-27	38.364	75.171	4023	5.0	2.70	0.0	0.990	38.97±1.18	KNSTD	7.77±0.26	7.52±0.39	Chi-squared: 0.48 Skewness: +0.65 Outlier: 0 Wt. mean: 7.77±0.26 ka Ar. mean: 7.80±0.26 ka Peak: 7.72 ka	7.26±0.38	7.65±0.55	7.77±0.63	7.30±0.62	7.27±0.64	7.70±1.10	8.20±1.10	7.58±0.98	7.45±0.23	7.60±0.23	7.14±0.2
Seong et al., 2009	Olimde 4 Stage	m6A	MUST-28	38.364	75.171	4024	5.0	2.70	0.0	0.990	41.41±1.09	KNSTD		7.98±0.42		7.61±0.42	8.07±0.61	8.18±0.68	7.74±0.64	7.72±0.67	8.20±1.20	8.60±1.20	8.00±1.00	7.96±0.21	8.12±0.21	7.59±0.2
Seong et al., 2009	Olimde 4 Stage	m6A	MUST-29	38.364	75.171	4025	5.0	2.70	0.0	0.990	40.06±1.09	KNSTD		7.72±0.4		7.4±0.39	7.82±0.59	7.96±0.62	7.49±0.62	7.46±0.65	7.90±1.20	8.60±1.20	7.84±0.21	7.84±0.21	7.33±0.2	
Seong et al., 2009	Olimde 4 Stage	m6A	MUST-30	38.364	75.171	4026	5.0	2.70	0.0	0.990	42.23±1.09	KNSTD		8.2±0.44		7.84±0.44	8.29±0.68	8.44±0.73	7.96±0.66	7.94±0.68	8.40±1.30	8.90±1.30	8.20±1.20	8.34±0.22	7.81±0.2	
Seong et al., 2009	Olimde 4 Stage	m6A	MUST-31	38.363	75.171	4028	5.0	2.70	0.0	0.990	38.97±0.99	KNSTD		7.57±0.38		7.3±0.37	7.70±0.57	7.70±0.57	7.30±0.60	7.32±0.63	7.80±1.10	8.20±1.10	7.63±0.98	7.50±0.19	7.67±0.20	7.20±0.1
Seong et al., 2009	Olimde 4 Stage	m5A	MUST-21	38.393	75.171	3862	5.0	2.70	0.0	1.000	39.15±0.99	KNSTD	7.74±0.24	8.11±0.43	Chi-squared: 0.41 Skewness: +0.12 Outlier: 0 Wt. mean: 7.74±0.24 ka Ar. mean: 7.74±0.24 ka Peak: 7.73 ka	7.79±0.44	8.25±0.64	8.40±0.72	7.88±0.66	7.86±0.68	8.40±1.30	8.90±1.30	8.20±1.10	8.17±0.21	8.26±0.21	7.72±0.2
Seong et al., 2009	Olimde 4 Stage	m5A	MUST-22	38.393	75.172	3864	5.0	2.70	0.0	1.000	36.62±0.99	KNSTD		7.6±0.39		7.35±0.38	7.76±0.56	7.88±0.66	7.37±0.61	7.34±0.64	7.90±1.20	8.30±1.20	8.00±1.10	7.55±0.21	7.69±0.21	7.22±0.2
Seong et al., 2009	Olimde 4 Stage	m5A	MUST-23	38.393	75.172	3862	5.0	2.70	0.0	1.000	35.63±1.27	KNSTD		7.4±0.4		7.19±0.39	7.58±0.57	7.70±0.64	7.18±0.61	7.15±0.65	7.70±1.10	8.10±1.10	7.54±0.98	7.39±0.26	7.48±0.27	7.03±0.2
Seong et al., 2009	Olimde 4 Stage	m5A	MUST-24	38.393	75.171	3862	5.0	2.70	0.0	1.000	36.44±1.36	KNSTD		7.56±0.43		7.70±0.60	7.86±0.65	7.34±0.64	7.31±0.67	7.80±1.20	8.30±1.20	8.00±1.00	7.52±0.28	7.65±0.29	7.19±0.2	
Seong et al., 2009	Olimde 4 Stage	m5A	MUST-25	38.393	75.171	3862	5.0	2.70	0.0	1.000	37.89±0.99	KNSTD		7.87±0.41		8.00±0.60	8.14±0.68	7.63±0.63	7.60±0.66	8.10±1.20	8.60±1.20	8.00±1.10	7.99±0.21	7.47±0.2		
Seong et al., 2009	Olimde 4 Stage	m5A	MUST-26	38.393	75.172	3861	5.0	2.70	0.0	1.000	38.16±0.99	KNSTD		7.92±0.41		7.61±0.42	8.06±0.61	8.20±0.69	7.69±0.64	7.66±0.66	8.20±1.30	8.60±1.30	8.00±1.10	7.95±0.21	8.06±0.21	7.53±0.2
Seong et al., 2007	Mungo 2 stage	m2G	K2-65	35.672	75.814	3113	3.0	2.70	0.0	0.800	36.17±0.90	KNSTD	6.63±0.30	14.7±0.7	Chi-squared: 0.68 Skewness: -1.13 Outlier: 2 Wt. mean: 6.63±0.30 ka Ar. mean: 6.64±0.30 ka Peak: 6.68 ka	15±0.81	15.90±1.20	16.10±1.30	14.60±1.10	14.90±1.20	16.10±2.30	16.40±2.30	15.90±2.10	14.44±0.36	14.24±0.30	14.25±0.3
Seong et al., 2007	Mungo 2 stage	m2G	K2-66	35.672	75.814	3128	3.0	2.70	0.0	0.800	14.47±0.90	KNSTD		6.17±0.41		6.42±0.44	6.54±0.76	6.62±0.82	5.88±0.58	5.76±0.61	6.40±1.00	7.00±1.00	6.50±1.10	6.54±0.41	6.19±0.39	5.64±0.3
Seong et al., 2007	Mungo 2 stage	m2G	K2-67	35.672	75.814	3122	3.0	2.70	0.0	0.800	15.37±0.90	KNSTD		6.6±0.44		6.86±0.46	7.14±0.64	7.26±0.68	6.53±0.58	6.42±0.65	7.00±1.10	7.00±1.10	7.00±1.00	7.00±0.41	6.67±0.39	6.11±0.3
Seong et al., 2007	Mungo 2 stage	m2G	K2-68	35.672	75.814	3113	3.0	2.70	0.0	0.800	16.28±0.90	KNSTD		6.87±0.44		7.14±0.47	7.44±0.64	7.50±0.68	6.60±0.60	6.53±0.67	7.20±1.10	7.00±1.10	7.00±1.00	7.25±0.40	6.95±0.39	6.40±0.3
Seong et al., 2007	Mungo 2 stage	m2G	K2-69	35.703	75.954	3109	3.5				18.99±0.90	KNSTD		7.99±0.52		8.23±0.62	8.64±0.85	8.73±0.91	7.67±0.71	7.67±0.74	8.70±1.50	9.20±1.50	8.60±1.30	8.09±0.39	8.47±0.40	7.51±0.3
Seong et al., 2007	Mungo 2 stage	m2G	K2-70	35.703	75.952	3106	2.0			0.790	16.28±0.90	KNSTD		6.93±0.44		7.18±0.47	7.49±0.65	7.55±0.68	6.64±0.58	6.58±0.67	7.20±1.00	8.00±1.20	7.00±1.00	7.29±0.41	6.99±0.39	6.45±0.3
Seong et al., 2007	Askole 2 stage	m2b	K2-116	35.292	75.662	2276	4.0	2.70	0.0	1.000	10.85±1.81	KNSTD	5.83±0.60	6.77±1.10	Chi-squared: 0.92 Skewness: +0.33 Outlier: 0 Wt. mean: 5.83±0.60 ka Ar. mean: 5.98±0.60 ka Peak: 5.68 ka	6.33±0.95	7.00±1.30	6.90±1.30	6.10±1.10	5.90±1.20	7.20±1.50	7.50±1.50	7.00±1.50	7.10±1.50	6.89±1.15	6.38±1.06
Seong et al., 2007	Askole 2 stage	m2b	K2-117	35.292	75.662	2276				1.000	8.14±1.00	KNSTD		5.40±0.61		4.97±0.59	5.35±0.33	5.35±0.36	4.68±0.35	4.50±0.36	5.44±0.66	5.66±0.66	5.40±0.61	0.00±0.00	0.00±0.00	
Seong et al., 2007	Askole 2 stage	m2b	K2-118	35.315	75.626	2276				1.000	9.95±1.00	KNSTD		6.34±0.61		5.90±0.56	6.46±0.53	6.45±0.58	5.60±0.40	5.49±0.44	6.60±1.10	7.00±1.10	6.56±0.98	0.00±0.00	0.00±0.00	
Seong et al., 2007	Askole 2 stage	m2b	K2-119	35.314	75.625	2276				1.000	8.14±1.00	KNSTD		5.40±0.61		4.97±0.58	5.35±0.33	5.35±0.36	4.68±0.35	4.49±0.36	5.44±0.66	5.66±0.66	5.40±0.61	0.00±0.00	0.00±0.00	
Seong et al., 2009	Olimde 5 stage	m6C'	MUST-76	38.292	75.025	4477	5.0	2.70	0.0	0.990	36.08±0.81	KNSTD	5.06±0.12	5.75±0.26	Chi-squared: 0.33 Skewness: +1.69 Outlier: 0 Wt. mean: 5.06±0.12 ka Ar. mean: 5.05±0.12 ka Peak: 5.05 ka	5.55±0.31	5.53±0.31	5.55±0.44	5.51±0.44	5.30±0.46	5.50±0.82	5.83±0.82	5.40±0.62	5.61±0.13	5.72±0.13	5.27±0.1
Seong et al., 2009	Olimde 5 stage	m6C'	MUST-77	38.292	75.025	4473	5.0	2.70	0.0	0.990	30.47±0.90	KNSTD		4.98±0.26	Regional glacial stage: ~6.9–4.3 ka, Weighted mean: 5.13±1.11 ka, n: 17, Dispersion: 19 %, P(sig 2-tailed): 0.00	4.88±0.28	4.85±0.36	4.93±0.38	4.71±0.38	4.50±0.40	4.77±0.58	5.18±0.58	4.67±0.67	4.68±0.14	4.82±0.14	4.46±0.1
Seong et al., 2009	Olimde 5 stage	m6C'	MUST-78	38.293	75.024	4461	5.0	2.70	0.0	0.990	31.92±0.90	KNSTD		5.22±0.25		5.12±0.27	5.07±0.35	5.16±0.38	4.94±0.38	4.78±0.42	5.00±0.57	5.37±0.57	4.91±0.63	5.14±0.15	4.70±0.1	
Seong et al., 2009	Olimde 5 stage	m6C'	MUST-79	38.293	75.025	4473	5.0	2.70	0.0	0.990	30.38±0.90	KNSTD		4.96±0.25		4.87±0.27	4.83±0.36	4.92±0.38	4.70±0.39	4.50±0.40	4.76±0.59	5.17±0.59	4.66±0.66	4.66±0.14	4.81±0.10	4.45±0.1
Hedrick et al., 2011	KM-4 stage	mG2	TM-B	32.971	78.182	5306	2.0	2.70	0.0	1.000	47.04±8.73	07KNSTD	4.94±0.28	5.86±0.95	Chi-squared: 13.12 Skewness: +0.03 Outlier: 2 Wt. mean: 4.43±1.17 ka Ar. mean: 4.66±1.17 ka Peak: 4.93 ka	5.41±0.95	5.40±1.10	5.90±1.10	6.00±1.00	5.80±1.20	5.00±1.20	5.80±1.30		5.99±1.11	5.27±0.9	
Hedrick et al., 2011	KM-4 stage	mG2	TM-C	32.971	78.182	5309	3.0	2.70	0.0	1.000	207.93±15.08	07KNSTD		22.93±1.71		22.14±1.58	23.00±2.10	23.40±2.20	22.80±2.30	23.90±2.60	21.90±3.00	22.00±3.00	21.50±2.70	21.38±1.56	22.38±1.63	23.56±1.7
Hedrick et al., 2011	KM-4 stage	mG2	TM-D	32.971	78.182	5309	3.0	2.70	0.0	1.000	33.21±6.28	07KNSTD		4.35±0.78		4.54±0.81	4.34±0.98	4.00±1.07	4.07±0.75	3.80±0.78	3.90±1.20	4.40±1.20	4.30±0.82	4.27±0.81	3.75±0.7	
Hedrick et al., 2011	KM-4 stage	mG2	TM-F	32.971	78.181	5318	1.0	2.70	0.0	1.000	26.54±3.79	07KNSTD		3.45±0.49		3.59±0.52	3.34±0.52	3.41±0.56	3.28±0.51	2.98±0.49	3.11±0.64	3.43±0.64	3.08±0.54	3.33±0.48	3.34±0.48	2.93±0.4
This study	Neoglacial	mG2	KO-17	32.971	78.179	5331	3.0	2.7	0.0	0.984	23.57±0.97	07KNSTD		3.29±0.23		3.16±0.23	3.07±0.25	3.12±0.25	2.77±0.25	2.72±0.25	2.90±0.44	3.16±0.44	2.88±0.29	2.67±0.11	3.07±0.13	3.06±0.1
This study	Neoglacial	mG2	KO-18	32.971	78.178	5337	2.0	2.7	0.0	0.985	36.75±1.19	07KNSTD		4.93±0.28		4.74±0.28	4.80±0.39	4.90±0.40	4.45±0.34	4.19±0.37	4.38±0.69	4.32±0.66	4.85±0.69	4.12±0.13	4.70±0.15	4.77±0.1
This study	Neoglacial	mG2	KO-1501	32.972	78.182	5327	1.0	2.7	0.0	0.990	47.97±1.22	07KNSTD		6.05±0.3		5.92±0.3	5.89±0.46	5.91±0.54	5.61±0.41	5.42±0.46	5.52±0.84	5.84±0.84	5.45±0.58	5.33±0.14	6.06±0.16	6.14±0.1
This study	Neoglacial	mG2	KO-1502	32.972	78.181	5334	2.0	2.7	0.0	0.990	105.93±1.35	07KNSTD		12.37±0.7		12.42±0.7	13.12±0.99	13.44±0.91	12.25±0.93	12.06±0.99	12.10±1.70	11.90±1.50	11.86±0.15	12.44±0.16	12.18±0.1	
Seong et al., 2009	Olimde 6 stage	m5H	KONG_18	38.649	75.032	4057	5.0	2.70	0.0	1.000	22.33±0.72	KNSTD	4.32±0.09	4.43±0.24	Chi-squared: 0.19 Skewness: +0.42 Outlier: 2 Wt. mean: 4.32±0.09 ka Ar. mean: 4.32±0.09 ka Peak: 4.32 ka	4.38±0.27	4.30±0.44	4.39±0.46	4.20±0.34	4.02±0.36	4.31±0.69	4.78±0.69	4.22±0.66	4.17±0.14	4.23±0.14	3.95±0.1
Seong et al., 2009	Olimde 6 stage	m5H	KONG_19	38.649	75.032	4057	5.0	2.70	0.0	1.000	21.70±0.81	KNSTD		4.31±0.25		4.31±0.25	4.28±0.41	4.25±0.45	4.09±0.34	3.90±0.35	4.18±0.76	4.56±0.76	4.04±0.15	4.12±0.16	3.84±0.1	
Seong et al., 2009	Olimde 6 stage	m5H	KONG_20	38.649	75.032	4060	5.0	2.70	0.0	1.000	21.25±0.81	KNSTD		4.22±0.25		4.17±0.28	4.05±0.42	4.14±0.45	4.00±0.33	3.82±0.35	4.08±0.79	4.54±0.79	3.99±0.63	3.98±0.15	4.04±0.16	3.75±0.1
Seong et al., 2009	Olimde 6 stage	m5H	KONG_21	38.645	75.031	4039	5.0	2.70	0.0	1.000	5.43±0.54	KNSTD		1.06±0.12	Regional glacial stage: ~4.5–2.8 ka, Weighted mean: 3.87±0.58 ka, n: 5, Dispersion: 5 %, P(sig 2-tailed): 0.00	1.02±0.12	1.15±0.11	1.16±0.13	1.12±0.13	0.99±0.14	1.15±0.20	1.20±0.20	1.14±0.16	1.05±0.11	1.06±0.11	0.97±0.1
Seong et al., 2009	Olimde 6 stage	m5H	KONG_22	38.645	75.031	4042	5.0	2.70	0.0	1.000	28.39±0.90	KNSTD		5.55±0.27		5.45±0.27	5.41±0.36	5.53±0.42	5.29±0.44	5.40±0.76	5.40±0.62	5.45±0.17	5.50±0.18	5.06±0.1		
Seong et al., 2009	Olimde 6 stage	m6H	KONG_23	38.644	75.028	4008	5.0	2.70	0.0	1.000	17.63±0.72	KNSTD	3.95±0.25	3.62±0.21	Chi-squared: 2.17 Skewness: -1.73 Outlier: 3 Wt. mean: 3.95±0.25 ka Ar. mean: 3.97±0.25 ka Peak: 4.13 ka	3.58±0.24	3.44±0.28	3.50±0.33	3.45±0.29	3.30±0.30	3.48±0.64	3.84±0.64	3.42±0.46	3.31±0.14	3.41±0.14	3.20±0.1
Seong et al., 2009	Olimde 6 stage	m6H	KONG_24	38.643	75.028	4005	5.0	2.70	0.0	1.000	9.13±0.63	KNSTD		1.85±0.16		1.8±0.17	1.89±0.24	1.93±0.25	1.80±0.20	1.69±0.19	1.90±0.42	2.23±0.42	1.87±0.33	1.66±0.12	1.73±0.12	1.66±0.1
Seong et al., 2009	Olimde 6 stage	m6H	KONG_25	38.645	75.026	3999	5.0	2.70	0.0	1.000	20.25±0.63	KNSTD		4.14±0.22		4.1±0.25	4.00±0.40	4.07±0.45	3.94±0.31	3.76±0.33	4.02±0.75	4.48±0.75	3.94±0.59	3.93±0.12	3.98±0.13	3.69±0.12
Seong et al., 2009	Olimde 6 stage	m6H	KONG_26	38.645	75.026	3997	5.0	2.70	0.0	1.000	20.25±0.67	KNSTD		4.15±0.24		4.15±0.24	4.07±0.41	4.08±0.46	3.94±0.32	3.76±0.34	4.03±0.75	4.55±0.76	3.98±0.14	3.98±0.14	3.70±0.11	
Seong et al., 2009	Olimde 6 stage	m6H	KONG_27	38.646	75.026	4000	5.0	2.70	0.0	1.000	14.20±0.72	KNSTD		2.94±0.2		2.91±0.23	2.88±0.21	2.90±0.20	2.84±0.24	2.63±0.26	2.89±0.41	3.20±0.41	2.86±0.32	2.76±0.14	2.81±0.14	2.59±0.1
Seong et al., 2009	Olimde 6 stage	m6H	KONG_28	38.646	75.026	4000	5.0	2.70	0.0	1.000	6.96±0.54	KNSTD		1.4±0.13		1.44±0.21	1.43±0.15	1.44±0.15	1.42±0.14	1.29±0.15	1.46±0.34	1.62±0.34	1.44±0.26	1.28±0.10	1.33±0.10	1.27±0.1
Hedrick et al., 2011	PM-2 stage	N/A	India-10	33.245	78.200	4910	3.0	2.70	0.0	1.000	62.54±3.21		3.42±0.71	8.94±0.67	Chi-squared: 17.79 Skewness: +1.18 Outlier: 4 Wt. mean: 3.42±0.71 ka Ar. mean: 3.50±0.71 ka Peak: 2.80 ka	9.05±0.77	9.32±0.92	9.50±0.99	8.51±0.85	8.50±0.82	8.70±1.50	9.30±1.50	9.00±1.30	9.45±0.49	9.31±0.48	8.36±0.4
Hedrick et al., 2011	PM-2 stage	N/A	India-11	33.245	78.201	4905	3.0			1.000	24.59±2.50			3.45±0.45		6.44±0.46	6.41±0.73	6.54±0.77	5.99±0.58	5.85±0.62	6.00±1.30	6.60±1.30	5.91±0.88	6.33±0.45	5.77±0.4	
Hedrick et al., 2011	PM-2 stage	N/A	India-12	33.245	78.201	4904	3.0			1.000	20.84±1.97			3.25±0.33		3.40±0.36	3.17±0.37	3.23±0.37	3.10±0.34	2.81±0.35	3.00±0.52	3.32±0.52	3.00±0.35	3.14±0.30	2.77±0.2	
Hedrick et al., 2011	PM-2 stage	N/A	India-13	33.245	78.201	4899	2.0			1.000	307.50±7.55			39.27±1.69		37.82±2.04	36.50±2.40	37.20±2.60	37.70±2.70	42.00±3.60	36.30±4.40	35.50±4.10	36.25±0.90	38.26±0.95	41.32±1.0	
Hedrick et al., 2011	PM-2 stage	N/A	India-14	33.245	78.202	4886	2.0			1.000	5.45±1.22			0.81±0.19		0.84±0.2	1.01±0.14	1.01±0.16	0.92±0.17	0.74±0.18	0.95±0.25	0.97±0.21	0.89±0.20	0.73±0.1		
Hedrick et al., 2011	PM-2 stage		India-56	33.244	78.198	4924	3.0	2.70	0.0	1.000	29.04±0.75			4.46±0.22		4.65±0.26	4.50±0.40	4.58±0.43	4.17±0.31	3.92±0.33	4.16±0.74	4.65±0.74	4.11±0.65	4.42±0.11	4.35±0.11	3.85±0.10
Hedrick et al., 2011	PM-2 stage		India-57	33.245	78.199	4924	3.0	2.70	0.0	1.000	17.76±0.70			2.78±0.18		2.91±0.21	2.82±0.15	2.85±0.17	2.70±0.22	2.40±0.22	2.68±0.28	2.94±0.30	2.75±0.11	2.74±0.11	2.36±0.0	
Dortch et al., 2013	Ladakh Chang La cirque	N/A	Chang-1	34.040	77.930	5461	5.0	2.70	0.0	1.000	17.00±2.00		2.31±0.24	2.02±0.27	Chi-squared: 2.02 Skewness: +0.72 Outlier: 2 Wt. mean: 2.31±0.24 ka Ar. mean: 2.29±0.24 ka Peak: 2.15 ka	2.07±0.29	2.16±0.35	2.21±0.34	1.99±0.29	1.79±0.26	1.97±0.45	2.26±0.45	1.95±0.19	1.88±0.22	1.92±0.23	1.77±0.2
Dortch et al., 2013	Ladakh Chang La cirque	N/A	Chang-2	34.040	77.930	5459	3.0			1.000	20.00±2.00			2.36±0.28		2.44±0.31	2.51±0.26	2.56±0.24	2.34±0.31	2.08±0.27	2.31±0.39	2.54±0.40	2.29±0.23	2.34±0.23	2.05±0.2	
Dortch et al., 2013	Ladakh Chang La cirque	N/A	Chang-3	34.040	77.930	5458	4.0			1.000	22.00±1.00			2.65±0.18		2.73±0.21	2.71±0.16	2.75±0.18	2.59±0.22	2.30±0.21	2.53±0.33	2.80±0.33	2.51±0.12	2.62±0.12	2.27±0.10	
Dortch et al., 2013	Ladakh Chang La cirque	N/A	Chang-4	34.040	77.930	5460	5.0			1.000	55.00±2.00			6.27±0.31		6.31±0.33	6.20±0.60	6.39±0.67	5.96±0.48	5.77±1.20	6.52±1.20	5.77±0.76	6.44±0.24	5.72±0.2		
Dortch et al., 2013	Ladakh Chang La cirque	N/A	Chang-5	34.040	77.930	5462	4.0			1.000	18.00±1.00			2.13±0.16		2.13±0.16	2.28±0.23	2.33±0.22	2.10±0.22	1.88±0.19	2.08±0.36	2.37±0.36	2.05±0.34	1.99±0.11	2.02±0.11	1.85±0.10
Dortch et al., 2013	Ladakh Chang La cirque	N/A	Chang-6	34.040	77.930	5445	5.0			1.000	97.00±3.00			10.8±0.51	Regional glacial stage: ~2.7–1.8 ka, Weighted mean: 2.19±0.22 ka, n: 13, Dispersion: 3.1 %, P(sig 2-tailed): 0.00	10.7±0.54	11.19±0.92	11.00±0.90	10.48±0.93	10.90±1.60	10.30±1.60	10.93±0.34	11.03±0.34	10.17±0.3		
Seong et al., 2009	Olimde 7 stage	m7A	MUST-32	38.361	75.171	4082	5.0	2.70	0.0	0.990	10.76±0.54	KNSTD	2.19±0.07	2.15±0.16	Chi-squared: 0.19 Skewness: +1.07 Outlier: 1 Wt. mean: 2.19±0.07 ka Ar. mean: 2.20±0.07 ka Peak: 2.19 ka	2.1±0.17	2.24±0.23	2.28±0.26	2.11±0.21	1.94±0.19	2.22±0.34	2.54±0.34	2.19±0.35	1.93±0.10	2.00±0.10	1.91±0.10
Seong et al., 2009	Olimde 7 stage	m7A	MUST-33	38.361	75.171	4081	5.0	2.70	0.0	0.990	11.21±0.54	KNSTD		2.24±0.16		2.2±0.18	2.34±0.22	2.38±0.24	2.21±0.22	2.00±0.20	2.32±0.43	2.60±0.43	2.26±0.34	2.03±0.10	2.10±0.10	1.99±0.10
Seong et al., 2009	Olimde 7 stage	m7A	MUST-34	38.360	75.172	4094	5.0	2.70	0.0	0.990	11.66±0.54	KNSTD		2.32±0.17		2.69±0.19	2.72±0.17	2.76±0.18	2.64±0.22	2.43±0.22	2.71±0.32	3.00±0.32	2.68±0.32	2.62±0.11	2.62±0.11	2.39±0.10
Seong et al., 2009	Olimde 7 stage	m7A	MUST-35	38.359	75.172	4120	5.0	2.70	0.0	0.980	13.56±0.54	KNSTD		2.71±0.17		2.69±0.18	2.74±0.16	2.78±0.18	2.66±0.22	2.45±0.21	2.62±0.32	3.20±0.32	2.71±0.32	3.00±0.32	2.68±0.32	2.62±0.1
Seong et al., 2009	Olimde 7 stage	m7A	MUST-36	38.356	75.173	4167	5.0	2.70	0.0	0.990	11.48±0.54	KNSTD		2.19±0.15		2.15±0.17	2.26±0.23	2.30±0.23	2.12±0.21	1.97±0.19	2.26±0.34	2.50±0.34	2.18±0.35	1.97±0.09	2.00±0.09	1.91±0.0
Seong et al., 2009	Olimde 7 stage	m7A	MUST-37	38.356	75.173	4176	5.0	2.70	0.0	0.990	11.30±0.45	KNSTD		2.15±0.14		2.15±0.14	2.23±0.22	2.28±0.24	2.10±0.24	1.95±0.18	2.21±0.33	2.54±0.33	2.18±0.35	1.92±0.08	2.00±0.08	1.91±0.0
Seong et al., 2009	Olimde 7 stage	m7A	MUST-38	38.355	75.173	4180	5.0	2.70	0.0	0.990	11.21±0.81	KNSTD		2.12±0.16		2.12±0.16	2.18±0.24	2.23±0.22	2.09±0.25	1.92±0.18	2.21±0.33	2.50±0.34	2.18±0.35	1.90±0.14	1.98±0.14	1.91±0.0
This study	Late Holocene	mG1	KO-14	32.967	78.179	5374	3.0	2.7	0.0	0.961	17.10±0.72	07KNSTD	2.10±0.34	2.36±0.19	Chi-squared: 9.37 Skewness: -1.07 Outlier: 2 Wt. mean: 2.10±0.34 ka	2.27±0.19	2.43±0.19	2.47±0.21	2.24±0.22	1.98±0.18	2.22±0.37	2.49±0.37	2.21±0.33	1.95±0.08	2.20±0.09	2.20±0.0
This study	Late Holocene	mG1	KO-15	32.968	78.180	5366	3.0	2.7	0.0	0.966	4.93±0.26	07KNSTD		0.64±0.05		0.62±0.05	0.82±0.06	0.82±0.08	0.73±0.06	0.57±0.06	0.74±0.12	0.72±0.10	0.56±0.03	0.72±0.04	0.73±0.0	
This study	Late Holocene	mG1	KO-16	32.968	78.180	5366	4.0	2.7	0.0	0.966	3.87±0.32	07KNSTD		0.5±0.06		0.48±0.06	0.66±0.07	0.67±0.09	0.58±0.06	0.45±0.05	0.59±0.10	0.57±0.10	0.59±0.09	0.44±0.04	0.57±0.03	0.58±0.0
This study	Late Holocene	mG1	KO1601	32.968	78.180	5374	2.0	2.7	0.0	0.966	13.40±0.39	07KNSTD		1.79±0.12		1.73±0.12	1.86±0.17	1.90±0.19	1.71±0.14	1.53±0.13	1.69±0.32	1.92±0.32	1.68±0.24	1.51±0.04	1.65±0.05	1.63±0.05

The following is a large multi-column data table (cosmogenic ^{10}Be exposure ages). Columns left-to-right: Reference | Local glacial stage | Sample code | Sample ID | Lat (°N) | Long (°E) | Elevation (m) | Thickness (cm) | Density | Erosion | Shielding | ^{10}Be age (ka) | Standard | Regional glacial stage / statistics | (grouped mean) | individual / scaling-model ages (ka).

Reference	Local stage	Code	Sample	Lat	Long	Elev	Thk	Dens	Er	Shield	Age/std	Std	Mean	Ages (ka, various scaling models)
This study	Late Holocene	mG1	KO1602	32.967	78.180	5388	1.5	2.7	0.0	0.954	18.94±0.71	07KNSTD		2.61±0.19	2.51±0.19 2.63±0.16 2.67±0.18 2.47±0.22 2.17±0.19 2.42±0.36 2.69±0.36 2.41±0.31 2.14±0.08 / 2.53±0.10 / 2.51±0.0 — Ar. Mean: 2.25±0.34 ka, Peak: 2.48 ka !
Seong et al., 2009	Olimde 7 stage	m7H	KONG_14	38.644	75.041	4168	5.0	2.70	0.0	1.000	9.58±0.99	KNSTD	1.66±0.14	1.78±0.21	1.72±0.22 1.80±0.26 1.80±0.30 1.76±0.24 1.63±0.23 1.81±0.49 2.12±0.49 1.78±0.34 1.58±0.16 / 1.67±0.17 / 1.60±0.1 — Chi-squared: 0.73
Seong et al., 2009	Olimde 7 stage	m7H	KONG_15	38.644	75.040	4178	5.0	2.70	0.0	1.000	5.15±0.90	KNSTD		0.94±0.17	0.89±0.17 1.05±0.14 1.06±0.16 1.02±0.17 0.87±0.18 1.04±0.21 1.08±0.21 1.03±0.18 0.97±0.17 / 0.97±0.17 / 0.86±0.1 — Skewness: −1.63 ka
Seong et al., 2009	Olimde 7 stage	m7H	KONG_16	38.644	75.040	4179	5.0	2.70	0.0	1.000	9.40±0.90	KNSTD		1.74±0.19	1.68±0.2 1.75±0.26 1.79±0.26 1.72±0.22 1.59±0.21 1.76±0.45 2.06±0.45 1.73±0.32 1.54±0.15 / 1.63±0.16 / 1.56±0.1 — Outlier: 1
Seong et al., 2009	Olimde 7 stage	m7H	KONG_17	38.643	75.039	4178	5.0	2.70	0.0	1.000	7.96±0.99	KNSTD		1.46±0.2	1.4±0.2 1.49±0.21 1.52±0.21 1.47±0.21 1.35±0.22 1.50±0.41 1.68±0.41 1.48±0.27 1.31±0.16 / 1.38±0.17 / 1.32±0.1 — Wt. mean: 1.66±0.14 ka, Ar. Mean: 1.46±0.14 ka
Seong et al., 2009	Olimde 7 stage of	m3I	KONG_35	38.709	75.280	3320	5.0	2.70	0.0	0.930	5.07±0.34	KNSTD	1.35±0.36	0.93±0.18	0.94±0.18 1.08±0.17 1.09±0.18 1.02±0.17 0.89±0.19 0.88±0.19 1.09±0.24 1.15±0.24 0.99±0.18 / 0.97±0.17 / 0.87±0.1
Seong et al., 2009	Olimde 7 stage of	m3I	KONG_36	38.709	75.280	3328	5.0	2.70	0.0	0.930	5.33±0.63	KNSTD		1.67±0.22	1.66±0.23 1.74±0.29 1.76±0.32 1.65±0.25 1.53±0.24 1.79±0.48 2.06±0.48 1.77±0.36 1.53±0.18 / 1.56±0.19 / 1.50±0.1 — Skewness: −0.03
Seong et al., 2009	Olimde 7 stage	m3I	KONG_37	38.711	75.280	3309	5.0	2.70	0.0	0.930	5.70±0.54	KNSTD		1.81±0.2	1.8±0.21 1.90±0.26 1.92±0.29 1.78±0.23 1.65±0.22 1.90±0.43 2.25±0.43 1.92±0.36 1.67±0.16 / 1.69±0.16 / 1.62±0.1 — Outlier: 1
Seong et al., 2009	Olimde 7 stage	m3I	KONG_38	38.714	75.280	3299	5.0	2.70	0.0	0.930	3.53±0.63	KNSTD		1.11±0.21	1.09±0.21 1.21±0.21 1.22±0.23 1.16±0.22 1.03±0.22 1.23±0.37 1.31±0.37 1.22±0.26 1.10±0.20 / 1.09±0.20 / 1.01±0.1 — Wt. mean: 1.39±0.36 ka
Seong et al., 2009	Olimde 7 stage	m3I	KONG_41	38.738	75.273	3118	5.0	2.70	0.0	0.930	1.27±0.45	KNSTD		0.43±0.16	0.43±0.16 0.56±0.22 0.56±0.22 0.50±0.18 0.41±0.17 0.55±0.22 0.63±0.22 0.55±0.21 0.43±0.16 / 0.43±0.16 / — — Ar. Mean: 1 ka !
Orr et al., 2017	N/A	mS3	ZK36	34.004	77.402	5280	3.0	2.70	0.0	0.960	16.20±1.20	07KNSTD	1.33±0.12	2.22±0.18	2.14±0.20 2.31±0.24 2.43±0.24 1.94±0.21 1.68±0.20 1.98±0.24 2.28±0.23 2.18±0.23 2.01±0.13 / 2.04±0.15 / 1.87±0.1 !
Orr et al., 2017	N/A	mG1	ZK36	34.004	77.461	5294	3.0	2.70	0.0	1.000	10.50±0.70	07KNSTD	1.33±0.12	1.29±0.11	1.41±0.12 1.5±0.15 1.20±0.12 1.34±0.12 1.26±0.11 1.35±0.15 / 1.36±0.12 / 1.23±0.08 — Regional glacial stage: ~1.8–0.9 ka; Weighted mean: 1.15±0.39 ka; n: 23; Dispersion: 25%; P(sig 2-tailed): 0.00
Orr et al., 2017	Late Holocene	nS2	STOK-1401	33.987	77.456	5329	3.0	2.7	0.0	0.964	15.57±0.51	07KNSTD	2.06±0.14	2.00±0.14 2.16±0.21 2.21±0.23 1.98±0.18 1.78±0.16 1.97±0.37 2.26±0.37 1.90±0.30 1.75±0.06 / 1.90±0.06 / 1.87±0.0 — Chi-squared: 21.83
Orr et al., 2017	Late Holocene	nS2	STOK-1402	33.988	77.456	5330	3.0	2.7	0.0	0.967	11.72±0.58	07KNSTD	1.48±0.12	1.59±0.14 1.61±0.13 1.50±0.12 1.33±0.13 1.48±0.30 1.60±0.30 1.31±0.07 / 1.43±0.07 / 1.38±0.0 — Skewness: +0.34
Orr et al., 2017	Late Holocene	nS2	STOK-1403	33.988	77.457	5323	1.0	2.7	0.0	0.969	14.65±0.65	07KNSTD	1.89±0.14	1.84±0.14 2.00±0.20 2.00±0.20 1.82±0.16 1.64±0.15 1.81±0.37 2.08±0.37 1.79±0.28 1.62±0.07 / 1.75±0.08 / 1.72±0.0 — Outlier: 3
Orr et al., 2017	Late Holocene	nS2	STOK-1404	33.988	77.457	5328	2.0	2.7	0.0	0.969	2.08±0.09	07KNSTD	0.25±0.02	0.25±0.02 0.34±0.04 0.35±0.04 0.32±0.03 0.24±0.02 0.30±0.05 0.29±0.05 0.30±0.04 0.23±0.01 / 0.32±0.01 / — — Wt. mean: 1.2±0.05 ka
Orr et al., 2017	Late Holocene	mS1	STOK-1405	33.987	77.460	5370	2.0	2.7	0.0	0.980	7.64±0.31	07KNSTD	1.2±0.05	0.93±0.07	0.92±0.07 1.08±0.07 1.10±0.07 1.02±0.07 0.84±0.08 1.02±0.13 1.05±0.13 1.00±0.10 0.82±0.03 / 0.98±0.04 / 0.98±0.0 — Ar. Mean: 1.4±0.05 ka
Orr et al., 2017	Late Holocene	mS1	STOK-1406	33.987	77.460	5314	2.5	2.7	0.0	0.980	4.54±0.22	07KNSTD		0.56±0.04	0.55±0.04 0.73±0.06 0.74±0.07 0.65±0.06 0.51±0.05 0.66±0.11 0.64±0.11 0.66±0.10 0.50±0.02 / 0.63±0.03 / 0.65±0.0 — Outlier: 1
Orr et al., 2017	Late Holocene	mS1	STOK-1407	33.987	77.461	5340	3.0	2.7	0.0	0.978	1.25±0.21	07KNSTD		0.14±0.03	0.14±0.03 0.20±0.03 0.21±0.03 0.19±0.04 0.14±0.03 0.18±0.04 0.17±0.04 0.18±0.04 0.14±0.02 / 0.19±0.03 / — — Peak: 1.97 ka !
Orr et al., 2017	Late Holocene	mS1	STOK-1408	33.987	77.461	5308	3.0	2.7	0.0	0.978	9.31±0.72	07KNSTD		1.19±0.11	1.17±0.11 1.29±0.13 1.31±0.11 1.23±0.11 1.06±0.12 1.21±0.24 1.28±0.24 1.21±0.14 1.04±0.08 / 1.16±0.09 / 1.14±0.0
This study	Late Holocene	mS1	STOK-1516	33.987	77.460	5303	3.0	2.7	0.0	0.977	7.37±0.65	07KNSTD		0.94±0.1	0.92±0.1 1.09±0.08 1.10±0.09 1.02±0.09 0.84±0.10 1.02±0.15 1.05±0.15 1.05±0.15 0.83±0.07 / 0.98±0.09 / 0.99±0.0
Seong et al., 2007	Askole 3 stage	m1H	K2-90	35.688	75.927	3095	3.0	2.70	0.0	0.960	1.81±0.90	KNSTD	1.03±0.28	0.70±0.34	0.66±0.32 0.84±0.07 0.84±0.07 0.74±0.05 0.60±0.05 0.83±0.14 0.83±0.14 0.83±0.11 0.00±0.00 / 0.00±0.00 / 0.00±0.0 — Chi-squared: 0.82
Seong et al., 2007	Askole 3 stage	m1H	K2-91	35.695	75.927	3096	3.0	2.70	0.0	0.960	3.62±0.90	KNSTD		1.34±0.35	1.41±0.38 1.49±0.39 1.50±0.34 1.36±0.34 1.22±0.35 1.50±0.60 1.70±0.60 1.30±0.33 1.28±0.32 / 1.28±0.32 / 1.20±0.3 — Skewness: −0.08
Seong et al., 2007	Askole 3 stage	m1H	K2-92	35.687	75.926	3094	3.0	2.70	0.0	0.960	2.71±0.90	KNSTD		1.05±0.36	1.00±0.34 1.16±0.07 1.16±0.08 1.07±0.07 0.92±0.07 1.16±0.18 1.22±0.18 1.16±0.13 0.00±0.00 / 0.00±0.00 / 0.00±0.0 — Outlier: 2
Seong et al., 2007	Askole 3 stage	m1H	K2-93	35.686	75.926	3090	2.0	2.70	0.0	0.960	7.23±0.90	KNSTD		2.75±0.37	2.94±0.41 2.88±0.33 2.90±0.31 2.70±0.40 2.43±0.39 2.90±0.54 3.16±0.54 2.88±0.41 2.77±0.35 / 2.66±0.33 / 2.38±0.3 — Wt. mean: 1.03±0.28 ka
Seong et al., 2007	Askole 3 stage	m1H	K2-94	35.294	75.925	3096	3.0	2.70	0.0	0.960	3.62±0.90	KNSTD		1.34±0.35	1.41±0.39 1.39 1.50±0.34 1.36±0.34 1.22±0.35 1.50±0.60 1.70±0.60 1.50±0.43 1.30±0.33 / 1.28±0.32 / 1.20±0.3 — Ar. Mean: 1.03±0.28 ka
Seong et al., 2007	Askole 3 stage	m1H	K2-95	35.292	75.662	3087	3.0	2.70	0.0	0.960	1.81±0.90	KNSTD		0.72±0.35	0.68±0.33 0.86±0.07 0.87±0.08 0.76±0.05 0.62±0.05 0.85±0.14 0.86±0.14 0.86±0.12 0.00±0.00 / 0.00±0.00 / 0.00±0.0 — Peak: 1.02 ka
Seong et al., 2007	Askole 3 stage	m1H	K2-96	35.292	75.662	3116	3.0	2.70	0.0	0.970	4.52±0.90	KNSTD		1.67±0.35	1.78±0.39 1.85±0.49 1.87±0.52 1.65±0.38 1.51±0.36 1.86±0.62 2.11±0.62 1.88±0.52 1.61±0.32 / 1.56±0.31 / 1.48±0.3
This study	Late Holocene	mM2	KO1	32.932	78.214	5532	3.0	2.7	0.0	0.991	20.44±0.66	07KNSTD	0.99±0.07	2.56±0.19	2.46±0.19 2.59±0.18 2.63±0.17 2.42±0.21 2.13±0.19 2.37±0.33 2.63±0.33 2.30±0.30 2.10±0.07 / 2.48±0.08 / 2.44±0.0 — Chi-squared: 0.90
This study	Late Holocene	mM2	KO-2	32.932	78.214	5541	6.0	2.7	0.0	0.991	9.03±0.53	07KNSTD		1.09±0.09	1.07±0.09 1.21±0.08 1.23±0.11 1.14±0.09 0.96±0.10 1.12±0.16 1.16±0.16 1.12±0.12 0.95±0.06 / 1.09±0.07 / 1.08±0.0 — Skewness: −0.17
This study	Late Holocene	mM2	KO-3	32.931	78.214	5548	4.0	2.7	0.0	0.991	8.18±0.39	07KNSTD		0.98±0.07	0.95±0.07 1.12±0.06 1.13±0.08 1.05±0.08 0.86±0.08 1.04±0.13 1.06±0.13 1.00±0.10 0.85±0.04 / 1.01±0.05 / 1.01±0.0 — Outlier: 1
This study	Late Holocene	mM2	MENTOK-1505	32.931	78.215	5569	2.0	2.7	0.0	0.991	8.76±0.32	07KNSTD		1.02±0.07	1.00±0.07 1.15±0.07 1.17±0.08 1.08±0.08 0.90±0.08 1.07±0.13 1.10±0.13 1.07±0.11 0.89±0.03 / 1.04±0.04 / 1.04±0.0 — Ar. Mean: 1.00±0.07 ka
This study	Late Holocene	mM2	MENTOK-1506	32.931	78.215	5574	1.0	2.7	0.0	0.992	7.84±0.50	07KNSTD		0.90±0.08	0.88±0.08 1.06±0.07 1.08±0.08 0.99±0.09 0.80±0.08 0.98±0.15 1.00±0.15 0.99±0.11 0.78±0.06 / 0.95±0.06 / 0.96±0.0 — Peak: 1 ka !
This study	Late Holocene	mM1	KO-7	32.933	78.214	5524	6.0	2.7	0.0	1.000	2.04±0.14	07KNSTD	0.67±0.07	0.24±0.02	0.23±0.02 0.32±0.03 0.33±0.04 0.30±0.03 0.22±0.02 0.28±0.05 0.28±0.05 0.28±0.05 0.22±0.01 / 0.30±0.02 / — — Chi-squared: 1.47
This study	Late Holocene	mM1	KO-8	32.933	78.214	5516	2.5	2.7	0.0	1.000	5.92±0.55	07KNSTD		0.69±0.08	0.68±0.08 0.88±0.11 0.90±0.11 0.79±0.09 0.62±0.08 0.79±0.15 0.78±0.15 0.78±0.15 0.61±0.06 / 0.77±0.07 / 0.78±0.0 — Skewness: −1.71
This study	Late Holocene	mM1	KO-9	32.934	78.215	5503	1.0	2.7	0.0	1.000	6.00±0.24	07KNSTD	0.67±0.07	0.70±0.05	0.68±0.05 0.89±0.08 0.91±0.07 0.79±0.06 0.62±0.06 0.80±0.13 0.79±0.13 0.80±0.10 0.61±0.02 / 0.78±0.03 / 0.79±0.0 — Outlier: 1; Wt. mean: 0.67±0.07 ka; Ar. Mean: 0.64±0.07 ka
This study	Late Holocene	mM1	KO10	32.934	78.215	5503	1.0	2.7	0.0	1.000	4.73±0.67	07KNSTD		0.54±0.09	0.53±0.09 0.72±0.10 0.73±0.11 0.63±0.10 0.49±0.08 0.64±0.13 0.62±0.13 0.64±0.13 0.48±0.07 / 0.62±0.09 / 0.63±0.0 — Peak: 0.69 ka
Seong et al., 2009	Olimde 8 stage	m8A	MUST-39	38.353	75.171	4228	5.0	2.70	0.0	1.000	2.62±0.45	KNSTD	0.66±0.22	0.46±0.08	0.46±0.08 0.58±0.12 0.59±0.12 0.54±0.10 0.40±0.09 0.56±0.12 0.54±0.12 0.55±0.12 0.43±0.08 / 0.52±0.09 / 0.43±0.0 — Chi-squared: 10.19
Seong et al., 2009	Olimde 8 stage	m8A	MUST-40	38.353	75.171	4227	5.0	2.70	0.0	1.000	5.52±0.45	KNSTD		0.99±0.09	0.95±0.1 1.10±0.08 1.10±0.08 1.06±0.11 0.92±0.11 1.08±0.17 1.12±0.17 1.01±0.08 / 1.01±0.08 / 0.90±0.0 — Skewness: −1.08
Seong et al., 2009			MUST-41	38.353	75.170	4238									— Outlier: 0; Wt. mean: 0.66±0.22 ka; Ar. Mean: 0.69±0.22 ka
	Olimde 8 stage	m8A					5.0	2.70	0.0	1.000	3.53±0.36	KNSTD		0.62±0.07	0.62±0.07 0.76±0.10 0.77±0.11 0.71±0.09 0.58±0.06 0.73±0.15 0.72±0.15 0.73±0.11 0.70±0.07 — Peak: 0.60 ka !
Saha et al. (2015)	N/A	N/A	ZK73	32.7927	77.4293	4757	5.0	2.70	0.0	1.000	3.10±0.50	KNSTD	0.59±0.11	0.51±0.09	0.52±0.09 0.68±0.14 0.72±0.11 0.59±0.10 0.47±0.08 0.62±0.12 0.61±0.12 0.62±0.13 0.60±0.10 / 0.58±0.09 / 0.46±0.0 — Chi-squared: 2.13
Saha et al. (2015)	N/A	N/A	ZK74	32.7929	77.4292	4764	5.0	2.70	0.0	1.000	4.40±0.70	KNSTD		0.72±0.12	0.75±0.13 0.93±0.12 0.97±0.13 0.82±0.13 0.66±0.12 0.86±0.20 0.87±0.20 0.87±0.18 0.83±0.13 / 0.81±0.13 / 0.65±0.1 — Skewness: !; Outlier: !; Wt. mean: 0.59±0.11 ka; Ar. Mean: 0.62±0.11 ka; Peak: 0.54 ka
Saha et al. (2015)	N/A	N/A	ZK75	32.7929	77.4292	4749	5.0	2.70	0.0	1.000	159.70±7.00	07KNSTD		23.16±1.31	22.67±1.3 23.60±1.80 24.80±1.80 23.10±1.90 24.30±2.20 22.90±3.20 23.00±3.20 22.50±2.90 21.82±0.96 / 22.56±1.00 / 23.84±1.0
Dortch et al., 2013	Pangong high cirque	N/A	Pang-25	33.890	78.430	5375	5.0	2.70	0.0	1.000	14.47±3.62	KNSTD	0.50±0.09	1.79±0.48	1.84±0.5 1.90±0.51 1.94±0.63 1.77±0.52 1.59±0.46 1.74±0.69 1.99±0.69 1.72±0.55 1.67±0.42 / 1.70±0.43 / 1.57±0.3 — Chi-squared: 0.63
Dortch et al., 2013	Pangong high cirque	N/A	Pang-26	33.890	78.430	5368	5.0	2.70	0.0	1.000	4.52±0.90	KNSTD		0.54±0.12	0.54±0.12 0.73±0.16 0.73±0.16 0.64±0.15 0.50±0.12 0.64±0.18 0.63±0.18 0.65±0.17 0.64±0.13 / 0.62±0.12 / 0.49±0.1 — Skewness: 0
Dortch et al., 2013	Pangong high cirque	N/A	Pang-27	33.890	78.430	5371	5.0	2.70	0.0	1.000	5.43±1.81	KNSTD		0.65±0.22	0.66±0.23 0.84±0.30 0.86±0.28 0.76±0.26 0.60±0.23 0.77±0.30 0.75±0.30 0.77±0.27 0.75±0.25 / 0.74±0.25 / 0.59±0.2 — Outlier: 2
Dortch et al., 2013	Pangong high cirque	N/A	Pang-28	33.890	78.430	5363	5.0	2.70	0.0	1.000	14.47±1.81	KNSTD		1.8±0.24	1.84±0.27 1.91±0.30 1.94±0.34 1.77±0.29 1.60±0.25 1.75±0.46 2.00±0.46 1.73±0.35 1.68±0.21 / 1.71±0.21 / 1.57±0.2 — Wt. mean: 0.50±0.09 ka; Ar. Mean: 0.54±0.09 ka
Dortch et al., 2013	Pangong high cirque	N/A	Pang-29	33.890	78.430	5360	4.0	2.70	0.0	1.000	3.62±0.90	KNSTD		0.43±0.11	0.43±0.11 0.57±0.17 0.58±0.18 0.51±0.13 0.40±0.11 0.52±0.15 0.51±0.15 0.52±0.15 0.52±0.13 / 0.51±0.13 / 0.39±0.1 — Peak: 0.50 ka !
Seong et al., 2009	Olimde 8 stage	m6C	MUST-52	38.285	75.023	4580	5.0	2.70	0.0	1.000	1.18±0.36	KNSTD	0.48±0.13	0.16±0.06	0.16±0.06 0.22±0.08 0.23±0.09 0.22±0.07 0.16±0.06 0.21±0.07 0.18±0.07 0.20±0.08 0.00±0.00 / 0.00±0.00 / 0.00±0.0 — Chi-squared: 4.19
Seong et al., 2009	Olimde 8 stage	m6C	MUST-53	38.285	75.026	4568	5.0	2.70	0.0	1.000	2.89±0.36	KNSTD		0.43±0.06	0.4±0.05 0.54±0.07 0.55±0.07 0.50±0.07 0.41±0.07 0.51±0.11 0.50±0.11 0.51±0.09 0.50±0.06 / 0.49±0.06 / 0.40±0.0 — Skewness: +0.14
Seong et al., 2009	Olimde 8 stage	m6C	MUST-54	38.287	75.024	4524	5.0	2.70	0.0	1.000	2.26±0.45	KNSTD		0.34±0.07	0.34±0.07 0.44±0.09 0.45±0.09 0.41±0.08 0.32±0.07 0.42±0.11 0.41±0.10 0.40±0.08 / 0.40±0.08 / 0.32±0.0 — Outlier: 1; Wt. mean: 0.48±0.13 ka; Ar. Mean: 0.51±0.13 ka
Seong et al., 2009	Olimde 8 stage	m6C	MUST-55	38.287	75.025	4504	5.0	2.70	0.0	1.000	4.34±0.45	KNSTD		0.68±0.08	0.64±0.08 0.81±0.10 0.82±0.12 0.76±0.10 0.63±0.09 0.78±0.16 0.78±0.16 0.77±0.13 0.73±0.08 / 0.73±0.08 / 0.62±0.0 — Peak: 0.42 ka !
Seong et al., 2009	Olimde 8 stage		MUST-56	38.287	75.025	4511	5.0	2.70	0.0	1.000	3.71±0.45	KNSTD		0.57±0.08	0.54±0.07 0.70±0.08 0.71±0.10 0.66±0.11 0.54±0.08 0.67±0.13 0.65±0.13 0.67±0.13 0.64±0.08 / 0.63±0.08 / 0.53±0.0 — Regional glacial stage: <1 ka; Weighted mean: 0.37±0.20 ka; n: 29; Dispersion: 43%; P(sig 2-tailed): 0.00
Lee et al., 2014	Lonp stage	TG-3	NK29	34.056	75.918	3679	2.5	2.70	0.0	0.957	1.56±0.05	07KNSTD	0.47±0.10	0.43±0.03	0.44±0.03 0.57±0.04 0.57±0.05 0.50±0.04 0.40±0.04 0.54±0.08 0.54±0.08 0.55±0.08 0.51±0.02 / 0.49±0.02 / 0.39±0.0 — Chi-squared: 12.53; Skewness: !; Outlier: 0; Wt. mean: 0.47±0.10 ka; Ar. Mean: 0.53±0.10 ka
Lee et al., 2014	Lonp stage	TG-3	NK30	34.055	75.917	3720	4.0	2.70	0.0	0.957	2.26±0.18	07KNSTD		0.62±0.06	0.65±0.07 0.80±0.08 0.81±0.07 0.71±0.08 0.57±0.06 0.77±0.14 0.77±0.14 0.78±0.11 0.72±0.06 / 0.68±0.05 / 0.56±0.0 — Peak: !
This study	Late Holocene	mA2c	LATO-1409	33.685	77.595	5314	3.0	2.7	0.0	0.959	265.10±5.64	07KNSTD	0.45±0.16	27.56±1.52	29.25±1.52 28.30±1.90 28.80±2.10 29.00±2.10 31.10±2.60 27.50±3.40 27.10±3.40 26.90±3.20 30.65±0.66 / 28.48±0.61 / 26.35±0.5 — Chi-squared: 24.25
This study	Late Holocene	mA2c	LATO-1410	33.685	77.595	5321	2.5	2.7	0.0	0.959	21.86±0.77	07KNSTD		3.04±0.21	2.93±0.21 2.91±0.16 2.93±0.20 2.83±0.21 2.53±0.23 2.75±0.29 2.99±0.29 2.73±0.29 2.49±0.10 / 2.88±0.11 / 2.86±0.1 — Skewness: 0.94
This study	Late Holocene	mA2c	LATO-1411	33.685	77.595	5315	2.0	2.7	0.0	0.959	29.63±1.78	07KNSTD		4.06±0.32	3.92±0.32 3.82±0.41 3.91±0.46 3.71±0.32 3.43±0.35 3.53±0.68 3.92±0.68 3.49±0.51 3.37±0.20 / 3.86±0.23 / 3.86±0.2 — Outlier: 3
This study	Late Holocene	mA2c	LATO-1412	33.685	77.596	5315	1.0	2.7	0.0	0.958	2.76±0.15	07KNSTD		0.35±0.03	0.34±0.03 0.46±0.04 0.47±0.05 0.42±0.03 0.32±0.03 0.41±0.07 0.40±0.07 0.41±0.07 0.31±0.02 / 0.41±0.02 / 0.42±0.0 — Wt. mean: 0.45±0.16 ka
This study	Late Holocene	mA2c	LATO-1413	33.685	77.596	5317	2.0	2.7	0.0	0.960	5.77±0.20	07KNSTD		0.74±0.06	0.73±0.06 0.93±0.06 0.94±0.06 0.83±0.07 0.67±0.06 0.85±0.15 0.85±0.15 0.85±0.11 0.66±0.02 / 0.81±0.03 / 0.83±0.0 — Ar. Mean: 0.52±0.16 ka
This study	Late Holocene	mA2c	LATO-1414	33.685	77.595	5314	2.0	2.7	0.0	0.960	3.76±0.18	07KNSTD		0.48±0.03	0.47±0.03 0.60±0.04 0.61±0.04 0.55±0.03 0.44±0.04 0.56±0.09 0.55±0.09 0.55±0.09 0.43±0.02 / 0.55±0.03 / 0.56±0.0 — Peak: !
This study	Late Holocene	mA2c	LATO-1415	33.682	77.592	5366	3.0	2.7	0.0	0.959	13.31±0.31	07KNSTD	0.26±0.06	1.78±0.11	1.72±0.11 1.84±0.16 1.88±0.17 1.71±0.14 1.53±0.13 1.68±0.32 1.92±0.32 1.67±0.24 1.51±0.04 / 1.64±0.04 / 1.60±0.0 — Chi-squared: 6.78
This study	Late Holocene	mA1	LATO-1416	33.682	77.592	5358	4.0	2.7	0.0	0.951	1.66±0.18	07KNSTD		0.21±0.03	0.20±0.03 0.28±0.04 0.29±0.04 0.26±0.04 0.19±0.03 0.25±0.05 0.24±0.05 0.24±0.05 0.19±0.02 / 0.26±0.03 / — — Skewness: +1.70
This study	Late Holocene	mA1	LATO-1417	33.683	77.592	5348	2.0	2.7	0.0	0.951	2.74±0.10	07KNSTD		0.35±0.03	0.34±0.03 0.46±0.04 0.47±0.04 0.42±0.03 0.32±0.03 0.41±0.07 0.40±0.07 0.41±0.06 0.31±0.01 / 0.41±0.02 / 0.42±0.0 — Outlier: 2
This study	Late Holocene	mA1	LATO-1418	33.683	77.592	5351	3.0	2.7	0.0	0.946	1.79±0.14	07KNSTD		0.22±0.03	0.22±0.03 0.30±0.03 0.31±0.03 0.29±0.03 0.21±0.02 0.28±0.05 0.27±0.05 0.28±0.05 0.21±0.02 / 0.26±0.03 / — — Ar. Mean: 0.26±0.06 ka; Peak: 0.22 ka !
This study	Late Holocene	mA1	LATO-1419	33.683	77.592	5339	3.0	2.7	0.0	0.952	24.66±1.85	07KNSTD		3.43±0.32	3.31±0.32 3.20±0.32 3.26±0.35 3.15±0.32 2.87±0.32 3.00±0.48 3.31±0.48 2.97±0.32 2.82±0.21 / 3.19±0.24 / 3.16±0.2
Hedrick et al., 2011	PM-3 stage	N/A	India-45	33.226	78.166	5266	3.0	2.70	0.0	1.000	4.45±0.30	07KNSTD	0.26±0.04	0.55±0.05	0.57±0.05 0.75±0.07 0.76±0.07 0.66±0.07 0.52±0.05 0.67±0.11 0.65±0.11 0.68±0.11 0.66±0.04 / 0.65±0.04 / 0.51±0.0 — Chi-squared: 2.22
Hedrick et al., 2011	PM-3 stage	N/A	India-46	33.226	78.167	5263	3.0	2.70	0.0	1.000	1.82±0.21	07KNSTD		0.22±0.03	0.23±0.03 0.31±0.03 0.31±0.05 0.29±0.04 0.21±0.03 0.27±0.05 0.26±0.05 0.27±0.05 0.00±0.00 / 0.29±0.03 / 0.21±0.0 — Skewness: −1.09
Hedrick et al., 2011	PM-3 stage	N/A	India-47	33.226	78.167	5257	3.0	2.70	0.0	1.000	11.74±0.47	07KNSTD		1.52±0.1	1.57±0.11 1.64±0.15 1.67±0.16 1.53±0.12 1.36±0.12 1.52±0.30 1.70±0.30 1.52±0.19 1.44±0.06 / 1.46±0.06 / 1.34±0.0 — Outlier: 3
Hedrick et al., 2011	PM-3 stage	N/A	India-48	33.226	78.167	5267	3.0	2.70	0.0	1.000	10.22±0.48	07KNSTD		1.3±0.09	1.32±0.1 1.43±0.12 1.46±0.12 1.30±0.10 1.17±0.11 1.33±0.26 1.44±0.26 1.33±0.16 1.25±0.06 / 1.27±0.06 / 1.15±0.0 — Wt. mean: 0.26±0.04 ka; Ar. Mean: 0.28±0.04 ka
Hedrick et al., 2011	PM-3 stage	N/A	India-49	33.226	78.167	5260	4.0	2.70	0.0	1.000	2.40±0.31	07KNSTD		0.29±0.04	0.33±0.04 0.41±0.06 0.42±0.07 0.38±0.05 0.29±0.04 0.37±0.07 0.36±0.07 0.37±0.07 0.37±0.05 / 0.37±0.05 / 0.28±0.0 — Peak: 0.29 ka !
Hedrick et al., 2011	PM-3 stage	N/A	India-50	33.226	78.167	5265	3.0	2.70	0.0	1.000	2.55±0.34	07KNSTD		0.32±0.05	0.31±0.05 0.42±0.06 0.44±0.07 0.40±0.06 0.30±0.05 0.39±0.08 0.38±0.08 0.39±0.07 0.36±0.05 / 0.37±0.05 / 0.29±0.0
This study	Late Holocene	mH1a	HAMTAH-1405	32.272	77.357	4014	2.0	2.7	0.0	0.943	8.89±0.19	07KNSTD	0.18±0.11	0.23±0.05	0.31±0.05 0.30±0.06 0.31±0.05 0.27±0.06 0.20±0.05 0.28±0.08 0.27±0.08 0.28±0.07 — Chi-squared: 8.55
This study	Late Holocene	mH1a	HAMTAH-1406	32.272	77.358	4023	1.0	2.7	0.0	0.944	1.56±0.41	07KNSTD		0.40±0.11	0.37±0.10 0.52±0.13 0.52±0.14 0.45±0.11 0.35±0.10 0.48±0.15 0.47±0.15 0.49±0.14 0.34±0.09 / 0.44±0.12 / 0.46±0.1 — Skewness: +0.87
This study	Late Holocene	mH1a	HAMTAH-1408	32.269	77.358	4111	2.5	2.7	0.0	0.948	9.06±0.55	07KNSTD		2.35±0.22	2.21±0.18 2.44±0.22 2.47±0.24 2.17±0.24 1.90±0.20 2.32±0.36 2.33±0.32 1.91±0.12 / 2.11±0.13 / 2.21±0.1 — Outlier: 2
This study	Late Holocene	mH1a	HAMTAH-1410	32.268	77.359	4125	2.5	2.7	0.0	0.954	0.60±0.10	07KNSTD		0.14±0.03	0.13±0.03 0.19±0.04 0.19±0.04 0.17±0.03 0.13±0.02 0.17±0.04 0.17±0.04 — Ar. Mean: 0.26±0.11 ka
This study	Late Holocene	mH1a	HAMTAH-1502	32.270	77.358	3861	2.0	2.7	0.0	0.923	2.57±0.25	07KNSTD		0.74±0.09	0.70±0.07 0.92±0.08 0.93±0.09 0.80±0.09 0.65±0.08 0.87±0.17 0.88±0.17 0.89±0.14 0.63±0.06 / 0.78±0.08 / 0.82±0.0 — Peak: 0.15 ka !

a Reported [Be-10] values have been corrected from background Be-10 detected in procedural blanks

All ages, local and regional glacial stages, weighted [Wt.] and arithmetic [Ar.] means, median, and peaks are reported in thousand years with ± 1σ

! Undefined peak/age statistics is not possible

Note: Blue coloured samples are identified as outliers and removed from further analysis

Scaling models: Lifton-Sato-Dunai (LSD; Lifton et al., 2014 [SA and SF in Marrero et al., 2016]), Lal and Stone time-dependent (Lm; Balco et al., 2008), Lal and Stone time-independent (St; Lal, 1991; Stone, 2000), Desilets (De; Desilets et al., 2006), Dunai (Du; Dunai, 2001), Lifton (Li; Lifton et al., 2005, 2008)

S4: Holocene boulder ages (published and new) are compared using different online age calculators and scaling schemes with reference to the LSD (Lifton-Sato-Dunai) scheme using the CREp calculator (used in this study). Scaling schemes are also compared across different latitudes and altitudes to examine any influence of the geomagnetic field and atmospheric pressure, respectively. Note that in most cases the relative age difference (including ±1σ uncertainties) is <10% except for altitude
<3000 m asl. Samples collected <3000 m asl are Central Karakoram samples dated prior to AD 2000 when analytical uncertainties (±1σ uncertainties) are larger than at present.
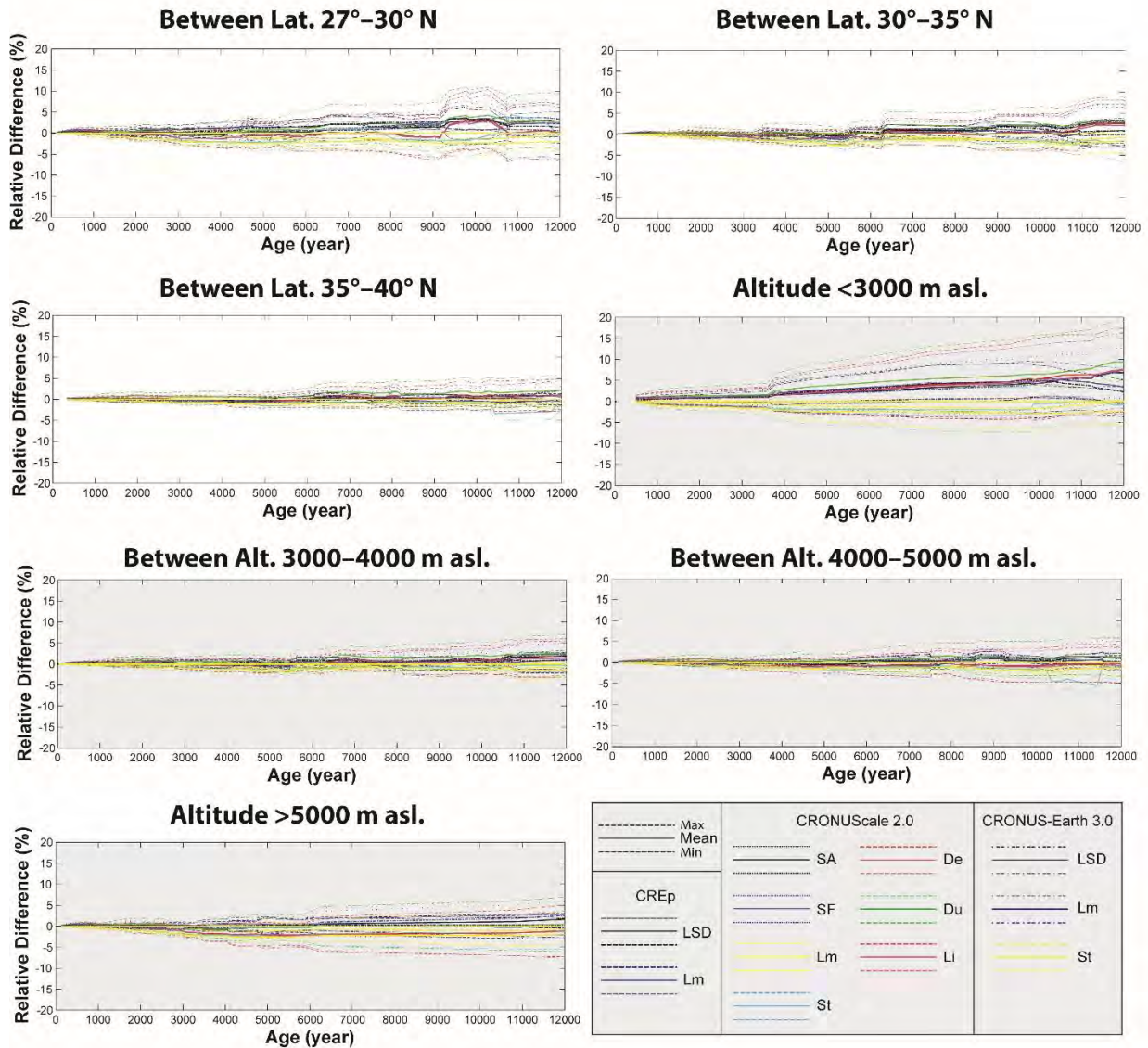
S5: Comparison of the influence of different erosion rates using the 57 Holocene [10]Be surface exposure ages in our study. Note that even with an erosion rate of 10 mm ka[-1], the percent difference in the calculated exposure age compared to zero erosion for a boulder eroding for <12 ka is <10%.
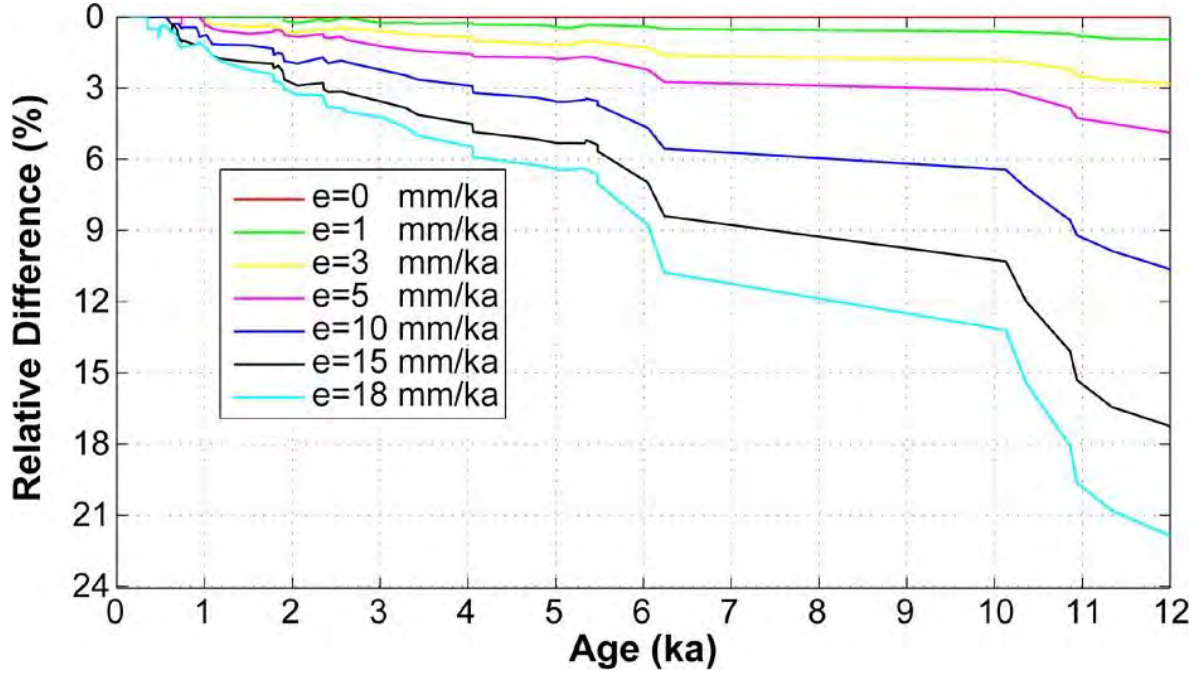
Table S7 Reconstructed ELAs and ΔELAs in the numerically dated (10Be) glaciated valleys at the NW end of the Himalaya and Tibet

Glaciated Valley	Glacial Stage	Mean moraine age (ka)	Glacier area (km2)	Mean slope (°)	Mean Aspect	Head (m a.s.l.)	Toe (m a.s.l.)	MELM (m a.s.l.)	Area-Altitude AA (m a.s.l.)	Area-Accumulation ratio			Toe-Headwall altitude ratio			Mean ELA (m a.s.l.)	ΔELA (m)
										AAR (0.5)	AAR (0.6)	AAR (0.7)	THAR (0.3)	THAR (0.4)	THAR (0.5)		
Alay Range (Koksu Valley)	Present		17.7	23	NNE	4917	3621	4059	4180	4209	4159	4099	4019	4149	4280	4144±78	
	AV	14.02±0.59	25.7	27	NE	4921	3442	-	4060	4129	4029	3899	3893	4041	4190	4034±101	122±36
Muztag Ata and Kongur Shan, NW Tibet	Present		47.4	30	N	6853	2773	3809	3972	3829	3729	3559	4003	4411	4820	4017±383	
	Olimde 7 stage (m3I)	1.35±0.10	57.7	32	N	6873	2462	-	3870	3769	3619	3449	3792	4233	4675	3915±382	131±47
Muztag Ata and Kongur Shan, NW Tibet	Present		6.8	56	WSW	7349	4271	5609	5998	6259	5979	5609	5203	5511	5820	5749±311	
	Olimde 7 stage (m7H)	1.66±0.12	8.1	53	WSW	7349	4054	-	5772	6029	5659	5229	5049	5379	5710	5547±316	222±93
Muztag Ata and Kongur Shan, NW Tibet	Present		5.9	48	WSW	6847	4300	5809	6030	6189	5989	5809	5068	5324	5580	5725±355	
	Olimde 6 stage (m5H)	4.32±0.14	6.7	47	WSW	6852	4003	-	5866	6099	5879	5629	4864	5149	5435	5560±407	153±37
	Olimde 6 stage (m6H)	3.95±0.13	7.0	46	WSW	6852	3919	-	5793	6059	5829	5539	4801	5095	5390	5501±409	212±49
	Olimde 4 stage (m4H)	7.98±0.18	8.8	43	WSW	6839	3591	-	5437	5759	5279	4529	4574	4899	5225	5100±421	612±294
	Olimde 2 stage (m3H)	13.01±0.38	9.2	42	W	6852	3515	-	5377	5679	5069	4469	4521	4855	5190	5023±409	690±309
Muztag Ata and Kongur Shan, NW Tibet	Present		3.5	45	WNW	6991	4348	4969	5602	5459	5119	4849	5144	5409	5675	5278±282	
	Olimde 8 stage (m6C)	0.48±0.04	4.4	48	WNW	7008	4273	-	5528	5389	4970	4769	5101	5375	5650	5255±294	68±38
	Olimde 2 stage (m5C)	11.66±0.41	5.1	45	WNW	7008	4209	-	5375	5089	4789	4599	5052	5333	5615	5122±325	201±117
Muztag Ata and Kongur Shan, NW Tibet	Present		8.9	46	N	6069	4237	4729	4936	4829	4749	4669	4791	4975	5160	4855±150	
	Olimde 8 stage (m8A)	0.66±0.05	11.3	45	N	6075	4152	-	4860	4779	4689	4559	4735	4927	5120	4810±167	63±22
	Olimde 7 stage (m7A)	2.19±0.07	12.3	44	N	6075	4018	-	4803	4739	4619	4499	4637	4843	5050	4741±166	131±24
	Olimde 4 Stage (m6A)	7.77±0.18	12.4	43	N	6075	3982	-	4796	4729	4610	4489	4616	4825	5035	4729±165	144±26
	Olimde 4 stage (m5A)	7.74±0.17	15.9	42	N	6075	3787	-	4621	4559	4409	4229	4476	4705	4935	4562±209	311±64
Muztag Ata and Kongur Shan, NW Tibet	Present		24.0	29	SW	6667	4257	4969	5236	5369	5219	4909	4985	5227	5470	5173±188	
	Olimde 3 stage (m3F)	10.25±0.21	44.0	27	SW	6682	3586	-	4734	4609	4400	4169	4519	4829	5140	4629±290	574±181
Muztag Ata and Kongur Shan, NW Tibet	Present		13.2	46	SSW	6711	4601	4979	5316	5229	5109	4940	5242	5453	5665	5242±226	
	Olimde 3 stage (m3F´)	9.71±0.20	39.2	30	WSW	6747	3410	-	4501	4489	4209	3929	4415	4750	5085	4483±342	797±129
Muztag Ata and Kongur Shan, NW Tibet	Present		5.8	48	W	6815	4258	4949	5488	5389	5129	4899	5027	5283	5540	5213±231	
	Olimde 5 stage (m6C´´)	5.06±0.15	7.9	53	W	6865	4059	-	5306	5150	4879	4669	4902	5183	5465	5079±255	172±66
Great Bogchigir Valley	Present		5.2	30	ENE	5324	4599	4919	4968	4979	4949	4899	4818	4891	4965	4924±50	
	BO8 stage	13.21±0.56	8.1	31	NE	5326	4425	-	4882	4919	4850	4760	4702	4793	4885	4827±72	97±24
Batura - Hunza Valley	Present		199.2	29	ESE	7606	2502	3489	4341	4159	3839	3599	4042	4553	5065	4136±485	
	Batura stage (t6)	14.3±0.5	277.0	32	ESE	7617	2455	-	4276	4089	3789	3549	4040	4527	5045	4188±456	40±23
Central Karakoram	Askole 2 stage (m2b)	5.83±0.33	-	-	-	-	-	-	-	-	-	-	-	-	-	-	-
Central Karakoram	Present		1.5	19	NNE	5173	4290	4829	4827	4829	4789	4759	4557	4646	4735	4746±92	
	Mungo 2 stage (m2G)	6.63±0.22	3.1	24	N	5202	2991	-	4310	4649	4359	3820	3662	3883	4105	4113±323	622±250
	Mungo 2 stage (m1G)	13.76±0.22	5.0	25	N, NW	5202	2889	-	3875	3489	3339	3249	3585	3817	4050	3629±273	1105±300
Central Karakoram	Present		386.9	13	SE	6260	3027	4449	4792	4900	4790	4592	4001	4325	4650	4562±276	
	Askole 3 stage (m1H)	1.03±0.16	396.7	13	SE	6262	2977	-	4769	4889	4779	4559	3966	4295	4625	4555±299	24±9
	Mungo 2 stage (m3I)	13.02±0.38	402.8	13	SE	6262	2977	-	4744	4879	4769	4519	3966	4295	4625	4542±294	36±17
	Mungo 2 stage (m2I)	14.08±0.42	406.5	13	SE	6262	2977	-	4730	4870	4759	4499	3966	4295	4625	4535±290	44±23
	Mungo 2 stage (m1I)	14.98±0.32	413.5	13	SE	6262	2977	-	4710	4860	4739	4459	3966	4295	4625	4522±286	57±36
Central Karakoram	Present		8.7	20	NNE	5840	4224	4939	5101	5129	5079	4989	4715	4877	5040	4984±129	
	Mungo 2 stage (m1E)	12.41±0.46	12.7	23	NNE, NW	5840	2643	-	4524	4969	4759	4219	3609	3929	4250	4323±436	667±312
Central Karakoram	Present		9.1	20	N	5718	4019	4689	4916	4949	4899	4779	4532	4703	4875	4793±134	
	Mungo 2 stage (m1F)	13.42±0.38	12.8	23	NNE	5718	2873	-	4568	4769	4529	4289	3734	4019	4305	4316±325	491±196
Central Karakoram	Present		4.0	25	SSE	5700	3877	4509	4893	4979	4819	4590	4428	4611	4795	4703±183	
		14.61±0.42	6.3	27	SSE	5724	2408	-	4338	4539	4349	4089	3405	3737	4070	4075±363	655±208
Ladakh cirque, Ladakh range	Present		0.2	63	N	5776	5407	5529	5596	5599	5550	5529	-	-	-	5561±31	
	Ladakh Chang La cirque	2.31±0.10	0.4	55	N	5776	5376	-	5553	5529	5499	5469	-	-	-	5513±32	56±10
Ladakh cirque, Ladakh range	Present		0.8	49	NNE	5984	5386	5679	5673	5679	5649	5600	5569	5629	5690	5646±40	
	Pangong high cirque	0.50±0.07	1.8	47	NE	5997	4844	-	5517	5559	5459	5390	5197	5313	5430	5409±114	232±83
Nun-Kun massif	Present		4.6	39	NNE	5571	4238	4629	4905	4909	4759	4549	4641	4775	4910	4760±133	
	Lonp stge (TG-3)	0.47±0.03	7.5	41	NE	5575	3277	-	4605	4539	4489	4409	3969	4199	4430	4377±204	401±172
Stok Kangri, Zanskar	Present		0.6	36	NE	5721	5288	5459	5507	5509	5489	5439	-	-	-	5481±27	
	mS1	1.20±0.48	0.9	34	NE	5748	5234	-	5456	5439	5409	5379	-	-	-	5421±29	65±11
Stok valley, Zanskar	mG1		0.6	30	NE	5649	5258	5479	5510	5520	5499	5469	-	-	-	5495±19	
	mG1	1.33±0.12	0.8	31	NE. E	5649	5149	-	5455	5469	5449	5409	-	-	-	5446±22	54±4
Amda Kangri, Lato	Present		1.1	22	ENE	5743	5312	5489	5538	5529	5509	5469	-	-	-	5504±24	
	mA1	0.26±0.08	1.4	25	ENE	5764	5298	-	5533	5529	5499	5469	-	-	-	5511±27	4±4
	mA2c	0.45±0.02	1.6	25	ENE	5764	5264	-	5511	5519	5479	5439	-	-	-	5487±31	21±7
Puga Valley, Zanskar	Present		0.8	23	NNE	6099	5686	5839	5893	5889	5850	5819	-	-	-	5858±29	
	PM-3 stage	0.26±0.02	7.3	23	NNE, NE	6101	5199	-	5647	5630	5579	5539	5472	5563	5655	5584±61	264±13
	PM-2 stage	3.42±0.13	10.3	21	NE	6101	4797	-	5480	5529	5439	5299	5192	5323	5455	5388±111	426±58
Mentok Kangri, Karzok	Present		2.5	33	NE	6003	5482	5659	5740	5739	5719	5689	-	-	-	5709±31	
	mM1	0.67±0.09	2.8	34	NE	6003	5447	-	5714	5720	5699	5669	-	-	-	5701±20	21±3
	mM2	0.99±0.08	4.1	30	NE	6003	5378	-	5685	5679	5650	5620	5568	5631	5695	5647±41	63±6
Gomuche Kangri, Karzok	Present		1.5	42	N	6084	5381	5649	5873	5929	5889	5839	5599	5669	5740	5773±117	
	mG1	2.10±0.42	1.8	42	N	6084	5332	-	5805	5889	5819	5660	5564	5639	5715	5727±107	64±50
	mG2 (or KM-4)	4.40±1.17	2.1	39	NNE	6084	5206	-	5732	5829	5649	5530	5473	5561	5650	5632±113	159±77
Yunam valley, Zanskar	Present		1.3	26	ENE	5601	5179	5369	5409	5399	5379	5359	-	-	-	5383±19	
	Youngest	0.59±0.07	2.4	28	ENE	5640	4698	-	5231	5309	5219	5119	4984	5079	5175	5159±100	167±53
Lahul Himalaya, Nn India	Present		7.2	33	NE	5378	3649	4639	4382	4349	4269	4159	4171	4345	4520	4354±153	
	Kulti glacial stage	11.64±0.57	18.0	54	NE	5378	2756	-	3854	3749	3620	3479	3548	3811	4075	3734±189	580±76
Lahul Himalaya, Nn India	Present		5.3	36	NE	5746	3972	4639	4960	5019	4969	4889	4513	4691	4870	4819±170	
	Kulti glacial stage	14.02±0.51	7.5	49	NNE	5746	2933	-	4530	4879	4609	4289	3785	4067	4350	4358±334	486±181
Lahul Himalaya, Nn India	Present		68.3	26	E	6002	4187	4909	5170	5219	5119	4999	4735	4917	5100	5021±151	
	Kulti glacial stage	14.45±0.7	110.9	29	E, SE	6002	3971	-	4822	4799	4549	4339	4588	4791	4995	4698±202	339±207
Lahul Himalaya, Nn India	Present		0.8	36	NE	4225	3470	3749	3776	3729	3719	3699	3698	3774	3850	3749±47	
	Kulti glacial stage	13.64±0.59	12.7	46	E, ESE	4782	2411	-	3404	3599	3289	2909	3130	3367	3605	3329±231	420±199
Hamtah Valley, Lahul	Present		4.0	27	NW	5011	4056	4569	4459	4479	4429	4380	4347	4443	4540	4456±70	
	mH1a	0.18±0.13	5.6	29	NW	5063	3941	-	4407	4429	4389	4259	4285	4397	4510	4382±79	57±28
	mH3	10.42±0.42	6.6	30	NNW	5063	3688	-	4332	4389	4240	4119	4103	4241	4380	4258±108	182±57

S8: Evidence showing post depositional hillslope contamination in the Hamtah m_{H3} (1, 3) and Lato m_{A3} (4, 5) moraines. In Hamtah valley, we sampled mostly from the ridge crests that are away from hillslope deposits and distinctly separated by prominent ablation valley (2, 3). In Lato valley, the south facing slope is likely contaminated by hillslope deposits (4, 5) and contains more high relief boulders (6) than their northern face (7). The end moraine is steep and contains several well striated lodged boulders on its surface (8) suggesting their glacial origin.
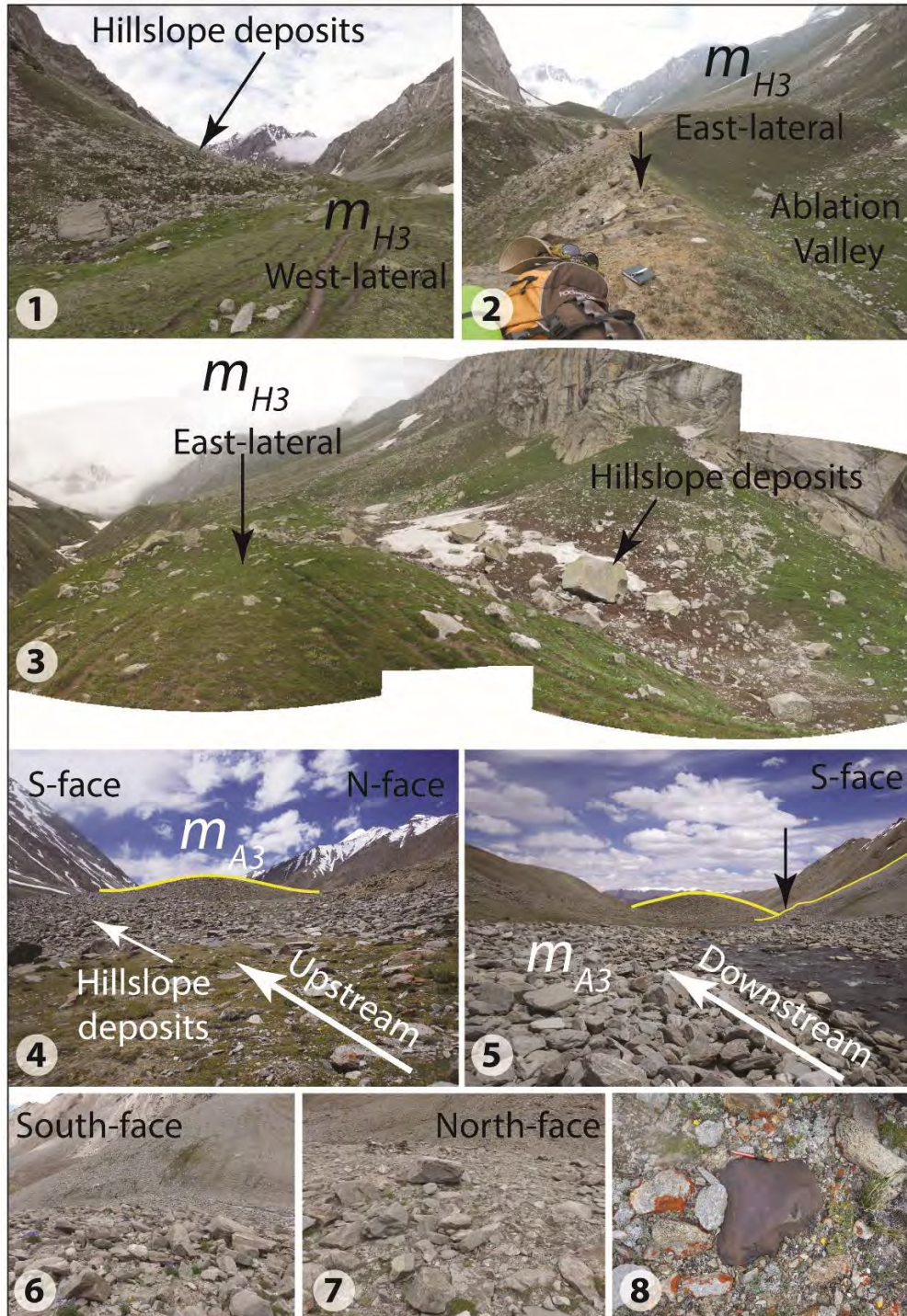
S9: Maps showing equilibrium line altitude depressions (ΔELAs) in the NW Himalaya and Tibet during different regional stages of glacier advances. ΔELAs are superimposed on reanalysis average precipitation data generated from CRU CL 2.0 for the period between 1961 and 1990 after New et al., 2002.
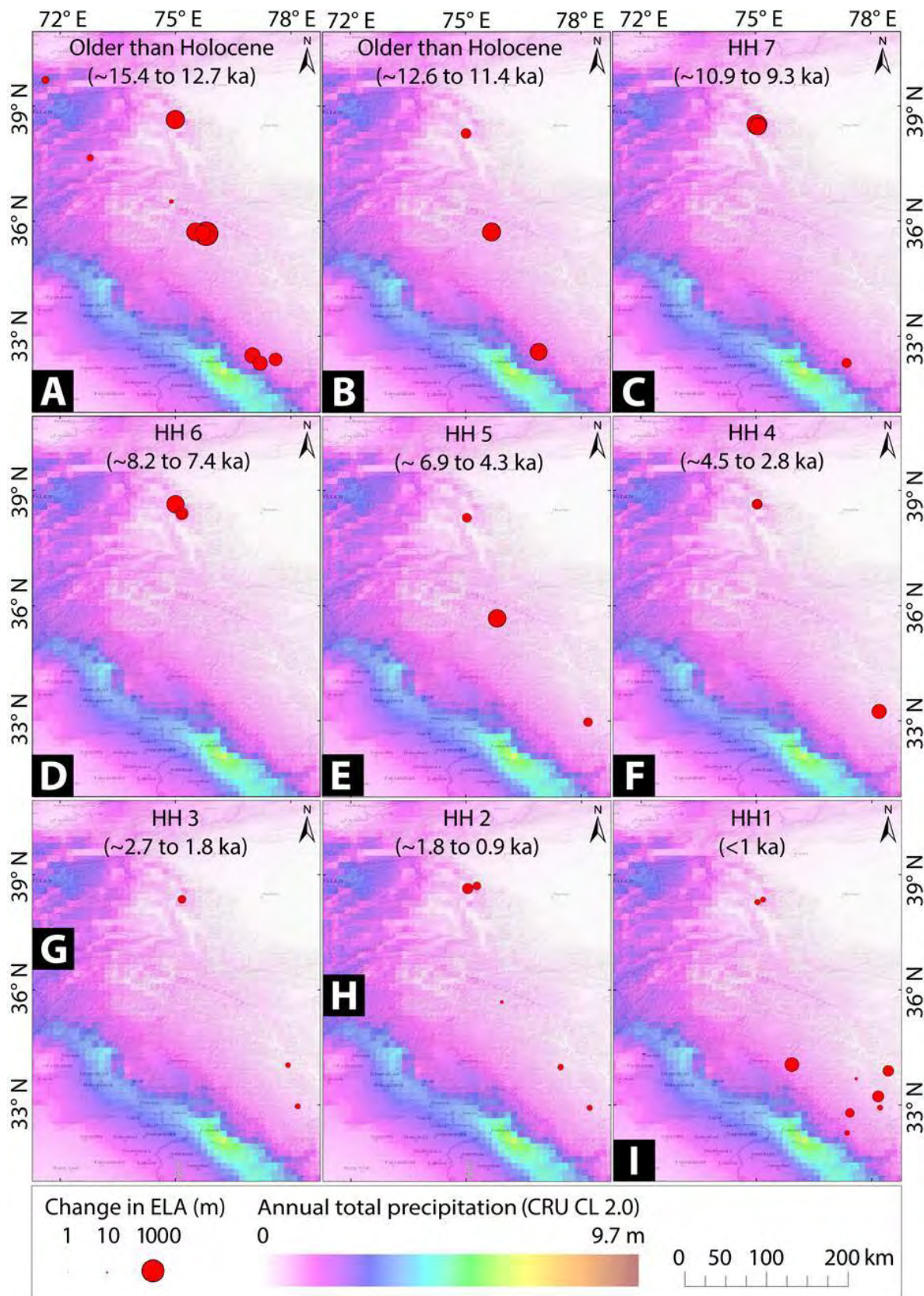
11.2 Appendix A2 (Supplementary materials for Paper II)

List of supplementary materials.

S1. Regional glacial history in the Chandra valley and in the Nun Kun massif

S2. Moraine and boulder characteristics in the study areas.

S3. Age Calculation

S4. Be-10 surface-exposure ages (in thousands of years before AD2016, labeled 'ka'±1σ) from 32 glaciated valleys at the NW end of the Himalaya and Tibet. Sample data, regional and local glacial stages, and associated age statistics are highlighted.

S5. Published AAR and THAR ratios used in this study for diverse regions (Table 2 and DR 4).

S6. Reconstructed ELAs across the Himalayan-Tibetan orogen.

S7. Modern glacier hypsometry in all the studied valleys.

S8. Age Calculation

S9. Sampled glaciers (RGI 6.0) used for climatic zonation.

S10. The linear inverse flow model

S11. Preserved moraines in the Kulti valley, Lahul Himal, and Parkachik valley, Nun Kun massif.

S12. Regional glacial stages using a radial plotter.

S13. Regional glacial stages using probability density function.

S1. Regional glacial history in the Chandra valley (A) and in the Nun Kun massif (B).
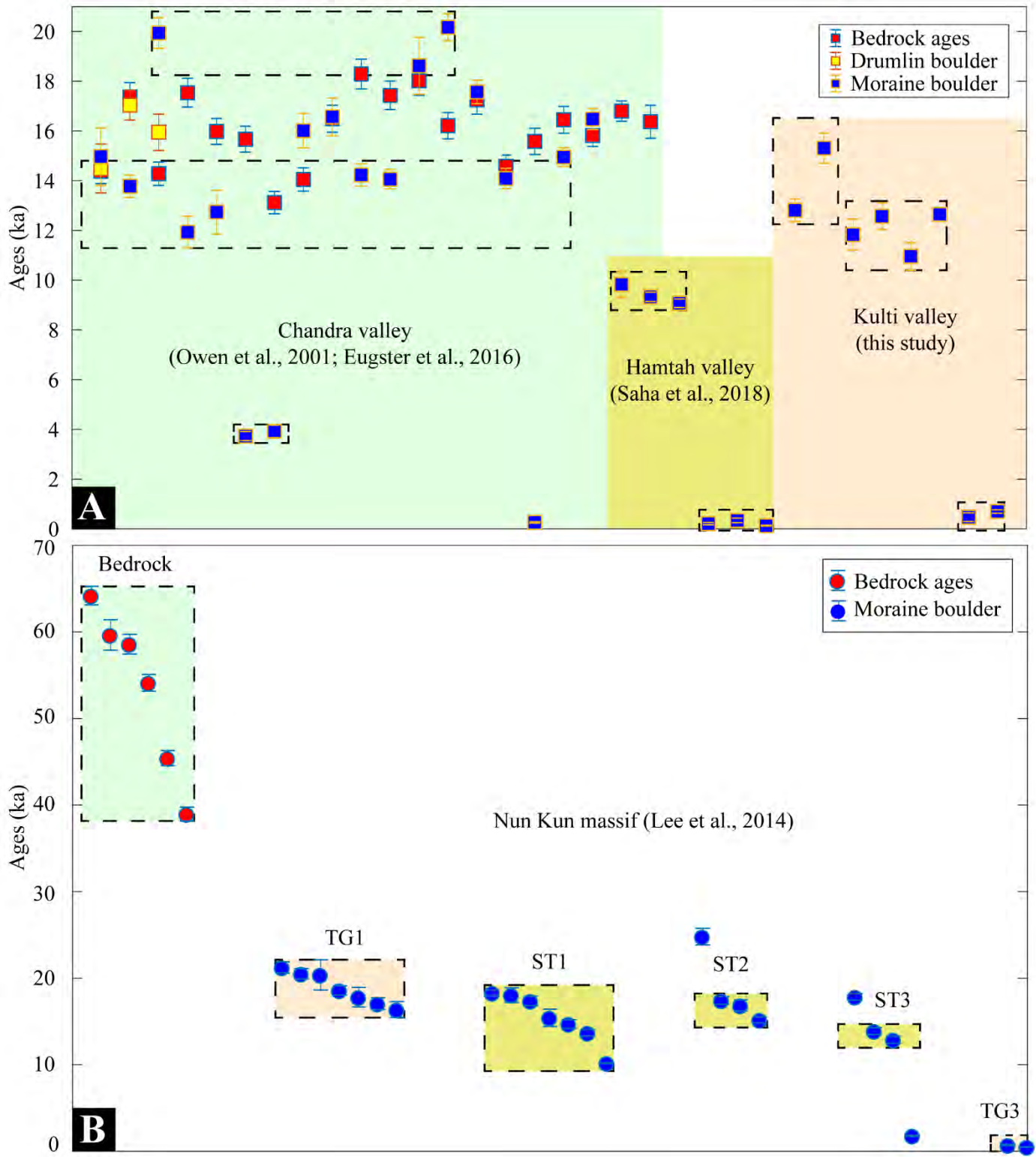
S2. Moraine and boulder characteristics in the study areas.

Morpho stat.	Moraine characteristics	Moraine boulder characteristics
Kulti valley		
M$_{K1}$	Several small, subdued, and degrading hummocky ridges; devoid of any vegetation and lichens; difficult to sample due to destabilization of the hummocks and in some instances lack of large boulders; pebbly-sandy till matrix; some hummocky mounds are eroded by the meltwater stream.	Boulders on these moraines have poor-to-no varnishes; limited-to-no weathering; lithology: predominantly grey meta-siltstones, phyllites, biotite-schists, and granites; sub-angular to angular boulders; fresh fracture faces; not suitable for sampling.
M$_{K2a}$, M$_{K2b}$	Round crested two remnants of a laterofrontal rides are mapped; the crest is more rounded and consists of plenty of smaller size boulders just slightly off the crest; M$_{K2a}$ very small to sample; M$_{K2b}$ was mostly used for sampling; both the ridges are subdued but covered with grasses; small lichens (diameter >2 cm) are present on boulder surfaces; no hill slope contamination was observed; massive matrix supported pebbly/boulder diamicton.	Boulders are moderately stable, and inset within other boulders; poorly-developed to no varnish present and limited-to-no weathering; sub-rounded to sub-angular freshly fractured boulders; lithology: mostly phyllites, grey-siltstones, biotite-schists, and occasional granites; a granitic and vein quartz of a meta-siltstone were sampled
M$_{K3}$	The terminal moraine has partially blocked the valley and allowed an extensive braided/lacustrine-plain to develop up-valley; the moraine has steep slopes, and the morphology suggests its glacial origin (and not landslide rampart); a few striated boulders are observed lodged on the surface of the moraine; presently round crested; mostly covered with green grasses and shrubs, except the bare recent slope deposits; composed likely of matrix-supported pebbly diamicton.	Boulders on these moraines consists of iron cast (red) and varnished phyllitic and grayish siltstones at the surface; while some boulders are very large and sub-angular, majority of present moraine surface is covered with jagged and sharp-edged very angular boulders, likely associated with hillslope processes; no sample was collected due to possible hillslope contamination; hillslope deposits also indicate periglacial processes.
M$_{K4a}$, M$_{K4b}$, M$_{K4c}$	Three rounded lateral ridges are mapped and sampled to the NW of the meltwater stream; a faint moraine ridge to the SE is observed, mostly buried under hillslope deposits (debris and talus); the rides are covered under thick grasses and hence no exposure is available; the M$_{K4a}$ is subdued and small and consists of very small boulders; three samples were collected from the distant M$_{K4c}$ moraine and one from M$_{K4b}$; both the lateral moraines are well preserved and separated by possible moraine-dammed lacustrine deposits.	Boulders are few but, except M$_{K4a}$, mostly large and very well inset into the ride crests; predominantly sub-rounded to sub-angular in nature but have flat-tabular surfaces (often dipping); all the sample boulders are large blocks of gray meta-siltstones, mica-schists, and phyllites; we mostly targeted vein quartz for exposure age dating whenever possible.
M$_{K5}$	A series of well-developed, steep, and sharp-crested laterofrontal moraine ridges; Moraine ridges turn west abruptly at the front; moraine degradation is limited and is covered by lush green Alpine meadows; polished (phyllite) bedrock has protruded at some places, but highly fractured; massive matrix supported pebbly diamicton; the glacier must have blocked the main Chandra river in the past and hence deposited lacustrine sediments in the south facing flanks of the SE ridge.	NW ridge is devoid of large size boulders for exposure age sampling; SE ridge contains several large boulders, but slope contamination is more probable; six boulder samples were collected while mostly avoiding hillslope deposits (but they are often difficult to distinguish); boulders on these moraines have well-developed varnishes; mostly sub-rounded to sub-angular boulders with limited-to-no visible weathering; vein quartz is sampled whenever possible.

Parkachik valley

M_{P1a}, M_{P1b}	Samples were collected far from hillslope deposits along the front of the M_{P1b} west lateral moraine ridge; both west M_{P1a} and east M_{P1} lateral ridges are small and consists of smaller to no datable boulders; mostly sandy matrix with pebbles and boulders; ridge flanks facing the glacier is degrading, but the intact sharp crest of the M_{P1b} ridge suggest that the ridge likely has not undergone any post-depositional modification and stable; sporadic grasses can be seen but mostly devoid of vegetation.	Boulders on these moraines are fresh and have no varnishes; mostly sub-rounded to sub-angular quartzite and gneissic boulders; mostly very well to moderately well inset boulders on the ridge crest (M_{P1b}) showing no indication of boulder toppling; no lichen cover in these boulders; fresh tabular surfaces devoid of any detrital materials; fresh boulder surfaces suggest no erosion or weathering.
M_{P2a}, M_{P2b}, $M_{P2c,}$ M_{P2d}	Three rounded ridges are mapped in the east side of the valley; these ridges contain thin veneer of matrix-supported pebbly diamicton overlying the polished and weathered bedrock surfaces. The ridges are steep and discontinuous and more of a bedrock ridge than moraine; covered by grasses.	No large datable boulders were found; remaining boulders show evidence of thermal breakdown and frost shattering; polished but weathered granitic/gneissic bedrock is protruded near the valley wall.

S3. Age Calculation

07KNSTD (standard) is used to normalize our Be isotopic measurements (Nishiizumi et al., 2007). Residual boron contamination is likely negligible (S. Saha et al., 2018). Native ^{9}Be in nearby (uniform) lithology is also insignificant (~0.0190±0.0160 to 0.0015±0.0001 ppm in Orr, et al. 2017 and Saha et al., in preparation) to account for any adjustments in our calculated exposure ages. We have used the ICE-D database (http://calibration.ice-d.org/) derived global *in situ* ^{10}Be production rate (4.08±0.23 at/g/a), ERA40 atmospheric model (Uppala et al., 2005), and VDM2016 geomagnetic database (Lifton, 2016) to calculate our (CREp) exposure ages (Martin et al., 2016).

S4. Be-10 surface-exposure ages (in thousands of years before AD2016, labeled 'ka'±1σ) from 32 glaciated valleys at the NW end of the Himalaya and Tibet. Sample data, regional and local glacial stages, and associated age statistics are highlighted.

Reference	Local Glacial Stage	Glacial stage or moraine name	Sample ID	Latitude (DD)	Longitude (DD)	Elevation (m a.s.l.)	Sample thickness (cm)	Density (g cm-3)	Erosion (cm a-1)	Shielding correction	[10Be] ± 1σ (104 atoms g -1)a	AMS std	Local glacial stage (based on LSD ages in ka)	CREp LSD Age ± 1σ (ka)	CREp Basic Statistics	CREp Lm Age ± 1σ (ka)	CRONUScale SA Age ± 1σ (ka)	CRONUScale SF Age ± 1σ (ka)	CRONUScale Lm Age ± 1σ (ka)	CRONUScale St Age ± 1σ (ka)	CRONUScale De Age ± 1σ (ka)	CRONUScale Du Age ± 1σ (ka)	CRONUScale Li Age ± 1σ (ka)	CRONUS EARTH 3.0 LSD Age ± 1σ (ka)	CRONUS EARTH 3.0 Lm Age ± 1σ (ka)	CRONUS EARTH 3.0 St Age ± 1σ (ka)
Group 1(a): Arid and semiarid colder climatic region— Transhimalaya, NW Tibet, Pamir, and Tian Shan.																										
Zech (2012)	Kitschi-Kurumdu	M2	KI11	40.7827	75.4876	3870	3.0	2.7	0.0	1.000	61.87±2.54	07KNSTD		10.73±0.65		11.56±0.67	11.44±0.99	12.00±1.00	11.00±1.00	12.00±1.00	11.90±1.80	12.20±1.70	11.60±1.60	11.22±0.46	11.63±0.48	11.26±0.46
Zech (2012)	Kitschi-Kurumdu	M2	KI12	40.7827	75.4876	3870	3.0	2.7	0.0	1.000	98.67±3.54	07KNSTD		16.53±1.03	Chi-squared: 17.74 Skewness: -1.62 Outlier: 1 Wt. mean: 13.93±3.03 ka Ar. Mean: 15.16±3.03 ka Peak: !	18.01±0.99	17.50±1.30	17.80±1.50	18.30±1.60	18.20±1.50	18.30±2.60	18.40±2.50	17.90±2.30	16.41±0.59	17.61±0.64	17.98±0.65
Zech (2012)	Kitschi-Kurumdu	M2	KI13	40.7826	75.4869	3870	3.0	2.7	0.0	1.000	105.42±3.22	07KNSTD	15.16±3.03	17.63±1.04		19.16±0.98	18.50±1.40	18.90±1.40	19.60±1.70	19.30±1.50	19.40±2.60	19.40±2.60	19.00±2.30	17.43±0.54	18.74±0.58	19.22±0.59
Zech (2012)	Kitschi-Kurumdu	M2	KI14	40.7826	75.4869	3870	3.0	2.7	0.0	1.000	93.38±4.47	07KNSTD		15.73±1.06		17.11±1.07	16.60±1.40	16.90±1.50	17.30±1.60	17.30±1.50	17.40±2.60	17.50±2.50	17.00±2.30	15.60±0.75	16.73±0.80	17.01±0.82
Zech (2012)	Kitschi-Kurumdu	M2	KI21	40.7874	75.4728	3990	3.0	2.7	0.0	1.000	135.75±4.74	07KNSTD		20.73±1.19		22.71±1.20	21.60±1.60	22.00±1.80	23.70±2.10	22.90±1.90	22.80±3.30	22.60±3.20	22.10±2.80	20.52±0.72	22.23±0.78	23.26±0.82
Seong et al., 2007	Mungo 2 stage	m1I	K2-72	35.7030	75.9530	4209	2.0	2.70	0.0	1.000	82.28±1.81	KNSTD		14.65±0.68		14.4±0.74	15.30±1.10	15.50±1.20	14.60±1.10	14.50±1.20	15.00±2.00	15.00±2.00	14.80±1.80	13.86±0.31	14.23±0.31	14.23±0.31
Seong et al., 2007	Mungo 2 stage	m1I	K2-73	35.7040	75.9520	4213	2.0	2.70	0.0	1.000	84.09±1.81	KNSTD		14.91±0.69	Chi-squared: 0.17 Skewness: +0.97 Outlier: 1 Wt. mean: 14.98±0.29 ka Ar. Mean: 14.98±0.29 ka Peak: 14.95 ka	14.66±0.75	15.50±1.10	15.80±1.20	14.80±1.10	14.80±1.30	15.30±2.10	15.60±2.10	15.10±1.80	14.06±0.30	14.50±0.31	14.52±0.31
Seong et al., 2007	Mungo 2 stage	m1I	K2-74	35.7030	75.9520	4212	2.0	2.70	0.0	1.000	84.99±1.81	KNSTD		15.04±0.7		14.81±0.76	15.70±1.10	16.00±1.30	15.00±1.10	14.90±1.30	15.50±2.10	15.80±2.10	15.20±1.80	14.21±0.30	14.66±0.31	14.68±0.31
Seong et al., 2007	Mungo 2 stage	m1I	K2-75	35.7030	75.9480	4215	3.0	2.70	0.0	1.000	83.19±2.71	KNSTD	14.98±0.29	14.87±0.76		14.62±0.81	15.50±1.10	15.70±1.30	14.80±1.20	14.70±1.30	15.30±2.10	15.60±2.10	15.00±1.90	14.01±0.46	14.45±0.47	14.47±0.47
Seong et al., 2007	Mungo 2 stage	m1I	K2-76	35.7030	75.9470	4211	3.0	2.70	0.0	1.000	107.60±2.71	KNSTD		18.89±0.91		18.41±1	19.30±1.20	19.60±1.30	18.90±1.40	19.10±1.60	19.20±2.30	19.40±2.30	18.90±2.20	17.70±0.45	18.36±0.47	18.77±0.48
Seong et al., 2007	Mungo 2 stage	m1I	K2-77	35.7030	75.9430	4211	3.0	2.70	0.0	1.000	86.80±1.81	KNSTD		15.44±0.72		15.15±0.79	16.10±1.20	16.40±1.30	15.40±1.20	15.40±1.30	15.90±2.20	16.20±2.20	16.00±2.00	14.62±0.31	15.04±0.31	15.13±0.32
Seong et al., 2007	Mungo 2 stage	m1D (bedrock)	K2-23	35.7180	75.5200	2646	3.0	2.70	0.0	0.960	33.46±0.90	KNSTD		14.96±0.74		15.51±0.85	16.50±1.20	16.50±1.30	14.90±1.10	14.80±1.20	16.80±2.30	17.00±2.30	16.60±2.20	14.96±0.41	14.52±0.39	14.55±0.40
Seong et al., 2007	Mungo 2 stage	m1D (bedrock)	K2-24	35.7180	75.5200	2631	3.0	2.70	0.0	0.960	31.65±0.90	KNSTD		14.33±0.71	Chi-squared: 0.19 Skewness: +0.70 Outlier: 1 Wt. mean: 14.61±0.32 ka Ar. Mean: 14.62±0.32 ka Peak: 14.62 ka	14.92±0.83	15.80±1.20	15.90±1.30	14.30±1.10	14.20±1.20	16.10±2.30	16.30±2.30	16.00±2.10	14.37±0.41	13.91±0.40	13.89±0.40
Seong et al., 2007	Mungo 2 stage	m1D (bedrock)	K2-25	35.7180	75.5200	2631	3.0	2.70	0.0	0.960	30.74±0.90	KNSTD	14.62±0.32	13.96±0.72		14.55±0.8	15.40±1.10	15.50±1.20	13.90±1.10	13.80±1.20	15.70±2.20	15.90±2.20	16.00±2.00	13.98±0.41	13.60±0.40	13.49±0.40
Seong et al., 2007	Mungo 2 stage	m1D (bedrock)	K2-26	35.7190	75.5200	2650	3.0	2.70	0.0	0.960	32.55±0.90	KNSTD		14.57±0.71		15.09±0.84	16.00±1.20	16.10±1.30	14.50±1.20	14.40±1.20	16.40±2.30	16.60±2.30	16.20±2.10	14.58±0.41	14.11±0.39	14.12±0.39
Owen et al., 2002	Batura stage	t6	KK98-34a	36.5100	74.8900	2600	5.0	2.70	0.0	0.990	28.09±0.86	LLNL3000		12.69±0.68		13.14±0.76	14.00±1.10	14.00±1.20	12.50±1.10	12.40±1.10	14.30±2.00	15.00±2.00	14.10±1.80	12.88±0.40	12.49±0.39	12.16±0.38
Owen et al., 2002	Batura stage	t6	KK98-34b	36.5100	74.8900	2610	5.0	2.70	0.0	0.990	32.24±0.86	LLNL3000	14.30±0.01	14.31±0.7	Chi-squared: ! Skewness: ! Outlier: 1 Wt. mean: 14.30±0.01 ka Ar. Mean: 14.30±0.01 ka Peak: 14.30 ka	14.81±0.81	15.60±1.20	15.70±1.30	14.30±1.10	14.20±1.20	16.10±2.30	16.30±2.30	15.90±2.10	14.28±0.38	13.90±0.37	13.88±0.37
Owen et al., 2002	Batura stage	t6	KK98-35	36.5100	74.8900	2595	5.0	2.70	0.0	0.990	31.90±0.86	LLNL3000		14.29±0.71		14.8±0.81	15.60±1.20	15.70±1.20	14.20±1.10	14.10±1.20	16.10±2.30	16.30±2.30	15.90±2.10	14.28±0.39	13.88±0.38	13.86±0.38
Seong et al., 2007	Mungo 2 stage	m1I	K2-78	35.6950	75.9570	4225	2.0	2.70	0.0	1.000	84.99±1.81	KNSTD		14.96±0.69		14.73±0.76	15.60±1.10	15.90±1.20	14.90±1.10	14.80±1.30	15.40±2.10	15.70±2.10	15.10±1.80	14.12±0.30	14.57±0.31	14.59±0.31
Seong et al., 2007	Mungo 2 stage	m1I	K2-79	35.6940	75.9580	4221	2.0	2.70	0.0	1.000	80.47±1.81	KNSTD		14.26±0.67		14.02±0.76	15.00±1.00	15.20±1.10	14.20±1.10	14.10±1.20	15.00±1.90	15.00±1.90	14.50±1.80	13.59±0.31	13.89±0.31	13.84±0.31
Seong et al., 2007	Mungo 2 stage	m2I	K2-80	35.6940	75.9580	3823	3.0	2.70	0.0	0.810	64.20±1.81	KNSTD		17.14±0.87		16.99±0.96	18.00±1.30	18.20±1.40	17.10±1.40	17.20±1.50	18.00±2.40	18.20±2.40	17.70±2.20	16.31±0.46	16.61±0.47	16.86±0.48
Seong et al., 2007	Mungo 2 stage	m2I	K2-81	35.6930	75.9600	3821	3.0	2.70	0.0	0.810	66.01±1.81	KNSTD	14.08±0.23	17.6±0.89	Chi-squared: 0.11 Skewness: -1.29 Outlier: 5 Wt. mean: 14.08±0.23 ka Ar. Mean: 14.08±0.23 ka Peak: 14.09 ka	17.43±0.98	18.40±1.30	18.70±1.40	17.60±1.40	17.70±1.50	18.40±2.40	18.60±2.40	18.10±2.30	16.75±0.46	17.07±0.47	17.35±0.48
Seong et al., 2007	Mungo 2 stage	m2I	K2-82	35.6920	75.9600	3818	2.0	2.70	0.0	0.810	63.29±1.81	KNSTD		16.83±0.86		16.66±0.96	17.70±1.30	17.90±1.40	16.80±1.40	16.80±1.50	17.70±2.40	17.90±2.40	17.40±2.20	16.02±0.46	16.31±0.47	16.53±0.47
Seong et al., 2007	Mungo 2 stage	m2I	K2-83	35.6920	75.9610	3779	3.0	2.70	0.0	1.000	231.48±5.43	KNSTD		48.51±3.17		45.91±3.44	44.50±3.30	45.30±3.70	46.00±3.90	51.80±4.50	46.90±6.80	45.60±6.80	45.50±6.20	44.03±1.04	46.56±1.10	50.89±1.21
Seong et al., 2007	Mungo 2 stage	m2I	K2-84	35.6890	75.9410	3768	2.0	2.70	0.0	1.000	61.49±1.81	KNSTD		13.82±0.71		13.82±0.78	14.70±1.10	14.90±1.10	13.70±1.10	13.60±1.20	15.00±1.90	15.00±1.90	14.40±1.80	13.40±0.40	13.50±0.40	13.36±0.39
Seong et al., 2007	Mungo 2 stage	m2I	K2-85	35.6890	75.9410	3766	2.0	2.70	0.0	0.990	62.39±2.71	KNSTD		14.15±0.82		14.13±0.88	15.00±1.10	15.20±1.20	14.10±1.20	14.00±1.30	14.90±2.00	15.00±2.00	14.70±1.90	13.68±0.60	13.79±0.60	13.71±0.60
Abramowski et al., 2006	N/A	AV	AV1	39.6800	71.6200	3440	4.0	2.70	0.0	1.000	56.57±3.65	S555		13.82±1.02	Chi-squared: 0.04 Skewness: +0.07 Outlier: 0 Wt. mean: 14.02±0.21 ka Ar. Mean: 14.02±0.21 ka Peak: 14.02 ka	13.24±1.05	14.10±1.30	14.30±1.40	13.80±1.40	13.70±1.50	14.60±2.10	14.80±2.10	14.00±2.00	13.17±0.85	13.53±0.88	13.48±0.87
Abramowski et al., 2006	N/A	AV	AV2	39.6800	71.6200	3440	4.0	2.70	0.0	1.000	57.48±3.65	S555	14.02±0.16	14.02±1.01		13.45±1.04	14.30±1.30	14.50±1.40	14.10±1.40	13.90±1.50	14.90±2.20	15.00±2.20	15.00±2.00	13.35±0.85	13.71±0.87	13.69±0.87
Abramowski et al., 2006	N/A	AV	AV3	39.6800	71.6200	3440	4.0	2.70	0.0	1.000	58.39±3.65	S555		14.23±1.02		13.65±1.03	14.50±1.30	14.70±1.40	14.30±1.40	14.20±1.50	15.10±2.20	15.20±2.20	15.00±2.00	13.53±0.85	13.89±0.87	13.91±0.87
Seong et al., 2007	Mungo 2 stage	m1G	K2-48	35.6710	75.7990	3633	2.0	2.70	0.0	1.000	54.25±1.81	KNSTD		13.17±0.69		13.26±0.77	14.10±1.10	14.30±1.20	13.10±1.10	12.90±1.20	14.00±1.90	14.40±1.90	13.90±1.80	12.94±0.43	12.94±0.43	12.68±0.42
Seong et al., 2007	Mungo 2 stage	m1G	K2-49	35.6710	75.7990	3631	2.0	2.70	0.0	1.000	55.16±1.81	KNSTD		13.39±0.69		13.48±0.76	14.30±1.10	14.50±1.10	13.30±1.10	13.10±1.20	14.00±1.90	14.60±1.90	14.10±1.80	13.09±0.43	13.10±0.43	12.90±0.42
Seong et al., 2007	Mungo 2 stage	m1G	K2-50	35.6710	75.7990	3640	2.0	2.70	0.0	1.000	58.77±1.81	KNSTD		14.12±0.73		14.17±0.8	15.10±1.10	15.20±1.20	14.10±1.10	13.90±1.20	15.00±2.00	15.00±2.00	14.80±1.80	13.71±0.42	13.77±0.43	13.69±0.42
Seong et al., 2007	Mungo 2 stage	m1G	K2-51	35.6710	75.7990	3644	2.0	2.70	0.0	1.000	54.25±1.81	KNSTD		13.1±0.7	Chi-squared: 0.56 Skewness: -0.20 Outlier: 1 Wt. mean: 13.76±0.53 ka Ar. Mean: 13.77±0.53 ka Peak: 13.80 ka	13.18±0.77	14.00±1.10	14.20±1.10	13.00±1.10	12.80±1.10	14.00±1.90	14.40±1.90	13.80±1.80	12.89±0.43	12.88±0.43	12.60±0.42
Seong et al., 2007	Mungo 2 stage	m1G	K2-52	35.6670	75.7980	3636	2.0	2.70	0.0	1.000	54.25±1.81	KNSTD		13.15±0.7		13.24±0.77	14.10±1.10	14.30±1.20	13.00±1.10	12.90±1.20	14.00±1.90	14.40±1.90	13.90±1.80	12.93±0.43	12.92±0.43	12.66±0.42
Seong et al., 2007	Mungo 2 stage	m1G	K2-53	35.6670	75.7970	3643	4.0	2.70	0.0	1.000	58.77±1.81	KNSTD	13.77±0.53	14.33±0.72		14.38±0.79	15.20±1.10	15.40±1.20	14.30±1.20	14.10±1.20	15.20±2.10	15.60±2.10	15.00±1.90	13.85±0.43	13.92±0.43	13.90±0.43
Seong et al., 2007	Mungo 2 stage	m1G	K2-54	35.6660	75.7970	3824	3.0	2.70	0.0	1.000	43.40±0.90	KNSTD		9.86±0.47		9.96±0.54	10.40±0.86	10.56±0.93	9.47±0.84	9.39±0.79	10.30±1.60	10.80±1.60	10.10±1.40	10.16±0.21	10.02±0.21	9.23±0.19
Seong et al., 2007	Mungo 2 stage	m1G	K2-55	35.6660	75.7960	3825	5.0	2.70	0.0	1.000	64.20±1.81	KNSTD		14.32±0.7		14.28±0.77	15.10±1.10	15.40±1.20	14.20±1.10	14.10±1.20	15.10±2.00	15.00±2.00	14.90±1.80	13.78±0.39	13.92±0.39	13.89±0.39
Seong et al., 2007	Mungo 2 stage	m1G	K2-56	35.6680	75.7970	3881	2.0	2.70	0.0	1.000	66.01±1.81	KNSTD		13.96±0.7		13.9±0.78	15.00±1.00	15.00±1.10	13.90±1.10	13.80±1.20	15.00±1.90	15.00±1.90	14.50±1.80	13.48±0.37	13.64±0.38	13.52±0.37
Seong et al., 2007	Mungo 2 stage	m1G	K2-58	35.6940	75.7190	3879	2.0	2.70	0.0	1.000	65.10±2.71	KNSTD		13.8±0.79		13.75±0.84	14.60±1.10	14.80±1.20	13.70±1.20	13.60±1.30	14.50±2.00	15.00±2.00	14.30±1.90	13.33±0.56	13.48±0.56	13.34±0.56
Seong et al., 2007	Mungo 2 stage	m1G	K2-59	35.6940	75.7190	3811	3.0	2.70	0.0	1.000	65.10±1.81	KNSTD		14.38±0.7		14.32±0.77	15.20±1.10	15.40±1.20	14.30±1.10	14.20±1.20	15.10±2.00	15.00±2.00	14.90±1.80	13.82±0.39	13.96±0.39	13.94±0.39

Reference	Stage	Type	Sample	Lat	Lon	Elev		Dens		Shield	Conc	Std	Group mean	Age	Statistics											
Seong et al., 2007	Mungo 2 stage	m1F (bedrock)	K2-60	35.6940	75.7190	3031	2.0	2.70	0.0	0.940	37.07±0.90	KNSTD		13.43±0.64		13.81±0.75	15.00±1.00	14.80±1.10	13.30±1.10	13.20±1.10	14.80±2.00	15.00±2.00	14.60±1.80	13.38±0.33	13.12±0.32	12.94±0.32
Seong et al., 2007	Mungo 2 stage	m1F (bedrock)	K2-61	35.6940	75.7180	3032	2.0	2.70	0.0	0.930	36.17±0.90	KNSTD		13.25±0.64		13.63±0.74	14.00±1.00	14.60±1.10	13.10±1.10	13.00±1.10	15.00±1.90	14.90±1.90	14.50±1.80	13.21±0.33	12.98±0.33	12.75±0.32
Seong et al., 2007	Mungo 2 stage	m1F (bedrock)	K2-62	35.6720	75.8140	3017	2.0	2.70	0.0	0.940	34.36±1.81	KNSTD	13.44±0.19	12.63±0.86	Chi-squared: 0.08 Skewness: +0.16 Outlier: 1 Wt. mean: 13.42±0.19 ka Ar. Mean: 13.44±0.19 ka Peak: 13.43 ka	13.02±0.93	13.80±1.20	13.90±1.30	12.50±1.20	12.30±1.20	14.00±2.00	14.00±2.00	13.80±1.90	12.75±0.67	12.46±0.66	12.10±0.64
Seong et al., 2007	Mungo 2 stage	m1F (bedrock)	K2-63	35.6720	75.8140	2944	2.0	2.70	0.0	0.690	26.22±0.90	KNSTD		13.63±0.72		14.03±0.83	14.90±1.10	15.00±1.20	13.50±1.20	13.40±1.20	15.10±2.10	15.40±2.10	14.90±1.90	13.57±0.47	13.26±0.46	13.10±0.45
Röhringer et al., 2012	BO8 stage	N/A	BH12	37.6490	72.7800	4451	3.0	2.70	0.0	0.960	108.28±7.07	S555		16.81±1.26		15.79±1.21	16.80±1.60	17.10±1.60	16.80±1.70	16.90±1.80	16.80±2.50	17.00±2.50	16.40±2.30	15.30±1.00	16.32±1.07	16.58±1.09
Röhringer et al., 2012	BO8 stage	N/A	BH13	37.6490	72.7800	4451	2.0	2.70	0.0	0.960	87.05±3.45	S555	13.18±0.64	13.63±0.76	Chi-squared: 0.65 Skewness: ! Outlier: 1 Wt. mean: 13.21±0.64 ka Ar. Mean: 13.18±0.64 ka Peak: 13.20 ka	12.96±0.83	13.80±1.10	14.10±1.20	13.60±1.20	13.40±1.20	14.00±1.90	14.00±1.90	13.40±1.80	12.79±0.51	13.31±0.53	13.21±0.53
Röhringer et al., 2012	BO8 stage	N/A	BH14	37.6490	72.7800	4449	4.0	2.70	0.0	0.960	79.38±3.73	S555		12.73±0.82		12.02±0.84	12.90±1.10	13.10±1.20	12.60±1.20	12.50±1.20	13.00±1.90	13.10±1.90	12.50±1.70	12.11±0.57	12.56±0.59	12.25±0.58
Blomdin et al. (2016)	BOR 2	N/A	TS-C-12-023	41.8158	78.1151	3734	4.0	2.7	0.0	0.990	74.79±2.59	07KNSTD		13.53±0.82		14.75±0.79	14.30±1.10	14.60±1.20	14.80±1.30	14.90±1.20	15.10±2.20	15.20±2.10	14.70±1.90	13.63±0.47	14.49±0.50	14.57±0.51
Blomdin et al. (2016)	BOR 2	N/A	TS-C-12-025	41.8144	78.1118	3706	3.0	2.7	0.0	0.990	58.05±1.54	07KNSTD	13.08±2.13	10.73±0.59	Chi-squared: 10.59 Skewness: -0.93 Outlier: 0 Wt. mean: 12.56±2.13 ka Ar. Mean: 13.08±2.13 ka Peak: !	11.64±0.59	11.40±0.95	11.62±0.95	11.58±0.99	11.71±0.96	12.00±1.80	12.30±1.70	11.70±1.60	11.24±0.30	11.72±0.31	11.38±0.30
Blomdin et al. (2016)	BOR 2	N/A	TS-C-12-026	41.8143	78.1118	3706	1.0	2.7	0.0	1.000	84.79±1.37	07KNSTD		14.93±0.80		16.29±0.77	15.70±1.10	16.00±1.30	16.50±1.40	16.50±1.30	16.70±2.40	16.80±2.30	16.30±2.10	14.95±0.24	15.98±0.26	16.20±0.26
Seong et al., 2007	Mungo 2 stage	m3I	K2-86	35.6890	75.9410	3445	3.0	2.70	0.0	0.980	46.11±0.90	KNSTD		12.82±0.62		13±0.72	13.81±0.99	14.00±1.10	13.00±1.00	12.50±1.10	14.00±1.90	14.20±1.90	13.60±1.80	12.74±0.25	12.63±0.25	12.29±0.24
Seong et al., 2007	Mungo 2 stage	m3I	K2-87	35.6890	75.9410	3442	3.0	2.70	0.0	0.980	48.83±1.81	KNSTD		13.52±0.73		13.69±0.8	14.50±1.10	14.70±1.20	13.40±1.20	13.30±1.20	14.60±2.00	15.00±2.00	14.40±1.80	13.27±0.49	13.21±0.49	13.04±0.48
Seong et al., 2007	Mungo 2 stage	m3I	K2-88	35.6880	75.9270	3447	3.0	2.70	0.0	0.980	52.44±1.81	KNSTD	13.06±0.40	14.4±0.75	Chi-squared: 0.33 Skewness: +1.72 Outlier: 1 Wt. mean: 13.02±0.40 ka Ar. Mean: 13.06±0.40 ka Peak: 12.98 ka	14.56±0.82	15.40±1.10	15.60±1.30	14.30±1.20	14.20±1.30	15.50±2.20	15.80±2.20	15.30±1.90	13.98±0.48	13.98±0.48	13.97±0.48
Seong et al., 2007	Mungo 2 stage	m3I	K2-89	35.6880	75.9270	3441	3.0	2.70	0.0	0.980	46.11±0.90	KNSTD		12.85±0.62		13.02±0.71	14.00±1.00	14.00±1.10	13.00±1.00	12.50±1.10	14.00±1.90	14.20±1.90	13.70±1.80	12.76±0.25	12.65±0.25	12.32±0.24
Seong et al., 2009	Olimde 2 stage	m3H	KONG_5	38.6420	74.9950	3539	5.0	2.70	0.0	1.000	53.17±1.45	KNSTD		12.88±0.67		12.48±0.75	13.00±1.00	13.50±1.10	12.80±1.10	12.70±1.10	14.00±1.90	13.90±1.90	13.30±1.80	12.50±0.34	12.68±0.35	12.43±0.34
Seong et al., 2009	Olimde 2 stage	m3H	KONG_6	38.6420	74.9950	3539	5.0	2.70	0.0	1.000	53.71±1.45	KNSTD	13.01±0.14	12.99±0.66	Chi-squared: 0.04 Skewness: +0.54 Outlier: 0 Wt. mean: 13.01±0.14 ka Ar. Mean: 13.01±0.14 ka Peak: 13.01 ka	12.6±0.76	13.00±1.00	13.60±1.10	12.90±1.10	12.80±1.10	14.00±1.90	14.00±1.90	13.50±1.80	12.60±0.34	12.78±0.35	12.55±0.34
Seong et al., 2009	Olimde 2 stage	m3H	KONG_7	38.6420	74.9950	3542	5.0	2.70	0.0	1.000	54.61±1.45	KNSTD		13.15±0.66		12.8±0.76	14.00±1.00	13.80±1.10	13.10±1.10	13.00±1.10	14.00±1.90	14.20±1.90	13.70±1.80	12.74±0.34	12.93±0.34	12.74±0.34
Owen et al., 2002	Batura stage	t6	KK98-1	36.4600	74.9000	2550	3.0	2.70	0.0	1.000	42.30±0.90	LLNL3000		16.51±0.82		17.08±0.94	18.00±1.30	18.10±1.40	16.50±1.30	16.50±1.30	18.60±2.60	18.70±2.50	18.40±2.30	16.46±0.39	16.02±0.38	16.21±0.39
Owen et al., 2002	Batura stage	t6	KK98-2	36.4600	74.9000	2550	3.0	2.70	0.0	1.000	29.50±0.90	LLNL3000		11.75±0.65		12.29±0.78	13.10±1.10	13.10±1.20	12.00±1.10	12.00±1.10	13.00±2.00	13.70±1.90	13.20±1.80	12.20±0.42	11.73±0.40	11.29±0.42
Owen et al., 2002	Batura stage	t6	KK98-3	36.4600	74.9000	2550	3.0	2.70	0.0	1.000	47.10±1.80	LLNL3000	12.49±1.05	18.27±1.06	Chi-squared: ! Skewness: ! Outlier: 2 Wt. mean: 12.23±1.05 ka Ar. Mean: 12.49±1.05 ka Peak: 11.93	18.81±1.17	19.70±1.40	19.80±1.50	18.30±1.40	18.30±1.40	20.40±2.70	20.40±2.60	20.10±2.40	18.18±0.78	17.71±0.76	18.06±0.78
Owen et al., 2002	Batura stage	t6	KK98-4	36.4600	74.9000	2550	3.0	2.70	0.0	1.000	33.30±1.90	LLNL3000		13.23±0.94		13.74±1.01	14.60±1.30	14.60±1.40	13.10±1.30	13.10±1.30	15.00±2.20	15.20±2.10	15.00±2.00	13.37±0.81	12.96±0.78	12.75±0.81
Seong et al., 2007	Mungo 2 stage	m1E	K2-31	35.7210	75.6760	3164	2.0	2.70	0.0	0.940	36.17±0.90	KNSTD		12.18±0.65		12.52±0.74	13.00±1.00	13.40±1.10	12.05±0.97	12.00±1.00	13.00±1.90	13.80±1.90	13.20±1.80	12.36±0.31	12.09±0.30	11.67±0.29
Seong et al., 2007	Mungo 2 stage	m1E	K2-32	35.7220	75.6740	3166	3.0	2.70	0.0	0.940	5.43±0.90	KNSTD		1.99±0.36	Chi-squared: 0.25 Skewness: ! Outlier: 1 Wt. mean: 12.41±0.33 ka Ar. Mean: 12.41±0.33 ka Peak: 12.41 ka	2.11±0.4	2.23±0.47	2.24±0.48	1.96±0.41	1.79±0.36	2.23±0.53	2.50±0.53	2.22±0.53	1.93±0.32	1.86±0.31	1.76±0.29
Seong et al., 2007	Mungo 2 stage	m1E (bedrock)	K2-33	35.7240	75.6720	3052	4.0	2.70	0.0	0.960	35.26±0.90	KNSTD	12.41±0.33	12.64±0.65		12.99±0.75	14.00±1.00	13.90±1.10	12.00±1.00	12.30±1.10	14.00±1.90	14.30±1.90	13.80±1.80	12.73±0.33	12.46±0.32	12.10±0.31
Seong et al., 2009	Olimde 2 stage	m5C	MUST-72	38.2870	75.0110	4295	5.0	2.70	0.0	1.000	80.65±1.99	KNSTD		13.2±0.64		12.49±0.74	13.00±1.00	14.00±1.00	13.20±1.10	13.00±1.10	13.00±1.90	13.70±1.90	13.00±1.70	12.50±0.31	12.97±0.32	12.79±0.32
Seong et al., 2009	Olimde 2 stage	m5C	MUST-73	38.2860	75.0110	4298	5.0	2.70	0.0	1.000	69.62±1.72	KNSTD		11.43±0.54	Chi-squared: 0.46 Skewness: ! Outlier: 2 Wt. mean: 11.66±0.40 ka Ar. Mean: 11.71±0.40 ka Peak: 11.62 ka	10.92±0.56	11.60±0.89	12.27±0.91	11.37±0.95	11.24±0.94	11.60±1.60	12.00±1.60	11.40±1.50	11.22±0.28	11.50±0.29	11.02±0.27
Seong et al., 2009	Olimde 2 stage	m5C	MUST-74	38.2860	75.0110	4292	5.0	2.70	0.0	1.000	72.97±1.81	KNSTD	11.71±0.40	11.99±0.64		11.34±0.59	12.13±0.88	12.85±0.99	11.94±0.97	11.81±0.99	12.10±1.70	12.50±1.70	11.90±1.50	11.61±0.29	11.97±0.30	11.59±0.29
Seong et al., 2009	Olimde 2 stage	m5C	MUST-75	38.2860	75.0110	4293	5.0	2.70	0.0	1.000	74.14±2.89	KNSTD		12.19±0.73		11.48±0.69	12.30±0.98	13.00±1.10	12.00±1.00	12.00±1.10	12.30±1.80	12.70±1.80	12.10±1.60	11.73±0.46	12.13±0.48	11.77±0.46
Seong et al., 2009	Olimde 3 stage	m3F	MUST-1	38.4670	75.0610	3689	5.0	2.70	0.0	1.000	45.30±1.18	KNSTD		10.31±0.5	Chi-squared: 0.10 Skewness: +1.26 Outlier: 0 Wt. mean: 10.25±0.16 ka Ar. Mean:	10.04±0.57	10.56±0.87	10.74±0.96	10.08±0.88	9.97±0.86	10.80±1.60	11.20±1.60	10.60±1.50	10.34±0.27	10.40±0.27	9.79±0.26
Seong et al., 2009	Olimde 3 stage	m3F	MUST-2	38.4670	75.0620	3681	5.0	2.70	0.0	1.000	44.85±1.18	KNSTD	10.25±0.16	10.26±0.5		10±0.57	10.50±0.86	10.68±0.95	10.02±0.87	9.91±0.85	10.70±1.60	11.10±1.60	10.50±1.50	10.30±0.27	10.34±0.27	9.73±0.26
Seong et al., 2009	Olimde 3 stage	m3F	MUST-3	38.4650	75.0650	3700	5.0	2.70	0.0	1.000	46.66±1.45	KNSTD		10.54±0.53		10.22±0.59	10.81±0.91	11.00±1.00	10.33±0.92	10.20±0.90	11.00±1.60	11.40±1.60	10.80±1.50	10.60±0.33	10.66±0.33	10.02±0.31
Seong et al., 2009	Olimde 3 stage	m3F	MUST-4	38.4640	75.0650	3709	5.0	2.70	0.0	1.000	45.12±1.18	KNSTD		10.18±0.5		9.91±0.57	10.40±0.87	10.58±0.94	9.93±0.87	9.82±0.85	10.60±1.60	11.00±1.60	10.40±1.40	10.22±0.27	10.27±0.27	9.65±0.25

Reference	Stage	Code	Sample	Lat	Long	Elev	Thick	Dens	Sh	Corr	Concentration	Std	Mean	Age	Statistics											
Seong et al., 2009	Olimde 3 stage	m3F	MUST-5	38.4660	75.0620	3688	5.0	2.70	0.0	1.000	44.31±1.18	KNSTD		10.12±0.5	10.25±0.16 ka Peak: 10.24 ka	9.85±0.58	10.33±0.86	10.51±0.93	9.86±0.87	9.75±0.84	10.50±1.60	11.00±1.60	10.30±1.40	10.17±0.27	10.21±0.27	9.58±0.26
Seong et al., 2009	Olimde 3 stage	m3F	MUST-6	38.4670	75.0610	3685	5.0	2.70	0.0	1.000	44.12±1.09	KNSTD		10.1±0.5		9.83±0.57	10.31±0.85	10.49±0.93	9.83±0.86	9.73±0.83	10.50±1.60	10.90±1.60	10.30±1.40	10.16±0.25	10.19±0.25	9.56±0.24
Seong et al., 2009	Olimde 3 stage	m3F´	MUST-7	38.5110	75.0340	3535	5.0	2.70	0.0	1.000	42.23±1.54	KNSTD	9.69±0.34	10.43±0.55	Chi-squared: 0.43 Skewness: +0.21 Outlier: 1 Wt. mean: 9.71±0.34 ka Ar. Mean: 9.69±0.34 ka Peak: 9.70 ka	10.2±0.62	10.76±0.95	11.00±1.00	10.22±0.93	10.10±0.92	11.00±1.60	11.40±1.60	10.80±1.50	10.55±0.39	10.54±0.39	9.92±0.36
Seong et al., 2009	Olimde 3 stage	m3F´	MUST-8	38.5160	75.0320	3534	5.0	2.70	0.0	1.000	41.32±1.09	KNSTD		10.23±0.51		10.02±0.58	10.54±0.87	10.71±0.94	10.00±0.87	9.89±0.85	10.80±1.60	11.20±1.60	10.60±1.50	10.32±0.27	10.32±0.27	9.71±0.26
Seong et al., 2009	Olimde 3 stage	m3F´	MUST-9	38.5200	75.0310	3521	5.0	2.70	0.0	1.000	39.69±0.99	KNSTD		9.94±0.49		9.73±0.58	10.20±0.82	10.36±0.92	9.66±0.86	9.56±0.82	10.50±1.60	10.90±1.60	10.30±1.40	10.08±0.25	10.06±0.25	9.39±0.24
Seong et al., 2009	Olimde 3 stage	m3F´	MUST-10	38.5210	75.0320	3517	5.0	2.70	0.0	1.000	36.89±0.99	KNSTD		9.25±0.54		8.99±0.63	9.49±0.79	9.60±0.90	8.96±0.79	8.91±0.77	9.70±1.50	10.20±1.50	9.60±1.40	9.52±0.26	9.44±0.26	8.75±0.24
Seong et al., 2009	Olimde 3 stage	m3F´	MUST-11	38.5200	75.0340	3494	5.0	2.70	0.0	1.000	36.62±0.99	KNSTD		9.31±0.54		9.06±0.63	9.55±0.81	9.71±0.91	9.00±0.80	8.96±0.78	9.80±1.50	10.20±1.50	9.60±1.40	9.58±0.26	9.49±0.26	8.79±0.24
Seong et al., 2009	Olimde 3 stage	m3F´	MUST-12	38.5210	75.0340	3490	5.0	2.70	0.0	1.000	38.34±0.99	KNSTD		9.78±0.5		9.56±0.61	10.04±0.85	10.20±0.87	9.48±0.84	9.40±0.81	10.30±1.60	10.70±1.60	10.10±1.40	9.98±0.26	9.92±0.26	9.23±0.24
Seong et al., 2009	Olimde 3 stage	m3F´	MUST-13	38.5140	75.0350	3511	5.0	2.70	0.0	1.000	38.07±1.27	KNSTD		9.6±0.56		9.37±0.66	9.84±0.88	10.00±0.94	9.30±0.85	9.22±0.82	10.10±1.60	10.50±1.60	9.90±1.40	9.83±0.33	9.77±0.33	9.06±0.30
Seong et al., 2009	Olimde 3 stage	m3F´	MUST-14	38.5130	75.0350	3521	5.0	2.70	0.0	1.000	38.70±0.99	KNSTD		9.71±0.51		9.48±0.62	9.95±0.85	10.10±0.90	9.40±0.83	9.30±0.80	10.20±1.60	10.60±1.60	10.00±1.40	9.92±0.26	9.86±0.25	9.16±0.24
Seong et al., 2009	Olimde 4 Stage	m4H	KONG_8	38.6400	75.0030	3639	5.0	2.70	0.0	0.980	33.55±0.99	KNSTD		7.95±0.43	Chi-squared: 0.06 Skewness: +1.21 Outlier: 0 Wt. mean: 7.98±0.10 ka Ar. Mean: 7.98±0.10 ka Peak: 7.99 ka	7.68±0.44	8.14±0.64	8.30±0.70	7.72±0.65	7.70±0.67	8.30±1.30	8.80±1.30	8.20±1.10	8.03±0.24	8.08±0.24	7.56±0.23
Seong et al., 2009	Olimde 4 Stage	m4H	KONG_9	38.6400	75.0040	3637	5.0	2.70	0.0	0.980	33.09±0.99	KNSTD	7.98±0.10	7.86±0.42		7.59±0.43	8.05±0.62	8.17±0.67	7.63±0.64	7.60±0.67	8.20±1.30	8.70±1.30	8.10±1.10	7.92±0.24	7.98±0.24	7.47±0.23
Seong et al., 2009	Olimde 4 Stage	m4H	KONG_10	38.6400	75.0040	3638	5.0	2.70	0.0	0.980	33.82±0.99	KNSTD		8.01±0.44		7.74±0.44	8.21±0.65	8.34±0.73	7.79±0.66	7.77±0.68	8.40±1.30	8.90±1.30	8.30±1.10	8.10±0.24	8.15±0.24	7.63±0.23
Seong et al., 2009	Olimde 4 Stage	m4H	KONG_11	38.6410	75.0047	3639	5.0	2.70	0.0	0.980	33.64±1.09	KNSTD		7.97±0.44		7.71±0.45	8.16±0.63	8.29±0.75	7.74±0.66	7.72±0.68	8.40±1.30	8.80±1.30	8.20±1.10	8.05±0.26	8.10±0.26	7.58±0.25
Seong et al., 2009	Olimde 4 Stage	m4H	KONG_12	38.6410	75.0052	3641	5.0	2.70	0.0	0.980	34.54±0.99	KNSTD		8.17±0.44		7.9±0.46	8.36±0.66	8.50±0.79	7.94±0.67	7.92±0.69	8.60±1.30	9.00±1.30	8.40±1.20	8.25±0.24	8.30±0.24	7.78±0.22
Seong et al., 2009	Olimde 4 Stage	m4H	KONG_13	38.6410	75.0057	3652	5.0	2.70	0.0	0.980	33.73±1.63	KNSTD		7.94±0.51		7.66±0.5	8.12±0.72	8.25±0.78	7.71±0.73	7.69±0.75	8.30±1.30	8.80±1.30	8.20±1.10	8.01±0.39	8.07±0.39	7.55±0.37
Seong et al., 2009	Olimde 4 Stage	m6A	MUST-27	38.3640	75.1710	4023	5.0	2.70	0.0	0.990	38.97±1.18	KNSTD		7.52±0.39	Chi-squared: 0.48 Skewness: +0.65 Outlier: 0 Wt. mean: 7.77±0.29 ka Ar. Mean: 7.80±0.29 ka Peak: 7.72 ka	7.26±0.38	7.65±0.55	7.77±0.63	7.30±0.62	7.27±0.64	7.70±1.10	8.20±1.10	7.58±0.98	7.45±0.23	7.60±0.23	7.14±0.22
Seong et al., 2009	Olimde 4 Stage	m6A	MUST-28	38.3640	75.1710	4024	5.0	2.70	0.0	0.990	41.41±1.09	KNSTD		7.98±0.42		7.61±0.42	8.07±0.61	8.21±0.68	7.74±0.64	7.72±0.67	8.20±1.20	8.60±1.20	8.00±1.10	7.96±0.21	8.12±0.21	7.59±0.20
Seong et al., 2009	Olimde 4 Stage	m6A	MUST-29	38.3640	75.1710	4025	5.0	2.70	0.0	0.990	40.06±1.09	KNSTD	7.80±0.29	7.72±0.4		7.4±0.39	7.82±0.59	7.96±0.62	7.49±0.62	7.46±0.65	7.90±1.20	8.40±1.20	8.00±1.00	7.64±0.21	7.84±0.21	7.33±0.20
Seong et al., 2009	Olimde 4 Stage	m6A	MUST-30	38.3640	75.1710	4026	5.0	2.70	0.0	0.980	42.23±1.09	KNSTD		8.2±0.44		7.84±0.44	8.29±0.68	8.44±0.73	7.96±0.66	7.94±0.68	8.40±1.30	8.90±1.30	8.20±1.10	8.20±0.21	8.34±0.22	7.81±0.20
Seong et al., 2009	Olimde 4 Stage	m6A	MUST-31	38.3630	75.1710	4028	5.0	2.70	0.0	0.980	38.97±0.99	KNSTD		7.57±0.38		7.3±0.37	7.70±0.57	7.83±0.63	7.30±0.60	7.32±0.63	7.80±1.10	8.20±1.10	7.63±0.98	7.50±0.19	7.67±0.20	7.20±0.18
Seong et al., 2009	Olimde 4 Stage	m5A	MUST-21	38.393	75.171	3862	5.0	2.70	0.0	1.000	39.15±0.99	KNSTD		8.11±0.43	Chi-squared: 0.41 Skewness: +0.12 Outlier: 0 Wt. mean: 7.74±0.27 ka Ar. Mean: 7.74±0.27 ka Peak: 7.73 ka	7.79±0.44	8.25±0.64	8.40±0.72	7.88±0.66	7.86±0.68	8.40±1.30	8.90±1.30	8.20±1.10	8.17±0.21	8.26±0.21	7.72±0.20
Seong et al., 2009	Olimde 4 Stage	m5A	MUST-22	38.393	75.172	3864	5.0	2.70	0.0	1.000	36.62±0.99	KNSTD		7.6±0.39		7.35±0.38	7.76±0.56	7.88±0.66	7.37±0.61	7.34±0.64	7.90±1.20	8.30±1.20	8.00±1.00	7.55±0.21	7.69±0.21	7.22±0.20
Seong et al., 2009	Olimde 4 Stage	m5A	MUST-23	38.393	75.172	3862	5.0	2.70	0.0	1.000	35.63±1.27	KNSTD	7.74±0.27	7.4±0.4		7.19±0.39	7.58±0.57	7.70±0.64	7.18±0.63	7.15±0.65	7.70±1.10	8.10±1.10	7.54±0.98	7.39±0.26	7.48±0.27	7.03±0.25
Seong et al., 2009	Olimde 4 Stage	m5A	MUST-24	38.393	75.171	3862	5.0	2.70	0.0	1.000	36.44±1.36	KNSTD		7.56±0.43		7.33±0.42	7.70±0.60	7.86±0.65	7.34±0.64	7.31±0.67	7.80±1.20	8.30±1.20	8.00±1.00	7.52±0.28	7.65±0.29	7.19±0.27
Seong et al., 2009	Olimde 4 Stage	m5A	MUST-25	38.393	75.171	3862	5.0	2.70	0.0	1.000	37.89±0.99	KNSTD		7.87±0.41		7.56±0.42	8.00±0.60	8.14±0.68	7.63±0.63	7.60±0.66	8.10±1.20	8.60±1.20	8.00±1.10	7.88±0.21	7.99±0.21	7.47±0.20
Seong et al., 2009	Olimde 4 Stage	m5A	MUST-26	38.393	75.172	3861	5.0	2.70	0.0	1.000	38.16±0.99	KNSTD		7.92±0.41		7.61±0.42	8.20±0.69	8.20±0.69	7.69±0.64	7.66±0.66	8.20±1.30	8.60±1.30	8.00±1.10	7.95±0.21	8.06±0.21	7.53±0.20
Seong et al., 2007	Mungo 2 stage	m2G	K2-65	35.672	75.814	3113	3.0	2.70	0.0	0.800	36.17±0.90	KNSTD		14.7±0.7	Chi-squared: 0.68 Skewness: -1.13 Outlier: 2 Wt. mean: 6.63±0.35 ka Ar. Mean: 6.64±0.35 ka Peak: 6.68 ka	15±0.81	15.90±1.20	16.10±1.30	14.60±1.10	14.50±1.20	16.10±2.30	16.40±2.30	15.90±2.10	14.44±0.36	14.24±0.36	14.25±0.36
Seong et al., 2007	Mungo 2 stage	m2G	K2-66	35.672	75.814	3128	3.0	2.70	0.0	0.800	14.47±0.90	KNSTD		6.17±0.41		6.42±0.44	6.54±0.76	6.62±0.82	5.88±0.58	5.76±0.61	6.60±1.00	7.00±1.10	6.60±1.10	6.54±0.41	6.19±0.39	5.64±0.35
Seong et al., 2007	Mungo 2 stage	m2G	K2-67	35.672	75.814	3122	5.0	2.70	0.0	0.800	15.37±0.90	KNSTD	6.64±0.35	6.6±0.44		6.86±0.46	7.14±0.64	7.20±0.68	6.33±0.58	6.24±0.65	7.20±1.10	7.60±1.10	7.00±1.00	7.00±0.41	6.67±0.39	6.11±0.36
Seong et al., 2007	Mungo 2 stage	m2G	K2-68	35.672	75.814	3113	3.0	2.70	0.0	0.800	16.28±0.90	KNSTD		6.87±0.44		7.14±0.47	7.44±0.64	7.50±0.68	6.60±0.60	6.53±0.67	7.50±1.10	7.90±1.10	7.00±1.00	7.25±0.40	6.95±0.39	6.40±0.36
Seong et al., 2007	Mungo 2 stage	m2G	K2-69	35.703	75.954	3109	3.5	2.70	0.0	0.800	18.99±0.90	KNSTD		7.99±0.52		8.23±0.62	8.64±0.85	8.73±0.91	7.67±0.71	7.67±0.74	8.70±1.50	9.20±1.50	8.60±1.30	8.47±0.40	8.09±0.39	7.51±0.36
Seong et al., 2007	Mungo 2 stage	m2G	K2-70	35.703	75.952	3106	2.0	2.70	0.0	0.790	16.28±0.90	KNSTD		6.93±0.44		7.18±0.47	7.49±0.65	7.55±0.68	6.64±0.58	6.58±0.67	7.60±1.20	8.00±1.20	7.00±1.00	7.29±0.41	6.99±0.39	6.45±0.36
Seong et al., 2007	Askole 2 stage	m2b	K2-116	35.292	75.662	2276	4.0	2.70	0.0	1.000	10.85±1.81	KNSTD		6.77±1.01	Chi-squared: 0.92 Skewness: +0.33 Outlier: 0 Wt. mean: 5.83±0.69 ka Ar. Mean: 5.98±0.69 ka Peak: 5.68 ka	6.33±0.95	7.00±1.30	7.00±1.30	6.10±1.10	5.90±1.20	7.20±1.50	7.50±1.50	7.10±1.50	6.89±1.15	6.38±1.06	5.83±0.97
Seong et al., 2007	Askole 2 stage	m2b	K2-117	35.292	75.662	2276	5.0	2.70	0.0	1.000	8.14±1.00	KNSTD		5.40±0.61		4.97±0.59	5.35±0.33	5.35±0.36	4.68±0.35	4.50±0.36	5.44±0.66	5.66±0.66	5.40±0.61	0.00±0.00	0.00±0.00	0.00±0.00
Seong et al., 2007	Askole 2 stage	m2b	K2-118	35.315	75.626	2276	5.0	2.70	0.0	1.000	9.95±1.00	KNSTD	5.98±0.69	6.34±0.61		5.90±0.56	6.46±0.53	6.45±0.58	5.60±0.40	5.49±0.44	6.60±1.10	7.00±1.10	6.56±0.98	0.00±0.00	0.00±0.00	0.00±0.00
Seong et al., 2007	Askole 2 stage	m2b	K2-119	35.314	75.625	2276	5.0	2.70	0.0	1.000	8.14±1.00	KNSTD		5.40±0.61		4.97±0.58	5.35±0.33	5.35±0.36	4.68±0.35	4.49±0.36	5.44±0.66	5.66±0.66	5.40±0.61	0.00±0.00	0.00±0.00	0.00±0.00
Koppes et al. (2008)	Aksai	N/A	KTS98-CS-61b	41.00	76.05	3804	3.0	2.7	0.0	0.990	50.70±1.50	07KNSTD		9.24±0.64	Chi-squared: ! Skewness: ! Outlier: 2 Wt. mean: 5.69±0.16 ka Ar. Mean: 5.70±0.16 ka Peak: 5.68 ka	10.03±0.52	9.77±0.84	9.97±0.91	9.77±0.84	9.86±0.87	10.20±1.60	10.60±1.50	10.00±1.40	9.85±0.29	10.15±0.30	9.60±0.29
Koppes et al. (2008)	Aksai	N/A	KTS98-CS-62a	41.00	76.05	3879	3.0	2.7	0.0	0.990	32.00±1.00	07KNSTD		5.81±0.31		6.19±0.31	5.86±0.49	5.99±0.66	5.92±0.51	6.00±0.50	6.10±1.10	6.60±1.20	5.94±0.91	6.01±0.19	6.25±0.20	5.82±0.18
Koppes et al. (2008)	Aksai	N/A	KTS98-CS-62b	41.00	76.05	3879	3.0	2.7	0.0	0.989	30.50±0.90	07KNSTD	5.70±0.16	5.58±0.29		5.93±0.29	5.60±0.36	5.70±0.46	5.64±0.49	5.74±0.45	5.80±0.90	6.20±1.20	5.67±0.72	5.69±0.17	5.94±0.18	5.54±0.16
Koppes et al. (2008)	Aksai	N/A	KTS98-CS-66	40.98	76.15	3576	4.0	2.7	0.0	0.996	205.80±3.50	07KNSTD		39.33±2.00		42.39±1.97	39.30±2.80	40.00±3.00	45.40±3.80	41.90±3.10	42.00±6.00	41.70±5.90	41.00±5.00	38.49±0.66	41.39±0.71	44.56±0.77
Seong et al., 2009	Olimde 5 stage	m6C´	MUST-76	38.292	75.025	4477	5.0	2.70	0.0	0.990	36.08±0.81	KNSTD		5.75±0.26	Chi-squared: 0.33 Skewness: +1.69 Outlier: 1 Wt. mean: 5.06±0.14 ka Ar. Mean: 5.05±0.14 ka Peak: 5.05 ka	5.59±0.26	5.53±0.31	5.61±0.36	5.51±0.44	5.36±0.46	5.50±0.82	5.83±0.82	5.40±0.62	5.61±0.13	5.72±0.13	5.27±0.12
Seong et al., 2009	Olimde 5 stage	m6C´	MUST-77	38.292	75.025	4473	5.0	2.70	0.0	0.990	30.47±0.90	KNSTD		4.98±0.26		4.88±0.28	4.85±0.36	4.93±0.38	4.71±0.38	4.50±0.40	4.77±0.58	5.18±0.58	4.67±0.67	4.68±0.14	4.82±0.14	4.46±0.13
Seong et al., 2009	Olimde 5 stage	m6C´	MUST-78	38.293	75.024	4461	5.0	2.70	0.0	0.990	31.92±0.90	KNSTD	5.05±0.14	5.22±0.25		5.12±0.27	5.07±0.35	5.16±0.38	4.94±0.38	4.78±0.42	5.00±0.57	5.37±0.57	4.91±0.63	5.02±0.14	5.14±0.15	4.70±0.13
Seong et al., 2009	Olimde 5 stage	m6C´	MUST-79	38.293	75.025	4473	5.0	2.70	0.0	0.990	30.38±0.90	KNSTD		4.96±0.25		4.87±0.27	4.83±0.36	4.92±0.38	4.70±0.39	4.50±0.40	4.76±0.59	5.17±0.59	4.66±0.66	4.66±0.14	4.81±0.14	4.45±0.13
Hedrick et al., 2011	KM-4 stage	mG2	TM-B	32.971	78.182	5306	2.0	2.70	0.0	1.000	47.04±8.73	07KNSTD		5.86±0.95	Chi-squared: 13.12 Skewness: +0.03 Outlier: 2 Wt. mean: 4.43±1.17 ka Ar. Mean: 4.66±1.17 ka Peak: !	6±0.91	5.80±1.10	5.90±1.30	6.00±1.00	5.40±1.10	5.00±1.20	5.80±1.20	5.41±0.95	6.08±1.13	5.99±1.11	5.27±0.98
Hedrick et al., 2011	KM-4 stage	mG2	TM-C	32.971	78.182	5309	3.0	2.70	0.0	1.000	207.93±15.08	07KNSTD		22.93±1.71		22.14±1.58	23.00±2.10	23.40±2.20	22.80±2.30	23.90±2.60	21.90±3.00	22.00±3.00	21.50±2.70	21.38±1.56	22.38±1.63	23.56±1.72
Hedrick et al., 2011	KM-4 stage	mG2	TM-D	32.971	78.182	5309	3.0	2.70	0.0	1.000	33.21±6.28	07KNSTD	4.66±1.17	4.35±0.78		4.54±0.81	4.34±0.98	4.00±1.00	4.07±0.75	3.80±0.78	3.90±1.20	4.40±1.20	3.89±0.98	4.30±0.82	4.27±0.81	3.75±0.71
Hedrick et al., 2011	KM-4 stage	mG2	TM-F	32.971	78.181	5318	1.0	2.70	0.0	1.000	26.54±3.79	07KNSTD		3.45±0.49		3.59±0.52	3.34±0.52	3.41±0.56	3.28±0.51	2.98±0.49	3.11±0.64	3.43±0.64	3.08±0.54	3.33±0.48	3.34±0.48	2.93±0.42
Saha et al. (2018)	Neoglacial	mG2	KO-17	32.971	78.179	5331	3.0	2.7	0.0	0.984	23.57±0.97	07KNSTD		3.29±0.23	!	3.16±0.23	3.07±0.25	3.12±0.25	3.02±0.23	2.72±0.25	2.90±0.44	3.16±0.44	2.88±0.29	2.67±0.11	3.07±0.13	3.06±0.13

Reference	Stage	Unit	Sample	Lat	Long	Elev	Thick	Density	—	Shielding	Conc	Std	Group mean	Age	Statistics	Age1	Age2	Age3	Age4	Age5	Age6	Age7	Age8	Age9	Age10	Age11
Saha et al. (2018)	Neoglacial	mG2	KO-18	32.971	78.178	5337	2.0	2.7	0.0	0.985	36.75±1.19	07KNSTD		4.93±0.28		4.74±0.28	4.80±0.39	4.90±0.40	4.45±0.34	4.19±0.37	4.38±0.69	4.85±0.69	4.32±0.66	4.12±0.13	4.70±0.15	4.77±0.15
Saha et al. (2018)	Neoglacial	mG2	KO-1501	32.972	78.182	5327	1.0	2.7	0.0	0.990	47.97±1.22	07KNSTD		6.05±0.3		5.92±0.3	5.89±0.46	6.01±0.54	5.61±0.41	5.42±0.46	5.52±0.84	5.84±0.84	5.45±0.58	5.33±0.14	6.06±0.16	6.14±0.16
Saha et al. (2018)	Neoglacial	mG2	KO-1502	32.972	78.181	5334	2.0	2.7	0.0	0.990	105.93±1.35	07KNSTD		12.37±0.7		12.42±0.7	13.12±0.99	13.40±1.10	12.25±0.93	12.06±0.99	12.10±1.70	12.60±1.70	11.90±1.50	11.86±0.15	12.44±0.16	12.18±0.16
Seong et al., 2009	Olimde 6 stage	m5H	KONG_18	38.649	75.032	4057	5.0	2.70	0.0	1.000	22.33±0.72	KNSTD		4.43±0.24	Chi-squared: 0.19; Skewness: +0.42; Outlier: 2; Wt. mean: 4.32±0.11 ka; Ar. Mean: 4.32±0.11 ka; Peak: 4.32 ka	4.38±0.27	4.30±0.44	4.39±0.46	4.20±0.34	4.02±0.36	4.31±0.69	4.78±0.69	4.22±0.66	4.17±0.14	4.23±0.14	3.95±0.13
Seong et al., 2009	Olimde 6 stage	m5H	KONG_19	38.649	75.032	4057	5.0	2.70	0.0	1.000	21.70±0.81	KNSTD		4.31±0.25		4.27±0.28	4.16±0.43	4.25±0.45	4.09±0.34	3.90±0.36	4.18±0.76	4.65±0.76	4.09±0.66	4.06±0.15	4.12±0.16	3.84±0.14
Seong et al., 2009	Olimde 6 stage	m5H	KONG_20	38.649	75.032	4060	5.0	2.70	0.0	1.000	21.25±0.81	KNSTD	4.32±0.11	4.22±0.25		4.17±0.28	4.05±0.42	4.14±0.45	4.00±0.33	3.82±0.35	4.08±0.79	4.54±0.79	3.99±0.63	3.98±0.15	4.04±0.16	3.75±0.14
Seong et al., 2009	Olimde 6 stage	m5H	KONG_21	38.645	75.031	4039	5.0	2.70	0.0	1.000	5.43±0.54	KNSTD		1.06±0.12		1.02±0.12	1.15±0.11	1.16±0.13	1.12±0.13	0.99±0.14	1.15±0.20	1.20±0.20	1.14±0.16	1.05±0.11	1.06±0.11	0.97±0.10
Seong et al., 2009	Olimde 6 stage	m5H	KONG_22	38.645	75.031	4042	5.0	2.70	0.0	1.000	28.39±0.90	KNSTD		5.55±0.27		5.45±0.27	5.41±0.36	5.48±0.38	5.29±0.44	5.15±0.46	5.40±0.76	5.76±0.76	5.34±0.62	5.45±0.17	5.50±0.18	5.06±0.16
Seong et al., 2009	Olimde 6 stage	m6H	KONG_23	38.644	75.028	4008	5.0	2.70	0.0	1.000	17.63±0.72	KNSTD		3.62±0.21		3.58±0.24	3.44±0.28	3.50±0.33	3.45±0.29	3.30±0.30	3.48±0.64	3.84±0.64	3.42±0.46	3.31±0.14	3.41±0.14	3.20±0.13
Seong et al., 2009	Olimde 6 stage	m6H	KONG_24	38.643	75.028	4005	5.0	2.70	0.0	1.000	9.13±0.63	KNSTD		1.85±0.16	Chi-squared: 2.17; Skewness: -1.73; Outlier: 3; Wt. mean: 3.95±0.30 ka; Ar. Mean: 3.97±0.30 ka; Peak: 4.13 ka	1.8±0.17	1.89±0.24	1.93±0.25	1.80±0.20	1.69±0.19	1.90±0.42	2.23±0.42	1.87±0.29	1.66±0.12	1.73±0.12	1.66±0.12
Seong et al., 2009	Olimde 6 stage	m6H	KONG_25	38.645	75.026	3999	5.0	2.70	0.0	1.000	20.25±0.63	KNSTD		4.14±0.22		4.1±0.25	4.00±0.40	4.07±0.45	3.94±0.31	3.76±0.33	4.02±0.75	4.48±0.75	3.94±0.59	3.93±0.12	3.98±0.13	3.69±0.12
Seong et al., 2009	Olimde 6 stage	m6H	KONG_26	38.645	75.026	3997	5.0	2.70	0.0	1.000	20.25±0.72	KNSTD	3.97±0.30	4.15±0.24		4.12±0.27	3.99±0.41	4.08±0.46	3.94±0.32	3.76±0.34	4.03±0.75	4.48±0.75	3.90±0.60	3.93±0.14	3.98±0.14	3.70±0.13
Seong et al., 2009	Olimde 6 stage	m6H	KONG_27	38.646	75.026	4000	5.0	2.70	0.0	1.000	14.20±0.72	KNSTD		2.94±0.2		2.91±0.23	2.88±0.21	2.90±0.20	2.84±0.24	2.63±0.26	2.89±0.41	3.20±0.41	2.86±0.32	2.76±0.14	2.81±0.14	2.59±0.13
Seong et al., 2009	Olimde 6 stage	m6H	KONG_28	38.646	75.026	4000	5.0	2.70	0.0	1.000	6.96±0.54	KNSTD		1.4±0.13		1.35±0.13	1.44±0.15	1.47±0.17	1.42±0.14	1.29±0.15	1.46±0.34	1.62±0.34	1.44±0.21	1.28±0.10	1.33±0.10	1.27±0.10
Hedrick et al., 2011	PM-2 stage	N/A	India-10	33.2450	78.2000	4910	3.0	2.70	0.0	1.000	62.54±3.21	07KNSTD		8.94±0.67		9.05±0.77	9.32±0.92	9.50±0.99	8.51±0.85	8.50±0.82	8.70±1.50	9.30±1.50	8.60±1.30	9.45±0.49	9.31±0.48	8.36±0.43
Hedrick et al., 2011	PM-2 stage	N/A	India-11	33.2450	78.2010	4905	3.0	2.70	0.0	1.000	42.94±2.96	07KNSTD		6.3±0.45	Chi-squared: 17.79; Skewness: +1.18; Outlier: 4; Wt. mean: 3.42±0.87 ka; Ar. Mean: 3.50±0.87 ka; Peak: 2.80 ka	6.44±0.46	6.41±0.73	6.54±0.77	5.99±0.58	5.85±0.62	6.00±1.30	6.60±1.30	5.91±0.88	6.59±0.46	6.48±0.45	5.75±0.40
Hedrick et al., 2011	PM-2 stage	N/A	India-12	33.2450	78.2010	4904	2.0	2.70	0.0	1.000	20.84±1.97	07KNSTD		3.25±0.33		3.4±0.36	3.17±0.37	3.23±0.37	3.10±0.34	2.81±0.35	3.00±0.52	3.32±0.52	2.99±0.34	3.15±0.30	3.14±0.30	2.77±0.26
Hedrick et al., 2011	PM-2 stage	N/A	India-13	33.2450	78.2010	4899	2.0	2.70	0.0	1.000	307.50±7.55	07KNSTD	3.50±0.87	39.27±1.69		37.82±2.04	36.50±2.40	37.20±2.60	37.70±2.70	42.00±3.60	36.30±4.40	35.50±4.40	35.50±4.10	36.25±0.90	38.26±0.95	41.32±1.03
Hedrick et al., 2011	PM-2 stage	N/A	India-14	33.2440	78.2020	4886	2.0	2.70	0.0	1.000	5.45±1.22	07KNSTD		0.81±0.19		0.84±0.2	1.01±0.14	1.02±0.16	0.92±0.17	0.74±0.18	0.95±0.25	0.97±0.25	0.89±0.20	0.91±0.21	0.89±0.20	0.73±0.16
Hedrick et al., 2011	PM-2 stage	N/A	India-56	33.2440	78.1980	4924	3.0	2.70	0.0	1.000	29.04±0.75	07KNSTD		4.46±0.22		4.65±0.26	4.50±0.40	4.58±0.43	4.17±0.31	3.92±0.33	4.16±0.74	4.65±0.74	4.11±0.65	4.42±0.11	4.35±0.11	3.85±0.10
Hedrick et al., 2011	PM-2 stage	N/A	India-57	33.2450	78.1990	4921	3.0	2.70	0.0	1.000	17.76±0.70	07KNSTD		2.78±0.18		2.91±0.21	2.82±0.15	2.85±0.17	2.70±0.22	2.40±0.22	2.68±0.28	2.93±0.28	2.70±0.30	2.75±0.11	2.74±0.11	2.36±0.09
Dortch et al., 2013	Ladakh Chang La cirque	N/A	Chang-1	34.0400	77.9300	5461	5.0	2.70	0.0	1.000	17.00±2.00	07KNSTD		2.02±0.27		2.07±0.29	2.16±0.35	2.21±0.34	1.99±0.29	1.79±0.26	1.97±0.45	2.26±0.45	1.95±0.39	1.88±0.22	1.92±0.23	1.77±0.21
Dortch et al., 2013	Ladakh Chang La cirque	N/A	Chang-2	34.0400	77.9300	5459	3.0	2.70	0.0	1.000	20.00±2.00	07KNSTD		2.36±0.28	Chi-squared: 2.02; Skewness: +0.72; Outlier: 2; Wt. mean: 2.31±0.28 ka; Ar. Mean: 2.29±0.28 ka; Peak: 2.15 ka	2.44±0.31	2.51±0.26	2.55±0.26	2.34±0.31	2.08±0.27	2.31±0.39	2.59±0.39	2.30±0.40	2.29±0.23	2.34±0.23	2.05±0.21
Dortch et al., 2013	Ladakh Chang La cirque	N/A	Chang-3	34.0400	77.9300	5458	4.0	2.70	0.0	1.000	22.00±1.00	07KNSTD		2.65±0.18		2.73±0.21	2.71±0.16	2.75±0.18	2.59±0.22	2.30±0.21	2.53±0.33	2.80±0.33	2.51±0.32	2.62±0.12	2.64±0.12	2.27±0.10
Dortch et al., 2013	Ladakh Chang La cirque	N/A	Chang-4	34.0400	77.9300	5460	5.0	2.70	0.0	1.000	55.00±2.00	07KNSTD	2.29±0.28	6.27±0.31		6.31±0.33	6.20±0.60	6.39±0.67	5.96±0.48	5.81±0.52	5.77±1.20	6.20±1.20	5.68±0.67	6.48±0.24	6.44±0.24	5.72±0.21
Dortch et al., 2013	Ladakh Chang La cirque	N/A	Chang-5	34.0400	77.9300	5462	4.0	2.70	0.0	1.000	18.00±1.00	07KNSTD		2.13±0.16		2.18±0.19	2.28±0.23	2.33±0.22	2.10±0.22	1.88±0.19	2.08±0.36	2.37±0.36	2.05±0.34	1.99±0.11	2.02±0.11	1.85±0.10
Dortch et al., 2013	Ladakh Chang La cirque	N/A	Chang-6	34.0400	77.9300	5445	5.0	2.70	0.0	1.000	97.00±3.00	07KNSTD		10.8±0.51		10.7±0.54	11.19±0.92	11.00±1.00	10.48±0.93	10.30±0.90	10.30±1.60	10.90±1.60	10.10±1.50	10.93±0.34	11.03±0.34	10.17±0.32
Saha et al., 2018	Late Holocene	mG1	KO-14	32.9672	78.1794	5374	3.0	2.70	0.0	0.961	17.10±0.72	07KNSTD		2.36±0.19		2.27±0.19	2.43±0.19	2.47±0.21	2.24±0.22	1.98±0.18	2.22±0.37	2.49±0.37	2.21±0.33	1.95±0.08	2.20±0.09	2.20±0.09
Saha et al., 2018	Late Holocene	mG1	KO-15	32.9678	78.1796	5366	3.0	2.70	0.0	0.966	4.93±0.26	07KNSTD		0.64±0.05	Chi-squared: 9.37; Skewness: -1.07; Outlier: 2; Wt. mean: 2.10±0.42 ka; Ar. Mean: 2.25±0.42 ka; Peak: 2.48 ka !	0.62±0.05	0.82±0.06	0.83±0.08	0.73±0.06	0.57±0.06	0.74±0.12	0.72±0.12	0.74±0.10	0.56±0.03	0.72±0.04	0.73±0.04
Saha et al., 2018	Late Holocene	mG1	KO-16	32.9678	78.1796	5366	4.0	2.70	0.0	0.966	3.87±0.32	07KNSTD	2.25±0.42	0.5±0.06		0.48±0.06	0.66±0.07	0.67±0.09	0.58±0.06	0.45±0.05	0.59±0.10	0.57±0.10	0.59±0.09	0.44±0.04	0.57±0.05	0.58±0.05
Saha et al., 2018	Late Holocene	mG1	KO1601	32.9680	78.1796	5374	2.0	2.70	0.0	0.966	13.40±0.39	07KNSTD		1.79±0.12		1.73±0.12	1.86±0.17	1.90±0.19	1.71±0.14	1.53±0.13	1.69±0.32	1.92±0.32	1.68±0.24	1.51±0.04	1.65±0.05	1.63±0.05
Saha et al., 2018	Late Holocene	mG1	KO1602	32.9671	78.1800	5388	1.5	2.70	0.0	0.954	18.94±0.71	07KNSTD		2.61±0.19		2.51±0.19	2.63±0.16	2.67±0.18	2.47±0.22	2.17±0.19	2.42±0.36	2.69±0.36	2.41±0.31	2.14±0.08	2.53±0.10	2.51±0.09
Seong et al., 2009	Olimde 7 stage	m7A	MUST-32	38.3610	75.1710	4082	5.0	2.70	0.0	0.990	10.76±0.54	KNSTD		2.15±0.16		2.1±0.17	2.24±0.23	2.28±0.26	2.11±0.21	1.94±0.19	2.22±0.34	2.54±0.34	2.19±0.35	1.93±0.10	2.00±0.10	1.91±0.10
Seong et al., 2009	Olimde 7 stage	m7A	MUST-33	38.3610	75.1710	4081	5.0	2.70	0.0	0.990	11.21±0.54	KNSTD		2.24±0.16	Chi-squared: 0.19; Skewness: +1.07; Outlier: 1; Wt. mean: 2.19±0.07 ka; Ar. Mean: 2.20±0.07 ka; Peak: 2.19 ka	2.2±0.18	2.34±0.22	2.38±0.24	2.21±0.22	2.00±0.20	2.32±0.34	2.63±0.34	2.29±0.35	2.03±0.10	2.10±0.10	1.99±0.10
Seong et al., 2009	Olimde 7 stage	m7A	MUST-34	38.3600	75.1720	4094	5.0	2.70	0.0	0.990	11.66±0.54	KNSTD		2.32±0.17		2.28±0.19	2.40±0.20	2.45±0.22	2.29±0.23	2.10±0.20	2.39±0.35	2.70±0.35	2.36±0.33	2.11±0.10	2.19±0.10	2.06±0.10
Seong et al., 2009	Olimde 7 stage	m7A	MUST-35	38.3590	75.1720	4120	5.0	2.70	0.0	0.980	13.56±0.54	KNSTD	2.20±0.07	2.71±0.17		2.69±0.19	2.72±0.17	2.76±0.18	2.64±0.22	2.43±0.22	2.71±0.32	3.00±0.32	2.68±0.32	2.58±0.10	2.62±0.11	2.39±0.10
Seong et al., 2009	Olimde 7 stage	m7A	MUST-36	38.3560	75.1730	4167	5.0	2.70	0.0	0.990	11.48±0.54	KNSTD		2.19±0.15		2.15±0.18	2.29±0.24	2.32±0.22	2.16±0.22	1.99±0.19	2.26±0.34	2.58±0.34	2.23±0.33	1.97±0.09	2.05±0.10	1.95±0.09
Seong et al., 2009	Olimde 7 stage	m7A	MUST-37	38.3560	75.1730	4176	5.0	2.70	0.0	0.990	11.30±0.45	KNSTD		2.15±0.14		2.1±0.16	2.23±0.22	2.28±0.24	2.10±0.20	1.95±0.18	2.21±0.33	2.54±0.33	2.18±0.35	1.92±0.08	2.00±0.08	1.91±0.08
Seong et al., 2009	Olimde 7 stage	m7A	MUST-38	38.3550	75.1730	4180	5.0	2.70	0.0	0.990	11.21±0.81	KNSTD		2.12±0.19		2.08±0.21	2.21±0.26	2.24±0.28	2.09±0.25	1.93±0.22	2.19±0.39	2.51±0.39	2.15±0.38	1.90±0.14	1.98±0.14	1.89±0.14
Seong et al., 2009	Olimde 7 stage	m7H	KONG_14	38.6440	75.0410	4168	5.0	2.70	0.0	1.000	9.58±0.99	KNSTD		1.78±0.21		1.72±0.22	1.80±0.26	1.80±0.30	1.76±0.24	1.63±0.23	1.81±0.49	2.12±0.49	1.78±0.34	1.58±0.16	1.67±0.17	1.60±0.17
Seong et al., 2009	Olimde 7 stage	m7H	KONG_15	38.6440	75.0400	4178	5.0	2.70	0.0	1.000	5.15±0.90	KNSTD		0.94±0.17	Chi-squared: 0.75; Skewness: -1.63 ka; Outlier: 1; Wt. mean: 1.66±0.17 ka; Ar. Mean: 1.66±0.17 ka; Peak: 1.70 ka	0.89±0.17	1.05±0.14	1.06±0.16	1.02±0.17	0.87±0.18	1.04±0.21	1.08±0.21	1.03±0.18	0.97±0.17	0.97±0.17	0.86±0.15
Seong et al., 2009	Olimde 7 stage	m7H	KONG_16	38.6440	75.0400	4179	5.0	2.70	0.0	1.000	9.40±0.90	KNSTD	1.66±0.17	1.74±0.19		1.68±0.2	1.75±0.26	1.79±0.26	1.72±0.22	1.59±0.21	1.76±0.45	2.06±0.45	1.73±0.32	1.54±0.15	1.63±0.16	1.56±0.15
Seong et al., 2009	Olimde 7 stage	m7H	KONG_17	38.6430	75.0390	4178	5.0	2.70	0.0	1.000	7.96±0.99	KNSTD		1.46±0.2		1.4±0.2	1.49±0.21	1.52±0.21	1.47±0.21	1.35±0.22	1.50±0.41	1.68±0.41	1.48±0.27	1.31±0.16	1.38±0.17	1.32±0.17
Orr et al., 2017	Late Holocene	mS2	STOK-1401	33.9873	77.4557	5329	3.0	2.70	0.0	0.964	15.57±0.51	07KNSTD		2.06±0.14		2.00±0.14	2.16±0.21	2.21±0.23	1.98±0.18	1.78±0.16	1.97±0.37	2.26±0.37	1.90±0.30	1.75±0.06	1.90±0.06	1.87±0.06
Orr et al., 2017	Late Holocene	mS2	STOK-1402	33.9879	77.4557	5330	3.0	2.70	0.0	0.967	11.72±0.58	07KNSTD		1.51±0.12		1.48±0.12	1.59±0.14	1.61±0.13	1.50±0.12	1.33±0.13	1.48±0.30	1.60±0.30	1.50±0.20	1.31±0.07	1.43±0.07	1.38±0.07
Orr et al., 2017	Late Holocene	mS2	STOK-1403	33.9883	77.4570	5323	1.0	2.70	0.0	0.969	14.65±0.65	07KNSTD		1.89±0.14	Chi-squared: 21.83; Skewness: +0.34; Outlier: 3	1.84±0.14	2.00±0.20	2.00±0.20	1.82±0.16	1.64±0.15	1.81±0.37	2.08±0.37	1.79±0.28	1.62±0.07	1.75±0.08	1.72±0.08
Orr et al., 2017	Late Holocene	mS2	STOK-1404	33.9882	77.4571	5328	2.0	2.70	0.0	0.969	2.08±0.09	07KNSTD		0.25±0.02		0.25±0.02	0.34±0.04	0.35±0.04	0.32±0.03	0.24±0.02	0.30±0.05	0.29±0.05	0.30±0.04	0.23±0.01	0.32±0.01	±
Orr et al., 2017	Late Holocene	mS1	STOK-1405	33.9872	77.4601	5370	2.0	2.70	0.0	0.980	7.64±0.31	07KNSTD	1.42±0.48	0.93±0.07		0.92±0.07	1.08±0.07	1.10±0.07	1.02±0.07	0.84±0.08	1.02±0.13	1.05±0.13	1.00±0.10	0.82±0.03	0.98±0.04	0.98±0.04
Orr et al., 2017	Late Holocene	mS1	STOK-1406	33.9870	77.4600	5314	2.5	2.70	0.0	0.980	4.54±0.22	07KNSTD		0.56±0.04		0.55±0.04	0.73±0.06	0.74±0.07	0.65±0.06	0.51±0.05	0.66±0.11	0.64±0.11	0.66±0.10	0.50±0.02	0.63±0.03	0.65±0.03
Orr et al., 2017	Late Holocene	mS1	STOK-1407	33.9871	77.4608	5340	3.0	2.70	0.0	0.978	1.25±0.21	07KNSTD		0.14±0.03	Peak: !	0.14±0.03	0.20±0.03	0.21±0.03	0.19±0.04	0.14±0.03	0.18±0.04	0.17±0.04	0.18±0.04	0.14±0.02	0.19±0.03	±
Orr et al., 2017	Late Holocene	mS1	STOK-1408	33.9871	77.4606	5308	3.0	2.70	0.0	0.978	9.31±0.72	07KNSTD		1.19±0.11		1.17±0.11	1.29±0.13	1.31±0.11	1.23±0.11	1.06±0.12	1.21±0.24	1.28±0.24	1.21±0.14	1.04±0.08	1.16±0.09	1.14±0.09
Saha et al., 2018	Late Holocene	mS1	STOK-1516	33.9872	77.4599	5303	3.0	2.70	0.0	0.977	7.37±0.65	07KNSTD		0.94±0.1		0.92±0.1	1.09±0.09	1.10±0.09	1.02±0.09	0.84±0.10	1.02±0.15	1.05±0.15	1.02±0.11	0.83±0.07	0.98±0.09	0.99±0.09

Reference	Landform	Group	Sample	Lat	Lon	Elev	Thick	Dens	f1	f2	Conc	Std	Group age	Age	Statistics	A1	A2	A3	A4	A5	A6	A7	A8	A9	A10	A11
Seong et al., 2009	Olimde 7 stage	m3I	KONG_35	38.7090	75.2800	3326	5.0	2.70	0.0	0.930	3.07±0.54	KNSTD		0.95±0.18		0.94±0.18	1.08±0.17	1.09±0.18	1.02±0.17	0.88±0.19	1.09±0.24	1.13±0.24	1.08±0.19	0.99±0.18	0.97±0.17	0.87±0.15
Seong et al., 2009	Olimde 7 stage of	m3I	KONG_36	38.7090	75.2800	3328	5.0	2.70	0.0	0.930	5.33±0.63	KNSTD		1.67±0.22	Chi-squared: 4.58 Skewness: -0.03 Outlier: 1	1.66±0.23	1.74±0.29	1.76±0.32	1.65±0.25	1.53±0.24	1.79±0.48	2.06±0.48	1.77±0.36	1.53±0.18	1.56±0.19	1.50±0.18
Seong et al., 2009	Olimde 7 stage of	m3I	KONG_37	38.7110	75.2800	3309	5.0	2.70	0.0	0.930	5.70±0.54	KNSTD	1.39±0.42	1.81±0.2	1.35±0.42 ka Ar. Mean: 1.39±0.42 ka	1.8±0.21	1.90±0.26	1.92±0.29	1.78±0.23	1.65±0.22	1.90±0.43	2.25±0.43	1.92±0.36	1.67±0.16	1.69±0.16	1.62±0.15
Seong et al., 2009	Olimde 7 stage of	m3I	KONG_38	38.7140	75.2800	3299	5.0	2.70	0.0	0.930	3.53±0.63	KNSTD		1.11±0.21	Peak: 1.02 ka !	1.09±0.21	1.21±0.21	1.22±0.23	1.16±0.22	1.03±0.22	1.23±0.37	1.31±0.37	1.22±0.26	1.10±0.20	1.09±0.20	1.01±0.18
Seong et al., 2009	Olimde 7 stage of	m3I	KONG_41	38.7380	75.2730	3118	5.0	2.70	0.0	0.930	1.27±0.45	KNSTD		0.43±0.16		0.43±0.16	0.56±0.20	0.56±0.22	0.50±0.18	0.41±0.17	0.55±0.22	0.54±0.22	0.55±0.21	0.00±0.00	0.00±0.00	0.00±0.00
Orr et al., 2017	N/A	mG1	ZK34	34.0043	77.4618	5280	3.0	2.70	0.0	0.960	16.20±1.20	07KNSTD	1.33±0.12	2.22±0.18	!	2.14±0.20	2.31±0.24	2.45±0.24	1.94±0.21	2.16±0.26	1.98±0.24	2.28±0.25	2.18±0.25	2.01±0.15	2.04±0.15	1.87±0.14
Orr et al., 2017	N/A	mG1	ZK36	34.0042	77.4610	5294	3.0	2.70	0.0	1.000	10.50±0.70	07KNSTD		1.33±0.12		1.29±0.11	1.41±0.12	1.5±0.15	1.20±0.12	1.36±0.12	1.26±0.11	1.35±0.15	1.36±0.12	1.23±0.08	1.26±0.08	1.16±0.07
Seong et al., 2007	Askole 3 stage	m1H	K2-90	35.6880	75.9270	3095	3.0	2.70	0.0	0.970	1.81±0.90	KNSTD		0.70±0.34		0.66±0.32	0.84±0.07	0.84±0.07	0.74±0.05	0.60±0.05	0.83±0.14	0.83±0.14	0.83±0.11	0.00±0.00	0.00±0.00	0.00±0.00
Seong et al., 2007	Askole 3 stage	m1H	K2-91	35.6950	75.9270	3096	3.0	2.70	0.0	0.960	3.62±0.90	KNSTD		1.34±0.35	Chi-squared: 0.82 Skewness: -0.08 Outlier: 2	1.41±0.38	1.49±0.39	1.50±0.34	1.36±0.34	1.22±0.35	1.50±0.60	1.70±0.60	1.50±0.43	1.30±0.33	1.28±0.32	1.20±0.30
Seong et al., 2007	Askole 3 stage	m1H	K2-92	35.6870	75.9260	3094	3.0	2.70	0.0	0.960	2.71±0.90	KNSTD		1.05±0.36	Wt. Mean: 1.03±0.28 ka	1.00±0.34	1.16±0.07	1.16±0.08	1.07±0.07	0.92±0.07	1.16±0.18	1.22±0.18	1.16±0.13	0.00±0.00	0.00±0.00	0.00±0.00
Seong et al., 2007	Askole 3 stage	m1H	K2-93	35.6860	75.9260	3090	2.0	2.70	0.0	0.960	7.23±0.90	KNSTD	1.03±0.28	2.75±0.37	Ar. Mean: 1.03±0.28 ka	2.94±0.41	2.88±0.33	2.90±0.31	2.70±0.40	2.43±0.39	2.90±0.54	3.16±0.54	2.88±0.41	2.77±0.35	2.66±0.33	2.38±0.30
Seong et al., 2007	Askole 3 stage	m1H	K2-94	35.6880	75.9250	3096	3.0	2.70	0.0	0.960	3.62±0.90	KNSTD		1.34±0.35	Peak: 1.02 ka	1.41±0.38	1.49±0.39	1.50±0.34	1.36±0.34	1.22±0.35	1.50±0.60	1.70±0.60	1.50±0.43	1.30±0.33	1.28±0.32	1.20±0.30
Seong et al., 2007	Askole 3 stage	m1H	K2-95	35.2920	75.6620	3087	3.0	2.70	0.0	0.960	1.81±0.90	KNSTD		0.72±0.35		0.68±0.33	0.86±0.07	0.87±0.08	0.76±0.05	0.62±0.05	0.85±0.14	0.86±0.14	0.86±0.12	0.00±0.00	0.00±0.00	0.00±0.00
Seong et al., 2007	Askole 3 stage	m1H	K2-96	35.2920	75.6620	3116	3.0	2.70	0.0	0.970	4.52±0.90	KNSTD		1.67±0.35		1.78±0.39	1.85±0.49	1.87±0.52	1.65±0.38	1.51±0.36	1.86±0.62	2.11±0.62	1.85±0.52	1.61±0.32	1.56±0.31	1.48±0.30
Saha et al., 2018	Late Holocene	mM2	KO1	32.9321	78.2143	5532	3.0	2.7	0.0	1.000	20.44±0.66	07KNSTD		2.56±0.19		2.46±0.19	2.59±0.18	2.63±0.17	2.42±0.21	2.13±0.19	2.37±0.33	2.63±0.33	2.30±0.30	2.10±0.07	2.48±0.08	2.44±0.08
Saha et al., 2018	Late Holocene	mM2	KO-2	32.9317	78.2143	5541	6.0	2.7	0.0	1.000	9.03±0.53	07KNSTD		1.09±0.09	Chi-squared: 0.90 Skewness: -0.17 Outlier: 1	1.07±0.09	1.21±0.08	1.23±0.11	1.14±0.09	0.96±0.10	1.12±0.16	1.16±0.16	1.12±0.12	0.95±0.06	1.09±0.07	1.08±0.06
Saha et al., 2018	Late Holocene	mM2	KO-3	32.9314	78.2142	5548	4.0	2.7	0.0	0.991	8.18±0.39	07KNSTD		0.98±0.07	Wt. mean: 0.99±0.08 ka	0.95±0.07	1.12±0.06	1.13±0.08	1.05±0.08	0.86±0.08	1.04±0.13	1.06±0.13	1.00±0.10	0.85±0.04	1.01±0.05	1.01±0.05
Saha et al., 2018	Late Holocene	mM2	MENTOK-1505	32.9312	78.2145	5569	2.0	2.7	0.0	0.991	8.76±0.32	07KNSTD	1.00±0.08	1.02±0.07	Ar. Mean: 1.00±0.08 ka	1.00±0.07	1.15±0.07	1.17±0.08	1.08±0.08	0.90±0.08	1.07±0.13	1.10±0.13	1.07±0.11	0.89±0.03	1.04±0.04	1.04±0.04
Saha et al., 2018	Late Holocene	mM2	MENTOK-1506	32.9311	78.2145	5574	1.0	2.7	0.0	0.992	7.84±0.50	07KNSTD		0.90±0.08	Peak: 1.00 ka	0.88±0.08	1.06±0.07	1.08±0.08	0.99±0.09	0.80±0.08	0.98±0.15	1.00±0.15	0.99±0.11	0.78±0.05	0.95±0.06	0.96±0.06
Seong et al., 2009	Olimde 8 stage	m8A	MUST-39	38.3530	75.1710	4228	5.0	2.70	0.0	1.000	2.62±0.45	KNSTD		0.46±0.08	Chi-squared: 10.19 Skewness: +1.08 Outlier: 0	0.44±0.08	0.58±0.12	0.59±0.12	0.54±0.10	0.44±0.09	0.56±0.12	0.54±0.12	0.55±0.12	0.53±0.09	0.52±0.09	0.43±0.07
Seong et al., 2009	Olimde 8 stage	m8A	MUST-40	38.3530	75.1710	4227	5.0	2.70	0.0	1.000	5.52±0.45	KNSTD		0.99±0.09	Wt. mean: 0.66±0.27 ka	0.95±0.1	1.09±0.10	1.10±0.08	1.06±0.11	0.92±0.11	1.08±0.17	1.12±0.17	1.07±0.13	1.01±0.08	1.01±0.08	0.90±0.07
Seong et al., 2009	Olimde 8 stage	m8A	MUST-41	38.3530	75.1700	4238	5.0	2.70	0.0	1.000	3.53±0.36	KNSTD	0.69±0.27	0.62±0.07	Ar. Mean: 0.69±0.27 ka Peak: 0.60 ka !	0.6±0.07	0.76±0.10	0.77±0.11	0.71±0.09	0.58±0.08	0.73±0.15	0.72±0.15	0.73±0.11	0.70±0.07	0.68±0.07	0.57±0.06
Saha et al., 2018	Late Holocene	mM1	KO-7	32.9328	78.2136	5524	6.0	2.7	0.0	1.000	2.04±0.14	07KNSTD		0.24±0.02		0.23±0.02	0.32±0.03	0.33±0.04	0.30±0.03	0.22±0.02	0.28±0.05	0.27±0.05	0.28±0.05	0.22±0.01	0.30±0.02	±
Saha et al., 2018	Late Holocene	mM1	KO-8	32.9333	78.2136	5516	2.5	2.7	0.0	1.000	5.92±0.55	07KNSTD		0.69±0.08	Chi-squared: 1.47 Skewness: -1.71 Outlier: 1	0.68±0.08	0.88±0.11	0.90±0.10	0.79±0.09	0.62±0.08	0.79±0.15	0.78±0.15	0.80±0.11	0.61±0.06	0.77±0.07	0.78±0.07
Saha et al., 2018	Late Holocene	mM1	KO-9	32.9341	78.2147	5503	1.0	2.7	0.0	1.000	6.00±0.24	07KNSTD		0.70±0.05	Wt. mean: 0.67±0.09 ka	0.68±0.05	0.89±0.08	0.91±0.07	0.79±0.06	0.62±0.06	0.80±0.13	0.79±0.13	0.80±0.10	0.61±0.02	0.78±0.03	0.79±0.03
Saha et al., 2018	Late Holocene	mM1	KO10	32.9345	78.2148	5503	1.0	2.7	0.0	1.000	4.73±0.67	07KNSTD	0.64±0.09	0.54±0.09	Ar. Mean: 0.64±0.09 ka Peak: 0.69 ka	0.53±0.09	0.72±0.10	0.73±0.11	0.63±0.10	0.49±0.08	0.64±0.13	0.62±0.13	0.64±0.13	0.48±0.07	0.62±0.09	0.63±0.09
Blomdin et al. (2016)	Bordoo Valley	BOR 1	TS-C-12-027	41.8125	78.1319	3775	2.00	2.70	0.00	0.990	2.52±0.37	07KNSTD		0.45±0.07		0.50±0.08	0.60±0.10	0.61±0.07	0.48±0.08	0.58±0.09	0.60±0.12	0.56±0.11	0.59±0.11	0.56±0.08	0.55±0.08	0.47±0.07
Blomdin et al. (2016)	Bordoo Valley	BOR 1	TS-C-12-028	41.8124	78.1314	3776	2.00	2.70	0.00	0.990	28.96±1.26	07KNSTD		5.40±0.32	Chi-squared: 10.96 Skewness: +1.23 Outlier: 0	5.78±0.33	5.50±0.40	5.54±0.39	5.51±0.51	5.61±0.48	5.69±0.84	6.00±1.00	5.55±0.66	5.54±0.24	5.76±0.25	5.41±0.24
Blomdin et al. (2016)	Bordoo Valley	BOR 1	TS-C-12-029	41.8121	78.1299	3759	2.50	2.70	0.00	0.990	17.23±1.01	07KNSTD		3.34±0.26	Wt. mean: 0.65±0.23 ka	3.61±0.26	3.34±0.28	3.40±0.32	3.32±0.33	3.48±0.32	3.50±0.55	3.79±0.57	3.41±0.47	3.22±0.19	3.43±0.20	3.26±0.19
Blomdin et al. (2016)	Bordoo Valley	BOR 1	TS-C-12-030	41.8122	78.1301	3766	2.60	2.70	0.00	0.990	3.16±0.42	07KNSTD	0.64±0.23	0.57±0.08	Ar. Mean: 0.64±0.23 ka Peak: !	0.64±0.09	0.75±0.10	0.76±0.09	0.61±0.10	0.73±0.10	0.75±0.14	0.72±0.16	0.74±0.13	0.69±0.09	0.69±0.09	0.60±0.08
Blomdin et al. (2016)		BOR 1	TS-C-12-031	41.8124	78.1305	3769	2.00			0.980	4.95±0.22	07KNSTD		0.90±0.07		1.01±0.07	1.07±0.07	1.09±0.09	0.95±0.09	1.08±0.08	1.10±0.14	1.11±0.16	1.08±0.13	0.99±0.04	1.02±0.05	0.94±0.04
Dortch et al., 2013	Pangong high cirque	N/A	Pang-25	33.8900	78.4300	5375	5.0	2.70	0.0	1.000	14.47±3.62	KNSTD		1.79±0.48		1.84±0.5	1.90±0.51	1.94±0.63	1.77±0.52	1.59±0.46	1.74±0.69	1.99±0.69	1.72±0.55	1.67±0.42	1.70±0.43	1.57±0.39
Dortch et al., 2013	Pangong high cirque	N/A	Pang-26	33.8900	78.4300	5368	5.0	2.70	0.0	1.000	4.52±0.90	KNSTD		0.54±0.11	Chi-squared: 0.63 Skewness: 0 Outlier: 2	0.54±0.12	0.72±0.15	0.73±0.16	0.64±0.15	0.50±0.12	0.64±0.18	0.63±0.18	0.65±0.17	0.64±0.13	0.62±0.12	0.49±0.10
Dortch et al., 2013	Pangong high cirque	N/A	Pang-27	33.8900	78.4300	5371	5.0	2.70	0.0	1.000	5.43±1.81	KNSTD		0.65±0.22	Wt. mean: 0.50±0.11 ka	0.66±0.23	0.84±0.30	0.86±0.28	0.76±0.26	0.60±0.23	0.77±0.30	0.75±0.30	0.77±0.27	0.75±0.25	0.74±0.25	0.59±0.20
Dortch et al., 2013	Pangong high cirque	N/A	Pang-28	33.8900	78.4300	5363	5.0	2.70	0.0	1.000	14.47±1.81	KNSTD	0.54±0.11	1.8±0.24	Ar. Mean: 0.54±0.11 ka Peak: 0.50 ka	1.84±0.27	1.91±0.31	1.95±0.34	1.77±0.29	1.60±0.26	1.75±0.46	2.00±0.46	1.73±0.35	1.68±0.21	1.71±0.21	1.57±0.20
Dortch et al., 2013	Pangong high cirque	N/A	Pang-29	33.8900	78.4300	5360	4.0	2.70	0.0	1.000	3.62±0.90	KNSTD		0.43±0.11		0.43±0.11	0.57±0.17	0.58±0.18	0.51±0.13	0.40±0.11	0.52±0.15	0.50±0.15	0.52±0.15	0.52±0.13	0.51±0.13	0.39±0.10
Saha et al., 2018	Late Holocene	mA2c	LATO-1409	33.6851	77.5953	5314	3.0	2.70	0.0	0.959	265.10±5.64	07KNSTD		27.56±1.52		29.25±1.52	28.30±1.90	28.80±2.10	29.00±2.10	31.10±2.60	27.50±3.40	27.10±3.40	26.90±3.20	30.65±0.66	28.48±0.61	26.35±0.56
Saha et al., 2018	Late Holocene	mA2c	LATO-1410	33.6851	77.5953	5321	2.5	2.70	0.0	0.959	21.86±0.87	07KNSTD		3.04±0.21	Chi-squared: 24.25 Skewness: 0.94 Outlier: 3	2.93±0.21	2.91±0.16	2.94±0.18	2.83±0.21	2.53±0.23	2.75±0.29	2.99±0.29	2.73±0.29	2.49±0.10	2.88±0.11	2.86±0.11
Saha et al., 2018	Late Holocene	mA2c	LATO-1411	33.6851	77.5952	5315	2.0	2.70	0.0	0.959	29.63±1.78	07KNSTD		4.06±0.32	Wt. mean: 0.45±0.20 ka	3.92±0.32	3.82±0.41	3.91±0.46	3.71±0.32	3.43±0.35	3.53±0.68	3.92±0.68	3.49±0.51	3.37±0.20	3.86±0.23	3.86±0.23
Saha et al., 2018	Late Holocene	mA2c	LATO-1412	33.6850	77.5957	5315	1.0	2.70		0.958	2.76±0.15	07KNSTD	0.52±0.20	0.35±0.03	Ar. Mean: 0.52±0.20 ka	0.34±0.03	0.46±0.04	0.47±0.05	0.42±0.03	0.32±0.03	0.41±0.07	0.40±0.07	0.41±0.07	0.31±0.02	0.41±0.02	0.42±0.02
Saha et al., 2018	Late Holocene	mA2c	LATO-1413	33.6849	77.5957	5317	2.0	2.70		0.959	5.77±0.20	07KNSTD		0.74±0.06	Peak: !	0.73±0.06	0.93±0.06	0.94±0.06	0.83±0.07	0.67±0.06	0.85±0.15	0.85±0.15	0.85±0.11	0.66±0.02	0.81±0.03	0.83±0.03
Saha et al., 2018	Late Holocene	mA2c	LATO-1414	33.6851	77.5954	5314	2.0	2.70		0.960	3.76±0.18	07KNSTD		0.48±0.03		0.46±0.03	0.62±0.06	0.64±0.07	0.56±0.05	0.43±0.04	0.56±0.09	0.55±0.09	0.57±0.08	0.43±0.02	0.55±0.03	0.56±0.03
Seong et al., 2009	Olimde 8 stage	m6C	MUST-52	38.2850	75.0230	4580	5.0			1.000	1.18±0.36	KNSTD		0.16±0.06	Chi-squared: 4.19 Skewness: +0.14 Outlier: 1	0.16±0.05	0.22±0.08	0.23±0.09	0.22±0.07	0.16±0.06	0.21±0.07	0.18±0.07	0.20±0.07	0.00±0.00	0.00±0.00	0.00±0.00
Seong et al., 2009	Olimde 8 stage	m6C	MUST-53	38.2850	75.0260	4568	5.0			1.000	2.89±0.36	KNSTD		0.43±0.06	Wt. mean: 0.48±0.15 ka	0.4±0.05	0.54±0.07	0.55±0.07	0.50±0.07	0.41±0.07	0.51±0.11	0.50±0.11	0.51±0.09	0.50±0.06	0.49±0.06	0.40±0.05
Seong et al., 2009	Olimde 8 stage	m6C	MUST-54	38.2870	75.0240	4524	5.0			1.000	2.26±0.45	KNSTD	0.51±0.15	0.34±0.07	Ar. Mean:	0.32±0.07	0.44±0.09	0.45±0.09	0.41±0.08	0.32±0.08	0.42±0.11	0.39±0.11	0.41±0.10	0.41±0.08	0.40±0.08	0.32±0.06
Seong et al., 2009	Olimde 8 stage	m6C	MUST-55	38.2870	75.0250	4504	5.0			1.000	4.34±0.45	KNSTD		0.68±0.08		0.64±0.08	0.81±0.10	0.82±0.12	0.76±0.10	0.63±0.09	0.78±0.16	0.78±0.16	0.77±0.13	0.74±0.08	0.73±0.08	0.62±0.07

Reference	Location	Code	Sample	Lat	Long	Elev	Thick	Density	Shield	Scaling	Conc.	Standard	Group age	Age	Statistics											
Seong et al., 2009	Olimde 8 stage	m6C	MUST-56	38.2870	75.0250	4511	5.0	2.70	0.0	1.000	3.71±0.45	KNSTD		0.57±0.08	0.51±0.15 ka Peak: 0.42 ka !	0.54±0.07	0.70±0.08	0.71±0.10	0.66±0.11	0.54±0.08	0.67±0.13	0.65±0.13	0.67±0.13	0.64±0.08	0.63±0.08	0.53±0.06
Koppes et al. (2008)	Ala Archa	N/A	KTS98-CS-101	42.52	74.51	3246	2.0	2.70	0.0	0.929	1.20±0.30	07KNSTD	0.49±0.25	0.31±0.08	Chi-squared: ! Skewness: ! Outlier: 0 Wt. mean: 0.43±0.25 ka Ar. Mean: 0.49±0.25 ka Peak: !	0.32±0.09	0.41±0.09	0.41±0.10	0.32±0.08	0.40±0.10	0.41±0.11	0.37±0.12	0.40±0.10	0.39±0.10	0.38±0.09	0.32±0.08
Koppes et al. (2008)	Ala Archa	N/A	KTS98-CS-102	42.52	74.51	3180	1.5	2.70	0.0	0.913	2.50±0.40	07KNSTD		0.67±0.11		0.73±0.12	0.83±0.14	0.84±0.13	0.70±0.13	0.82±0.13	0.87±0.19	0.85±0.20	0.85±0.17	0.77±0.12	0.78±0.13	0.69±0.11
Li et al., 2014	LIA	Daxi	1#-10-18	43.115	86.825	3686	3.0	2.70	0.0	0.972	1.66±0.18	07KNSTD		0.30±0.03		0.33±0.04	0.42±0.05	0.42±0.06	0.33±0.04	0.42±0.05	0.42±0.08	0.37±0.08	0.41±0.07	0.41±0.04	0.40±0.04	0.32±0.04
Li et al., 2014	LIA	Daxi	1#-10-19	43.115	86.825	3691	2.0	2.70	0.0	0.972	2.00±0.18	07KNSTD	0.33±0.02	0.35±0.03	Chi-squared: 0.49 Skewness: -1.19 Outlier: 0 Wt. mean: 0.33±0.02 ka Ar. Mean: 0.33±0.02 ka Peak: !	0.40±0.04	0.50±0.06	0.51±0.04	0.39±0.05	0.49±0.05	0.50±0.09	0.45±0.09	0.49±0.08	0.47±0.04	0.47±0.04	0.38±0.04
Li et al., 2014	LIA	Daxi	1#-10-20	43.115	86.825	3694	1.0	2.70	0.0	0.972	1.93±0.45	07KNSTD		0.34±0.08		0.38±0.09	0.47±0.13	0.48±0.14	0.37±0.09	0.47±0.10	0.47±0.13	0.43±0.14	0.47±0.13	0.46±0.11	0.45±0.10	0.37±0.09
Li et al., 2014	LIA	Daxi	1#-10-21	43.115	86.825	3698	3.5	2.70	0.0	0.972	1.84±0.22	07KNSTD		0.33±0.04		0.36±0.05	0.46±0.05	0.47±0.07	0.36±0.05	0.46±0.06	0.46±0.09	0.42±0.09	0.45±0.08	0.44±0.05	0.43±0.05	0.36±0.04
Hedrick et al., 2011	PM-3 stage	N/A	India-45	33.2260	78.1660	5266	3.0	2.70	0.0	1.000	4.45±0.30	07KNSTD		0.55±0.05		0.57±0.05	0.75±0.07	0.76±0.07	0.66±0.07	0.52±0.05	0.67±0.11	0.65±0.11	0.68±0.11	0.66±0.04	0.65±0.04	0.51±0.03
Hedrick et al., 2011	PM-3 stage	N/A	India-46	33.2260	78.1670	5263	3.0	2.70	0.0	1.000	1.82±0.21	07KNSTD		0.22±0.03	Chi-squared: 2.22 Skewness: -1.09 Outlier: 3 Wt. mean: 0.26±0.05 ka Ar. Mean: 0.28±0.05 ka Peak: 0.29 ka !	0.23±0.03	0.31±0.03	0.31±0.05	0.29±0.04	0.21±0.03	0.27±0.05	0.26±0.05	0.27±0.05	0.00±0.00	0.29±0.03	0.21±0.02
Hedrick et al., 2011	PM-3 stage	N/A	India-47	33.2260	78.1670	5257	3.0	2.70	0.0	1.000	11.74±0.47	07KNSTD		1.52±0.1		1.57±0.11	1.64±0.15	1.67±0.16	1.53±0.12	1.36±0.12	1.52±0.30	1.70±0.30	1.52±0.19	1.44±0.06	1.46±0.06	1.34±0.05
Hedrick et al., 2011	PM-3 stage	N/A	India-48	33.2260	78.1670	5267	2.0	2.70	0.0	1.000	10.22±0.48	07KNSTD	0.28±0.05	1.3±0.09		1.32±0.1	1.43±0.12	1.46±0.12	1.30±0.10	1.17±0.11	1.33±0.26	1.44±0.26	1.33±0.16	1.25±0.06	1.27±0.06	1.15±0.05
Hedrick et al., 2011	PM-3 stage	N/A	India-49	33.2260	78.1670	5260	4.0	2.70	0.0	1.000	2.40±0.31	07KNSTD		0.29±0.04		0.3±0.04	0.41±0.06	0.42±0.07	0.38±0.05	0.28±0.04	0.37±0.07	0.36±0.07	0.37±0.07	0.38±0.05	0.37±0.05	0.28±0.04
Hedrick et al., 2011	PM-3 stage	N/A	India-50	33.2260	78.1670	5265	3.0	2.70	0.0	1.000	2.55±0.34	07KNSTD		0.32±0.05		0.32±0.05	0.44±0.07	0.44±0.07	0.40±0.06	0.30±0.05	0.39±0.08	0.38±0.08	0.39±0.08	0.40±0.05	0.39±0.05	0.29±0.04
Saha et al., 2018	Late Holocene	mA2c	LATO-1415	33.6822	77.5920	5366	3.0	2.70	0.0	0.950	13.31±0.31	07KNSTD		1.78±0.11		1.72±0.11	1.84±0.16	1.88±0.17	1.71±0.14	1.53±0.13	1.68±0.32	1.92±0.32	1.67±0.24	1.51±0.04	1.64±0.04	1.60±0.04
Saha et al., 2018	Late Holocene	mA1	LATO-1416	33.6822	77.5921	5358	4.0	2.70	0.0	0.950	1.66±0.18	07KNSTD		0.21±0.03	Chi-squared: 6.78 Skewness: +1.70 Outlier: 2 Wt. mean: 0.26±0.08 ka Ar. Mean: 0.26±0.08 ka Peak: 0.22 ka !	0.20±0.03	0.28±0.04	0.29±0.04	0.26±0.04	0.19±0.03	0.25±0.05	0.24±0.05	0.25±0.04	0.19±0.02	0.26±0.03	±
Saha et al., 2018	Late Holocene	mA1	LATO-1417	33.6826	77.5920	5348	2.0	2.70	0.0	0.951	2.74±0.10	07KNSTD	0.26±0.08	0.35±0.03		0.34±0.03	0.46±0.04	0.47±0.04	0.42±0.03	0.32±0.03	0.41±0.07	0.40±0.07	0.41±0.06	0.31±0.01	0.41±0.02	0.42±0.02
Saha et al., 2018	Late Holocene	mA1	LATO-1418	33.6826	77.5921	5351	3.0	2.70	0.0	0.946	1.79±0.14	07KNSTD		0.22±0.03		0.22±0.03	0.30±0.03	0.31±0.03	0.29±0.03	0.21±0.02	0.27±0.05	0.26±0.05	0.27±0.05	0.21±0.02	0.28±0.02	±
Saha et al., 2018	Late Holocene	mA1	LATO-1419	33.6827	77.5920	5339	3.0	2.70	0.0	0.952	24.66±1.85	07KNSTD		3.43±0.32		3.31±0.32	3.20±0.32	3.26±0.35	3.15±0.32	2.87±0.32	3.00±0.48	3.31±0.48	2.97±0.32	2.82±0.21	3.19±0.24	3.16±0.24

Group 2(a): Transitional climatic region—western Himalaya

Reference	Location	Code	Sample	Lat	Long	Elev	Thick	Density	Shield	Scaling	Conc.	Standard	Group age	Age	Statistics											
Owen et al. (2010)	N/A	M5	Na104	30.4365	81.4479	5499	2.0	2.70	0.0	1.000	132.16±3.34	07KNSTD		15.26±0.81		15.11±0.70	16.00±0.38	16.30±0.38	15.00±0.34	15.00±0.38	15.00±0.32	15.20±0.31	14.50±0.32	14.55±0.37	14.89±0.37	14.74±0.37
Owen et al. (2010)	N/A	M5	Na105	30.4364	81.4475	5501	1.0	2.70	0.0	1.000	79.56±2.02	07KNSTD		9.85±0.56	Chi-squared: 0.54 Skewness: +0.28 Outlier: 2 Wt. mean: 15.23±0.60 ka Ar. Mean: 15.30±0.60 ka Peak: 15.18 ka	9.54±0.53	9.83±0.27	10.04±0.27	8.97±0.25	8.93±0.23	8.80±0.24	9.50±0.25	8.70±0.23	10.02±0.26	9.95±0.26	8.78±0.22
Owen et al. (2010)	N/A	M5	Na106	30.4363	81.4484	5499	2.5	2.70	0.0	1.000	137.55±3.55	07KNSTD	15.30±0.60	15.91±0.88		15.73±0.76	16.70±0.38	17.00±0.38	15.70±0.38	15.70±0.41	15.30±0.34	15.80±0.36	15.10±0.33	15.07±0.39	15.45±0.39	15.41±0.40
Owen et al. (2010)	N/A	M5	Na107	30.4365	81.4488	5500	2.0	2.70	0.0	1.000	165.76±4.02	07KNSTD		18.73±0.99		18.60±0.88	19.40±0.33	19.70±0.32	18.50±0.39	18.80±0.46	18.00±0.38	18.40±0.35	17.80±0.38	17.80±0.43	18.21±0.43	18.49±0.45
Owen et al. (2010)	N/A	M5	Na108	30.4373	81.4464	5497	1.0	2.70	0.0	0.989	125.31±3.15	07KNSTD		14.72±0.75		14.50±0.67	15.30±0.34	15.60±0.35	14.40±0.33	14.30±0.36	14.00±0.32	14.60±0.30	13.90±0.31	13.91±0.35	14.25±0.35	14.02±0.35
This study	Lateglacial	Mk5	S19	32.3833	77.2783	3255	2.0	2.70	0.0	1.000	22.80±0.69	07KNSTD		8.92±0.63		8.33±0.46	9.20±0.29	9.28±0.29	7.96±0.24	8.00±0.24	9.10±0.28	9.60±0.29	9.00±0.28	9.18±0.28	8.51±0.28	7.85±0.24
This study	Lateglacial	Mk5	S20	32.3833	77.2783	3258	2.0	2.70	0.0	1.000	4.73±0.45	07KNSTD		2.11±0.25	Chi-squared: ! Skewness: ! Outlier: 4 Wt. mean: 14.28±2.06 ka Ar. Mean: 14.65±2.06 ka Peak: !	1.95±0.22	2.21±0.22	2.23±0.21	1.91±0.18	1.73±0.17	2.15±0.22	2.39±0.21	2.16±0.22	1.94±0.19	1.83±0.19	1.70±0.16
This study	Lateglacial	Mk5	S21	32.3833	77.2783	3256	2.0	2.70	0.0	1.000	32.03±1.14	07KNSTD	14.65±2.06	13.19±0.78		12.54±0.72	14.00±0.45	14.10±0.45	12.00±0.43	12.20±0.44	14.00±0.45	14.20±0.43	13.70±0.45	12.81±0.46	12.41±0.46	11.99±0.43
This study	Lateglacial	Mk5	S22	32.3833	77.2783	3268	2.0	2.70	0.0	1.000	44.85±1.78	07KNSTD		16.11±1.01		15.33±0.86	17.00±0.60	17.20±0.60	15.30±0.56	15.30±0.61	16.80±0.61	17.20±0.59	16.70±0.60	15.31±0.61	14.93±0.61	15.02±0.60
This study	Lateglacial	Mk5	S23	32.3833	77.2783	3272	2.0	2.70	0.0	1.000	3.16±0.30	07KNSTD		1.28±0.14		1.20±0.13	1.38±0.12	1.40±0.10	1.24±0.10	1.08±0.10	1.35±0.12	1.45±0.15	1.36±0.12	1.21±0.11	1.17±0.11	1.06±0.10
This study	Lateglacial	Mk5	S24	32.3833	77.2783	3274	3.0	2.70	0.0	1.000	3.06±3.93	07KNSTD		1.25±1.6		1.16±1.49	1.40±1.61	1.40±1.66	1.20±1.28	1.10±1.35	1.30±1.51	1.40±1.93	1.30±1.52	1.18±1.52	1.14±1.52	1.03±1.33
Owen et al. (2001)	Kulti glacial stage	N/A	L44	32.4000	77.6000	4070	5.0	2.70	0.0	0.990	66.21±1.90	LLNL3000	14.45±0.70	14.45±0.7	!	14.83±0.8	15.60±1.20	15.80±1.30	14.40±1.10	14.30±1.30	15.10±2.10	15.60±2.10	15.00±1.80	14.08±0.41	14.07±0.41	14.02±0.40
Scherler et al. (2010)	Tons Valley	(location C)	DS6-27A	31.1246	78.3825	3010	2.0	2.70	0.0	0.960	34.84±0.54	07KNSTD		13.99±0.64	Chi-squared: ! Skewness: ! Outlier: 0 Wt. mean: 14.06±0.10 ka Ar. Mean: 14.06±0.10 ka Peak: 14.06 ka	14.93±0.76	15.70±1.10	15.70±1.20	13.90±1.10	13.90±1.10	15.50±2.20	15.90±2.20	15.40±1.90	14.20±0.22	13.68±0.21	13.59±0.22
Scherler et al. (2010)	Tons Valley	(location C)	DS6-27B	31.1246	78.3825	3010	2.0	2.70	0.0	0.960	35.25±0.54	07KNSTD	14.06±0.10	14.13±0.63		15.05±0.76	15.80±1.10	15.90±1.30	14.10±1.10	14.10±1.10	15.60±2.20	16.10±2.30	15.60±1.90	14.37±0.22	13.80±0.21	13.75±0.22
Owen et al. (2001)	Kulti glacial stage	N/A	L24	32.5000	77.0000	2985	5.0	2.70	0.0	0.860	7.09±0.35	LLNL3000		3.6±0.23		3.93±0.28	3.76±0.39	3.79±0.42	3.40±0.30	3.16±0.31	3.72±0.74	4.06±0.74	3.71±0.56	3.74±0.18	3.47±0.17	3.10±0.15
Owen et al. (2001)	Kulti glacial stage	N/A	L25	32.5000	77.0000	2985	5.0	2.70	0.0	0.930	8.04±0.52	LLNL3000		3.77±0.28	Chi-squared: 0.05 Skewness: ! Outlier: 2 Wt. mean: 14.02±0.16 ka Ar. Mean: 14.03±0.16 ka Peak: 14.03 ka	4.11±0.34	3.96±0.47	4.00±0.50	3.57±0.35	3.31±0.36	3.90±0.79	4.28±0.79	3.90±0.64	3.92±0.25	3.66±0.24	3.25±0.21
Owen et al. (2001)	Kulti glacial stage	N/A	L28	32.5000	77.0000	3000	5.0	2.70	0.0	0.900	33.02±1.04	LLNL3000	14.03±0.16	14.14±0.73		14.95±0.84	15.80±1.20	15.90±1.30	14.10±1.20	14.00±1.20	15.70±2.30	16.00±2.30	16.00±2.00	14.24±0.45	13.77±0.43	13.70±0.43
Owen et al. (2001)	Kulti glacial stage	N/A	L29	32.5000	77.0000	2985	5.0	2.70	0.0	0.970	34.66±0.95	LLNL3000		13.91±0.7		14.76±0.8	15.50±1.20	15.60±1.20	13.80±1.10	13.70±1.20	15.40±2.20	15.80±2.20	15.30±1.90	14.02±0.39	13.58±0.37	13.47±0.37
Owen et al. (2001)	Kulti glacial stage	N/A	L10	32.3000	77.2000	2390	5.0	2.70	0.0	0.990	25.76±1.99	LLNL3000	13.95±0.88	14.57±1.18	Chi-squared: 1.11 Skewness: !	15.67±1.35	16.60±1.80	16.60±1.90	14.50±1.60	14.40±1.70	16.70±2.60	16.90±2.60	16.60±2.50	14.98±1.16	14.11±1.09	14.15±1.10

Reference	Stage	Location	Sample ID	Lat	Long	Elev	Thick	Density	Erosion	Shielding	Concentration	Standard	Group mean	Age	Statistics											
Owen et al. (2001)	Kulti glacial stage	N/A	L12	32.3000	77.2000	2415	5.0	2.70	0.0	0.990	23.77±0.78	LLNL3000		13.33±0.68	Outlier: 0; Wt. mean: 13.64±0.88 ka; Ar. Mean: 13.95±0.88 ka; Peak: 13.47 ka	14.41±0.8	15.20±1.10	15.20±1.20	13.20±1.10	13.10±1.20	15.20±2.10	15.50±2.10	15.10±1.90	13.79±0.45	13.05±0.43	12.85±0.42
Barnard et al. (2004b)	N/A	Moraine m2	NDL15	30.4600	80.1300	3720	5.0	2.70	0.0	0.980	9.20±1.30	LLNL3000		2.50±0.4		2.75±0.44	2.69±0.37	2.71±0.37	2.46±0.37	2.46±0.37	2.58±0.49	2.81±0.44	2.59±0.45	2.63±0.37	2.54±0.36	2.14±0.37
Barnard et al. (2004b)	N/A	Moraine m2	NDL16	30.4500	80.1300	3817	5.0	2.70	0.0	0.980	0.40±0.20	LLNL3000		0.09±0.05		0.09±0.05	0.14±0.08	0.14±0.08	0.12±0.08	0.12±0.08	0.12±0.07	0.12±0.07	0.13±0.07	0.11±0.05	0.10±0.05	0.08±0.04
Barnard et al. (2004b)	N/A	Moraine m2	NDL23	30.4500	80.1400	3968	5.0	2.70	0.0	0.990	17.60±0.60	LLNL3000		4.14±0.23	Chi-squared: !; Skewness: !; Outlier: 5; Wt. mean: 13.71±0.69 ka; Ar. Mean: 13.71±0.69 ka; Peak: !	4.5±0.27	4.30±0.40	4.32±0.42	3.90±0.40	3.90±0.40	4.04±0.69	4.45±0.75	4.04±0.62	4.29±0.15	4.13±0.14	3.57±0.15
Barnard et al. (2004b)	N/A	Moraine m2	NDL29	30.4300	80.1600	3497	5.0	2.70	0.0	0.970	50.00±1.50	LLNL3000	13.71±0.69	13.71±0.69		14.51±0.78	15.10±1.10	15.30±1.20	13.60±1.10	13.60±1.10	14.80±2.10	15.00±2.00	14.70±1.80	13.83±0.42	13.46±0.41	13.29±0.42
Barnard et al. (2004b)	N/A	Moraine m2	NDL30	30.4300	80.1600	3476	5.0	2.70	0.0	0.970	17.10±0.50	LLNL3000		5.21±0.25		5.59±0.28	5.41±0.34	5.45±0.37	4.88±0.34	4.88±0.34	5.27±0.69	5.58±0.59	5.27±0.61	5.56±0.16	5.27±0.15	4.59±0.16
Barnard et al. (2004b)	N/A	Moraine m2	NDL32	30.4100	80.1600	3397	5.0	2.70	0.0	0.970	12.10±0.50	LLNL3000		3.94±0.23		4.32±0.29	4.09±0.42	4.13±0.43	3.73±0.42	3.73±0.42	3.95±0.68	4.33±0.74	3.96±0.61	4.13±0.17	3.91±0.16	3.39±0.17
Murari et al. (2014)	mm1	N/A	KAL25	30.7283	79.0198	4405	1.5	2.70	0.0	0.980	69.96±3.50	07KNSTD		13.36±0.82	Chi-squared: 0.67; Skewness: +0.41; Outlier: 0; Wt. mean: 13.58±0.66 ka; Ar. Mean:13.62±0.66 ka; Peak: 13.53 ka	13.81±0.91	14.50±1.20	14.70±1.20	13.20±1.20	13.20±1.20	13.80±2.10	14.00±2.00	13.70±1.90	13.21±0.66	13.18±0.66	12.87±0.66
Murari et al. (2014)	mm1	N/A	KAL26	30.7281	79.0198	4412	3.0	2.70	0.0	0.979	66.50±2.66	07KNSTD		12.9±0.75		13.3±0.8	14.00±1.10	14.20±1.20	12.70±1.10	12.70±1.10	13.00±2.00	13.80±1.90	13.10±1.80	12.88±0.52	12.81±0.51	12.35±0.52
Murari et al. (2014)	mm1	N/A	KAL27	30.7280	79.0189	4411	2.0	2.70	0.0	0.972	71.69±2.87	07KNSTD	13.62±0.66	13.78±0.76		14.21±0.84	14.90±1.10	15.10±1.20	13.70±1.10	13.70±1.10	14.20±2.10	14.70±1.90	14.10±1.80	13.60±0.55	13.57±0.54	13.31±0.55
Murari et al. (2014)	mm1	N/A	KAL28	30.7271	79.0205	4378	3.0	2.70	0.0	0.980	74.41±3.72	07KNSTD		14.45±0.86		14.89±0.96	15.60±1.30	15.80±1.40	14.40±1.30	14.40±1.30	14.90±2.10	15.40±2.10	14.80±1.90	14.12±0.71	14.12±0.71	14.03±0.71
Lee et al., 2013	Anantick stage	ST-3	NK1	34.0466	75.9473	3506	3.5	2.70	0.0	0.970	66.36±1.41	07KNSTD		18.32±0.86	Chi-squared: !; Skewness: !; Outlier: 2; Wt. mean: 13.53±0.88 ka; Ar. Mean: 13.55±0.88 ka; Peak: 13.46 ka	18.67±0.98	19.60±1.20	19.70±1.30	18.30±1.20	18.30±1.20	19.50±2.50	19.70±2.30	19.30±2.20	17.88±0.38	17.76±0.38	18.13±0.38
Lee et al., 2013	Anantick stage	ST-3	NK2	34.0466	75.9473	3506	4.5	2.70	0.0	0.950	58.09±2.28	07KNSTD		16.62±0.95		17.01±1.06	18.00±1.40	18.20±1.50	16.60±1.40	16.60±1.40	17.90±2.60	18.20±2.40	17.70±2.30	16.26±0.64	16.13±0.63	16.33±0.64
Lee et al., 2013	Anantick stage	ST-3	NK3	34.0466	75.9473	3506	3.0	2.70	0.0	0.970	45.52±1.40	07KNSTD	13.55±0.88	12.92±0.69		13.27±0.75	14.00±1.00	14.30±1.10	12.70±1.00	12.70±1.00	14.00±2.00	14.40±1.90	13.80±1.80	12.90±0.40	12.72±0.39	12.37±0.40
Lee et al., 2013	Anantick stage	ST-3	NK4	34.0466	75.9473	3506	3.0	2.70	0.0	0.970	50.47±1.44	07KNSTD		14.17±0.71		14.56±0.78	15.40±1.10	15.60±1.20	14.10±1.10	14.10±1.10	15.30±2.10	15.60±2.10	15.10±1.80	13.91±0.40	13.81±0.40	13.72±0.40
This study	YD/Early Holocene	Mk4	S2	32.4000	77.2850	3522	2.0	2.70	0.0	0.913	36.64±1.92	07KNSTD		11.96±0.86	Chi-squared: 2.06; Skewness: -0.94; Outlier: 0; Wt. mean: 12.06±0.99 ka; Ar. Mean: 12.18±0.99 ka; Peak: !	11.42±0.71	12.70±0.63	12.80±0.64	11.30±0.60	11.10±0.59	12.40±0.61	12.90±0.63	12.30±0.60	11.83±0.62	11.52±0.62	10.92±0.58
This study	YD/Early Holocene	Mk4	S3	32.4000	77.2850	3527	2.0	2.70	0.0	0.915	39.64±1.69	07KNSTD		12.9±0.85		12.29±0.76	13.60±0.54	13.70±0.54	12.00±0.49	12.00±0.51	13.00±0.54	13.80±0.51	13.20±0.53	12.57±0.54	12.23±0.54	11.76±0.50
This study	YD/Early Holocene	Mk4	S5	32.4000	77.2850	3526	2.0	2.70	0.0	0.915	32.65±1.65	07KNSTD	12.18±0.99	10.86±0.65		10.33±0.63	11.30±0.57	11.50±0.56	10.00±0.54	9.87±0.50	11.10±0.56	11.60±0.53	11.00±0.56	10.96±0.56	10.49±0.56	9.69±0.49
This study	YD/Early Holocene	Mk4	S6	32.4000	77.2850	3528	2.0	2.70	0.0	0.915	39.99±0.85	07KNSTD		12.99±0.72		12.40±0.63	14.00±0.27	13.80±0.27	12.24±0.25	12.00±0.26	13.00±0.27	13.90±0.26	13.30±0.27	12.65±0.27	12.32±0.27	11.86±0.25
Owen et al. (2001)	Kulti glacial stage	N/A	L20	32.6000	76.9000	2865	5.0	2.70	0.0	0.900	24.20±1.30	LLNL3000		11.34±0.71	Chi-squared: 0.54; Skewness: !; Outlier: 0; Wt. mean: 11.64±0.59 ka; Ar. Mean: 11.76±0.59 ka; Peak: 11.54 ka	12.1±0.89	12.80±1.20	12.90±1.30	11.20±1.10	11.00±1.10	13.00±2.00	13.00±2.00	12.70±1.80	11.93±0.64	11.40±0.61	10.83±0.58
Owen et al. (2001)	Kulti glacial stage	N/A	L21	32.6000	76.9000	2700	5.0	2.70	0.0	1.000	26.28±1.82	LLNL3000	11.76±0.59	12.18±0.96		13.08±1.08	13.80±1.40	13.90±1.50	12.10±1.30	11.90±1.40	13.80±2.10	14.20±2.10	14.00±2.00	12.74±0.88	12.11±0.84	11.69±0.81
Scherler et al. (2010)	Tons Valley	location D	DS6-35	31.0789	78.4548	3642	2.5	2.70	0.0	0.980	1.67±0.11	07KNSTD		0.53±0.05	Chi-squared: !; Skewness: !; Outlier: 1; Wt. mean: 11.09±0.50 ka; Ar. Mean: 11.09±0.50 ka; Peak: !	0.50±0.04	0.69±0.08	0.72±0.06	0.57±0.08	0.57±0.08	0.64±0.11	0.63±0.11	0.65±0.11	0.6±0.04	0.57±0.04	0.45±0.03
Scherler et al. (2010)	Tons Valley	location D	DS6-37	31.0776	78.4564	3658	2.5	2.70	0.0	0.980	37.02±0.63	07KNSTD	11.09±0.50 ka	11.09±0.50		10.55±0.46	11.56±0.89	12.14±0.89	10.19±0.89	10.19±0.89	11.20±1.70	11.80±1.60	11.10±1.60	11.±0.19	10.78±0.18	9.92±0.17
Saha et al., 2018	Early Holocene	mH3	HAMTAH-1401	32.3005	77.3684	3783	1.5	2.7	0.0	0.897	37.33±1.91	07KNSTD		10.94±0.66		10.48±0.62	11.40±1.10	11.60±1.10	10.00±1.00	10.02±0.96	11.10±1.70	11.60±1.70	11.00±1.60	9.83±0.51	10.69±0.55	11.03±0.57
Saha et al., 2018	Early Holocene	mH3	HAMTAH-1402	32.3006	77.3685	3769	2.0	2.7	0.0	0.887	19.86±1.69	07KNSTD		6.24±0.51	Chi-squared: 0.48; Skewness: +1.16; Outlier: 3; Wt. mean: 10.42±0.48 ka; Ar. Mean: 10.48±0.48 ka; Peak: 10.37 ka	5.93±0.48	6.18±0.75	6.26±0.77	5.61±0.57	5.45±0.64	6.00±1.30	6.50±1.30	5.95±0.94	5.35±0.46	6.00±0.51	6.33±0.54
Saha et al., 2018	Early Holocene	mH3	HAMTAH-1403	32.2998	77.3670	3808	1.0	2.7	0.0	0.879	58.05±2.35	07KNSTD		16.18±1.03		15.67±0.87	17.10±1.30	17.30±1.40	15.60±1.30	15.70±1.40	16.70±2.30	17.10±2.30	16.50±2.20	15.36±0.62	15.24±0.62	15.36±0.62
Saha et al., 2018	Early Holocene	mH3	HAMTAH-1404	32.2992	77.3662	3808	2.0	2.7	0.0	0.879	12.21±0.57	07KNSTD	10.48±0.48	4.05±0.28		3.79±0.23	3.87±0.38	3.90±0.40	3.60±0.30	3.31±0.31	3.70±0.73	4.12±0.73	3.72±0.54	3.25±0.15	3.71±0.18	3.87±0.18
Saha et al., 2018	Early Holocene	mH3	HAMTAH-1503	32.2942	77.3647	4112	3.0	2.7	0.0	0.898	41.47±0.86	07KNSTD		10.36±0.53		10.02±0.47	10.76±0.89	10.91±0.97	9.57±0.86	9.50±0.80	10.30±1.60	10.90±1.60	10.20±1.50	9.33±0.19	10.21±0.21	10.48±0.22
Saha et al., 2018	Early Holocene	mH3	HAMTAH-1504	32.2954	77.3655	4083	3.0	2.7	0.0	0.879	38.89±0.73	07KNSTD		10.13±0.54		9.77±0.47	10.46±0.86	10.61±0.94	9.28±0.82	9.23±0.77	10.00±1.60	10.60±1.60	9.90±1.40	9.07±0.17	10.01±0.19	10.23±0.19
Scherler et al. (2010)	Tons Valley	location F'	DS6-48	31.1458	78.4346	3544	2.5	2.70	0.0	0.970	34.43±0.55	07KNSTD		10.51±0.46	Chi-squared: !; Skewness: !; Outlier: 0; Wt. mean: 10.25±0.35 ka; Ar. Mean: 10.26±0.35 ka; Peak: 10.25 ka	11.08±0.5	11.56±0.88	11.67±0.96	10.15±0.88	10.15±0.88	11.20±1.70	11.80±1.60	11.20±1.60	11.12±0.18	10.74±0.17	9.89±0.18
Scherler et al. (2010)	Tons Valley	location F'	DS6-49	31.1461	78.4327	3514	2.0	2.70	0.0	0.970	32.17±0.59	07KNSTD	10.26±0.35 ka	10.01±0.45		10.61±0.51	10.94±0.92	11.05±0.97	9.56±0.92	9.56±0.92	10.60±1.70	11.20±1.70	10.60±1.50	10.70±0.20	10.19±0.19	9.35±0.20

Reference	Glacial stage	Location	Sample	Lat	Long	Elev	Thick	Dens		Shield	Conc	Standard	Mean age	Age	Statistics											
Murari et al. (2014)	N/A	mk1	KAL29	30.7301	79.0635	3648	2.5	2.70	0.0	0.948	35.72±3.21	07KNSTD		10.66±0.92	Chi-squared: 0.64 Skewness: -1.12 Outlier: 1 Wt. mean: 10.29±0.83 ka Ar. Mean: 10.25±0.83 ka Peak: 10.38 ka	11.18±1.02	11.70±1.30	11.80±1.40	10.30±1.30	10.30±1.30	11.00±2.00	11.90±1.90	11.30±1.80	11.22±1.01	10.88±0.98	10.04±1.01
Murari et al. (2014)	N/A	mk1	KAL30	30.7296	79.0635	3650	2.5	2.70	0.0	0.948	57.92±9.85	07KNSTD		16.47±2.63		17.29±2.7	18.10±2.90	18.30±2.90	16.50±2.90	16.50±2.90	17.60±3.60	18.10±3.50	17.50±3.40	16.43±2.81	16.06±2.74	16.29±2.81
Murari et al. (2014)	N/A	mk1	KAL31	30.7295	79.0635	3642	2.5	2.70	0.0	0.944	36.63±8.06	07KNSTD	10.25±0.83	10.95±2.3		11.46±2.34	12.00±2.60	12.20±2.60	10.70±2.60	10.70±2.60	12.00±3.00	12.20±2.90	11.60±2.90	11.44±2.52	11.13±2.46	10.37±2.52
Murari et al. (2014)	N/A	mk1	KAL32	30.7287	79.0635	3641	2.5	2.70	0.0	0.940	29.59±3.85	07KNSTD		8.98±1.25		9.67±1.33	9.80±1.60	9.90±1.60	8.50±1.60	8.50±1.60	9.00±2.00	10.00±2.00	9.40±1.90	9.84±1.28	9.32±1.21	8.42±1.28
Murari et al. (2014)	N/A	mk1	KAL33	30.7295	79.0635	3643	2.0	2.70	0.0	0.944	32.61±1.63	07KNSTD		9.85±0.64		10.43±0.66	11.00±1.00	10.80±1.10	9.37±1.00	9.37±1.00	10.30±1.70	11.00±1.70	10.30±1.50	10.48±0.53	10.08±0.51	9.18±0.53
Murari et al. (2014)	N/A	mk1	KAL34	30.7244	79.0652	3605	3.0	2.70	0.0	0.958	35.71±1.79	07KNSTD		10.82±0.62		11.33±0.7	12.00±1.00	12.00±1.10	10.00±1.00	10.00±1.00	11.50±1.80	12.10±1.70	11.50±1.60	11.34±0.57	11.01±0.55	10.21±0.57
Owen et al. (2010)	N/A	M7	Na64	30.4704	81.2058	5195	2.0	2.70	0.0	0.980	26.50±0.66	07KNSTD		4.29±0.25	Chi-squared: ! Skewness: ! Outlier: 2 Wt. mean: 8.71±0.55 ka Ar. Mean: 8.75±0.55 ka Peak: 8.68 ka	4.06±0.20	3.98±0.11	4.07±0.11	3.81±0.08	3.50±0.09	3.62±0.09	3.98±0.11	3.60±0.09	4.11±0.10	4.06±0.10	3.42±0.09
Owen et al. (2010)	N/A	M7	Na66	30.4711	81.2056	5159	5.0	2.70	0.0	0.978	82.78±2.37	07KNSTD		12.00±0.74		11.72±0.60	12.52±0.34	12.70±0.35	11.55±0.33	11.35±0.33	11.60±0.32	12.20±0.30	11.40±0.32	11.82±0.34	11.91±0.34	11.19±0.32
Owen et al. (2010)	N/A	M7	Na67	30.4712	81.2056	5154	2.0	2.70	0.0	0.978	57.37±2.22	07KNSTD	8.75±0.55	8.36±0.60		8.12±0.48	8.41±0.35	8.57±0.35	7.68±0.29	7.70±0.30	7.80±0.29	8.40±0.31	8.00±0.28	8.57±0.33	8.41±0.33	7.57±0.29
Owen et al. (2010)	N/A	M7	Na68	30.4712	81.2056	5154	1.0	2.70	0.0	0.978	62.51±1.84	07KNSTD		9.14±0.66		8.77±0.54	9.14±0.29	9.30±0.30	8.31±0.26	8.33±0.25	8.40±0.25	9.00±0.27	8.30±0.25	9.42±0.28	9.25±0.28	8.18±0.24
Barnard et al. (2004a)	Kedar glacial stage	N/A	BH19	30.9436	78.9520	4323	5.0	2.70	0.0	0.970	47.24±1.13	LLNL3000		8.59±0.48	Chi-squared: ! Skewness: ! Outlier: 0 Wt. mean: 8.22±0.45 ka Ar. Mean: 8.28±0.45 ka Peak: 8.15 ka	9.06±0.63	9.17±0.81	9.32±0.88	8.20±0.81	8.20±0.81	8.70±1.40	9.30±1.50	8.60±1.30	9.32±0.22	8.92±0.21	8.07±0.22
Barnard et al. (2004a)	Kedar glacial stage	N/A	BH20	30.9442	78.9505	4242	5.0	2.70	0.0	0.970	42.00±1.00	LLNL3000	8.28±0.45	7.96±0.4		8.31±0.52	8.46±0.71	8.60±0.80	7.54±0.71	7.54±0.71	8.10±1.20	8.70±1.30	8.00±1.10	8.49±0.20	8.20±0.20	7.46±0.20
Scherler et al. (2010)	Tons Valley	Location F	DS6-54/64	31.1487	78.4268	3504	2.5	2.70	0.0	0.980	20.22±0.52	07KNSTD		6.41±0.29	Chi-squared: 4.00 Skewness: +0.21 Outlier: 0 Wt. mean: 6.00±0.54 ka Ar. Mean: 6.09±0.54 ka Peak: !	6.81±0.35	6.80±0.60	6.92±0.65	6.08±0.60	6.08±0.60	6.70±1.10	7.23±0.98	6.62±0.97	6.90±0.18	6.54±0.17	5.87±0.18
Scherler et al. (2010)	Tons Valley	Location F	DS6-61	31.1459	78.4278	3412	2.0	2.70	0.0	0.950	19.69±0.47	07KNSTD		6.68±0.3		7.12±0.36	7.22±0.54	7.28±0.59	6.35±0.54	6.35±0.54	7.10±1.10	8.00±1.00	7.00±1.00	7.20±0.17	6.82±0.16	6.17±0.17
Scherler et al. (2010)	Tons Valley	Location F	DS6-63	31.1493	78.4279	3516	2.5	2.70	0.0	0.970	17.36±0.44	07KNSTD		5.64±0.25		6.03±0.3	5.87±0.45	5.93±0.49	5.30±0.45	5.30±0.45	5.73±0.76	6.10±1.10	5.71±0.66	6.05±0.15	5.70±0.14	5.06±0.15
Scherler et al. (2010)	Tons Valley	Location F	DS05-05B	31.1489	78.4272	3495	2.5	2.70	0.0	0.980	17.28±0.43	07KNSTD	6.09±0.54	5.63±0.24		6.02±0.3	5.86±0.43	5.92±0.48	5.30±0.43	5.30±0.43	5.72±0.75	6.10±1.10	5.70±0.66	6.03±0.15	5.68±0.14	5.04±0.15
Srivastava (2012; Sci. report)	Shivling glacial stage	N/A	MILAP4	30.9964	78.9308	3029	5.0	2.70	0.0	0.918	10.70±0.38	07KNSTD		5.48±0.28	Chi-squared: 0.63 Skewness: -0.86 Outlier: 0 Wt. mean: 5.23±0.27 ka Ar. Mean: 5.22±0.27 ka Peak: 5.27 ka	5.04±0.28	5.33±0.35	5.36±0.39	4.73±0.37	4.50±0.40	5.25±0.68	5.54±0.58	5.20±0.60	5.41±0.19	5.04±0.19	4.43±0.16
Srivastava (2012; Sci. report)	Shivling glacial stage	N/A	MILAP5	30.9971	78.9274	3012	5.0	2.70	0.0	0.907	9.66±0.31	07KNSTD		5.13±0.29		4.68±0.29	5.00±0.38	5.02±0.38	4.39±0.34	4.17±0.36	4.91±0.71	5.24±0.61	4.91±0.63	5.02±0.16	4.60±0.16	4.09±0.13
Srivastava (2012; Sci. report)	Shivling glacial stage	N/A	MILAP8	30.9971	78.9311	3021	2.0	2.70	0.0	0.899	10.68±0.61	07KNSTD		5.48±0.35		5.04±0.35	5.30±0.40	5.36±0.43	4.72±0.42	4.51±0.45	5.25±0.71	5.54±0.61	5.24±0.63	5.41±0.31	5.03±0.31	4.42±0.26
Srivastava (2012; Sci. report)	Shivling glacial stage	N/A	MIALP10	30.9968	78.9289	3017	2.0	2.70	0.0	0.911	10.50±0.62	07KNSTD	5.22±0.27	5.35±0.35		4.89±0.35	5.20±0.40	5.24±0.42	4.60±0.42	4.39±0.44	5.13±0.71	5.44±0.62	5.12±0.64	5.28±0.31	4.87±0.31	4.30±0.25
Srivastava (2012; Sci. report)	Shivling glacial stage	N/A	MILAP11	30.9967	78.9284	3022	2.0	2.70	0.0	0.907	10.44±0.58	07KNSTD		5.33±0.35		4.89±0.35	5.20±0.41	5.22±0.41	4.59±0.41	4.37±0.43	5.11±0.71	5.42±0.62	5.11±0.63	5.26±0.29	4.85±0.29	4.29±0.24
Srivastava (2012; Sci. report)	Shivling glacial stage	N/A	MILAP12	30.9968	78.9277	3017	2.0	2.70	0.0	0.905	9.68±0.43	07KNSTD		5.02±0.32		4.57±0.32	4.90±0.40	4.92±0.41	4.30±0.36	4.07±0.38	4.80±0.73	5.15±0.64	4.80±0.66	4.88±0.22	4.49±0.22	3.99±0.18
Srivastava (2012; Sci. report)	Shivling glacial stage	N/A	MILAP13	30.9969	78.9272	3039	2.0	2.70	0.0	0.907	9.25±0.57	07KNSTD		4.76±0.36		4.33±0.36	4.62±0.46	4.65±0.48	4.07±0.36	3.83±0.39	4.52±0.76	4.90±0.73	4.50±0.70	4.56±0.28	4.25±0.28	3.76±0.23
Owen et al. (2010)	N/A	M8	Na58	30.4683	81.2064	5325	5.0	2.70	0.0	1.000	38.41±1.64	07KNSTD		5.63±0.30	Chi-squared: ! Skewness: ! Outlier: 0 Wt. mean: 4.92±0.88 ka Ar. Mean: 5.01±0.88 ka Peak: !	5.41±0.28	5.38±0.17	5.45±0.17	5.04±0.19	4.78±0.20	4.97±0.18	5.34±0.16	4.93±0.18	5.62±0.24	5.54±0.24	4.71±0.20
Owen et al. (2010)	N/A	M8	Na59	30.4683	81.2050	5325	1.0	2.70	0.0	1.000	29.51±0.83	07KNSTD	5.01±0.88	4.39±0.26		4.16±0.21	4.08±0.12	4.17±0.13	3.89±0.09	3.56±0.10	3.70±0.10	4.05±0.13	3.66±0.11	4.20±0.12	4.15±0.12	3.50±0.10
Srivastava (2012; Sci. report)	Gangotri glacial stage	N/A	MILAP2	30.7633	79.0775	4343	5.0	2.70	0.0	0.980	9.83±0.29	07KNSTD		2.41±0.18	Chi-squared: ! Skewness: ! Outlier: 0 Wt. mean: 2.08±0.35 ka Ar. Mean: 2.16±0.35 ka Peak: !	2.22±0.18	2.43±0.19	2.50±0.20	2.20±0.20	1.94±0.17	2.28±0.36	2.52±0.33	2.29±0.32	2.26±0.07	2.17±0.07	1.91±0.06
Srivastava (2012; Sci. report)	Gangotri glacial stage	N/A	MILAP3	30.9129	79.0783	4335	5.0	2.70	0.0	0.980	7.98±0.26	07KNSTD	2.16±0.35	1.91±0.13		1.80±0.13	1.97±0.18	2.00±0.18	1.76±0.15	1.58±0.14	1.84±0.29	2.06±0.35	1.85±0.27	1.76±0.06	1.72±0.06	1.55±0.05
Scherler et al. (2010)	Tons Valley	Location G	DS6-57	31.1418	78.4536	3636	2.5	2.70	0.0	0.950	1.37±0.05	07KNSTD		0.42±0.03	Chi-squared: ! Skewness: ! Outlier: 0 Wt. mean: 0.55±0.34 ka Ar. Mean: 0.66±0.34 ka Peak: !	0.44±0.03	0.58±0.05	0.59±0.06	0.49±0.05	0.49±0.05	0.54±0.08	0.53±0.08	0.55±0.08	0.51±0.02	0.49±0.02	0.38±0.02
Scherler et al. (2010)	Tons Valley	Location G	DS6-58	31.1418	78.4531	3623	2.5	2.70	0.0	0.940	2.82±0.08	07KNSTD	0.66±0.34	0.9±0.05		0.96±0.07	1.10±0.07	1.11±0.06	0.98±0.07	0.98±0.07	1.06±0.12	1.09±0.14	1.07±0.11	0.99±0.03	0.95±0.03	0.80±0.03
Saha et al. (2015)	N/A	N/A	ZK73	32.7927	77.4293	4757	5.0	2.70	0.0	1.000	3.10±0.50	07KNSTD	0.62±0.15	0.51±0.09	Chi-squared: 2.13 Skewness: ! Outlier: 1	0.52±0.09	0.68±0.14	0.72±0.11	0.59±0.10	0.47±0.08	0.62±0.12	0.61±0.12	0.62±0.13	0.60±0.10	0.58±0.09	0.46±0.07
Saha et al. (2015)	N/A	N/A	ZK74	32.7929	77.4292	4764	5.0	2.70	0.0	1.000	4.40±0.70	07KNSTD		0.72±0.12		0.75±0.13	0.93±0.12	0.97±0.13	0.82±0.13	0.66±0.12	0.86±0.20	0.87±0.20	0.87±0.18	0.83±0.13	0.81±0.13	0.65±0.10

Reference	Stage	Sub-location	Sample	Lat	Lon	Elev	Thick	Density	(col)	Shielding	Conc	Standard	Group age	Age	Statistics	A1	A2	A3	A4	A5	A6	A7	A8	A9	A10	A11
Saha et al. (2015)	N/A	N/A	ZK75	32.7929	77.4292	4749	5.0	2.70	0.0	1.000	159.70±7.00	07KNSTD		23.16±1.31	Wt. mean: 0.59±0.15 ka / Ar. Mean: 0.62±0.15 ka / Peak: 0.54 ka	22.67±1.3	23.60±1.80	24.80±1.80	23.10±1.90	24.30±2.20	22.90±3.20	23.00±3.20	22.50±2.90	21.82±0.96	22.56±1.00	23.84±1.05
Barnard et al. (2004b)	N/A	Moraine m4	NDL2	30.4500	80.1200	3534	5.0	2.70	0.0	0.970	1.40±0.50	LLNL3000	0.60±0.28	0.4±0.15	Chi-squared: ! / Skewness: ! / Outlier: 0 / Wt. mean: 0.62±0.28 ka / Ar. Mean: 0.60±0.28 ka / Peak: !	0.43±0.16	0.56±0.24	0.56±0.25	0.47±0.24	0.47±0.24	0.52±0.22	0.51±0.21	0.53±0.23	±	±	±
Barnard et al. (2004b)	N/A	Moraine m4	NDL4	30.4500	80.1200	3522	5.0	2.70	0.0	0.960	2.70±0.40	LLNL3000		0.79±0.13		0.86±0.14	1.01±0.14	1.02±0.14	0.89±0.14	0.89±0.14	0.97±0.18	0.99±0.21	0.99±0.16	0.92±0.14	0.87±0.13	0.71±0.14
Barnard et al. (2004a)	Gangotri glacial stage	N/A	BH29	30.9450	79.0615	3973	5.0	2.70	0.0	0.970	3.12±0.84	LLNL3000	0.56±0.30	0.71±0.2	Chi-squared: 4.45 / Skewness: +0.86 / Outlier: 0 / Wt. mean: 0.49±0.30 ka / Ar. Mean: 0.56±0.30 ka / Peak: !	0.75±0.21	0.93±0.21	0.94±0.21	0.80±0.21	0.80±0.21	0.87±0.29	0.87±0.31	0.89±0.28	0.82±0.22	0.79±0.21	0.63±0.22
Barnard et al. (2004a)	Gangotri glacial stage	N/A	BH30	30.9449	79.0616	3956	5.0	2.70	0.0	0.970	1.53±0.67	LLNL3000		0.34±0.16		0.37±0.16	0.48±0.26	0.49±0.22	0.41±0.26	0.41±0.26	0.44±0.24	0.43±0.23	0.45±0.24	0.43±0.19	0.41±0.18	0.31±0.19
Barnard et al. (2004a)	Gangotri glacial stage	N/A	BH31	30.9448	79.0616	3973	5.0	2.70	0.0	0.970	1.12±0.68	LLNL3000		0.26±0.16		0.24±0.15	0.35±0.26	0.35±0.27	0.31±0.26	0.31±0.26	0.32±0.23	0.31±0.23	0.32±0.23	1.07±0.17	1.04±0.17	0.90±0.17
Barnard et al. (2004a)	Gangotri glacial stage	N/A	BH32	30.9448	79.0619	3956	5.0	2.70	0.0	0.970	4.37±0.70	LLNL3000		1.01±0.17		1.07±0.19	1.20±0.17	1.21±0.21	1.08±0.17	1.08±0.17	1.14±0.22	1.18±0.24	1.15±0.21	0.51±0.02	0.49±0.02	0.38±0.02
Srivastava (2012; Sci. report)	Gangotri glacial stage	N/A	Milap7	30.9454	79.0600	3935	2.0	2.70	0.0	0.949	1.69±0.07	07KNSTD		0.47±0.04		0.44±0.04	0.61±0.06	0.62±0.06	0.52±0.04	0.41±0.04	0.57±0.09	0.55±0.09	0.58±0.08	0.54±0.02	0.52±0.02	0.40±0.02
Lee et al., 2014	Lonp stage	TG-3	NK29	34.0559	75.9181	3679	2.5	2.70	0.0	0.957	1.56±0.05	07KNSTD	0.53±0.13	0.43±0.03	Chi-squared: 12.53 / Skewness: ! / Outlier: 0 / Wt. mean: 0.47±0.13 ka / Ar. Mean: 0.53±0.13 ka / Peak: !	0.44±0.03	0.57±0.04	0.57±0.05	0.50±0.04	0.40±0.04	0.54±0.08	0.54±0.08	0.55±0.08	0.51±0.02	0.49±0.02	0.39±0.01
Lee et al., 2014	Lonp stage	TG-3	NK30	34.0548	75.9173	3720	4.0	2.70	0.0	0.957	2.26±0.18	07KNSTD		0.62±0.06		0.65±0.07	0.80±0.08	0.81±0.07	0.71±0.08	0.57±0.06	0.77±0.14	0.77±0.14	0.78±0.11	0.72±0.06	0.68±0.05	0.56±0.04
This study	LIA	Mk2	S9	32.4233	77.3067	3676	2.0	2.70	0.0	0.917	1.27±0.46	07KNSTD	0.51±0.16	0.40±0.15	Chi-squared: ! / Skewness: ! / Outlier: 0 / Wt. mean: 0.57±0.16 ka / Ar. Mean: 0.51±0.16 ka / Peak: 0.61 ka	0.37±0.14	0.52±0.19	0.53±0.19	0.45±0.14	0.35±0.13	0.49±0.18	0.48±0.17	0.50±0.18	0.47±0.17	0.44±0.17	0.35±0.13
This study	LIA	Mk2	S10	32.4233	77.3067	3678	2.0	2.70	0.0	0.913	1.95±0.19	07KNSTD		0.62±0.08		0.59±0.07	0.79±0.07	0.80±0.06	0.68±0.07	0.54±0.05	0.75±0.07	0.74±0.07	0.76±0.07	0.70±0.07	0.66±0.07	0.53±0.05
Owen et al. (2010)	N/A	M9	Na54	30.4637	81.2157	5503	1.0	2.70	0.0	0.947	2.98±0.39	07KNSTD	0.46±0.10	0.38±0.06	Chi-squared: 2.57 / Skewness: +1.65 / Outlier: 0 / Wt. mean: 0.46±0.10 ka / Ar. Mean: 0.46±0.10 ka / Peak: !	0.39±0.06	0.54±0.08	0.55±0.08	0.47±0.08	0.47±0.08	0.47±0.10	0.45±0.09	0.48±0.10	0.47±0.06	0.47±0.06	0.35±0.06
Owen et al. (2010)	N/A	M9	Na55	30.4635	81.2157	5520	1.5	2.70	0.0	0.947	3.09±0.55	07KNSTD		0.39±0.08		0.41±0.08	0.55±0.10	0.57±0.12	0.48±0.10	0.48±0.10	0.48±0.12	0.46±0.11	0.49±0.11	0.49±0.09	0.49±0.09	0.36±0.09
Owen et al. (2010)	N/A	M9	Na56	30.4629	81.2157	5509	2.0	2.70	0.0	0.928	4.09±0.36	07KNSTD		0.54±0.06		0.57±0.06	0.75±0.07	0.76±0.08	0.65±0.07	0.65±0.07	0.66±0.13	0.62±0.11	0.67±0.12	0.65±0.06	0.65±0.06	0.49±0.06
Owen et al. (2010)	N/A	M9	Na57	30.4632	81.2155	5508	1.0	2.70	0.0	0.933	6.69±0.86	07KNSTD		0.89±0.13		0.93±0.14	1.08±0.12	1.10±0.10	1.00±0.12	1.00±0.12	1.00±0.15	1.00±0.18	1.00±0.14	0.98±0.13	0.98±0.13	0.79±0.13
Murari et al. (2014)	mk2	N/A	KAL35	30.7448	79.6503	3841	4.0	2.70	0.0	0.953	1.81±0.41	07KNSTD	0.31±0.17	0.51±0.13	Chi-squared: 19.33 / Skewness: +1.73 / Outlier: 2 / Wt. mean: 0.22±0.17 ka / Ar. Mean: 0.31±0.17 ka / Peak: !	0.54±0.13	0.71±0.13	0.72±0.14	0.59±0.13	0.59±0.13	0.65±0.19	0.64±0.18	0.67±0.19	0.61±0.14	0.59±0.13	0.46±0.14
Murari et al. (2014)	mk2	N/A	KAL36	30.7454	79.0652	3853	5.0	2.70	0.0	0.950	0.80±0.09	07KNSTD		0.22±0.03		0.24±0.03	0.31±0.04	0.32±0.05	0.28±0.04	0.28±0.04	0.29±0.06	0.28±0.06	0.29±0.05	±	0.27±0.03	0.21±0.00
Murari et al. (2014)	mk2	N/A	KAL37	30.7462	79.0655	3884	3.0	2.70	0.0	0.959	72.22±22.22	07KNSTD		17.93±4.86		18.64±4.86	19.40±4.40	19.60±4.50	17.90±4.40	17.90±4.40	18.90±5.40	19.30±4.90	18.70±5.20	17.75±5.49	17.45±5.49	17.83±5.51
Murari et al. (2014)	mk2	N/A	KAL38	30.7473	79.0661	3909	5.0	2.70	0.0	0.959	0.80±0.08	07KNSTD		0.21±0.02		0.23±0.03	0.31±0.03	0.31±0.03	0.27±0.03	0.27±0.03	0.28±0.05	0.27±0.05	0.28±0.05	±	0.26±0.03	0.20±0.00
Murari et al. (2014)	mk2	N/A	KAL39	30.7478	79.0662	3915	2.5	2.70	0.0	0.096	1.22±0.22	07KNSTD		3.47±0.61		3.75±0.67	3.50±0.65	3.55±0.72	3.30±0.65	3.30±0.65	3.35±0.78	3.66±0.86	3.35±0.75	3.29±0.59	3.17±0.57	2.79±0.59
Saha et al., 2018	Late Holocene	mH1a	HAMTAH-1405	32.2725	77.3574	4014	2.0	2.70	0.0	0.943	0.89±0.19	07KNSTD	0.26±0.13	0.23±0.05	Chi-squared: 8.55 / Skewness: +0.87 / Outlier: 2 / Wt. mean: 0.18±0.13 ka / Ar. Mean: 0.26±0.13 ka / Peak: 0.15 ka !	0.21±0.05	0.30±0.06	0.31±0.05	0.27±0.06	0.20±0.05	0.28±0.08	0.27±0.08	0.28±0.08	±	0.26±0.00	0.20±0.04
Saha et al., 2018	Late Holocene	mH1a	HAMTAH-1406	32.2722	77.3575	4023	1.0	2.70	0.0	0.944	1.56±0.41	07KNSTD		0.40±0.11		0.37±0.10	0.52±0.13	0.52±0.14	0.45±0.11	0.35±0.10	0.48±0.15	0.47±0.15	0.49±0.14	0.34±0.09	0.44±0.12	0.46±0.12
Saha et al., 2018	Late Holocene	mH1a	HAMTAH-1408	32.2686	77.3585	4111	2.5	2.70	0.0	0.954	9.06±0.55	07KNSTD		2.35±0.22		2.21±0.18	2.44±0.22	2.47±0.24	2.17±0.24	1.90±0.20	2.32±0.36	2.58±0.36	2.33±0.32	1.91±0.12	2.11±0.13	2.21±0.14
Saha et al., 2018	Late Holocene	mH1a	HAMTAH-1410	32.2678	77.3589	4125	2.5	2.70	0.0	0.948	0.60±0.10	07KNSTD		0.14±0.03		0.13±0.03	0.19±0.04	0.19±0.04	0.17±0.03	0.13±0.02	0.17±0.04	0.17±0.04	0.17±0.04	0.13±0.02	0.16±0.03	±
Saha et al., 2018	Late Holocene	mH1a	HAMTAH-1502	32.2703	77.3579	3861	2.0	2.70	0.0	0.923	2.57±0.25	07KNSTD		0.74±0.09		0.70±0.07	0.92±0.08	0.93±0.09	0.80±0.09	0.65±0.08	0.87±0.17	0.88±0.17	0.89±0.14	0.63±0.06	0.78±0.08	0.82±0.08
Scherler et al. (2010)	Tons Valley	Location E	DS6-32	31.0715	78.4992	4071	3.0	2.70	0.0	0.950	1.21±0.06	07KNSTD	0.26±0.08	0.31±0.02	Chi-squared: ! / Skewness: ! / Outlier: 0 / Wt. mean: 0.28±0.08 ka / Ar. Mean: 0.26±0.08 ka / Peak: !	0.29±0.02	0.41±0.04	0.44±0.04	0.36±0.04	0.36±0.04	0.38±0.06	0.37±0.06	0.39±0.06	0.37±0.02	0.36±0.02	0.27±0.01
Scherler et al. (2010)	Tons Valley	Location E	DS6-33	31.0715	78.4977	4046	2.0	2.70	0.0	0.970	0.77±0.09	07KNSTD		0.18±0.02		0.2±0.03	0.26±0.03	0.27±0.04	0.23±0.03	0.23±0.03	0.23±0.05	0.23±0.05	0.24±0.04	±	0.22±0.03	0.17±0.00
Owen et al. (2010)	N/A	M10	Na48	30.4633	81.2169	5508	2.0	2.70	0.0	0.946	2.90±0.41	07KNSTD	0.24±0.15	0.39±0.06	Chi-squared: 10.04 / Skewness: +0.20 / Outlier: 2 / Wt. mean: 0.22±0.15 ka / Ar. Mean:	0.37±0.06	0.53±0.08	0.54±0.07	0.46±0.06	0.34±0.05	0.46±0.07	0.44±0.06	0.47±0.07	0.47±0.07	0.46±0.07	0.34±0.05
Owen et al. (2010)	N/A	M10	Na49	30.4634	81.2168	5506	1.0	2.70	0.0	0.946	22.99±0.65	07KNSTD		3.40±0.21		3.24±0.17	3.09±0.08	3.15±0.09	3.07±0.08	2.71±0.08	2.87±0.06	3.08±0.08	2.86±0.06	3.18±0.09	3.17±0.09	2.67±0.08
Owen et al. (2010)	N/A	M10	Na50	30.4634	81.2169	5509	1.5	2.70	0.0	0.946	0.75±0.27	07KNSTD		0.09±0.04		0.09±0.03	0.14±0.05	0.14±0.05	0.12±0.04	0.09±0.03	0.12±0.04	0.11±0.04	0.12±0.04	±	0.12±0.00	0.09±0.03
Owen et al. (2010)	N/A	M10	Na52	30.4640	81.2170	5514	1.5	2.70	0.0	0.952	28.09±0.69	07KNSTD		4.09±0.24		3.87±0.18	3.75±0.10	3.83±0.10	3.65±0.08	3.30±0.08	3.39±0.08	3.70±0.09	3.36±0.08	3.92±0.10	3.90±0.10	3.24±0.08

Owen et al. (2010)	N/A	M10	Na53	30.4638	81.2159	5509	2.0	2.70	0.0	0.955	1.78±0.12	07KNSTD		0.23±0.02	0.24±0.15 ka Peak: !	0.22±0.02	0.32±0.02	0.33±0.02	0.29±0.02	0.21±0.01	0.28±0.02	0.26±0.02	0.28±0.02	±	±	0.21±0.01
Srivastava (2012; Sci. report)	Bhujbas glacial stage	N/A	MILAP1	30.9395	79.0635	3908	5.0	2.70	0.0	0.947	0.71±0.05	07KNSTD	0.21±0.02	0.21±0.02	!	0.19±0.02	0.27±0.03	0.27±0.03	0.24±0.03	0.18±0.02	0.25±0.04	0.24±0.04	0.25±0.04	±	0.23±0.00	0.18±0.01
Murari et al. (2014)	mbd1	N/A	KAL18	30.7565	78.9629	4132	2.0	2.70	0.0	0.949	0.86±0.12	07KNSTD		0.2±0.03		0.22±0.03	0.29±0.05	0.29±0.05	0.25±0.05	0.25±0.05	0.26±0.06	0.25±0.06	0.26±0.06	±	0.25±0.04	0.19±0.00
Murari et al. (2014)	mbd1	N/A	KAL19	30.7585	78.9627	4182	2.0	2.70	0.0	0.937	1.07±0.08	07KNSTD	0.21±0.02	0.23±0.02		0.26±0.03	0.35±0.04	0.36±0.04	0.31±0.04	0.31±0.04	0.32±0.06	0.31±0.05	0.33±0.05	±	0.31±0.02	0.23±0.00
Murari et al. (2014)	mbd1	N/A	KAL20	30.7567	78.9628	4115	2.0	2.70	0.0	0.940	3.64±0.30	07KNSTD		0.9±0.09	Chi-squared: 0.61 Skewness: +1.73 Outlier: 1 Wt. mean: 0.22±0.02 ka Ar. Mean: 0.21±0.02 ka Peak: 0.22 ka	0.96±0.1	1.11±0.08	1.12±0.09	1.00±0.08	1.00±0.08	1.05±0.13	1.08±0.15	1.06±0.12	1.00±0.08	0.97±0.08	0.81±0.08
Murari et al. (2014)	mbd1	N/A	KAL21	30.7567	78.9653	4108	2.0	2.70	0.0	0.939	0.86±0.12	07KNSTD		0.2±0.03		0.22±0.03	0.30±0.05	0.30±0.05	0.26±0.05	0.26±0.05	0.27±0.06	0.26±0.06	0.27±0.06	±	0.26±0.04	0.19±0.00
Murari et al. (2014)	mbd2	N/A	KAL1	30.7778	78.9515	3641	1.5	2.70	0.0	0.937	0.99±0.08	07KNSTD		0.3±0.03		0.32±0.03	0.43±0.05	0.44±0.05	0.37±0.05	0.37±0.05	0.40±0.07	0.39±0.07	0.41±0.07	0.39±0.03	0.37±0.03	0.28±0.03
Murari et al. (2014)	mbd2	N/A	KAL2	30.7777	78.9512	3650	2.0	2.70	0.0	0.923	1.14±0.12	07KNSTD		0.35±0.04	Chi-squared: 103.54 Skewness: +0.58 Outlier: 0 Wt. mean: 0.07±0.15 ka Ar. Mean: 0.16±0.15 ka Peak: !	0.36±0.05	0.50±0.06	0.51±0.05	0.43±0.06	0.43±0.06	0.46±0.09	0.45±0.08	0.47±0.08	0.45±0.05	0.42±0.04	0.33±0.05
Murari et al. (2014)	mbd2	N/A	KAL3	30.7782	78.9506	3646	1.5	2.70	0.0	0.935	0.25±0.03	07KNSTD	0.16±0.15	0.07±0.01		0.08±0.01	0.11±0.01	0.11±0.01	0.09±0.01	0.09±0.01	0.10±0.02	0.10±0.02	0.10±0.02	0.10±0.01	0.09±0.01	0.07±0.01
Murari et al. (2014)	mbd2	N/A	KAL4	30.7782	78.9504	3657	1.5	2.70	0.0	0.923	0.05±0.02	07KNSTD		0.02±0.01		0.02±0.01	0.02±0.01	0.02±0.01	0.02±0.01	0.02±0.01	0.02±0.01	0.02±0.01	0.02±0.01	0.02±0.01	0.02±0.01	0.02±0.01
Murari et al. (2014)	mbd2	N/A	KAL5	30.7782	78.9533	3644	5.0	2.70	0.0	0.929	0.24±0.03	07KNSTD		0.07±0.01		0.08±0.02	0.11±0.01	0.11±0.01	0.09±0.01	0.09±0.01	0.10±0.02	0.09±0.02	0.10±0.02	0.10±0.01	0.09±0.01	0.07±0.01
Murari et al. (2014)	mbd3	N/A	KAL10	30.7839	78.9511	3579	3.0	2.70	0.0	0.937	0.62±0.12	07KNSTD		0.19±0.04		0.21±0.05	0.28±0.07	0.28±0.07	0.24±0.07	0.24±0.07	0.26±0.07	0.25±0.07	0.26±0.07	±	0.24±0.05	0.18±0.00
Murari et al. (2014)	mbd3	N/A	KAL11	30.7838	78.9509	3576	2.5	2.70	0.0	0.937	0.70±0.09	07KNSTD		0.22±0.03	Chi-squared: 71.63 Skewness: -1.57 Outlier: 2 Wt. mean: 0.06±0.10 ka Ar. Mean: 0.15±0.10 ka Peak: !	0.24±0.03	0.32±0.05	0.32±0.05	0.28±0.05	0.28±0.05	0.29±0.06	0.28±0.06	0.30±0.06	±	0.27±0.03	0.21±0.00
Murari et al. (2014)	mbd3	N/A	KAL12	30.7836	78.9507	3568	2.0	2.70	0.0	0.937	4.73±0.25	07KNSTD	0.15±0.10	1.59±0.12		1.72±0.14	1.79±0.18	1.81±0.17	1.58±0.18	1.58±0.18	1.72±0.26	1.90±0.34	1.73±0.25	1.60±0.08	1.51±0.08	1.39±0.08
Murari et al. (2014)	mbd3	N/A	KAL13	30.7834	78.9504	3571	3.0	2.70	0.0	0.943	6.93±0.31	07KNSTD		2.38±0.17		2.61±0.21	2.60±0.20	2.60±0.20	2.34±0.20	2.34±0.20	2.51±0.36	2.74±0.34	2.52±0.31	2.51±0.11	2.36±0.11	2.04±0.11
Murari et al. (2014)	mbd3	N/A	KAL14	30.7831	78.9501	3571	2.5	2.70	0.0	0.938	0.10±0.01	07KNSTD		0.03±0.01		0.03±0.01	0.05±0.01	0.05±0.01	0.04±0.01	0.04±0.01	0.04±0.01	0.04±0.01	0.04±0.01	0.04±0.01	0.04±0.00	0.03±0.01
Murari et al. (2014)	mbd4	N/A	KAL7	30.7898	78.9522	3635	3.0	2.70	0.0	0.911	0.68±0.12	07KNSTD		0.21±0.04	Chi-squared: ! Skewness: ! Outlier: 0 Wt. mean: 0.06±0.11 ka Ar. Mean: 0.13±0.11 ka Peak: !	0.23±0.04	0.31±0.04	0.31±0.05	0.27±0.04	0.27±0.04	0.28±0.07	0.27±0.07	0.29±0.07	±	0.26±0.00	0.20±0.04
Murari et al. (2014)	mbd4	N/A	KAL9	30.7897	78.9523	3637	3.0	2.70	0.0	0.911	0.17±0.03	07KNSTD	0.13±0.11	0.05±0.01		0.06±0.02	0.08±0.02	0.08±0.02	0.07±0.02	0.07±0.02	0.07±0.02	0.07±0.02	0.07±0.02	0.07±0.01	0.06±0.01	0.05±0.01
This study	MP1	Late Holocene	PAR1	34.0835	75.9998	3700	2.0	2.70	0.0	0.968	0.56±0.06	07KNSTD		0.15±0.02	Chi-squared: 5.44 Skewness: -0.86 Outlier: 0 Wt. mean: 0.15x±0.05 ka Ar. Mean: 0.16±0.05 ka Peak: 0.17 ka	0.14±0.02	0.20±0.03	0.20±0.03	0.18±0.03	0.14±0.02	0.19±0.04	0.18±0.04	0.19±0.03	0.19±0.02	0.18±0.02	0.14±0.02
This study	MP1	Late Holocene	PAR2	34.0844	76.0001	3687	3.0	2.70	0.0	0.973	0.33±0.08	07KNSTD		0.09±0.02		0.08±0.02	0.12±0.03	0.12±0.03	0.11±0.03	0.08±0.02	0.11±0.03	0.10±0.03	0.11±0.03	0.11±0.02	0.10±0.02	0.08±0.02
This study	MP1	Late Holocene	PAR3	34.0846	76.0002	3678	3.5	2.70	0.0	0.974	0.71±0.05	07KNSTD	0.16±0.05	0.19±0.02		0.19±0.02	0.26±0.03	0.26±0.03	0.24±0.03	0.18±0.02	0.24±0.04	0.23±0.04	0.24±0.04	0.25±0.01	0.23±0.01	0.18±0.01
This study	MP1	Late Holocene	PAR6	34.0850	76.0004	3667	2.0	2.70	0.0	0.969	0.74±0.12	07KNSTD		0.21±0.04		0.19±0.04	0.27±0.04	0.27±0.04	0.24±0.04	0.18±0.03	0.25±0.06	0.24±0.06	0.25±0.06	0.26±0.03	0.24±0.03	0.18±0.03

Group 3(a): Wet and warm climatic region—central and eastern Himalaya

Kong et al. (2009b)	No stage name given	Ganhaizi	YN-62	27.1217	100.2547	3070	2.0	2.70	0.0	1.000	32.70±2.00	NIST_Certified		13.97±0.96	Chi-squared: ! Skewness: ! Outlier: 0 Wt. mean: 12.97±1.41 ka Ar. Mean: 12.97±1.41 ka Peak: !	15.12±1.11	15.30±1.30	15.30±1.40	14.00±1.30	14.00±1.30	15.00±2.20	15.50±2.30	15.00±2.00	14.54±0.89	13.87±0.85	13.49±0.89
Kong et al. (2009b)	No stage name given	Ganhaizi	YN-63	27.1218	100.2543	3060	2.0	2.70	0.0	1.000	27.60±2.00	NIST_Certified	12.97±1.41	11.97±0.96		13.13±1.1	13.10±1.40	13.20±1.50	11.90±1.40	11.90±1.40	12.80±2.20	13.40±2.20	13.00±2.00	12.78±0.93	12.13±0.88	11.44±0.93
Kong et al. (2009b)	No stage name given	Ganheba	YN-64	27.0523	100.2555	2930	2.0	2.70	0.0	1.000	22.10±0.80	NIST_Certified		10.58±0.53	Chi-squared: ! Skewness: ! Outlier: 0 Wt. mean: 11.62±1.94 ka Ar. Mean: 11.96±1.94 ka Peak: !	11.45±0.64	11.00±1.00	11.40±1.10	10.26±1.00	10.26±1.00	11.10±1.90	11.70±1.80	11.20±1.70	11.31±0.41	10.88±0.40	9.88±0.41
Kong et al. (2009b)	No stage name given	Ganheba	YN-65	27.0530	100.2543	2960	2.0	2.70	0.0	1.000	29.10±1.00	NIST_Certified	11.96±1.94	13.33±0.68		14.55±0.81	14.60±1.10	14.70±1.20	13.30±1.10	13.30±1.10	14.30±2.10	15.00±2.00	14.40±1.90	13.92±0.48	13.30±0.46	12.80±0.48
Kong et al. (2009b)	No stage name given	N/A	YN-48	27.0383	100.1137	2440	2.0	2.70	0.0	0.990	2.36±0.24	NIST_Certified		1.64±0.2	!	1.89±0.23	1.75±0.21	1.75±0.21	1.60±0.21	1.60±0.21	1.70±0.30	1.86±0.35	1.75±0.28	1.79±0.18	1.66±0.17	1.43±0.18
Kong et al. (2009b)	No stage name given	N/A	YN-50	27.0380	100.0973	2210	2.0	2.70	0.0	0.990	30.20±0.60	NIST_Certified	!	20.93±0.87		22.78±1.14	23.10±1.70	23.00±1.80	20.80±1.70	20.80±1.70	23.20±3.30	23.40±3.30	23.00±3.00	21.96±0.44	20.50±0.41	21.15±0.44
Pratt-Sitaula (2005)	Younger Dryas	Yak Glacier lower	Be-425	28.6856	84.1772	4581	1.5	2.65	0.0	0.971	95.62±2.10	LLNL3000		15.19±0.68	Chi-squared: ! Skewness: ! Outlier: 1 Wt. mean: 11.39±1.29 ka Ar. Mean: 11.66±1.29 ka Peak: !	15.78±0.84	16.40±1.30	16.60±1.30	15.20±1.30	15.20±1.30	15.40±2.10	16.00±2.30	15.30±1.90	14.99±0.33	14.97±0.33	14.84±0.33
Pratt-Sitaula (2005)	Younger Dryas	Yak Glacier lower	Be-426	28.6846	84.1777	4530	1.5	2.65	0.0	0.971	75.23±2.00	LLNL3000		12.57±0.65		13.11±0.72	13.50±1.10	13.70±1.20	12.00±1.10	12.00±1.10	12.60±1.90	13.00±2.00	12.60±1.70	12.74±0.34	12.61±0.34	11.95±0.34
Pratt-Sitaula (2005)	Younger Dryas	Yak Glacier lower	Be-427	28.6838	84.1788	4496	1.5	2.65	0.0	0.971	62.10±1.58	LLNL3000	11.66±1.29	10.75±0.48		11.18±0.51	11.39±0.98	12.00±1.00	10.36±0.98	10.36±0.98	10.60±1.80	11.40±1.70	10.60±1.60	11.17±0.29	11.04±0.28	10.02±0.29
Pratt-Sitaula (2005)	Early Holocene	Lyapche Glacier	Be-218	28.6987	84.2545	3815	4.0	2.70	0.0	0.931	41.83±1.18	LLNL3000	11.54±0.80	10.75±0.49	Chi-squared: 2.02 Skewness: +0.02	11.32±0.56	11.59±0.96	12.00±1.00	10.39±0.96	10.39±0.96	11.10±1.80	11.80±1.70	11.10±1.60	11.27±0.32	11.01±0.31	10.07±0.32

Reference	Stage	Site	Sample	Lat	Long	Elev (m)	Thick	Density		Shield	Concentration	Std	Group mean	Age	Statistics											
Pratt-Sitaula (2005)	Early Holocene	Lyapche Glacier	Be-219	28.6987	84.2545	3815	4.0	2.70	0.0	0.931	27.48±0.80	LLNL3000		7.14±0.34	Outlier: 1 Wt. mean: 11.38±0.80 ka Ar. Mean: 11.54±0.80 ka Peak: 11.20 ka	7.61±0.43	7.47±0.59	7.55±0.63	6.76±0.59	6.76±0.59	7.20±1.10	7.80±1.10	7.16±0.99	7.63±0.22	7.32±0.21	6.61±0.22
Pratt-Sitaula (2005)	Early Holocene	Lyapche Glacier	Be-220	28.6987	84.2545	3815	3.0	2.70	0.0	0.940	46.65±1.31	LLNL3000		11.54±0.56		12.35±0.75	13.00±1.00	12.80±1.10	11.42±1.00	11.42±1.00	12.10±1.80	12.80±1.90	12.10±1.60	12.04±0.34	11.71±0.33	11.03±0.34
Pratt-Sitaula (2005)	Early Holocene	Lyapche Glacier	Be-221	28.6987	84.2545	3815	3.0	2.70	0.0	0.940	49.85±1.35	LLNL3000		12.34±0.67		13.12±0.73	13.50±1.10	13.60±1.20	12.18±1.10	12.18±1.10	13.00±2.00	13.60±1.90	12.90±1.80	12.75±0.35	12.39±0.34	11.79±0.35
Abramowski (2004)	LT3: Langtang Stage	N/A	LT32	28.2000	85.6200	3853	2.5	2.70	0.0	0.968	43.10±1.70	S555		10.96±0.55	Chi-squared: 0.55 Skewness: -0.59 Outlier: 1 Wt. mean: 10.87±0.43 ka Ar. Mean: 10.90±0.43 ka Peak: 10.87 ka	11.55±0.68	12.00±1.00	11.90±1.10	11.00±1.00	11.00±1.00	11.30±1.80	12.00±1.70	11.30±1.70	11.43±0.45	11.20±0.44	10.30±0.45
Abramowski (2004)	LT3: Langtang Stage	N/A	LT33	28.2000	85.6200	3851	2.5	2.70	0.0	0.957	40.30±1.60	S555		10.45±0.55		11.1±0.59	11.00±1.00	11.30±1.10	10.06±1.00	10.06±1.00	10.70±1.80	11.40±1.70	10.70±1.60	11.08±0.44	10.79±0.43	9.75±0.44
Abramowski (2004)	LT3: Langtang Stage	N/A	LT35	28.2000	85.6200	3846	1.0	2.70	0.0	0.978	45.80±2.10	S555	10.90±0.43	11.3±0.62		12.03±0.83	12.30±1.10	12.40±1.20	11.10±1.10	11.10±1.10	11.80±1.90	12.40±1.80	11.80±1.70	11.78±0.54	11.50±0.53	10.74±0.54
Abramowski (2004)	LT3: Langtang Stage	N/A	LT36	28.2000	85.6200	3846	2.0	2.70	0.0	0.920	19.20±0.80	S555		5.5±0.28		5.9±0.33	5.51±0.36	5.56±0.39	5.16±0.36	5.16±0.36	5.30±0.70	5.66±0.72	5.31±0.62	5.88±0.25	5.65±0.24	4.82±0.25
Pratt-Sitaula (2011)	Early-mid Holocene	Syaktan Glacier	Be-226	28.6882	84.0234	4500	3.0	2.65	0.0	0.969	52.35±1.63	LLNL3000		9.25±0.58	Chi-squared: 3.38 Skewness: +0.97 Outlier: 1 Wt. mean: 9.51±0.91 ka Ar. Mean: 9.48±0.91 ka Peak: 9.08 ka	9.86±0.59	9.62±0.93	10.00±1.00	8.72±0.93	8.72±0.93	9.00±1.50	9.70±1.60	8.90±1.40	9.96±0.31	9.73±0.30	8.55±0.31
Pratt-Sitaula (2011)	Early-mid Holocene	Syaktan Glacier	Be-227	28.6882	84.0234	4500	3.0	2.65	0.0	0.969	61.14±1.66	LLNL3000		10.72±0.49		11.16±0.52	11.35±0.97	12.00±1.00	10.32±0.97	10.32±0.97	10.60±1.70	11.30±1.70	10.50±1.60	11.15±0.30	11.02±0.30	9.99±0.30
Pratt-Sitaula (2011)	Early-mid Holocene	Syaktan Glacier	Be-228	28.6944	84.0253	4744	3.0	2.65	0.0	0.962	58.76±1.65	LLNL3000	9.48±0.91	9.39±0.56		9.91±0.56	9.68±0.93	9.86±0.99	8.81±0.93	8.81±0.93	8.90±1.50	9.70±1.60	8.90±1.40	10.00±0.28	9.84±0.28	8.63±0.28
Pratt-Sitaula (2011)	Early-mid Holocene	Syaktan Glacier	Be-229	28.6944	84.0253	4744	3.0	2.65	0.0	0.962	54.11±1.59	LLNL3000		8.54±0.5		9.07±0.65	8.83±0.83	9.00±0.89	8.10±0.83	8.10±0.83	8.20±1.30	8.90±1.40	8.10±1.20	9.23±0.27	8.96±0.26	7.94±0.27
Pratt-Sitaula (2011)	Early-mid Holocene	Danfe Glacier	Be-433	28.4735	84.3172	4009	1.5	2.75	0.0	0.917	37.42±0.96	LLNL3000		8.73±0.52	Chi-squared: 0.53 Skewness: -0.35 Outlier: 1 Wt. mean: 8.82±0.36 ka Ar. Mean: 8.87±0.36 ka Peak: 8.82 ka	9.48±0.63	9.21±0.86	9.35±0.92	8.28±0.86	8.28±0.86	8.70±1.50	9.50±1.50	8.70±1.30	9.59±0.25	9.16±0.24	8.14±0.25
Pratt-Sitaula (2011)	Early-mid Holocene	Danfe Glacier	Be-434	28.4739	84.3165	4057	1.0	2.75	0.0	0.945	37.99±0.98	LLNL3000		8.33±0.44		8.98±0.63	8.80±0.80	8.90±0.88	7.92±0.80	7.92±0.80	8.30±1.40	9.00±1.40	8.30±1.20	9.11±0.24	8.65±0.22	7.79±0.24
Pratt-Sitaula (2011)	Early-mid Holocene	Danfe Glacier	Be-435	28.4741	84.3163	4068	2.0	2.75	0.0	0.945	40.08±1.03	LLNL3000		8.85±0.53		9.59±0.6	9.33±0.86	9.47±0.94	8.39±0.86	8.39±0.86	8.80±1.50	9.60±1.50	8.80±1.30	9.71±0.25	9.31±0.24	8.25±0.25
Pratt-Sitaula (2011)	Early-mid Holocene	Danfe Glacier	Be-437	28.4734	84.3178	3978	2.0	2.75	0.0	0.916	38.65±0.99	LLNL3000	8.87±0.36	9.28±0.55		9.99±0.56	9.78±0.92	9.92±0.97	8.76±0.92	8.76±0.92	9.30±1.60	10.00±1.60	9.30±1.40	10.03±0.26	9.71±0.25	8.59±0.26
Pratt-Sitaula (2011)	Early-mid Holocene	Danfe Glacier	Be-438	28.4784	84.3126	4213	1.0	2.75	0.0	0.962	45.56±1.17	LLNL3000		9.19±0.55		9.87±0.56	9.60±0.90	9.78±0.98	8.67±0.90	8.67±0.90	9.10±1.60	9.80±1.60	9.00±1.40	9.95±0.26	9.65±0.25	8.50±0.26
Pratt-Sitaula (2011)	Early-mid Holocene	Danfe Glacier	Be-439	28.4784	84.3126	4215	1.0	2.75	0.0	0.962	42.92±0.94	LLNL3000		8.57±0.47		9.25±0.63	9.00±0.80	9.14±0.89	8.13±0.80	8.13±0.80	8.50±1.40	9.20±1.50	8.50±1.20	9.38±0.21	8.97±0.20	8.00±0.21
Pratt-Sitaula (2011)	Early-mid Holocene	Danfe Glacier	Be-440	28.4789	84.3116	4249	2.0	2.75	0.0	0.980	46.68±1.20	LLNL3000		9.17±0.54		9.83±0.57	9.57±0.89	9.73±0.98	8.63±0.89	8.63±0.89	9.00±1.50	9.80±1.60	9.00±1.40	9.92±0.26	9.63±0.25	8.47±0.26
Pratt-Sitaula (2005)	Early-mid Holocene	Yak upper	Be-420	28.6915	84.1773	4821	1.0	2.65	0.0	0.977	60.89±1.57	LLNL3000		9.05±0.55	Chi-squared: 0.75 Skewness: -1.14 Outlier: 0 Wt. mean: 8.64±0.40 ka Ar. Mean: 8.72±0.40 ka Peak: 8.74 ka	9.6±0.6	9.33±0.86	9.51±0.94	8.52±0.86	8.52±0.86	8.60±1.40	9.30±1.50	8.50±1.30	9.75±0.25	9.57±0.25	8.36±0.25
Pratt-Sitaula (2005)	Early-mid Holocene	Yak upper	Be-421	28.6908	84.1778	4798	1.0	2.65	0.0	0.977	60.40±1.55	LLNL3000		9.07±0.55		9.63±0.6	9.36±0.87	9.54±0.95	8.54±0.87	8.54±0.87	8.60±1.50	9.40±1.50	8.60±1.30	9.77±0.25	9.58±0.25	8.38±0.25
Pratt-Sitaula (2005)	Early-mid Holocene	Yak upper	Be-422	28.6903	84.1786	4770	1.0	2.65	0.0	0.977	57.58±1.48	LLNL3000		8.7±0.52		9.25±0.64	9.01±0.82	9.18±0.92	8.23±0.82	8.23±0.82	8.30±1.40	9.10±1.40	8.30±1.20	9.42±0.24	9.20±0.24	8.09±0.24
Pratt-Sitaula (2005)	Early-mid Holocene	Yak upper	Be-423	28.6894	84.1800	4702	2.0	2.65	0.0	0.977	55.33±1.43	LLNL3000	8.72±0.40	8.69±0.52		9.28±0.64	9.01±0.82	9.18±0.92	8.22±0.82	8.22±0.82	8.30±1.40	9.10±1.40	8.30±1.20	9.43±0.24	9.19±0.24	8.09±0.24
Pratt-Sitaula (2005)	Early-mid Holocene	Yak upper	Be-424	28.6894	84.1800	4702	1.0	2.65	0.0	0.977	52.00±1.31	LLNL3000		8.09±0.42		8.53±0.56	8.35±0.71	8.50±0.82	7.67±0.71	7.67±0.71	7.80±1.20	8.50±1.30	7.70±1.10	8.65±0.22	8.42±0.21	7.54±0.22
Gayer et al. (2006)	N/A	M3	GA24	28.2320	85.1880	4490	3.0	2.70	0.0	0.990	31.78±3.24	NIST_27900		6.58±0.62	Chi-squared: ! Skewness: ! Outlier: 0 Wt. mean: 7.08±0.64 ka Ar. Mean: 7.04±0.64 ka Peak: 7.17 ka	6.96±0.65	6.62±0.87	6.73±0.92	6.21±0.87	6.21±0.87	6.20±1.20	6.80±1.40	6.20±1.10	7.01±0.72	6.82±0.70	5.96±0.72
Gayer et al. (2006)	N/A	M3	GA54	28.2270	85.1880	4434	3.0	2.70	0.0	0.980	35.74±2.41	NIST_27900	7.04±0.64	7.49±0.56		7.96±0.65	7.71±0.77	7.83±0.83	7.08±0.77	7.08±0.77	7.30±1.20	7.90±1.20	7.20±1.10	8.02±0.54	7.77±0.53	6.95±0.54
Zech et al. (2009)	Lete	N/A	LE12	28.6240	83.6420	2440	2.0	2.70	0.0	0.9660	8.97±2.02	07KNSTD	6.36±1.21	6.36±1.21	!	5.73±1.13	6.10±1.50	6.10±1.50	5.30±1.30	5.50±1.20	6.00±1.70	6.50±1.90	6.00±1.60	6.37±1.44	5.84±1.32	5.15±1.16
Barnard et al. (2006)	Langtang glacial stage	N/A	KTM25	28.2100	85.4700	3230	5.0	2.70	0.0	0.850	14.00±1.90	LLNL3000		5.75±0.68	Chi-squared: ! Skewness: ! Outlier: 0 Wt. mean: 5.31±0.40 ka Ar. Mean: 5.47±0.40 ka Peak: 5.47 ka	6.28±0.74	5.88±0.94	6.00±1.00	5.45±0.94	5.45±0.94	5.70±1.10	6.20±1.50	6.00±1.00	6.28±0.85	5.91±0.80	5.13±0.85
Barnard et al. (2006)	Langtang glacial stage	N/A	KTM26	28.2100	85.4700	3239	5.0	2.70	0.0	0.850	12.40±0.80	LLNL3000	5.47±0.40	5.19±0.35		5.65±0.38	5.31±0.45	5.34±0.48	4.87±0.45	4.87±0.45	5.18±0.75	5.52±0.66	5.19±0.68	5.60±0.36	5.32±0.34	4.52±0.36
Abramowski (2004)	N/A	MK4: LIA	MK41	28.3300	84.7600	3900	4.0	2.70	0.0	1.000	24.90±2.20	S555		6.29±0.52	Chi-squared: 2.83 Skewness: +1.35 Outlier: 1 Wt. mean: 5.05±0.92 ka Ar. Mean: 4.99±0.92 ka Peak: !	6.71±0.57	6.39±0.79	6.47±0.83	5.94±0.79	5.94±0.79	6.10±1.10	6.70±1.40	6.00±1.00	6.75±0.60	6.51±0.58	5.67±0.60
Abramowski (2004)	N/A	MK4: LIA	MK42	28.3300	84.7600	3900	4.0	2.70	0.0	1.000	10.10±1.50	S555		2.76±0.44		3.05±0.49	2.79±0.37	2.81±0.36	2.69±0.37	2.69±0.37	2.70±0.50	2.88±0.43	2.68±0.47	2.90±0.43	2.83±0.42	2.30±0.43
Abramowski (2004)	N/A	MK4: LIA	MK43	28.3300	84.7600	3900	4.0	2.70	0.0	1.000	18.00±1.40	S555		4.79±0.39		5.21±0.41	4.80±0.50	4.89±0.52	4.47±0.50	4.47±0.50	4.59±0.82	5.01±0.74	4.60±0.74	5.13±0.40	4.89±0.38	4.10±0.40
Abramowski (2004)	N/A	MK4: LIA	MK44	28.3300	84.7600	3900	4.0	2.70	0.0	1.000	15.40±2.40	S555	4.99±0.92	4.14±0.62		4.55±0.68	4.12±0.85	4.18±0.84	3.90±0.85	3.90±0.85	3.90±0.94	4.30±1.10	3.90±0.90	4.34±0.68	4.19±0.65	3.50±0.68
Abramowski (2004)	N/A	MK4: LIA	MK45	28.3300	84.7600	3900	4.0	2.70	0.0	1.000	17.80±3.40	S555		4.74±0.82		5.17±0.85	4.78±0.96	5.00±1.00	4.43±0.96	4.43±0.96	4.50±1.20	5.00±1.10	4.60±1.20	5.06±0.97	4.83±0.92	4.05±0.97
Barnard et al. (2006)	Langtang glacial stage	N/A	KTM19	28.2100	85.5100	3581	5.0	2.70	0.0	0.950	14.50±0.90	LLNL3000	4.60±0.33	4.60±0.33	Chi-squared: ! Skewness: ! Outlier: 2 Wt. mean:	5.05±0.35	4.66±0.49	4.70±0.50	4.30±0.49	4.30±0.49	4.46±0.78	4.88±0.76	4.48±0.71	4.92±0.31	4.65±0.29	3.93±0.31
Barnard et al. (2006)	Langtang glacial stage	N/A	KTM20	28.2100	85.5100	3507	5.0	2.70	0.0	0.950	2.50±0.70	LLNL3000		0.80±0.24		0.87±0.26	1.00±0.21	1.01±0.23	0.89±0.21	0.89±0.21	0.96±0.26	0.97±0.32	0.98±0.25	0.92±0.26	0.88±0.25	0.70±0.26

Barnard et al. (2006)	Langtang glacial stage	N/A	KTM21	28.2100	85.5100	3510	5.0	2.70	0.0	0.950	3.90±0.70	LLNL3000		1.25±0.24	4.60±0.33 ka Ar. Mean: 4.60±0.33 ka Peak: !	1.38±0.28	1.41±0.27	1.42±0.28	1.29±0.27	1.29±0.27	1.40±0.30	1.44±0.38	1.38±0.28	1.30±0.23	1.24±0.22	1.10±0.23
Abramowski (2004)	N/A	LT6	LT61	28.2100	85.5300	3523	1.5	2.70	0.0	0.957	12.90±0.80	S555	4.42±0.15	4.31±0.31		4.76±0.35	4.36±0.47	4.40±0.49	4.05±0.47	4.05±0.47	4.18±0.75	4.59±0.81	4.19±0.68	4.57±0.28	4.34±0.27	3.67±0.28
Abramowski (2004)	N/A	LT6	LT63	28.2100	85.5300	3525	1.0	2.70	0.0	0.941	13.40±0.70	S555		4.52±0.29	Chi-squared: ! Skewness: ! Outlier: 0 Wt. mean: 4.42±0.15 ka Ar. Mean: 4.42±0.15 ka Peak: 4.43 ka	4.97±0.33	4.59±0.45	4.63±0.46	4.23±0.45	4.23±0.45	4.40±0.75	4.82±0.74	4.41±0.67	4.82±0.25	4.55±0.24	3.85±0.25
Zech et al. (2009)	Neoglacial	N/A	DK21	28.6020	84.4590	3150	2.0	2.70	0.0	0.911	4.86±1.35	S555		2.05±0.61		2.32±0.7	2.26±0.75	2.28±0.72	2.03±0.75	2.03±0.75	2.19±0.76	2.40±0.73	2.22±0.72	2.18±0.61	2.00±0.56	1.78±0.61
Zech et al. (2009)	Neoglacial	N/A	DK22	28.6020	84.4590	3150	2.0	2.70	0.0	0.911	3.22±0.87	S555	1.70±0.50	1.34±0.38	Chi-squared: ! Skewness: ! Outlier: 0 Wt. mean: 1.54±0.50 ka Ar. Mean: 1.70±0.50 ka Peak: 1.43 ka	1.48±0.43	1.52±0.39	1.50±0.40	1.37±0.39	1.37±0.39	1.47±0.44	1.57±0.53	1.49±0.43	1.40±0.38	1.31±0.36	1.18±0.38
Barnard et al. (2006)	Yala I glacial stage	Yala I	KTM4	28.2100	85.5600	3924	5.0	2.70	0.0	0.970	2.50±0.80	LLNL3000		0.62±0.21		0.68±0.23	0.83±0.29	0.84±0.28	0.72±0.29	0.72±0.29	0.77±0.27	0.76±0.30	0.80±0.27	0.73±0.23	0.72±0.23	0.55±0.18
Barnard et al. (2006)	Yala I glacial stage	Yala I	KTM5	28.2100	85.5600	3922	5.0	2.70	0.0	0.970	4.40±1.20	LLNL3000		1.12±0.31	Chi-squared: 0.61 Skewness: +1.21 Outlier: 0 Wt. mean: 0.72±0.20 ka Ar. Mean: 0.76±0.20 ka Peak: 0.68 ka	1.22±0.35	1.28±0.36	1.29±0.31	1.18±0.36	1.18±0.36	1.21±0.35	1.26±0.44	1.23±0.35	1.15±0.31	1.12±0.31	0.96±0.26
Barnard et al. (2006)	Yala I glacial stage	Yala I	KTM6	28.2100	85.5600	3923	5.0	2.70	0.0	0.970	2.20±0.80	LLNL3000	0.76±0.20	0.55±0.21		0.6±0.22	0.74±0.26	0.75±0.29	0.63±0.26	0.63±0.26	0.69±0.32	0.67±0.31	0.72±0.26	0.65±0.24	0.63±0.24	0.48±0.18
Barnard et al. (2006)	Yala I glacial stage	Yala I	KTM7	28.2100	85.5700	3840	5.0	2.70	0.0	0.980	2.70±0.90	LLNL3000		0.7±0.24		0.76±0.26	0.92±0.25	0.93±0.26	0.79±0.25	0.79±0.25	0.86±0.33	0.84±0.35	0.88±0.32	0.81±0.27	0.79±0.27	0.61±0.20
Barnard et al. (2006)	Yala I glacial stage	Yala I	KTM8	28.2100	85.5700	3838	5.0	2.70	0.0	0.980	2.80±0.80	LLNL3000		0.72±0.22		0.79±0.24	0.94±0.21	0.95±0.22	0.82±0.21	0.82±0.21	0.89±0.30	0.88±0.32	0.91±0.22	0.83±0.24	0.81±0.24	0.63±0.18
Barnard et al. (2006)	Yala I glacial stage	Yala I	KTM9	28.2100	85.5700	3839	5.0	2.70	0.0	0.980	3.30±1.00	LLNL3000		0.86±0.27		0.94±0.29	1.05±0.26	1.06±0.27	0.95±0.26	0.95±0.26	1.00±0.27	1.02±0.31	1.02±0.26	0.96±0.29	0.93±0.29	0.74±0.23
Heimsath and McGlynn (2008)	N/A	E moraine crest	NP222	28.6350	84.0420	4000	1.5	2.70	0.0	0.910	4.35±0.65	LLNL3000		1.1±0.18		1.18±0.2	1.30±0.20	1.27±0.21	1.15±0.20	1.15±0.20	1.19±0.22	1.23±0.29	1.21±0.22	1.14±0.17	1.11±0.17	0.95±0.17
Heimsath and McGlynn (2008)	N/A	E moraine crest	NP223	28.6350	84.0420	3813	1.5	2.70	0.0	0.912	2.31±0.36	LLNL3000		0.62±0.1		0.67±0.11	0.83±0.16	0.84±0.15	0.72±0.16	0.72±0.16	0.78±0.16	0.76±0.18	0.80±0.16	0.74±0.12	0.72±0.11	0.56±0.12
Heimsath and McGlynn (2008)	N/A	E moraine crest	NP233	28.6350	84.0420	4275	1.5	2.70	0.0	0.907	1.51±0.34	LLNL3000		0.31±0.07	Chi-squared: 5.54 Skewness: -1.07 Outlier: 3 Wt. mean: 0.55±0.16 ka Ar. Mean: 0.55±0.16 ka Peak: !	0.34±0.08	0.44±0.11	0.45±0.11	0.39±0.11	0.39±0.11	0.40±0.12	0.39±0.12	0.41±0.12	0.40±0.09	0.40±0.09	0.29±0.09
Heimsath and McGlynn (2008)	N/A	E moraine crest	NP234	28.6350	84.0420	4216	1.5	2.70	0.0	1.000	2.48±0.20	LLNL3000	0.55±0.16	0.49±0.05		0.53±0.06	0.68±0.09	0.70±0.08	0.58±0.09	0.58±0.09	0.62±0.12	0.60±0.10	0.64±0.11	0.60±0.05	0.59±0.05	0.45±0.05
Heimsath and McGlynn (2008)	N/A	E moraine crest	NP235	28.6350	84.0420	4157	1.5	2.70	0.0	0.910	0.74±0.06	LLNL3000		0.16±0.02		0.18±0.02	0.23±0.03	0.23±0.03	0.20±0.03	0.20±0.03	0.21±0.04	0.20±0.03	0.21±0.04	0.21±0.02	0.20±0.02	0.15±0.02
Heimsath and McGlynn (2008)	N/A	W moraine crest	NP212	28.6410	84.0438	3844	1.5	2.70	0.0	1.000	2.65±0.16	LLNL3000		0.64±0.05		0.7±0.06	0.85±0.08	0.87±0.09	0.74±0.08	0.74±0.08	0.80±0.12	0.78±0.13	0.82±0.11	0.76±0.05	0.74±0.05	0.57±0.05
Heimsath and McGlynn (2008)	N/A	W moraine crest	NP213	28.6410	84.0438	3797	1.5	2.70	0.0	0.935	0.70±0.18	LLNL3000		0.18±0.04		0.2±0.05	0.25±0.08	0.26±0.08	0.22±0.08	0.22±0.08	0.23±0.08	0.23±0.08	0.24±0.08	0.23±0.06	0.22±0.06	0.17±0.06
Heimsath and McGlynn (2008)	N/A	W moraine crest	NP214	28.6410	84.0438	3669	1.5	2.70	0.0	0.943	1.98±0.14	LLNL3000		0.72±0.07		0.66±0.06	0.77±0.06	0.78±0.06	0.65±0.06	0.52±0.04	0.72±0.05	0.70±0.05	0.74±0.05	0.78±0.06	0.75±0.06	0.59±0.04

Group 2(b): Transitional climatic region—central and eastern Himalaya

Schaefer et al. (2008)	Fu Qu valley, Puluo moraine sequence	Puluo 2 moraine	Ny-12-1	28.1680	85.9330	4261	2.5	2.70	0.0	0.978	66.54±2.93	S555		13.42±0.75		14.07±0.88	15.30±1.50	15.50±1.60	14.20±1.50	14.20±1.50	14.60±2.30	15.20±2.20	14.50±2.10	13.50±0.60	13.32±0.59	12.86±0.60
Schaefer et al. (2008)	Fu Qu valley, Puluo moraine sequence	Puluo 2 moraine	Ny-12-2	28.1680	85.9330	4261	2.5	2.70	0.0	0.978	65.58±2.62	S555		13.23±0.72	Chi-squared: 0.41 Skewness: +1.30 Outlier: 0 Wt. mean: 13.34±0.58 ka Ar. Mean: 13.47±0.58 ka Peak: 13.27 ka	13.91±0.85	14.30±1.20	14.40±1.20	13.10±1.20	13.10±1.20	13.50±2.10	14.00±2.00	13.40±1.90	13.32±0.54	13.15±0.53	12.67±0.54
Schaefer et al. (2008)	Fu Qu valley, Puluo moraine sequence	Puluo 2 moraine	Ny-13	28.1680	85.9330	4273	4.0	2.70	0.0	0.978	70.95±5.11	S555	13.47±0.58	14.29±1.07		14.97±1.19	14.40±1.20	14.60±1.20	13.30±1.20	13.30±1.20	13.70±2.10	14.00±2.00	13.60±1.90	14.22±1.03	14.07±1.02	13.80±1.03
Schaefer et al. (2008)	Fu Qu valley, Puluo moraine sequence	Puluo 2 moraine	Ny-14-1	28.1680	85.9330	4265	6.1	2.70	0.0	0.978	47.58±2.62	S555		10.19±0.66		10.8±0.65	29.10±2.30	29.50±2.50	27.90±2.30	27.90±2.30	28.20±3.90	28.50±3.80	27.90±3.50	10.82±0.60	10.52±0.58	9.44±0.60
Schaefer et al. (2008)	Fu Qu valley, Puluo moraine sequence	Puluo 2 moraine	Ny-14-2	28.1680	85.9330	4265	6.1	2.70	0.0	0.978	62.00±2.48	S555		12.93±0.75		13.59±0.8	20.00±1.40	20.20±1.50	18.90±1.40	18.90±1.40	19.20±2.60	19.70±2.30	19.10±2.30	13.05±0.52	12.91±0.52	12.32±0.52
Finkel et al. (2003)	Chhukung glacial stage	N/A	E79	27.9200	86.8100	4624	5.0	2.70	0.0	0.974	67.90±1.70	LLNL3000		11.40±0.51	Chi-squared: 0.04 Skewness: -1.15 Outlier: 0 Wt. mean: 11.50±0.11 ka Ar. Mean: 11.52±0.11 ka Peak: 11.49 ka	11.93±0.72	12.12±0.94	12.00±1.00	11.20±0.94	11.20±0.94	11.30±1.80	12.00±1.70	11.20±1.60	11.69±0.29	11.63±0.29	10.79±0.29
Finkel et al. (2003)	Chhukung glacial stage	N/A	E80	27.9200	86.8100	4624	5.0	2.70	0.0	0.974	69.00±3.10	LLNL3000	11.52±0.11	11.55±0.66		12.13±0.83	12.30±1.10	12.50±1.20	11.40±1.10	11.40±1.10	11.50±1.90	12.20±1.80	11.40±1.70	11.85±0.53	11.78±0.53	10.97±0.53
Finkel et al. (2003)	Chhukung glacial stage	N/A	E81	27.9200	86.8100	4628	5.0	2.70	0.0	0.974	69.50±2.70	LLNL3000		11.61±0.64		12.21±0.8	12.40±1.10	12.60±1.20	11.00±1.10	11.00±1.10	11.50±1.80	12.20±1.80	11.50±1.70	11.91±0.46	11.83±0.46	11.02±0.46
Finkel et al. (2003)	Chhukung glacial stage	N/A	E29	27.9000	86.8700	4755	5.0	2.70	0.0	0.986	133.80±1.60	LLNL3000		19.77±0.82	Chi-squared: ! Skewness: ! Outlier: 1 Wt. mean: 10.97±0.03 ka Ar. Mean: 10.97±0.03 ka Peak: 10.96 ka	20.38±0.91	20.50±1.10	20.80±1.30	19.60±1.10	19.60±1.10	19.50±2.30	20.00±2.10	19.40±2.10	19.50±0.23	19.39±0.23	19.83±0.23
Finkel et al. (2003)	Chhukung glacial stage	N/A	E30	27.9000	86.8700	4837	5.0	2.70	0.0	0.986	72.00±2.20	LLNL3000	10.97±0.03	10.99±0.49		11.37±0.57	11.50±0.97	12.00±1.00	10.63±0.97	10.63±0.97	10.60±1.80	11.30±1.70	10.50±1.60	11.30±0.35	11.27±0.35	10.26±0.35
Finkel et al. (2003)	Chhukung glacial stage	N/A	E31	27.9000	86.8700	4812	5.0	2.70	0.0	0.986	70.80±1.60	LLNL3000		10.95±0.46		11.31±0.53	11.44±0.96	12.00±1.00	10.57±0.96	10.57±0.96	10.50±1.80	11.30±1.70	10.50±1.60	11.27±0.26	11.23±0.25	10.20±0.26
Owen et al. (2005)	Local LGM	Local LGM moraines	GS17	29.6122	102.1035	1858	5.0	2.70	0.0	0.948	14.59±0.80	LLNL3000	10.10±0.73	11.25±0.7	Chi-squared: 0.89 Skewness: +1.03 Outlier: 0 Wt. mean:	12.65±0.95	12.70±1.30	12.50±1.30	11.10±1.30	11.10±1.30	12.80±2.10	13.10±2.10	12.70±1.90	12.34±0.68	11.32±0.62	10.75±0.68
Owen et al. (2005)	Local LGM	Local LGM moraines	GS19	29.6118	102.1048	1864	5.0	2.70	0.0	0.968	13.52±0.90	LLNL3000		10.3±0.75		11.42±0.88	11.40±1.30	11.30±1.30	10.00±1.30	10.00±1.30	12.00±2.00	11.90±1.90	11.50±1.80	11.32±0.76	10.44±0.70	9.72±0.76

Owen et al. (2005)	Local LGM	Local LGM moraines	GS20	29.6118	102.1051	1884	5.0	2.70	0.0	0.965	12.86±1.10	LLNL3000		9.79±0.94	10.28±0.73 ka Ar. Mean: 10.10±0.73 Peak: 10.12 ka	10.93±0.93	10.70±1.50	10.60±1.50	9.40±1.50	9.40±1.50	10.90±2.10	11.00±2.00	10.80±1.90	10.90±0.94	9.96±0.85	9.15±0.94
Owen et al. (2005)	Local LGM	Local LGM moraines	GS19R	29.6118	102.1048	1864	5.0	2.70	0.0	0.968	12.85±1.02	LLNL3000		9.87±0.89		11.02±0.9	10.90±1.40	10.80±1.40	9.50±1.40	9.50±1.40	11.00±2.10	11.00±2.00	10.90±1.90	10.98±0.87	10.03±0.80	9.23±0.87
Owen et al. (2005)	Local LGM	Local LGM moraines	GS20R	29.6115	102.1051	1884	5.0	2.70	0.0	0.965	12.27±1.18	LLNL3000		9.31±1		10.49±0.99	10.20±1.50	10.10±1.50	8.90±1.50	8.90±1.50	10.30±2.10	11.00±2.00	10.30±1.90	10.42±1.00	9.53±0.92	8.73±1.00
Owen et al. (2005)	N/A	"Recessional moraine"	GS14	29.5700	102.0200	1670	5.0	2.70	0.0	1.000	8.80±0.66	LLNL3000	6.03±1.97	7.42±0.6	Chi-squared: ! Skewness: ! Outlier: 0 Wt. mean: 6.22±1.97 ka Ar. Mean: 6.03±1.97 ka Peak: !	8.42±0.82	8.08±0.97	7.98±0.99	7.12±0.97	7.12±0.97	8.20±1.50	8.60±1.50	8.20±1.40	8.43±0.63	7.51±0.56	6.97±0.63
Owen et al. (2005)	N/A	"Recessional moraine"	GS15	29.5900	102.0200	1670	5.0	2.70	0.0	1.000	5.13±0.79	LLNL3000		4.64±0.69		5.28±0.73	4.90±0.85	4.85±0.89	4.43±0.85	4.43±0.85	5.00±1.00	5.00±1.00	4.92±0.99	5.27±0.81	4.70±0.73	4.06±0.81
Finkel et al. (2003)	Thuklha glacial stage	N/A	E61	27.9100	86.8900	5005	5.0	2.70	0.0	0.979	29.70±2.20	LLNL3000		4.73±0.37	Chi-squared: 1.08 Skewness: -0.55 Outlier: 0 Wt. mean: 4.39±0.32 ka Ar. Mean: 4.43±0.32 ka Peak: 4.42 ka	5.04±0.39	4.53±0.53	4.61±0.55	4.36±0.53	4.36±0.53	4.12±0.78	4.55±0.84	4.10±0.71	4.91±0.36	4.85±0.36	3.95±0.36
Finkel et al. (2003)	Thuklha glacial stage	N/A	E62	27.9100	86.8800	4955	5.0	2.70	0.0	0.979	27.40±1.10	LLNL3000	4.43±0.32	4.47±0.25		4.78±0.29	4.26±0.41	4.35±0.44	4.14±0.41	4.14±0.41	3.88±0.67	4.29±0.76	3.90±0.60	4.61±0.19	4.55±0.18	3.72±0.19
Finkel et al. (2003)	Thuklha glacial stage	N/A	E63	27.9100	86.8800	5032	5.0	2.70	0.0	0.979	25.70±1.50	LLNL3000		4.09±0.28		4.39±0.33	3.82±0.41	3.90±0.45	3.82±0.41	3.82±0.41	3.49±0.59	3.83±0.68	3.48±0.53	4.19±0.25	4.17±0.24	3.37±0.25
Owen et al. (2009)	N/A	T5c	Ron-25	28.1423	86.8536	5242	2.5	2.70	0.0	0.980	20.00±1.00	KNSTD		3.02±0.2		3.22±0.24	2.84±0.18	2.88±0.21	2.89±0.18	2.89±0.18	2.63±0.35	2.90±0.30	2.63±0.31	3.05±0.15	3.06±0.15	2.44±0.15
Owen et al. (2009)	N/A	T5c	Ron-26	28.1424	86.8535	5240	3.5	2.70	0.0	0.980	22.10±0.70	KNSTD		3.35±0.19		3.58±0.22	3.07±0.26	3.13±0.27	3.17±0.26	3.17±0.26	2.86±0.33	3.07±0.47	2.86±0.29	3.38±0.11	3.39±0.11	2.72±0.11
Owen et al. (2009)	N/A	T5c	Ron-27	28.1427	86.8540	5247	5.0	2.70	0.0	0.980	8.00±0.60	KNSTD		1.16±0.1	Chi-squared: 1.18 Skewness: +0.38 Outlier: 4 Wt. mean: 3.19±0.23 ka Ar. Mean: 3.18±0.23 ka Peak: 3.14 ka	1.22±0.12	1.28±0.12	1.30±0.12	1.22±0.12	1.22±0.12	1.17±0.16	1.20±0.18	1.19±0.14	1.17±0.09	1.18±0.09	0.99±0.09
Owen et al. (2009)	N/A	T5c	Ron-28	28.1431	86.8544	5244	3.0	2.70	0.0	0.980	23.00±1.00	KNSTD		3.47±0.21		3.69±0.24	3.17±0.29	3.24±0.31	3.27±0.29	3.27±0.29	2.93±0.32	3.20±0.50	2.93±0.28	3.52±0.15	3.54±0.15	2.81±0.15
Owen et al. (2009)	N/A	T5c	Ron-29	28.1432	86.8539	5240	1.0	2.70	0.0	0.980	19.70±1.10	KNSTD	3.18±0.23	2.93±0.22		3.13±0.24	2.79±0.21	2.80±0.20	2.83±0.21	2.83±0.21	2.58±0.35	2.81±0.35	2.58±0.31	2.98±0.17	3.00±0.17	2.37±0.17
Owen et al. (2009)	N/A	T5c	Ron-30	28.1436	86.8540	5245	3.0	2.70	0.0	0.980	20.60±1.00	KNSTD		3.12±0.2		3.32±0.23	2.90±0.18	2.94±0.19	2.97±0.18	2.97±0.18	2.70±0.36	2.91±0.29	2.70±0.31	3.13±0.15	3.14±0.15	2.52±0.15
Owen et al. (2009)	N/A	T5c	Ron-31	28.1432	86.8523	5193	4.5	2.70	0.0	0.950	8.40±0.60	KNSTD		1.29±0.11		1.36±0.13	1.38±0.13	1.40±0.12	1.32±0.13	1.32±0.13	1.27±0.19	1.32±0.23	1.29±0.16	1.28±0.09	1.28±0.09	1.10±0.09
Owen et al. (2009)	N/A	T5c	Ron-32	28.1432	86.8523	5190	0.5	2.70	0.0	0.950	8.10±0.80	KNSTD		1.2±0.14		1.27±0.15	1.31±0.13	1.33±0.15	1.25±0.13	1.25±0.13	1.21±0.18	1.24±0.23	1.22±0.16	1.20±0.12	1.20±0.12	1.02±0.12
Owen et al. (2009)	N/A	T5c	Ron-33	28.1428	86.8523	5195	1.0	2.70	0.0	0.960	9.40±0.50	KNSTD		1.38±0.1		1.46±0.12	1.47±0.13	1.50±0.13	1.41±0.13	1.41±0.13	1.35±0.18	1.43±0.24	1.36±0.17	1.38±0.07	1.37±0.07	1.18±0.07
Owen et al. (2009)	N/A	T6	Ron-61	28.1363	86.8515	5175	1.5	2.70	0.0	0.980	14.30±0.50	KNSTD		2.14±0.14	Chi-squared: 0.51 Skewness: -1.49 Outlier: 0 Wt. mean: 2.06±0.09 ka Ar. Mean: 2.08±0.09 ka Peak:2.05 ka	2.29±0.17	2.17±0.21	2.20±0.20	2.11±0.21	2.11±0.21	1.96±0.32	2.19±0.36	1.96±0.29	2.16±0.08	2.14±0.08	1.78±0.08
Owen et al. (2009)	N/A	T6	Ron-62	28.1364	86.8515	5178	5.0	2.70	0.0	0.980	12.90±0.40	KNSTD		1.98±0.11		2.11±0.15	2.00±0.18	2.04±0.21	1.93±0.18	1.93±0.18	1.81±0.28	2.01±0.32	1.82±0.25	1.97±0.06	1.94±0.06	1.65±0.06
Owen et al. (2009)	N/A	T6	Ron-63	28.1364	86.8515	5174	2.5	2.70	0.0	0.980	13.90±0.70	KNSTD	2.08±0.09	2.11±0.16		2.25±0.19	2.12±0.21	2.17±0.24	2.06±0.21	2.06±0.21	1.90±0.30	2.14±0.36	1.92±0.29	2.10±0.11	2.08±0.11	1.74±0.11
Owen et al. (2005)	Neoglacial	Neoglacial moraines	GS1	29.5699	101.9855	3174	5.0	2.70	0.0	0.924	3.11±0.39	LLNL3000		1.17±0.16		1.29±0.18	1.34±0.16	1.35±0.17	1.24±0.16	1.24±0.16	1.32±0.21	1.34±0.25	1.30±0.20	1.25±0.16	1.18±0.15	1.05±0.16
Owen et al. (2005)	Neoglacial	Neoglacial moraines	GS2	29.5699	101.9855	3160	5.0	2.70	0.0	0.939	4.79±0.61	LLNL3000		1.84±0.25	Chi-squared: 0.31 Skewness: +0.72 Outlier: 2 Wt. mean: 1.06±0.10 ka Ar. Mean: 1.04±0.10 ka Peak: 1.06 ka	2.03±0.3	1.90±0.30	1.90±0.30	1.83±0.30	1.83±0.30	1.88±0.37	2.04±0.48	1.89±0.35	1.94±0.25	1.81±0.23	1.60±0.25
Owen et al. (2005)	Neoglacial	Neoglacial moraines	GS3	29.5758	102.0037	3056	5.0	2.70	0.0	0.942	2.46±0.32	LLNL3000		0.98±0.14		1.07±0.16	1.17±0.16	1.18±0.17	1.06±0.16	1.06±0.16	1.10±0.20	1.10±0.20	1.16±0.19	1.06±0.14	1.02±0.13	0.87±0.14
Owen et al. (2005)	Neoglacial	Neoglacial moraines	GS4	29.5758	102.0037	3056	5.0	2.70	0.0	0.942	8.20±1.40	LLNL3000	1.04±0.10	3.39±0.58		3.77±0.64	3.29±0.67	3.31±0.71	3.29±0.67	3.29±0.67	3.24±0.81	3.48±0.87	3.24±0.77	3.73±0.64	3.51±0.60	2.89±0.64
Owen et al. (2005)	Neoglacial	Neoglacial moraines	GS8	29.5768	102.0031	2972	5.0	2.70	0.0	0.976	2.14±1.01	LLNL3000		0.95±0.44		1.01±0.47	1.07±0.42	1.07±0.42	0.95±0.42	0.95±0.42	1.04±0.42	1.04±0.44	1.06±0.42	1.0±0.51	1.03±0.49	0.89±0.42
Owen et al. (2005)	Neoglacial	Neoglacial moraines	GS9	29.5769	102.0031	2959	5.0	2.70	0.0	1.000	2.71±0.29	LLNL3000		1.07±0.13		1.18±0.15	1.26±0.14	1.26±0.15	1.14±0.14	1.14±0.14	1.23±0.19	1.24±0.22	1.25±0.18	1.15±0.12	1.09±0.12	0.95±0.12
Owen et al. (2005)	Little Ice Age	Little Ice Age moraines	GS5	29.5713	101.9990	3010	5.0	2.70	0.0	0.936	1.03±0.30	LLNL3000		0.41±0.12		0.45±0.14	0.59±0.19	0.60±0.17	0.49±0.19	0.49±0.19	0.56±0.22	0.54±0.21	0.58±0.22	±	0.49±0.00	0.37±0.11
Owen et al. (2005)	Little Ice Age	Little Ice Age moraines	GS6	29.5717	101.9989	2988	5.0	2.70	0.0	0.932	7.84±2.95	LLNL3000	0.46±0.06	3.41±1.25	Chi-squared: ! Skewness: ! Outlier: 1 Wt. mean: 0.48±0.06 ka Ar. Mean: 0.46±0.06 ka Peak: 0.49 ka	3.8±1.37	3.30±1.50	3.30±1.50	3.30±1.50	3.30±1.50	3.30±1.50	3.50±1.70	3.30±1.50	3.69±1.39	3.46±1.39	2.86±1.08
Owen et al. (2005)	Little Ice Age	Little Ice Age moraines	GS7	29.5703	101.9989	2979	5.0	2.70	0.0	0.927	1.21±0.13	LLNL3000		0.5±0.06		0.54±0.07	0.72±0.09	0.72±0.09	0.59±0.09	0.59±0.09	0.68±0.14	0.65±0.13	0.71±0.11	0.62±0.07	0.59±0.06	0.45±0.07
Owen et al. (2009)	N/A	T7	Ron-51	28.1298	86.8531	5216	3.5	2.70	0.0	0.970	1.10±0.80	KNSTD		0.18±0.13		0.16±0.11	0.21±0.17	0.22±0.18	0.19±0.17	0.19±0.17	0.18±0.15	0.18±0.15	0.19±0.15	0.2±0.16	±	0.15±0.11
Owen et al. (2009)	N/A	T7	Ron-53	28.1294	86.8542	5213	2.3	2.70	0.0	0.970	2.00±0.20	KNSTD		0.27±0.03	Chi-squared: 12.31 Skewness: +1.32 Outlier: 0 Wt. mean: 0.34±0.19 ka Ar. Mean: 0.33±0.19 ka Peak: !	0.28±0.03	0.38±0.06	0.39±0.06	0.35±0.06	0.35±0.06	0.33±0.07	0.32±0.06	0.34±0.06	0.35±0.04	0.00±0.00	0.25±0.04
Owen et al. (2009)	N/A	T7	Ron-55	28.1296	86.8560	5225	2.0	2.70	0.0	0.970	3.90±0.30	KNSTD	0.33±0.19	0.55±0.05		0.58±0.06	0.74±0.07	0.75±0.07	0.65±0.07	0.65±0.07	0.66±0.12	0.62±0.11	0.68±0.12	0.65±0.05	0.66±0.05	0.48±0.05

Group 1(b): Arid and semiarid colder climatic region—southern and northeastern Tibet

Wang et al. (2013)	Qitai Valley	Group D moraines	DLJ-09	35.5577	102.7354	3828	2.1	2.65	0.0	0.991	60.58±1.72	07KNSTD	13.45±0.25	13.27±0.66	Chi-squared: ! Skewness: !	13.28±0.73	13.60±1.10	13.80±1.20	13.20±1.10	13.20±1.10	13.50±2.10	14.00±1.90	13.30±1.90	13.12±0.37	13.14±0.37	12.79±0.37

Reference	Location	Group	Sample	Lat	Lon	Elev					Conc	Standard	Group mean	Age	Statistics											
Wang et al. (2013)	Qitai Valley	Group D moraines	DLJ-17	35.5583	102.7351	3816	2.2	2.65	0.0	0.991	61.81±1.71	07KNSTD		13.62±0.67	Outlier: 0 Wt. mean: 13.44±0.25 ka Ar. Mean: 13.45±0.25 ka Peak: 13.44 ka	13.62±0.74	13.90±1.10	14.10±1.20	13.60±1.10	13.60±1.10	13.90±2.10	14.00±2.00	13.70±1.90	13.41±0.37	13.46±0.37	13.14±0.37
Laserre et al. (2002)	N/A	unnamed moraine	LLL1	37.5300	101.8500	3900	4.0	2.70	0.0	1.000	33.87±2.34	LLNL3000		6.18±0.45		6.15±0.44	5.78±0.58	5.88±0.65	5.99±0.58	5.99±0.58	5.90±0.99	6.40±1.20	5.78±0.84	6.42±0.44	6.34±0.44	5.70±0.44
Laserre et al. (2002)	N/A	unnamed moraine	LLL2	37.5300	101.8500	3920	4.0	2.70	0.0	1.000	47.33±2.34	LLNL3000		8.3±0.57		8.09±0.59	7.93±0.75	8.09±0.85	8.12±0.75	8.12±0.75	8.10±1.30	8.70±1.40	8.00±1.20	8.41±0.42	8.48±0.42	7.89±0.42
Laserre et al. (2002)	N/A	unnamed moraine	LLL3	37.5300	101.8500	3980	4.0	2.70	0.0	1.000	76.03±3.86	LLNL3000		12.79±0.85		12.35±0.88	12.60±1.20	12.80±1.30	12.70±1.20	12.70±1.20	12.70±2.10	13.00±2.00	12.50±1.80	12.46±0.63	12.71±0.65	12.30±0.63
Laserre et al. (2002)	N/A	unnamed moraine	LLL4	37.5300	101.8500	3980	4.0	2.70	0.0	1.000	46.79±2.33	LLNL3000		7.98±0.53		7.75±0.52	7.59±0.69	7.74±0.75	7.78±0.69	7.78±0.69	7.80±1.30	8.30±1.30	7.60±1.10	8.07±0.40	8.16±0.41	7.56±0.40
Laserre et al. (2002)	N/A	unnamed moraine	LLL5	37.5300	101.8500	3990	4.0	2.70	0.0	1.000	85.54±4.69	LLNL3000		14.16±0.93	Chi-squared: 1.66 Skewness: -0.95 Outlier: 6 Wt. mean: 13.04±1.05 ka Ar. Mean:13.16±1.05 ka Peak: 13.44 ka	13.69±0.95	14.00±1.30	14.30±1.40	14.20±1.30	14.20±1.30	14.20±2.20	14.60±2.10	14.00±2.00	13.58±0.75	13.93±0.77	13.77±0.75
Laserre et al. (2002)	N/A	unnamed moraine	LLL6	37.5300	101.8500	4000	4.0	2.70	0.0	1.000	18.93±1.05	LLNL3000		3.45±0.25		3.5±0.27	3.15±0.29	3.21±0.29	3.37±0.29	3.37±0.29	3.21±0.48	3.49±0.54	3.15±0.43	3.48±0.19	3.45±0.19	3.02±0.19
Laserre et al. (2002)	N/A	unnamed moraine	LLL7	37.5300	101.8500	4000	4.0	2.70	0.0	1.000	28.30±2.12	LLNL3000	13.16±1.05	5.06±0.4		5.11±0.4	4.76±0.51	4.84±0.52	4.80±0.51	4.80±0.51	4.79±0.79	5.21±0.68	4.70±0.73	5.20±0.39	5.11±0.38	4.52±0.39
Laserre et al. (2002)	N/A	unnamed moraine	LLL8	37.5300	101.8500	4000	4.0	2.70	0.0	1.000	68.32±3.95	LLNL3000		11.38±0.76		11.09±0.76	11.20±1.10	11.40±1.30	11.40±1.10	11.40±1.10	11.40±1.90	11.80±1.80	11.10±1.70	11.30±0.66	11.45±0.66	10.93±0.66
Laserre et al. (2002)	N/A	unnamed moraine	LLL9	37.5300	101.8500	4000	4.0	2.70	0.0	1.000	77.98±4.34	LLNL3000		12.96±0.89		12.55±0.94	12.70±1.30	13.00±1.40	12.90±1.30	12.90±1.30	12.90±2.10	13.30±2.10	12.60±1.90	12.61±0.70	12.87±0.72	12.48±0.70
Laserre et al. (2002)	N/A	unnamed moraine	LLL10	37.5300	101.8500	4000	4.0	2.70	0.0	1.000	85.94±4.29	LLNL3000		14.16±0.89		13.68±0.9	14.00±1.30	14.20±1.30	14.20±1.30	14.20±1.30	14.20±2.20	14.50±2.10	14.00±2.00	13.57±0.68	13.93±0.70	13.76±0.68
Laserre et al. (2002)	N/A	unnamed moraine	LLL10b	37.5300	101.8500	4000	4.0	2.70	0.0	1.000	81.59±4.20	LLNL3000		13.50±0.86		13.06±0.91	13.30±1.30	13.60±1.30	13.50±1.30	13.50±1.30	13.50±2.20	14.00±2.00	13.00±2.00	13.03±0.67	13.34±0.69	13.06±0.67
Laserre et al. (2002)	N/A	unnamed moraine	LLL11	37.5300	101.8500	4000	4.0	2.70	0.0	1.000	26.98±1.59	LLNL3000		4.83±0.34		4.88±0.35	4.54±0.48	4.63±0.49	4.64±0.48	4.64±0.48	4.58±0.77	5.02±0.67	4.49±0.69	4.94±0.29	4.84±0.29	4.31±0.29
Owen et al. (2003a)	Halong glacial stage	N/A	A29	34.8400	99.5800	3945	5.0	2.70	0.0	0.994	66.00±2.00	LLNL3000		12.36±0.68		12.46±0.77	12.70±1.10	12.90±1.10	12.00±1.10	12.00±1.10	12.50±1.90	13.10±1.90	12.30±1.70	12.40±0.38	12.34±0.38	11.83±0.38
Owen et al. (2003a)	Halong glacial stage	N/A	A30	34.8400	99.5800	3945	5.0	2.70	0.0	0.994	74.00±2.00	LLNL3000		13.74±0.68	Chi-squared: 4.68 Skewness: -1.47 Outlier: 0 Wt. mean: 13.28±1.26 ka Ar. Mean: 12.89±1.26 ka Peak: 13.40 ka	13.8±0.76	14.20±1.10	14.40±1.20	13.70±1.10	13.70±1.10	14.00±2.10	14.50±1.90	13.80±1.90	13.53±0.37	13.57±0.37	13.27±0.37
Owen et al. (2003a)	Halong glacial stage	N/A	A31	34.8400	99.5700	3970	5.0	2.70	0.0	0.995	71.00±2.00	LLNL3000	12.89±1.26	13.06±0.66		13.13±0.74	13.40±1.10	13.70±1.20	13.00±1.10	13.00±1.10	13.20±2.10	13.80±1.90	13.00±1.80	12.96±0.37	12.97±0.37	12.55±0.37
Owen et al. (2003a)	Halong glacial stage	N/A	A32	34.8400	99.5700	3980	5.0	2.70	0.0	0.996	77.00±3.00	LLNL3000		13.98±0.79		14.01±0.85	14.40±1.10	14.60±1.20	14.00±1.10	14.00±1.10	14.20±2.10	15.00±2.00	14.00±1.90	13.72±0.54	13.79±0.54	13.53±0.54
Owen et al. (2003a)	Halong glacial stage	N/A	A37	34.8400	99.5500	4045	5.0	2.70	0.0	0.996	77.00±4.00	LLNL3000		13.58±0.86		13.61±0.91	14.00±1.30	14.20±1.30	13.50±1.30	13.50±1.30	13.70±2.20	14.00±2.00	13.00±2.00	13.33±0.70	13.41±0.70	13.09±0.70
Owen et al. (2003a)	Halong glacial stage	N/A	A38	34.8400	99.5500	4055	5.0	2.70	0.0	0.995	59.00±2.00	LLNL3000		10.60±0.53		10.71±0.57	11.00±1.00	10.90±1.10	10.35±1.00	10.35±1.00	10.50±1.70	11.10±1.70	10.30±1.60	10.92±0.37	10.79±0.37	9.98±0.37
Owen et al. (2005)	Intermediate age	Un-named moraine	PR35	28.8947	90.2299	4914	5.0	2.70	0.0	0.972	81.90±2.47	LLNL3000		11.66±0.6		12.13±0.76	12.24±0.99	12.50±1.10	11.51±0.99	11.51±0.99	11.30±1.80	12.10±1.70	11.20±1.70	11.88±0.36	11.89±0.36	11.10±0.36
Owen et al. (2005)	Intermediate age	Un-named moraine	PR36	28.8957	90.2294	4897	5.0	2.70	0.0	0.964	74.80±2.47	LLNL3000		10.99±0.5	Chi-squared: 1.56 Skewness: +0.80 Outlier: 0 Wt. mean: 11.32±0.70 ka Ar. Mean: 11.47±0.70 ka Peak: 11.04 ka	11.32±0.58	11.00±1.00	11.60±1.10	10.66±1.00	10.66±1.00	10.50±1.80	11.30±1.70	10.40±1.60	11.29±0.37	11.26±0.37	10.29±0.37
Owen et al. (2005)	Intermediate age	Un-named moraine	PR37	28.8958	90.2293	4891	5.0	2.70	0.0	0.968	85.60±2.11	LLNL3000	11.47±0.70	12.38±0.65		12.89±0.74	13.00±1.10	13.20±1.20	12.18±1.10	12.18±1.10	12.00±1.80	12.80±1.90	11.90±1.60	12.54±0.31	12.52±0.31	11.77±0.31
Owen et al. (2005)	Intermediate age	Un-named moraine	PR38	28.8960	90.2292	4878	5.0	2.70	0.0	0.968	73.20±1.77	LLNL3000		10.86±0.47		11.2±0.5	11.19±0.95	11.40±1.10	10.47±0.95	10.47±0.95	10.30±1.70	11.10±1.70	10.20±1.60	11.18±0.27	11.14±0.27	10.12±0.27
Owen et al. (2003c)	Gangshiga valley	Holocene moraine	Q21	37.7000	101.5900	4190	5.0	2.70	0.0	0.980	64.00±2.00	LLNL3000		10.08±0.53	Chi-squared: ! Skewness: ! Outlier: 1 Wt. mean: 10.08±0.53 ka Ar. Mean: 10.08±0.53 ka Peak: !	9.75±0.6	9.50±0.90	10.00±1.00	9.86±0.90	9.86±0.90	9.70±1.60	10.20±1.60	9.50±1.50	10.06±0.32	10.19±0.32	9.52±0.32
Owen et al. (2003c)	Gangshiga valley	Holocene moraine	Q23	37.7000	101.4600	4180	5.0	2.70	0.0	1.000	28.00±1.00	LLNL3000	10.08±0.53	4.61±0.25		4.63±0.28	4.26±0.41	4.36±0.44	4.43±0.41	4.43±0.41	4.29±0.72	4.75±0.72	4.19±0.64	4.58±0.16	4.56±0.16	4.10±0.16
Owen et al. (2003a)	Halong glacial stage	N/A	A1	34.8900	99.4400	4285	5.0	2.70	0.0	0.997	26.00±1.00	LLNL3000		4.46±0.26		4.65±0.29	4.21±0.42	4.30±0.45	4.26±0.42	4.26±0.42	4.11±0.72	4.61±0.76	4.04±0.64	4.58±0.18	4.44±0.17	3.90±0.18
Owen et al. (2003a)	Halong glacial stage	N/A	A2	34.8800	99.4500	4335	5.0	2.70	0.0	0.998	34.00±1.00	LLNL3000		5.54±0.26	Chi-squared: ! Skewness: ! Outlier: 3 Wt. mean: 9.22±1.70 ka Ar. Mean: 9.48±1.70 ka Peak: !	5.67±0.27	5.29±0.35	5.37±0.38	5.29±0.35	5.29±0.35	5.20±0.70	5.60±0.60	5.11±0.62	5.78±0.17	5.65±0.17	4.97±0.17
Owen et al. (2003a)	Halong glacial stage	N/A	A3	34.8800	99.4500	4340	5.0	2.70	0.0	0.995	11.00±1.00	LLNL3000	9.48±1.70	1.83±0.2		1.89±0.21	1.80±0.21	1.84±0.24	1.84±0.21	1.84±0.21	1.78±0.31	1.99±0.43	1.76±0.28	1.79±0.16	1.77±0.16	1.61±0.16
Owen et al. (2003a)	Halong glacial stage	N/A	A4	34.8800	99.4300	4285	5.0	2.70	0.0	0.998	67.00±2.00	LLNL3000		10.68±0.51		10.71±0.55	10.68±0.98	10.90±1.10	10.43±0.98	10.43±0.98	10.40±1.70	11.10±1.70	10.20±1.50	10.93±0.33	10.87±0.33	10.06±0.33
Owen et al. (2003a)	Halong glacial stage	N/A	A5	34.8800	99.4300	4285	5.0	2.70	0.0	0.998	52.00±1.00	LLNL3000		8.28±0.41		8.27±0.5	8.09±0.69	8.25±0.74	8.00±0.69	8.00±0.69	8.00±1.20	8.60±1.30	7.80±1.10	8.57±0.17	8.49±0.16	7.80±0.17
Owen et al. (2006b)	N/A	M2 moraines	PR1	35.7046	94.2506	4546	5.0	2.70	0.0	0.970	53.08±5.61	LLNL3000		7.52±0.81		7.4±0.77	7.34±0.98	7.00±1.00	7.00±0.98	7.00±0.98	7.20±1.40	7.80±1.40	7.10±1.30	7.58±0.80	7.67±0.81	7.07±0.80
Owen et al. (2006b)	N/A	M2 moraines	PR2	35.7049	94.2506	4548	5.0	2.70	0.0	0.970	129.72±5.77	LLNL3000		17.54±1.06	Chi-squared: ! Skewness: ! Outlier: 1 Wt. mean: 8.13±0.74 ka Ar. Mean: 8.04±0.74 ka Peak: 8.25 ka	16.95±1.09	17.50±1.40	17.90±1.60	17.60±1.40	17.60±1.40	17.20±2.60	17.60±2.50	16.90±2.30	16.43±0.73	17.16±0.77	17.32±0.73
Owen et al. (2006b)	N/A	M2 moraines	PR3	35.7040	94.2503	4588	5.0	2.70	0.0	0.970	61.90±3.69	LLNL3000	8.04±0.74	8.56±0.68		8.39±0.73	8.30±0.90	8.52±0.99	8.29±0.90	8.29±0.90	8.20±1.40	8.80±1.50	8.00±1.20	8.74±0.52	8.79±0.53	8.09±0.52
Owen et al. (2005)	Youngest	Un-named moraine	PR31	28.8907	90.2281	4980	5.0	2.70	0.0	0.963	25.90±2.38	LLNL3000	3.28±0.74	4.12±0.39	Chi-squared: 6.20 Skewness: +1.38 Outlier: 0 Wt. mean:	4.41±0.43	3.82±0.55	3.90±0.58	3.86±0.55	3.86±0.55	3.51±0.67	3.90±0.80	3.49±0.61	4.24±0.39	4.19±0.39	3.43±0.39
Owen et al. (2005)	Youngest	Un-named moraine	PR33	28.8892	90.2285	4994	5.0	2.70	0.0	0.951	18.50±1.01	LLNL3000		3.02±0.22		3.23±0.24	2.82±0.19	2.86±0.21	2.90±0.19	2.90±0.19	2.64±0.36	2.88±0.31	2.64±0.32	3.08±0.17	3.07±0.17	2.47±0.17

| Owen et al. (2005) | Youngest | Un-named moraine | PR34 | 28.8889 | 90.2285 | 4989 | 5.0 | 2.70 | 0.0 | 0.957 | 16.70±1.09 | LLNL3000 | | 2.7±0.23 | 3.05±0.74 ka
Ar. Mean:
3.28±0.74 ka
Peak: ! | 2.9±0.25 | 2.60±0.22 | 2.64±0.24 | 2.64±0.22 | 2.64±0.22 | 2.41±0.37 | 2.67±0.39 | 2.42±0.33 | 2.79±0.18 | 2.80±0.18 | 2.22±0.18 |

a   Reported [Be-10] values have been corrected from background Be-10 detected in procedural blanks

All ages, local and regional glacial stages, weighted [Wt.] and arithmatic [Ar.] means, median, and peaks are reported in thousand years with ± 1σ

!   Undefined peak/age statistics is not possible

Note: Blue coloured samples are identified as outliers and removed from further analysis

Scaling models: Lifton-Sato-Dunai (LSD; Lifton et al., 2014 [SA and SF in Marrero et al., 2016]), Lal and Stone time-dependent (Lm; Balco et al., 2008), Lal and Stone time-independent (St; Lal, 1991; Stone, 2000), Desilets (De; Desilets et al., 2006), Dunai (Du; Dunai, 2001), Lifton (Li; Lifton et al., 2005, 2008)

S5. Published AAR and THAR ratios used in this study for diverse regions (Table 2 and DR 4).

Study	Region	AAR	THAR
Northwestern Tibet			
Scherler et al. (2011)	Hindu Kush	0.46	-
Xu et al. (2013)	Northwestern Tibet	0.45–0.70	-
The Karakoram and the Northwestern Himalaya			
Porter (1970), Richards et al. (2000), Dortch et al. (2011)	Swat Himalaya	0.60±0.10	-
Fort (1983), Burbank and Fort (1985), Bovard (2001)	Sub-polar glaciers in Ladakh region.	0.65	0.40
Benn et al. (2005), Sharma et al. (2016)	Sarchu, Zanskar	0.55–0.65	0.50–0.60
Owen et al. (1996), Damm (1997), Tylor and Mitchel (2000)	Zanskar and Lahul	0.65	0.40–0.50
Orr et al. (2017, 2018)	Zanskar	0.40, 0.50, 0.60	0.40–0.50
Scherler et al. (2011)	Karakoram	0.58	-
Shi and Zhang	Batura, Karakoram	0.50	-
Chaturvedi et al. (2014)	Karakoram	0.58–0.70	-
Deswal et al. (2017)	Miyar valley	0.44, 0.56, 0.60	0.5–0.6
De Terra and Paterson (1939), Holmes and Street-Perrott (1989)	Kashmir Himalaya	-	0.40
Scott (1992), Richards et al. (2000, 2001), Phillips et al. (2000)	Nanga Parbat and Middle Indus Valley	-	0.40
Western Himalaya			
Schaefer et al. (2008)	Garhwal Himalaya	-	0.40–0.50
Andrew (1975), Sharma and Owen (1996), Barnard et al. (2004)	Garhwal Himalaya	0.60, 1.3	0.50
Dhobal et al. (2008)	Garhwal Himalaya (debris-covered glaciers)	~0.61–0.70	0.50–0.60
Nainwal et al. (2006)	Garhwal Himalaya	0.60±0.05	-
Mehta et al. (2012)	Garhwal Himalaya	~0.45	-
Scherler et al. (2010)	Garhwal Himalaya	0.45, 0.55, 0.65	0.50–0.60
Kulkarni (1992)	Debris covered glaciers in the Western Himalaya	0.43–0.47	-
Benn and Lehmkuhl (2000)	Debris covered glaciers in the Karakoram, Nepal to clean glaciers in Tibet	0.44–0.67	-
Scherler et al. (2011)	Western Himalaya	0.48±26	-
Central Himalaya			
Kaser and Osmaston (2002)	Tropical debris-covered glaciers	0.65–0.70	-
Williams (1983), Zheng (1988), Burbank and Cheng (1991), Burbank and Kang (1991), Shiraiwa and Watanable (1991), Shiraiwa (1993), Fort (1995), Mann et al. (1996), Finkel et al. (2003)	Debris covered glaciers in the Nepal Himalaya	0.60–0.65	-

254

Scherler et al. (2011)	North and South, Central Himalaya	0.42–0.60	-
Porter (1975)	Mid- and High-latitude glaciers	0.55–0.65	-
Pant et al. (2006)	Uttaranchal, Central Himalaya	0.45	-
Pratt-Sitaula (2005 PhD)	Nepal Himalaya	0.6 (present), 0.45–0.70 (predicted)	-
Gayer et al. (2006)	Ganesh Himal, Nepal	0.65	0.40
Eastern Himalaya and the Southeastern Tibet			
Zhang (1988), Yang et al. (2008)	Eastern Himalaya	0.60	-
Smiraglia (1997)	Eastern Himalaya	0.67	-
Shangzhe et al. (2010)	Boduizanbo basin, Southeastern Tibet	0.60	-
Isacks et al. (1995)	Bhutan Himalaya	-	0.50
Northeastern and Central Tibet			
Benn and Lehmkuhl (2000)	Quilian Mountains	0.69	-
Scherler et al. (2011)	West Kunlun Shan	0.80	-
Gross et al. (1976)	Central and High Asia	0.67	-
Owen et al. (2003)	Northeastern edge of Tibetan Plateau	0.50–0.80	-
Dyurgerov et al. (1995), Kunakhovitch and Sokalskaya (1997)	Tien Shan	0.65	-
Meier and Post (1962), Hawkins (1985), Benn and Lehmkuhl (2000), Owen and Benn (2005)	Variety of glaciers in the Himalaya and Tibet	0.50–0.80	0.30–0.50
Heyman (2014)	Tibet	-	0.50

S6. Reconstructed ELAs across the Himalayan-Tibetan orogen.

Glaciated Valley	Glacial Stage	Mean moraine age (ka)	Head (m asl)	Toe (m asl)	MELM (m asl)	Area-Altitude AA (m asl)	Area-Accumulation ratio			Toe-Headwall altitude ratio			Mean ELA (m asl)	ΔELA (m)
							AAR (0.50)	AAR (0.60)	AAR (0.70)	THAR (0.30)	THAR (0.40)	THAR (0.50)		
Group 1(a): Arid and semiarid colder climatic region— Transhimalaya, NW Tibet, Pamir, and Tian Shan.														
Bordoo Valley, Tian Shan	Present	-	4467	3870	4100	4188	4199	4159	4109	4037	4113	4190	4137±56	-
	BOR 1	0.64±0.23	4458	3745	-	4135	4159	4109	4039	3974	4059	4145	4089±67	54±10
	BOR 2	13.08±2.13	4452	3629	-	4044	4079	3979	3869	3890	3987	4085	3990±86	152±46
Kitschi-Kurumdu, Tian Shan	M2	15.16±3.03	4268	3787	-	3999	3969	3930	3899	-	-	-	3949±44	-
Ala Archa, Kyrgyz Tian Shan	Present	-	4299	3722	3950	4004	3989	3949	3889	3907	3973	4040	3963±50	-
	Ala Archa	0.49±0.25	4258	3400	-	3765	3739	3659	3569	3669	3769	3870	3720±97	244±50
Aksai valley, Kyrgyz Tian Shan	Present	-	4139	3843	4100	4006	3989	3979	3949	-	-	-	4005±57	-
	Aksai	5.70±0.16	4072	3408	-	3700	3689	3629	3549	3602	3683	3765	3660±71	339±46
Daxi valley, Tian Shan	Present	-	4400	3801	4000	4075	4049	4019	3969	3972	4043	4115	4030±50	-
	LIA	0.33±0.02	4390	3684	-	4013	3999	3949	3909	3909	3989	4070	3977±58	58±9
Alay Range (Koksu Valley)	Present	-	4917	3621	4059	4180	4209	4159	4099	4019	4149	4280	4144±84	-
	AV	14.02±0.16	4921	3442	-	4060	4129	4029	3899	3893	4041	4190	4034±110	122±39
Muztag Ata and Kongur Shan, NW Tibet			6853	2773	3809	3972	3829	3729	3559	4003	4411	4820	4017±409	-
	Olimde 7 stage (m3I)	1.39±0.42	6873	2462	-	3870	3769	3619	3449	3792	4233	4675	3915±413	131±51
Muztag Ata and Kongur Shan, NW Tibet	Present	-	7349	4271	5609	5998	6259	5979	5609	5203	5511	5820	5749±332	-
	Olimde 7 stage (m7H)	1.66±0.17	7349	4054	-	5772	6029	5659	5229	5049	5379	5710	5547±341	222±100
Muztag Ata and Kongur Shan, NW Tibet	Present	-	6847	4300	5809	6030	6189	5989	5809	5068	5324	5580	5725±379	-
	Olimde 6 stage (m5H)	4.32±0.11	6852	4003	-	5866	6099	5879	5629	4864	5149	5435	5560±440	153±40
	Olimde 6 stage (m6H)	3.97±0.30	6852	3919	-	5793	6059	5829	5539	4801	5095	5390	5501±442	212±53
	Olimde 4 stage (m4H)	7.98±0.10	6839	3591	-	5437	5759	5279	4529	4574	4899	5225	5100±454	612±317
	Olimde 2 stage (m3H)	13.01±0.14	6852	3515	-	5377	5679	5069	4469	4521	4855	5190	5023±442	690±334
Muztag Ata and Kongur Shan, NW Tibet	Present	-	6991	4348	4969	5602	5459	5119	5119	5144	5409	5675	5278±301	-
	Olimde 8 stage (m6C)	0.51±0.15	7008	4273	-	5528	5389	4970	4769	5101	5375	5650	5255±317	68±42
	Olimde 2 stage (m5C)	11.71±0.40	7008	4209	-	5375	5089	4789	4599	5052	5333	5615	5122±352	201±126
Muztag Ata and Kongur Shan, NW Tibet	Present	-	6069	4237	4729	4936	4829	4749	4669	4791	4975	5160	4855±160	-
	Olimde 8 stage (m8A)	0.69±0.27	6075	4152	-	4860	4779	4689	4559	4735	4927	5120	4810±181	63±24
	Olimde 7 stage (m7A)	2.20±0.07	6075	4018	-	4803	4739	4619	4499	4637	4843	5050	4741±180	131±26
	Olimde 4 Stage (m6A)	7.80±0.29	6075	3982	-	4796	4729	4610	4489	4616	4825	5035	4729±179	144±28
	Olimde 4 Stage (m5A)	7.74±0.27	6075	3787	-	4621	4559	4409	4229	4476	4705	4935	4562±225	311±69
Muztag Ata and Kongur Shan, NW Tibet	Present	-	6667	4257	4969	5236	5369	5219	4909	4985	5227	5470	5173±201	-
	Olimde 3 stage (m3F)	10.25±0.16	6682	3586	-	4734	4609	4400	4169	4519	4829	5140	4629±313	574±196
Muztag Ata and Kongur Shan, NW Tibet	Present	-	6711	4601	4979	5316	5229	5109	4940	5242	5453	5665	5242±241	-
	Olimde 3 stage (m3F′)	9.69±0.34	6747	3410	-	4501	4489	4209	3929	4415	4750	5085	4483±370	797±140
Muztag Ata and Kongur Shan, NW Tibet	Present	-	6815	4258	4949	5488	5389	5129	4899	5027	5283	5540	5213±247	-
	Olimde 5 stage (m6C′)	5.05±0.14	6865	4059	-	5306	5150	4879	4669	4902	5183	5465	5079±276	172±72
Great Bogchigir Valley	Present	-	5324	4599	4919	4968	4979	4949	4899	4818	4891	4965	4924±54	-
	BO8 stage	13.18±0.64	5326	4425	-	4882	4919	4850	4760	4702	4793	4885	4827±78	97±26

Glaciated Valley	Glacial Stage	Mean moraine age (ka)	Head (m asl)	Toe (m asl)	MELM	AA	AAR (0.45)	AAR (0.55)	AAR (0.65)	THAR (0.40)	THAR (0.50)	THAR (0.60)	Mean ELA	ΔELA
Group 1(a): Arid and semiarid colder climatic region— Transhimalaya, NW Tibet, Pamir, and Tian Shan.														
Batura - Hunza Valley	Present	-	7606	2502	3489	4341	4359	3979	3719	4553	5065	5576	4385±689	-
	Batura stage (t6)	14.30±0.01	7617	2455	-	4276	4279	3919	3659	4527	5045	5562	4467±653	46±26
Batura - Hunza Valley	Present	-	6070	3226	4900	4966	5049	4859	4469	4481	4965	5448	4892±315	-
	Batura stage (t6)	12.49±1.05	7112	2542	-	4862	5009	4799	4249	4403	4900	5396	4803±381	88±61
Central Karakoram	Askole 2 stage (m2b)	5.98±0.69	-	-	-	-	-	-	-	-	-	-	-	-
Central Karakoram	Present	-	5173	4290	4829	4827	4859	4809	4779	4646	4735	4824	4789±69	-
	Mungo 2 stage (m2G)	6.64±0.35	5202	2991	-	4310	4729	4559	4089	3883	4105	4326	4286±291	497±232
	Mungo 2 stage (m1G)	13.77±0.53	5202	2889	-	3875	3639	3389	3289	3817	4050	4282	3763±353	1020±366
Central Karakoram	Present	-	6260	3027	4449	4792	4959	4839	4719	4325	4650	4974	4713±231	-
	Askole 3 stage (m1H)	1.03±0.28	6262	2977	-	4769	4949	4829	4689	4295	4625	4954	4730±228	21±8
	Mungo 2 stage (m3I)	13.06±0.40	6262	2977	-	4744	4939	4820	4669	4295	4625	4954	4721±226	30±13
	Mungo 2 stage (m2I)	14.08±0.23	6262	2977	-	4730	4939	4819	4649	4295	4625	4954	4716±226	35±21
	Mungo 2 stage (m1I)	14.98±0.29	6262	2977	-	4710	4929	4809	4619	4295	4625	4954	4706±225	45±32
Central Karakoram	Present	-	5840	4224	4939	5101	5159	5099	5039	4877	5040	5202	5057±108	-
	Mungo 2 stage (m1E)	12.41±0.33	5840	2643	-	4524	5029	4889	4509	3929	4250	4570	4529±370	545±293
Central Karakoram	Present	-	5718	4019	4689	4916	4979	4929	4839	4703	4875	5046	4872±125	-
	Mungo 2 stage (m1F)	13.44±0.19	5718	2873	-	4568	4859	4649	4409	4019	4305	4590	4486±271	413±186
Central Karakoram	Present	-	5700	3877	4509	4893	5050	4909	4709	4611	4795	4978	4807±186	-
		14.62±0.32	5724	2408	-	4338	4659	4429	4199	3737	4070	4402	4262±296	587±162
Ladakh cirque, Ladakh range	Present	-	5776	5407	5529	5596	5609	5570	5539	-	-	-	5529±110	-
	Ladakh Chang La cirque	2.29±0.28	5776	5376	-	5553	5549	5519	5480	-	-	-	5525±34	53±8
Ladakh cirque, Ladakh range	Present	-	5984	5386	5679	5673	5690	5659	5629	5629	5690	5750	5675±39	-

Location	Stage	Age			MELM	AA	AAR (0.45)	AAR (0.55)	AAR (0.65)	THAR (0.40)	THAR (0.50)	THAR (0.60)	Mean ELA	ΔELA
	Pangong high cirque	0.54±0.11	5997	4844	-	5517	5589	5509	5420	5313	5430	5546	5475±93	199±72
Stok Kangri, Zanskar	Present	-	5721	5288	5459	5507	5519	5499	5459	-	-	-	5489±28	-
	mS1	1.42±0.48	5748	5234	-	5456	5449	5419	5399	-	-	-	5431±27	65±13
Stok valley, Zanskar	mG1		5649	5258	5479	5510	5539	5509	5479	-	-	-	5503±25	-
	mG1	1.33±0.12	5649	5149	-	5455	5499	5459	5430	-	-	-	5461±29	49±6
Amda Kangri, Lato	Present	-	5743	5312	5489	5538	5539	5519	5489	-	-	-	5515±25	-
	mA1	0.26±0.08	5764	5298	-	5533	5539	5519	5489	-	-	-	5523±25	1±3
	mA2c	0.52±0.20	5764	5264	-	5511	5529	5489	5459	-	-	-	5497±30	24±10
Puga Valley, Zanskar	Present	-	6099	5686	5839	5893	5909	5870	5839	-	-	-	5870±32	-
	PM-3 stage	0.28±0.05	6101	5199	-	5647	5659	5609	5559	5563	5655	5746	5634±64	259±15
	PM-2 stage	3.50±0.87	6101	4797	-	5480	5569	5489	5369	5323	5455	5586	5467±96	401±55
Mentok Kangri, Karzok	Present	-	6003	5482	5659	5740	5759	5729	5709	-	-	-	5719±38	-
	mM1	0.64±0.09	6003	5447	-	5714	5739	5710	5679	-	-	-	5711±25	24±5
	mM2	1.00±0.08	6003	5378	-	5685	5689	5669	5639	5631	5695	5758	5681±42	64±8
Gomuche Kangri, Karzok	Present	-	6084	5381	5649	5873	5939	5909	5869	5669	5740	5810	5807±110	-
	mG1	2.25±0.42	6084	5332	-	5805	5909	5859	5739	5639	5715	5790	5779±91	50±39
	mG2 (or KM-4)	4.66±1.17	6084	5206	-	5732	5869	5739	5579	5561	5650	5738	5695±107	134±78

Group 2(a): Transitional climatic region—western Himalaya

Location	Stage	Age			MELM	AA	AAR (0.45)	AAR (0.55)	AAR (0.65)	THAR (0.40)	THAR (0.50)	THAR (0.60)	Mean ELA	ΔELA
Nun-Kun massif	Anantick stage (ST-3)	13.55±0.88			-	3685	3699	3639	3569	3705	3795	3884	3711±102	-
Nun-Kun massif	Present	-	5571	4238	4629	4905	5000	4830	4629	4775	4910	5044	4840±156	-
	Lonp stge (TG-3)	0.53±0.13	5575	3277	-	4605	4629	4509	4469	4199	4430	4660	4500±158	370±133
Yunam valley, Zanskar	Present	-	5601	5179	5369	5409	5410	5389	5369	-	-	-	5389±20	-
	Youngest	0.62±0.15	5640	4698	-	5231	5329	5269	5159	5079	5175	5270	5216±84	147±58
Lahul Himalaya, Nn India	Present	-	5378	3649	4639	4382	4389	4319	4219	4345	4520	4694	4438±164	-
	Kulti glacial stage	11.76±0.59	5378	2756	-	3854	3869	3689	3559	3811	4075	4338	3885±256	525±104
Lahul Himalaya, Nn India	Present	-	5746	3972	4639	4960	5049	4999	4939	4691	4870	5048	4899±157	-
	Kulti glacial stage	14.03±0.16	5746	2933	-	4530	4949	4659	4499	4067	4350	4632	4527±274	410±163
Lahul Himalaya, Nn India	Present	-	6002	4187	4909	5170	5269	5169	5060	4917	5100	5282	5109±142	-
	Kulti glacial stage	14.45±0.70	6002	3971	-	4822	4929	4650	4439	4791	4995	5198	4832±245	306±212
Lahul Himalaya, Nn India	Present	-	4225	3470	3749	3776	3739	3720	3709	3774	3850	3926	3780±73	-
	Kulti glacial stage	13.95±0.88	4782	2411	-	3404	3639	3419	3099	3367	3605	3842	3482±238	303±184
Hamtah Valley, Lahul	Present	-	5011	4056	4569	4459	4509	4449	4399	4443	4540	4636	4500±78	-
	mH1a	0.26±0.13	5063	3941	-	4407	4559	4409	4319	4397	4510	4622	4460±106	30±41
	mH3	10.48±0.48	5063	3688	-	4332	4419	4319	4180	4241	4380	4518	4341±112	149±47
Sonapani glacier, Kulti Valley, Lahul Himalaya	Present	-	5465	3901	4640	4815	4929	4819	4719	4533	4690	4846	4749±127	-
	mK1	-	5478	3601	-	4727	4879	4759	4590	4403	4585	4766	4673±157	92±31
	mK2	0.51±0.16	5478	3662	-	4704	4859	4739	4569	4397	4580	4762	4659±154	106±30
	mK3	-	5498	3631	-	4662	4839	4709	4529	4387	4575	4762	4638±153	127±38
	mK4	12.18±0.99	5474	3432	-	4641	4829	4699	4500	4255	4460	4664	4578±188	186±62
	mK5	15.30±0.60	5498	3151	-	4598	4809	4659	4469	4099	4335	4570	4506±232	259±109
Tons Valley, Garhwal Himalaya, Nn. India	Present	-	5883	3848	4679	4570	4449	4320	4259	4665	4870	5074	4611±274	-
	Location G	0.66±0.34	5883	3519	-	4433	4319	4249	4119	4467	4705	4942	4462±281	139±39
	Location F	6.09±0.54	5883	3277	-	4329	4269	4140	4049	4323	4585	4846	4363±271	238±59
	Location F'	10.26±0.35	5883	3211	-	4286	4250	4109	4020	4287	4555	4822	4333±273	268±63
Tons Valley, Garhwal Himalaya, Nn. India	Present	-	5924	4014	4680	5078	5199	5109	4989	4783	4975	5166	4997±183	-
	Location E	0.26±0.08	5955	3884	-	4997	5170	5039	4889	4717	4925	5132	4981±154	61±25
	Location D	11.09±0.50	5955	3527	-	4879	5109	4969	4719	4501	4745	4988	4844±204	198±69
	Location C	14.06±0.10	5955	3352	-	4166	4189	4059	3939	4065	4370	4674	4209±245	834±228
Gangotri, Garhwal Himalaya, Nn India	Present	-	6429	4581	4900	5084	5059	4969	4899	5093	-	-	5001±90	-
	Kedar glacial stage	8.28±0.45	6429	4218	-	5053	5030	4949	4869	5003	-	-	4981±74	40±28
Gangotri, Garhwal Himalaya, Nn India	Present	-	7003	4017	4900	5151	5149	5000	4879	5215	-	-	5049±143	-
	Bhujbas glacial stage	0.21±0.02	7004	3870	-	5132	5139	4990	4859	-	-	-	5050±124	15±6
	Gangotri glacial stage	0.56±0.30	7004	3874	-	5122	5129	4989	4859	-	-	-	5036±114	20±7
	Gangotri glacial stage	2.16±0.35	7010	3792	-	5101	5119	4979	4849	-	-	-	5023±111	33±12
	Shivling glacial stage	5.22±0.27	7010	2980	-	4998	5079	4939	4789	-	-	-	4900±178	94±41
Bhillanganga and Dudhanga valleys, Sn. Garhwal Himalaya	Present	-	6068	3806	4710	4956	5069	4919	4710	4717	4945	5172	4900±175	-
	mbd4	0.13±0.11	6068	3566	-	4918	5049	4889	4659	4573	4825	5058	4853±184	74±50
	mbd3	0.15±0.10	6082	3526	-	4871	5019	4849	4609	4534	4810	5066	4822±181	104±41
	mbd2	0.16±0.15	6082	3459	-	4840	4999	4819	4569	4511	4775	5038	4793±198	134±45
Bhillanganga and Dudhanga valleys, Sn. Garhwal Himalaya	Present	-	5616	4523	5019	5092	5079	5049	5019	4969	5080	5190	5062±66	-
	mbd1	0.21±0.02	5616	3776	-	5005	5060	5029	4999	4519	4705	4890	4887±202	182±188
Kedarnath, Sn. Garhwal Himalaya	Present	-	6136	3805	4730	4985	5189	4959	4730	4745	4980	5214	4941±195	-
	mk2	0.31±0.17	6136	3597	-	4897	5089	4830	4619	4619	4875	5130	4866±201	106±17
	mk1	10.25±0.83	6136	3180	-	4466	4519	4179	4039	4368	4665	4962	4457±306	515±206

					MELM	AA	AAR (0.50)	AAR (0.60)	AAR (0.70)	THAR (0.30)	THAR (0.40)	THAR (0.50)	Mean ELA	ΔELA
Mayalil, Sn. Garhwal Himalaya	Present	-	5121	4620	4839	4893	4919	4869	4839	-	-	-	4872±35	-
	mm1	13.62±0.66	5121	4327	-	4758	4809	4759	4699	4649	4730	4810	4745±58	124±16
Nanda Devi, Garhwa, Nn Indial	Present	-	6862	3560	4879	5080	5279	4929	4639	4884	5215	5546	5056±285	-
	Moraine m4	0.60±0.28	6875	3478	-	4984	5169	4729	4549	4839	5180	5520	4996±325	86±60
	Moraine m2	13.71±0.69	6870	3432	-	4954	5119	4699	4529	4815	5160	5504	4971±356	113±66
Muguru valley, Gurla Mandhata	Present	-	6739	5621	5969	6190	6249	6159	6079	6077	6190	6302	6152±106	-
	M10	0.24±0.15	6739	5489	-	6115	6189	6089	5969	5981	6110	6238	6099±99	79±18
	M9	0.46±0.10	6753	5430	-	6062	6119	5999	5869	5962	6095	6228	6048±117	130±45
	M8	5.01±0.88	6760	5262	-	5935	5949	5829	5739	5869	6020	6170	5930±139	248±81
	M7	8.75±0.55	6760	5207	-	5904	5920	5800	5699	5767	5935	6102	5875±133	303±62
Muguru valley, Gurla Mandhata	Present	-	6108	5728	5960	5985	6019	5989	5959	-	-	-	5982±25	-
	M5	15.30±0.60	6108	5474	-	5756	5759	5659	5599	-	-	-	5693±78	295±61

Group 3(a): Wet and warm climatic region—central and eastern Himalaya					MELM	AA	AAR (0.50)	AAR (0.60)	AAR (0.70)	THAR (0.30)	THAR (0.40)	THAR (0.50)	Mean ELA	ΔELA
Lete valley, Annapurna, Nepal		6.363±1.21	-	-	-	-	-	-	-	-	-	-	-	-
Ganhaizi and Ganheba, southeastern Tibet	Present	-	5108	4502	4670	4841	4839	4819	4779	4667	4743	4820	4772±72	-
	Ganhaizi	12.97±1.41	5108	2907	-	3998	3940	3559	3219	3554	3789	4025	3726±296	1061±273
	Ganheba	11.96±1.94	5174	2955	-	3715	3429	3359	3309	3608	3861	4115	3628±292	1159±301
Annapurna Range, Nepal	Syaktan glacier (Present)	-	5311	4987	5099	5144	5139	5109	5079	-	-	-	5114±27	-
	Syaktan glacier stage	9.48±0.91	5589	3722	-	4789	4899	4709	4539	4290	4477	4665	4624±205	384±124
Annapurna Range, Nepal	Lyapche glacier (Present)	-	6583	4764	5559	5734	5729	5639	5519	5315	5497	5680	5584±142	-
	Lyapche glacier stage	11.54±0.80	6641	3549	-	5380	5559	5439	5269	4479	4789	5100	5145±387	443±265
Annapurna Range, Nepal	Yak glacier (Present)	-	5144	4870	4979	5012	5009	4989	4969	-	-	-	4992±19	-
	Yak upper	8.72±0.40	5173	4440	-	4882	4929	4869	4789	4662	4736	4810	4811±92	128±41
	Yak lower	11.66±1.29	5179	4388	-	4821	4849	4789	4699	4629	4709	4790	4755±78	205±46
Annapurna Range, Nepal	Danfe Glacier (Present)	-	5420	4621	5029	5000	4899	4849	4809	4869	4949	5030	4929±85	-
	Danfe glacier stage	8.87±0.36	5446	4009	-	4457	4319	4269	4229	4444	4589	4735	4435±181	480±119
Milarepa's Glacier, Annapurna Range, Nepal	Present	-	5386	3879	4439	4551	4399	4359	4319	4334	4487	4640	4441±112	-
	N/A	0.55±0.16	5504	3513	-	4469	4379	4329	4239	4116	4315	4515	4337±135	104±73
Dudh Khola Valley, Annapurna, Nepal	Present	-	6673	3552	4529	5295	5679	4929	4529	4495	4807	5120	4923±423	-
	Neoglacial	1.70±0.50	6673	3084	-	5196	5559	4689	4449	4166	4525	4885	4781±474	198±98
Macha Khola Valley, Gorkha Himal, Nepal	Present	-	5268	4916	5049	5079	5079	5059	5039	-	-	-	5061±18	-
	MK4: LIA	4.99±0.92	5304	3735	-	4523	4659	4379	4079	4210	4367	4525	4392±199	654±230
Mailun Khola, Ganesh Himal, Nepal	Present	-	5530	4799	5089	5144	5149	5119	5069	5021	5095	5170	5107±48	-
	M3	7.04±0.64	5562	4257	-	5024	5090	5019	4939	4652	4783	4915	4917±153	192±119
Langtang Valley, Langtang Himal, Nepal	Present	-	6319	3983	4909	4861	4769	4629	4439	4691	4925	5160	4798±218	-
	Yala I	0.76±0.20	6328	3774	-	4648	4509	4339	4229	4547	4803	5060	4591±280	191±71
	LT6	4.42±0.15	6328	3506	-	4491	4329	4189	4049	4358	4641	4925	4426±292	356±77
Langtang Valley, Langtang Himal, Nepal	Present	-	6514	4392	5239	5369	5429	5309	5149	5035	5247	5460	5280±143	-
	Langtang Stage (LT3)	10.90±0.43	6525	3915	-	5169	5259	5069	4869	4702	4963	5225	5037±204	249±55
Langtang Valley, Langtang Himal, Nepal	Present	-	6563	4369	5139	5195	5069	5020	4949	5029	5249	5470	5140±166	-
	Langtang glacial stage II	4.60±0.33	6563	3344	-	4747	4869	4619	4449	4315	4637	4960	4657±226	484±163
	Langtang glacial stage I	5.47±0.40	6563	3079	-	4374	4499	4049	3419	4126	4475	4825	4252±448	888±315
Nyalam County, Sn Xixabangma, Sn Tibet	Fu Qu glacier (Present)	-	5566	4446	4929	4845	4709	4620	4579	4788	4901	5015	4798±153	-
	Puluo 1 moraine	!	5552	4013	-	4509	4439	4379	4329	4481	4635	4790	4509±158	271±39

Group 2(b): Transitional climatic region—central and eastern Himalaya					MELM	AA	AAR (0.50)	AAR (0.60)	AAR (0.70)	THAR (0.30)	THAR (0.40)	THAR (0.50)	Mean ELA	ΔELA
Rongbuk valley, N. Mt. Everest	Present	-	6847	5203	5609	5881	5859	5799	5719	5704	5869	6035	5809±132	-
	T7	0.33±0.19	6847	5162	-	5844	5839	5769	5669	5676	5845	6015	5808±119	30±11
	T6	2.08±0.09	6847	5128	-	5840	5839	5759	5659	5648	5821	5995	5794±120	44±13
	T5c	3.18±0.23	6847	5098	-	5832	5830	5759	5650	5627	5803	5980	5783±120	55±17
Khumbu Himal, Nepal	Present	-	7680	4855	5249	5521	5339	5280	5229	5708	5991	6275	5574±388	-
	Chhukung glacial stage	11.52±0.11	7699	4392	-	5477	5329	5259	5209	5392	5723	6055	5492±300	128±134
Khumbu Himal, Nepal	Present	-	5837	4760	5039	5025	4989	4959	4899	5087	5196	5305	5062±132	-
	Chhukung glacial stage	10.97±0.03	5870	4675	-	5004	4969	4929	4879	5039	5159	5280	5037±139	29±10
Khumbu Himal, Nepal	Present	-	6749	4926	5209	5381	5249	5179	5119	5478	5661	5845	5390±256	-
	Thuklha glacial stage	4.43±0.32	6800	4867	-	5361	5210	5140	5070	5451	5645	5840	5388±280	28±15
Hailuogou Valley, Gonga Shan, SE Tibet	Present	-	7331	2963	5080	5188	5219	5119	5039	4280	4714	5155	4974±321	-
	Little Ice Age moraines	0.46±0.06	7354	2911	-	5103	5190	5099	4999	4251	4695	5140	4925±339	34±24
	Neoglacial moraines	1.04±0.10	7354	2799	-	4931	5130	5040	4849	4167	4623	5080	4831±339	128±69
	Recessional moraine	6.03±1.97	7354	2482	-	4750	5099	4969	4149	3950	4437	4925	4611±440	348±262

Group 1(b): Arid and semiarid colder climatic region—southern and northeastern Tibet					MELM	AA	AAR (0.60)	AAR (0.70)	AAR (0.80)	THAR (0.30)	THAR (0.40)	THAR (0.50)	Mean ELA	ΔELA
	Local LGM moraines	10.10±0.73	7354	1697	-	4071	3769	3309	2969	3397	3963	4530	3715±529	1244±550
Dalijia Shan, NE Tibet	Group D moraines	13.45±0.25	4460	3725	4029	4079	4029	3949	3879	3951	4025	4100	4005±74	-
Xiying He valley, Qilian Shan, NE Tibet	Present	-	4729	4152	4379	4471	4439	4399	4349	-	-	-	4407±48	-
	N/A	13.16±1.05	4729	3397	-	3836	3689	3629	3579	3801	3935	4070	3791±174	731±65
NW Menyuan, Qilian Shan, NE Tibet	Gangshiga glacier (Present)	-	4812	4465	4579	4620	4599	4559	4519	-	-	-	4575±39	-
	Holocene moraine	10.08±0.53	4832	4320	-	4506	4459	4409	4379	-	-	-	4438±56	136±15
Anyemaqen Mountains	Halong glacial I (Present)	-	6183	4443	4939	5140	5339	4959	4729	4971	5145	5320	5068±207	-
	Halong glacial stage	9.48±1.70	6183	4428	-	4675	5109	4780	4639	4957	5133	5310	4943±255	143±167
Anyemaqen Mountains	Halong glacial II (Present)	-	6005	4549	4884	5347	5069	4989	4879	4987	5133	5280	5071±173	-
	Halong glacial stage	13.89±1.26	6006	3940	-	5268	4419	4309	4199	4564	4772	4980	4644±384	453±229
Kunlun Shan (northern slopes)	Present	-	5935	4593	5119	5861	5329	5239	5119	5001	5135	5270	5259±264	-
	M2 moraines	8.04±0.74	5960	4405	-	5693	5129	4999	4849	4877	5033	5190	5110±285	169±71
Karola Pass, Mt. Kaluxung, Sn Tibet	Present	-	6604	4860	5549	5861	5909	5789	5639	5385	5560	5735	5678±177	-
	Youngest	3.28±0.74			-	5754	5809	5629	5469	5369	5549	5730	5616±161	81±71
	Oldest	11.47±0.70	6623	4806	-	5200	5749	5529	5389	5355	5537	5720	5497±198	200±229

- No data
m asl Meter above sea level
Note: The present here refers to the year 2016 AD

S7. Modern glacier hypsometry in all the studied valleys. Each glaciated area is named after the [10]Be dated sample referred in Table S4.
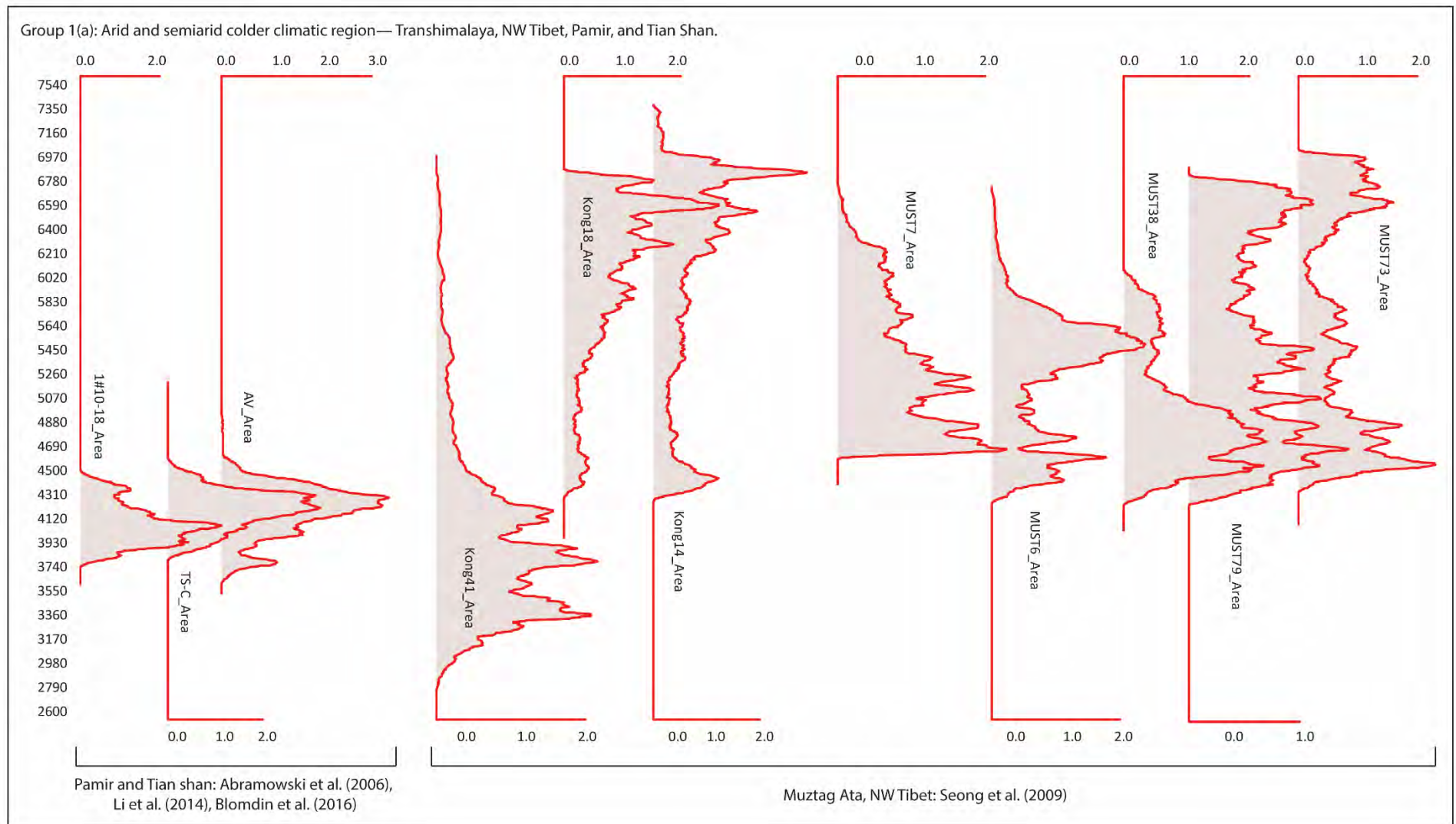
Group 1(a): Arid and semiarid colder climatic region— Transhimalaya, NW Tibet, Pamir, and Tian Shan.

Pamir: Röhringer et al. (2012) Northern Karakoram: Owen et al., (2002) Central Karakoram: Seong et al. (2007)
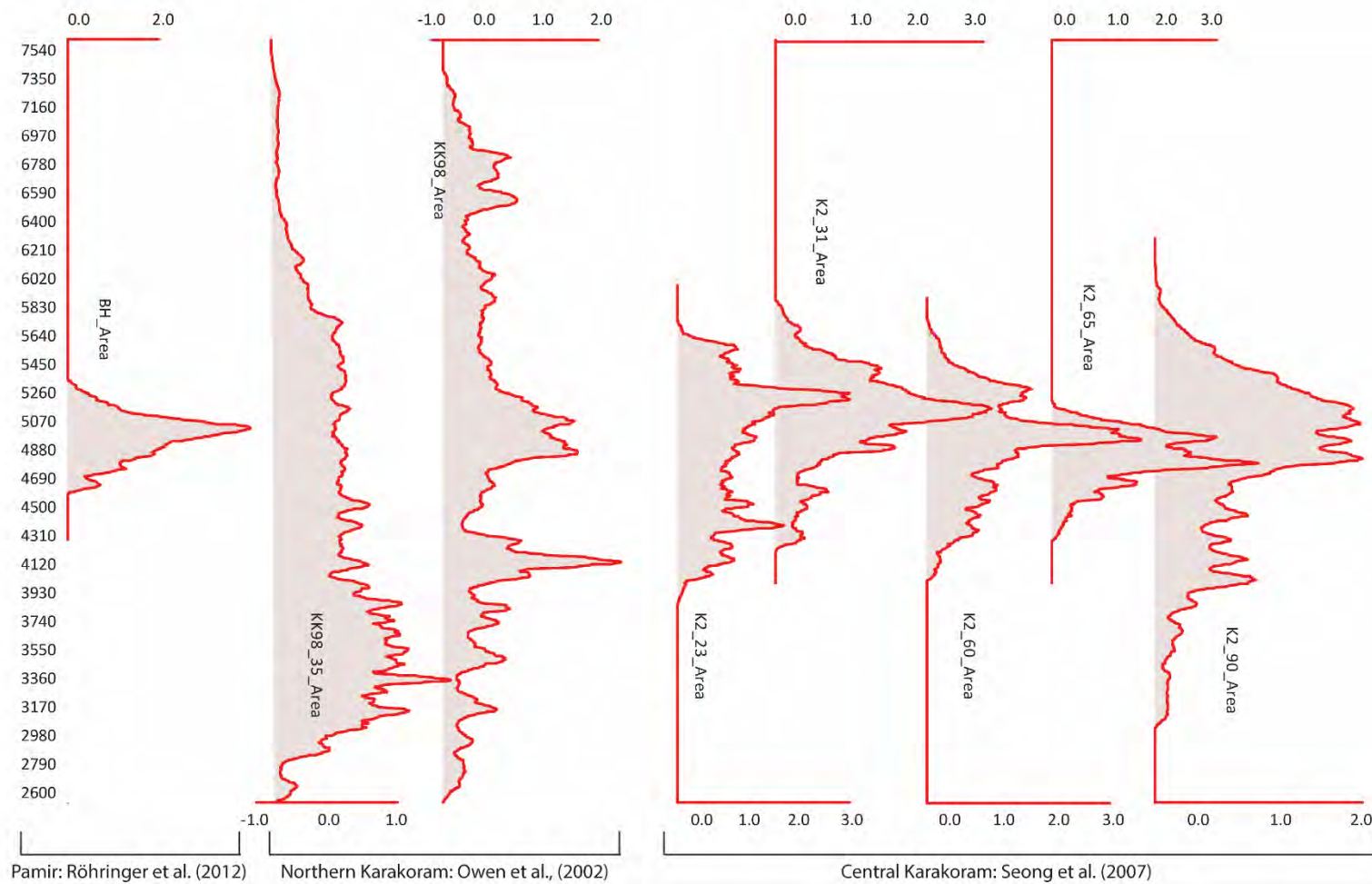
Group 1(a): Arid and semiarid colder climatic region— Transhimalaya, NW Tibet, Pamir, and Tian Shan.
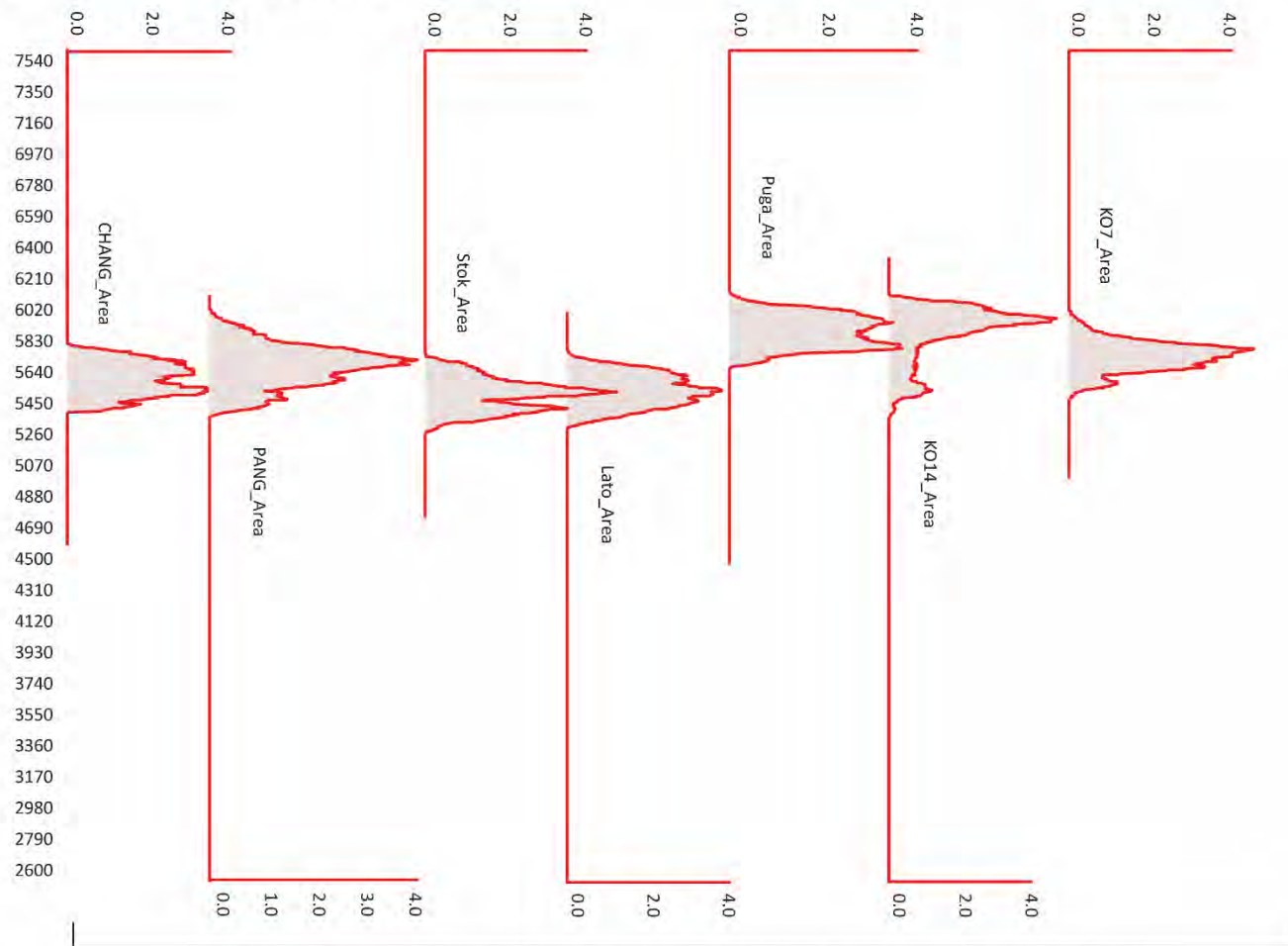
Ladakh and Zanskar Range: Hedrick et al. (2011); Dortch et al. (2013), Orr et al. (2017, 2018), Saha et al. (2018)

Group 1(b): Arid and semiarid colder climatic region—northeastern Tibet
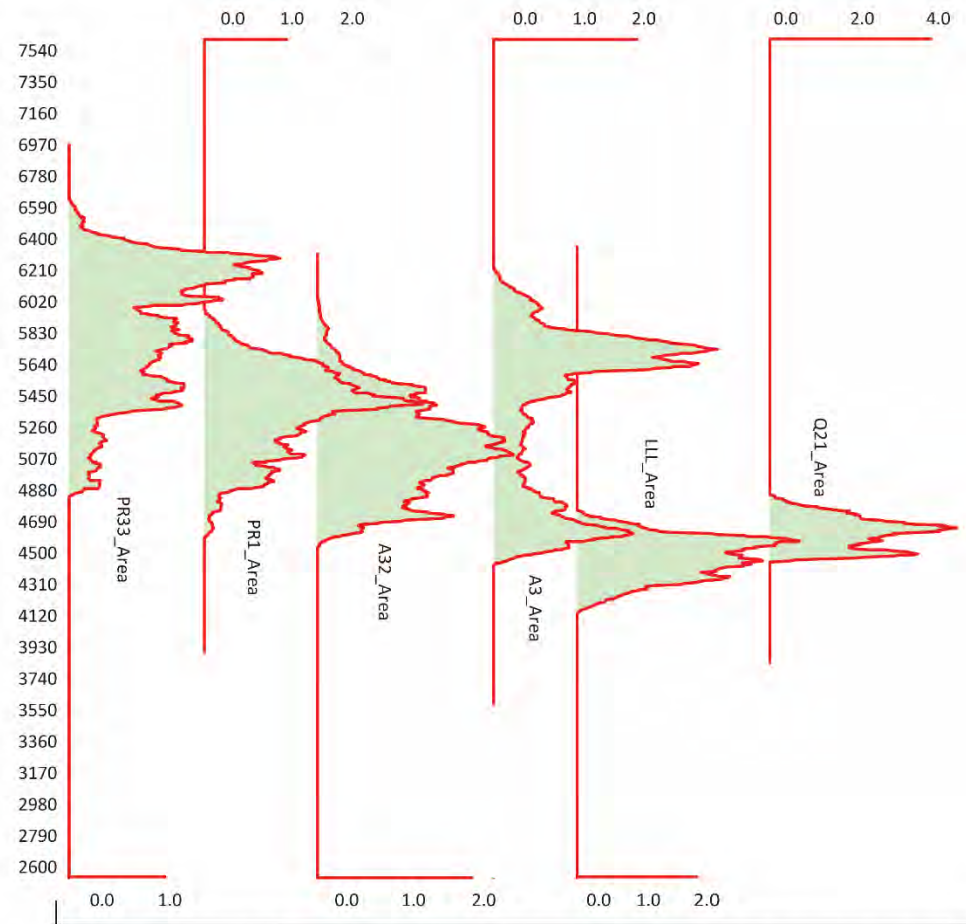
NE Tibet: Laserre et al. (2002), Owen et al. (2003a), Owen et al. (2003c), Owen et al. (2005), Owen et al. (2006b)

Group 2(a): Transitional climatic region—western Himalaya
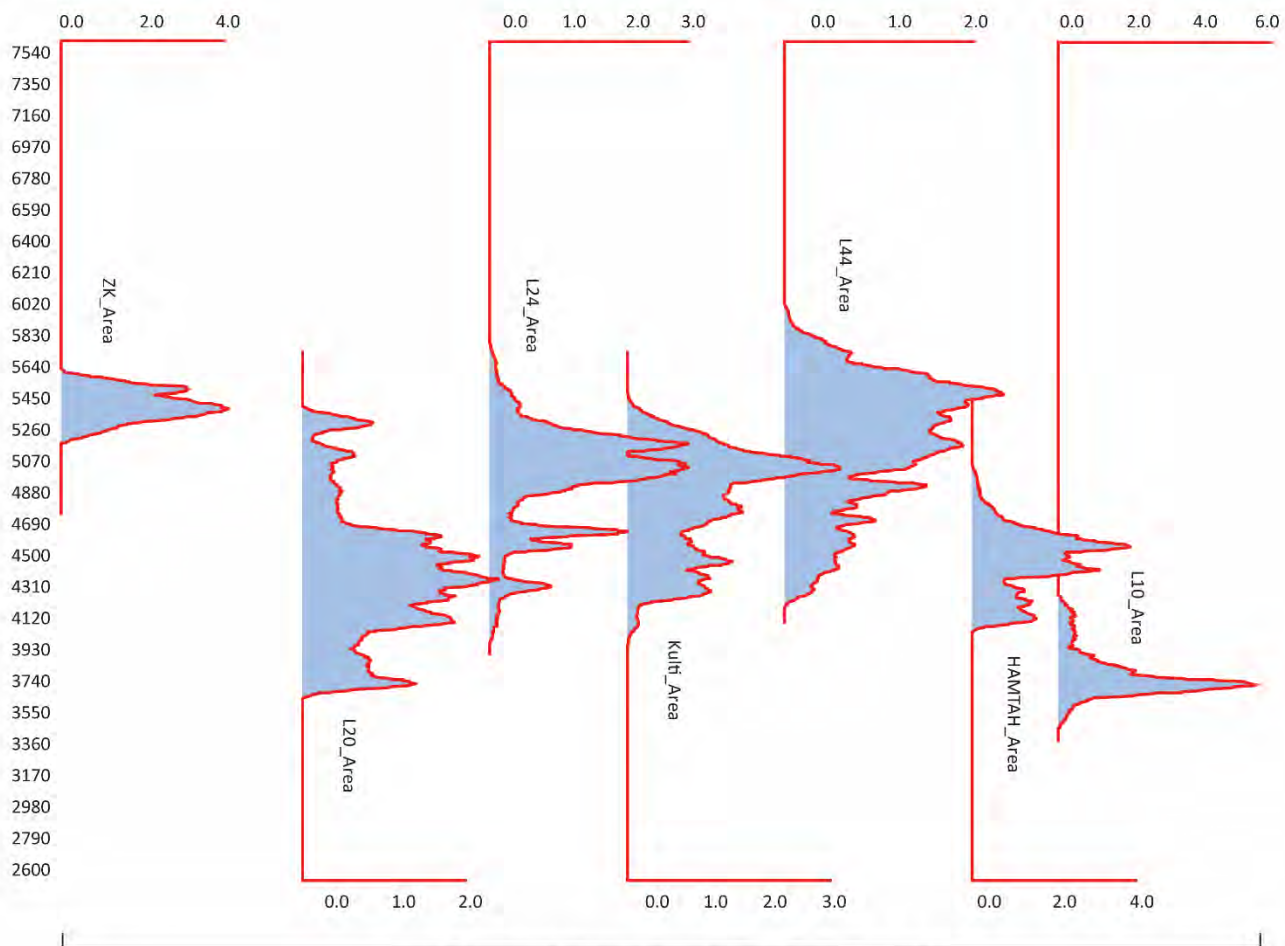
Lahul: Owen et al. (2001), Saha et al. (2015, 2018), This study

264

Group 2(a): Transitional climatic region—western Himalaya
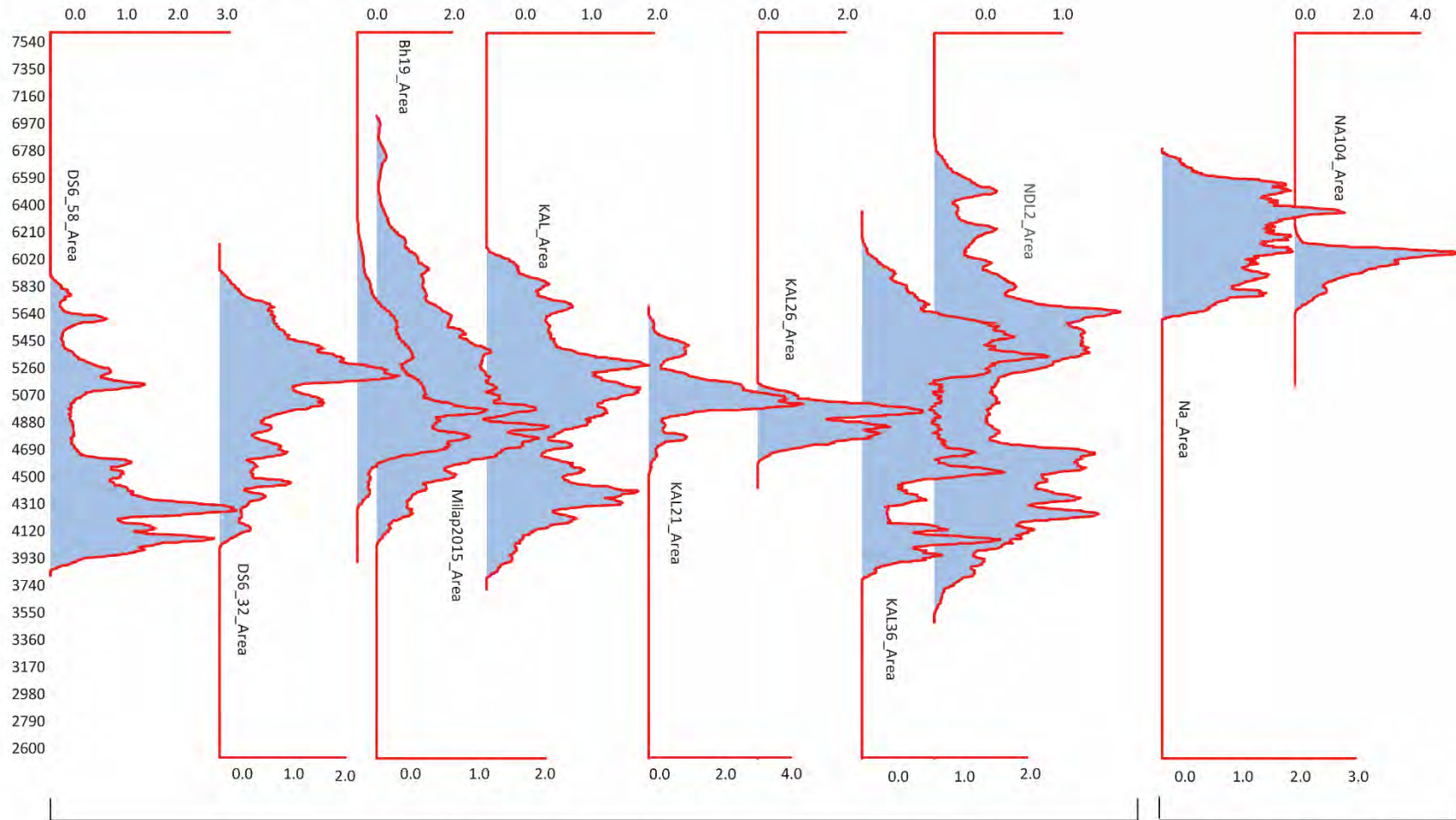
Garhwal Himalaya: Barnard et al. (2004a, b), Scherler et al. (2010), Srivastava (2012), Murari et al. (2014)

Gurla Mandhata: Owen et al. (2010)

265

Group 2(b): Transitional climatic region—central Himalaya
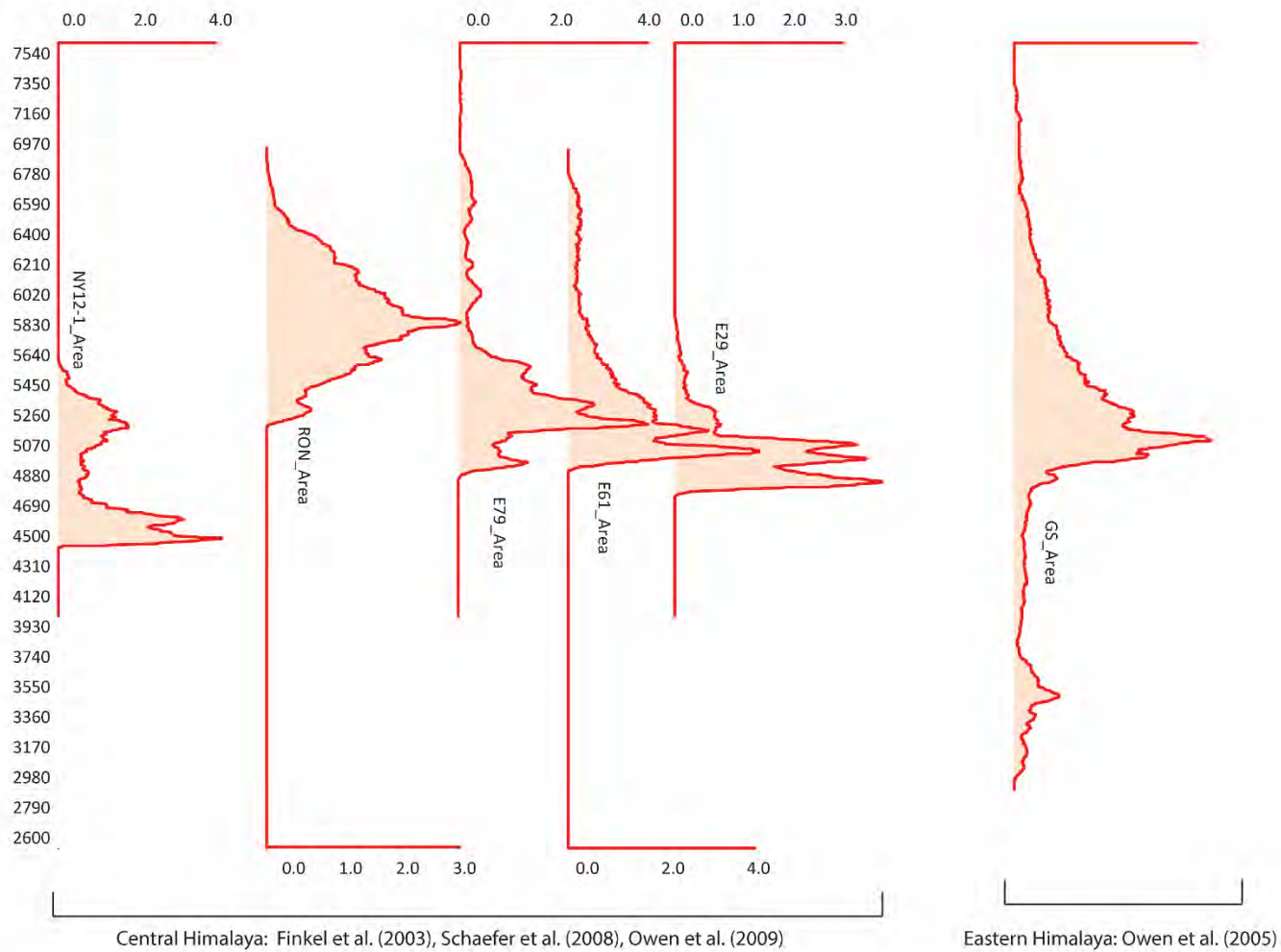
Central Himalaya: Finkel et al. (2003), Schaefer et al. (2008), Owen et al. (2009)

Eastern Himalaya: Owen et al. (2005)

266

Group 3(a): Wet and warm climatic region—central and eastern Himalaya
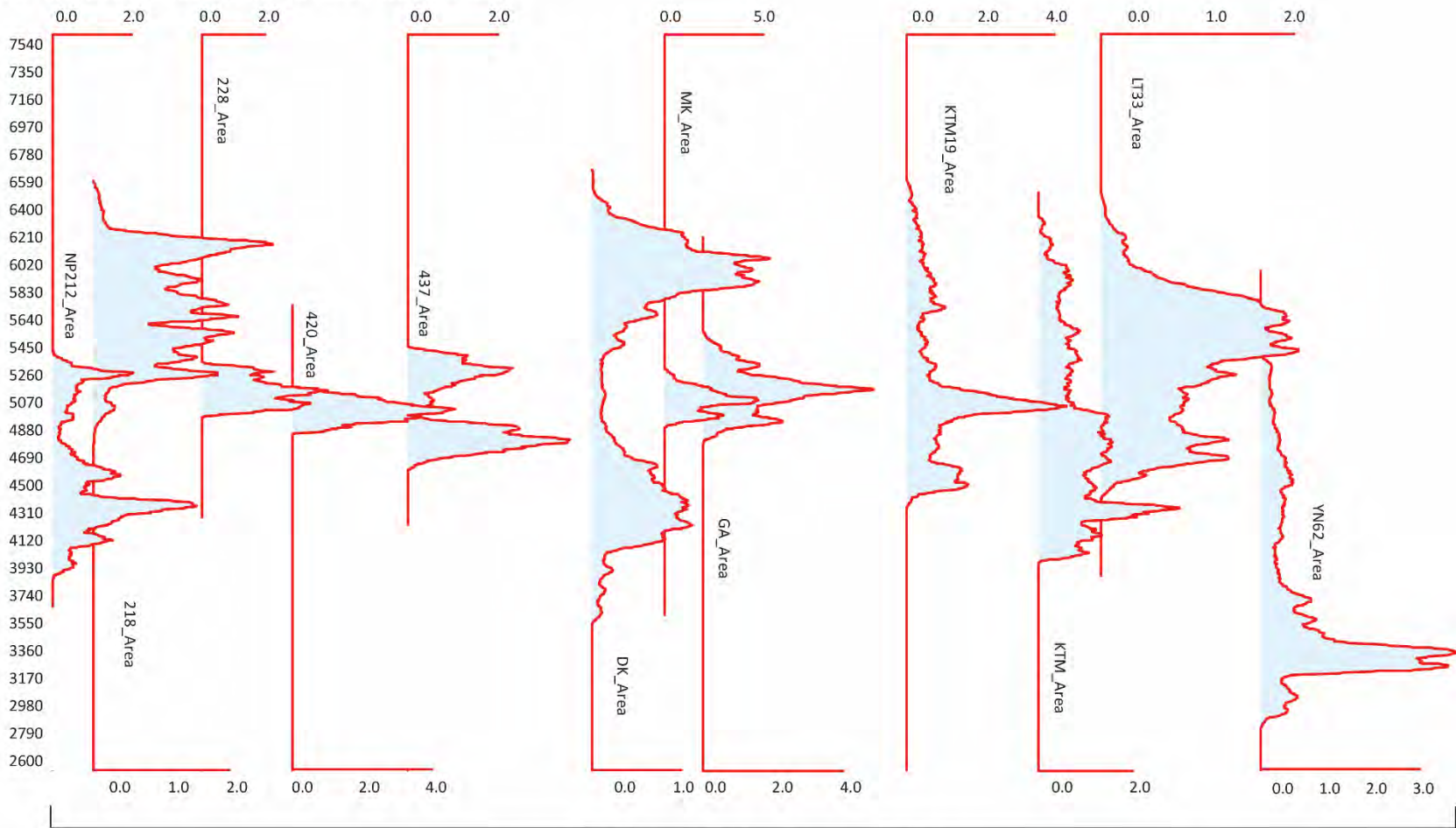
Central & eastern Himalaya: Abramowski (2004),
Pratt-Sitaula (2005), Barnard et al. (2006), Gayer et al. (2006), Heimsath and McGlynn (2008), Kong et al. (2009b), Zech et al. (2009), Pratt-Sitaula (2011)

267

S8. Climate Zonation

Both CRU CL 2.0 (10' latitude/longitude) reanalysis temperature (T in °C) data and TRMM derived precipitation (P in mm) data (4-km-horizontal x 250-m-vertical) are first rescaled to 18 x 18 km grid cell for each month; averaged over the period of 30 and 12 years, respectively. Approximately 42,511 glacier polygons (samples), derived from the Randolph Glacier Inventory (RGI 6.0), are then converted into points using the *Feature to Point* tool in ArcGIS. Subsequently, climate data are extracted for each point (glacier/sample) from the gridded datasets using the *Extract Multi Values to Points* tool. Nine climate parameters are derived from the primary data for each glacier (sample). These are,

1. Annual mean temperature ($T(x) = \sum_{x=1}^{12} \frac{T(x)}{12}$)   (3)
2. Annual temperature range ($T(x) = T(x)\ max. - T(x)\ min.$)   (4)
3. Annual total precipitation ($P^a(x) = \sum_{x=1}^{12} P(x)$)   (5)
4. Annual precipitation range ($P^r(x) = P(x)\ max. - P(x)\ min.$)   (6)
5. Total summer (monsoon) precipitation ($P^s(x) = \sum_{x=1}^{4} P(x)$) for *JJAS*   (7)
6. Total winter (westerlies) precipitation ($P^w(x) = \sum_{x=1}^{4} P(x)$) for *DJFM*   (8)
7. Seasonality Concentration Index ($SCI = \dfrac{\sqrt{\frac{1}{12-1}\sum_{x=1}^{12}(P(x)-\acute{P})^2}}{\acute{P}}$)   (9)

    where $\acute{P}$ is mean annual precipitation (Fujita, 2008)
8. Relative Entropy ($RE = \sum_{m=1}^{12} Pm(x)\ log_2\ (12\ Pm\ (x))$)   (10)

    where *m* is a month and $Pm(x) = \frac{P(x)}{\acute{P}}$ (Pascale et al., 2014) and
9. Dimensionless Seasonality Index ($DSI = RE\frac{\acute{P}}{\mathcal{R}}$)   (11)

    Where $\mathcal{R}$ is a constant scaling factor introduced to make precipitation dimensionless. We choose $\mathcal{R}$ as the maximum of ($\sum_{x=1}^{12} P(x)$) among all samples (glaciers) and equal to 9,659 mm.

SCI indicates relative precipitation variability in each month compared to mean annual (Fujita, 2008). *RE* is likely associated with the number of 'wet' months and reaches its maximum value of $log_2\ 12$ when annual precipitation is concentrated in one single month (Pascale et al., 2014). According to definition (11), *DSI* is zero when either $\acute{P}$ (completely dry location) or *RE* (P distributed uniformly throughout the year) are zero and maximum ($log_2\ 12$) when $\mathcal{R}$ is concentrated in a single month (ibid). Due to the nature, units, and dissimilar ranges of the climate parameters, all data (except *DSI*) are scaled to lie between 0 and 1, using the maximum value in the sample population for respective parameters (e.g., $T(x)/T(x)\ max.$).

We, after that, have performed Cluster Analysis (CA) which is often preferred to classify samples (glaciers) based on the degree of similarity among them concerning a defined set of parameters (Sagredo and Lowell, 2012; Zuming and Maohuan, 1989). Euclidean (linear) distances between any pair of glaciers in a multidimensional (in our case no. of dimensions are nine) Cartesian space are calculated in R (The R Core Team, 2018). Using the Unweighted Pair-Group Method with Arithmetic Averaging (UPGMA), finally, a cluster dendrogram is produced by groping the most similar (i.e., least linear distances) sets of glaciers together.

Principal Component Analysis (PCA) is also performed to correlate climate parameters and represent them as a smaller set of uncorrelated (orthogonal) variables called principal components (PCs; Sagredo and Lowell, 2012). PCs geometrically capture the directions of maximum variation in the data (Seaby and Henderson, 2014) and therefore, are used to compare and refine our CA generated groups.

Furthermore, the significance of our clusters is tested using the Pearson's product-moment correlation between the sample Euclidean and cophenetic distances. Higher positive correlation is expected for our CA groupings to be validated (ibid). We have also performed Analysis of Similarities (ANOSIM) between sample Euclidean distances and CA defined groups (with 600 permutations) to calculate *R*. Where the value of *R* (constrained between –1 to 1) is more positive, the samples within groups are more similar than would be expected by random chance (ibid). These statistical analyses are performed at the Ohio Supercomputer Center (OSC; Ohio Supercomputer Center. 1987; https://www.osc.edu/) due to its volume.

S9. Sampled glaciers (RGI 6.0) used for climatic zonation.
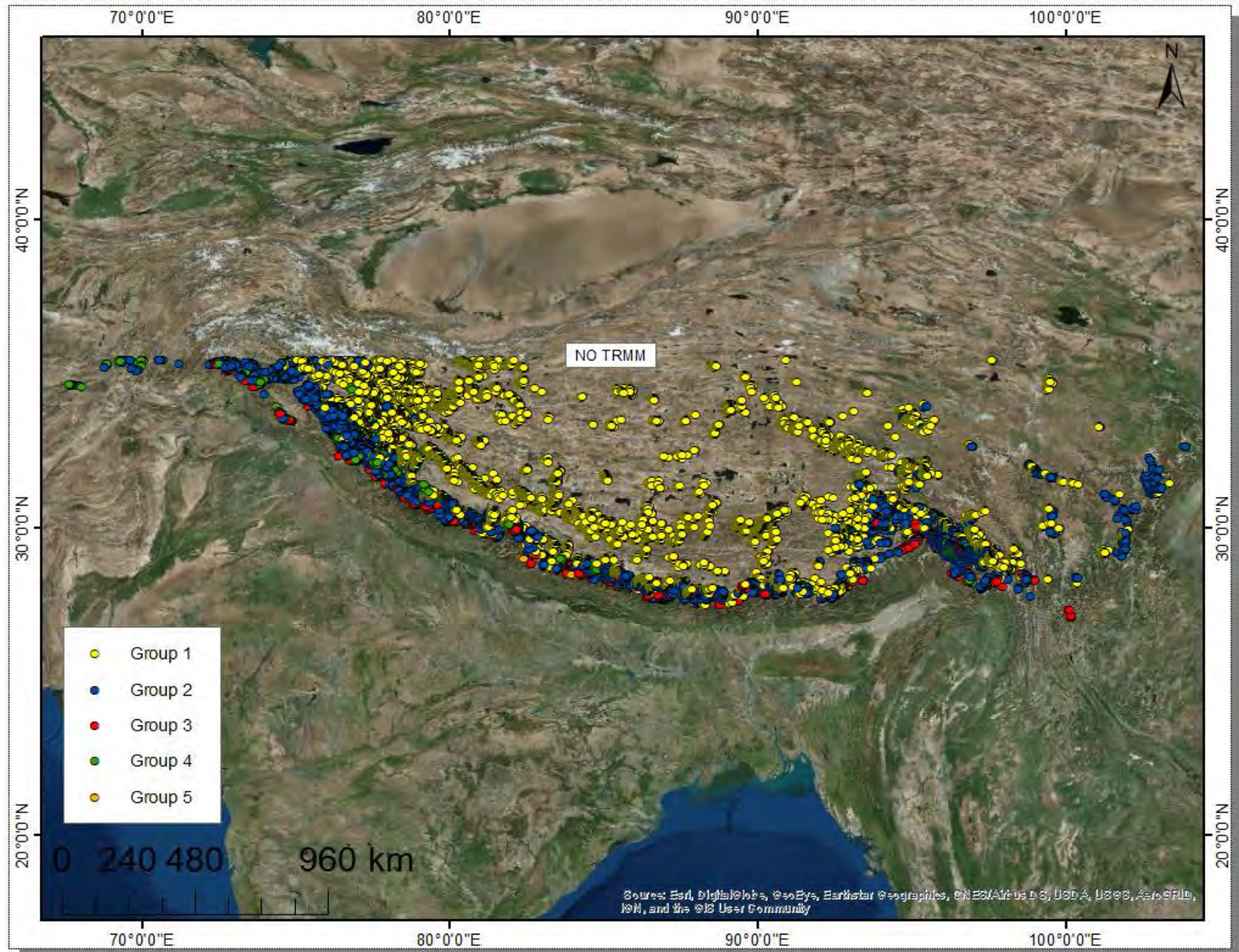
S10. Linear inverse flow model

Climate sensitivity (c) is calculated as $c = 2.3P^{0.6}s^{-1}$ (12)

and response time (τ) as $\tau = 13.6\beta^{-1}s^{-1}(1 + 20s)^{-1/2}L'^{1/2}$ (13)

Here, P is the annual climatological precipitation in m a^{-1}, s is the mean surface slope of the glacier in percent, L' is the present glacier length in m calculated along the medial flow line of the glacier, and β is the altitudinal mass-balance gradient, which is defined as $\beta = 0.006P^{1/2}$ (after Oerlemans, 2001, 2005). It is to be noted that these formulas and constants are obtained by calibrating a simple model of glacier dynamics against globally distributed glacier records (see Oerlemans et al., 1998; Oerlemans, 2001; Klok and Oerlemans, 2003). We are unable to calibrate the constants for our study areas due to lack of detailed (proxy or instrumental) long-term glacier length change and climatological data in the higher reaches. However, we argue that the (globally calibrated) inverse linear flow model is a simple first-order representation of the glacier length change with a corresponding change in temperature (T) given the climate sensitivity and the response time (i.e., the lag time) of the glacier. Since, we have averaged our reconstructed T regionally and have also provided ±30% change in P, given the large uncertainty in P during the Holocene in the orogen, we argue that the changing pattern of reconstructed T is useful for our understanding, if not exact. We have derived s and P for each glacier from the ASTER GDEM and the TRMM gridded cells, respectively. Also, we have calculated L for each glacier advance using preserved moraines that likely represent a steady-state scenario and hence, useful for our purpose.

S11. Preserved moraines in the Kulti valley, Lahul Himal, and Parkachik valley, Nun Kun massif.

Kulti valley

M_{K5}

M_{K5}

Glaciofluvial outwash terrace

I

J

Parkachik glacier

M_{P1}

M_{P2a}

M_{P2a}

M_{P2b}

M_{P2c}

Bedrock core

K

M_{P1b}

M_{P1a}

L

Bedrock core

M_{P2b}

M_{P2a}

M

272
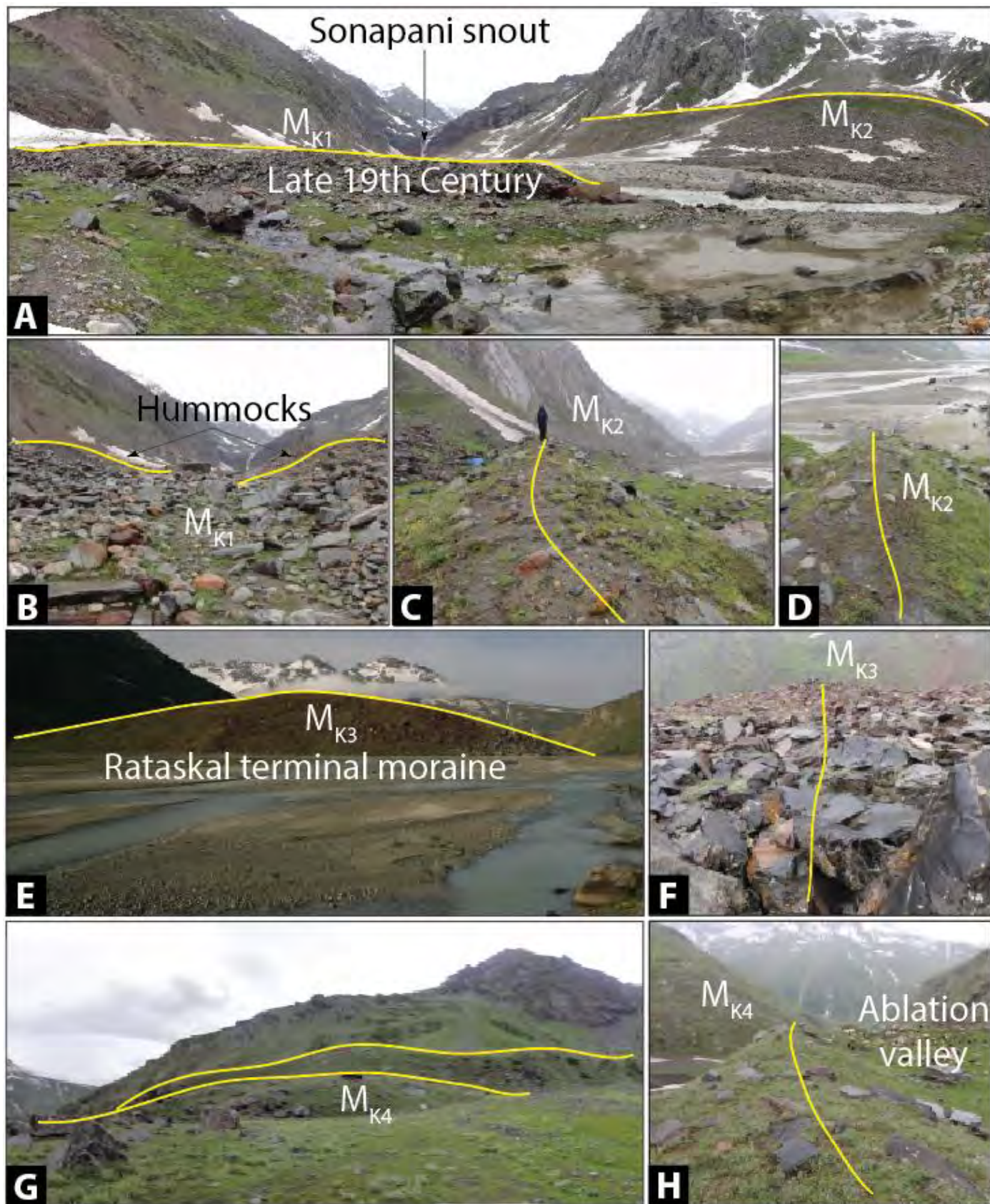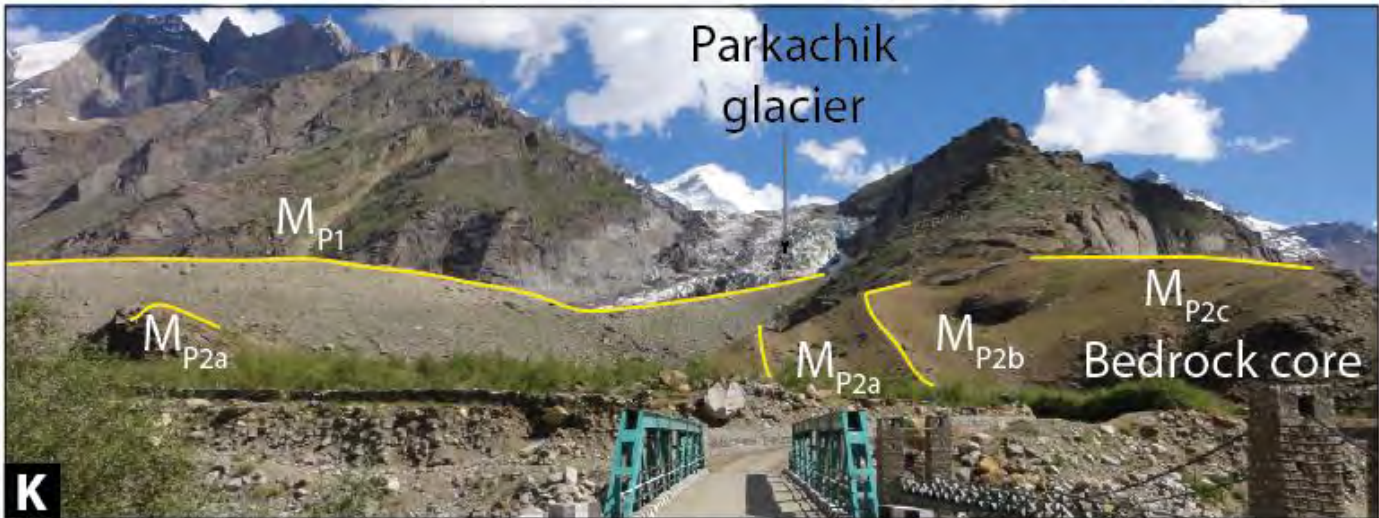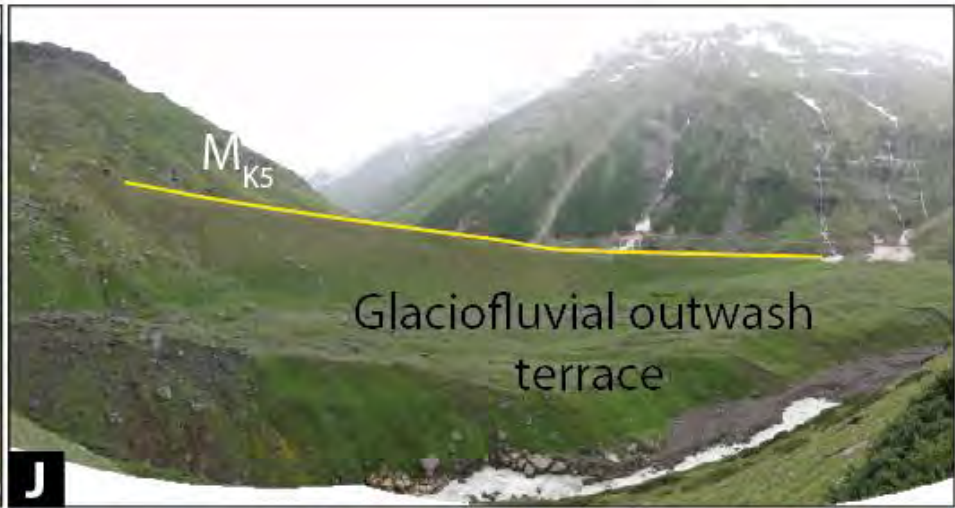
S12. Regional glacial stages using a radial plotter.
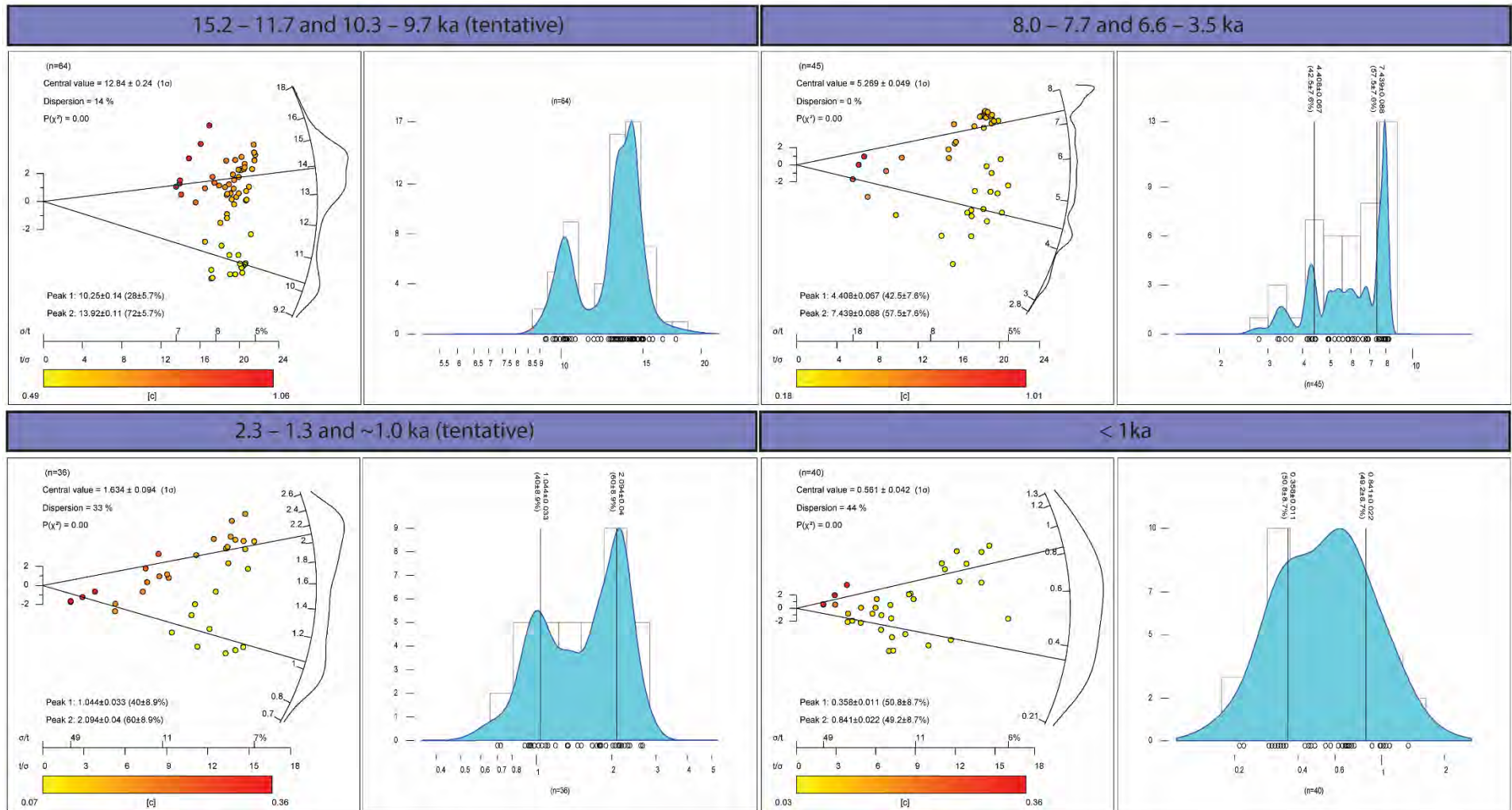
Group 2(a). Transitional western Himalaya

15.3 – 11.8 and 11.1 – 10.3 ka
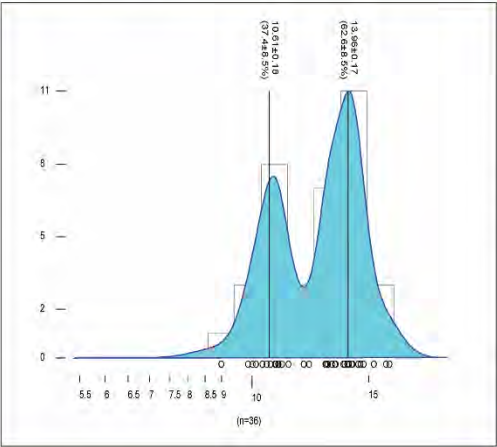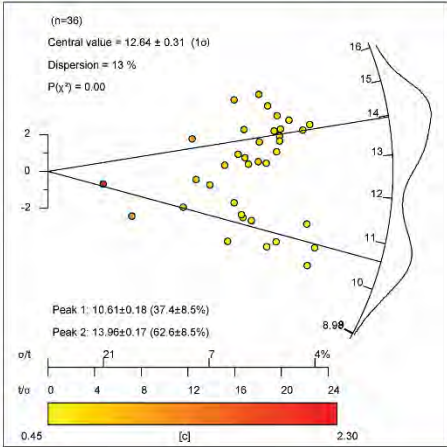
8.8 – 8.3 (tentative) and 6.1 – 5.0 ka
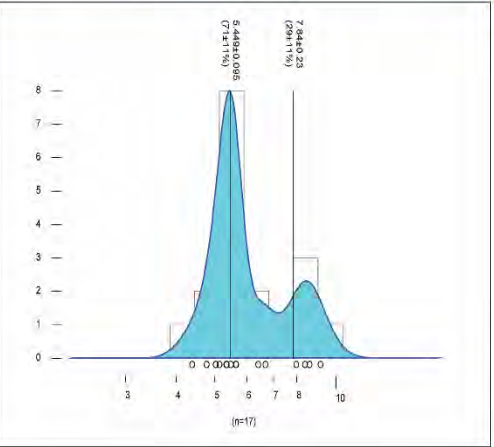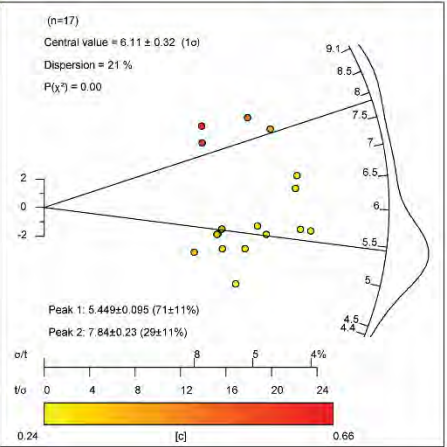
~2.2 and < 1 ka
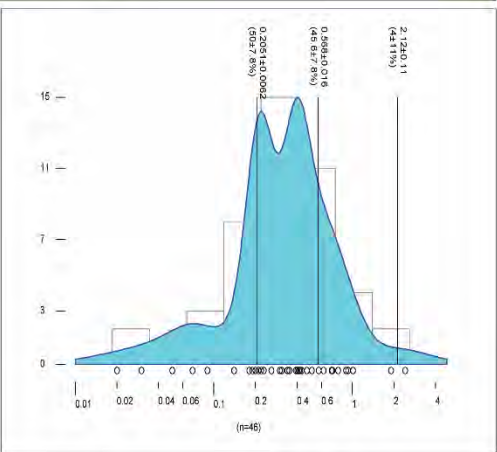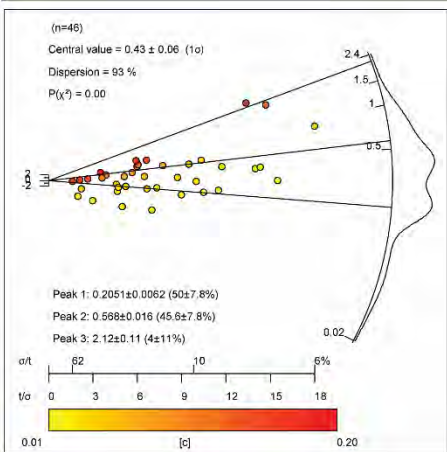
Group 3(a). Wet and warm central and eastern Himalaya

13.0 – 10.9 and 9.5 – 8.7 ka
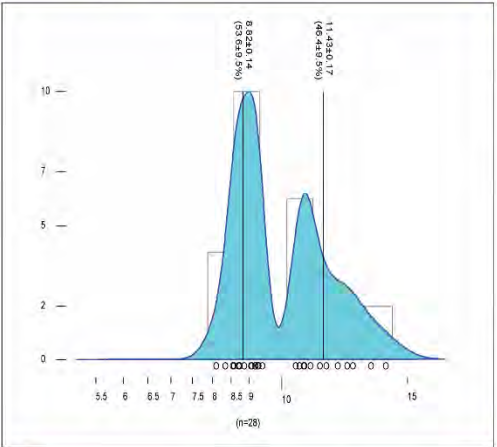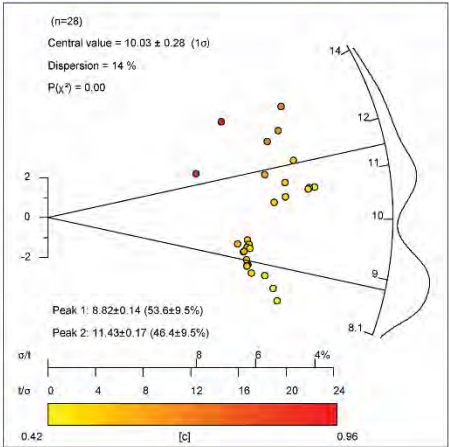
7.0 – 4.4, ~1.7 (tentative) and < 1 ka (tentative)
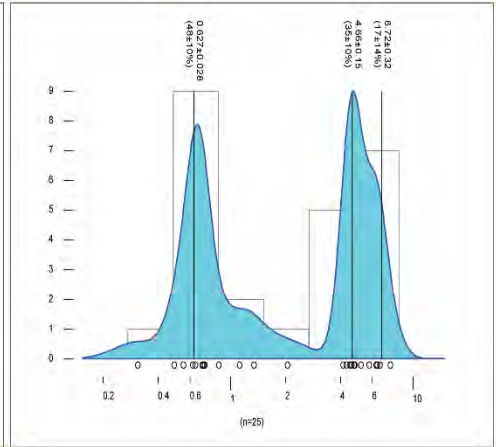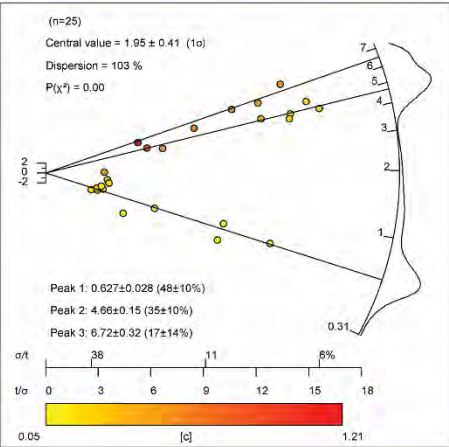
Group 2(b). Transitional central and eastern Himalaya

11.5 – 10.1 and 6.0 – 3.2 ka
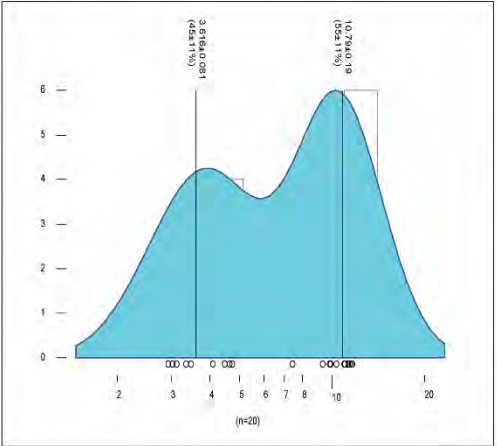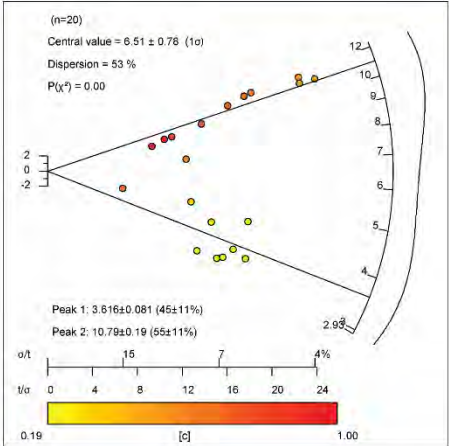
6.0 – 3.2, ~2.1 – 1.0 (tentative), and < 1 ka

275
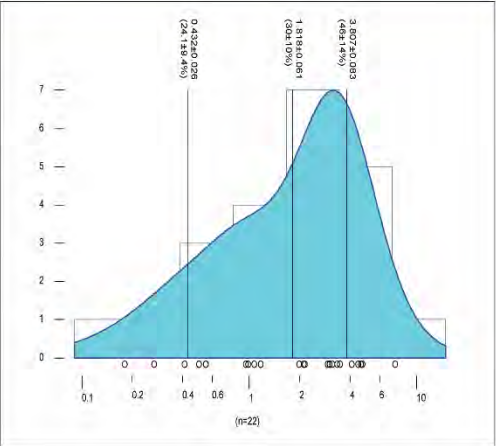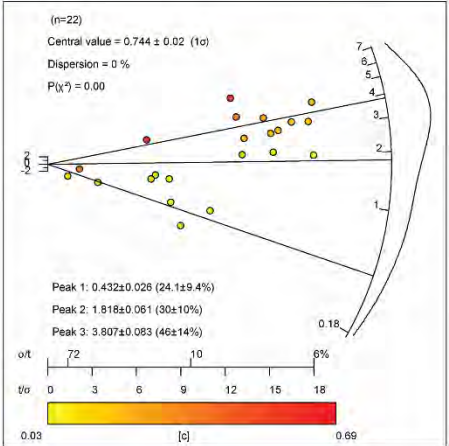
Group 1(b). Arid and semiarid southern and northeastern Tibet
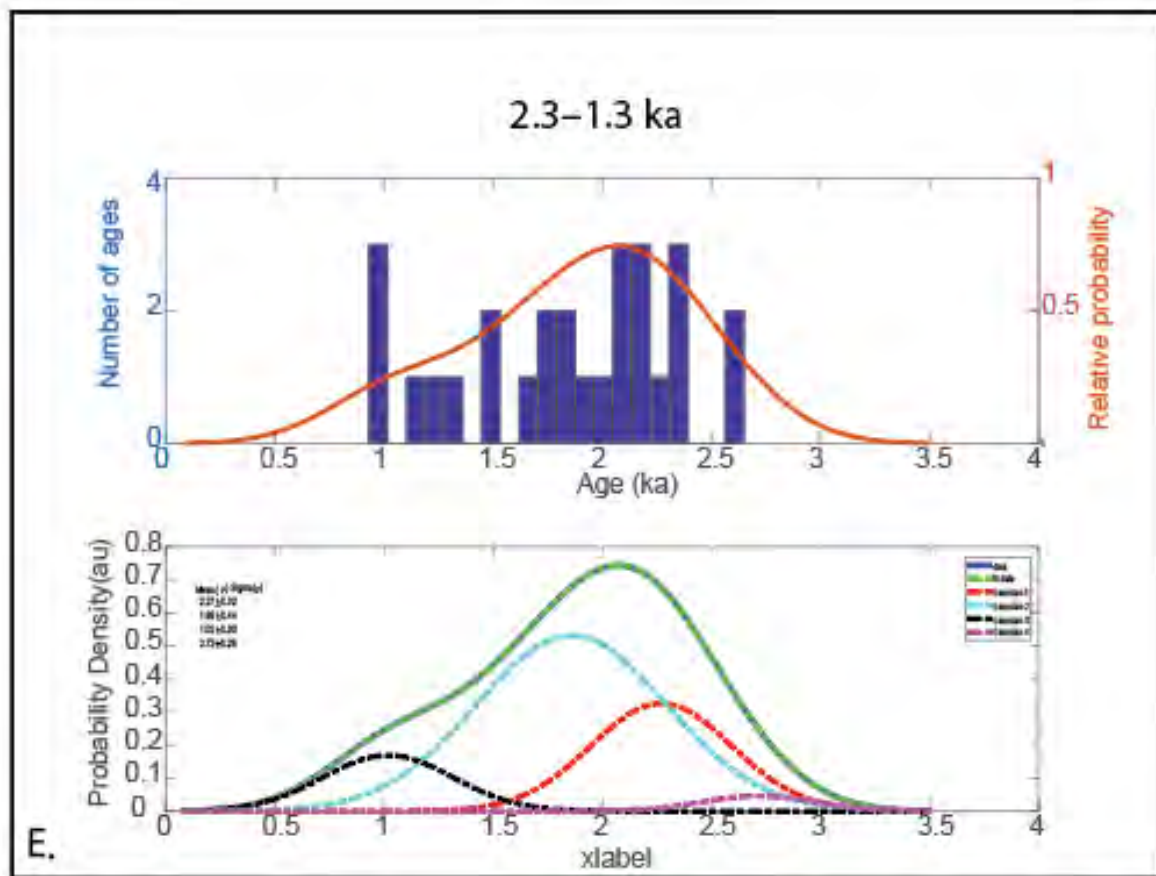
13.5 – 12.9 and 11.5 – 9.7 ka
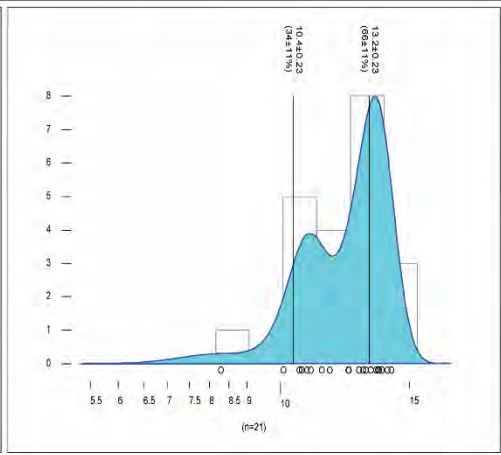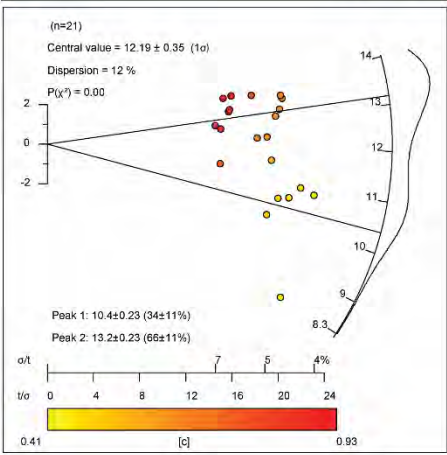
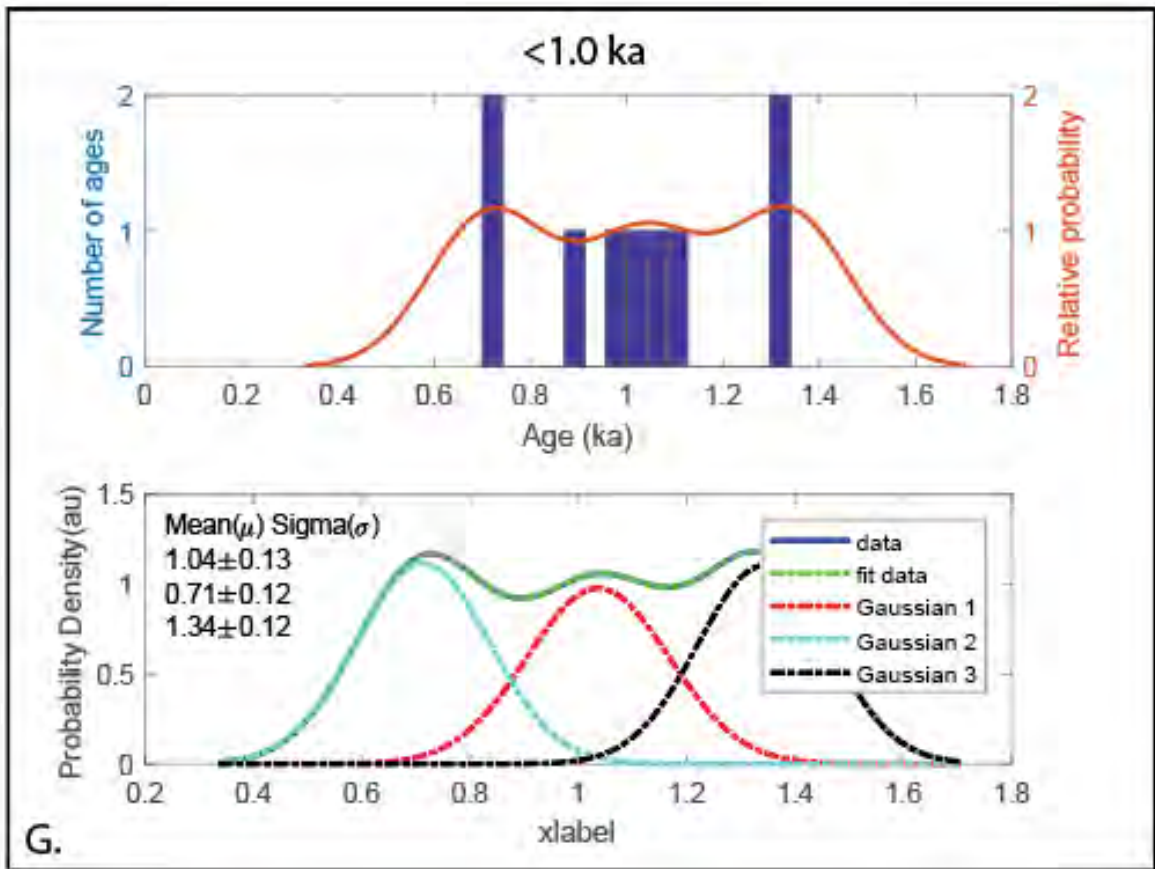~8.0 (tentative) and ~3.3 ka (tentative)
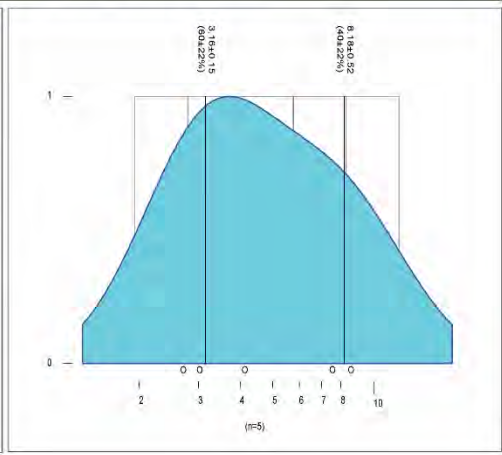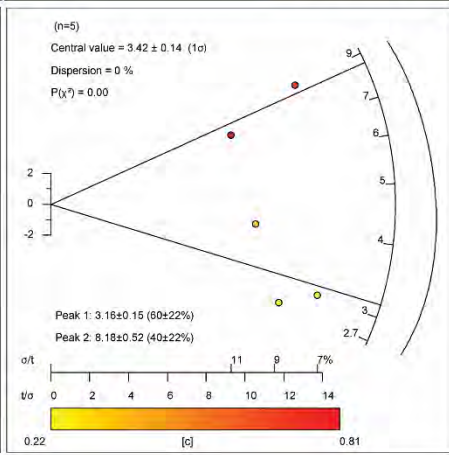
S13. Regional glacial stages using probability density function.

Arid and semiarid Transhimalaya, NW Tibet, Pamir, and Tian Shan
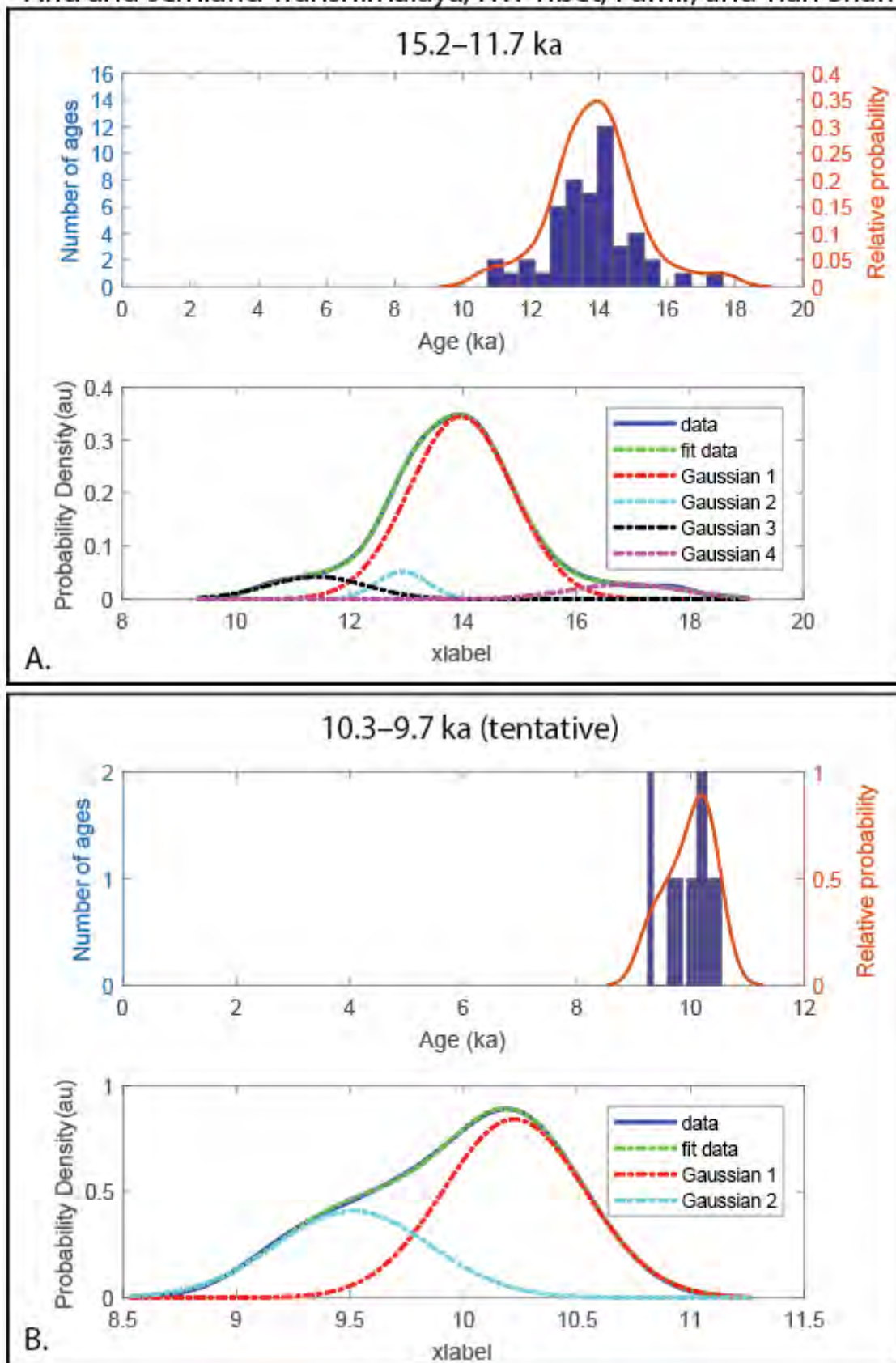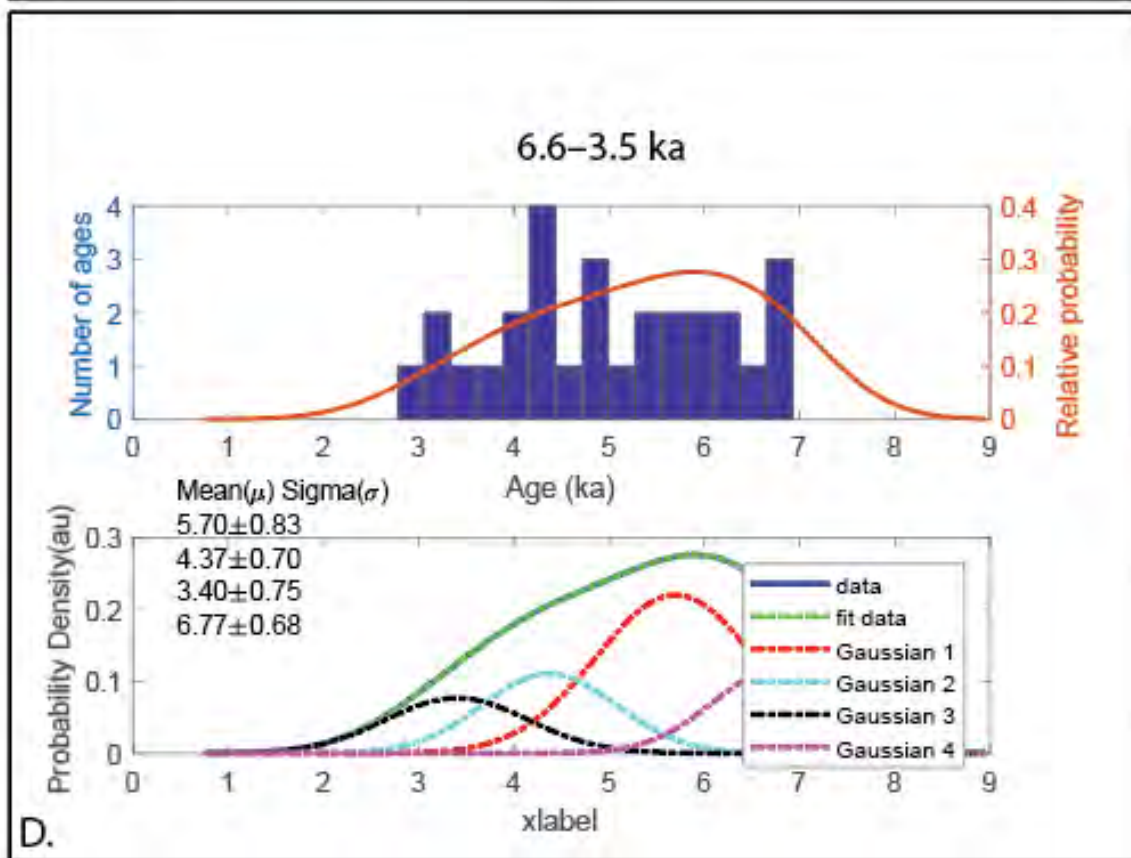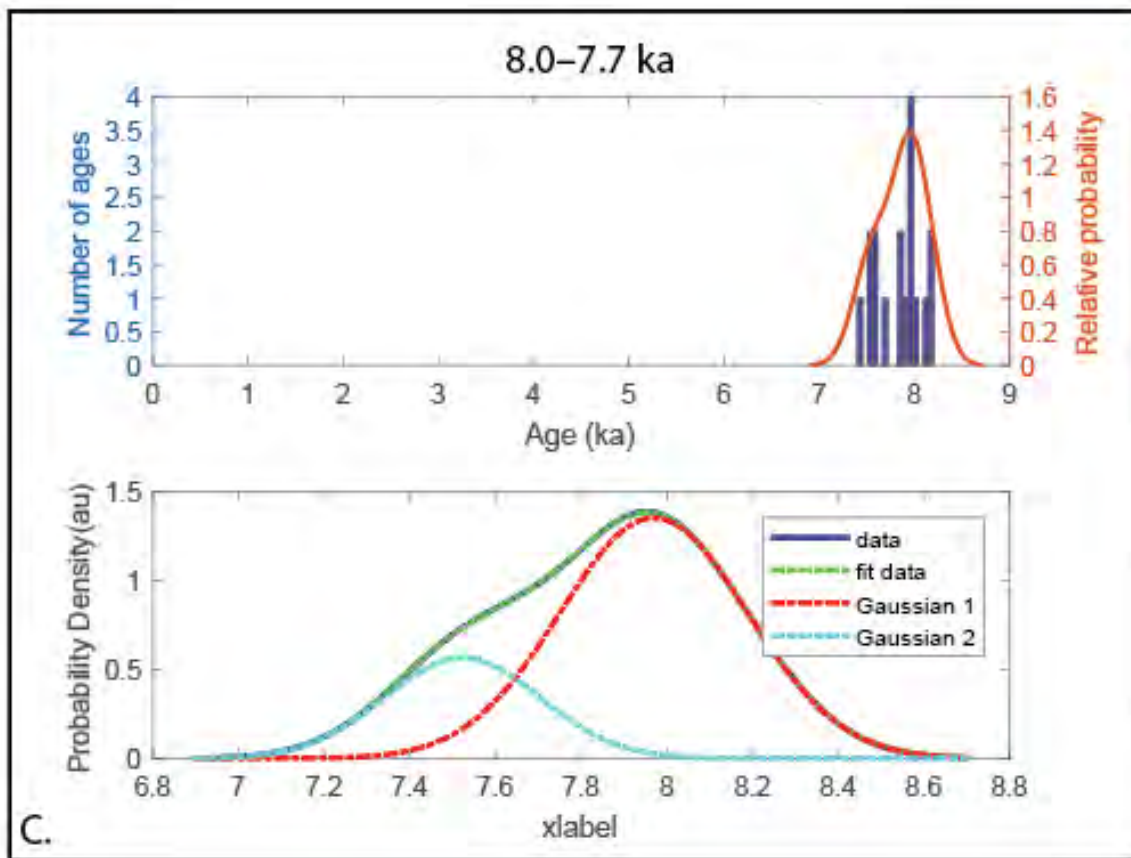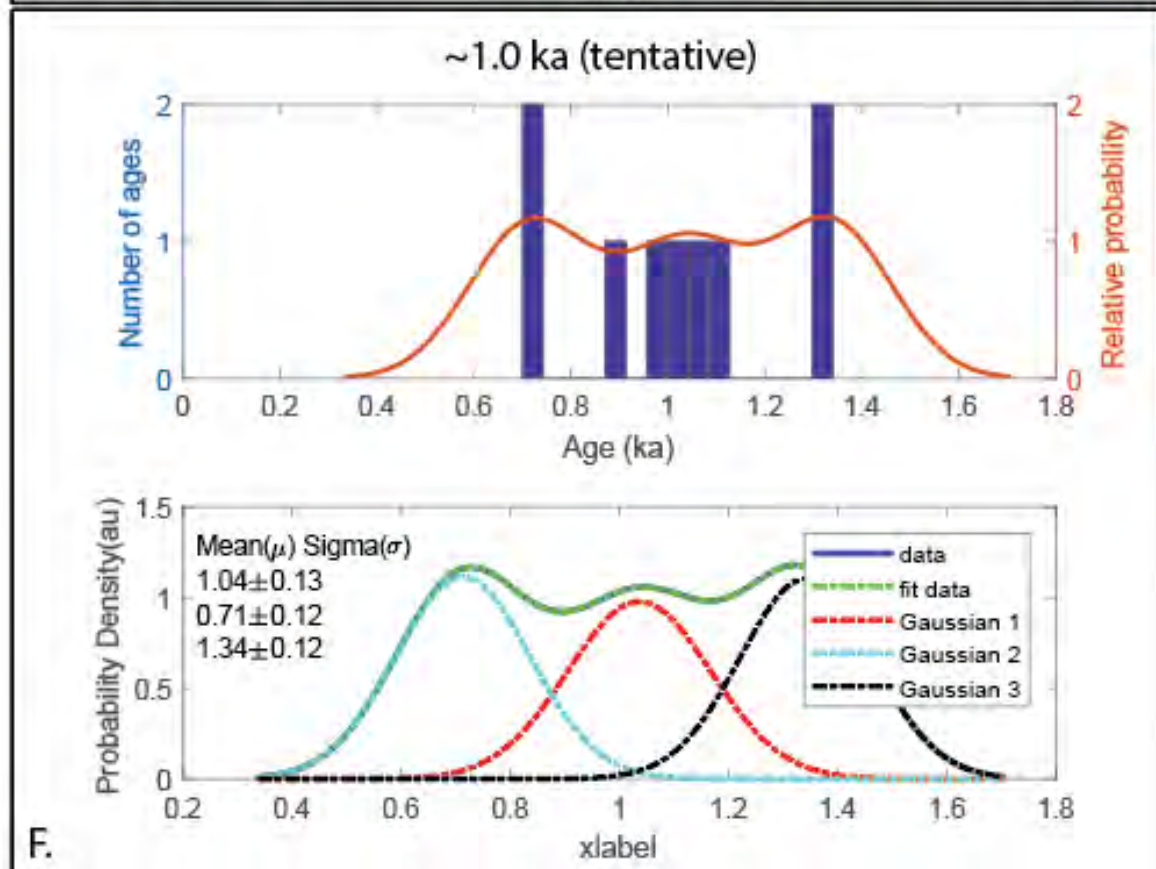
A. 15.2–11.7 ka

B. 10.3–9.7 ka (tentative)

C.

D.

2.3–1.3 ka

~1.0 ka (tentative)

Mean(μ) Sigma(σ)
1.04±0.13
0.71±0.12
1.34±0.12

data
fit data
Gaussian 1
Gaussian 2
Gaussian 3

E.

F.

Transitional western Himalaya

6.1–5.0 ka

J.

<1 ka

Mean(μ) Sigma(σ)
0.43±0.09
0.30±0.15
-0.97±0.07
0.70±0.13
0.98±0.10

K.

Wet and warm central and eastern Himalaya

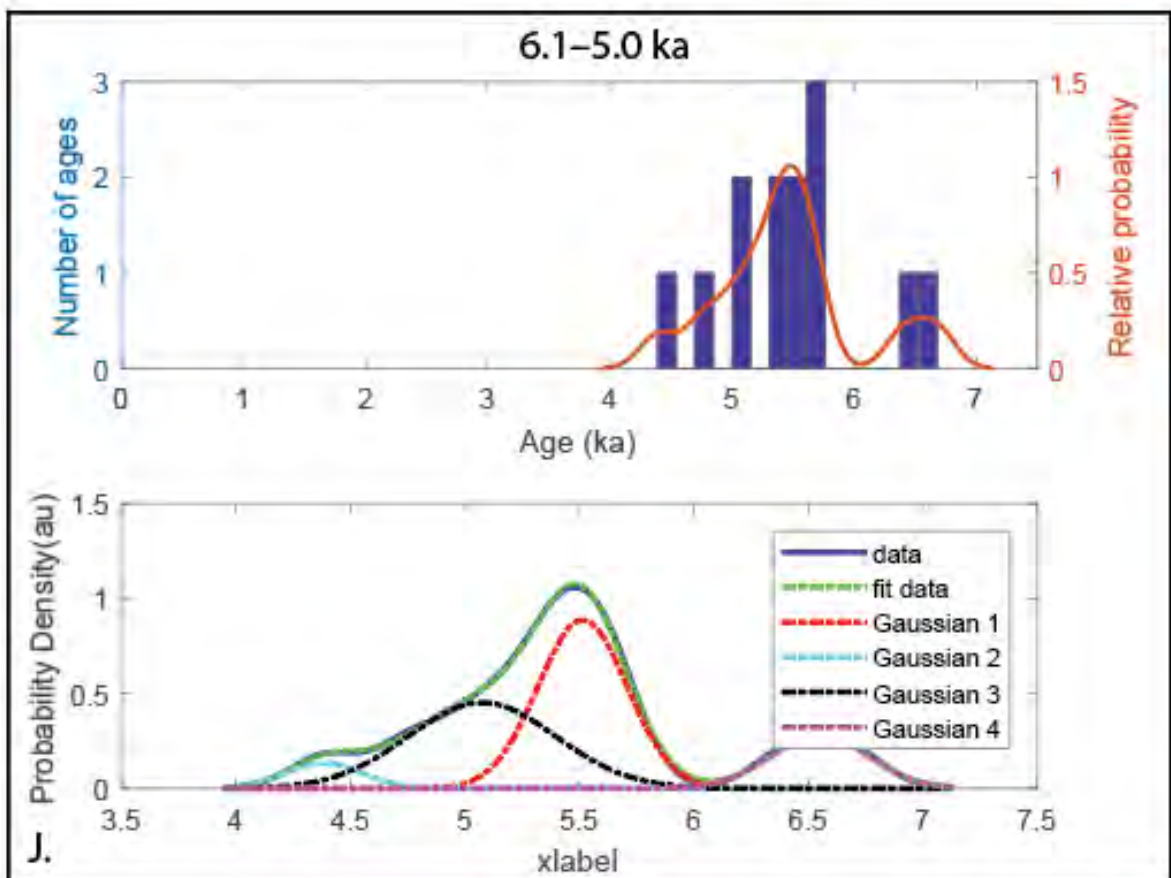## 13.0–10.9 ka
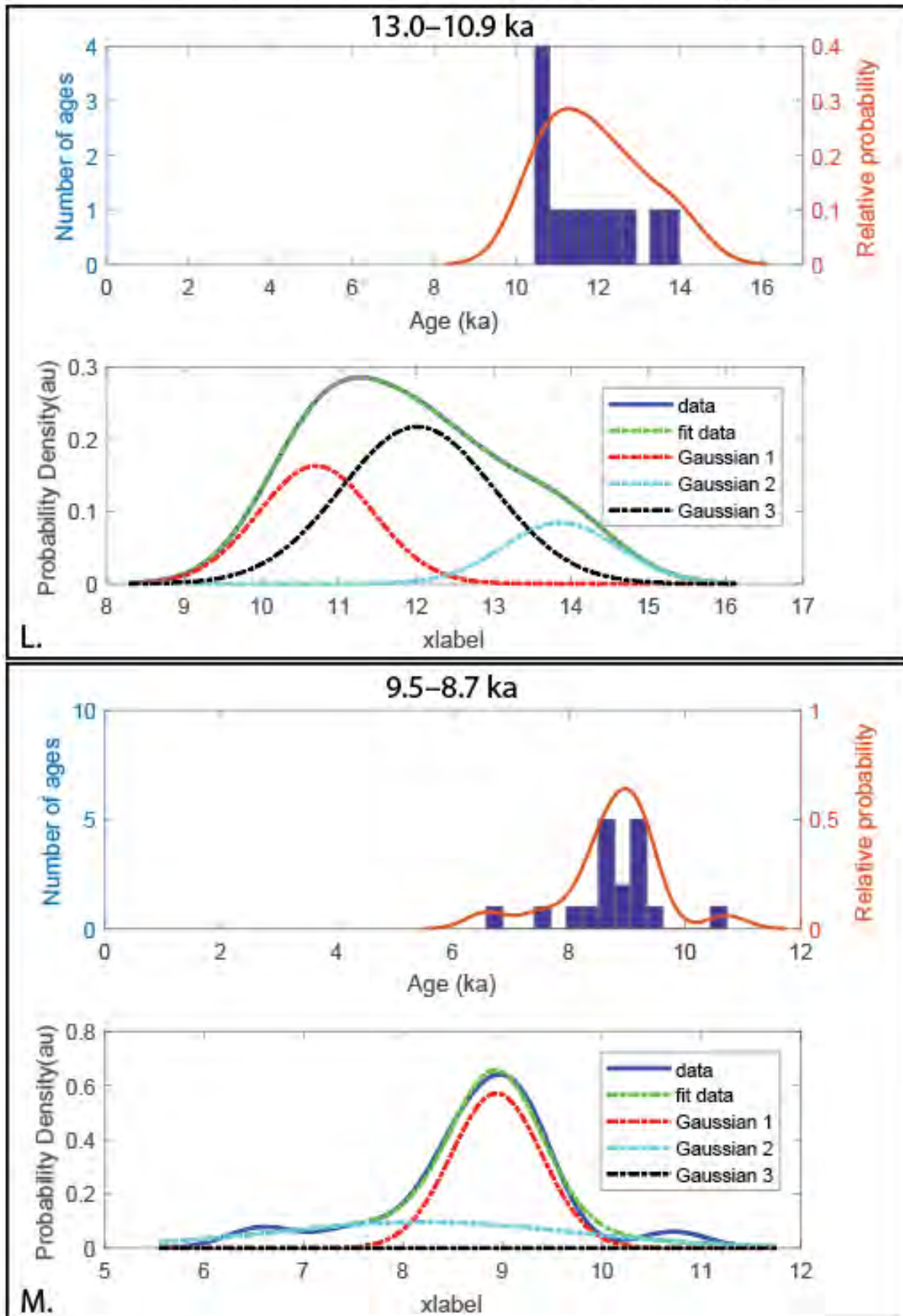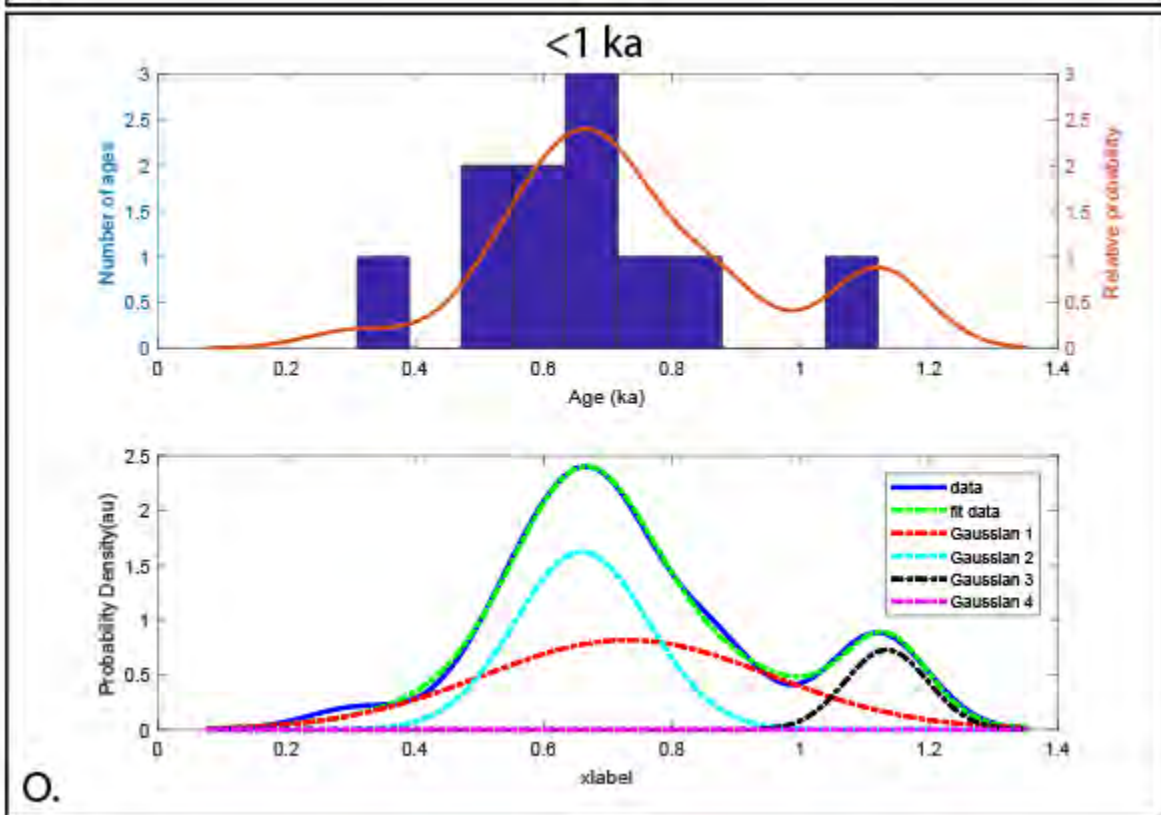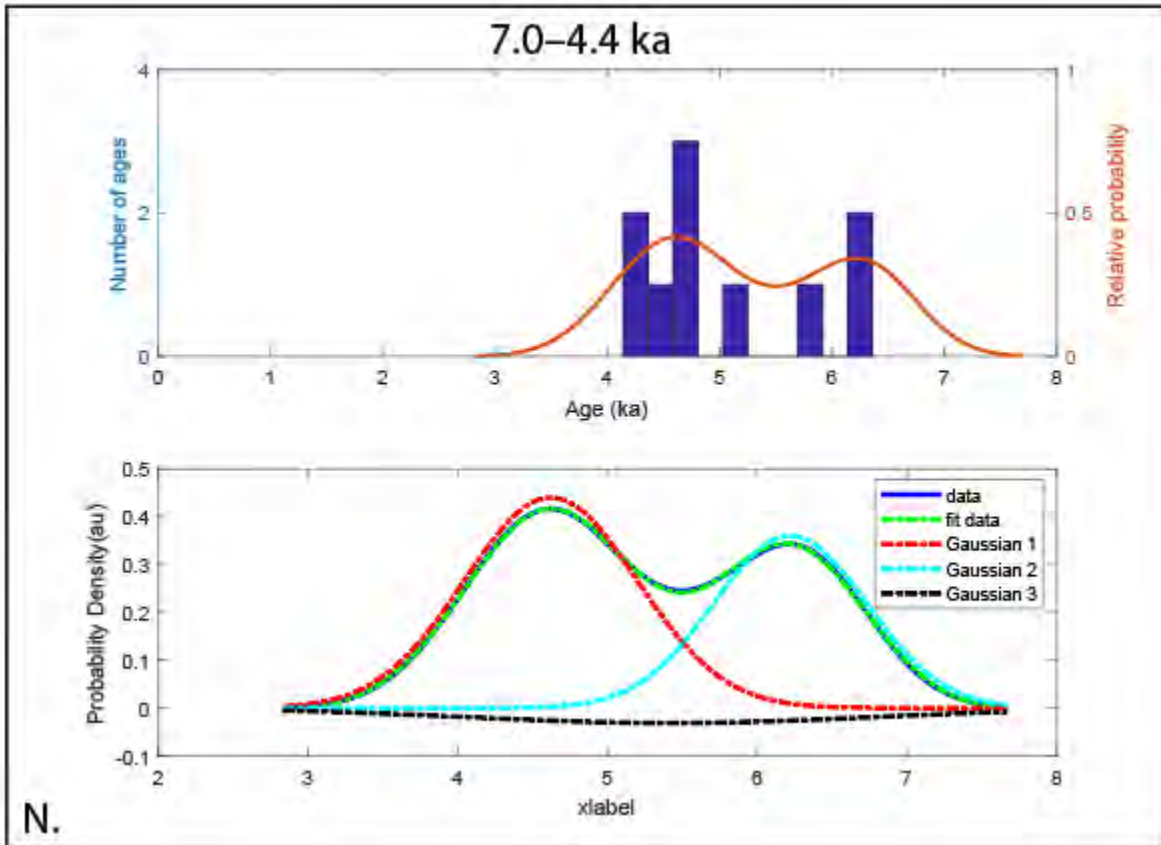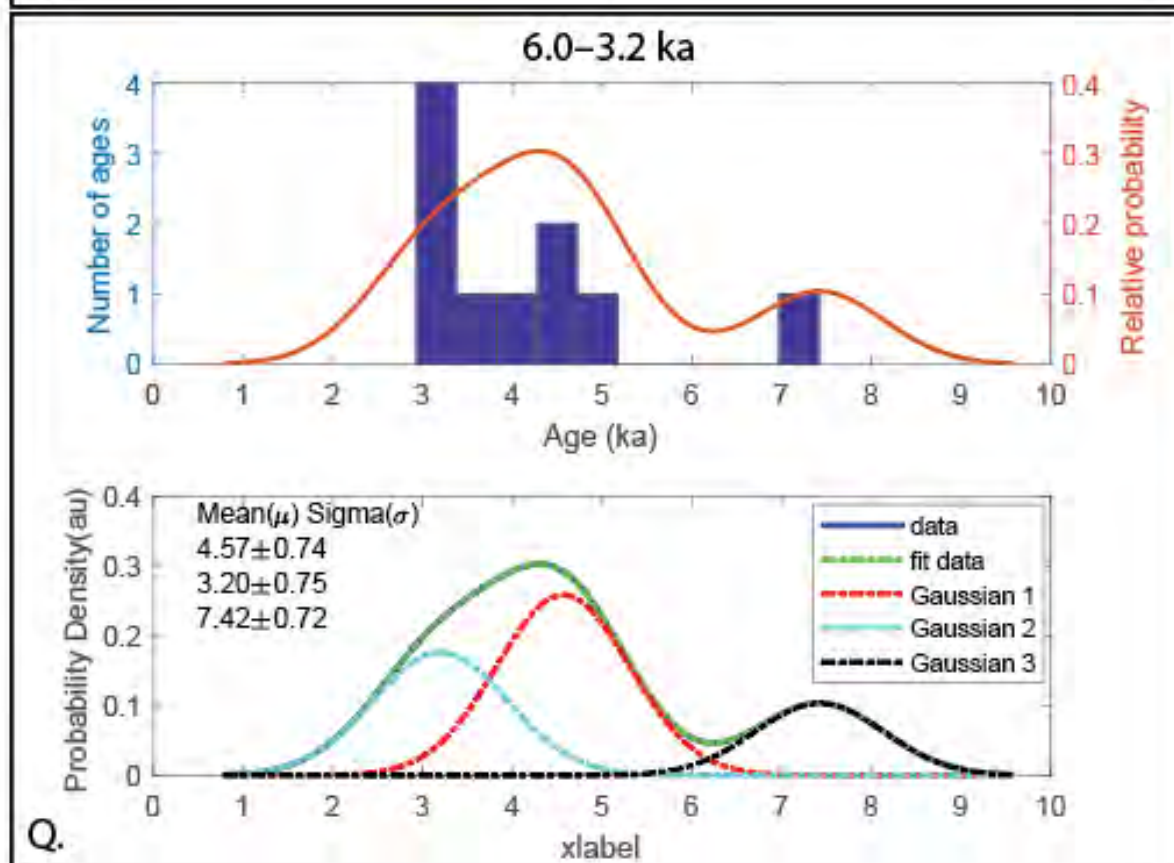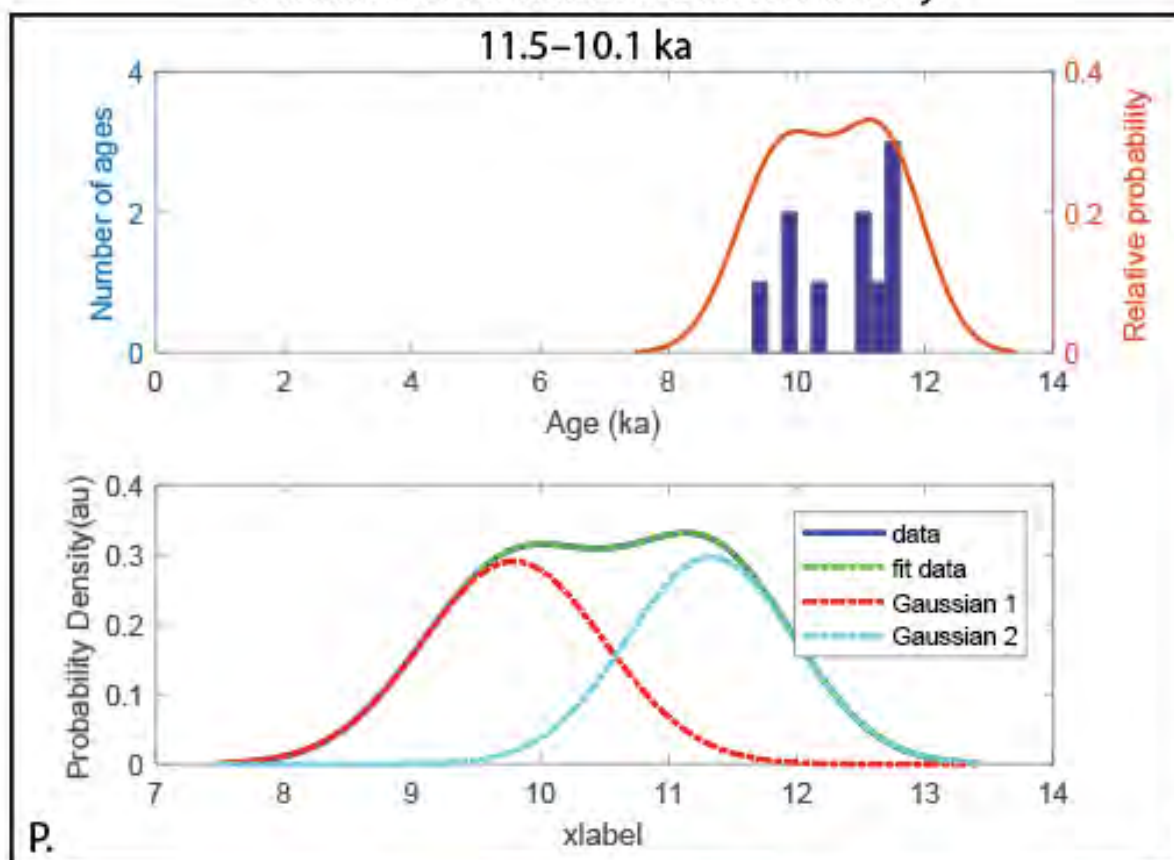

L.

9.5–8.7 ka

M.

N.

O.

Transitional central and eastern Himalaya

285

Transitional western Himalaya

13.5–12.9 ka

T.

11.5–9.5 ka

U.

287
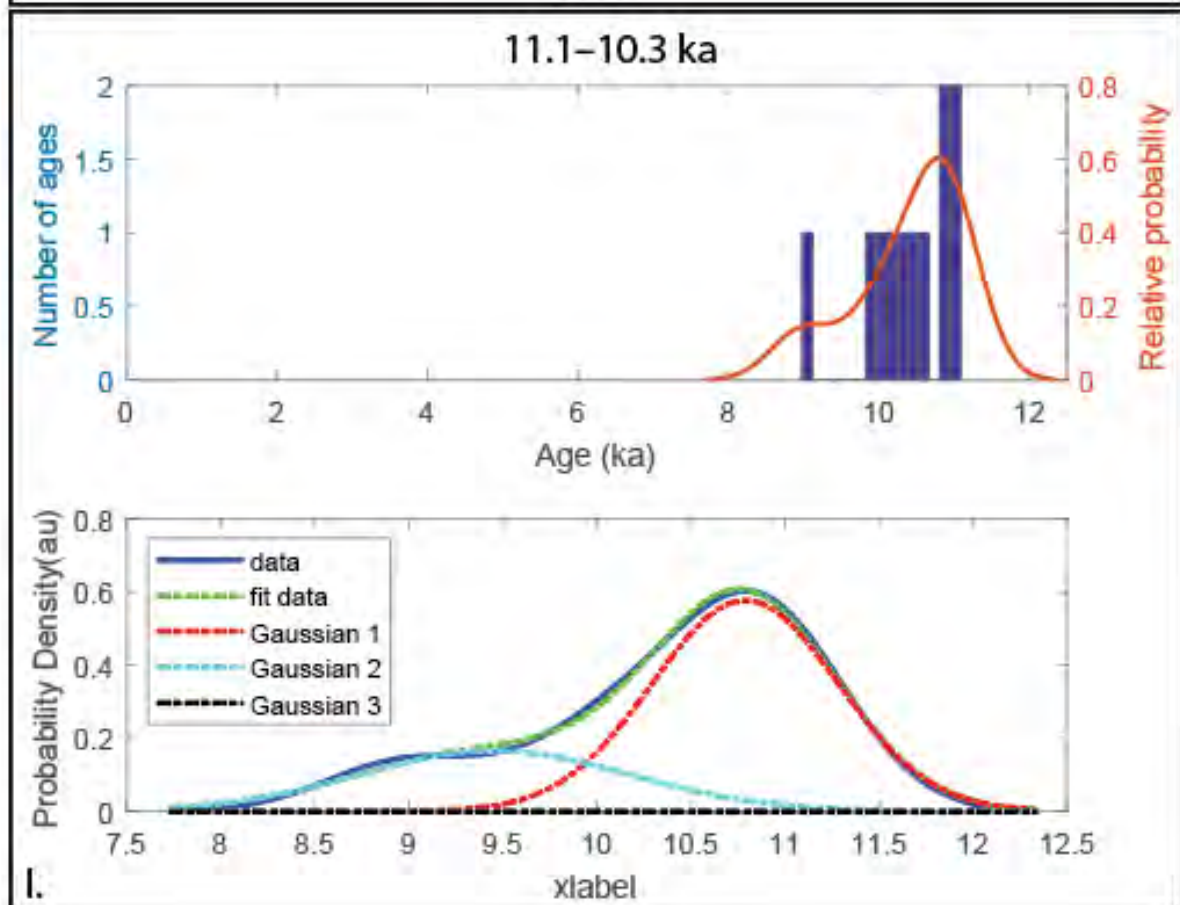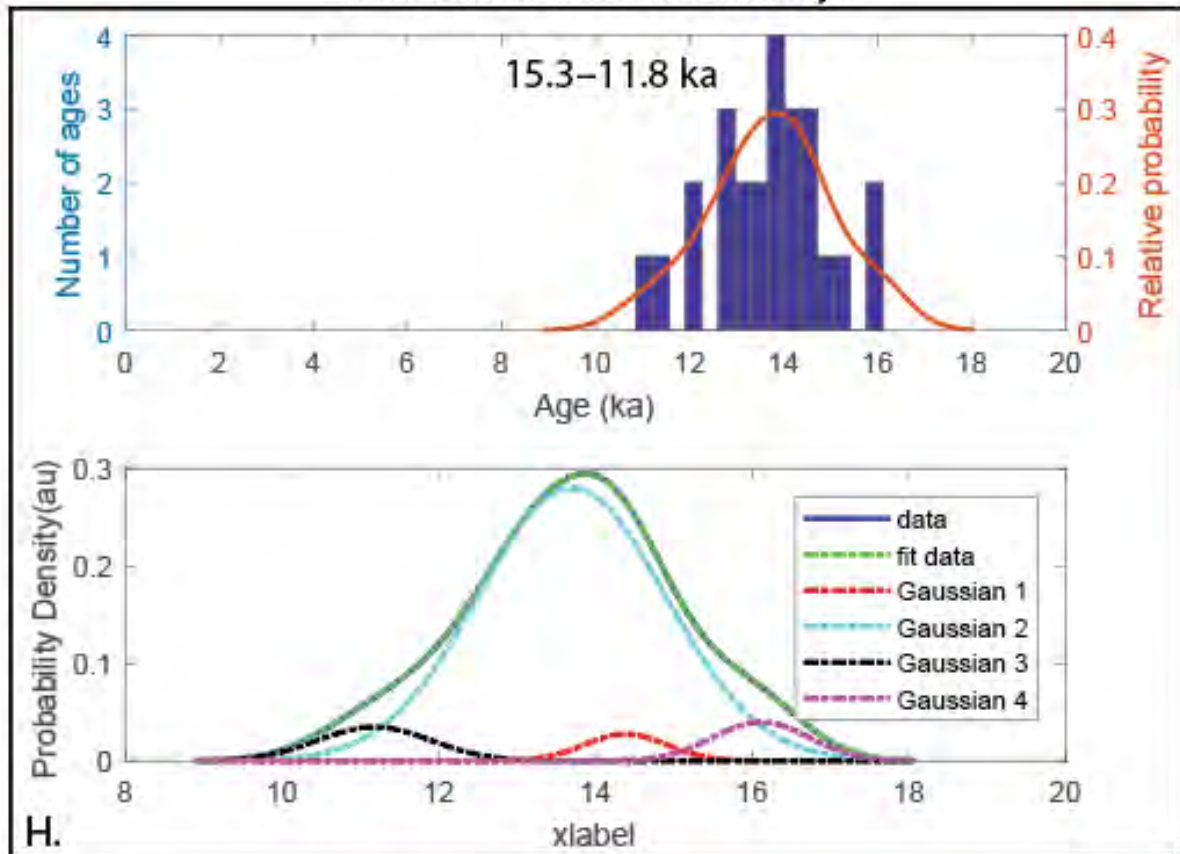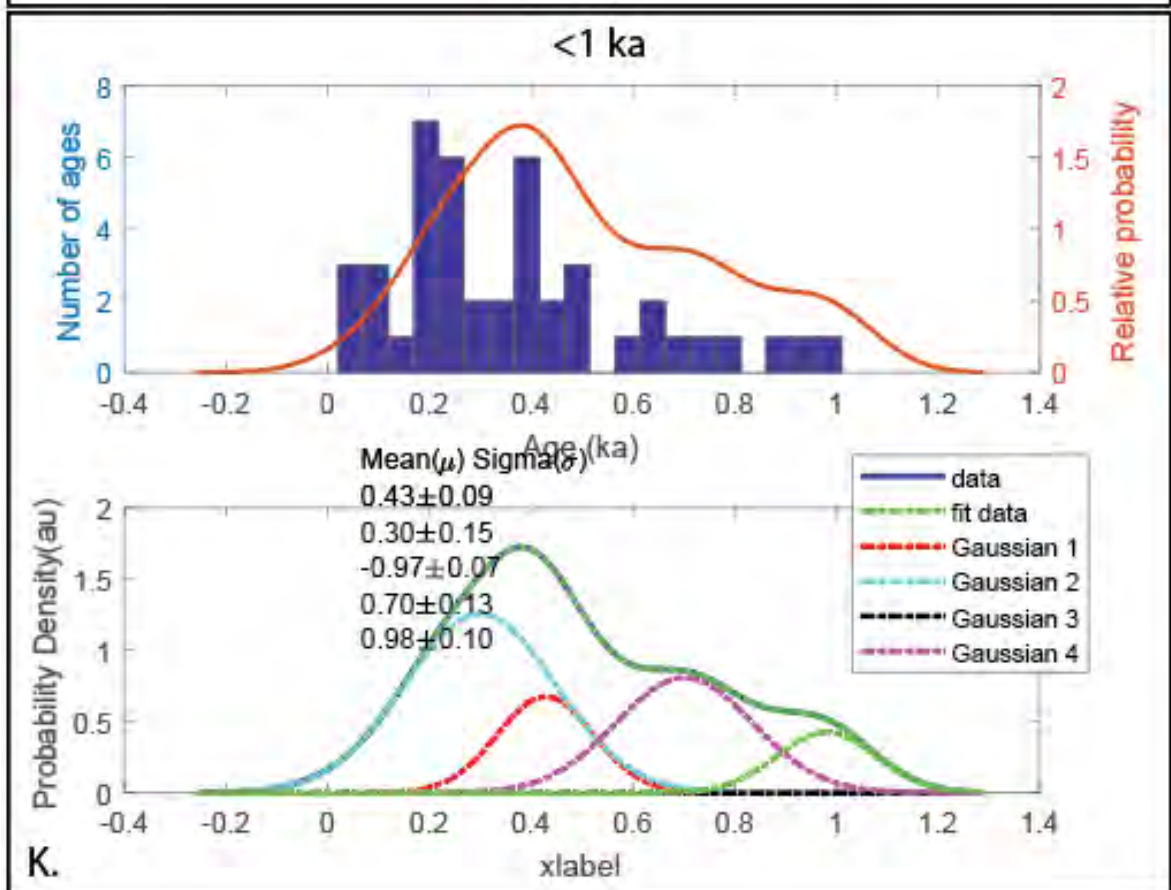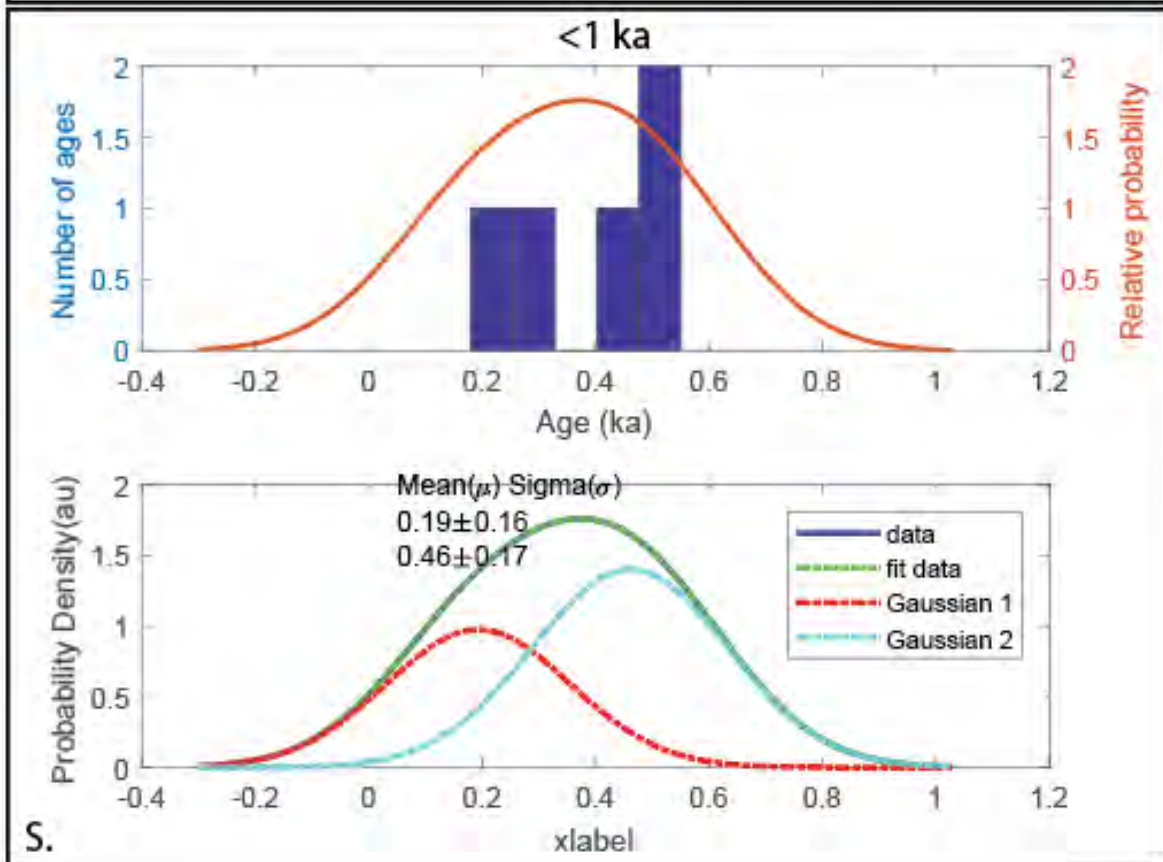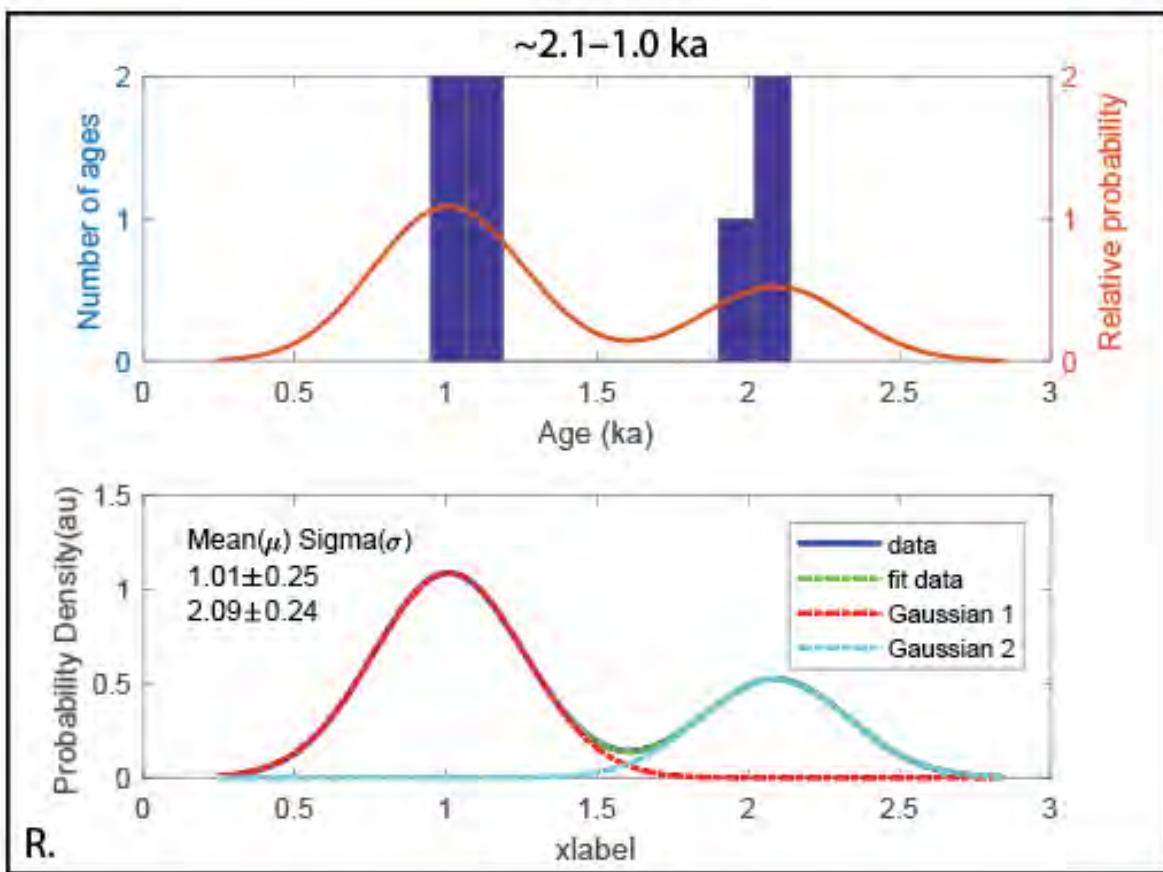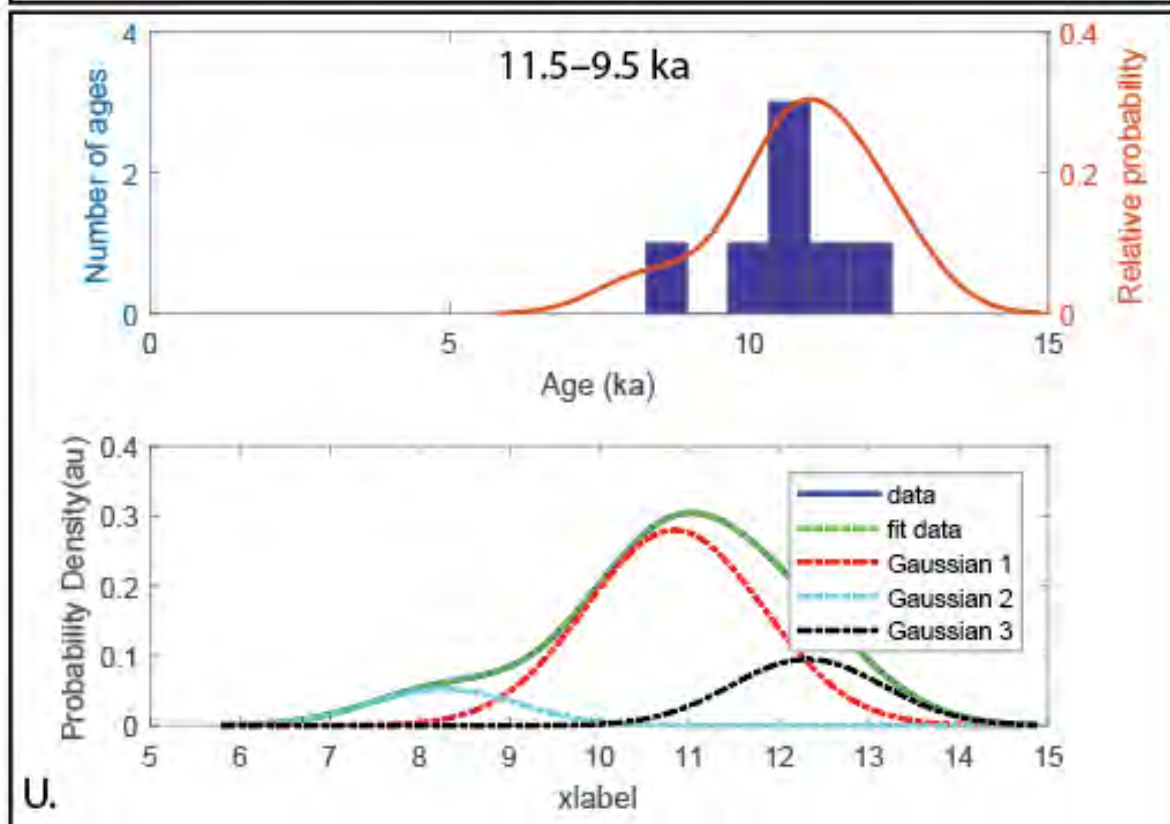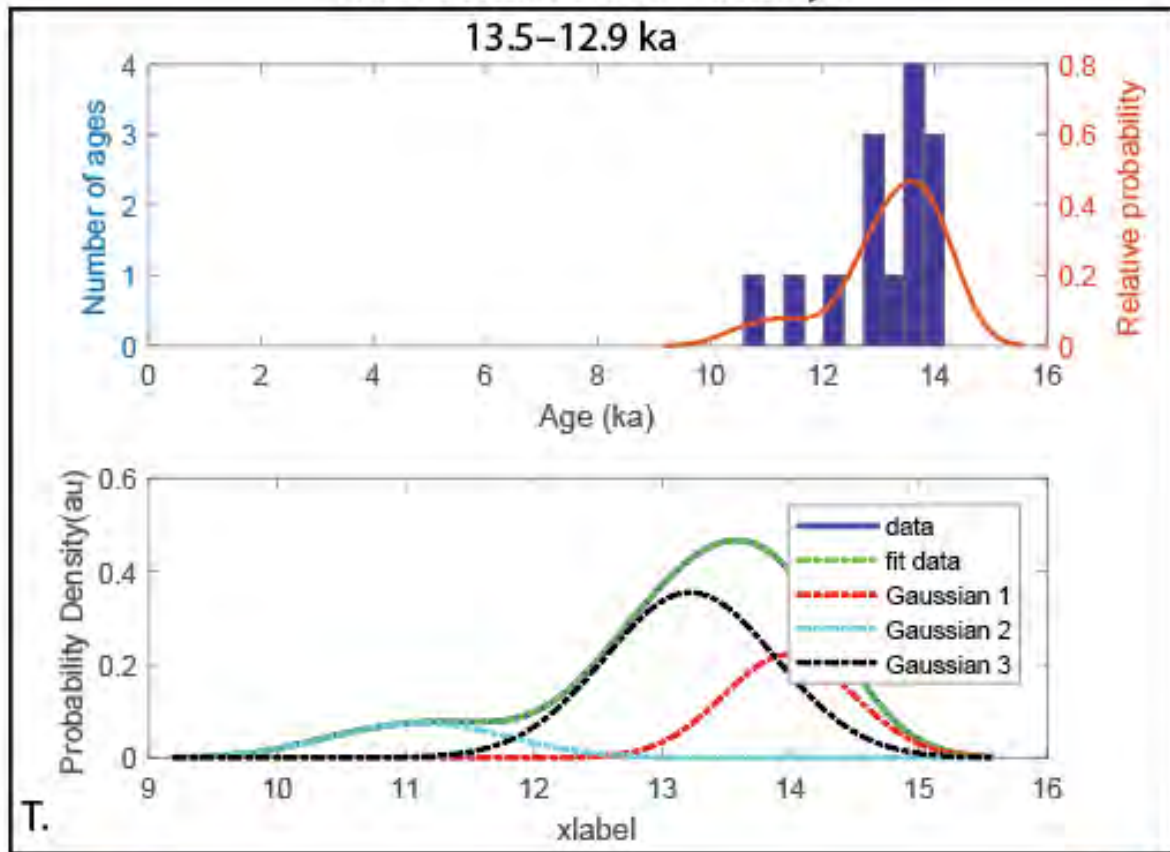
11.3 Appendix A3 (Supplementary materials for Paper III)

List of supplementary materials.

S1. Major geomorphic landforms of the Bhagirathi valley. A) Recent slope deposits and talus formation in the frontal section of M_{B4} and M_{B3}. B) Dissection of the frontal section of M_{B4} and M_{B3} by streams emanating from debris fans. C) Ablation valley separate M_{B2} from any slope contamination. D) Hummocks in the proglacial zone of Meru glacier. E) Active supraglacial zone of Meru glacier.

S2. Sampled moraine boulders for ^{10}Be dating in the study areas.

S3. Be-10 surface-exposure concentrations and ages (in thousands of years before AD2016, labeled 'ka'$\pm 1\sigma$) used in this study. Sample data, local glacial stages, ages, and associated age statistics are highlighted.

S4. A maximum spallogenic ^{10}Be concentration at the surface of a boulder; estimated assuming a ^{10}Be production rate of ~95.4 atoms/g SiO_2/a, density of 2.7 g cm^{-3}, decay constant of 4.99 x 10^{-7}, erosion rate of 0.2–0.5 mm a^{-1}, and spent ~0.5 ka on the supraglacial zone

S1. Major geomorphic landforms of the Bhagirathi valley. A) Recent slope deposits and talus formation in the frontal section of M_{B4} and M_{B3}. B) Dissection of the frontal section of M_{B4} and M_{B3} by streams emanating from debris fans. C) Ablation valley separate M_{B2} from any slope contamination. D) Hummocks in the proglacial zone of Meru glacier. E) Active supraglacial zone of Meru glacier.
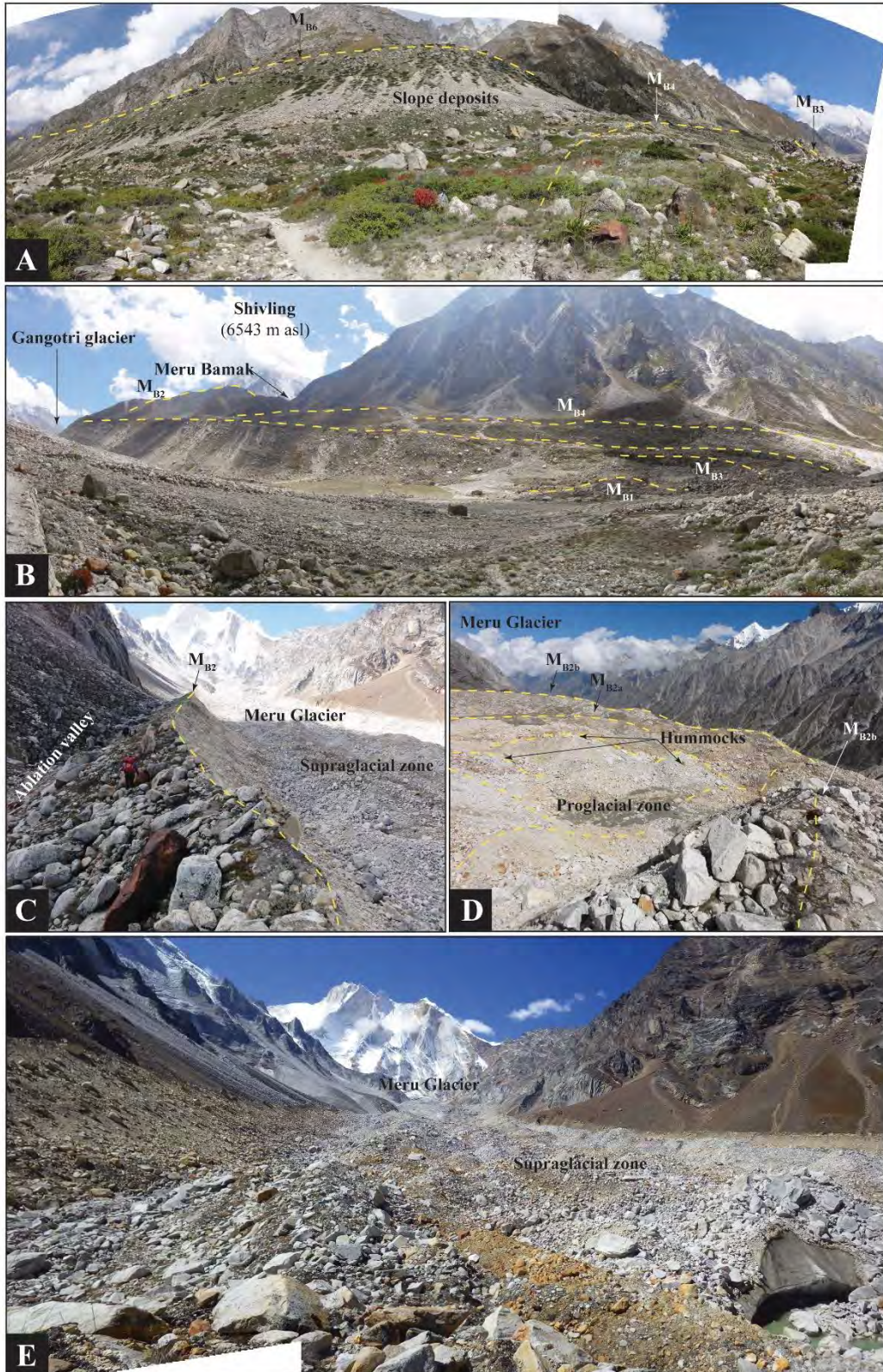
S2. Sampled moraine boulders for ^{10}Be dating in the study areas.

Table S3. Be-10 surface-exposure concentrations and ages (in thousands of years before AD2016, labeled 'ka'±1σ) used in this study. Sample data, local glacial stages, ages, and associated age statistics are highlighted.

Moraine morpho-stratigraphy	Sample ID	Material sampled	Latitude (DD N)	Longitude (DD E)	Elevation (m a.s.l.)	Sample thickness (cm)	Density (g cm⁻³)	Erosion (cm a⁻¹)	Shielding correction	[¹⁰Be] ± 1σ (10⁴ atoms g⁻¹)	AMS standard	Local glacial stage (based on LSD ages in ka)	CREp LSD Age ± 1σ (ka)[i]	CREp Basic age statistics	Lm Age ± 1σ (ka)[j]	CRONUS EARTH V 3.0 LSD Age ± 1σ (ka)[i]	Lm Age ± 1σ (ka)[j]	St Age ± 1σ (ka)[k]
Bhagirathi stage																		
M$_{B8}$	BH41^{ac}		30.9900	78.9400	3063	5.0	2.7	0.0	0.99	1.40±1.00	LLNL3000		0.63±0.45		0.58±0.41	0.61±0.43	0.57±0.40	0.46±0.33
M$_{B8}$	BH43^{ac}		31.0100	78.7100	2510	5.0	2.7	0.0	0.95	0.60±1.30	LLNL3000		0.39±0.85	? (incomplete	0.35±0.76	0.39±0.85	0.36±0.78	0.28±0.61
M$_{B8}$	BH44^{ac}	Moraine boulder	31.0100	78.7100	2499	5.0	2.7	0.0	0.95	3.50±1.10	LLNL3000	?	2.48±0.83	exposures/later	2.20±0.73	1.96±0.62	1.79±0.56	1.66±0.52
M$_{B8}$	BH45^{ac}		31.0100	78.7100	2490	5.0	2.7	0.0	0.95	1.20±1.10	LLNL3000		0.80±0.74	deposits)	0.73±0.67	0.76±0.69	0.70±0.64	0.57±0.52
M$_{B8}$	BH46^{ac}		31.0100	78.7100	2495	5.0	2.7	0.0	0.95	2.70±1.10	LLNL3000		1.89±0.81		1.69±0.70	1.49±0.61	1.38±0.56	1.28±0.52
Sudarshan stage																		
M$_{B7}$	BH35B^a		30.9500	79.0600	4093	5.0	2.7	0.0	0.970	94.0±2.8	LLNL3000B		20.82±1.01	Chi-squared: 14.14	20.34±0.96	17.81±0.53	17.64±0.53	18.03±0.54
M$_{B7}$	BH36^a		30.9500	79.0600	4112	5.0	2.7	0.0	0.970	69.5±1.9	LLNL3000		15.83±0.88	Dispersion: 13%	15.30±0.74	13.56±0.37	13.43±0.37	13.19±0.36
														Skewness: !				
														Outlier: 1				
M$_{B7}$	BH37^{ac}	Moraine boulder	30.9500	79.0600	4098	5.0	2.7	0.0	0.970	51.3±1.5	LLNL3000	18.3±3.5	12.15±0.76	Wt. mean: 18.0±3.5 ka	11.63±0.58	10.99±0.32	10.71±0.31	9.79±0.29
														Ar. Mean: 18.3±3.5 ka				
														Peak: !				
Kedar stage																		
M$_{B6}$	BH19^a		30.9400	78.9500	4323	5.0	2.7	0.0	0.970	49.3±1.2	LLNL3000		8.59±0.48	Chi-squared: 1.05	9.06±0.63	9.32±0.22	8.92±0.21	8.07±0.22
														Dispersion: 0%				
														Skewness: !				
														Outlier: 0				
M$_{B6}$	BH20^a	Moraine boulder	30.9400	78.9500	4242	5.0	2.7	0.0	0.970	43.8±1	LLNL3000	8.3±0.4	7.96±0.4	Wt. mean: 8.2±0.4 ka	8.31±0.52	8.49±0.20	8.20±0.20	7.46±0.20
														Ar. Mean: 8.3±0.4 ka				
														Peak: 8.24 ka				
Shivling stage																		
M$_{B5}$	Milap4^b		30.9964	78.9308	3029	5.0	2.7	0.0	0.918	10.70±0.38^g	07KNSTD		5.48±0.28	Chi-squared: 0.63	5.04±0.28	5.41±0.19	5.04±0.19	4.43±0.16
M$_{B5}$	Milap5^b		30.9971	78.9274	3012	5.0	2.7	0.0	0.907	9.66±0.31^g	07KNSTD		5.13±0.29	Dispersion: 0%	4.68±0.29	5.02±0.16	4.60±0.16	4.09±0.13
M$_{B5}$	Milap8^b		30.9971	78.9311	3021	2.0	2.7	0.0	0.899	10.68±0.61^g	07KNSTD		5.48±0.35	Skewness: -0.86	5.04±0.35	5.41±0.31	5.03±0.31	4.42±0.26
M$_{B5}$	Milap10^b		30.9968	78.9289	3017	2.0	2.7	0.0	0.911	10.50±0.62^g	07KNSTD		5.35±0.35	Outlier: 0	4.89±0.35	5.28±0.31	4.87±0.31	4.30±0.25
M$_{B5}$	Milap11^b	Moraine boulder	30.9967	78.9284	3022	2.0	2.7	0.0	0.907	10.44±0.58^g	07KNSTD	5.2±0.3	5.33±0.35	Wt. mean: 5.2±0.3 ka	4.89±0.35	5.26±0.29	4.85±0.29	4.29±0.24
M$_{B5}$	Milap12^b		30.9968	78.9277	3017	2.0	2.7	0.0	0.905	9.68±0.43^h	07KNSTD		5.02±0.32	Ar. Mean: 5.2±0.3 ka	4.57±0.32	4.88±0.22	4.49±0.22	3.99±0.18
M$_{B5}$	Milap13^b		30.9969	78.9272	3039	2.0	2.7	0.0	0.907	9.25±0.57^g	07KNSTD		4.76±0.36	Peak: 5.25 ka	4.33±0.36	4.56±0.28	4.25±0.28	3.76±0.23
Gangotri stage																		
M$_{B4}$	Milap2^b		30.7633	79.0775	4343	5.0	2.7	0.0	0.980	9.83±0.29^h	07KNSTD2		2.41±0.18	Chi-squared: 5.63	2.22±0.14	2.26±0.07	2.17±0.07	1.91±0.06
M$_{B4}$	Milap3^b		30.9129	79.0783	4335	5.0	2.7	0.0	0.980	7.98±0.26^h	07KNSTD		1.91±0.13	Dispersion: 9.2%	1.80±0.11	1.76±0.06	1.72±0.06	1.55±0.05
														Skewness: !				
														Outlier: 1				
M$_{B4}$	Milap7^{bc}	Moraine boulder	30.9454	79.0600	3935	2.0	2.7	0.0	0.949	1.69±0.07^g	07KNSTD	2.2±0.4	0.47±0.04	Wt. mean: 2.1±0.4 ka	0.44±0.03	0.54±0.02	0.52±0.02	0.40±0.02
														Ar. Mean: 2.2±0.4 ka				
														Peak: !				
Bhujbasa stage																		
M$_{B3}$	BH26^a		30.9400	79.0600	3917	5.0	2.7	0.0	0.97	5.8±0.3	LLNL3000		1.70±0.14		1.58±0.11	1.37±0.07	1.33±0.07	1.21±0.06
M$_{B3}$	BH27^a		30.9400	79.0600	3918	5.0	2.7	0.0	0.97	10.2±0.4	LLNL3000		3.10±0.21	Chi-squared: 30.57	2.86±0.18	2.61±0.10	2.52±0.10	2.13±0.08
M$_{B3}$	BH29^a		30.9400	79.0600	3973	5.0	2.7	0.0	0.97	3.3±0.9	LLNL3000		0.71±0.2	Dispersion: 41%	0.75±0.21	0.82±0.22	0.79±0.21	0.63±0.22
M$_{B3}$	BH30^{ac}		30.9400	79.0600	3956	5.0	2.7	0.0	0.97	1.6±0.7	LLNL3000		0.34±0.16	Skewness: 0.93	0.37±0.16	0.43±0.19	0.41±0.18	0.31±0.19
M$_{B3}$	BH31^{ac}		30.9400	79.0600	3973	5.0	2.7	0.0	0.97	1.2±0.7	LLNL3000		0.26±0.16	Outlier: 4	0.24±0.15	1.07±0.17	1.04±0.17	0.90±0.17
M$_{B3}$	BH32^a	Moraine boulder	30.9400	79.0600	3956	5.0	2.7	0.0	0.97	4.6±0.7	LLNL3000	0.8±0.3	1.01±0.17	Wt. mean: 0.7±0.3 ka	1.07±0.19	0.51±0.02	0.49±0.02	0.38±0.02
M$_{B3}$	Gang1		30.9149	79.0780	4294	1.5	2.7	0.0	0.963	2.57±0.15^d	07KNSTD		0.59±0.05	Ar. Mean: 0.8±0.3 ka	0.56±0.05	0.66±0.04	0.64±0.04	0.50±0.03
M$_{B3}$	Gang2		30.9140	79.0785	4328	3.0	2.7	0.0	0.960	5.17±0.17^d	07KNSTD		1.21±0.08	Peak: 0.95 ka	1.14±0.08	1.16±0.04	1.14±0.04	1.01±0.03
M$_{B3}$	Gang3		30.9139	79.0786	4327	2.5	2.7	0.0	0.960	2.05±0.16^e	07KNSTD		0.46±0.05		0.43±0.05	0.54±0.04	0.52±0.04	0.40±0.03
M$_{B3}$	Gang4		30.9116	79.0797	4337	1.0	2.7	0.0	0.964	3.90±0.13^e	07KNSTD		0.89±0.06		0.83±0.06	0.94±0.03	0.92±0.03	0.74±0.03
M$_{B3}$	Gang5^c		30.9140	79.0785	4329	3.0	2.7	0.0	0.960	13.29±0.43^f	07KNSTD		3.31±0.21		3.09±0.21	3.09±0.10	3.03±0.10	2.60±0.08
Meru stage																		
M$_{B2}$	Gang6		30.9114	79.0699	4519	3.0	2.7	0.0	0.958	0.63±0.08^f	07KNSTD		0.12±0.02	Chi-squared: 36.52	0.11±0.02	0.16±0.02	0.15±0.02	0.11±0.02
M$_{B2}$	Gang7		30.9078	79.0675	4569	3.0	2.7	0.0	0.916	1.79±0.10^e	07KNSTD		0.38±0.03	Dispersion: 49%	0.35±0.03	0.45±0.02	0.43±0.02	0.33±0.02
M$_{B2}$	Gang8		30.9058	79.0656	4598	2.5	2.7	0.0	0.910	2.21±0.11^e	07KNSTD		0.45±0.04	Skewness: -0.98	0.43±0.04	0.53±0.03	0.52±0.03	0.40±0.02
														Outlier: 0				
M$_{B2}$	Gang9	Moraine boulder	30.9045	79.0643	4614	2.0	2.7	0.0	0.909	1.49±0.30^d	07KNSTD	0.3±0.1	0.30±0.06	Wt. mean: 0.2±0.1 ka	0.29±0.06	0.37±0.07	0.36±0.07	0.27±0.05
														Ar. Mean: 0.3±0.1 ka				
														Peak: 0.35 ka				
Gaumukh recessional stage																		

	Sample ID	Material sampled	Latitude	Longitude	Elevation					$[^{10}Be] \pm 1\sigma$	AMS standard		^{10}Be Age	Statistics				
M_{B1c}	Milap1[b]		30.9395	79.0635	3908	5.0	2.7	0.0	0.947	0.71±0.05[h]	07KNSTD		0.21±0.02	Chi-squared: 4.20	0.19±0.02	-	0.23±0.00	0.18±0.01
M_{B1c}	Gang15		30.9394	79.0651	3914	2.0	2.7	0.0	0.936	0.94±0.07[d]	07KNSTD		0.26±0.03	Dispersion: 18%	0.24±0.03	0.32±0.03	0.31±0.03	0.23±0.02
M_{B1c}	Gang16		30.9393	79.0650	3915	2.0	2.7	0.0	0.936	0.65±0.23[d]	07KNSTD		0.18±0.07	Skewness: 1.24	0.17±0.07	0.23±0.08	0.21±0.08	0.16±0.06
M_{B1c}	Gang17		30.9391	79.0645	3912	2.0	2.7	0.0	0.952	0.76±0.02[e]	07KNSTD		0.21±0.02	Outlier: 1	0.20±0.02	0.26±0.01	0.25±0.01	0.18±0.01
M_{B1c}	Gang18[c]		30.9390	79.0644	3911	2.0	2.7	0.0	0.948	14.86±0.41[f]	07KNSTD	0.2±0.1	4.51±0.26	Wt. mean: 0.2±0.1 ka	4.18±0.26	4.31±0.12	4.14±0.12	3.60±0.10
M_{B1c}	Gang19		30.9390	79.0644	3911	2.5	2.7	0.0	0.952	1.22±0.04[e]	07KNSTD		0.34±0.03	Ar. Mean: 0.2±0.1 ka / Peak: 0.25 ka	0.32±0.03	0.41±0.02	0.39±0.02	0.30±0.01
M_{B1a}	Gang10	Moraine boulder	30.9355	79.0711	3932	1.0	2.7	0.0	0.918	0.79±0.04[e]	07KNSTD		0.22±0.02	Chi-squared: 1.19	0.21±0.02	0.27±0.01	0.26±0.01	0.19±0.01
M_{B1a}	Gang12		30.9362	79.0702	3932	1.0	2.7	0.0	0.919	0.77±0.01[e]	07KNSTD		0.22±0.01	Dispersion: 0%	0.20±0.01	0.27±0.003	0.25±0.003	0.19±0.002
M_{B1a}	Gang13		30.9363	79.0697	3924	2.0	2.7	0.0	0.935	0.85±0.05[f]	07KNSTD		0.24±0.02	Skewness: 0.85 / Outlier: 0	0.22±0.02	0.29±0.02	0.28±0.02	0.21±0.01
M_{B1a}	Gang14		30.9363	79.0691	3927	3.0	2.7	0.0	0.937	0.93±0.07[f]	07KNSTD	0.2±0.0	0.26±0.03	Wt. mean: 0.2±0.0 ka / Ar. Mean: 0.2±0.0 ka / Peak: 0.23 ka	0.24±0.03	0.32±0.02	0.30±0.02	0.23±0.02

Reference	Sample ID	Material sampled	Latitude (DD N)	Longitude (DD E)	Elevation (m a.s.l.)					$[^{10}Be] \pm 1\sigma$ $(10^4$ atoms g$^{-1})$	AMS standard		^{10}Be Age $\pm 1\sigma$ (ka)[i]					
Gangotri supraglacial sediment																		
	G_{sup1}		30.9000	79.0900	4315	-	-	-	-	1.1±0.2	07KNSTD	-	0.24±0.05	-	-	-	-	-
	G_{sup2}		30.9000	79.0800	4280	-	-	-	-	1.6±0.3	07KNSTD	-	0.36±0.07	-	-	-	-	-
Orr et al. (in prep)	G_{sup3}	Supraglacial sediment	30.8900	79.0900	4325	-	-	-	-	2.7±0.3	07KNSTD	-	0.59±0.08	-	-	-	-	-
	G_{sup4}		30.9000	79.0900	4285	-	-	-	-	2.5±0.3	07KNSTD	-	0.55±0.08	-	-	-	-	-
	G_{sup5}		30.9200	79.0800	4130	-	-	-	-	2.6±0.3	07KNSTD	-	0.63±0.08	-	-	-	-	-
	G_{sup6}		30.9200	79.0800	4130	-	-	-	-	1.5±0.4	07KNSTD	-	0.35±0.10	-	-	-	-	-
Gangotri proglacial sediment																		
Barnard et al. (2004)	BH25	Supraglacial sediment	30.9300	79.8000	3960	-	-	-	-	3.9±0.5	LLNL3000	-	1.05±0.15	-	-	-	-	-
Alaska supraglacial debris																		
	Shadows Glacier M1-left		62.4980	-152.6788	961	-	-	-	-	1.50±0.21	07KNSTD	-	1.29±0.2	-	-	-	-	-
	Shadows Glacier M1-right		62.4980	-152.6788	961	-	-	-	-	2.05±0.16	07KNSTD	-	1.80±0.18	-	-	-	-	-
	Shadows Glacier M5		62.4980	-152.6788	961	-	-	-	-	1.74±0.15	07KNSTD	-	1.51±0.16	-	-	-	-	-
	Shadows Glacier M8-left		62.4980	-152.6788	961	-	-	-	-	1.62±0.23	07KNSTD	-	1.40±0.22	-	-	-	-	-
	Shadows Glacier M8-right		62.4980	-152.6788	961	-	-	-	-	2.94±0.36	07KNSTD	-	2.62±0.36	-	-	-	-	-
	Shadows mean (SM-mean)		62.4980	-152.6788	961	-	-	-	-	1.97±0.53	07KNSTD	-	1.72±0.48	-	-	-	-	-
	Trident Glacier T1		62.4654	-152.5255	804	-	-	-	-	0.80±0.10	07KNSTD	-	0.79±0.11	-	-	-	-	-
Ward and Anderson (2011)	Trident Glacier T2-mean	Supraglacial debris	62.4654	-152.5255	804	-	-	-	-	0.79±0.21	07KNSTD	-	0.78±0.21	-	-	-	-	-
	Trident Glacier T2A (subsample)		62.4654	-152.5255	804	-	-	-	-	0.56±0.07	07KNSTD	-	0.56±0.07	-	-	-	-	-
	Trident Glacier T2B (subsample)		62.4654	-152.5255	804	-	-	-	-	0.71±0.10	07KNSTD	-	0.70±0.10	-	-	-	-	-
	Trident Glacier T2C (subsample)		62.4654	-152.5255	804	-	-	-	-	0.54±0.07	07KNSTD	-	0.54±0.07	-	-	-	-	-
	Trident Glacier T2D (subsample)		62.4654	-152.5255	804	-	-	-	-	0.78±0.07	07KNSTD	-	0.77±0.08	-	-	-	-	-
	Trident Glacier T2E (subsample)		62.4654	-152.5255	804	-	-	-	-	1.38±0.14	07KNSTD	-	1.37±0.16	-	-	-	-	-
	Caldwell Glacier C1		62.3835	-152.7072	937	-	-	-	-	2.27±0.14	07KNSTD	-	2.04±0.18	-	-	-	-	-
	Caldwell Glacier C2		62.3835	-152.7072	937	-	-	-	-	1.58±0.09	07KNSTD	-	1.39±0.11	-	-	-	-	-
Annapurna supraglacial (active ice) debris																		
	NP 215		28.6308	84.0386	4288	-	-	-	-	1.53±0.23	LLNL3000	-	0.36±0.06	-	-	-	-	-
	NP 216		28.6308	84.0386	4288	-	-	-	-	5.72±0.90	LLNL3000	-	1.42±0.25	-	-	-	-	-
	NP 217		28.6308	84.0386	4217	-	-	-	-	1.80±0.44	LLNL3000	-	0.44±0.11	-	-	-	-	-
	NP 218		28.6308	84.0386	4062	-	-	-	-	2.00±0.22	LLNL3000	-	0.53±0.07	-	-	-	-	-
	NP 220		28.6308	84.0386	3921	-	-	-	-	4.31±0.41	LLNL3000	-	1.28±0.14	-	-	-	-	-
	NP 221		28.6308	84.0386	3862	-	-	-	-	1.44±0.10	LLNL3000	-	0.42±0.04	-	-	-	-	-
Heimsath and McGlynn (2008)	NP 225	Supraglacial debris	28.6308	84.0386	3800	-	-	-	-	2.21±0.19	LLNL3000	-	0.69±0.07	-	-	-	-	-
	NP 226		28.6308	84.0386	3862	-	-	-	-	1.81±0.12	LLNL3000	-	0.54±0.05	-	-	-	-	-
	NP 227		28.6308	84.0386	4000	-	-	-	-	2.19±0.20	LLNL3000	-	0.61±0.07	-	-	-	-	-
	NP 228		28.6308	84.0386	4000	-	-	-	-	0.24±0.15	LLNL3000	-	0.06±0.04	-	-	-	-	-
	NP 229		28.6308	84.0386	4000	-	-	-	-	0.75±0.15	LLNL3000	-	0.20±0.04	-	-	-	-	-
	NP 230		28.6308	84.0386	4306	-	-	-	-	5.40±0.31	LLNL3000	-	1.32±0.11	-	-	-	-	-
	NP 231		28.6308	84.0386	4306	-	-	-	-	1.19±0.08	LLNL3000	-	0.27±0.02	-	-	-	-	-
	NP 232		28.6308	84.0386	4306	-	-	-	-	0.74±0.08	LLNL3000	-	0.16±0.02	-	-	-	-	-
Annapurna ridge crest																		
	NP 236		28.6278	84.0389	4069	-	-	-	-	33.60±1.88	LLNL3000	-	8.54±0.73	-	-	-	-	-
Heimsath and McGlynn (2008)	NP 239	Bedrock	28.6278	84.0389	4723	-	-	-	-	23.30±1.36	LLNL3000	-	4.82±0.34	-	-	-	-	-
	NP 240		28.6278	84.0389	4897	-	-	-	-	2.16±0.147	LLNL3000	-	0.37±0.04	-	-	-	-	-
	NP 241		28.6278	84.0389	4718	-	-	-	-	151.00±8.88	LLNL3000	-	24.07±1.66	-	-	-	-	-

Reference	Sample ID	Type	Lat	Long	Elev						Standard							
	NP 242		28.6278	84.0389	4858	-	-	-	-	43.50±2.42	LLNL3000	-	7.54±0.52	-	-	-	-	-

Annapurna rockfall debris

Reference	Sample ID	Type	Lat	Long	Elev						Standard							
Heimsath and McGlynn (2008)	NP 203	Debris	28.6278	84.0389	4288	-	-	-	-	14.20±0.79	LLNL3000	-	3.71±0.27	-	-	-	-	-
	NP 205		28.6278	84.0389	4302	-	-	-	-	18.00±1.00	LLNL3000	-	4.59±0.32	-	-	-	-	-
	NP 206		28.6278	84.0389	4540	-	-	-	-	29.60±1.72	LLNL3000	-	6.25±0.4	-	-	-	-	-
	NP 211		28.6278	84.0389	4610	-	-	-	-	3.36±0.216	LLNL3000	-	0.69±0.06	-	-	-	-	-

Chorabari supraglacial (active ice) boulders

Reference	Sample ID	Type	Lat	Long	Elev						Standard							
Murari et al. (2014)	KAL40	Supraglacial boulder	30.7481	79.0658	3904	2.5	2.7	0.0	1.000	0.25±0.03	07KNSTD	-	0.06±0.02	-	0.06±0.01	0.08±0.01	0.07±0.01	0.06±0.01
	KAL41		30.7485	79.0642	3892	4.0	2.7	0.0	1.000	0.79±0.31	07KNSTD	-	0.22±0.08	-	0.20±0.08	0.26±0.10	0.25±0.10	0.19±0.07
	KAL42		30.7472	79.0636	3853	2.5	2.7	0.0	1.000	2.19±0.90	07KNSTD	-	0.62±0.26	-	0.58±0.24	0.69±0.28	0.66±0.27	0.52±0.22

Baltoro supraglacial (active ice) debris

Reference	Sample ID	Type	Lat	Long	Elev						Standard							
Seong et al. (2009a)	K2E-1	Supraglacial debris	35.7040	76.1610	4484	-	-	-	-	5.78±0.34	07KNSTD	-	0.96±0.08	-	-	-	-	-
	K2E-2		35.7080	76.1660	4483	-	-	-	-	4.68±0.31	07KNSTD	-	0.77±0.07	-	-	-	-	-
	K2E-3		35.7440	76.2360	5216	-	-	-	-	4.61±0.6	07KNSTD	-	0.53±0.08	-	-	-	-	-
	K2E-4		35.7490	76.2430	5218	-	-	-	-	5.87±0.32	07KNSTD	-	0.68±0.06	-	-	-	-	-
	K2E-5		35.7030	76.2210	5075	-	-	-	-	4.67±0.43	07KNSTD	-	0.57±0.07	-	-	-	-	-
	K2E-6		35.7030	76.2230	5091	-	-	-	-	4.42±0.27	07KNSTD	-	0.54±0.05	-	-	-	-	-
	K2E-7		35.7000	76.2250	5127	-	-	-	-	9.97±0.44	07KNSTD	-	1.23±0.09	-	-	-	-	-
	K2E-8		35.7230	76.2520	4659	-	-	-	-	5.23±0.35	07KNSTD	-	0.79±0.07	-	-	-	-	-
	K2E-9		35.7220	76.2580	4641	-	-	-	-	5.32±0.33	07KNSTD	-	0.82±0.07	-	-	-	-	-
	K2E-12		35.7330	76.3160	4103	-	-	-	-	6.75±0.44	07KNSTD	-	1.38±0.12	-	-	-	-	-
	K2E-20		35.7650	76.5350	4655	-	-	-	-	11.68±2.19	07KNSTD	-	1.84±0.38	-	-	-	-	-
	K2E-23		35.7580	76.5360	4643	-	-	-	-	4.22±0.36	07KNSTD	-	0.64±0.07	-	-	-	-	-
	K2E-24		35.8210	76.5130	4869	-	-	-	-	15.54±0.75	07KNSTD	-	2.23±0.18	-	-	-	-	-
	K2E-25		35.8220	76.5160	4877	-	-	-	-	6.04±0.61	07KNSTD	-	0.82±0.10	-	-	-	-	-

[a] Data from Barnard et al. (2004)
[b] Data from Srivastava (2012)
[c] Outliers removed
[d] Ratios are corrected from background ^{10}Be: 1.51±0.41 and 2.49±0.39 (^{10}Be/^{9}Be ± 1σ (10^{-15}))
[e] Ratios are corrected from background ^{10}Be: 1.37±0.68 and 1.04±0.39 (^{10}Be/^{9}Be ± 1σ (10^{-15}))
[f] Ratios are corrected from background ^{10}Be: 0.87±0.29 and 0.64±0.24 (^{10}Be/^{9}Be ± 1σ (10^{-15}))
[g] Ratios are corrected from background ^{10}Be: 2.39±1.01 (^{10}Be/^{9}Be ± 1σ (10^{-15}))
[h] Ratios are corrected from background ^{10}Be: 4.33±2.18 and 3.10±1.03 (^{10}Be/^{9}Be ± 1σ (10^{-15}))
[i] Lifton-Sato-Dunai (LSD) scaling model
[j] Lal and Stone time-dependent (Lm) scaling model
[k] Lal and Stone time-independent (St) scaling model
- No data

S4. A maximum spallogenic ^{10}Be concentration at the surface of a boulder; estimated assuming a ^{10}Be production rate of ~95.4 atoms/g SiO$_2$/a, density of 2.7 g cm^{-3}, decay constant of 4.99 x 10^{-7}, erosion rate of 0.2–0.5 mm a^{-1}, and spent ~0.5 ka on the supraglacial zone.